Author:
Scott, Louis M

Title:
The interplay between innate immunity and metabolism in the retinal pigment epithelium

The interplay between innate immunity and metabolism in the retinal pigment epithelium

Louis McCullum Scott

A dissertation submitted to University of Bristol in accordance with the requirements for award of degree of Doctor of Philosophy in the Faculty of Medicine and Dentistry

Translational Health Sciences

August 2019

Word Count: 98,190

Abstract

All cells must be able to tailor their energetic resources to different conditions both in quiescent and stress contexts. The retinal pigment epithelium (RPE) provides a highly dynamic model system to study basic cellular metabolism due to its extremely active mitochondrial capacity, which maintains retinal homeostasis and compensates the noxious effects of oxidative damage to the tissue. RPE stress, inflammasome activation and metabolic alterations with mitochondrial dysfunction have been implicated in retinal diseases. However, the causal link between stress, metabolic alterations and retinal degeneration remains unclear.

There are important symbiotic interactions between immune responses and core intracellular metabolic pathways. Specific alterations in metabolism couple to immune effector functions, most notably resulting in a programmed production of distinct sets of cytokines. To this end, immune cells with different functions use several different metabolic pathways to generate adequate levels of energy stores to (A) support survival and (B) to facilitate the highly expensive production of numerous biosynthetic intermediates. Conversely, evidence suggests that intracellular metabolites themselves may modulate immune function. This thesis highlights the interplay between immune responses and cellular metabolism in the RPE (a non-haemopoietic innate immune cell responsible for immune privilege in the retina). Key components of the RPE innate immune response are responsible for the remodelling of metabolic pathways through innate immune receptor signalling and nuclear control over protein expression.

A decline in mitochondrial capacity with age may limit the ability of a cell to divert energy sources and maintain optimum retinal health. The data presented suggest that the activity of the energy sensor AMP-activated kinase (AMPK) is fundamental to maintaining innate immune and metabolic function within the RPE. AMPK acts as a “built-in brake system” to limit aerobic glycolysis and anabolic metabolism, whilst simultaneously increasing mitochondrial function. During innate immune activation, altering the activation state of AMPK allows different Toll-like receptor (TLR) agonists to elicit alternate RPE metabolic phenotypes.

Data presented have identified the “alarmin” interleukin-33 (IL-33) as a key regulatory node of RPE metabolism. Activation of the IL-33/ST2 axis is supported metabolically by mitochondrial respiration. Through bolstering mitochondrial activity, exogenous IL-33

administration protects RPE cells against oxidative damage, accompanied by the increased expression of PGC-1α and other metabolic regulators. In addition to its extracellular function, endogenous IL-33 expression status influences metabolic regulation in RPE cells. IL-33 loss constrains oxidative glucose catabolism, as IL-33 was found to regulate pyruvate import into the mitochondria through the mitochondrial pyruvate carrier (MPC) complex. In contrast, cells overexpressing IL-33 display increased expression of MPC complex components and activity of pyruvate dehydrogenase to facilitate increased pyruvate flux into the TCA cycle.

IL-33 retains its nuclear localisation *in vitro* under multiple conditions of inflammatory stress and interacts with a dynamic network of proteins. Moreover, it is observed that nuclear IL-33 regulates protein expression of human and murine RPE cells and contributes to the regulation of metabolic enzyme splicing. These support the current view of IL-33 as a dual function protein with functional roles in the nucleus. As IL-33 and its nuclear interactions are enhanced or dampened in response to inflammatory cues, this indicates that intrinsic IL-33 acts as a key node to maintain cellular metabolic profiles and likely facilitate innate immune responses separate from its extracellular functions.

Acknowledgements

First and foremost, I would like to thank Andrew Dick for providing me the opportunity to work on this thesis. As a mentor, he has provided the perfect balance between support, encouragement and inspiration, challenging me to think beyond the simplest answer and giving me the confidence to express my thoughts and develop independently. Despite juggling about a thousand jobs and different research projects, he still retains the laid-back nature one can only find in the surfers of Hawaii's north shore. An absolute "dude" to put it simply.

I would like to acknowledge Sofia Theodoropolou in her role as my second PhD supervisor.

I am indebted to the support given from Emma Vincent throughout my thesis. Whether that be the continued scientific advice, kind words of encouragement or just eagerness to grab a beer, nachos and a chat!

I would like to thank Lindsay Nicholson for his encouraging jokes about how metabolism is not important. Jokes aside, I am grateful for all his advice and praise during my time here. Most notably, I am incredibly thankful that he kindly agreed to give up his time to give feedback on the early drafts of this thesis.

I would like to thank Dave Copland for his continued help and support throughout my PhD. I doubt any of this work could have happened without his guidance.

Everyone in the Ophthalmology research group (past and present) have made this an enjoyable and stimulating place to work. I would like to thank so many of them for their help, encouragement and general banter that's kept me going through this project. I would like to thank Richard Lee, Jian Liu, Lauren Schewitz-Bowers, Kepeng Ou, Lydia Bradley and Colin Chu. Most importantly, I would like to thank the other "dream team" members Amy Ward and Oli Bell for all your support.

A huge thank you to Mathew Campbell and team in Trinity College Dublin for everything *Il33*$^{-/-}$, to Chris Neal for the electron microscopy, to Kate Heesom for the proteomics advice, Luc Choinière for the mass spec and Nick Jones for assistance in so many aspects of this thesis.

I am so grateful to all my friends and family who continued to support me and realised that it wasn't that they were less important than the job, but rather the job was so important to me. Especially my mum, dad and grandparents for their love and support, despite having no clue

what I have been doing all this time. To Joséphine Thouvenin, Damian Mayo, Nathan Simmonds-Buckley, Ross Falco, Eli Wellstead and Lucy Troman for keeping me sane.

None of this work would have been possible without the kind donations given by the Macular Society, most importantly Lady Wall and her inspiring determination to fight macular degeneration.

Author’s declaration

I declare that the work in this dissertation was carried out in accordance with the requirements of the University's *Regulations and Code of Practice for Research Degree Programmes* and that it has not been submitted for any other academic award. Except where indicated by specific reference in the text, the work is the candidate's own work. Work done in collaboration with, or with the assistance of, others, is indicated as such. Any views expressed in the dissertation are those of the author.

SIGNED: ..... DATE:.....

Table of Contents

List of figures

List of abbreviations

2DG	2-deoxyglucose
3-PG	3-phosphoglycerate
Aβ	Amyloid beta
ADP	Adenosine diphosphate
ACAVDL	Very-long chain specific acyl-coA dehydrogenase
ACC	Acetyl CoA carboxylase
AICAR	5-Aminoimidazole-4-carboxamide ribonucleotide
AP	Alternate pathway
AP-1	Activator protein 1
APC	Antigen presenting cell
AMD	Age-related macular degeneration
AMP	Adenosine monophosphate
AMPK	AMP-activated kinase
ASC	Apoptosis-associated Speck-like protein
ATP	Adenosine triphosphate
BAX	BCL-2-associated X protein
BCL2	B-cell lymphoma 2
BCLXL	B-cell lymphoma extra-large
BGLOB	Beta-globulin
BIR	Baculoviral inhibitor of apoptosis repeat
BM	Bruch's membrane
BMDM	Bone-marrow-derived macrophages
BMMC	Bone-marrow-derived mast cells
Bregs	Regulatory B-cells
CARD	Caspase-recruitment domain
CEP	Carboxyethylpyrrole
CD	Cluster of differentiation
CFH	Complement factor H
ChIP	Chromatin immunoprecipitation

CNV	Choroidal neovascularisation
COX2	Cytochrome C oxidase
CP	Classical pathway
CpG	CpG oligodeoxynucleotide
CPT1	Carnitine palmitoyl transferase I
CRegs	Complement regulatory factors
CTL	Cytotoxic lymphocytes
CXCL	C-X-C motif chemokine
Cybrid	Cytoplasmic hybrid
CYTB	Cytochrome B
DAMP	Danger associated molecular pattern
DAVID	Database for Annotation, Visualization and Integrated Discovery
DMSO	Dimethylsufoxide
dsRNA	Double stranded RNA
ECAR	Extracellular acidification rate
ELISA	Enzyme-linked immunosorbent assay
ERR	Estrogen-related receptor
ETC	Electron transport chain
FACS	Fluorescence-activated cell sorting
FAD	Flavin adenine dinucleotide
FCCP	P-trifluoromethoxyphenylhydrazone
FcεR1	Fcε receptor 1
FDR	False discovery rate
FGF	Fibroblast growth factor
FH	Fumarate hydratase
FOXO1	Forkhead box protein O1
GA	Geographic atrophy
GAPDH	Glyceraldehyde-3-phosphate dehydrogenase
GCMS	Gas chromatography coupled to mass spectrometry
GFAP	Glial fibrillary acidic protein
GLUT1	Glucose transporter 1

GM-CSF	Granulocyte-macrophage-colony-stimulating factor
GWAS	Genome-wide association studies
H_2O_2	Hydrogen peroxide
HDAC	Histone deacetylase
HIF-1α	Hypoxia inducible factor 1 alpha
HMBG1	High mobility group box 1 protein
hnRNP	Heterogeneous nuclear ribonucleoprotein
ICL2	Type 2 innate lymphoid cell
IDH	Isocitrate dehydrogenase
Ig	Immunoglobulin
INF	Interferon
IL	Interleukin
IL-1R	Interleukin receptor
IL-1RA	Interleukin-1 receptor agonist
IL-1RAcP	IL-1 receptor accessory protein
IRAK	Interleukin-1 receptor-associated kinase
IRF	Interferon-regulatory factor
KD	Knockdown
LANA	Latency-associated nuclear antigen
LC	Liquid chromatography
LP	Lectin pathway
LPS	Lipopolysaccharide
LRR	Leucine-rich repeated
MAC	Membrane attack complex
MACS	Magnetic-activated cell sorting
MAPK	Mitogen activated protein kinase
MASP	Mannose-binding lectin serine peptidase
MBL	Mannose-binding lectin
MCT1	Monocarboxylate transporter 1
MFN	Mitofusin
MHC	Major-histocompatibility complex

MID	Mass isotopomer distributions
MIO-M1	Moorfields/Institute of Ophthalmology- Müller 1
MMPs	Extracellular matrix metalloproteinases
MPC	Mitochondrial pyruvate carrier
Mreg	Regulatory macrophage
MS	Mass-spectroscopy
mtDNA	Mitochondrial DNA
mTOR	Mammalian target of rapamycin
mTORC	mTOR complex
MyD88	Myeloid differentiation factor 88
NAD	Nicotinamide adenine dinucleotide
nAMD	Neovascular AMD
NDUFB8	NADH dehydrogenase ubiquinone 1 beta subcomplex subunit 8
NF1	Nuclear factor 1
NF-κB	Nuclear factor kappa B
NK	Natural killer cell
NLR	NOD-like receptor
NRF	Nuclear respiratory factor
NOD	Nucleotide binding domain
NOX	NADPH oxidase
OCR	Oxygen consumption rate
OMM	Outer mitochondrial membrane
OXPHOS	Oxidative phosphorylation
P53	Tumour suppressor p53
PAMP	Pathogen associated molecular pattern
PC	Pyruvate carboxylase
PDH	Pyruvate dehydrogenase
PDK	Pyruvate dehydrogenase kinase
PEDF	Pigment epithelium-derived factor
PER	Proton efflux rate
PFK	Phosphofructokinase

PFKFB1	6-phosphofructo-2-kinase/fructose-2,6-biphosphatase 1
PGC-1	PPARγ coactivator 1
PI3K	Phosphoinositide 3-kinase
PINK-1	PTEN-induced kinase
PKM	Pyruvate kinase muscle isoform
POS	Photoreceptor outer segments
PPAR	Peroxisome proliferator-activated receptor
PPP	Pentose phosphate pathway
PRR	Pattern-recognition receptor
PTB	Polypyrimidine tract binding protein
Raptor	Regulatory protein associated of mTOR
Rictor	Rapamycin-insensitive companion of mTOR
RIPK3	Receptor-interacting serine/threonine-protein kinase 3
RNA-seq	RNA sequencing
ROS	Reactive oxygen species
RPE	Retinal pigment epithelium
RPE65	Retinoid isomerohydrolase
SAM	S-adenosylmethionine
SDH	Succinate dehydrogenase
siRNA	Small interfering RNA
SIRT1	Sirtuin 1
SITA	Stable isotope tracing
SNP	Single nucleotide polymorphism
SOD	Superoxide dismutase
SRSF3	Serine/arginine-rich splicing factor 3
ST2	Suppression of tumorigenicity 2
STAT	Signal transducer and activator of transcription
STING	Stimulator of interferon genes
TFAM	Mitochondrial transcription factor A
TGFβ	Transforming growth factor-β
Th	T helper

TIGAR	TP53-induced glycolysis and apoptosis regulator
TIMPs	Tissue inhibitor of matrix metallo-proteases
TIR	Toll/IL-1 receptor
T-mem	Memory T-cell
TMT	Tandem mass-tagging
TNF	Tumour necrosis factor
TRAF	TNF receptor-associated factor 6
Tregs	Regulatory T-cells
TRIF	Toll/IL-1 domain-containing adaptor-inducing interferon-β
TLR	Toll-like receptor
UCP1	Uncoupling protein 1
UQCRC2	Cytochrome b-c1 complex subunit 2
VEGF	Vascular endothelial growth factor
WDFY1	WD repeat and FYVE domain containing 1
WDR82	WD Repeat Domain 82
XF	Extracellular flux

Chapter 1. Introduction

1.1. Primer

The retina is referred to as an "immune privileged" tissue, where homeostasis is maintained through both hemopoietic immune cells such as microglia and innate immune-competent tissue resident cells such as the retinal pigment epithelium (RPE) [1]. RPE are integral in the maintenance of immunity within the retina, generating a diverse cytokine and chemokine output that contributes to defence against foreign antigens [1, 2]. The RPE is highly differentiated and considered to be a post-mitotic single cell layer that performs a host of functions critical to retinal homeostasis, including the maintenance of the visual cycle and photoreceptor phagocytosis [3]. RPE cells are highly metabolically active whilst providing critical metabolic support through the directional transport of glucose and lactate to fuel the outer retina and photoreceptors in particular [4]. Defects in RPE metabolic and mitochondrial function, associated with low grade inflammation or with age-related decline, are associated with retinal degenerative diseases including age-related macular degeneration (AMD) [2].

Cellular intrinsic and extrinsic signals regulate the activity of metabolic pathways to couple the growth and survival needs of the cell and consequently regulates the generation of key products to fulfil these needs. In the context of immunity, metabolic changes directly influence immune cell effector functions. The flexibility to switch between multiple biochemical pathways maintains intracellular adenosine triphosphate (ATP) levels for energy demanding processes, including cell proliferation, growth and immune-modulation *via* cytokine production [5]. Understanding how immune competent tissue-resident cells, like RPE, manage energy consumption to potentially support the maintenance of outer retinal function is crucial. Recently, data shows that RPE cells utilise reductive carboxylation [6] that supports redox homeostasis. This in turn is re-enforced by the documented disproportionate damage to mitochondrial DNA in the RPE of individuals with AMD, corroborating a causal link. Therefore, a possible explanation is that photoreceptors, which mainly rely on RPE lactate, starve when RPE mitochondria fail and the RPE becomes more dependent on glycolysis, preventing glucose from reaching the retina. Furthermore, as the retina ages, RPE become increasingly susceptible to the cumulative effects of oxidative stress, as a result of their high metabolic demand [7]. As a result of this, adaptive and innate immune functions are disturbed, leading to an imbalanced environment unable to control cell death, tissue dysfunction or up-regulate inflammatory responses [1].

Interleukin-33 (IL-33), a member of the IL-1 family, is a type 2 cytokine that is constitutively expressed in the inner retina, RPE and choroid [8] as well as in epithelial cells, endothelial cells, and fibroblasts

[9]. IL-33 either functions as an “alarmin” molecule released from necrotic barrier cells following cellular damage [9] or is retained within the nucleus of cells to control gene expression [10]. However, the mechanisms controlling the later remain poorly understood. Extracellular IL-33 binds to its cognate receptor, formed of a heterodimeric complex of suppression of tumorigenicity 2 (ST2) and IL-1 receptor accessory protein (IL-1RAcP), to activate mitogen activated protein kinase (MAPK) and nuclear factor kappa B (NF-κB) signalling pathways [11]. The role of IL-33 has been recognized in several diseases, such as, chronic gastrointestinal inflammation [12], allergic diseases/ anaphylaxis [13], cardiovascular disease [14], choroidal angiogenesis [8] and Alzheimer’s [15]. In experimental autoimmune uveitis, IL-33 moderates disease severity [16]. In a phototoxic model of retinal degeneration, IL-33 contributed to an upregulated chemokine and cytokine output from Müller Glia, leading to the recruitment of mononuclear phagocytes, and ultimately contributing to photoreceptor loss and diminished retinal integrity [17].

It has been previously shown that Toll-like receptors (TLR) ligands (TLR-3, -4) induce up-regulation of IL-33 in RPE cells without cell death [8]. Recent exploitation of the cytoplasmic hybrid (cybrid) technique for representative mitochondrial DNA (mtDNA) haplotypes of AMD populations, revealed alterations in IL-33 expression and altered bioenergetics [18]. This, coupled with novel epigenetic roles for IL-33 as shown in the maintenance of mitochondrial function in adipose tissue [19] and the observation that a deficiency in the IL-33/ST2 axis reshapes mitochondrial metabolism in macrophages, prompts the questions: (1) do aspects of the innate immune system (e.g. endogenous vs exogenous IL-33 and TLR signalling) regulate metabolism in the RPE and (2) if so, what are the implications for degenerative diseases such as AMD whereby metabolic dysfunction drives disease progression?

1.2. The eye

The eye is a highly organized and complex structure, which reflects its specialized function for photoreception. Light energy from the environment passes through the ocular media and concentrates on the macula (a specialized area of the retina attributed with a dense population of photoreceptors for high visual acuity). Upon reaching the macular, light is transduced by specialized nerve cells (rod photoreceptors and cones) into nerve impulses in the form of an action potential. These are then relayed to the optic nerve and subsequently to the brain, whereby the neuronal signals

are appreciated as vision [20]. The retinal anatomy is comprised of several layers: an internal limiting membrane, nerve fibre layer, a ganglion cell layer, the inner and outer plexiform layers, the photoreceptor layer, the RPE, Bruch's membrane and the choroidal vasculature (which together form the choroid) and the sclera. (Fig. 1.1). Müller glia are observed in the inner nuclear layer as the supporting glia cell. Bipolar cells, horizontal cells and amacrine cells also aid neural support to the inner nuclear layer. Blood is directed to the neural retina by retinal blood vessels, originating from the central retinal artery and supplying the choroidal network. The choroid has a specific VEGF-controlled vasculature with caveola and in distinct layers with fibroblasts, mast cells, macrophages and dendritic cell populations [21]. Transport across the inner retinal vasculature is mediated by retinal endothelial cell tight junctions and by the Bruch's membrane (BM) which comprise the inner blood-retinal barrier; the RPE comprise the outer-blood-retinal barrier. Integrity of the blood-retinal barrier is an important physiological barrier which maintains ion, protein, nutrient and water flux between the choroidal blood and the retina [20]. Optimal vision is dependent on effective function in the retina, particularly that of the macula. Damage to any structure on the visual axis, from the cornea to photoreception in the retina, likely leads to aberrations in or loss of vision.

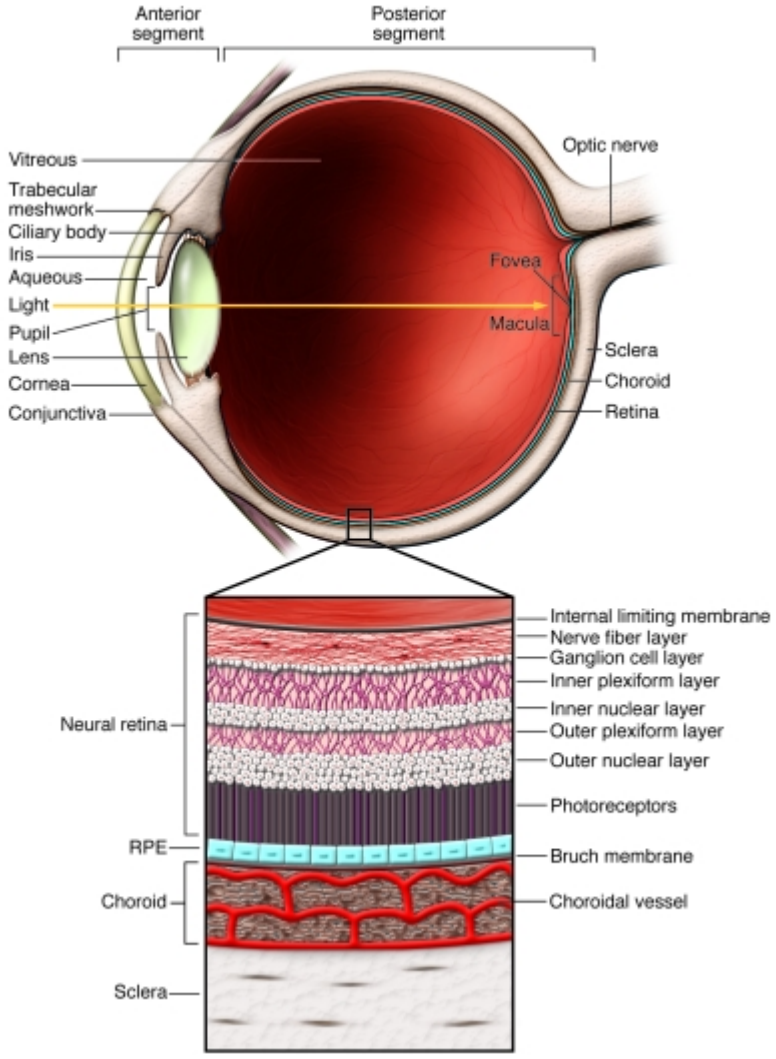

Figure 1.1. Schematic of the eye and major anatomical structures of the retina:

Light enters the eye through the lens and passes through the ocular media before concentrating on the macula. Photoreceptors interpret the photons of light as an action potential which is transmitted to the brain *via* the optic nerve. The retinal architecture is comprised of (from anterior to posterior) an internal limiting membrane, nerve fibre layer, a ganglion cell layer, the inner and outer plexiform layers, the photoreceptor layer, the retinal pigment epithelium (RPE), Bruch's membrane and the choroidal vasculature (which together form the choroid) and the sclera. Damage to the structures along the visual axis likely manifests in visual impairment. This figure schematic is reproduced from [22].

1.3. Retinal pigment epithelium

Situated between the photoreceptors and the choroidal vasculature is the highly organized monolayer of neuroectodermally-derived pigmented cells, termed the RPE (Fig. 1.1) [23]. In terms of its orientation, the apical membrane of the RPE faces the photoreceptor outer segments, whereas its basolateral membrane faces Bruch's membrane and separates the RPE from the endothelium of the choriocapillaris [3]. On the basolateral membrane of RPE cells, numerous highly convoluted invaginations increase the overall surface area for optimal absorption of oxygen and nutrients [24]. The apical surface contains numerous microvilli which maximize the surface area of plasma membrane surrounding photoreceptor outer segments (POS) in order to maximize transepithelial flux and augment phagocytosis [24] (Fig. 1.2). The RPE layer encompasses the optic nerve to the ora serrata and subsequently continues as the pigment epithelia of the ciliary body [23]. There are typically around three and a half million RPE in a human adult eye and this population remains stable throughout young adult life [23]. Studies investigating mitosis and proliferation in RPE cells indicate that very low levels of RPE are retained in the cell cycle, with the RPE considered to be a post-mitotic terminally differentiated cell [23]. The high abundance of pigment in the RPE monolayer results in the absorption of light energy focused onto the macula by the lens [24]. The dark pigment of the RPE is attributed to the large distribution of melanin granules within the cells [24]. RPE exhibit a basal nucleus and a high level of mitochondria which reflect the high metabolic rate of the cells. Additionally, the cells have an abundance of smooth endoplasmic reticulum and lysosomes [24].

The primary role of the RPE is in the preservation and survival of the overlying photoreceptors. The RPE facilities the absorption of fluid, ions and nutrients (such as glucose, fatty acids, amino acids and retinol) from the choroidal blood flow to supply the photoreceptors. The passage across the RPE occurs *via* lateral plasma membrane barrier junctions and transporters located in the apical and basal membranes. Metabolic end products, such as lactate from the highly glycolytic photoreceptors, is removed from the sub-retinal space *via* the lactate/H^+ co-transporter monocarboxylate transporter 1 (MCT1) [4, 25]. The RPE expresses transporters for multiple amino acids including alanine, taurine, glutamine and leucine [26]. The high expression of glucose transporter 1 (GLUT1) on both apical and basal membranes permits the passive "trans-RPE" flux of glucose from the choroid to the photoreceptors [27]. A continuous cycle of retinal exchange occurs between the photoreceptors and the RPE [3]. As photoreceptors themselves cannot metabolize *trans*-retinal (occurring post light absorption) into 11-*cis*-retinal, isomerization occurs in the RPE (*via* the RPE-specific isomerase retinoid isomerohydrolase (RPE65)) and is then transported back to the photoreceptors. This permits the

preservation of photoreceptor excitability and is a mechanism identified as the “visual cycle of retinal” [3]. The RPE plays a key role in the phagocytosis of POS. During a lifetime, it is estimated that each RPE cell consumes over 45 outer segments, whereby daily renewal processes result in ~10% of photoreceptor volume shed and phagocytosed [28]. Consumed POS are degraded through a combination of over 40 different lysosomal protease enzymes, the most prominent of these in the RPE is cathepsin D [29]. Daily internalization of POS and rapid proteasomal degradation in RPE cells, in conjunction with the observation that *in vivo* RPE are terminally differentiated and therefore post-mitotic, indicates that these cells have an enormous proteolytic burden [30]. Indeed, the RPE exhibits one of the highest phagocytic capacities of cells in the body [30]. Processed outer segment end-products are degraded and recycled quickly in young healthy RPE. However, with time, incompletely degraded photoreceptor material is accumulated in the form of lipofuscin, lipid-containing residues of lysosomal digestion [31].

The retina is the single neural tissue with constant direct exposure to visible light. This combined with the high oxygen consumption and electron transport chain (ETC) activity of RPE cells lead to a high production rate of reactive oxygen species (ROS) and photo-oxidized lipids with noxious potential for retinal cells [32]. There are various types of ROS, including both superoxide radicals (O^{-}_{2}), hydroxyl ions (OH^{-}) and non-radicals, such as hydrogen peroxide (H_2O_2) [33]. Additionally, phagocytosis of POS creates high levels of ROS *via* the respiratory burst, increasing H_2O_2 production over nine-fold [34, 35]. The RPE plays a critical role in protecting against high levels of oxidative stress and photo-oxidation and this is achieved by multiple defence mechanisms. The first line of defence is the presence of the multiple pigments (melanin, zeaxanthin and lipofuscin) which act as an optical filter to limit the absorption of damaging blue wavelengths before reaching the sensory neurons [35]. Another line of defence is comprised of both enzymatic and non-enzymatic antioxidant systems, which facilitate the immediate removal of ROS [32]. Antioxidant enzymes, such as superoxide dismutase (SOD)-1 and -2, catalase and glutathione peroxidase are expressed at high levels in the RPE [36]. Smaller non-enzymatic antioxidant, such as carotenoids, vitamin C, vitamin E and ubiquinol are accumulated in the RPE and support the enzymes as direct radical scavengers [32, 33].

The RPE have a key role in the secretion of various soluble growth factors, survival factors and signalling molecules which are essential for the maintenance of structural integrity of the retina, photoreceptors and the choriocapillaris. The importance of secretion direction from the RPE is often overlooked, with many proteins exhibiting a preferential secretion by either the apical or basolateral

membrane to promote either photoreceptors or the choroidal blood flow, respectively [37]. RPE cells basolaterally secrete various types of tissue inhibitor of matrix metallo-proteases (TIMPs) to facilitate the remodelling and health of the choroidal vasculature *via* limiting the action of extracellular matrix metalloproteinases (MMPs) [3]. Multiple MMPs and TIMPs are apically secreted by the RPE to support the turnover and maintenance of the interphotoreceptor matrix [37]. Interestingly, it is proposed that RPE secrete certain MMPs and TIMPs in different directions depending on various environmental cues, such as cytokine signalling [37]. Moreover, the RPE secretes fibroblast growth factors (FGFs), transforming growth factor-β (TGF-β), endothelin 1, cystatin C, vascular endothelial growth factor (VEGF) and pigment epithelium-derived factor (PEDF) which regulate optimal circulation and stabilization of the endothelium and choriocapillaris on the basolateral side, and avert angiogenesis on the apical side [3, 37]. Additionally, PEDF is secreted preferentially on the apical side of RPE, where it acts as a neurotropic survival factor for photoreceptors [38]. αB crystallin is a cytoprotective molecular chaperone released from the apical side of RPE cells under stress stimuli, which inhibits caspase-3-mediated apoptosis in photoreceptors, conferring a survival advantage [39].

Natural regulatory mechanisms are present to regulate inflammation in the ocular microenvironment, including the anatomical restriction of lymphatics into the retina through the blood-retinal barrier. As previously discussed, RPE constitute part of the blood-retinal barrier preventing movement of cells into the eye from the bloodstream [40]. To this end, the eye is referred to as an organ exhibiting immune privilege. Innate immune responses in the retina are therefore maintained though tissue-resident myeloid cells (macrophages/microglia) and innate immune competent - but not haematopoietically-derived - cells, such as the RPE [41]. Multiple lines of evidence suggest an immunoregulatory function of the RPE which endeavours to maintain tissue homeostasis under stress. For example, RPE cells suppress the activation of cluster of differentiation (CD)4+ and CD8+ T-cells through TGF-β [42, 43] and elicit the expression of various suppressive anti-inflammatory cytokines [44]. The RPE cell expresses innate TLRs, functional NOD-like receptors (NLRs) and complement system components, but also exhibits adaptive immune functions, such as major-histocompatibility complex (MHC) class I and II antigens expression and contribution as retinal antigen-presenting cell (APC) [44-48]. Furthermore, the RPE has a vast output of immuno-stimulatory chemokines and cytokines, including both anti-inflammatory: TGF-β, interleukin (IL)-11, interleukin-1-receptor agonist (IL-1RA) and interferon(IFN)-β, and pro-inflammatory: IL-6, IL-15, tumour necrosis factor (TNFα), IL-1α/β, IL-8, IL-18, monocyte chemotactic protein (MCP)-1, granulocyte-macrophage-colony-stimulating factor (GM-CSF), C-X-C motif chemokine (CXCL)-10 CXCL-11 and IL-33 [44, 47, 49], which permit predominantly immune regulatory signalling networks between RPE cells and other retinal innate

immune cells. In addition to their rich expression of cytokines, RPE cells also express functional cytokine/chemokine receptors to respond to many of the above listed cytokines, but similarly others, such as IFN-γ, IL-22, IL-4, IL-13, IL-10 and IL-17 [8, 48-51].

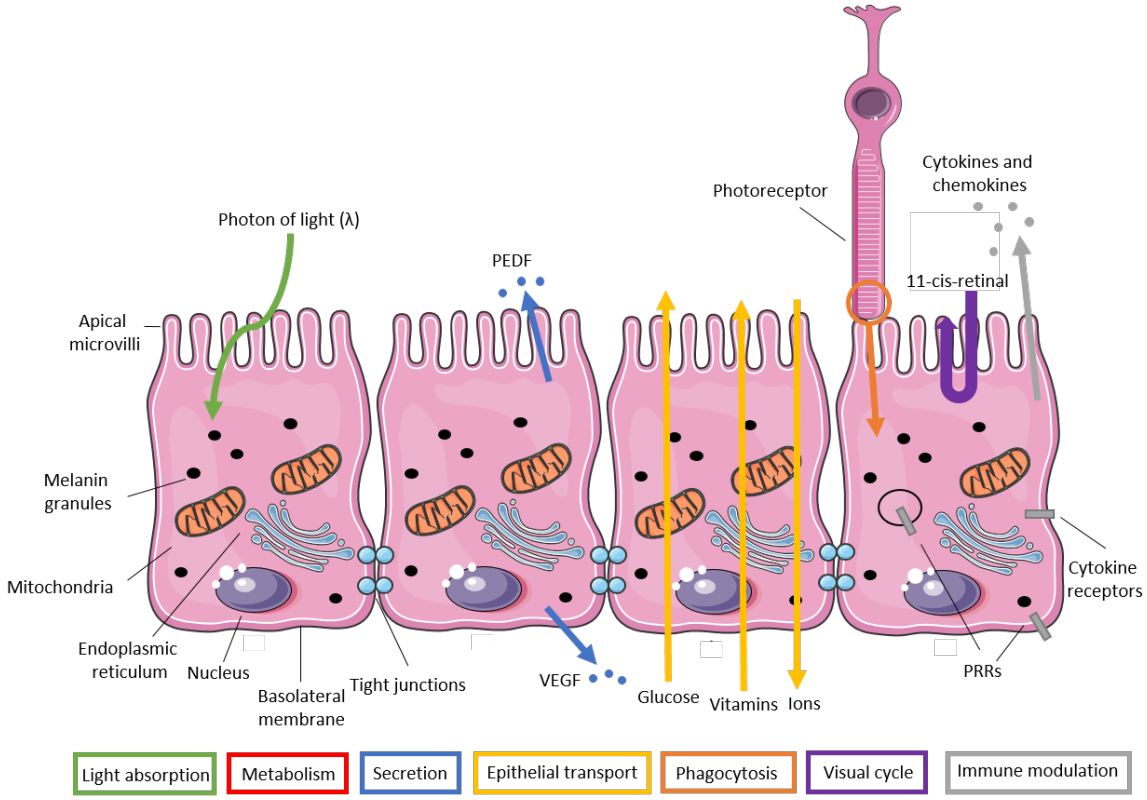

Figure 1.2. Summary of the retinal pigment epithelium and its functions:

The RPE is a monolayer of cells located between the choroid and photoreceptors. RPE cells have a polarized morphology with apical microvilli projections extending out between the rods and cones for functional support. RPE cells are interconnected by the expression of tight junctions. The RPE has multiple important functions in the maintenance of homeostasis and functional support to both the choroid and photoreceptors. These functions include: the absorption of photons of light in pigmented granules, metabolic support of the retina, secretion of factors which regulate the health of both photoreceptors and the choroidal vasculature, trans-epithelial movement of nutrients, ions and metabolic waste products, phagocytosis of old rod outer segments, re-isomerization of 11-*cis*-retinal to complete the visual cycle and maintenance of immune privilege through the expression of innate-immune receptor complexes/secretion of immune-modulating cytokines and chemokines. PEDF, pigment epithelium-derived factor; VEGF, vascular endothelial growth factor; PRR, pattern-recognition receptors. Adapted from [3].

1.4. Age-related macular degeneration

The leading cause of irreversible blindness within the western world can be attributed to AMD. The disease refers to the progressive deterioration of the macula occurring predominantly in the older population (post 60 years of age). The annual global economic cost of AMD is estimated to be in excess of US$300 billion, with over 30 million individuals worldwide suffering from visual defects by cause of AMD [2]. With a progressive increase in the ageing population, it is anticipated that there will be a 50% increase its prevalence by 2050 [52]. AMD is classified into two distinct subsets: neovascular age-related macular degeneration (nAMD) (wet) and geographic atrophy (GA) (advanced dry), both of which lead to significant visual impairment. nAMD is characterised by abnormal growth of blood vessels from the choriocapillaris into the retina. Whilst the fundamental biology remains uncertain, molecular therapies which target VEGF (a pro-angiogenic factor) are successful in preventing disease progression in a large proportion of patients [53]. Granting current anti-VEGF therapies have revolutionized treatment strategies for nAMD, there remains no approved cure for the dry form, largely due to a scarcity of suitable molecular targets. The early stages of GA are characterized by insoluble extracellular lipid deposits (drusen), which accumulate between the RPE and BM [54]. GA develops following the development of drusen, and refers to large confluent areas of RPE detachment and cell death, and atrophy of RPE, the overlying photoreceptor and the choriocapillaris [55]. This ultimately confers reduced visual function, with GA accounting for around 50% of legal blindness associated with AMD [2]. The influence of innate immunity (mainly that of the complement system and pattern recognition receptors (PRR)) are widely accepted as central to the progression of dry AMD development [2, 56]. Yet, as AMD development is long and insidious, it is likely that altered immune responses occur as a result of disparity between protective responses (in place to maintain tissue homeostasis) and chronic parainflammatory responses, secondary to a lifetime of oxidative damage within the retina, mainly in the RPE [57].

1.5. Innate immunity

1.5.1. Pattern-recognition receptors

Innate immune responses are evolutionarily perfected; conserved across the animal kingdom, these non-clonal inflammatory responses recognize pathogen associated molecular patterns (PAMPs) and self-derived danger associated molecular patterns (DAMPs) to produce an immediate output of co-stimulatory chemokines and cytokines [58]. Innate immune responses differ from adaptive immunity in the sense that their recognition of biological material (proteins, lipids, DNA and carbohydrates) is not antigen specific and therefore lacks the requirement of anergy and clonal expansion. Whilst macrophages and dendritic cells are essential within innate immunity, "non-immunological" cells such as fibroblasts, endothelial and epithelial cells contribute through the expression of germline-encoded PRR [58]. Once activated by ligand recognition, downstream responses are initiated through complex signalling pathways. Cytokines and chemokines produced from PRR signalling promote the activation of antigen presenting cells (e.g. dendritic cells), initiating the adaptive immune response through constant gene re-arrangement in B and T-lymphocytes [59]. To date, a plethora of PRR and their distinct activation pathways have been uncovered, including members of TLR and NLR families.

1.5.1.1. Toll-like receptors

TLRs are transmembrane proteins capable of PAMP recognition both extracellularly, and within endosomes; there are currently 10 TLR observed in humans, and 12 in mice [60]. Each extracellular receptor domain recognizes a specific PAMP, so that the TLR family is capable of recognizing a variety of bacteria, viral and other pathogens [61]. Expression of TLRs 1-6 and 8-10 gene transcripts, and proteins for TLRs 1-6 and 9 have been observed in human RPE [62], with TLRs 2-4, -6 and -9 exhibiting functional responses to synthetic ligands [62, 63]. Interestingly, TLR-3 and -4 are noted to have the highest expression of any TLR in the RPE [45, 62]. Considering these observations noted within the literature - and the fact that I will only examine the effect of TLR-3 and -4 signalling in this body of work – I will only address these receptors in this section. However, readers are directed to the following reviews for a more comprehensive view on signalling through other TLRs ([60, 64]).

Lipopolysaccharide (LPS), a classically described PAMP, is one of the best studied stimuli of the inflammatory response. It is a structural component of the outer membrane of Gram-negative bacteria, recognized by TLR-4. TLR-4 signalling is preceded by a cascade of events, starting with the interaction of LPS-binding protein with LPS. This facilitates the transfer of LPS to the TLR-4 complex

through the involvement of the glycoprotein CD14. Upon activation, the TLR-4 complex undergoes dimerization; this subsequently activates a pro-inflammatory response through myeloid differentiation factor 88 (MyD88) and Toll/IL-1 domain-containing adaptor-inducing IFN-β (TRIF) - dependent cytokine production.

Once activated through specific recognition of viral double-stranded RNA (dsRNA), TLR-3 signalling is initiated through the activation of TRIF which subsequently leads to the nuclear translocation of NF-kB and IFN-regulatory factor-3 (IRF-3) promoting the expression of type 1 IFN genes and other cytokines/chemokines essential for mediating viral defence [45, 65].

1.5.1.2. Nod-like receptors and the inflammasome complex

NLR are cytoplasmic receptors shown to initiate host responses to a wide range of bacterial and viral ligands, there are currently 22 identified NLR in humans [60]. The NLR family share a conserved structure, with three distinct domains: the nucleotide-binding domain (NOD), an N-terminal protein-protein interaction domain which initiates downstream signalling and a C-terminal leucine-rich repeated (LRR) region responsible for PAMP and DAMP recognition [66]. NLR family members can be subcategorized into 4 subfamilies on the basis of their N-terminal domains, these include: acidic transactivation, pyrin, caspase-recruitment domain (CARD) and baculoviral inhibitor of apoptosis repeat (BIR)-like domain [67]. The most studied and well-known NLR family member is NLRP3, which forms a multiprotein immune platform. The inflammasome is an essential part of caspase-1 activation through autocatalysis, allowing the post-translational processing and secretion of pro-inflammatory cytokines IL-1β, IL-18 and IL-33 [68]. Formation of the inflammasome occurs through NLRP1/NLRP3/NLRC4 oligomerization and recruitment of pro-caspase-1 and the apoptosis-associated Speck-like protein (ASC). ASC proteins contain a CARD that allows the amplification of caspase-1 activation [69]. The general mechanism of canonical inflammasome activation by PAMPs and DAMPs remains elusive to date. Multiple models have been advocated, including K^+ efflux, Ca^{2+}/ cAMP signalling, autophagic processing of subcellular material, ROS, altered glycolytic flux, mitochondrial dysfunction and release of oxidised mtDNA, cathepsin activity and NLRP3 deubiquitination [70-74]. Altogether, the literature implies that the NLRP3 inflammasome acts following energetic stress and sub-cellular damage as opposed to an immunological receptor complex. Whilst the NLRP1, NLRP3 and NLRC4 are well known as critical inflammasome components along with ASC/CARD domains, it is noted that roles for additional components (including NLRP6) are now emerging [75]. In addition to

this, it is essential to note that whilst caspase-1 inflammasomes have been extensively studied, additional initiator caspases have also been identified allowing inflammasome complexes to operate in a non-canonical caspase-1-independent manner [76].

1.5.2. Complement system

The complement system is a significant component of innate immune responses, providing an initial defence response that targets and destroys microbial pathogens. It is comprised of a series of plasma proteins which undergo a sequential enzymatic-activation cascade (complement activation pathway), ultimately leading to opsonization of extracellular pathogens and their phagocytic removal [77]. Activation is divided into four key stages: initiation of complement activity, C3 convertase activation, C5 convertase activation and the ultimate formation of a lytic membrane attack complex (MAC). The activity of the complement pathway is attenuated through multiple mechanisms, including reduced half-lives of activated components and a number of soluble complement regulatory factors (CRegs) [78]. Collectively, the complement system is formed of over sixty proteins, of which nine components are central to the cascade (C1-C9) (Fig. 1.3). Numerous activation products, inhibitory factors/regulators (a key and AMD-relevant example includes complement factor H (CFH)), proteases and receptors for effector products (e.g. C5aR) are also included. Complement components are produced primarily in hepatocytes; however, recent studies have identified that key complement components (regulatory proteins) can be produced by the RPE, suggestive of local regulation in order to maintain immune homeostasis [79].

The complement activation process occurs through three dissimilar pathways (alternate (AP), lectin (LP) and classical (CP)) initiated by differing stimuli, but ultimately converging at central complement protein C3 [80]. The CP is initiated in response to antibodies bound to a pathogen or directly to a pathogen surface. The binding of initial component C1q to antibody complexes triggers proteolytic cleavage of downstream steps. The lectin pathway is initiated though the activity of mannose-binding lectin (MBL) and ficolins which bind PAMPS on pathogen surfaces. Key proteases associated with these PRR (e.g. MASP1) trigger the cleavage of C4 and C2. Finally, the alternative pathway is initiated by the spontaneous cleavage and activation of C3, permitting the binding of complement factor B (CFB) and activation of C3 convertase. Following the cleavage of C3 (and generation of C3 convertase from each pathway), activated proteins C3a, C3b, C5a lead to the formation of the MAC (C5b-9) [77]. Interestingly, in the genetic absence of C3, thrombin (coagulation protein) can substitute as a C5-

convertase [81]. Dysregulation of complement is amplified in the pathogenesis of multiple diseases, including rheumatoid arthritis, multiple sclerosis and AMD [56, 82]. More information on how complement dysregulation is observed in AMD can be found in section 1.5.4.

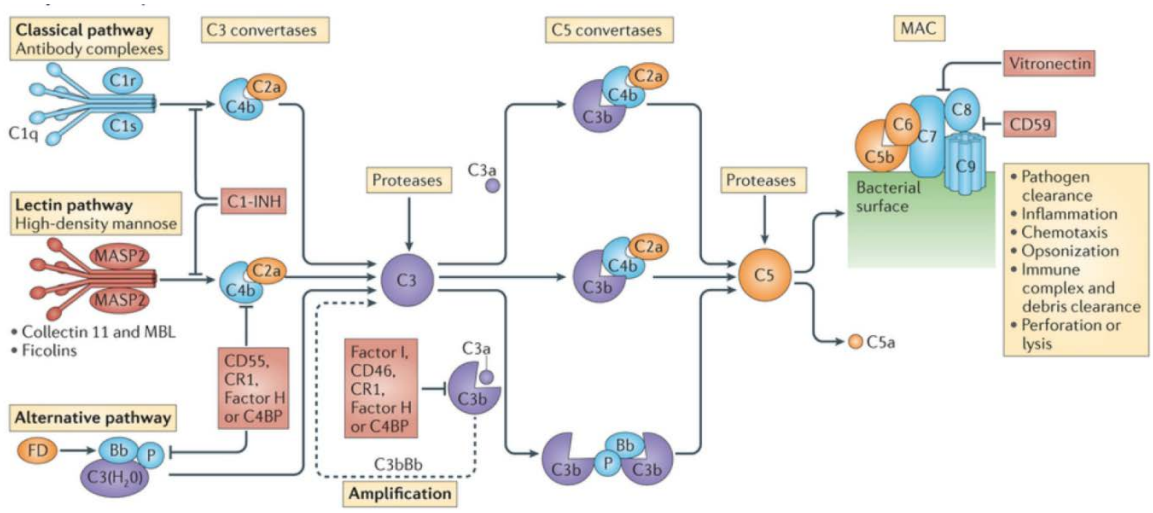

Figure 1.3. An overview of the systemic complement system:

The complement system is initiated by three pathways (alternative, classical and lectin) and leads to a sequential activation cascade of downstream components. The classical pathway involves the binding of antibody-antigen complexes to C1, which itself has three components (C1q, C1r and C1s). The pathway corms a C3 convertase C4b2a, which cleaves C3 into two subsequent fragments. C3b attaches to pathogen surfaces to start the opsonization process whilst C3a activates mast cells. The C3 convertase C4b2a is similarly formed through the lectin pathway: mannose binding lectin binds mannose residues on a pathogen surface, which in turn activate associated serine proteases and C4 and C2. The alternative pathway generates the C3 convertase C3bBb. Activation is succeeded by an amplification reaction to generate additional C3 convertases and C3b. Subsequent C5 convertase formation (C4bC2aC3b for classical and lectin pathways, and C3bBbC3b for the alternative pathway) generates the potent inflammatory C5a anaphylatoxin and C5b. C5b initiates the formation of the membrane attack complex through the recruitment of C6, C7, C8 and C9 components to the bacterial surface. This complex inserts into cell membranes leading to cell lysis through pore formation. Self-tissue is protected from the deposition of complement components through extracellular and cell-surface regulators (e.g. complement factor 1, CD46 and C1 inhibitor). Convertases are regulated by through decay-accelerating factors (e.g. C4b-binding protein and complement factor H) which inhibit their biological activity and thus attenuate complement cascade. MASP, mannose lectin activated serine protease; MAC, membrane attack complex; C1-INH, complement inhibitor. This figure schematic is reproduced from [82].

1.5.3. Para-inflammation

It is argued that between a true acute inflammatory state and basal homeostasis conferred by the immune system, there exists an intermediate stage termed “para-inflammation” [83]. This para-inflammatory state exists as part of the adaptive immune response, instigated to combat low-level cellular stresses and danger signalling. It is generally perceived that an inflammatory response is advantageous, bestowing defence against pathogenic infection, only when this response becomes dysfunctional and uncontrolled will immune-mediated disorders such as infection and autoimmune disorders emancipate. Yet as Medzhitof states, “inflammatory responses are only known in pathological settings, and there is no clear understanding of their physiological counterparts” [83]. A mass of compelling experimental evidence suggests that inflammation, evolving to restore homeostasis may underlie the basis of human diseases such as obesity, gout and degenerative disorders [83-85]. RPE are subjected to accumulated oxidative damage from a lifetime of exposure to oxidative stress, the build-up of free radicals and oxidized lipoproteins [86]. This combined with RPE degeneration, complement activation and alterations to BM structure leave the retina extremely susceptible to the development of chronic inflammation [1]. The switch from a “para-inflammatory” environment – serving to protect tissue integrity – to that of low grade persistent inflammation within the aging retina has been postulated to be a likely mechanism of AMD pathogenesis; it is unknown if the RPE continues to adapt and protect the retina prior to this switch, or whether cellular stresses to the RPE will lead to an amplification of tissue damage [41].

1.5.4. Innate inflammation in the pathogenesis of AMD

An efficient immune response is essential in the maintenance of visual homeostasis and the preservation of the retinal environment in response to microbial invasion, but more likely (considering the retina is located in a site of immune privilege) tissue destruction and “sterile” inflammation [2]. In chronic conditions “sterile” inflammation occurs following uncontrolled activation of PRR *via* self-derived ligands. Putative endogenous ligands could be either proteins, polysaccharides, phospholipids, nucleic acids, extracellular matrix components and proteoglycans [87]. Degenerating RPE-derived drusen components are likely drivers of innate sterile immune responses within the eye which manifest as TLR activation [41]. Inflammation is an adaptive response to tissue stress, so when tissues are exposed to noxious environmental stressors, cell mediated response pathways (e.g inflammasome activation, autophagy or bioenergetic adaptations) are activated to promote survival and tissue homeostasis. As previously discussed, failure to maintain low-grade immune responses below a certain threshold may upset the balance between tissue homeostasis and overt

parainflammation, leading to chronic inflammatory dysfunction in degenerative diseases, such as AMD. Indeed, recent genome-wide association studies (GWAS) have demonstrated the prominent role of the innate immune system during AMD pathogenesis; with genes and single nucleotide polymorphisms (SNPs) identified within the complement pathways [88-90], chemokine receptors [91, 92] and innate endotoxin PRR [93, 94].

In the context of AMD, there is reported cross-talk between the complement system and TLR signalling, with drusen component (and complement activation product) C5a reported to induced TLR-4 upregulation and downstream cytokine expression in an MAPK dependent manner [95]. TLR-4 has been suggested to mediate POS phagocytosis through CD36 scavenger receptor clustering in RPE [96]. Direct TLR-4 stimulation in Müller glial cells/photoreceptors has been shown to contribute to photoreceptor degeneration however, the same study suggested a novel role in regulating photoreceptor survival through LPS-mediated pre-conditioning and the suppression of WNT/TNFα signalling [97]. Whilst polymorphisms in TLR-4 were previously associated with AMD [94], it is interesting to note that follow-up studies have yet to find a genetic association with coding SNPs and AMD susceptibility [98, 99]. A pathogenic role for TLR-3 may lie in the accumulation of *Alu*-repeat derived dsRNA observed in GA, a result of reduced processing activity of DICER1 (a microRNA processing enzyme) [100]. In addition to this, ultraviolet light has been shown to potently damage self-non-coding RNA leading to increased TLR-3 activation [101], a phenomenon with direct relevance to RPE cell loss in AMD. The implication of TLR-3 polymorphisms in the pathogenesis GA has been met with some controversy. The hypomorphic SNP rs3775291 (L412F) was proposed to confer a degree of protection to carriers against GA, suggesting deleterious involvement of TLR-3 signalling within macular degeneration [93]. However, later genetic association studies failed to identify a significant correlation between the TLR-3 variant and a protective phenotype [99, 102]. Recent meta-analyses have confirmed the association of L412F with GA through "pooling" the surrounding literature, leading on to speculating a protective mechanism for the SNP through decreased affinity for dsRNA [103]. L412F however, is proposed as an associative marker in Caucasians but not Asians, with only a small influence on disease susceptibility [104]. A recent study has implicated a protective role for TLR-3 signalling in oxidative stress, mediated by the downstream transcription factor signal transducer and activator of transcription (STAT)3; stimulation *via* commercial TLR-3 agonist Poly (I:C) (dsRNA) rescued photoreceptor degeneration and conferred additional protection to cultured RPE [105]. Similarly to what is observed in TLR-4 and TLR-9 preconditioning for photoreceptor protection and induced tolerance within autoimmune diseases, respectively; it appears that the timing of preconditioning is essential for conferring protection [97, 106].

The inflammasome complex is activated during AMD development through a capacity to recognize extracellular drusen deposits, leaving to a release of IL-18 and IL-1β [47]. NLRP3 has recently been implicated in the pathogenesis of AMD, a result attributed to a range of factors including: drusen components, mitochondrial dysfunction and *Alu* RNA [47, 107-110]. Drusen components isolated from AMD eyes were observed to prime the NLRP3 complex leaving to increased IL-18, IL-1β and cleaved caspases. Moreover, common drusen-associated components complement component C1Q and oxidized carboxyethylpyrrole (CEP)-adducts, prime and activate the NLRP3 inflammasome, respectively [47]. In experimental choroidal neovascularisation (CNV) (used as a model of wet AMD) disease development was intensified in *Nlrp3*$^{-/-}$ mice, yet this was not observed in *Il1r1*$^{-/-}$ mice. IL-18, when processed into its mature form can act as an antiangiogenic factor reducing CNV both alone, and in combination with a murine specific anti-VEGF antibody. It was further observed that IL-18 from bone marrow derived hematopoietic cells had the potential to protect against CNV [111]. Whilst its activation is evident in both GA and neovascular AMD, there remains controversy to whether a protective or pathogenic role can be attributed. Theoretically, the initial activation of NLRP3 must be protective, to preserve tissue integrity in response to danger-associated signalling. Only when clinical disease manifestations lead to an uncontrolled inflammatory response NLRP3 activation may be classified as an "immunotherapeutic target". Drusen, as a hallmark of AMD progression, displays a protein-rich composition of complement factors and amyloid beta (Aβ) [112, 113]. When isolated from human eyes, and used as an isolated C1Q component alone, both were capable of eliciting NLRP3 activation and leading to the secretion of IL-1β and IL-18 from LPS-primed macrophages and murine bone-marrow-derived-macrophages (BMDM) [47]. Aβ 1-40 was observed in both *in vitro* and *in vivo* studies to upregulate inflammasome activity through the expression of *IL-1β*, *IL-18*, *NLRP3* and *CASP-1* within the RPE and choroid [107]. The fluorophore A2E, a major component of lipofuscin (and ultimately drusen), was observed to activate the NLRP3 inflammasome and increase the production of IL-1β following its endocytosis into RPE cells [114]. In addition to this, A2E can initiate oxidative damage and complement activation within RPE [115], with oxidative damage identified as a prominent up-regulator of *NLRP3* expression [109]. DICER1 deficiency and the accumulation of *Alu* RNA is well noted within GA [100] and has been recently shown to activate the NLRP3 inflammasome independently of TLR signalling. Cytotoxicity conferred by the *Alu* RNA was identified to occur through MyD88 and the downstream secretion of IL-18 however, mitochondrial ROS were identified as the initial priming event for NLRP3 activation [110]. Although suppression of the NLRP3 inflammasome certainly appears to be an attractive therapeutic for the treatment of AMD, as discussed earlier, the initial activation is almost certainly in place to preserve tissue health in pre-clinical disease.

A large proportion of the molecular constituents of drusen are complement-activation products, these include complement regulators, activators and terminal pathway proteins [116]. This indicates a role for complement-mediated local inflammation in the early stages of AMD development. Genetic studies have identified significant associations between complement sequence gene polymorphisms and AMD risk, including SNPs in complement factor H (CFH), CFB, C3 and C2 [117-119]. CFH is one of most widely recognized pre-disposing genetic factor for AMD development [120]. Heterozygotic CFH mice develop characteristics of early AMD pathogenesis when fed on a high fat, cholesterol rich diet mimicking the environmental pressures of western societies with increased AMD prevalence [121]. CFH regulates complement activation at sites of tissue inflammation following injury or during degradation [56]. In humans, an amino acid substitution from histidine to tyrosine in the binding domain of CFH leads to the expression of an alternative variant (H402) which poorly regulates the AP of complement activation [122]. Uncontrolled complement activation is suggested to dysregulate immune homeostasis which in turn may manifest into the early stages AMD development [56]. The involvement of CFH and other complement pathway genes highlights the role of innate immunity in AMD. Despite a mass of both genetic and clinical data pointing to a role of low-grade chronic inflammation in the pathogenesis of AMD, the underlying molecular mechanisms are yet to be fully elucidated

1.6. The Interleukin-1 cytokine family

The IL-1 family of cytokines are a group of cytokines with a key role in the regulation of inflammatory responses or sterile inflammation. The IL-1 family consists of 11 members that can be separated into sub-families based on their pre-processed forms and bioactivities (Fig. 1.3) [123]. They share a highly conserved gene arrangement, allowing the formation of a 12-stranded beta-barrel [124]. IL-1 family members differ in their signalling pathways and the mechanism whereby they are processed to mature bioactive forms. Inflammasome cytokines IL-1β and IL-18 are initially translated as inactive pro-peptides (pro- IL-1β -18) that require cleavage by caspases mediated by NLRP3 for both secretion and biological activity [125]. In contrast, processing of pro-IL-1α precursor occurs in an inflammasome-independent manner through a calcium-dependent cysteine protease, calpain [126]. IL-1α and IL-1β exert their pro-inflammatory effector functions through the activation of NF-kB, following binding to the IL-1 receptor 1 (IL-1R1) and IL-1RAcP complex [127, 128]. IL-18 confers more complexity to its signalling, in the sense that it can initiate Th1 and Th2 responses [129]. The IL-18R complex consists of two domains - IL-18Rα (ligand binding domain) and IL-18Rβ (co-receptor domain) [130] - which

following the binding of IL-18 form a heterodimer complex to initiate downstream signalling cascades through MAPK and p38 pathways as opposed to NF-kB activation in IL-1R transduction [130].

IL-18 subfamily member IL-37 suppresses innate inflammatory responses through binding to interleukin 18 binding protein (IL-18BP), forming a complex that inhibits IL-18 signalling [131]. The processed IL-37 acts as a dual function cytokine (like IL-1α and IL-33) displaying intracellular and extracellular anti-inflammatory properties initiated through nuclear translocation [131].

The third IL-36 family subset contains members with the smallest pre-processed peptides [132]. This sub-family includes cytokines IL-36α, IL-36β, IL-36γ, IL-36RA and IL-38 that initiate hyper-reactive and inflammatory responses through the IL-36R/ IL-RAcP signalling complex [132]. IL-36RA and IL-38 both share significant sequence homology with the IL-1RA, allowing them to initiate antagonistic activities through preventing the recruitment of IL-RAcP. (See Fig. 1.4.).

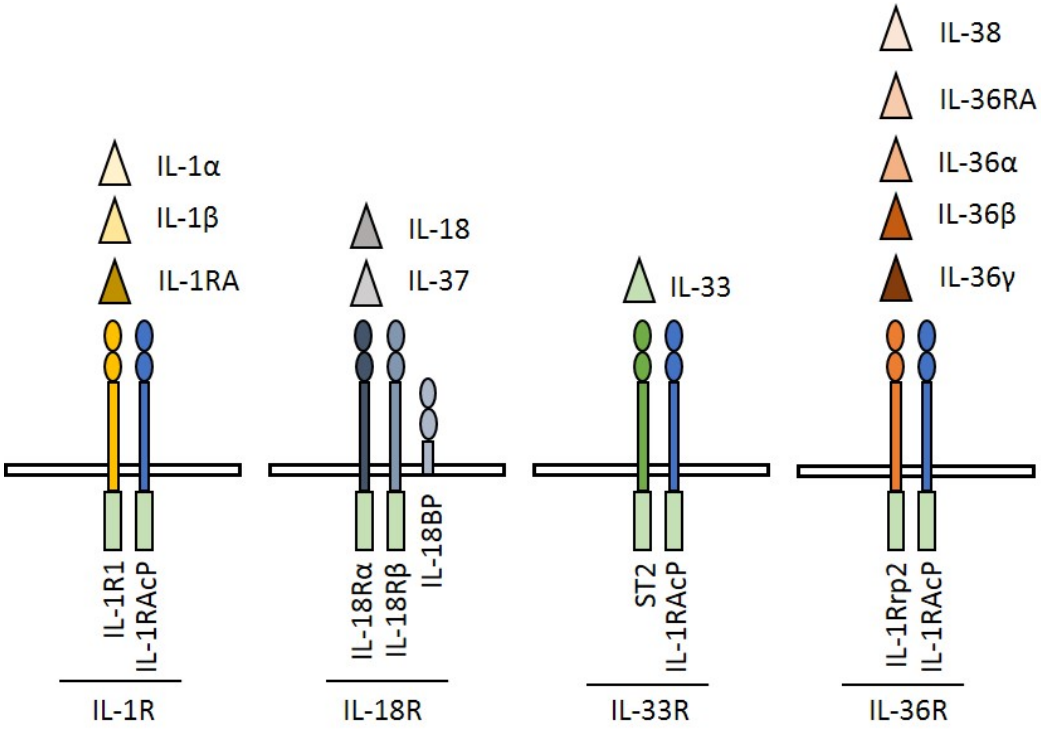

Figure 1.4. A schematic of ligands and their receptor chains in the IL-1 family:

The IL-1 family consists of 11 ligands, further separated into their respective sub-families on the basis their pre-processed form and bioactivities. The IL-1 subfamily contains cytokines with a larger precursor peptide length such as IL-1α, IL-1β and IL-33. The IL-18 family have smaller pro-peptides and includes both IL-18 and IL-37. Additionally, there is a third IL-36 family subset containing members with the smallest pre-processed peptides. There are 7 agonists (IL-1α, IL-1β, IL-18, IL-33, IL-36α, β and γ), three receptor antagonists (IL-1Ra, IL-36Ra and IL-38) and one anti-inflammatory member (IL-37). IL-1α, IL-1β and IL-1Ra signal through a receptor complex formed of IL-1R1 and a co-receptor IL-1RAcP. IL-33 signals through the ST2 IL-1RAcP complex. IL-18 signals through a receptor complex comprised of IL-18Rα, β and the IL-18BP; IL-37 on the other hand, requires only IL-18Rα. IL-36α, β and γ signal through the IL-36R/IL-1RAcP-receptor complex. IL-36RA and IL-38 signal through IL-36R without the need for a co-receptor. IL, interleukin; IL-1R, interleukin-1-receptor; IL-1RAcP, interleukin-1-receptor accessory protein; IL-18R, interleukin-18-receptor; ST2, suppression of tumorigenicity 2; IL-1Rrp2, interleukin-1-receptor related protein 2; IL-RA, interleukin receptor agonist. Adapted from [11].

1.7. Interleukin-33

IL-33 is a member of the larger IL-1 superfamily of cytokines and is only observed in placental mammals [19, 133]. Constitutive nuclear expression of IL-33 is observed at high levels in multiple cell types in both human and murine tissues [134]. Prior to its establishment as an IL-1 family member in 2005 [133], IL-33 was first identified and cloned from canine vasospastic cerebral arteries [135]. It was later described as a nuclear factor observed in high endothelial venules, where it was recognized as NF-HEV [136]. Expression of IL-33 is observed predominantly in barrier endothelial cells, epithelial cells and fibroblasts [14, 133, 136, 137]; additionally, adaptive and innate immunological cells such as dendritic cells, monocytes and macrophages have been shown to express IL-33, [138-140]. IL-33 is typically associated with T helper (Th) 2 responses initiated through its IL-1 receptor related protein ST2 present on effector cells (mast cells, eosinophils, basophils, natural killer (NK) cells and macrophages) [133]. Trans-membrane ST2 is also expressed on a variety of non-immune cells, and therefore has been speculated to influence pathogenic inflammatory responses in a number of disease models [17, 125, 141, 142], yet on the contrary, protective novel roles for IL-33 have been suggested in the attenuation of disease development [8, 14, 15, 143-145]. In addition to this, pro-IL-33 is speculated to have a nuclear function in the regulation of gene expression, yet this is currently warranting further investigation. An overview of IL-33 biology is shown in Fig. 1.5.

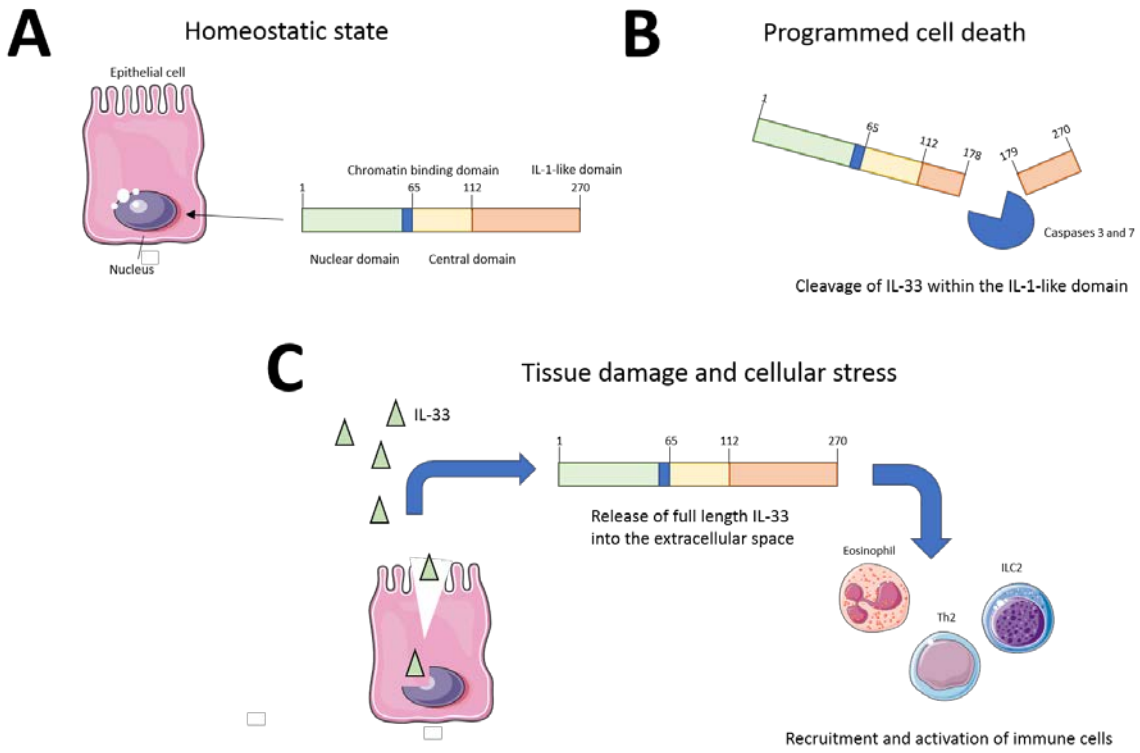

Figure 1.5. Biology of the nuclear alarmin IL-33:

(A) During homeostasis IL-33 is constitutively expressed at high levels in epithelial barrier cells where it acts (*via* poorly defined mechanisms) to control the epigenome. (B) In apoptotic cell death, IL-33 is released from cells and is processed by inflammasome-derived caspases 3 and 7. Processed IL-33 has no biological activity and is unable to activate its cognate receptor ST2. (C) Mechanical damage, cellular stress or exposure to allergens or viruses leads to the extracellular release of full-length bioactive IL-33. IL-33 alerts the immune system of tissue damage by activating multiple ST2-expressing cells such as mast cells, Th2 T-cells and ILC2s. IL, interleukin; ST2, suppression of tumorigenicity 2; Th2, T-helper cell type 2; ILC2, type 2 innate lymphoid cell. Adapted from [146].

1.7.1. The Interleukin-33:ST2 signalling axis

The IL-33 receptor ST2 is active in the form of a heterodimeric complex comprised of a ligand (cytokine) binding chain (IL-1R4) and an accessory chain (IL-1R3) [147]. Both chains contain intracellular Toll/IL-1 receptor (TIR) and extracellular immunoglobulin-like (Ig) domains [124]. The Ig domains, along with a highly homologous receptor accessory protein (IL-1RAcP) induce the dimerization of the two TIR domains following binding of agonist IL-33 [148]. The presence of IL-1RAcP is imperative for linking the binding of IL-33 and ST2, acting as a common β-chain for IL-33Rα and three other IL-1 receptor family members [149]. The ST2/IL-1RAcP complex allows IL-33 to initiate its downstream functions through downstream kinases NF-kB and various MAP kinases (ERK1, ERK2 and p38) [133]. The recruitment of TNF receptor-associated factor 6 (TRAF6) is a crucial mediator in the initiation of IL-1/TLR signalling and it appears that IL-33 requires the ubiquitin ligase effector function of TRAF6 in the initiation of ST2 signalling [150] (See Fig. 1.6).

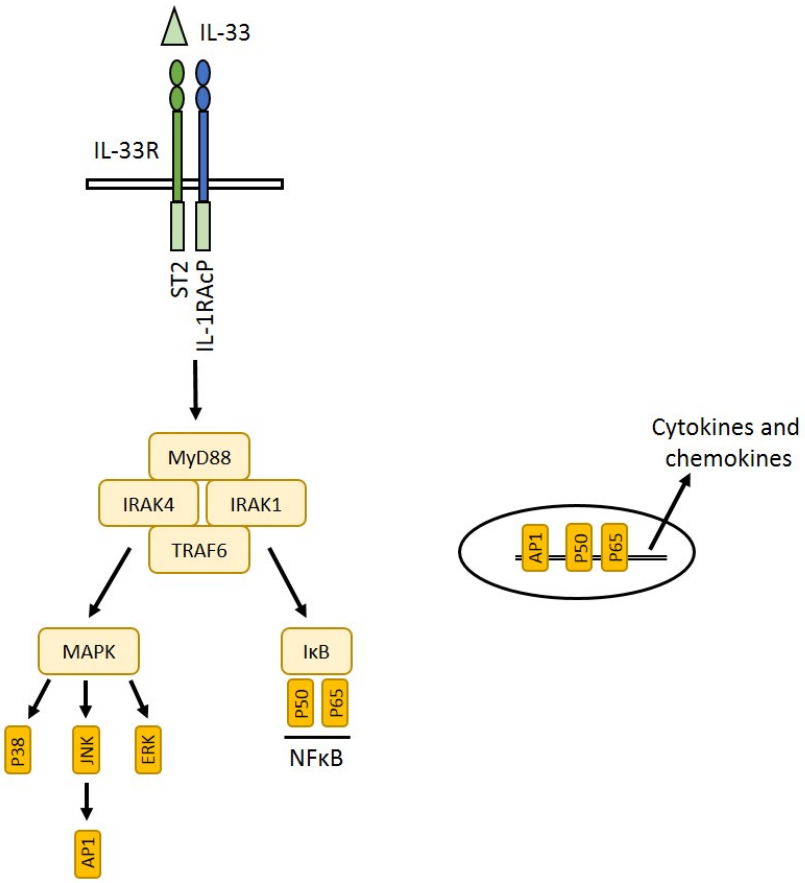

Figure 1.6. A schematic of the IL-33/ST2 signalling axis:

IL-33 binds to its cognate receptor formed as a dimer complex of ST2 and IL-1RAcP.The binding of IL-33 to ST2 initiates the recruitment of MYD88, IRAK1 and IRAK4 which lead to the activation of NF-κB and MAPK pathways, respectively. MAPK activation leads to the activation of P38, JNK and ERK pathways. JNK activation results in activation of the transcription factor AP1. The transcription factors AP1 and NF-κB translocate to the nucleus whereby they promote the expression of relevant cytokines and chemokines. ST2, suppression of tumorigenicity 2; IL-1RAcP, interleukin-1-receptor accessory protein; MYD88, myeloid differentiation primary-response protein 88; IRAK, interleukin-1-receptor associated kinase; NF-κB, nuclear factor kappa B; MAPK, mitogen activated protein kinase pathway; AP1, activated protein-1. Adapted from [151].

1.7.1.1. Interleukin-33 signalling on lymphoid cells

The alarmin activity of IL-33 potently enhances the lymphoid arm of the immune system. Although ST2 was first described on Th2 cells [152, 153], expression is observed on type 2 innate lymphoid cells (ICL2) [154], NK cells [155], NK T cells [156], activated Th1 cells [157], cytotoxic CD8 T cells [158], regulatory T cells (Tregs) [159], B1 cells [160] and regulatory B cells (Bregs) [161].

Th2 and GATA+ Treg cells constitutively express ST2 at high levels; In cytotoxic lymphocytes (CTL) and Th1 cells, ST2 expression is activation-dependent (albeit at lower levels than Th2 subsets) [157, 162, 163]. IL-33/ST2 signalling in T-cells initiates downstream effector functions through activation of the phosphoinositide 3-kinase (PI3K) and mammalian target of rapamycin (mTOR) signalling pathway [164]. IL-33 is essential for promoting the primary differentiation of both CD4 and CD8 subsets, acting to extend their cytokine production capacity and effector functions [162]. In Th1 cells, IL-33 signalling and activation of STAT4 increases the production of T-bet (a critical factor for Th1 differentiation) [157]. In the Th2 subset, IL-33 and IL-2/STAT5 signalling converge on GATA3 to promote Th2 differentiation [165]; the activation of GATA3 in Treg cells lead to increased FOXP3 expression [159]. Whilst IL-33 appears to be a key co-stimulator of various T-cell subsets, additional roles for the cytokine have been suggested in both clonal expansion and maturation of functional CTL and Th1 subsets, increasing expression of pro-survival proteins and proliferation [157, 158]. Indeed, lack of IL-33/ST2 signalling weakens the capacity of CTL to kill LCMW infected cells and impairs the antiviral cytokine output of Th1 cells [158]. Additionally, IL-33 has been observed to initiate antigen-independent cytokine production from Th2 cells *in vitro* through solely ST2 activation [166] and with a co-stimulatory activation of STAT5 *via* IL-2 [165].

Unlike T cells, murine NK cell differentiation and development does not appear to involve IL-33/ST2 signalling, with ST2 deficient cells observed to differentiate into a memory pool [167]. Whilst not essential for NK survival, activation and IFN-γ production, IL-33 signalling is critical for the expansion of a Ly45H+ subset following *in vivo* cytomegaloviral infection [167]. IL-33 acts synergistically with IL-12 to further upregulate IFN-γ production in human NK cells [155]. In both murine NK cells and murine invariant NK cells, on the contrary to instigating a Th2 response, IL-33 stimulation upon TCR engagement also lead to an increased IFN-γ output in conjunction with IL-12 [156]. Further provoking the hypothesis that IL-33 may act as a co-stimulatory factor during adaptive immune responses.

Peripheral B cells can be subdivided into two main classes: the B1 subset, which function as an long-lived and self-renewing APC and innate immune effector) and the B2 subset (the "classical subset"), which responds to antigen stimulation to undergo IgH class switching and affinity development *via* T-cell dependent mechanisms [168]. ST2 is expressed exclusively on the B1 subset [160]. IL-33 activates murine B1 cells, enhancing proliferation, IgM synthesis and Th2 cytokine output in a IL-5/IL-5R dependent mechanism [160]. In addition to their activation by IL-33, B cells purportedly (through an unidentified secretory mechanism) release IL-33 following Notch-1 activation to modulate and co-stimulate T-cell responses [169]. Alike the Treg subset, a Breg can be found in the B lineage. These cells have gained increased attention due to their immunoregulatory and suppressive capacity [170]. IL-33 elicits the generation of a phenotypically distinct murine Breg subset, of which protects against inflammatory bowel disease in an IL-10-dependent manner [161].

ILCs are mucosal effector cells differentiated from common lymphoid progenitors; however, unlike adaptive lymphocytes, ILCs do not have the capacity to rapidly rearrange cell-surface receptors to recognize non-self-antigens [171]. ILCs express a similar range of transcriptional regulators to their adaptive counterparts to control a large cytokine repertoire [171].

GATA3+ ILC2s are highly responsive to IL-33 *in vivo* and *in vitro* because of their high ST2 expression [172]; indeed, IL-33 is the "hallmark activator" of both peripheral and bone marrow ILC2s [173]. Similarly (to Th2 T-cells), IL-33/ST2 signalling engages the activation of the PI3K/mTOR signalling pathway [164]. IL-33 is reported to have a critical role in the trafficking of ILC2s from the bone marrow into the peripheral tissues, yet not in their differentiation status, proliferative capacity or cytokine profile [174]. Interestingly, the IL-33/ICL2 axis appears to play a vital role in acute wound healing facilitating re-epithelialization of damaged surfaces [175].

1.7.1.2. Interleukin-33 signalling on myeloid cells

The ST2 receptor is highly expressed on several myeloid derived immune cells associated with allergy (mast cells, eosinophils and basophils). The most well studied of these are eosinophils, of which IL-33 plays a critical role in both development within the bone marrow and activation. During the early stages of cellular differentiation, IL-33 regulates the expansion of an eosinophil precursor [176]. By upregulating the expression of the IL-5R and IL-5, IL-33 ensures commitment to the eosinophil lineage [176, 177]. IL-33 acts potently on mature eosinophils to increase their cytokine production, CD11b

and CD69 expression, degranulation capacity, and the expression of several adhesion factors (CXCL8/ CCR3) that enhance eosinophil survival [178-181]. Administration of IL-33 drives eosinophilia *in vivo* likely due to augmented eosinophil survival [133, 182].

Not unlike eosinophils, basophils are also cellular targets of IL-33 and once activated, increase their cytokine production and expression of several adhesion factors (e.g. CXCL8) that enhance their survival [98-100]. IL-33 promotes the secretion of IL-4, IL-13 and IL-8 from human basophils in co-operation with either IL-3 or Fcε receptor 1 (FcεRI) [183]. Direct stimulation of human basophils with IL-33 is reported to have no observable effect on their degranulation or attraction *in vitro* [184]. Yet in conjunction with immunoglobulin (Ig)E receptor stimulation, IL-33 augments basophil degranulation [185]. Independently of FcεRI, IL-33 regulates the synthesis of leukotrienes *via* alternate mechanisms to IL-3, yet lacks the ability to efficiently prime human basophils for their C5a-induced leukotriene generation [183]. Additionally, IL-33 exerts effects on the migratory capacity of human basophils by inducing the expression of CD11b in human basophils and adhesiveness to nearby endothelial cells [184].

IL-33 acts on ST2 expressing neutrophils to promote migration and recruitment through the upregulation of CXCL1, CXCR2 and CXCR3 [186, 187]. *In vivo* the recruitment of neutrophils appears to be dependent on the MC release of TNFα [188]. On the contrary, IL-33 deficient mice have been shown exhibit increased neutrophil migratory capacity, increased production of IL-6 and TNFα, but reduced IFN-γ [189]. Direct effects of IL-33 are observed in the activation of neutrophils; IL-33 polarises neutrophils *via* C-Jun and NF-kB to a novel IL-33 subpopulation exhibiting a characteristic IL-4, IL-13, IL-9 and IL-5 cytokine output [190]. Indirect IL-33-induced IL-5 production in neutrophils has previously been observed through the regulation of ILC2-dependent IL-5 production [191]. Indirectly action of IL-33 on neutrophils is described *via* an ILC2-IL-13-STAT6-dependent mechanism. This results in the generation of an immunosuppressive neutrophil population exhibiting high levels of IL-10 and arginase-1 [192].

Mast cells express the ST2 receptor at high level and represents a murine lineage marker [193]. IL-33 activation of ST2 can initiate signalling through two independent pathways depending on the enzymatic activity of the receptor tyrosine kinase, c-Kit. If c-Kit is enzymatically inactive, IL-33 signalling occurs through the PI3K/mTOR axis in a similar fashion to TLR activation. However, when c-

Kit is in the active conformation at the ST2/IL1-RAcP complex, STAT3 is activated following IL-33 stimulation [194]. IL-33 is involved in the mast cell maturation process, and in conjunction with thymic stromal lymphopoietin, enhances the maturation of a CD34+ precursor and expression of tryptase (an early marker of differentiation status [195]. In addition to this, IL-33 signalling increases mast cell survival by upregulating B-cell lymphoma extra-large (BCLXL) expression and attenuating apoptosis [196]. IL-33 directly acts on mast cells to increase cytokine production [197, 198] and can augment TLR or FcεRI-dependent cytokine production [199]. The IL-33-induced release of IL-2 from mast cells mediates the expansion of both Treg and Th17 populations in a context-dependent manner [200, 201]. IL-33 signalling *per se* activates mast cells without degranulation [199, 202]. The consensus is that IL-33 may act in conjunction with IgE to augment the extent of mast cell degranulation but not kinetics [203]. Interestingly, it is suggested that the effects of IL-33 on IgE production, mast cell degranulation and anaphylaxis, appear to be mediated through downstream IL-4 release and signalling [204]. The IL-33/ST2 axis may be critical in the response to tissue damage; with the release of IL-33 from necrotic cells activating mast cells to initiate inflammatory responses in response to injury [205].

Macrophages can be broadly classified into two subsets: classically activated (M1), defined by their potent type 1 inflammatory responses, TLR expression and inducible NO synthase (iNOS) expression; or alternatively activated (M2) macrophages, defined by their roles in type 2 immune responses and tissue repair, secretion of high amounts IL-10, and induction by IL-4 and IL-13 [206] (see Fig. 1.7.). IL-33 was observed to polarize macrophages into an alternatively activated phenotype (expressing IL-4R, arginase-1, CCL24 and CCL-17 during airway inflammation *via* an IL-13-dependent mechanism [101]. IL-33 is reported to reduce the expression of IL-1β, IL-12, IFN-γ and TNFα, whilst increasing the expression of IL-13, IL-4 and IL-10 from macrophages *in vitro* [207]. Additionally, IL-33 can augment the expression of M2 marker expression when treated in combination with IL-4/IL-13; yet further reduces expression when skewed to an M1 phenotype in conjunction with LPS [208].

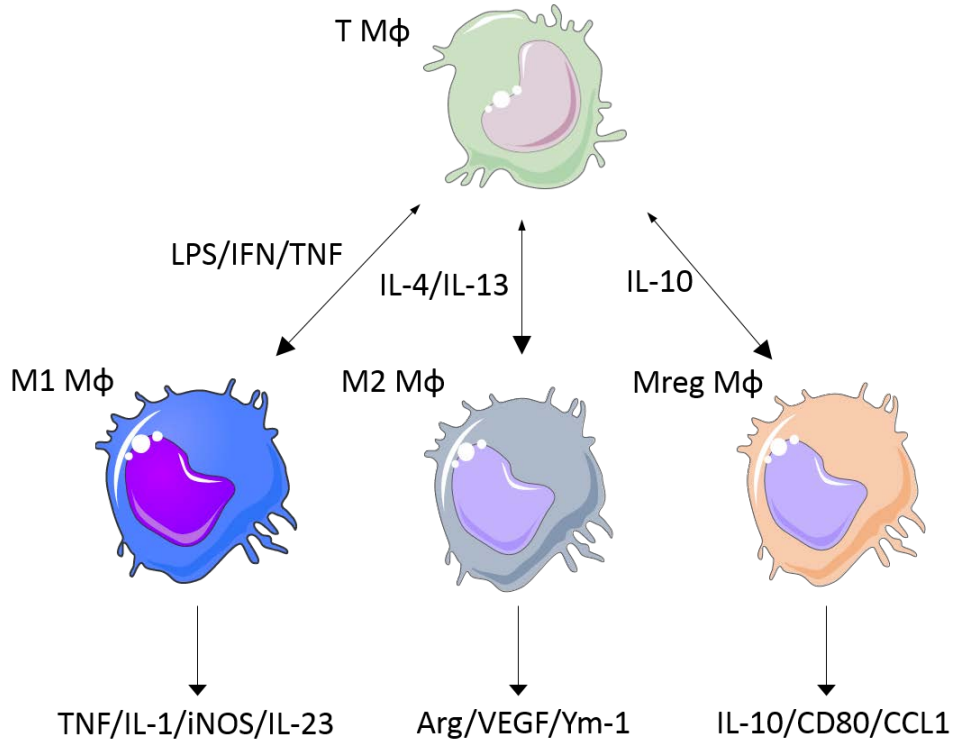

Figure 1.7. Macrophage subsets: "M1", "M2" and "Mreg":

Tissue-resident macrophages can be polarised into three major subsets based on cytokine production and cell surface markers. Classically activated "M1" macrophages are polarised by LPS, IFN-γ or IFN-γ in combination with TNFα. These cells generate high levels of inducible nitric oxide synthase and MHC II along with a vast output of proinflammatory cytokines (TNFα, IL-1, IL-6, IL-23, IL-12 and CCL2) which facilitate their role in pathogen clearance and sustaining a Th1 response. Alternatively activated "M2" macrophages are generated through stimulation with IL-4 and/or IL-13. These cells are associated with tissue resolving and Th2 responses and express high levels of arginase-1 and VEGF. Regulatory "Mreg" macrophages are produced in response to either TLR ligation with IL-10 or glucocorticoids. These cells have a cytokine signature defined by high levels of IL-10 production.

Whilst there is limited research concerning the effects of IL-33 on dendritic cells, it appears to play a key role in their generation and activation. In a murine *in vitro* dendritic cell culture system, IL-33 was observed to augment the generation of CD11+ cells *via* an indirect mechanism involving GM-CSF [209]. Dendritic cells expressing ST2 (albeit at low levels) increase their MHC II expression following IL-33 exposure, leading to T-cell-dependent cytokine production in a co-culture system [102]. IL-33-stimulated dendritic cells lead to the selective expansion of a Treg population through the indirect secretion of IL-2 [210]. Furthermore, the activation of dendritic cells by IL-33 both *in vitro* and *in vivo* primes naïve T-cells to a Th2 phenotype, with a robust expression of IL-5 and IL-13 [211]. Interestingly, the identification of a novel IL-33-ST2-MyD88-STAT1 axis drives dendritic cell activation and maturation, ultimately leading to increased anti-tumour immunity *in vivo* [212].

1.7.1.3. Interleukin-33 signalling in non-haemopoietic cells

Whilst most literature concerning the IL-33/ST2 axis has focused on hematopoietic immune cells, it is essential to note many non-haemopoietic innate immune competent cells also respond to IL-33. ST2 expression is observed in fibroblasts [8, 150, 213], epithelial cells [8, 214, 215], osteoblasts [216], some endothelial cell populations [8, 217-219] , hepatocytes [220], myocytes [14, 221] smooth muscle cells [218], and Müller glia [222].

IL-33/ST2 signalling in fibroblasts drives the activation of NF-kB, p38 and JNK through IRAK and TRAF6, leading to the secretion of MCP1, MCP3 and IL-6 [150]. IL-33 is observed to affect the migratory capacity of choroidal fibroblasts through modulating the expression of migratory factors MMP2, MMP9, TIMP1 and TIMP2 [8]. In rheumatoid arthritis-derived synovial fibroblasts, extracellular IL-33 diminishes MMP1 and IL-6 expression, whilst endogenous IL-33 appears to have a broader role in the regulation of TNFα-induced pro-inflammatory, migratory and destructive signalling mediators [223]. Additionally, IL-33 promotes the expression of fibronectin and type-1 collagens to facilitate airway remodelling [224].

ST2 expression is observed at high levels in epithelial stem cells and progenitor cells; this appears to be essential for reprogramming undifferentiated epithelial progenitors into the secretory intestinal epithelial lineage through the IL-33-mediated suppression of Notch signalling [225]. Fully differentiated epithelial cells respond to IL-33 *in vitro*, producing IL-6, IL-8 and MCP-1, both independently and in conjunction with IL-4 [214]. Endogenous IL-33 appears to regulate the

expression of the epithelial adhesion molecule E-cadherin, and induction of chemokines and surfactants following cryptococcal infection in the lung epithelium [226]. IL-33 enhances epithelial cell proliferation and gut mucus production *in vivo* [133], *Ex vivo* human epithelial cultures respond to IL-33 and produce anti-inflammatory mediators IL-1RA, IL-18BPa, IL-1RAcP and sST2 [227].

In quiescent endothelial cells, endogenous IL-33 production is dependent on Notch-1 signalling [228]. Nuclear IL-33 expression in human endothelial cells is absent upon cytokine/ pro-angiogenic stimulation, with expression only observed at confluence, whereby cells are in a G0/G1 state [229]. Furthermore, IL-33 expression correlates with cell-cycle determinants (cyclin-dependent kinase inhibitor P27KIP1) [228], suggesting either cell cycle status may be critical for constitutive IL-33 expression or, IL-33 may have a regulatory role in endothelial cell cycle progression. Stimulation of human endothelial has been found to increase the expression of IL-6, IL-8 and MCP-1, and induce NF-kB translocation [219]. Endothelial cell activation and upregulation of adhesion molecules (ICAM-1, VCAM-1 and E-selectin) which facilitate leukocyte adherence *in vitro* has also been described [219]. A recent study utilising a proteome-based approach to IL-33/ST2 signalling in endothelial cells identified a large array of proteins differentially regulated by extracellular IL-33 [230]. IL-33 stimulation primarily induces changes in NF-kB signalling, chemokine and cytokine expression, cell adhesion and cell surface receptor expression, and antigen processing [230].

1.7.2. Interleukin-33 processing and release

Similarly, to other IL-1 family cytokines IL-1β and IL-18, IL-33 lacks a signal sequence required for secretion through the Golgi apparatus and endoplasmic reticulum [231, 232] and is consequently synthesized as a pro-peptide (pro-IL-33). It was initially proposed that IL-33, like IL-1β and IL-18 required cleavage for release and bioactivity because of a lack of clear signal peptide. IL-33 was later found to not require inflammasome activation, with optimum bioactivity occurring at full-length; [233]. Whilst pro-IL-33 contains residues denoting a caspase-1 cleavage site, the processed forms of the peptide are unable to activate ST2, it is therefore speculated that caspase-1 is involved in the attenuation and inactivation of IL-33 signalling [232, 233]. In addition to this, caspase-3 and -7 are reported to mediate proteolysis of pro-IL-33 during apoptosis to suppress the pro-inflammatory properties of the cytokine [231, 234]. Neutrophil-derived proteases (elastase, cathepsin G) initiate N-terminal cleaving of IL-33 (at sites between residues 109-95) yielding forms with an increased potency for ST2 activation [235]. Endogenous calpains and exogenous extracellular allergy proteases in airway

epithelial cells are reported to process IL-33 to increase its alarmin activity, yet systematic analysis of the both proteolysis sites and the structure of the processed forms remain unknown [236, 237]. These results suggest that IL-33 is bioactive in its unprocessed form; endogenous and exogenous proteases may be utilized to enhance/dampen the IL-33/ST2 signalling axis depending on certain micro-environmental cues.

Because of its constitutive expression and lack of signal peptide, it is proposed that IL-33 functions as an alarmin molecule, released into the extracellular space (*via* poorly defined mechanisms) following cellular necrosis or mechanical damage [146]. Release of endogenous IL-33 has been observed both *in vitro* (following mechanical disruption [233], induction of oxidative stress by hydrogen peroxide [234], viral infection [238] and formation of cellular pores by streptolysin O [234]) and *in vivo* (following viral infection of both human primary bronchial epithelial cells [238] and in nasal fluid of asthmatic subjects following rhinovirus infection [239].

A fungal allergen is reported to elicit the release of IL-33 in the absence of cell death through extracellular ATP release, ROS generation and changes in intracellular calcium concentrations both *in vitro* and *in vivo* [240, 241]. It has been suggested that extracellular ATP exposure or pharmacological modulation of intracellular calcium may lead to the release of IL-33; however, the capacity of these agents to prompt nuclear-cytoplasmic translocation has not been confirmed in other studies [242]. Additionally, many studies have not confirmed specificity of IL-33 detection in an IL-33 deficient system or considered cellular necrosis/cell death which may account for the release [243].

1.7.3. Regulation of Interleukin-33

As one of the most biologically potent families of cytokines, control over the IL-1 family members is exerted through a variety of mechanisms including: signal peptide processing (in a caspase-dependent or independent manner as noted in the previous sections), extracellular signalling inhibitors, soluble decoy receptors and natural receptor agonists to block or diminish the affinities of receptor complexes for their intended ligands [123, 132]. IL-33 is not an exception to this phenomenon, with many counter-regulatory strategies exhibited to control its downstream signalling.

Before the discovery of IL-33, the soluble form of ST2 (sST2), was observed to inhibit LPS-induced production of pro-inflammatory cytokines from macrophages, in addition to halting the toxicity conferred by the administration of LPS [244]. Whilst it was already known that alternative splicing of the ST2 receptor generated a soluble form [213, 245], it was not until the identification of IL-33 as the natural ligand for ST2, that sST2 was classified as a decoy receptor for IL-33-dependent signalling [133]. sST2 is extracellularly identical to its membrane bound counterpart except for nice amino acids at the C-terminus [246]. Lacking the transmembrane and intracellular TIR receptor domains, the upregulation of sST2 expression allows sequestration of IL-33, decreasing its ST2L/IL-1RAcP binding probability [247]. A protective role for sST2 was originally suggested in the context of attenuating the severity inflammatory and auto-inflammatory conditions, based on its anti-inflammatory properties [244, 248].

IL-1RAcP facilitates the binding between IL-33 and ST2, acting as a common β-chain for IL-33Rα and three other IL-1 receptor family members [149]. Alternative splicing leads to the generation of two IL-1RAcP variants, one membrane bound and the other soluble. The soluble form ((s)IL-1RAcP) contributes to counter-regulation through increasing the affinity of IL-1 cytokines to the IL-1R2 decoy receptor [249]. In the negative-regulation of IL-33 signalling, sIL-1RAcP forms a complex with sST2, and together bind IL-33 [11]. SIGIRR (single immunoglobulin IL-1R-related molecule)/TIR8 (Toll IL-1R8). SIGIRR/TIR8 has been identified as a negative regulator of TLR-4, TLR-9 and IL-1R signalling [250, 251]. SIGIRR/TIR8 inhibits IL-33 signalling through an interaction with the ST2 receptor complex and subsequent interaction between respective extracellular Ig domains and intracellular TIR domains [250]. In addition to this, negative-regulation of IL-33 signalling can be exerted through the posttranslational modification of ST2L; the over-expression of E3 ubiquitin ligase (FBXL19) lead to the poly-ubiquitination of ST2L and proteasome-dependent degradation, lessening lung inflammation and severity of lung injury in a murine model [252].

Whilst little is known about the biological half-life and natural degradation of IL-33 when released from cells, a recent study has identified cysteine oxidation as a mechanism to inactivate IL-33. Free cysteine residues in the c-terminal are rapidly oxidized into two disulphide which disrupt the conformation of IL-33 and lead to disruption of the ST2 interaction [236]. It is interesting to note that other IL-1 family members (IL-1α, IL-1β, IL-18 and IL-36) exhibit free cysteine residues in their c-terminal domain [236, 253] , suggesting a biologically conserved mechanism to control their potent activity.

1.7.4. Nuclear interleukin-33

IL-33 shares many features with IL-1 superfamily member IL-1α, including potent biological immune activity and nuclear localization, leading to its classification as a "dual-function cytokine" [133, 254]. Whilst IL-1α is targeted to the nuclei *via* a classical nuclear localization sequence [255], IL-33 contains a helix-loop-helix bipartite DNA-binding homeodomain within residues (1-56) [254]. It was originally suggested that IL-33 may influence transcriptional repression through an association with heterochromatin [254, 256]. However, the nuclear functions of IL-33 remain diverse and incompletely understood to date.

A formation of an IL-33:SUV39H1 histone methyltransferase complex reportedly allows IL-33 to bind multiple homeobox binding motifs in the promoter regions of *IL1RL1, IL6 and CCL5* repressing their transcription in human atrial endothelium [254, 257]. IL-33 has been reported to directly bind a conserved non-coding sequence before the translation initiation site in the *IL13* gene in HEK293T cells to directly activate its transcription [258]. Additionally, IL-33 is suggested to repress the transcriptional activity of NF-kB by sequestering the p65 subunit in endothelium [10] and fibroblast-like synoviocytes [259]. Yet in contrast, IL-33 is reported to bind to the NF-kB promoter region to enhance its transcription [260]. A recent study has identified a large IL-33 nuclear interactome in squamous cell carcinoma cells, with a large array of transcriptional regulators and chromatin remodelling factors which converge on the modulation of NF-kB activity and downstream gene targets [261]. The identification of co-localization of IL-33 within both membrane-bound cytoplasmic vesicles/ nuclear euchromatin [262] question the original theory of IL-33 acting as a transcriptional repressor and may support the role of IL-33 in enhancing gene expression.

Despite the broad range of transcriptional associations, nuclear roles for IL-33 remain unknown in certain cell types [230]. In a recent study, IL-33 was transduced in an oesophageal epithelial cell line lacking constitutive expression of the protein. Following RNA sequencing, no global gene changes in the transcriptional profile of the cells was observed. Moreover, utilizing fluorescence recovery after photobleaching it was observed that IL-33 exhibited a reduced intranuclear mobility compared to other transcriptional factors such as IL-1α and high mobility group box protein 1 (HMBG1) [263]. Additionally, another study utilizing a global proteomics approach following IL-33 knockdown by siRNA observed no observable changes to the endothelial proteome [230]. These two studies advocate a

lack of nuclear function for the cytokine and speculate nuclear localization is an evolutionary adaptation whereby cells can sequester the cytokine in order to suppress its potent extracellular activities.

The consensus still remains that IL-33 functions as an epigenetic regulator or a chromatin "insulator" protein [262]. These factors play a role in the modification of higher-order chromatin structure and the regulation of gene expression, with common molecular mechanisms found in modulating chromatin accessibility, long-range interactions with distant elements or compartmentalization of interphasic chromatin with nuclear pore complexes or additional nuclear structures [264]. There remains however, a desperate requirement for the utilization of a MeDIP/ChIP-seq/microarray-based sequencing approach to determine the magnitude of IL-33 regulation at an epigenetic level.

1.7.5. Role of interleukin-33 in disease

Studies have started to uncover the potential of IL-33 signalling, with elevated antagonistic sST2 levels correlating with disease severity in a wide range of disorders including diabetes, systemic lupus erythematosus, sepsis, preeclampsia, cardiovascular disease and obesity [14, 265-269]. In the case of cardiovascular disease, sST2 levels are increased following myocardial infarctions and negatively correlate with patient outcome, suggesting the potential of sST2 as a diagnostic marker. Recombinant IL-33 administration following transverse aortic constriction attenuated hypertrophy and fibrosis, indicating a protective role for IL-33 in regulating myocardial mechanical strain [14]. Interestingly, common genetic variation in IL-33/ST2 signalling has been identified, with multiple SNPs identified in the locus of ST2. Five of these missense variants were mapped to the intracellular region of ST2 and conferred a phenotype of increased sST2 production [270]. As increased sST2 may be precarious in multiple disease settings, screening for SNPs in this gene may be an attractive avenue for predicting clinical outcomes, especially in cardiovascular disease and degenerative disorders.

IL-33 plays a fundamental role in the defence against helminth infection. Administration of recombinant IL-33 to mice infected with *Truchris muris* conferred increased protection against disease severity through a Th2 mediated response [271]. Mice lacking IL-33 exhibited an incompetence for removal of *Strongyloides venezuelenis* and *Nippostrongylus brasiliensis* [272, 273]. As a Th2 response is essential for removal of parasites, this further supports the crucial role of IL-33 in the activation of mast cells and ICL2 which mediate helminth removal [172, 274]. In the context of protozoa infection,

a Th1 response is protective whereas Th2 initiation exacerbates; IL-33 as a potent activator of Th2 immunity worsens disease severity. Indeed, patients with leishmania show high serum concentrations of IL-33 [275]. In a murine model of fungal infection with *Canadia albicans* recombinant IL-33 administration instigates increased fungicidal activity on neutrophils which contribute to removal of fungal aggregations [276]. A similar phenomenon was observed in *Canadia neoformans* infection *in vivo*, where mice deficient in ST2 had amplified fungal development within their lungs [277]. In bacterial infections the IL-33/ST2 axis is critical in host defence, through enhancing the antimicrobial capacity of macrophages and neutrophils [278, 279]. It appears that following sepsis recovery, high serum levels of IL-33 may contribute to prolonged immune suppression through enhanced numbers of IL-10-producing Tregs [134].

A plethora of literature has described the roles of IL-33 within allergic diseases. Genetic polymorphisms in *IL33* and *IL1RL1* are supposed drivers of allergic susceptibility [134]. Indeed, in the serum samples of asthma patients increased IL-33 protein is observed and correlates robustly with severity [280]. Treatment of mice with recombinant IL-33 leads to the development of acute eosinophil/IL-13-mediated allergic inflammatory responses and airway inflammation dependent on ILC2 [133, 281]. Atopic dermatitis is associated with *ST2* polymorphisms which drives increased IL-33 specificity and IL-33/ST2 signalling [282, 283]. Additionally, IL-33 expression is increased in dermatitis patients [282] and intradermal administration of IL-33 drives an atopic dermatitis-like inflammatory phenotype with neutrophil and eosinophil accretion [187]. Increased IL-33 is observed in rhinitis and conjunctivitis and augments the release of histamine/chemoattractants, which drive eosinophil and basophil accumulation and inflammation at early stages in the disease [284]. Interestingly, the exposure of IL-33 to allergen proteases leads to cleavage of a central IL-33 domain with increased potency for initiating Th2 responses [285]. This has been shown to be prevented by the generation of a novel antibody to the IL-33 protease “sensor” domain which blocks allergen-associated inflammation [285].

1.7.6. Interleukin-33 and implications for AMD

IL-33 and ST2 are constitutively expressed across the retina and choroid by a range of cells, including, Müller cells, RPE, retinal and choroidal endothelial cells [8, 17]. RPE are critical to the maintenance of immune homeostasis within the retina, stimulation with agonists for TLR-4 and TLR-3 have been shown to up-regulate the expression of IL-33 and ST2L [8, 286]. IL-33 subsequently acts on multiple cells within the retina to propagate immune responses and initiate cellular signalling processes, many

of which have yet to be uncovered. Whilst literature surrounding the influence of this "novel" cytokine in the development of AMD is limited, it appears from other discoveries of context-dependent functions of IL-33, particularly in the CNS [145, 287], that many pleiotropic alarmins with functions in attenuating tissue injury should not be overlooked prior to adequate investigation.

IL-33 has recently been implicated in the development of AMD. In a phototoxic model of retinal degeneration, stress to the retina - in the form of constant bright light – was shown to increase the release of IL-33 from Müller cells. Once activated in an autocrine-dependent manner, IL-33 contributed to an upregulated chemokine and cytokine output, leading to the recruitment of mononuclear phagocytes, and ultimately contributing to photoreceptor loss and diminished retinal integrity. This phenomenon was attenuated by the knockdown of ST2 and led to reduced expression of CCL2, IL-6 and IL-1β. An increased expression of IL-33 and IL-33^{+} Müller cells was found in the macula and central retina of AMD cases [17]. A later study observed the TLR-dependent up-regulation of IL-33 by RPE without any influence on cell viability; intravitreal administration of IL-33 was shown not to affect the retinal integrity or thickness. Moreover, in stark contrast, IL-33 did not lead to the accumulation of Iba^{+} macrophage or CD45^{+}/CD11b^{+}/Ly6C+ monocyte within the retina (even when administered 500-times greater than the therapeutic dose) [8]. As IL-33 is released from RPE and Müller cells without cell death, it is likely that this is an adaptive response to maintain homeostasis. The release of IL-33 following exposure to light may have evolved to combat the recurrent minor cell damage and tissue injury faced by the retina.

It is proposed that dry AMD may be classified as a precursor state to wet AMD, with significant overlap in the underlying biological mechanisms and clinical manifestations [2]. However, as anti-VEGF treatments have proved successful in preventing disease progression of wet AMD, there remain no viable therapeutic options for those unresponsive to anti-VEGF. Additionally, it is suggested that long term anti-VEGF treatment leads to inner retina degeneration, as well as increased choroidal fibrosis.

A novel role for IL-33 has been observed, reducing the manifestations of nAMD. IL-33 was shown to attenuate angiogenesis with exogeneous administration of recombinant human (rh)IL-33 protecting against CNV; interestingly, it was observed that a lower dose was more effective at suppressing CNV [8], suggesting greater doses of IL-33 may elicit negative-regulatory mechanisms to balance excessive inflammation.

The retina has a massive metabolic throughput, entailing more oxidative damage than any other tissue; the effects of prolonged oxidative stress, through the high production of ROS over a lifetime are sorely felt as the retina ages. Whilst para-inflammation has evolved to combat noxious damage, a dysregulated para-inflammatory environment can contribute to macular degeneration [57]. IL-33 may exert potential anti-oxidative roles through the direct upregulation of SOD activity in the context of chronic heart failure [288]. In addition to this, the IL-33/ST2 axis has been proposed to affect the cellular concentrations of magnesium and reduced glutathione, both key mediators of cellular anti-oxidative capacities [289].

The predominant clinical hallmark of AMD progression is the deposition of drusen between the RPE and Bruch's membrane/choroid [113]. Recent studies identified common characteristics between the progression of AMD and Alzheimer's, with the presence of Aβ observed within both drusen and senile neuronal plaques [290]. The RPE and retinal ganglion cells contribute to Aβ production and accumulation in the posterior eye [290]. Elevated levels are observed in the aging retina and correlate strongly with the development of AMD. As the retina can be viewed as an extension of the neuronal environment, many findings and therapeutic strategies for targeting neurodegeneration may have direct applicability to AMD treatment. IL-33 has recently shown to reduce the accumulation of both soluble Aβ and Aβ plaques through the recruitment of phagocytic microglia [15].

Microglia activated through ST2/p38 were shown to increase the expression of CD68 scavenger receptor, promoting phagolysomal activity to clear Aβ deposits, even at later stages of disease progression [15]. In addition to this, through polarization of microglia to an M2 phenotype and the induction of Treg proliferation, IL-33 reduces the expression of pro-inflammatory cytokines [15, 145]. Polymorphisms of IL-33 may confer a reduced risk of AD development with increased sST2 correlated with mild cognitive decline in humans [291]. It is plausible that in an ocular setting, impaired IL-33 signalling may contribute to the aggregation of Aβ, implicating IL-33 as an attractive therapeutic outlook for AMD.

1.8. Metabolism

Cells extract energy and reducing power from their environment, this energy is necessary for the synthesis of higher order macromolecules such as proteins and DNA. Energy-generating processes are comprised of a highly integrated network of chemical reactions, which collectively are known as a cell's metabolic pathways. Intrinsic and extrinsic signals regulate the activity (and/or expression) of enzymes and therefore flux through these metabolic pathways to accommodate the growth and survival requirements under quiescent or stress contexts. The free energy donor in all energy-requiring processes is ATP. Energy is liberated in its hydrolysis to form ADP and P_i. Whereas an input of free energy is required for the reverse reaction. Electron donors such as nicotinamide adenine dinucleotide (NAD)+ and flavin adenine dinucleotide (FAD)+ provide the reductive power to facilitate ATP production. The basic strategy of metabolism is to form reduced ATP, NADH and other "building blocks" for biosynthesis. ATP synthesis is the end point extraction from the breakdown of foodstuffs (such as saccharides, amino acids and lipids) into smaller molecules which in the context of aerobic metabolism, converge on the citric acid (TCA) (commonly known as Krebs) cycle and oxidative phosphorylation (OXPHOS). The interconnected nature of various metabolic pathways (through shared metabolites, fuel inputs and endpoints) indicates the complex metabolic interplay which occurs in cells. Six key pathways: glycolysis, the TCA cycle, fatty acid synthesis, fatty acid oxidation, the pentose phosphate pathway and amino acid degradation have an important role in energy metabolism, the generation of products which influence cell survival responses to stress and forming a skeleton of core pathways in a cell (Fig. 1.8.).

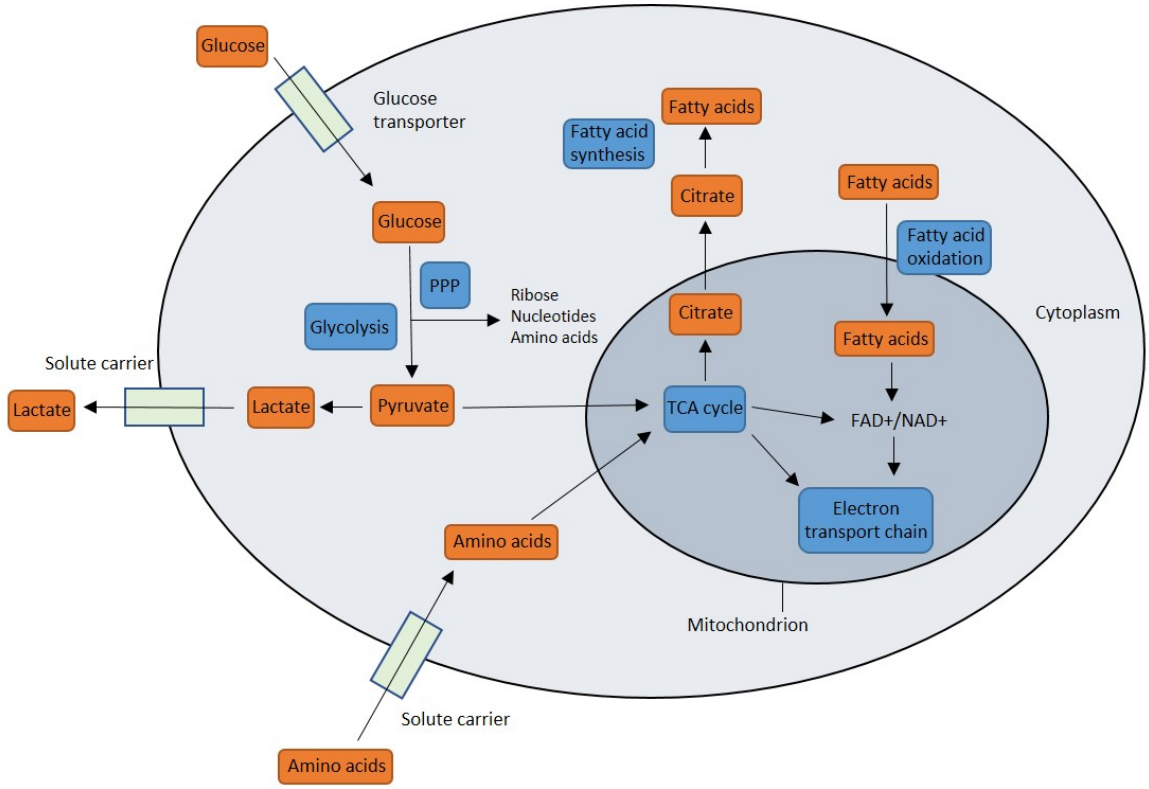

Figure 1.8. A schematic of core metabolic pathways:

Glucose enters a cell *via* a glucose transporter and is metabolised though the glycolysis pathway to yield pyruvate. Pyruvate can either be converted to lactate and secreted from a cell or can enter the TCA cycle where reduced NADH and $FADH_2$ are generated for utilisation in the ETC. Glycolytic carbon can also be diverted into the pentose phosphate pathway to generate ribonucleotides, amino acids and the electron carrier NADH. Amino acids are taken up through their respective solute carriers and feed into the mitochondrial TCA cycle either through pyruvate or glutamine. Citrate is withdrawn from the TCA cycle and is used in the synthesis of fatty acids. Fatty acid oxidation generates reduced NADH and $FADH_2$, which again drive mitochondrial ATP production in the ETC. The TCA cycle, fatty acid oxidation and the ETC are all oxygen-dependent pathways. Glycolysis, amino acid metabolism, fatty acid synthesis and the PPP are oxygen-independent pathways. PPP, pentose phosphate pathway; FAD, flavin adenine dinucleotide; NAD, nicotinamide adenine dinucleotide. Blue squares represent metabolic pathways, light green squares represent transporters and orange squares represent metabolites. Adapted from [5].

1.8.1. Glycolysis

Glycolysis is a universal pathway in biological systems and refers to the collective sequence of reactions involved in the conversion of glucose into pyruvate. In aerobic organisms, glycolysis is a preface to the TCA cycle and the ETC, which maximises the potential free energy available from a single glucose molecule. In mammalian cells, glycolysis begins with the intracellular uptake of glucose across the plasma membrane *via* the activity of several glucose transporters (GLUT1-5) [292]. The subsequent intracellular processing reactions occur within the cytosol and are divided into two sections (Fig. 1.9.). The bioenergetically expensive first stage sees the consumption of two molecules of ATP, as glucose is converted into fructose-1,6-bisphosphate. In the first step, glucose is rapidly phosphorylated by the action of hexokinase which catalyses the transfer of a phosphate from ATP to glucose, consuming one ATP molecule but preventing the exit of glucose from the cell. The next step involves the isomerisation of glucose-6-phosphate into fructose-6-phosphate by phosphoglucose isomerase. Fructose-6-phosphate is phosphorylated into fructose-1,6-bisphosphate by phosphofructokinase (PFK). This is the rate limiting step in the glycolytic pathway and is critically dependent on the level of activity of phosphofructokinase, which is allosterically regulated by changes to the ATP/AMP ratio. In this reaction another molecule of ATP is consumed as a phosphate is transferred to fructose-6-phosphate. The second stage of glycolysis consists of four reactions which collectively generate four molecules of ATP per glucose molecule. The second stage starts with the hydrolysis of fructose-1,6-bisphosphate into glyceraldehyde-3-phosphate and dihydroxyacetone phosphate by aldolase. These two molecules are isomers (glyceraldehyde-3-phosphate is an aldose whereas dihydroxyacetone phosphate is a ketose sugar) so a supplementary reaction is required to convert dihydroxyacetone phosphate into glyceraldehyde-3-phosphate. This isomerisation is catalysed by triose phosphate isomerase and allows the biproduct of this reaction to enter the main glycolytic pipeline rather than requiring a complete set of reactions to yield pyruvate. Accordingly, two molecules of glyceraldehyde-3-phosphate are formed from fructose-1,6-bisphosphate from this section of glycolysis. Up to this point, no energy has been extracted from the metabolism of glucose, but energy has been exploited in the form of two ATP molecules. The preceding steps permit ATP production *via* the generation of “high potential phosphorylated molecules”. Glyceraldehyde-3-phosphate is first converted into 1,3-bisphosphoglycerate through the activity of glyceraldehyde-3-phosphate dehydrogenase (GAPDH). The product of this reaction (1,3-bisphosphoglycerate) exhibits a high phosphoryl transfer potential due to an acyl phosphate group (a mixed anhydride of phosphoric and carboxylic acid). The next step sees the high phosphoryl transfer potential of 1,3-bisphosphoglycerate used to phosphorylate ADP and concurrently reduce NAD+ to NADH. This reaction is catalysed by phosphoglycerate kinase and leads to the generation of the next glycolytic

metabolite, 3-phosphoglycerate. As there are two molecules of glyceraldehyde-3-phosphate formed from glucose, two molecules of ATP are formed in this step. The next reaction involves the intramolecular rearrangement of 3-phosphoglycerate into 2-phosphoglycerate *via* phosphoglycerate mutase. 2-phosphoglycerate is subsequently dehydrated yielding phosphoenolpyruvate and a molecule of H_2O. The dehydration of 2-phosphoglycerate by enolase and the formation of an enol phosphate increases the phosphate group transfer potential present on phosphoenolpyruvate. In the final reaction of glycolysis, the high potential phosphoryl group of this group is transferred to ADP, forming the final molecules of ATP. This reaction is catalysed by pyruvate kinase and forms a molecule of pyruvate. Once again, as two molecules of phosphoenolpyruvate are formed from a single molecule of glucose, a total of two molecules of ATP are formed in this stage [292].

Glycolytic metabolism is relatively inefficient in terms of the ATP generation compared to the TCA cycle and ETC, yielding only two molecules of ATP per glucose unit. Whilst inefficient in terms of net ATP yield, glycolysis provides advantages to cells as it permits the reduction of NAD+ to NADH, used by many enzymes as a co-factor. To maintain flux through the glycolytic pathway, cells frequently reduce pyruvate to lactate through lactate dehydrogenase A (LDHA). This is coupled to the oxidation of NADH to maintain constitutive NAD+ levels. Glycolysis has key survival advantages for cells requiring a rapid generation of ATP for growth and proliferation. Glycolysis generates ATP at a rate over 10-times faster than the complete mitochondrial oxidation to CO_2 and ATP [293]. In addition to this, glycolytic metabolism provides the biosynthetic precursors for the synthesis of ribose for nucleotides (*via* the pentose-phosphate pathway) and the amino acid serine (*via* the serine biosynthesis pathway which diverts from 3-phosphoglycerate). Consequently, highly glycolytic metabolism is associated with the phenotype of rapidly proliferating cells.

1.8.2. The pentose phosphate pathway

The pentose phosphate pathway branches off the main glycolytic pathway at glucose-6-phosphate. This pathway permits a “metabolic diversion” of intermediates from glycolysis towards the synthesis of ribose-5-phosphate and NADPH. The production of nucleotides and amino acids require the synthesis of ribose. This is termed the non-oxidative branch of the pentose phosphate pathway and is critical for both cell growth and proliferation. This pathway is much more active when more ribose-5-phosphate than NADPH is required. A different function of the pathway is active when cells require more NADPH than ribose-5-phosphate: the oxidative branch. NADPH has a key role in the maintenance of redox homeostasis within a cell and is also required for fatty acid synthesis [5, 292]. The oxidative branch generates 12 NADPH molecules per molecule of glucose. The interplay between glycolysis and the pentose phosphate pathway allows cells to continuously meet their demands of NADPH, ATP, pyruvate and ribose.

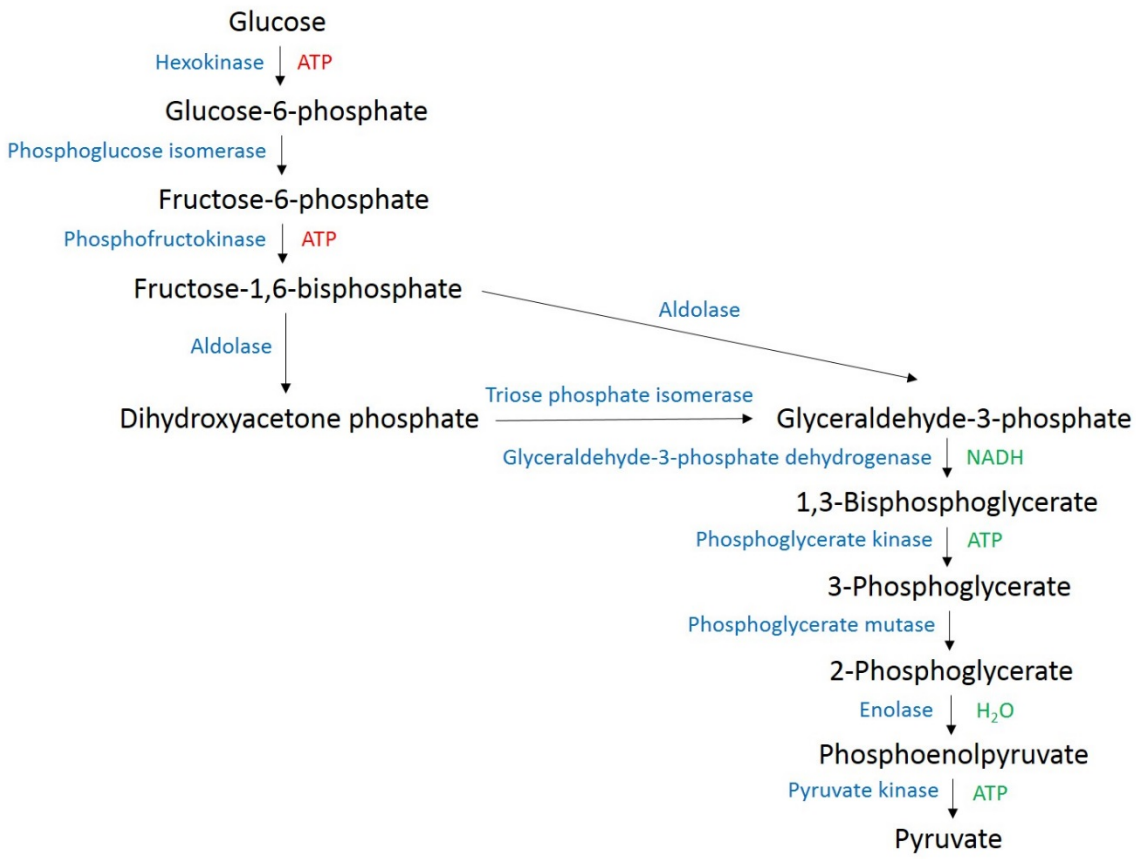

Figure 1.9. The glycolytic pathway:

Glycolysis refers to the catabolism of a glucose molecule to yield two molecules of pyruvate, two molecules of ATP, reduced NADH and a molecule of H_2O. Glucose is first phosphorylated into glucose-6-phosphate by hexokinase, this step consumes one molecule of ATP. Glucose-6-phosphate is then isomerized into fructose-6-phosphate by phosphoglucose isomerase. Phosphofructokinase is responsible for the addition of another phosphate group to fructose-6-phosphate, yielding fructose-1,6-bisphosphate. Fructose-1,6-bisphosphate is split into a molecule of dihydroxyacetone phosphate and a molecule of glyceraldehyde-3-phosphate by aldolase. Dihydroxyacetone phosphate is isomerized into a second molecule of glyceraldehyde-3-phosphate by triose phosphate isomerase. Glyceraldehyde-3-phosphate is converted to 1,3-bisphosphoglycerate by glyceraldehyde-3-phosphate dehydrogenase, yielding NADH. 1,3-Bisphosphoglycerate is dephosphorylated into 3-phosphoglycerate by phosphoglycerate kinase, this step yields one molecule of ATP. 3-Phosphoglycerate is isomerized into 2-phosphoglycerate by phosphoglycerate mutase. Enolase catalyses an aldol condensation reaction which produces phosphoenolpyruvate and a molecule of H_2O. The final step of glycolysis sees the dephosphorylation of phosphoenolpyruvate into pyruvate. This step is catalysed by pyruvate kinase and yields one molecule of ATP. ATP, adenine triphosphate; NADH, nicotinamide adenine dinucleotide. Red writing corresponds to consumption and green writing corresponds to production. Adapted from [292].

1.8.3. The TCA cycle

The preceding section considered the glycolytic pathway, whereby glucose is catabolised into pyruvate yielding a small amount of ATP. Under aerobic conditions, the TCA cycle is the subsequent pathway in the generation of additional ATP from a single molecule of glucose (see Fig. 1.10). The TCA cycle acts as a common pathway for the oxidation of all fuel molecules (amino acids, fatty acids and carbohydrates). Most of these molecules enter the cycle in the form of acetyl CoA, however other TCA metabolites serve as additional entry points. Unlike the reactions of the glycolysis pathway, the TCA cycle occurs within the mitochondria of cells [292].

The first entry point of the TCA cycle is the formation of acetyl coenzyme A (CoA) from pyruvate. This step bridges glycolysis and the TCA cycle, permitting the full oxidation of glucose. In order to first enter the TCA cycle, pyruvate must first be imported into the mitochondria through the mitochondrial pyruvate carrier complex (MPC) consisting of components MPC1/2 [294]. Once inside the mitochondrial matrix, the pyruvate dehydrogenase complex catalyses the oxidative decarboxylation of pyruvate to form acetyl CoA and CO_2. This reaction is the first to generate a molecule of reduced NADH for later utilisation in the ETC. The cycle starts with the condensation of a two-carbon acetyl CoA molecule with a four-carbon molecule (oxaloacetate) to yield citrate and CoA. This step is catalysed by the enzyme citrate synthase. Citrate requires isomerization into isocitrate prior to undergoing oxidative carboxylation in the forthcoming step. The isomerisation is catalysed by aconitase which utilises inorganic Fe-S clusters to facilitate dehydration and the successive rehydration of citrate. In the next step, isocitrate undergoes an oxidative carboxylation reaction to produce α-ketoglutarate and a molecule of CO_2. This reaction is catalysed by isocitrate dehydrogenase and is the second reaction to generate a molecule of reduced NADH. The next step of the cycle is another oxidation decarboxylation reaction, forming succinyl CoA from α-ketoglutarate. The reaction is catalysed by the α-ketoglutarate dehydrogenase complex and in a similar manner provides a molecule of reduced NADH and a molecule of CO_2. A high energy thioester bond is formed in the formation of succinyl CoA. The cleavage of this bond is coupled to the phosphorylation of GDP in the following step of the cycle. Succinyl CoA synthetase catalyses this reaction and leads to the formation of a four-carbon succinate molecule, GTP and CoA. GTP can be used for cellular signal transduction or can be readily converted into a molecule of ATP *via* the activity of nucleoside diphosphokinase. Succinate is oxidised to fumarate by the enzyme succinate dehydrogenase. The oxidation of this reaction is coupled to the reduction of acceptor FAD+ into $FADH_2$, which is later utilised in the ETC. Fumarate produced in this reaction is utilised in the next step of the cycle. Fumarase catalyses the

stereospecific trans hydration of fumarate to produce malate. The final step of the TCA cycle involves the oxidation of malate to form oxaloacetate. This reaction is catalysed by malate dehydrogenase and is the final NADH-producing reaction in the cycle, using NAD+ as a hydrogen acceptor. The oxaloacetate produced in this reaction condensates with an acetyl unit, and another turn of the cycle will occur. The TCA cycle collectively yields four molecules of NADH (three from the cycle and one from the formation of acetyl CoA), one molecule of reduced $FADH_2$ and one molecule of GTP from a single molecule of pyruvate. Additionally, the three carbons of pyruvate are lost as three molecules of CO_2 during one turn of the cycle [292].

Whilst the discussion of the TCA cycle so far has concentrated on the TCA cycle as a major catabolic pathway in the generation of ATP, it is important to highlight that the TCA cycle is a key provider of intermediates for biosynthetic pathways. For example, many amino acids are derivatives of either oxaloacetate or α-ketoglutarate, citrate provides acetyl groups for fatty acid synthesis and moreover, succinyl CoA provides the carbon skeleton required for the synthesis of porphyrins. Considering the observations that biosynthetic pathways feed of the TCA cycle, how is it that cycling continues and metabolite pools are replenished, when the starting point is *via* the entry of acetyl CoA? Hypothetically, if all the oxaloacetate was utilised in the generation of amino acids, one would assume that the TCA cycle would terminate unless new anaplerotic oxaloacetate was formed. In order to replenish oxaloacetate levels to a basal level, pyruvate is carboxylated into oxaloacetate through the pyruvate carboxylase complex, which serves as an additional entry point of pyruvate into the TCA cycle [295]. Additionally, as briefly highlighted, and discussed in the forthcoming section, glutamine metabolism can support the TCA cycle through entry at α-ketoglutarate [292].

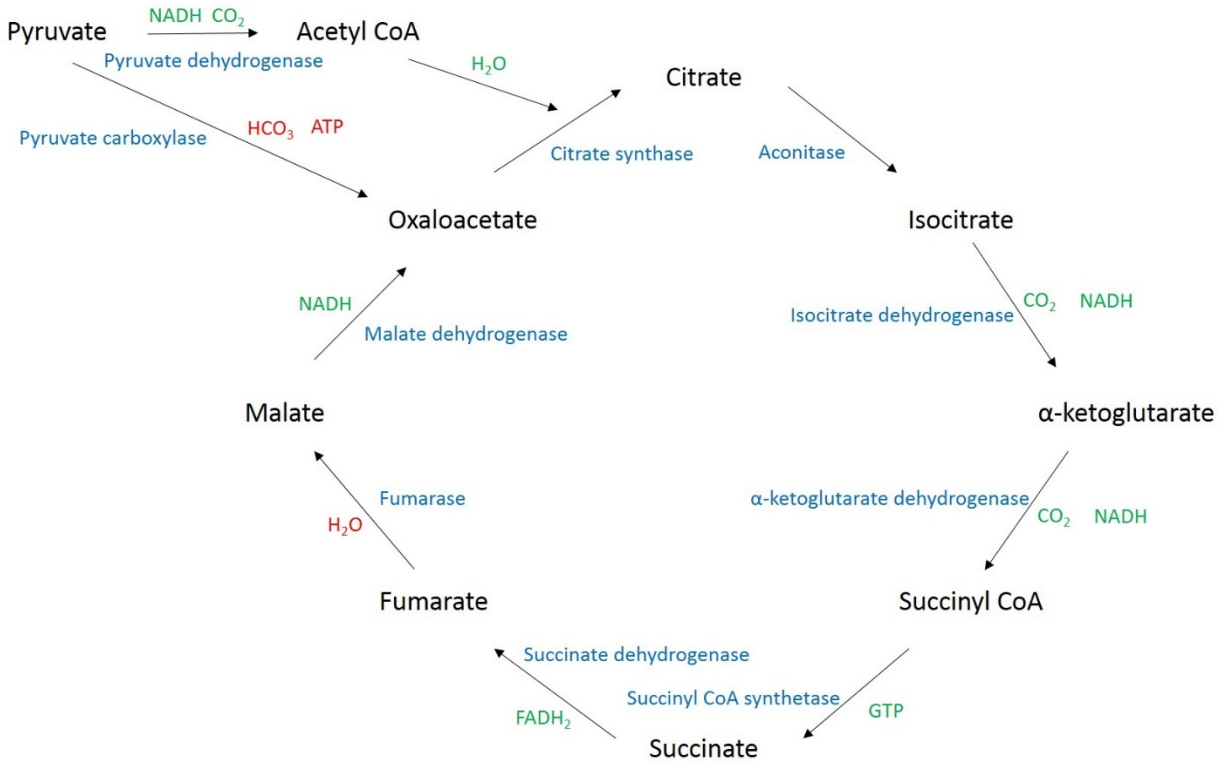

Figure 1.10. The TCA cycle:

Prior to entry into the TCA cycle, a three-carbon pyruvate molecule undergoes an oxidative decarboxylation into acetyl CoA by pyruvate dehydrogenase. This step generates one molecule of CO_2 and a molecule of NADH. In the first step of the TCA cycle, a four-carbon oxaloacetate condenses with a two-carbon acetyl unit to produce the six-carbon citrate. This step is catalysed by citrate synthase. Citrate is isomerized into isocitrate by aconitase. Isocitrate undergoes oxidative decarboxylation to produce a five-carbon α-ketoglutarate, CO_2 and a molecule of NADH. This step is catalysed by the enzyme isocitrate dehydrogenase. α-Ketoglutarate is immediately oxidatively carboxylated to yield a four-carbon compound (succinyl CoA), CO_2 and a molecule of NADH. This step is catalysed by the enzyme α-ketoglutarate dehydrogenase. In the next step, succinyl CoA synthetase catalyses the hydrolysis of succinyl CoA to succinate, which provides one molecule of GTP. Succinate is oxidised into fumarate by the enzyme succinate dehydrogenase. This reaction provides reduced equivalents in the form of $FADH_2$. In the next step, fumarase catalyses the hydration of fumarate into malate. Malate is subsequently oxidised by malate dehydrogenase to provide another molecule of NADH and the original four-carbon starting molecule, oxaloacetate. Pyruvate may enter the TCA cycle as oxaloacetate through a reaction catalysed by pyruvate carboxylase and requiring ATP and bicarbonate. ATP, adenosine triphosphate; NADH, nicotinamide adenine dinucleotide; GTP, guanosine triphosphate; $FADH_2$, flavin adenine dinucleotide; HCO_3, bicarbonate. Red writing corresponds to consumption and green writing corresponds to production. Adapted from [292].

1.8.4. Amino acid metabolism

In contrast to fatty acids, amino acids are unable to be stored or excreted, therefore when produced in excess amino acids provide key metabolite precursors within cells. In each case, the amino group is removed as urea and the residual core carbon molecules are converted into metabolic intermediates. Ultimately, the strategy of amino acid metabolism is to convert amino acids into a major metabolite which can either be converted to glucose or fatty acids or provide energy in the form of ATP *via* the TCA cycle. There is a degree of biochemical efficiency in the carbon skeleton which allows a diverse set of over 20 core amino acids to be catabolised into seven molecules (Fig. 1.11.). Amino acids which are metabolised into either acetyl CoA or acetoacetyl CoA are referred to as ketogenetic as they lead to the conversion of ketone bodies. On the other hand, amino acids that enter core metabolic pathways *via* pyruvate, α-ketoglutarate, succinyl CoA, fumarate or oxaloacetate are termed glucogenic, as glucose synthesis from their TCA cycle intermediates is permitted through conversion to phosphoenolpyruvate. Amino acids are split into families based on number of carbons (e.g C3, C4 and C5) present in their core skeleton and this underlies their respective degradation pathways. The C3 family, consisting of alanine, serine, cysteine, threonine, glycine and tryptophan, use the three-carbon molecule pyruvate. The C4 family, consisting of aspartate and asparagine, are transaminated for entry at the four-carbon TCA metabolite oxaloacetate. Aspartate can additionally be converted into fumarate *via* the coupling of the TCA and urea cycles. The C5 family sees the entry of several amino acids into the TCA cycle, first through conversion to glutamate and then through oxidative deamination to C. This pathway has significance as it involves the metabolism of glutamine, the most abundant amino acid present in the body with key roles in cell proliferation [296]. Glutamine undergoes catabolism to α-ketoglutarate *via* glutamine anaplerosis, a process comprising of two deamination reactions [297] . The first of these generates glutamate from glutamine through the enzyme glutaminase. α-Ketoglutarate is formed *via* the action of either glutamate dehydrogenase or transaminases. Non-polar amino acids such as methionine, isoleucine and valine require succinyl CoA as a point of entry into the TCA cycle [292].

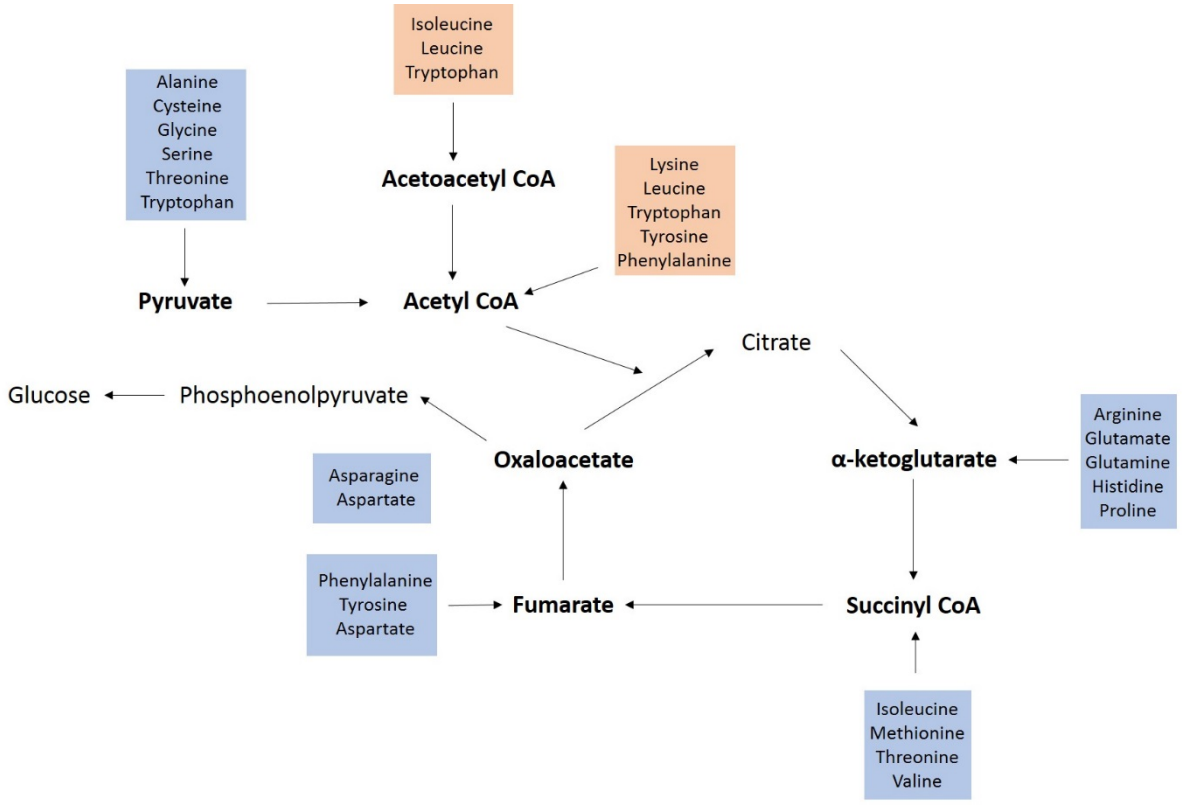

Figure 1.11. Fates of amino acid carbon skeletons:

Bold metabolites represent the entry points for the fundamental amino acids. Glucogenic amino acids are shaded in blue, whereas ketogenic amino acids are shaded orange. Alanine, cysteine, glycine, serine, threonine and tryptophan enter at pyruvate; isoleucine, leucine and tryptophan enter at acetoacetyl CoA; lysine, leucine, tryptophan, tyrosine and phenylalanine enter at acetyl CoA; arginine, glutamate, glutamine, histidine and proline enter at α-ketoglutarate; isoleucine, methionine, threonine and valine enter at succinyl CoA; phenylalanine, tyrosine and aspartate enter at fumarate; asparagine and aspartate enter at oxaloacetate. CoA, coenzyme A. Adapted from [292].

1.8.5. Fatty acid oxidation

Fatty acids are a class of biomolecules with a long hydrocarbon chain and a terminal carboxyl group [292]. Whilst fatty acids play key biological roles in the synthesis of phospholipids, glycolipids and cholesterol, and act as intracellular signalling intermediates, they provide key fuel molecules for oxidation within the mitochondria, *via* a process termed either β-oxidation or fatty acid oxidation. Prior to oxidisation, fatty acids must be first attached through a thioester linkage reaction to a molecule of CoA. This reaction is catalysed by acyl CoA synthetase and occurs on the outer mitochondrial membrane. Once activated, long-chain acyl CoA fatty acids are transported across the inner mitochondrial membrane into the mitochondrial matrix for further processing. Carnitine palmitoyl transferase I (CPT1) is the translocase enzyme responsible for the movement of long chain acyl units across the inner mitochondrial matrix [292]. This step constitutes the rate limiting step in the process of long chain β-oxidation [298]. Fatty acid molecules having six or fewer carbon atoms in their aliphatic tail diffuse passively across the mitochondrial membrane without the need of a transporter. Once in the mitochondrial matrix, the saturated acyl CoA chain is degraded (two carbons at a time) through the β-oxidation pathway to produce $FADH_2$, NADH and Acetyl CoA. In the first step, acyl CoA is oxidised to enoyl CoA by acyl CoA dehydrogenase. This step uses FAD+ as an electron acceptor and is subsequently reduced to $FADH_2$. In the next step, enoyl CoA hydratase catalyses the hydration of enoyl CoA to form 3-hydroxyacyl CoA. A second oxidation step then takes place as 3-hydroxyacyl CoA is converted to 3-ketoacyl CoA. This step is catalysed by 3-hydroxyacyl CoA dehydrogenase and generates NADH, which acts as an electron acceptor from the oxidised 3-hydroxyacyl CoA. In the final step, β-ketothiolase catalyses a thiolysis reaction, cleaving an acetyl CoA group from the end of the fatty acid chain. The reduced electron carriers $FADH_2$ and NADH are imminently utilised to generate ATP in the ETC. The oxidation of fatty acids generates a high energy yield in terms of net ATP production. Indeed, the complete oxidation of a molecule of palmitate (a sixteen-carbon fatty acid chain) yields a total of 106 ATP molecules [292]. This accounts to almost three-times the amount of ATP generated in glycolysis, thus is a robust pathway to generate ATP [299].

1.8.6. The electron transport chain

To this point, only a small amount of ATP has been generated in glycolysis; the TCA cycle and fatty acid oxidation pathways do not generate ATP themselves, but rather produce energy-rich molecules NADH and $FADH_2$. The process of mitochondrial OXPHOS couples the transfer of electrons from NADH and $FADH_2$ *via* a series of electron carriers located in the inner mitochondrial membrane, to the final electron acceptor O_2. This process generates large quantities of ATP, with 32 of the 36 molecules formed from the complete oxidation of glucose generated in this pathway [292].

The electrons from NADH enter the ETC at complex I (also known as NADH-Q-reductase) and are immediately transferred a series of iron-sulphur (Fe-S) clusters. From here, electrons are transferred to the electron carrier ubiquinone. The flow of electrons from complex I to ubiquinone is accompanied by the pumping of four protons (H^+) from the matrix across the inner mitochondrial membrane. Complex II (succinate-Q-reductase) catalyses the transfer of electrons from $FADH_2$ to its Fe-S clusters and then on to ubiquninone. Unlike the oxidation of NADH, the transfer of electrons from $FADH_2$ does not lead to the pumping of H^+ across the inner mitochondrial membrane. So subsequently, less ATP is produced per $FADH_2$ molecule than that of NADH. The reduced ubiquinone molecule passes its electrons into the second of the three proton pumps present in the ETC (complex III; cytochrome reductase), which facilitates the transfer of two H^+ across from the matrix. Complex IV (cytochrome oxidase) catalyses the final transfer of electrons from complex III to the final acceptor molecular oxygen, forming two molecules of H_2O. This reaction leads to the concomitant pumping of H^+ into the intermembrane space. As the electrons have passed through the ETC complexes I to IV, an electrochemical H^+ gradient is formed across the inner mitochondrial membrane (Fig. 1.12). The electrochemical gradient provides a proton-motive force which drives the conversion of ATP from ADP in the ATP synthase complex. The complex is formed of an F_0 subunit which permits H^+ passage through the membrane, and an F_1 subunit which sequentially releases tightly bound ATP molecules from three binding sites. The flow of electrons from a molecule of NADH to molecular oxygen generates a proton gradient adequate to produce 2.5 ATP molecules. $FADH_2$ on the other hand, only generates a proton gradient enough for the synthesis of 1.5 ATP [292]. Under normal conditions, electron flux through the ETC is tightly coupled to the synthesis of ATP. This respiratory coupling can be disrupted, and maximal respiration is stimulated by chemical uncouplers such as p-trifluoromethoxyphenylhydrazone (FCCP), or thermogenic uncoupling proteins such as uncoupling protein-1 (UCP1) [300, 301].

Under aerobic conditions, quiescent cells typically favour the utilization of oxygen dependent OXPHOS in order to maximize the yield of ATP production. Anaerobic conditions lead to an increased output of lactate as the cell derives its energy production solely from glycolysis. Yet, even in the absence of oxygen deprivation or mitochondrial dysfunction, cells may preferentially undertake glycolytic metabolism [302]. The switch from OXPHOS to glycolysis under these conditions is characteristic of the “Warburg effect”, where cancer cells are reprogrammed to increase glycolytic flux under aerobic conditions to meet their energetic requirements within minutes [302]. Whilst glycolysis may be inefficient in terms of ATP generation (2 ATP generated per glucose molecule compared to 36 in OXPHOS), it can utilize glucose 12 times faster [303, 304]. Energetically, this makes perfect sense, increased glycolysis allows a rapid proliferation and the production of bio-effectors to be achieved within cancer cells, a feat that OXPHOS would be unable to match.

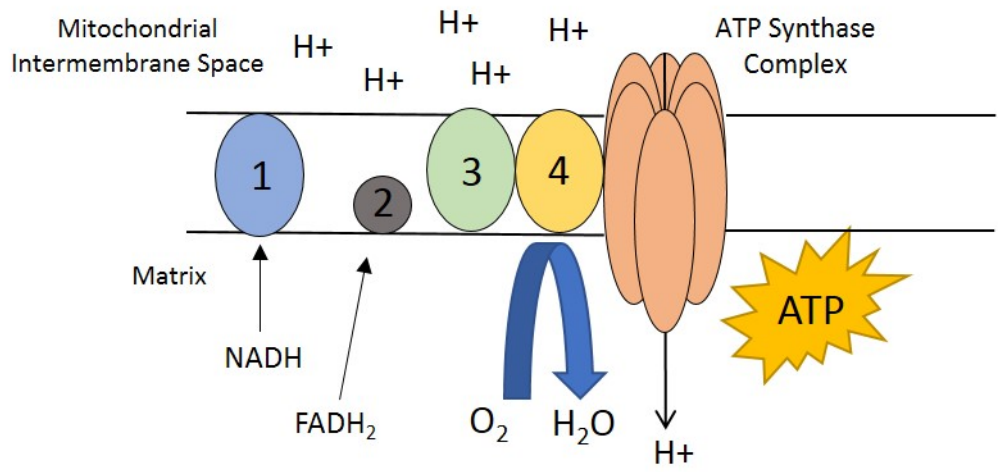

Figure 1.12. The electron transport chain:

The main pathway of ATP generation in cells occurs through mitochondrial OXPHOS. This involves the transfer of electrons from reduced equivalents ($FADH_2$ and NADH), through the multi-subunit ETC complexes (I to IV) to the final electron acceptor, molecular oxygen (O_2). NADH transfers its electrons to complex I, whereas $FADH_2$ transfers its electrons to complex II. Upon receiving electrons, complexes I, III and IV are responsible for pumping protons (H^+) from the mitochondrial matrix to the intermembrane space. This generates an electrochemical gradient across the inner mitochondrial membrane. The ATP synthase complex exploits this proton gradient to facilitate ATP production as protons flow back to the matrix. ATP, adenosine triphosphate; NADH, nicotinamide adenine dinucleotide; $FADH_2$, flavin adenine dinucleotide.

1.8.7. Fatty acid synthesis

The synthesis of fatty acids allows cells to produce lipids which are physiologically relevant for components of phospholipids, lipophilic modifiers of proteins, glycolipids, hormones and intracellular messengers. Fatty acids are synthesised in the cytosol and utilises products derived from multiple metabolic pathways, namely glycolysis, the TCA cycle and the pentose phosphate pathway. The malate pyruvate shuttle is used to transfer acetyl groups from the mitochondria to the cytosol in the form of TCA-derived citrate. Once in the cytosol, the enzyme ATP-citrate lyase is responsible for the conversion of citrate into oxaloacetate and acetyl CoA. Synthesis starts with the rate limiting carboxylation of acetyl CoA to malonyl CoA by acetyl CoA carboxylase (ACC). Then, the fatty acid synthase complex catalyses the NADPH-dependent elongation of the fatty acid chain to yield products such as palmitate. Fatty acid synthesis and β-oxidation are both reciprocally regulated through the ACC complex to ensure that both pathways are not occurring simultaneously [5, 292].

1.8.8. Regulation of cellular metabolism

Cells must be able to rapidly adapt to changes in their environment and respond to perturbations in energy status. Metabolism is constantly reprogrammed in cells to maintain metabolic homeostasis and provide enough ATP for cellular functions. In order to bolster flux through a given pathway, cells can either increase the amount of a rate limiting enzyme, for example: phosphofructokinase in glycolysis or CPT1 in the oxidation of long chain acyl fatty acids or use activators to convert an enzyme into its active formation, such as AMPK, which will be discussed later. Conversely, the same principles apply if a cell intends to stop given pathway, by reducing the expression of key enzymes and/or altering their active state, flux through the pathway will be reduced. Feedback inhibition permits the fine-tuning of metabolic pathways in response to concentrations of intermediate metabolites. For example, the first enzyme of glycolysis (hexokinase) is inhibited by its product glucose-6-phosphate.

1.8.5.1. Transcriptional regulation

The genes encoding metabolic pathway enzymes are frequently assumed to be regulated solely at the post-transcriptional level and therefore similarly expressed under diverse conditions and cell populations. This has led to many metabolic genes (such as GAPDH) used frequently experimentally as "housekeeping" controls. Whilst activity of metabolic enzymes is indeed regulated by "in pathway" mechanisms (such as feedback inhibition), it is becoming increasingly more appreciated that metabolic gene programs are regulated at the transcriptional level to control proliferation, differentiation and adaptive responses to cellular signalling. Many of the transcription factors which facilitate metabolic programming are well-characterised due to their roles in cancer metabolism and other programs (such as T-cell activation) which support dynamic proliferation. Oncogenic signalling is frequently associated with the reprogramming of pathways to facilitate enhanced nutrient attainment and integration of carbon into macromolecules to support cell growth (Fig. 1.13). This is associated with rapidly increased rates of both glycolysis and (in many cases) glutaminolysis [305].

The MYC oncogene is a transcription factor responsible for the modulation of global gene expression through transcriptional regulation [306]. MYC is located downstream of multiple signal transduction pathways receptive to extracellular stimuli, such as growth factors, cytokines, nutrient availability and extracellular matrix [306]. MYC directly binds DNA at proximal promotor regions, relieving pausing of the RNA polymerase complex, subsequently activating transcription. MYC is associated with the activation of transcriptional programs which favour aberrant cellular growth and proliferation in many biological systems [306, 307]. MYC induces the expression of numerous genes involved in the glycolysis and glutaminolysis pathways due to the presence of conserved MYC consensus binding sites in the promoter regions. In addition to this, MYC has been shown to induce the expression of genes involved in both nucleotide biosynthesis and the shuttling of citrate out of the TCA cycle to be used in lipid synthesis [306]. To support the increased metabolic demand MYC activation places on a cell, mitochondrial biogenesis is additionally upregulated to support biosynthetic pathways involving the TCA cycle [306].

Hypoxia inducible factor 1 alpha (HIF-1α) is another transcription factor involved in the cellular response to environmental changes. The HIF-1 complex consists of an O_2-regulated HIF-1α subunit and a constitutively expressed HIF-1β subunit [308]. Under conditions of low oxygen, degradation of the HIF-1α subunit is attenuated. The increased active HIF-1α binds HIF-1β to form a heterodimer (HIF-

1) with transcriptional properties. The HIF-1 complex binds to the promoter regions of (hypoxia-inducible) genes exhibiting a specific binding site and subsequently elicits broad transcriptional changes [309]. HIF-1 therefore translates information regarding oxygen state into specific gene expression programs which allow a cell to adapt to its environment. HIF-1 has a key role in the reprogramming of cells towards a pro-glycolytic phenotype by activating the transcription of glucose transporters and glycolytic enzymes [308]. Furthermore, the increased expression of pyruvate dehydrogenase kinase 1 (PDK1) by HIF-1 leads to the phosphorylation and inactivation of the pyruvate dehydrogenase (PDH) complex. As a result, pyruvate is shunted away from oxidation in the mitochondrial TCA cycle and is converted into lactate by LDHA [308]. Genetic or pharmacological inhibition of HIF-1 or PDK1 increases the oxygen consumption in cancer cells [310, 311].

The p53 tumour suppressor gene has long been characterised as a metabolic regulator with functions in promoting OXPHOS and suppression of aerobic glycolysis. P53 binds to and regulates the expression of over 500 genes, among these are key regulators of and genes within glycolysis, TCA cycle, lipid metabolism, amino acid metabolism, OXPHOS and ROS generation pathways [312]. In terms of glycolysis, the role of p53 be both inhibitory and promotive. For example, p53 promotes the expression TP53-induced glycolysis and apoptosis regulator (TIGAR) but decreases the expression of (GLUT1 and 4) and phosphoglycerate mutase. TIGAR lowers the intracellular concentrations of fructose-2,6-bisphosphate and therefore decreases glycolytic flux. As glycolysis is downregulated, more glucose can pass into the pentose phosphate pathway for the generation of NADPH [313]. P53 promotes OXPHOS by the induction of cytochrome c oxidase expression. In addition to this, p53 increases the transcription of genes involved in the metabolism of glutamine, subsequently increasing α-ketoglutarate levels and mitochondrial respiration [313].

Members of the peroxisome proliferator-activated receptor (PPAR)γ coactivator-1 (PGC-1) family of transcriptional coactivators (PGC-1α and PGC-1β) activate a cellular metabolic program of increased mitochondrial biogenesis, oxidative metabolism and fatty acid β-oxidation [314]. PGC-1α lacks histone-modifying enzymatic activities but directly binds DNA and interacts with a variety of chromatin remodelling complexes and transcriptional co-activators. These include the nuclear respiratory factors (NRF), PPARα and estrogen-related orphan nuclear receptor (ERR). PGC-1α promotes the expression of genes involved glutamine and β-oxidation metabolic pathways through interactions with ERRα and sirtuin (SIRT)-1, respectively [315, 316]. NRF-1 acts directly on the transcription of genes involved in the respiratory transport chain and therefore promotes increased biogenesis [316]. In addition to this,

PGC-1s have an important role in the defence against ROS (produced by bolstered mitochondrial activity) through the ability to directly induce the transcription of multiple antioxidant enzymes, such as SOD, catalase and glutathione peroxidases [317].

Enzymes involved in the modification of chromatin require cofactors or substrates that can be found in core metabolic pathways. These metabolites provide a mechanism to synchronize epigenetic regulation with the metabolic status of a cell. Such examples are the use of acetyl-CoA by histone acetyltransferases to acetylate and increase the accessibility of chromatin, and the use of NAD+ as a substrate for SIRTs (class III HDACs) to deacetylate and repress gene transcription [318]. SIRT1, 3 and 6 inhibit the proinflammatory transcription NF-kB, AP-1, and HIF-1a, and enhances oxidative metabolism [319]. Histone methylation is controlled by histone methyltransferases which use S-adenosylmethionine (SAM) as methyl donor. SAM is derived from the folate-mediated one carbon metabolism of amino acids serine and glycine [320]. Therefore, dietary amino acid availability directly affects the methylation status of chromatin [318].

In addition to the influence of metabolites of gene expression, many metabolic enzymes have been shown to “moonlight” and directly influence chromatin regulation, transcription and post-transcriptional control [318]. An example of this is in the nuclear interaction between fructose-1,6-bisphosphatase and HIF-1α. Fructose-1,6-bisphosphatase acts as a transcriptional corepressor of HIF-1α, binding to its inhibitory domain to facilitate silencing of hypoxia response DNA elements [321]. Other enzymes such as phosphofructokinase and pyruvate kinase isoform 2 (PKM2) lack DNA-binding domains but interact with other transcription factors, such as HIF-1α/MYC to regulate transcription [322]. Key metabolic enzymes such as GAPDH and enolase directly function as transcription factors through DNA-binding domains [322]. GAPDH localizes to the nucleus following phosphorylation by AMPK, whereby it activates SIRT1 to reprogram gene transcription in energy metabolism pathways [323]. In addition, GAPDH interacts with the p53 tumour suppressor complex to promote the expression of genes involved in oxidative metabolism [324]. Enolase directly binds to the *MYC* promotor to positively regulate its transcription and ultimately MYC-activated glycolysis [322]. LDHA orchestrates global histone deacetylation status through controlling NAD+ availability and interacting with SIRT1 [325]. Nuclear regulation of metabolic gene transcription is not just a phenomenon reserved to enzymes of the glycolytic pathway; malate dehydrogenase translocates to the nucleus of cells where it binds to p53-responsive elements, including promoter regions of TCA cycle enzymes and OXPHOS genes [326].

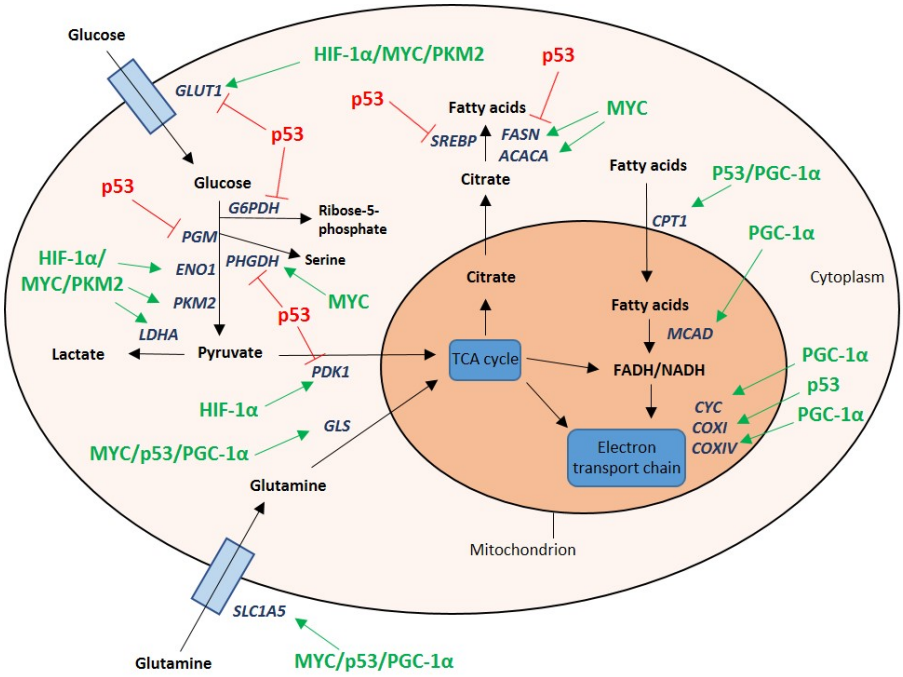

Figure 1.13. Transcriptional reprogramming of cell metabolism:

Metabolic reprogramming in cells is regulated by key transcription factors. P53 inhibits the expression of *GLUT1* and glycolytic enzyme *PGM*. P53 also inhibits the efflux of metabolites into pathways which feed of glycolysis. By inhibiting the transcription of *G6PDH* and *PHGDH*, p53 regulates the ox-PPP and serine biosynthesis, respectively. P53 promotes mitochondrial OXPHOS by inhibiting the expression of *PDK1* and promoting the expression of *COX1*. Moreover, p53 promotes the expression of genes involved in glutaminolysis (*SLC1A5* and *GS*) and FAO (*CPT1*), whilst inhibiting enzymes of the FAS pathway (*SREBP* and *FASN*). HIF-1α promotes a metabolic phenotype of aerobic glycolysis through increasing the expression of pro-glycolytic genes (*GLUT1*, *ENO1*, *PKM2*, *LDHA* and *PDK1*). PKM2 directly interacts with HIF-1α, activating the hypoxia response element required for HIF-1α binding to target genes. The MYC transcription factor alters the expression of key genes involved in glucose (*GLUT1*, *ENO1*, *PKM2*, *LDHA*) and glutamine metabolism (*SLC1A5* and *GS*), serine biosynthesis (*PHGDH*) and FAS (*FASN* and *ACACA*). PGC-1α increases the expression of genes involved FAO (*CPT1*), glutaminolysis (*SLC1A5* and *GS*) and the ETC (*COXIV* and *CYC*). HIF-1α, hypoxia inducible factor-1α; PGC-1α, peroxisome proliferator-activated receptor gamma coactivator 1α; oxPPP, oxidative pentose phosphate pathway; G6PDH, *Glucose-6-phosphate dehydrogenase; PGM,* Phosphoglycerate mutase; ENO1, enolase; PKM2, pyruvate kinase isoform 2; LDHA, lactate dehydrogenase A; PDK1, pyruvate dehydrogenase kinase; GLS, glutamine synthetase, SLC1A5, Solute Carrier Family 1 Member 5; NADH, nicotinamide adenine dinucleotide; $FADH_2$, flavin adenine dinucleotide; CYC, cytochrome C; COXI, cytochrome C oxidase I; COXIV, cytochrome C oxidase IV. Metabolites are noted in black text and genes of metabolic enzymes are noted by dark blue italic text. Green arrows represent positive regulation of a target gene by transcription factor(s). Red arrows represent negative regulation of a target gene by transcription factor(s). Adapted from [305].

1.8.5.2. Alternative splicing of the *PKM* gene

Pyruvate kinase is a rate-limiting enzyme in the glycolysis pathway, responsible for the irreversible catalysation of phosphoenolpyruvate into pyruvate [327]. This final reaction commits pyruvate to either oxidation in the TCA cycle or aerobic lactate production [328]. In mammals, four pyruvate kinase isoforms are observed, encoded by two different genes [329]. The *PKLR* gene encodes PKL and PKR which are expressed in the liver and erythrocytes, respectively. The *PKM* gene encodes the muscle isoforms PKM1 and PKM2 [330]. The expression of pyruvate kinase is tissue specific and is regulated by various mechanisms, including alternative splicing and the activity of upstream promotors. As PKL and PKR isoforms are restricted to the liver, kidneys, intestines and red blood cells (the later exclusively expressing PKR), PKM isoforms are expressed in the remaining terminally differentiated tissues. PKM1 and PKM2 are produced through the alternative splicing of mutually exclusive exons, identical in length but encode a 56-amino acid region that varies at 22 residues (Fig. 1.14) [330]. PKM1 contains exon 9, whereas PKM2 exclusively contains exon 10. Although both isoforms have equal catalytic functions in the glycolysis pathway, the extra 22 amino acids present in the PKM2 isoform lead to the addition of a fructose-1,6-bisphosphate binding pocket. The presence of this binding site renders the active PKM2 tetramer sensitive to the allosteric binding of fructose-1,6-bisphosphate [330]. The non-allosteric isoform PKM1 is constitutively expressed in tissues requiring a large demand of ATP, including both the muscle and brain [328]. PKM1 is thought to generate a bioenergetic profile in favour of oxidative phosphorylation and the entrance of pyruvate into the TCA cycle. In cancer cells, PKM2 is overexpressed at the expense of PKM1, regulated by the activity of MYC [331]. MYC promotes the transcription of heterogeneous nuclear ribonucleoproteins (hnRNPs) A1 and A2 and the polypyrimidine tract binding protein (PTB), which bind repressively to sequences flanking exon 9, resulting in exon 10 inclusion [331]. This leads to the inhibition of PKM1 and mRNA splicing and promotes PKM2 isoform expression. The serine/arginine-rich splicing factor 3 (SRSF3) has a key role in the splicing of PKM2 and binds to an exonic splicing enhancer found on *PKM* exon 10 [332]. How mRNA splicing controls the inclusion of PKM1 is not as well understood, in a large part because PKM1 is generally expressed at much lower levels within cells. In the A172 cell line, commonly used to study PKM1 expression, PKM1 expression is observed at 5% of total transcript levels [333].

Both PKM isomers are tetrameric proteins consisting of four identical subunits. Due to the splicing of different exons into in their mRNA transcripts, PKM1 and PKM2 exhibit differences in the encoded C domain of the monomer subunit, ultimately conferring altered stability to the tetramer. Physiologically, PKM1 protein constitutively arranges as a tetramer whereas PKM2 exists in either dimer or tetramer. The differences between dimer or tetramer conformation depend on the allosteric regulation fructose-1,6-bisphosphate [334]. This intermediate directly binds PKM2 and increases its

affinity for phosphoenolpyruvate, which in turn increases flux through the glycolysis pathway [335]. PKM1 on the other hand, is not significantly affected by fructose-1,6-bisphosphate [335]. The dimer conformation of PKM2 exhibits an activity of less than 10% of the tetramer [336]. Using this mechanism, reversible activation of PKM2 allows for dynamic regulation of enzymatic activity and an additional control point in the glycolysis pathway.

Inactivation of PKM2 allows for a build-up of phosphorylated glycolytic intermediates, which feed into the biosynthesis pathways of serine and nucleotides. Altering PKM expression status into the forced expression of PKM1 leads to an inability of cells to produce deoxynucleotides [337]. Typically, PKM2 expression is thought to be associated with rapidly proliferating cancer cells favouring anabolic metabolism. Phosphorylation and inactivation of PKM2 *via* tyrosine kinase signalling is critical for the entry of glucose-derived carbon into the pentose phosphate pathway to generate sufficient reducing potential to aid redox balance [338].

A multitude of recent work has identified multiple non-canonical functions for PKM2 in gene regulation, cell signalling and the cell cycle. For example, the PKM2 dimer is observed to interact with multiple tyrosine kinases including A-Raf and fibroblast growth factor receptor 1 [339]. PKM2 also functions as the cytosolic receptor for thyroid hormone [340]. Additionally, PKM2 translocates into the nucleus where it acts as a transcriptional co-activator and protein kinase involved in modulation of histone phosphorylation status [341]. PKM2 has been shown to interact with β-catenin, STAT3, NF-κB and OCT4 [334]. Nuclear PKM2 directly interacts with HIF-1α to promote the expression of target genes. This is achieved by enhancing the binding of HIF-1α to hypoxia response elements, ultimately conferring augmented transcription of glycolytic genes [342].

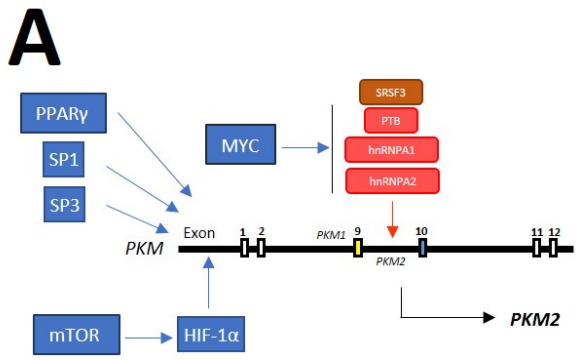

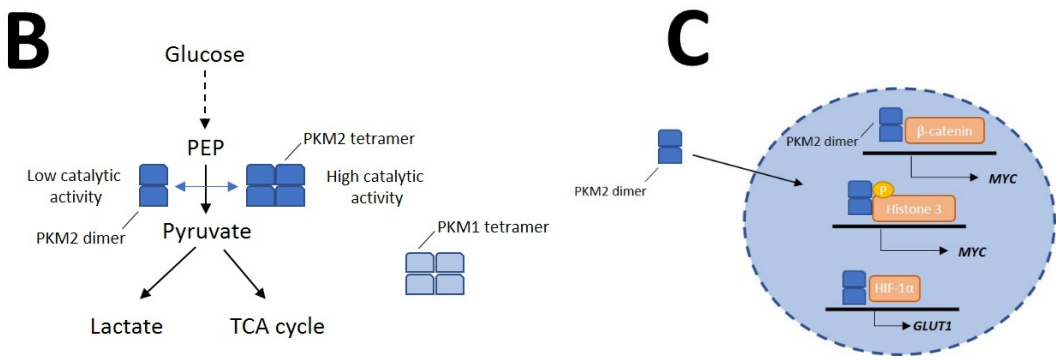
B
Glucose
PEP
PKM2 tetramer
Low catalytic activity
High catalytic activity
PKM2 dimer
Pyruvate
PKM1 tetramer
Lactate
TCA cycle
C
PKM2 dimer
PKM2 dimer
β-catenin
MYC
P
Histone 3
MYC
HIF-1α
GLUT1

Figure 1.14. Splicing and "moonlighting" of pyruvate kinase M2:

(A) Several transcription factors regulate the activity of the *PKM* promoter including: SP1, SP3, HIF-1α and PPARγ. PKM2 expression is regulated at the level of transcribed *PKM* mRNA *via* splicing. The splicing factors hnRNPA1, hnRNPA2, PTB and SRF3 bind to the mRNA transcript to favour the exclusion of exon 9 (PKM1) and inclusion of exon 10 (PKM2). HnRNPA1, hnRNPA2 and PTB are upregulated by the transcription factor MYC. (B) Pyruvate kinase catalyses the final rate-limiting step in the glycolysis pathway by catalysing a phosphoryl transfer reaction from phosphoenolpyruvate to ADP, to yield pyruvate and ATP. Allosteric control of PKM2 tetramerization regulates its enzymatic activity, with the PKM2 dimer exhibiting low catalytic activity compared to the tetramer. The PKM1 isoform lacks an allosteric control site and is therefore always present as a tetramer. (C) PKM2 has been found to translocate into the nucleus upon mitogenic stimuli. Once in the nucleus, PKM2 functions as a transcriptional activator by phosphorylating histones, indicating a crucial role in the epigenetic control of the Warburg effect through a MYC-dependent feedback loop. PKM2 directly interacts with HIF-1α to promote binding to hypoxia response DNA elements. HIF-1α, hypoxia inducible factor-1α; mTOR, mammalian target of rapamycin; SP1, specificity protein 1; SP3, specificity protein 3; PPARγ, peroxisome proliferator-activated receptor; PKM; pyruvate kinase muscle isoform; SRSF3, serine/arginine-rich splicing factor 3; PTB, polypyrimidine tract binding protein; hnRNPA1, heterogeneous nuclear ribonucleoprotein A1; hnRNPA2, heterogeneous nuclear ribonucleoprotein A2; PKM1, pyruvate kinase muscle isoform 1, PKM2; pyruvate kinase muscle isoform 2; PEP, phosphoenoylpyruvic acid. Adapted from [341].

1.8.5.3. AMP-activated kinase and mammalian target of rapamycin

The maintenance of cellular energy homeostasis is dependent on a number of regulatory strategies, including the trafficking and uptake of hexose sugars through various transporters, ATP production by glycolysis, Kreb's cycle and other catabolic pathways, OXPHOS, and the overall control of metabolic pathway flux by the governing activities of AMPK and mTOR [343-345]. The fundamental regulator of cellular metabolic homeostasis is AMPK. This evolutionarily conserved protein-kinase is observed in principally all eukaryotic cells where it exists as a heterodimeric complex comprised of catalytic α-subunits and regulatory β- and γ-subunits. The catalytic subunits contain a conserved Serine/Threonine (Ser/Thr) kinase at the amino terminus. Kinase activity of the AMPK complex increases 100-fold following the phosphorylation of Thr172 in the activation loop by the upstream kinase liver kinase B1 (LKB1). A high level of basal Thr172 phosphorylation is conferred by LKB1, with modulation initiated by the binding of AMP to the γ-subunit. AMP (or ADP) binding to the γ-subunit is indicative of bioenergetic stress; allosteric activation induces conformational changes to Thr172, leading to constitutive phosphorylation by LKB1. Allosteric binding of ATP to the γ-subunit promotes net dephosphorylation; this mechanism modulates kinase activity to the degree of energy impairment [344, 346]. Once activated, AMPK endeavours to restore energy balance by switching on catabolic pathways that generate ATP (e.g. glycolysis, fatty acid oxidation, glucose transporter trafficking to the plasma membrane, and mitochondrial biogenesis), whilst simultaneously inhibiting anabolic, ATP consuming pathways such as protein/sterol/fatty acid synthesis, which contribute to cell-cycle progression [344] (Fig. 1.15). This implicates AMPK activation with the phenotype of quiescent anti-inflammatory cells, preferentially favouring OXPHOS, rather than proliferative inflammatory cells undergoing glycolytic metabolism [345]. The result of AMPK activation is to conserve cellular energy prior to a bioenergetic crisis leading to cell death.

AMPK directly regulates the activity of ACC to control lipid biosynthesis. ACC mediates the conversion of acetyl CoA to malonyl CoA, which is directed to a carbon pool for lipid biosynthesis. Increased malonyl CoA levels simultaneously inhibits CPT1 and therefore lipid oxidation. Phosphorylation of Ser-79 by AMPK inhibits ACC, indirectly relieving the inhibition of CPT1 and directly inhibiting fatty acid synthesis. In addition to this, AMPK has been shown to promote glycolytic flux by phosphorylation of phosphofructokinase [347].

Another key metabolic pathway controlled by the activity of AMPK is autophagy, a natural mechanism of cell "self-devouring" which mediates the disassembly and recycling of intracellular components to promote cell survival. AMPK positively regulates autophagy through a direct interaction with the

autophagy initiating kinases ULK1 and ULK2 [348]. AMPK phosphorylates both kinases on multiple regulatory sites to promote autophagy in response to nutrient depletion and energetic stress [349]. Furthermore, AMPK may promote autophagy under energetic stress through inhibition of the mTOR complex 1 [350].

AMPK activation can be modulated by various compounds, including AICA-riboside, 2DG, metformin and dorsomorphin, which act either directly (influencing the phosphorylation of Thr172) or indirectly (*via* the ratio of intercellular AMP/ATP) [351].

mTOR is an evolutionarily conserved serine-threonine protein kinase belonging to the phospho-inositide 3-kinase (PI3K) family. mTOR integrates numerous biological signals to regulate an array of cellular functions including cell growth, apoptosis, protein synthesis, cytoskeletal reorganization and metabolism. mTOR forms the catalytic subunit of two distinct multi-protein complexes: mTOR Complex 1 (mTORC1) and 2 (mTORC2). mTORC1 is described by its three core proteins: mTOR, regulatory protein associated of mTOR (Raptor), and GβL. mTORC2 on the other hand, is comprised of mTOR, rapamycin-insensitive companion of mTOR (Rictor), mammalian stress-activated protein kinase interacting protein, protein observed with Rictor-1; mLST8; and Deptor [352, 353].

mTORC1 is the most well studied of the mTOR complexes and has many of its upstream and downstream signals well defined. mTORC1 incorporates key signals in the form of growth factors, energy status, oxygen tensions and amino acid abundances. Intracellular messengers such as insulin-like growth factors (IGF), interleukins, IFNs and chemokines have been shown to activate mTORC1 through AKT and PI3K pathways [343]. Additionally, TNFα activates IkB kinase-β which physically interacts with TSC1, leading to mTORC1 activation [354]. AMPK conveys information on bioenergetic status to mTORC1 through multiple pathways. The first of which sees phosphorylation of TSC2 by AMPK, this ultimately reduces mTORC1 activation through a lack of activity of TSC2 for Rheb [355]. In addition to this, AMPK phosphorylates Raptor on conserved Ser residues, leading to the inhibition of mTORC1 [356]. mTORC1 activity is influenced by intracellular amino acid concentrations *via* the nutrient sensing Rag GTPases [357]. Aerobic glycolysis in cells is positively regulated by mTORC1 through the transcriptional activation of multiple core glycolytic and pentose phosphate pathway enzymes [358]. Rapamycin treated cells have impaired upregulation of glucose transporters, glucose uptake and expression of glycolytic enzymes [359, 360]. mTORC1 interacts with core metabolic

transcription factors including HIF-1α and MYC to promote glycolytic metabolism [361]. mTORC1 increases the expression of HIF-1α mRNA, this in turn promotes a hypoxia-response pro-glycolytic gene program in cells [362]. mTORC1 is reported to regulate the expression of MYC *via* post-transcriptional modifications [363]. MYC is a key mTORC1 effector, leading to the splicing of PKM2 and an increased glycolytic flux [358]. In addition to its role in promoting glycolysis, mTORC1 is a key regulator of mitochondrial biogenesis and TCA cycle activity. Inhibiting mTORC1 through rapamycin drastically lowers mitochondrial oxygen consumption, cellular ATP levels, and is associated with a complete shift in the mitochondrial phosphoproteome [364]. Evidence suggests that dysregulated overexpression of glycolysis and OXPHOS genes are observed in T-cells with hyperactive mTOR activity [365].

Compared to mTORC1, relatively little is known about the biology of mTORC2. Due to an embryonic lethality caused by the deletion of mTORC2 components in mice and (up until very recently) a lack of specific inhibitors, knowledge of this complex has remained elusive [366]. Despite this, many important discoveries have highlighted a role for mTORC2 in the regulation of many core cellular processes, including cell survival and metabolic reprogramming. mTORC2 activates AKT on one of its key sites (Ser 473) to activate forkhead box protein O1 (FOXO1) and FOXO3a transcription factors, key transcriptional nodes in the regulation of genes involved in stress response and metabolism [367]. Interestingly, a lack of mTORC2 in T-cells appears to increase their metabolic capacity, both in terms of glycolysis and OXPHOS. This mechanism has yet to be elucidated, yet it is suggested to occur through stabilization of FOXO1 [368].

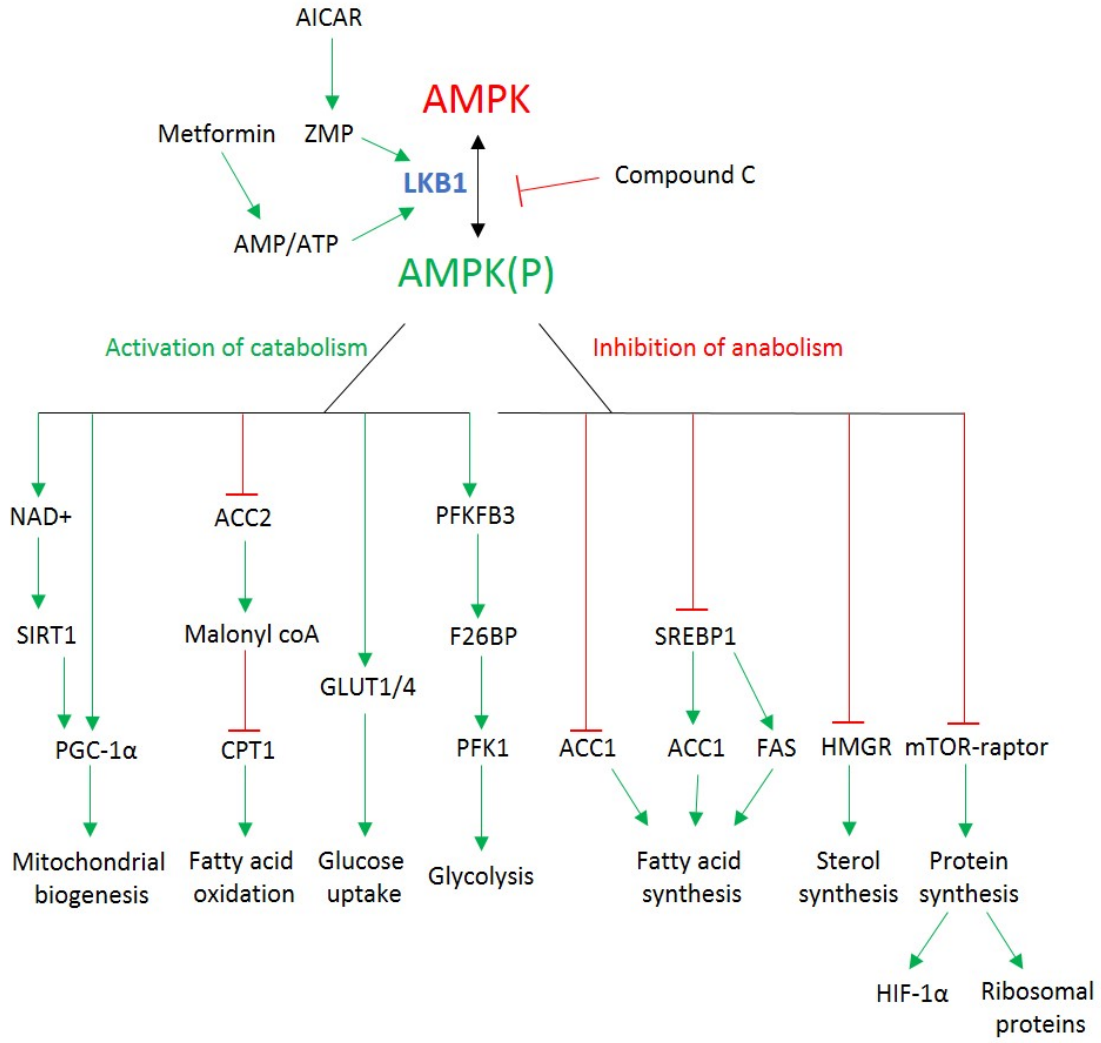

Figure 1.15. Regulation of AMP-activated kinase and its downstream pathways:

AMPK is activated by phosphorylation by LKB1. Binding of AMP/ADP (which increase in response to metformin) or ZMP (which increases in response to the modulation of purine biosynthesis by AICAR) to allosteric binding sites promote phosphorylation. Compound C inhibits AMPK activation. Once activated, AMPK activates catabolic pathways (left side) and inhibits anabolic pathways (right side). AMPK promotes both mitochondrial biogenesis and fatty acid oxidation, whilst down-regulating aerobic glycolysis through the inhibition of the mTORC1 complex (mTOR-raptor) and HIF-1α. HIF-1α, hypoxia inducible factor-1α; mTOR, mammalian target of rapamycin; NAD+, nicotinamide adenine dinucleotide; SIRT1, sirtuin 1; AICAR, 5-Aminoimidazole-4-carboxamide ribonucleotide; ZMP, 5-Aminoimidazole-4-carboxamide ribonucleotide; AMP, adenine monophosphate; ATP, adenine triphosphate; ACC2, acetyl-coenzyme A carboxylase-2, PGC-1α, peroxisome proliferator-activated receptor gamma coactivator 1α; CPT1, carnitine palmitoyl transferase 1; PFKFB3, fructose-2,6-biphosphatase 3; F26BP, fructose-2,6-biphosphate; PFK1, phosphofructokinase 1; ACC1, acetyl-coenzyme A carboxylase-1; SREBP1, sterol regulatory element binding transcription factor 1; FAS, fatty acid synthase; HMGR, 3-hydroxy-3-methylglutaryl-coenzyme A reductase; LKB1, liver kinase B1. Adapted from [345].

1.8.6. Metabolism of the retina and RPE

In humans, 14 plasma membrane transporters have been identified for the transport of monosaccharides and polyol sugars, and are encoded by the SCL2 gene family [369]. The RPE are reported to express a range of GLUT transporters during early development however, their sugar uptake post-maturation is restricted to the expression of GLUT1, GLUT11 and SGLT1 [370]. The predominant transporter in RPE is GLUT1 which facilitates the trans-epithelial uptake of substrates: glucose, galactose and mannose [369]; roles for transporters GLUT2-5 remain ambiguous, this could potentially be attributed to low basal expression [371, 372]. The presence of additional transporters has yet to be functionally documented in RPE.

The retina is dependent on glucose and other fuel sources from the choroidal blood flow. Before these nutrients can reach cells within the retina, they must first pass through the RPE monolayer. Glucose passes through the basolateral surface of the RPE and exits into the retina on the apical surface. Recent work in the laboratories of Hurley and Philp have led to the emergence of a concept of "metabolic coupling" between the RPE and the retina which provides an explanation to why RPE metabolic dysfunction has a global effect on retinal function [373, 374]. In a series of elegant experiments, Kanow et al., show that the retina and RPE function as part of a "metabolic ecosystem", whereby symbiotic metabolic relationships between each cell type are required for cell survival [4]. In this model, most of the glucose passes through the RPE to the photoreceptors and for the most part, is not required to support their metabolism. Photoreceptors use glucose as a major fuel source, exporting lactate as a product of glycolysis. Lactate is then used to fuel OXPHOS is neighbouring Müller glia and the RPE. It is of interest to note that the retina (along with tumours) were two tissues first identified by Otto Warburg in the 1920's to rely predominantly on aerobic glycolysis [375]. Accumulating evidence suggests that photoreceptors are the site of retinal aerobic glycolysis.

Metabolism in RPE cells is supported predominantly by their mitochondria. Studies show that mitochondria are abundant within RPE cells [376] and in culture, RPE cells exhibit high levels of oxygen consumption [377]. Lactate is suggested to be the most prominent RPE fuel source *in vivo* [4]. Indeed, lack of monocarboxylate lactate transporters can cause retinal dysfunction and degradation [378]. In addition to lactate, photoreceptors also supply the RPE with lipids

through phagocytosis of outer segments. These lipids serve as key substrates for beta-oxidation, producing acetyl-coA which feeds into the TCA cycle. Glutamine is another key fuel source used by the RPE, with studies indicating that the RPE has a high capacity for reductive carboxylation of a-ketoglutarate to isocitrate through isocitrate dehydrogenase 2 [6]. Reductive carboxylation appears to be a key pathway in the RPE to support mitochondrial metabolism and redox homeostasis. In the absence of reductive carboxylation, RPE function is impaired and oxidative damage to the RPE is augmented. Proline and taurine are key nutrients consumed by the RPE. Interestingly, studies have indicated that proline is the preferred fuel source of the RPE [379, 380]. Proline is taken up basolateral by RPE cells at levels ~7-fold greater than that of glucose. When inside the RPE, proline is utilised to generate TCA intermediates through both mitochondrial oxidative and reductive pathways. Proline-derived metabolites are exported preferentially to the apical side where they are used as a retinal fuel source. In addition to the metabolites discussed above, the RPE has been suggested to function based on glucose uptake and storage as glycogen, followed by glycogen utilisation [371]. Collectively, the metabolic program adopted by RPE cells *in vivo* appears to be that of mitochondrial OXPHOS, utilising multiple substrates to feed into the TCA cycle rather than the utilisation of glycolysis. Cultured RPE cells, however, are adept at utilising glycolysis, and produce high levels of lactate *in vitro* [381]. Despite their high capacity for glycolysis, it is unlikely to be used as a fuel source *in vivo*. Studies show that the RPE is unable to support the retina when forced to rely on glycolytic rather than mitochondrial metabolism [382]. Interestingly, activation of mTORC1 or the normoxic stabilisation of HIF-1α in RPE cells *in vivo* causes degeneration in the surrounding photoreceptors [383]. Activating AMPK or PGC-1α in RPE cells on the other hand, has been shown to improve mitochondrial function and in the case of AMPK activation, protect against photoreceptor damage [36, 384].

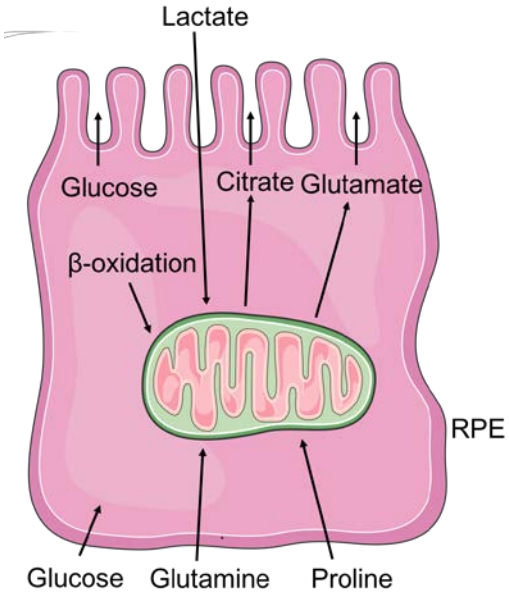

Figure 1.16. Metabolism of the RPE *in vivo*:

In a heathy retina, retinal pigment epithelium (RPE) cells take up glucose through GLUT1 transporters yet is not used as a metabolic substrate. Instead, glucose from the choroidal blood flow is shuttled to the photoreceptors for use in aerobic glycolysis. Lactate produced in the photoreceptors is taken up by RPE monocarboxylate transporters and enters the mitochondrial TCA cycle as pyruvate. Photoreceptors also supply the RPE with lipids from the degradation of photoreceptor outer segments. These lipids are used to generate ATP in mitochondrial β-oxidation. Glutamine enters the RPE through the SLC1A5 transporter and enters the TCA cycle as α-ketoglutarate. RPE cells use reductive carboxylation of α-ketoglutarate to support cellular functions. Proline imported into RPE cells can be catabolized into glutamate for mitochondrial intermediates. RPE cells export TCA intermediates to the retina as additional fuel sources. Adapted from [4].

1.8.7. Bioenergetic dysfunction in AMD

With progressing age, the observation that bioenergetic function declines is well documented [385]. Aging models of rats and mice have shown complexes I and IV of the ETC display reduced kinetic activity, whilst complexes II, III, and the F1-ATP-synthase complex remain largely unaffected [386, 387]. The impaired enzymatic functions of complexes I and IV compromise energy transduction through the ETC, and therefore decrease the ATP output of mitochondrial OXPHOS [385]. Additionally, aging results in increased ROS production, the accumulation of mtDNA mutations, and a decline in the function of CPT1 [86, 388, 389]. RPE are susceptible to reductions in bioenergetic fluxes because of their high metabolic capacity; there is now increasing evidence that mitochondrial health decline plays a prominent role in the pathogenesis of AMD [390, 391].

In addition to their role in energy production, mitochondria function as a signalling platform for retrograde/anterograde communication with the nucleus [392]. Under normal conditions, ROS act as an important signalling molecule in these processes. Communication between the two organelles is important for adjustments in nuclear and mitochondrial-encoded genes to accommodate cellular bioenergetic demands. Excessive ROS production, however, can damage mtDNA and mitochondrial proteins and lipids. Damage to the mitochondrial genome leads to defects in the expression of essential ETC components. Damage to the mitochondrial membrane can elicit the formation of mitochondrial permeability pores, reducing mitochondrial membrane potential and leading to the release of mitochondria-derived biomolecules such as mtDNA, apoptosis-inducing factor and cytochrome C [393]. Release of these molecules initiates apoptotic and inflammasome cascades, leading to cell death *via* pyroptosis [71].

Outcomes of ROS-mediated DNA damage include double and single strand breaks, in addition to the formation of DNA adducts. These DNA lesions can affect the interpretation and transmission of mitochondrial genetic material [394]. One repercussion of double-strand break repair is the 4977bp deletion of mtDNA, a common deletion zone observed in various post-mitotic tissues with a high-energy demand [395]. Age-dependent increases in 4977bp deletions have been observed in RPE from healthy and AMD donors [395]. Analysis of multiple AMD cohorts has shown that the degree of mtDNA damage is correlated to AMD severity [376]. Upon further investigation, it was found that sites of increased mitochondrial genome damage were localised to regions encoding 16S and 12S ribosomal

RNA [396], suggesting that the translation of various mitochondrial-encoded genes could be adversely affected. In addition to this, other significantly damaged regions in the AMD cohorts included genes encoding ETC subunits, potentially suggesting reduced ATP production. Recent studies have built on this, and shown using extracellular flux analysis, that RPE from AMD donors have significantly reduced mitochondrial OXPHOS [397, 398]. In both experimental systems used in these studies, there appears to be differences in how glycolytic metabolism is affected in AMD donor RPE cells. Further studies will be required to explore if other metabolic pathways support ATP synthesis with mitochondrial dysfunction.

In the context of the metabolic ecosystem discussed in the previous section [399], it is plausible that AMD-mediated dysfunction in RPE mitochondria would disrupt the energy balance, not just in RPE themselves, but in other cells in the retina which rely on the RPE for metabolic support. RPE cells rely predominantly on β-oxidation and oxidative metabolism of lactate and amino acids, such as proline and glutamine [6, 374, 379]. As mitochondria are the site of these key pathways, damage would likely cause defects in ATP production. It is suggested that defects in OXPHOS would force the RPE to rely on glycolytic metabolism to support cellular bioenergetics. As discussed previously, RPE cells are capable of utilising glycolysis and have a robust expression of key glycolytic enzymes [400]. *In vivo*, glycolysis is seldom used, with glucose shuttled through the RPE to fuel photoreceptors [4]. An increased RPE glycolytic program would have adverse effects for photoreceptors, which rely solely on glycolysis. A reduction in photoreceptor lactate production would reduce the available retina lactate pool for RPE cells to use as a fuel source, increasing their reliance on glycolysis, starving photoreceptors further and ultimately leading to degeneration and cell death. It is well known that AMD patients exhibit the degeneration of rods, which precedes the death of cones [401]. Interestingly, rods secrete thioredoxins to promote glucose uptake and augment cone glycolytic flux [402]. If one assumes the theory of a retinal metabolic ecosystem is true, and that metabolic reprogramming to glycolysis occurs following AMD-induced mitochondrial damage, a reduced flow of glucose to the photoreceptors could accelerate rod loss. With a higher density of cones to rods, fewer rods would thus be able to support cone metabolism, contributing to the loss of macular photoreceptors.

1.9. Immunometabolism

Cells of both the innate and adaptive immune system require the ability to rapidly respond to pathogenic insults, initiating responses such as antigen presentation, phagocytosis and the production of inflammatory/effector cytokines. Immunometabolism refers to the concept that metabolic

plasticity governs the ability of immune cells to quickly proliferate and initiate immunological responses, following exposure to pathogenic or noxious stimuli [5]. Lymphocytes (T-cells, B-cells and NK cells), macrophages and DC have all reported to undergo the Warburg effect when activated, facilitating the rapid output of cytokines and chemokines [403-407]. Indeed, the small molecule inhibitor of hexokinase (the enzyme responsible for catalysing the first step in glycolysis), 2-deoxyglucose (2DG), has been reported to inhibit inflammation in many contexts [408-411]. Recent studies have confirmed integration between metabolic reprogramming and immune function, with various immune cells exhibiting a "metabolic plasticity" [412]. This flexibility between ATP-generating pathways allows the functional demands of cells to be met, even under nutrient deprivation and hypoxic conditions [413]. Inflammation itself is a bioenergetically expensive process and in certain contexts elicits a switch from OXPHOS to aerobic glycolysis. This "Warburg-like" switch provides a rapid generation of ATP for cytokine production [414]. Metabolic reprogramming is observed in response to PRR stimulation of innate immune cells and Th1/Th17 proliferation [403-405]; a metabolic shift away from OXPHOS and Kreb's cycle, into glycolysis, supports an immediate ATP output that fuels the immune response. Cells involved in the attenuation of a pro-inflammatory environment, such as M2 macrophages, Tregs and CD8+ memory cells, and exhibit reduced glycolytic rates, favouring production of ATP through the utilization of Kreb's cycle and the ETC [404, 415]. The maintenance of cellular energy homeostasis within mammalian cells is controlled by the enzymatic activity of AMPK and mTOR [343, 344]. Studies have identified, that similar to the regulation of cancer cell proliferation, immune cells require a similar regulation of bioenergetic sourcing, controlled through AMPK and extracellular signal-transduction [345].

1.9.1. Metabolism of innate immune cells

Resting dendritic cells and macrophages rely predominantly on OXPHOS to generate ATP, yet upon activation of TLRs they undergo a switch in metabolic state towards a program of highly glycolytic metabolism [403, 416]. Activated cells display increased expression of various metabolic enzymes, increased lactate output and a decrease in mitochondrial OXPHOS. LPS activation of cells is a classic example of PAMP/TLR interaction inducing amplified cellular glycolytic flux in a HIF-1α/PI3K/AKT-dependent manner [417]. The increased output of lactate from glycolysis may contribute to immunological defence through its reported antimicrobial properties [418]. LPS-activated macrophages and dendritic cells increase the expression of glucose transporter GLUT1, facilitating enhanced glucose uptake [416]. Interestingly, TLR-9 stimulation of DC induce the expression of type-1 IFNs which modulate metabolism away from aerobic glycolysis, and towards OXPHOS of fatty acids and mitochondrial pyruvate [419]. Macrophages are differentially activated into the M1 (pro-

inflammatory) and M2 (anti-inflammatory) isoforms. These vary in their metabolic profile, with M1 macrophages relying heavily on Warburg metabolism as oppose to their OXPHOS-utilizing M2 counterparts [412]. This can be attributed to a number of mechanisms including, expression of highly active glycolytic enzyme ubiquitous phosphofructokinase (uPFK) in M1 macrophages compared to the less-active PFKFB1 in M2 and the induction of PKM2 which alters the expression of HIF1-α-dependent genes, including glycolytic enzymes and IL-1β [416]. M1 macrophages exhibit a "broken" TCA cycle which prevents coupling to OXPHOS. The broken cycle leads to an accumulation of citrate - a result of decreased *isocitrate lyase* expression – which facilitates fatty acid synthesis, antimicrobial itaconate synthesis and nitric oxide (NO) production [416]. NO is essential for prolonging the longevity of dendritic cells and M1 macrophages through inhibition of the terminal ETC electron acceptor, cytochrome c oxidase [420]. Without inhibition of cytochrome c oxidase, a rapid drop in mitochondrial membrane potential would occur, leading to the recruitment of (BCL-2-associated X protein) BAX to the mitochondria and the subsequent initiation of apoptosis cascades [165]. IL-10 limits the switch to aerobic glycolysis and blocks TLR activation of dendritic cells, implicating mitochondrial metabolism with an anti-inflammatory phenotype [403]. IL-4 activation of macrophages promotes the expression of PPARγ-coactivator-1β (PGC-1β) *via* STAT6; this ultimately leads to increased transcription of genes involved within fatty acid oxidation and mitochondrial biogenesis [421]. Phagocytic functions of immune-cells are mediated by Phox/NADPH oxidase (NOX)-dependent respiratory bursts, which generate mitochondrial ROS through complexes 1 and 2 of the ETC [422]. The upregulation of the pentose-phosphate pathway in M1 macrophages serves as an essential counter-regulatory mechanism of preventing tissue damage in response to rapid ROS generation through the generation of antioxidants and glutathione; this is modulated by the expression of carbohydrate kinase-like protein [423]. Mitochondrial stress and increased ROS production form a prominent danger signal in the activation of the NLRP3 inflammasome [69].

Studies of TLR-mediated changes in bioenergetic sourcing have primarily focused on immunological cells of the adaptive and innate immune system (T-cells, dendritic cells, macrophages). Whilst not strictly an immunological cell, RPE plays a pivotal role in the maintenance of ocular immune privilege; with an output of immuno-stimulatory chemokines and cytokines, APC functions, and a rich expression of TLR, RPE initiate cellular responses stretching beyond innate-frontline defence [45, 46]. Recent studies have shown that integrated immunological and metabolic pathways are observed in the RPE, indicating a translational aspect to much of the current research in immunometabolism. RPE are reported to undergo the Warburg effect following TLR activation *via* TLR-3 and TLR-4 agonists Poly (I:C) and LPS, respectively [286, 424]. This switch from OXPHOS into glycolytic metabolism was

accompanied by an increased expression of *GLUT1*, increased glucose consumption and lactate production.

1.9.2. AMPK activation in immune cells

AMPK activation elicits cell-cycle arrest and prevents metabolic adaptations occurring in proliferating cells, leading to the consensus that AMPK functions as a suppressor of tumorigenesis and inflammation [345]. The role of AMPK appears to be in the suppression of the "Warburg effect" upon immune cell activation and the continued usage of mitochondrial respiration, through creating a state of "pseudo-starvation" that mimics nutrient deprovision [345]. Indeed, glycolysis and the expression of glycolytic enzymes are elevated in T-cells from AMPK deficient mice [425]. Activation or inhibition of AMPK through small molecules have been reported to attenuate inflammatory responses in several settings. These include, inhibition of LPS-induced ROS-NF-kB signalling in macrophages; a reduced LPS-induced cytokine output of IL-1β IL-6 and IL-8 in the bovine endometrium; a suppression of IFN-γ production by CD8+ T effector cells; attenuation of disease severity in experimental autoimmune encephalomyelitis through the reduction of Th1 cytokines IFN-γ and TNF-α, whilst upregulating Th2 cytokines IL-4 and IL-10; prevention of LPS-induced inhibition of neutrophil chemotaxis and inflammatory responses, yet interestingly, AMPK activation facilitated enhanced phagocytic and bactericidal activity [426-430]. AMPK activation may facilitate a "pro-Warburg" phenotype in LPS-induced monocytes expressing inducible 6-phosphofructo-2-kinase variant PFKFB3 [431]. When phosphorylated by AMPK, its kinase activity is increased, resulting in amplified fructose-2,6-bisphosphate; this allosterically activates PFK1, leading to increased glycolytic metabolism under hypoxia [431]. It is argued that small molecule activators of AMPK may induce a state of pseudo-starvation conferring an anti-inflammatory phenotype [345]. As AMPK inhibitors confer a similar anti-inflammatory shift, it gives the impression that, the integration of energy metabolism and innate immunity depends on the activity of AMPK and the maintenance of cellular energy homeostasis. Disruption *via* inhibition or activation of AMPK may negatively impact the innate immune response. In addition to its roles in inflammation, AMPK has been shown to control several cellular processes in RPE, including phagocytosis of photoreceptors, permeability, and survival under oxidative stress [432, 433].

The mTOR complex unsurprisingly (given its central role in the regulation of cellular function), plays a key role in the development of immune cells. mTORC1 mediates metabolic activation networks in

response to TLR signalling [434] and promotes glycolytic metabolism in innate immune cells through the induction of HIF-1α and MYC which, in turn facilitate the upregulation of genes involved in glycolytic metabolism [306]. Additionally, mTORC1 promotes fatty acid and cholesterol synthesis for utilization in ER and Golgi synthesis, which promote secretion of pro-inflammatory mediators [434]. Initial studies focused on the immunosuppressive actions of rapamycin on the proliferation of T-cells and IL-2 production [435]. In innate immune cells, rapamycin promotes pro-inflammatory cytokine production and limits IL-10 production. mTORC1 limits the activation NF-kB whilst promoting the activity of STAT3 [436]. As mTORC1 signalling is reported to increase with RPE cell senescence [437], this gives an indication of how aging may negatively influence immune responses. The effects of rapamycin on immune cell metabolism were shown to be pivotal in the promotion of fatty acid oxidation [438]. Activation of macrophages by IL-4 is associated with enhanced fatty acid oxidation and increased glucose oxidative catabolism; recent studies have shown that mTORC2 is a key node in this metabolic reprogramming [439]. As previously discussed, a lack of mTORC1 regulation in T-cells leads to enhanced glycolytic metabolism and the failure of memory T-cell (T-mem) development [365]. Inhibition *via* the dual inhibitor Torrin1, but not rapamycin, has been reported to limit endometrial inflammatory responses [427]. The glycolytic enzyme hexokinase-1 has been observed to up regulate macrophage NLRP3 activation in a raptor/mTORC1-dependent manner [437].

1.9.3. Interleukin-33 and the control of cellular metabolic profiles

The previous sections have discussed how the metabolism of immune cells is modulated through external environmental cues (e.g. TLR, T-cell receptor or cytokine receptor-mediated signalling) and the roles of metabolic regulators (such as AMPK and mTOR) in initial immune cell metabolic adaptations and ultimately the regulation of immune responses. In this section I will focus entirely on the immunometabolic interactions of IL-33.

A recent study exploited the cytoplasmic hybrid (cybrid) technique [440] to generate RPE cell lines containing representative mtDNA haplotypes. These haplogroups were associated with protective (H haplogroup) or high risk (J haplogroup) AMD populations. The J haplogroup was found to exhibit reduced expression of seven mitochondrial genes involved in OXPHOS, including essential proteins of complexes I, IV, and F1-ATP-synthase [18]. It was additionally observed that the J haplogroup exhibited a reduced oxygen consumption rate (OCR) and extracellular acidification rate (ECAR)/OCR ratio, yet ATP turnover, and spare respiratory capacity remained constant when compared to the H haplogroup.

Interestingly, it was observed that the J haplogroup revealed an >2-fold reduction in the expression of IL-33, yet in response to oxidative stress, its expression was greater in the H haplogroup [18]. Although this study observed a correlation in the RPE metabolic phenotype and expression of IL-33, this finding was timely to another study suggesting a novel role for IL-33 in the regulation of thermogenesis and uncoupled mitochondrial respiration [19]. IL-33 was observed to be critical for the splicing of uncoupling protein 1 (*Ucp1)* mRNA in adipocytes, and the expression of functional UCP1. In addition to this, mitochondria from *Il33*$^{-/-}$ mice exhibited profound respiratory defects, including reduced OXPHOS, and enzymatic activity of ETC complexes II and IV. Further RNA-seq experiments identified an increased expression of genes involved in the catabolism of fatty acids, glucose and amino acids in *Il33*$^{-/-}$ mice [19]; this suggests a compensatory mechanism for defects in uncoupled respiration, upregulating flux through catabolic pathways to generate ATP.

Murine mast cells activated with exogenous IL-33 are reported to increase glycolysis, the expression of key glycolytic enzymes and OXPHOS [441]. Endogenous and exogenous IL-33 have been shown to up-regulate HIF-1α in synovial fibroblasts [442] and increase glycolysis in cancer cell lines [443]. Furthermore, IL-33 is proposed to be a key regulator of macrophage metabolism in response to LPS stimulation; cells with ST2 deficiency were associated with increased mitochondrial metabolism and IL-33 overexpressing cells displayed an augmented shift to aerobic glycolysis in response to LPS [444]. Although these studies support a role in the regulation of central carbon metabolism, the biology of IL-33 is clearly multifaceted, especially when we consider the influence of endogenous and exogenous forms. As IL-33 is not normally released from cells [9], it is of interest to understand how a lack of ST2 alters metabolic phenotypes [19, 444].

1.10. Thesis objectives

Experimental observations have demonstrated that inflammation plays a prominent role in the pathogenesis of AMD. The integration of immune responses and metabolic pathways has been demonstrated in immune cells, yet evidence of this is only just emerging within the retina. Bioenergetic dysfunction, para-inflammation and oxidative stress are linked with the exacerbation of age-related disorders. Whilst inflammation has the potential to mediate bioenergetic sourcing, mitochondria themselves appear to drive and regulate inflammatory signalling, suggesting a cyclic relationship between the two co-dependent processes. One consequence of a bioenergetic switch in the RPE is the concurrent production of IL-33. IL-33 is an immunomodulatory alarmin of the innate immune system, which targets a diverse array of cell types, and exhibits complex functions as both an

extracellular cytokine and as a nuclear regulator. Novel and protective roles for this cytokine are beginning to emerge in the context of degenerative disorders; it appears that IL-33 is essential for the prevention of ocular angiogenesis, Aβ clearance in the brain, and may attenuate the noxious effects of oxidative stress in the tissue. Whilst IL-33 appears to be an attractive therapeutic adjuvant, it should be noted that a vast proportion of its underlying biology remains undetermined to date. Little is known about the processing of IL-33, and mechanisms of its regulation through various endogenous peptides and decoy receptors. Additionally, the role of IL-33 within the nucleus and its influence on cellular metabolism remain ambiguous.

In summary the hypotheses, on which this thesis was based, were designed to focus on the integration between aspects of the innate immune response and cellular metabolism in the RPE:

1. Under conditions of tissue damage and parainflammatory stress, innate immune-derived signals elicit metabolic reprogramming in the RPE which impair its ability to provide functional support to the retina.

2. IL-33 is released following tissue damage and stress to maintain cellular and metabolic homeostasis in the RPE.

3. IL-33 functions as a key node in the metabolic regulation of the RPE, acting through both canonical (ST2-dependent) and non-canonical (ST2-independent) pathways.

To test these hypotheses, this thesis aimed to:

1. Investigate the metabolism of RPE in normal aged mice and examine if metabolic differentiation exists in the RPE after stress of immune system (Chapter 3 and 4).

2. Examine how IL-33 maintains RPE health under conditions of cellular stress (Chapter 4).

3. Explore the links between IL-33 and metabolic function in the RPE (Chapter 4 and 5).

4. Investigate the functional significance of IL-33 nuclear localisation in epithelial cells (Chapter 6 and 7).

Chapter 2. Materials and methods

2.1. Experimental models

2.1.1. Cell lines

Immortalized human retinal pigment epithelium (ARPE-19), a spontaneously formed mouse RPE cell line (B6-RPE07) [445], human colorectal adenocarcinoma (SW1463) [446] and human Müller glial **Moorfields/Institute of Ophthalmology- Müller 1** (MIO-M1) cell lines were cultured in DMEM (4.5mg/L) supplemented with 10% heat-inactivated foetal bovine serum (FBS), 2mM L-glutamine, 1mM sodium-pyruvate, 0.5µM 2-mercaptoethanol, 100U/ml penicillin, and 100µg/ml streptomycin. Cells were passaged with a split ratio of 1:4 using trypsin EDTA and allowed to recover for 2 days in complete medium prior to experiments. All cell lines were maintained at 37°C and were routinely screened for mycoplasma contamination. ARPE-19 cells were received as a kind gift from Dr. Gabi Braun (University of Bristol, UK). B6-RPE07 cells were received as a kind gift from Prof. Heping Xu (Queens University Belfast, UK). The human SW1463 was received as a kind gift from Prof. Ann Williams (University of Bristol, UK). The human **MIO-M1 was obtained from the UCL Institute of Ophthalmology, London, UK.** MIO-M1 express markers of mature Müller cells, including cellular retinaldehyde binding protein [CRALBP], glutamine synthetase, vimentin and epidermal growth factor receptor-[EGF-R] [447]. B6-RPE07, **MIO-M1 and** SW1463 **cells are female, and ARPE-19 are male.**

2.1.2. Primary cells

C57BL/6J mice were purchased from Charles River Laboratories, Margate, UK. All mice were maintained in the animal house facilities of the University of Bristol, according to Home Office Regulations. Animal husbandry and procedures complied with the ARVO (Association for Research in Vision and Ophthalmology) statement for the use of animals in ophthalmic and vision research. IL-33 knockout mice (*Il33*$^{-/-}$) were generated as described [448] at the animal house facilities of Trinity College Dublin and sent to the animal house facilities of the University of Bristol when required. ST2 knockout mice (*Il1rl1*$^{-/-}$) were generated as described [8] at the animal house facilities of the University of Bristol.

2.1.2.1. Primary RPE

Primary murine RPE cells were obtained as described [449]. Briefly, eyes were enucleated and cleaned using angles scissors to ensure than no connective tissue remained attached to the sclera. A large incision was made in the centre of the cornea so that the lens could be removed. Once removed, the eyes were incubated at 37°C in hyaluronidase for 45min, and in Hank's balanced salt solution (HBSS) with calcium, magnesium and 10mM HEPES for a further 30min. An incision was made beneath the ora serrata to remove the iris epithelium and cornea. The neural retina and the attachment to the optic nerve were removed. Eyecups were incubated at 37°C in trypsin EDTA for 45min. Eyecups were then transferred into HBSS with 20% FBS and shaken gently to allow the RPE to detach. The RPE sheets were incubated at 37°C in 1ml trypsin EDTA for 1min, 9ml primary RPE media was then added, centrifuged, and supernatant removed. The resulting RPE cells were resuspended in 200µL primary RPE media and homogenously mixed using a p200 pipette. Cells were used within 10 days of extraction. Cells were cultured in alpha-MEM, containing 1% N1 supplement, 1% glutamine-1% penicillin-streptomycin, 1% non-essential amino acid solution, 5% heat-inactivated foetal bovine serum (FBS), 20µg/L Hydrocortisone, 250mg/L Taurine and 13ng/L triiodo-thyronin. Purity was assessed by immunoblotting for RPE specific protein RPE65 and rhodopsin contamination from the neurosensory retina (Figure 2.1.).

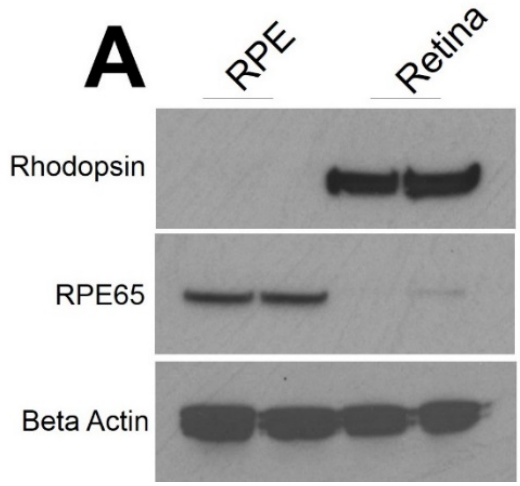

Figure 2.1. Isolation of primary RPE:

(A) Immunoblot of primary RPE purity with RPE65 and rhodopsin protein expression. Western blot analysis represents two individual mice.

2.1.2.2. Bone marrow derived mast cells

Bone marrow derived mast cells (BMMCs) were generated from C57BL/6 as described [194]. Briefly, legs were taken from mice and stripped of muscle. Under sterile conditions the bones were placed into a petri dish and cut at the end using angles scissors to expose the red marrow. Using a syringe and a 23-gauge needle DMEM was flushed through the bone until marrow was not visible. DMEM containing the cell suspension was spun at 14,000g for 5min in a centrifuge cooled to 4°C. The resulting cell pellet was resuspended in 15ml of DMEM containing IL-3 and dispensed into a cell culture flask. The cell suspension was left for 5 weeks (with bi-weekly passages) to allow the generation of a mast cell population. Prior to functional assays, mast cells were sorted into a viable population using a MACS dead cell removal kit and the purity was assessed by FACS based on CD117 (c-Kit) and CD45 (BD Bioscience, UK) cell surface marker expression.

2.2. Method details

2.2.1. Cell culture

Cells were seeded at a density of 100,000 per well of a 24 well plate and were exposed to different inflammatory stimuli; Poly (I:C) (high and low molecular weight), LPS, IL-33, peptidoglycan (PGN), CpG oligodeoxynucleotide (CpG), IL-1β, IL-4, IL-6 IL-10, IL-17A, IL-22, TNFα and IFN-γ. Poly (I:C) from Invivogen was used as a result of its highly referenced usage as a potent TLR-3 ligand within the literature [65, 450]. Ultrapure LPS (from E. coli O111:B4) from Invivogen was used as a result of its highly referenced usage as a potent TLR-4 ligand within the literature [451, 452]. Ultrapure LPS was used as opposed to the standard LPS-EB. Unlike the LPS-EB, Ultrapure LPS was further purified to remove other bacterial components such as lipopeptides which may activate TLR-2, ensuring TLR-4 specificity. Recombinant IL-33 was purchased from Enzo Life Science; this specific IL-33 was used so that the work from this thesis was in keeping with other published research [8]. Oxidative stress was induced by the addition of hydrogen peroxide (1mM). AMPK activity was modulated by activator AICAR (1mM), and inhibitor Compound C (40μM). Unstimulated controls and vehicle controls (DMSO) were always included. Further information regarding these agonists can be found in Table 2.4.1; page 109.

2.2.2. Protein isolation

2.2.2.1. Protein isolation from cell lines

Following treatment, total protein extraction was performed using Cell-Lytic-M (Thermo Fischer, UK) with the addition of Protease/Phosphatase Inhibitor Cocktail (Cell Signalling, UK). The resulting cell suspension was centrifuged for 15min at 14,000g in a centrifuge cooled to 4°C. A commercial nuclear extraction kit (Active Motif, Belgium) was used for the preparation of nuclear and cytoplasmic extracts as per the manufacturer's instructions. Briefly, cells were washed twice with 1ml of ice-cold PBS/phosphatase inhibitors and 0.3ml of ice-cold PBS/phosphatase inhibitors was added. Cells were removed from the cell culture plate by gentle scraping. Samples were pooled from 2 wells of a 24 well plate. The resulting cell suspension was centrifuged for 5min at 200g in a centrifuge cooled to 4°C. The supernatant was removed, and the pellet kept on ice prior to resuspension in 100µl hypotonic buffer containing 5% (vol/vol) detergent. The resulting cell suspension was centrifuged for 30s at 14,000g in a centrifuge cooled to 4°C. The supernatant was removed as the cytoplasmic fraction. The remaining pellet was resuspended in 25µL of complete lysis buffer and incubated for 30min on ice on a rocking platform. The resulting cell suspension was centrifuged for 10min at 14,000g in a centrifuge cooled to 4°C. The supernatant was removed as the nuclear fraction.

2.2.2.2. Isolation of RPE protein

RPE cell protein was isolated from mouse tissue as previously described [453]. In brief, eyes were enucleated and cleaned using angles scissors to ensure than no connective tissue remained attached to the sclera. A large incision was made in the centre of the cornea so that the lens could be removed. Once removed, four small slits were made into the RPE/choroid to flatten the tissue. The tissue was then transferred into a 1.5µL eppendorf containing 200µL of RIPA buffer with the addition of protease/phosphatase Inhibitor Cocktail for 30min on ice. After incubation, the tube was tapped gently fifty times to allow the RPE to be released into the lysis buffer. The choroid/sclera was then removed and the RPE was left on ice for a further 30min. Proteins were then extracted from the RIPA lysis buffer by first subjecting the lysate to one round of sonication for 20s and centrifuging for 15min at 14,000g and 4°C. The supernatant was removed and placed in a fresh pre-chilled eppendorf.

2.2.3. Western blot

Protein concentration was assessed using a bicinchonic acid (BCA) assay kit (Thermo Fischer, UK). 15µg of protein (to a total volume of 28µL), 2µL of β-mercaptoethanol (Sigma, UK) and 10µL of NuPage SDS buffer (Thermo Fischer, UK) were heated for 5min at 90°C. The denatured proteins were then added

to each well of a precast NuPage tris-glycine mini gel (Thermo Fischer, UK) with at least one well empty for the addition of protein standards. 500mL of 1X NuPage tris-glycine (Thermo Fischer, UK) was added to the mini-Tank (Thermo Fischer, UK) and SDS-page electrophoresis was performed for 45min at 200V/160mA. Following electrophoresis, the gel was submerged in 10% methanol for 10min. The precast gel coating was then cracked open and the gel removed. Dry blotting of proteins from mini gels was performed using an iBlot-2 dry blotting system (Thermo Fischer, UK). The iBlot-2 transfer stacks (Thermo Fischer, UK) and the pre-run gel were inserted into the iBlot-2 machine as per the manufacturer's instructions. A pre-designed method (20V for 2min, 23V for 3min and 25V for 2min) for a total of 7min was used to transfer proteins between 30-150kDa. Reducing the run time to 5-6mins was required for proteins <30kDa and an increase to 8-10min was required for proteins >150kDa. After transfer, the stacks were removed and the PVDF membrane was cut as required. The membrane was blocked in 5% milk/TBS for 2h at room temperature (R.T.). Immunoblotting was performed by the addition of a primary antibody to protein of interest overnight at 4°C (antibody concentrations detailed in Table 2.4.2; page 110). The membrane was then washed in TBS/Tween-20 for 5min three consecutive times. The membrane was then incubated at R.T. for 1h with a polyclonal HRP-conjugated secondary antibody. The membrane was then washed in TBS/Tween-20 for 5min three consecutive times. An electrochemiluminescence (ECL) was used to detect protein abundance in the membrane as per the manufacturer's instructions. In brief, membranes were incubated in 0.5mL of both ECL detection agent A and B (G.E. Healthcare, UK) for 1min at R.T. Protein expression was visualized using chemiluminescent film (G.E. Healthcare, UK) at increasing exposure time. Relative protein expression was calculated by normalization to beta actin, beta tubulin or histone 3.

2.2.4. RNA and DNA analysis

2.2.4.1. RNA isolation

RNA was isolated from cells using the RNeasy extraction kit (QIAGEN, UK). In brief, 100,000 cells were lysed directly in a 24-well plate with 350µL of RLT plus buffer, containing 3.5µL β-mercaptoethanol. The lysate was transferred into a fresh pre-chilled eppendorf and vortexed for 30s. The lysate was transferred to a gDNA eliminator spin column placed in a 2ml collection tube and centrifuged for 30s at 10,000g. The column was discarded and 350µL of 70% ethanol was added to the flow-through and mixed well by pipetting. 700µL of the sample was placed in a RNeasy spin column in a 2ml collection tube and centrifuged for 30s at 10,000g. The flow-through was discarded and 700µL of RW1 buffer was added to the RNAeasy spin column. This was centrifuged for 30s at 10,000g and the flow-through was discarded. 500µL of RPE buffer was added to the RNAeasy spin column and centrifuged for 30s at 10,000g. The flow-through was discarded and 500µL of RPE buffer was added to the RNAeasy spin column. This was centrifuged for 2min at 10,000g. The RNAeasy spin column was removed and placed into a new 2ml collection tube before centrifugation at full speed for 1min to further dry the membrane. The RNAeasy spin column was then placed into a new eppendorf. 30µL of RNase-free water was added directly to the spin column membrane and centrifuged for 1min at 10,000g to elute the RNA.

2.2.4.2. cDNA conversion

Purity and RNA concentration was assessed using a nanodrop 3000 spectrophotometer (Thermo Fischer, UK) and 1µg RNA was reverse-transcribed into cDNA using a SuperScript III First Strand Synthesis system (Thermo Fischer, UK). In brief, RNA, 1µl of 50µM oligo(dT), 1µl of 10mM dNTP mix and RNase-free water (up to 10µL) were added to a 0.2mL tube and incubated for 5min at 65°C and 5min on ice. A cDNA synthesis mix was prepared by adding the following components: 2µL of 10X RT buffer, 4µL of 25mM $MgCl_2$, 2µL of 0.1M DTT and 1µL reverse-transcriptase. The cDNA synthesis mix was added to the RNA/primer mixture, vortexed gently and collected by brief centrifugation. The subsequent mixture was incubated for 50min at 50°C followed by 5min at 85°C to generate cDNA.

2.2.4.3. RT-PCR

Resulting cDNA was diluted 1:20 and 2.5µL was added to a micro-amp optical 96-well reaction plate. 0.25µL of 100µM forward and reverse primers were also added to the cDNA, along with 2.5µL DNA-free water and 5µL SYBR-green reagent (Thermo Fischer, UK). cDNA was amplified in a StepOne Plus detection system (Thermo Fischer, UK). Cycling conditions: Heat ramp 95°C for 10min, extension (95°C for 15s, 60°C for 1min) for 45 cycles, melt curve 95°C for 15s, 60°C for 1min, 95°C for 15s. Relative gene expression was calculated by normalization to *βActin*. Primer sequences used are detailed in Table 2.4.3; page 111.

2.2.4.4. Mitochondrial DNA content

The content of mtDNA was examined as previously described using RT-PCR [397]. In brief, three sets of mitochondrial primers were used in the RT-PCR analysis. Total mtDNA copies were generated by amplifying two regions of the mitochondrial genome: cytochrome b and 16 S rRNA. An average of these were taken and normalised to cell number using the nuclear-encoded β-globulin gene.

2.2.5. Enzyme-linked immunosorbent assay (ELISA)

IL-33, IL-6 and ST2 release from supernatants, and IL-1β and malonyl CoA abundance in cell lysates were measured using commercially available ELISA kits (DuoSet, R&D Systems, UK; CUSABIO, UK). In brief, 50µL of capture antibody in PBS was added to Nunc "immuno" plates (VWR, UK) for overnight incubation at RT. Concentrations of all antibodies used for ELISA are detailed in Table 2.4.4, page 114. Antibody pre-coated plates were incubated with 1% bovine serum albumin (BSA; Sigma-Aldrich, UK) in PBS (PBSA) for 1h at RT to prevent antibody non-specificity. The plates were washed three times with 0.5% Tween-20 (Sigma-Aldrich, UK) in PBS; to remove excess liquid, plates were dabbed on tissue paper several times. Cell supernatants and recombinant protein standards were added for 2h at RT and washed prior to the addition of the detection antibody in PBSA for 2h at RT. After the next wash, 100ul of Extra-Avidin-Peroxidase (1:1000) was added for 20min at RT followed by three further washes. TMB substrate (BD Biosciences, UK) was added to permit the development of the peroxidase-linked chromogen, 2N H_2SO_4 was used to stop the reaction. The optical density was read at 450nm with a background absorbance read at 540nm. Concentrations in the supernatants were calculated by reference to the standard curve.

2.2.6. Immunoprecipitation

Immunoprecipitation was performed on both cell line protein lysates and primary lysates isolated from mice. Pre-clearing of the lysate was performed by adding 10µl of 50% Protein A agarose bead slurry (Cell Signalling, UK) to 200µl cell lysate at 1 mg/ml. The lysate was incubated with rotation at 4°C for 30min and centrifuged for 15min at 4°C. Immunoprecipitation was performed by adding an anti-IL-33 antibody (Nessy-1) at a 1:100 dilution and incubated with rotation at 4°C overnight. Protein A agarose (10µl of 50% bead slurry) was added and incubated with rotation for 3hr at 4°C. The lysate was centrifuged for 30s at 4°C and washed five times with 500µl of cell lysate buffer to yield the immunoprecipitate.

2.2.7. Proteomics

2.2.7.1. Tandem mass-tagging of pull-down

2.2.7.1.1. TMT labelling

Samples were digested with trypsin (2.5µg trypsin; 37°C, overnight), labelled with Tandem Mass Tag (TMT) six plex reagents according to the manufacturer's protocol (Thermo Fisher Scientific, UK) and the labelled samples pooled. The pooled sample was then evaporated to dryness, resuspended in 5% formic acid and then desalted using SepPak cartridges according to the manufacturer's instructions (Waters, USA)). Eluate from the SepPak cartridge was again evaporated to dryness and resuspended in 1% formic acid prior to analysis by nano-LC MSMS using an Orbitrap Fusion Tribrid Mass Spectrometer (Thermo Scientific, UK).

2.2.7.1.2. Nano-LC mass spectrometry

The pooled TMT-labelled sample was fractionated using an Ultimate 3000 nano-LC system in line with an Orbitrap Fusion Tribrid mass spectrometer (Thermo Scientific, UK). In brief, peptides in 1% (vol/vol) formic acid were injected onto an Acclaim PepMap C18 nano-trap column (Thermo Scientific, UK). After washing with 0.5% (vol/vol) acetonitrile 0.1% (vol/vol) formic acid peptides were resolved on a 250mm × 75µm Acclaim PepMap C18 reverse phase analytical column (Thermo Scientific, UK) over a 150 min organic gradient, using 6 gradient segments (5-9% solvent B over 2min, 9-25% B over 94min, 25-60%B over 23min, 60-90%B over 5min, held at 90%B for 5min and then reduced to 1%B over 2min) with a flow rate of 300nl min−1. Solvent A was 0.1% formic acid and Solvent B was aqueous 80% acetonitrile in 0.1% formic acid. Peptides were ionized by nano-electrospray ionization at 2.0kV using

a stainless-steel emitter with an internal diameter of 30µm (Thermo Scientific, UK) and a capillary temperature of 275°C.

All spectra were acquired using an Orbitrap Fusion Tribrid mass spectrometer controlled by Xcalibur 2.0 software (Thermo Scientific, UK) and operated in data-dependent acquisition mode using an SPS-MS3 workflow. FTMS1 spectra were collected at a resolution of 120 000, with an automatic gain control (AGC) target of 400,000 and a max injection time of 100ms. Precursors were filtered with an intensity range from 5000 to 1E20, according to charge state (to include charge states 2-6) and with monoisotopic precursor selection. Previously interrogated precursors were excluded using a dynamic window (60s +/-10ppm). The MS2 precursors were isolated with a quadrupole mass filter set to a width of 1.2m/z. ITMS2 spectra were collected with an AGC target of 10,000, max injection time of 70ms and CID collision energy of 35%.

For FTMS3 analysis, the Orbitrap was operated at 30,000 resolution with an AGC target of 50,000 and a max injection time of 105ms. Precursors were fragmented by high energy collision dissociation (HCD) at a normalised collision energy of 55% to ensure maximal TMT reporter ion yield. Synchronous Precursor Selection (SPS) was enabled to include up to 5 MS2 fragment ions in the FTMS3 scan.

2.2.7.1.3. Data analysis

The raw data files were processed and quantified using Proteome Discoverer software v2.1 (Thermo Scientific, UK) and searched against the UniProt Human or murine databases (downloaded 13/09/18: 152927 entries) using the SEQUEST algorithm. Peptide precursor mass tolerance was set at 10ppm, and MS/MS tolerance was set at 0.6Da. Search criteria included oxidation of methionine (+15.9949) as a variable modification and carbamidomethylation of cysteine (+57.0214) and the addition of the TMT mass tag (+229.163) to peptide N-termini and lysine as fixed modifications. Searches were performed with full tryptic digestion and a maximum of 2 missed cleavage events was allowed. The reverse database search option was enabled, and the data was filtered to satisfy a false discovery rate (FDR) of 5%.

2.2.7.2. Whole proteome analysis

2.2.7.2.1. TMT labelling and high pH reversed-phase chromatography

Aliquots of 100µg of six samples per experiment were digested with trypsin (2.5µg trypsin per 100µg protein; 37°C, overnight), labelled with TMT six plex reagents according to the manufacturer's protocol (Thermo Fisher Scientific, UK) and the labelled samples pooled.

An aliquot of the pooled sample was evaporated to dryness, resuspended in 5% formic acid and then desalted using a SepPak cartridge according to the manufacturer's instructions (Waters, USA). Eluate from the SepPak cartridge was again evaporated to dryness and resuspended in buffer A (20 mM ammonium hydroxide, pH 10) prior to fractionation by high pH reversed-phase chromatography using an Ultimate 3000 liquid chromatography system (Thermo Fisher Scientific, UK). In brief, the sample was loaded onto an XBridge BEH C18 Column (130Å, 3.5µm, 2.1mm X 150mm, Waters, UK) in buffer A and peptides eluted with an increasing gradient of buffer B (20mM Ammonium Hydroxide in acetonitrile, pH 10) from 0-95% over 60min. The resulting fractions were evaporated to dryness and resuspended in 1% formic acid prior to analysis by nano-LC MSMS using an Orbitrap Fusion Tribrid mass spectrometer (Thermo Scientific, UK). Nano-LC MSMS protocol is previously detailed (see section 2.2.7.1.2.).

2.2.7.2.2. Data analysis

The raw data files were processed and quantified using Proteome Discoverer software v1.4 (Thermo Scientific, UK) and searched against the UniProt Human database (downloaded September 2018: 152927 entries) or the Uniprot Mouse database (downloaded November 2018: 81925 entries) using the SEQUEST algorithm. Peptide precursor mass tolerance was set at 10ppm, and MS/MS tolerance was set at 0.6Da. Search criteria included oxidation of methionine (+15.9949) as a variable modification and carbamidomethylation of cysteine (+57.0214) and the addition of the TMT mass tag (+229.163) to peptide N-termini and lysine as fixed modifications. Searches were performed with full tryptic digestion and a maximum of 1 missed cleavage was allowed. The reverse database search option was enabled, and all peptide data was filtered to satisfy FDR of 5%.

2.2.8. Cell viability assays

Cell proliferation was assessed using the colorimetric MTT assay (Sigma Aldrich, UK) as per the manufacturer's instructions. Briefly, 10µL of the 12 mM MTT stock solution in 100µL of culture medium was added to cells and incubated at 37°C for 2h. After labelling the cells with MTT, all but

25µL of medium was from the wells. 50µL of DMSO was added and incubated 37°C for 30min; the resulting solution was transferred into a 96well plate. Absorbances were read at 540nm and expressed as a percentage of an untreated control. Cellular cytotoxicity was quantified using an LDH detection kit (Sigma Aldrich, UK) as per the manufacturer's instructions. Briefly, 50µL of cell culture supernatant was transferred to a 96well plate with 50µL of the reaction mixture and incubated 37°C for 30min. Absorbances were read at 450nm and expressed as relative to an untreated control.

2.2.9 *In vitro* genetic modulation

2.2.9.1. Small interfering RNA (siRNA)

Knock-down of IL-33 from ARPE-19 cells was achieved using the fast-forward transfection technique. Cells were seeded at a concentration of 55,000 per well of a 24 well plate in 0.5ml of culture medium with 1% FBS and no antibiotics. Cells were incubated for 1h at 37°C prior to transfection. The FlexiTube GeneSolution (QIAGEN, UK), as a specific mixture of four preselected siRNA duplexes was used to target different sequences of the human *IL33* gene. Each siRNA was diluted in 100µl of culture medium without serum and antibiotics (final concentration 20nM each siRNA). 6µl HiPerfect transfection reagent (QIAGEN, UK) was added to the siRNA, vortexed and left for 5min. 100µl of transfection complex was added to the cells and left for 48h at 37°C.

2.2.9.2. Clustered regularly interspaced short palindromic repeats (CRISPR)-cas9

For IL-33 overexpression in ARPE-19 cells, a CRISPR-cas9 activation plasmid was used to up-regulate the expression of the human *IL33* gene. A commercially available IL-33 activation plasmid was purchased from Santa Cruz Biotechnology. Cells were seeded at a concentration of 40,000 per well of a 24 well plate in 0.5ml of culture medium with 10% FBS and no antibiotics. Cells were incubated overnight at 37°C prior to transfection. Media was replaced just before transfection. For each transfection, 0.16µg of Plasmid DNA was diluted into 25µl plasmid transfection medium. Separately, 0.833µl of transfection reagent was diluted in 25µl plasmid transfection medium. Both solutions were left for 5min before combined, mixed and left for a further 30min. 50ul of transfection complex was added to the cells and left for 48h at 37°C.

2.2.10. Enzyme-based metabolic assays

2.2.10.1. Glucose consumption

Glucose consumption was assessed using a glucose coulometric assay kit (Thermo Fischer, UK) as per the manufacturer's instructions. Briefly, 15µL of cell culture supernatant was transferred to a 96well plate with 85µL of diluted assay buffer. 100µL of enzyme buffer was then added and incubated at 37°C for 10min. Absorbances were read at 520nm. Glucose consumption was calculated by subtracting the glucose concentration of samples from the glucose concentration of unconditioned media and expressed as relative to an untreated control.

2.2.10.2. Lactate assay

Extracellular lactate production was measured using a L-lactate fluorometric assay kit (Abcam, UK) as per the manufacturer's instructions. In brief, 20µL of cell culture supernatant was transferred to a 96well plate with 100µL diluted assay buffer, 20µL of cofactor mixture, 40µL of enzyme mixture and 20µL of fluorometric substrate. The plate was incubated for 20min at RT and read using an excitation wavelength at 530nm and an emission wavelength of 590nm. Lactate production was calculated by subtracting the lactate concentration of samples from the lactate concentration of unconditioned media and expressed as relative to an untreated control.

2.2.10.3. ATP and ADP assay

ATP and ADP measurements were quantified using an ATP/ADP fluorometric assay kit (Abcam, UK). In brief, cell supernatants were removed and 500µL of nucleotide releasing buffer was added to cells. 90µL of this buffer was transferred to a 96well plate and background ATP fluorescence was measured. 10µL of ATP-monitoring enzyme was added and left for 2min at RT. ATP fluorescence levels were then measured. The fluorescence levels were subsequently measured again to give background ADP fluorescence. 10µL of ADP converting enzyme was then added and left for 2min at RT. ADP fluorescence levels were then measured. ATP and ADP levels were calculated and expressed as the ratio ATP/ADP. Data is expressed as relative to an untreated control.

2.2.11. Extracellular flux (XF) analysis

Cell metabolism was assessed using a Seahorse XFp Extracellular Flux Analyzer (Agilent, UK). ARPE-19 and M1-MO were seeded at a density of 30,000 cells per well, 24h prior to analysis, with further treatments detailed in results. Cell tack was used to attach primary RPE and BMMC at a density of 50,000 to the XFp. Real time measurements of oxygen consumption rate (OCR) and extracellular

acidification rate (ECAR) (see Fig. 2.2.) were normalized to total protein content using a BCA assay. Pre-optimised injections specific for each assay were used. Cell Mito Stress kit injections: oligomycin (1µM) and antimycin A/rotenone (1µM). Glycolysis stress injections: glucose (10mM), oligomycin (1µM) and 2DG (1µM). Glycolysis rate injections: antimycin A/rotenone (1µM) and 2DG (1µM). UK5099 (5µM) was used to inhibit the mitochondrial pyruvate transporter MCP1. Etomoxir (10µM) was used to inhibit CPT1. Potassium dichloroacetate (20mM) was used to inhibit PDK1. XF medium included 25mM glucose, 1mM pyruvate, 2mM glutamine and 10% FBS in minimal DMEM at pH 7.4. Metabolic parameters were calculated using the formulae detailed in Table 2.4.5; page 115.

Different cell types vary in their metabolic profile and it was necessary to first characterise specific cell types with respect to basal and maximal OCR. In order to effectively assess the maximal respiratory function, the concentration of FCCP (required to uncouple the ETC) was determined empirically for both ARPE-19 and primary murine RPE. A XFp cartridge and cell culture plate were divided into two groups: a “low” concentration range (0.125, 0.25 and 0.5µM) and a “high” concentration range (0.5, 1 and 2µM) of FCCP. Each group was treated with 1µM oligomycin followed by three serial injections of FCCP at the different concentrations. The data was transformed into a dose curve of OCR vs [FCCP]. 0.5µM was chosen as the optimum dose for both cell types, as under these conditions it was the dose which elicited the maximal OCR response (Fig. 2.3A-B).

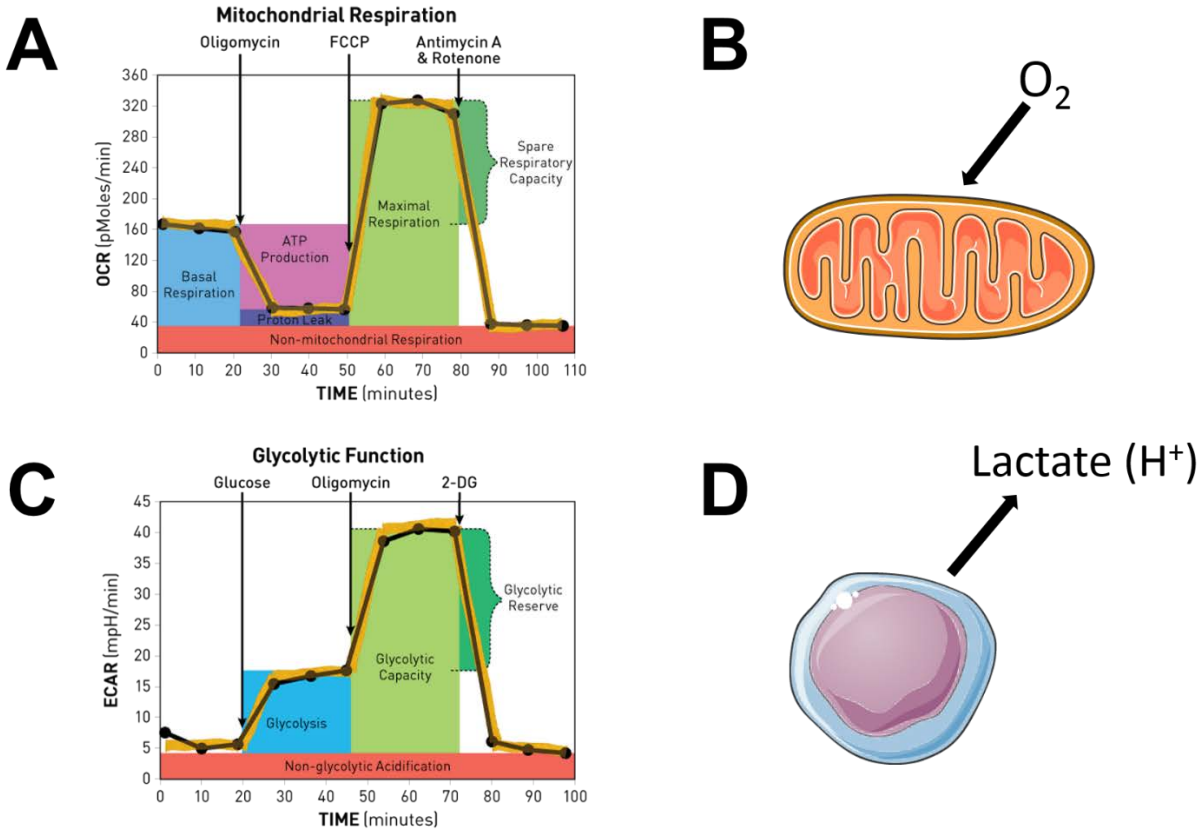

Figure 2.2. Using extracellular flux:

(A) Typical mitochondrial stress bioenergetic profile revealing numerous parameters such as maximal, basal and spare respiration rates. (B) Mitochondrial oxygen consumption. (C) Glycolytic stress profile showing basal glycolysis rate along with the capacity and reserve. (D) The glycolysis end-point metabolite lactate is released from cells and contributes to extracellular acidification. Adapted from Seahorse Bioscience.

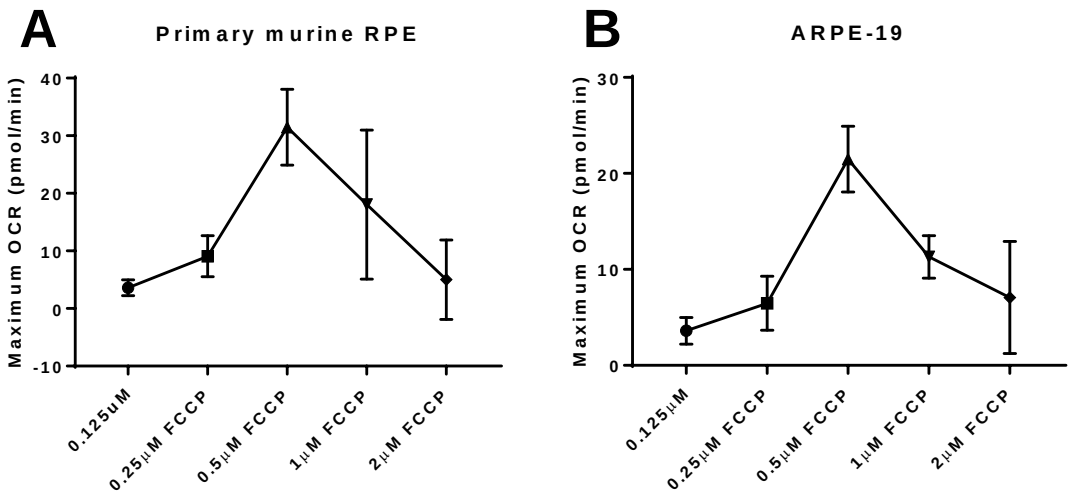

Figure 2.3. Optimisation of FCCP concentration:

A FCCP dose response was used to assess maximal mitochondrial respiration (OCR) on the XFp platform. (A) Maximal FCCP OCR data transformed into a dose response curve: OCR vs. [FCCP] for isolated primary murine RPE. (B) Maximal FCCP OCR data transformed into a dose response curve: OCR vs. [FCCP] for ARPE-19 cells.

2.2.12. Metabolomics

For stable isotope tracing (SITA) experiments, ARPE-19 cells were seeded at a concentration of 1,000,000 per well of a 6-well plate in 3ml of normal culture medium with 10% FCS and antibiotics and left for 24h to reach sub-confluency before treatment. Cells were washed twice with PBS before pulsing with [U-13C]-glucose medium (Cambridge Isotopes, UK) for 2h. SITA media contained 10mM [U-13C]-glucose, 2mM glutamine and 10% dialysed FBS. Cells were washed twice with saline and overlaid with 0.8ml of ice-cold methanol. The cells were subjected to three rounds of sonication and freeze-dried using a speed-vacuum centrifuge. Gas chromatography coupled to mass spectrometry (GCMS) was performed on the samples using previously detailed methods [311]. In brief, dried samples were re-suspended in 30µL anhydrous pyridine and added to GC-MS autoinjector ports holding 70µL N-(*tert*-butyldimethylsilyl)-N-methyltrifluoroacetamide derivatization reagent. The samples were first heated to 70°C for 1hr, 1µL aliquots were taken and injected for analysis. GC-MS data were collected on an Agilent 5975C series GC/MSD system (Agilent, Canada) functioning in election ionization mode (70 eV) with selective ion monitoring. Mass isotopomer distributions (MID) were derived using an algorithm developed at McGill University [454]. Relative metabolite levels were normalised to protein content (µg) using a BCA assay. This was performed in the Core Metabolomics Facility (McGill University, Canada) with the technical and scientific assistance of Dr. Emma Vincent (University of Bristol, UK) and Mr. Luc Choinière (McGill University, Canada).

2.2.13. Electron microscopy

2.2.13.1. *Ex vivo* electron microscopy

WT and *Il33*$^{-/-}$ mice eyes were enucleated with the anterior chamber removed and fixed in 2.5% glutaraldehyde in 0.1m phosphate buffer. Eyes were washed in buffer post fixation in Osmium tetroxide for 1 hour and enbloc stained with uranyl acetate prior to being dehydrated with ethanol and embedded in Epon-resin (TAAB, UK). After polymerisation the embedded eyes were trimmed to remove excess material revealing the retina and choroid layers these were sectioned transversely at 0.5µm for light microscopy. Suitable areas were selected for transmission electron microscopy and these were sectioned (80nm thick) and sectioned stained with uranyl acetate and lead citrate prior to observation in a Tecnai 12 microscope. This was performed in the Electron Microscopy unit of the Wolfson Bioimaging Facility (University of Bristol, UK) and assisted by Dr. Chris Neal as technical support.

2.2.13.2. *In vitro* electron microscopy

Cells were grown on 24-well plates. Cells were washed in buffer and fixed in phosphate buffered glutaraldehyde and post fixed using osmium tetroxide in the same buffer. Cells were stained with uranyl acetate and then after ethanol dehydration were infiltrated with Epon resin mix (TAAB, UK) and polymerised at 60°C for 2 days. Sections were cut at 70-80nm thickness using an Ultracut S ultramicrotome and stained with Reynolds' lead citrate and uranyl acetate. Sections were viewed and images recorded on a Tecnai T12 microscope (FEI).

2.2.14. Confocal microscopy

To prepare RPE/choroid sections, enucleated eyes were initially fixed in 4% formaldehyde overnight, cryosectioned and mounted onto poly-lysine coated slides. Mito Green™ (Thermo Fischer, UK) staining was used on fixed cells to visualise mitochondria. Slides were incubated for 1h in 20nM Mito Green™ and washed twice in PBS before imaging with a Leica TCS-SP2-AOBS confocal laser scanning microscope on a 488 nm argon laser line. Image analysis: Mitochondria density in confocal images were assessed using the Volocity® Image Analysis Software 6.3 (Perkin Elmer, UK).

2.2.15. Chromatin immunoprecipitation (ChIP) with parallel DNA sequencing

2.2.15.1. Interleukin-33 ChIP

ChIP assays were performed by Active Motif Epigenetic Services. In brief, ARPE-19 cells were fixed with 1% formaldehyde for 15min and quenched with 0.125M glycine. Chromatin was isolated by adding chromatin lysis buffer, followed by disruption with a Dounce homogenizer. Lysates were sonicated to shear the DNA to an average length of 300–500 bp. Genomic DNA (Input) was purified from an aliquot of chromatin and quantified on a Nanodrop spectrophotometer. Extrapolation to the original chromatin volume permitted quantitation of the total chromatin yield.

An aliquot of chromatin was precleared with protein G agarose beads. IL-33-bound genomic DNA regions were isolated using a Nessy-1 (mouse derived polyclonal anti-IL-33). After overnight incubation at 4°C, protein G agarose beads (Cell Signalling, UK) enabled isolation of IL-33-chromatin complexes. These were subsequently washed, eluted from the beads with SDS buffer, and subjected to RNase and proteinase K treatment. Crosslinks were removed by incubation overnight at 65°C, and immunoprecipitated DNA was purified by phenol-chloroform extraction and ethanol precipitation.

RT-PCR were performed in triplicate on specific genomic regions using SYBR green reagents (Thermo Fischer, UK). Data were normalized for primer efficiency by carrying out RT-PCR on input DNA with each primer pair.

2.2.15.2. DNA sequencing

ChIP and input DNAs were prepared for amplification by converting overhangs into phosphorylated blunt ends and adding an adenine to the 3' ends. Illumina adaptors were added, and the library was size-selected (175-225 bp) with an agarose gel. The adaptor-ligated libraries were amplified for 18 cycles. The resulting DNA libraries were purified, quantified by RT-PCR at the same specific genomic regions as the original ChIP DNA to assess amplification efficiency. Subsequently, DNA libraries were sequenced on the Illumina Genome Analyzer II (Illumina, UK). Reads were filtered to keep only those with > 70% of bases having Phred quality score of >20. These filtered reads were mapped to the human genome by GSNAP, allowing maximum of two mismatches. Mean fragment length was estimated using a correlation method applied in the 'chipseq' package from Bioconductor. Reads were then extended according to the estimated fragment length, and per base coverage was calculated through the extended reads. ChIP-seq enrichment regions for anti-IL-33 ChIP were identified using MACS 1.4. with a p-value threshold of $1x10^{-9}$ and enrichment threshold of 5. Mapping enrichment regions to different regions of the genome was performed with Genentech in-house software tools using R/Bioconductor.

2.3. Quantification and Statistical Analysis

2.3.1. ImageJ

Mitochondrial morphology was manually assessed using ImageJ software (NIH, USA). A scale was set by normalising the pixel distance to the scale provided (in nm) on each image. Area measurements were calculated by freehand selection around every whole mitochondrion observed in each image (Fig. 2.4A). Three separate measurements were taken the mean value was used as the area. Diameter measurements were calculated by freehand lines at the largest part of every whole mitochondrion observed in each image (Fig. 2.4B). Mitochondrial numbers were manually counted in each image which corresponded to a 4.95µm^2 (*ex vivo*) or 37µm^2 (*in vitro*) area of the RPE; only whole mitochondria were counted (Fig. 2.4C). Mitochondria were manually characterized into either (Fig. 2.4D) “short tubular”, (Fig. 2.4E) “fragmented” or (Fig. 2.4F) “long tubular” phenotypes.

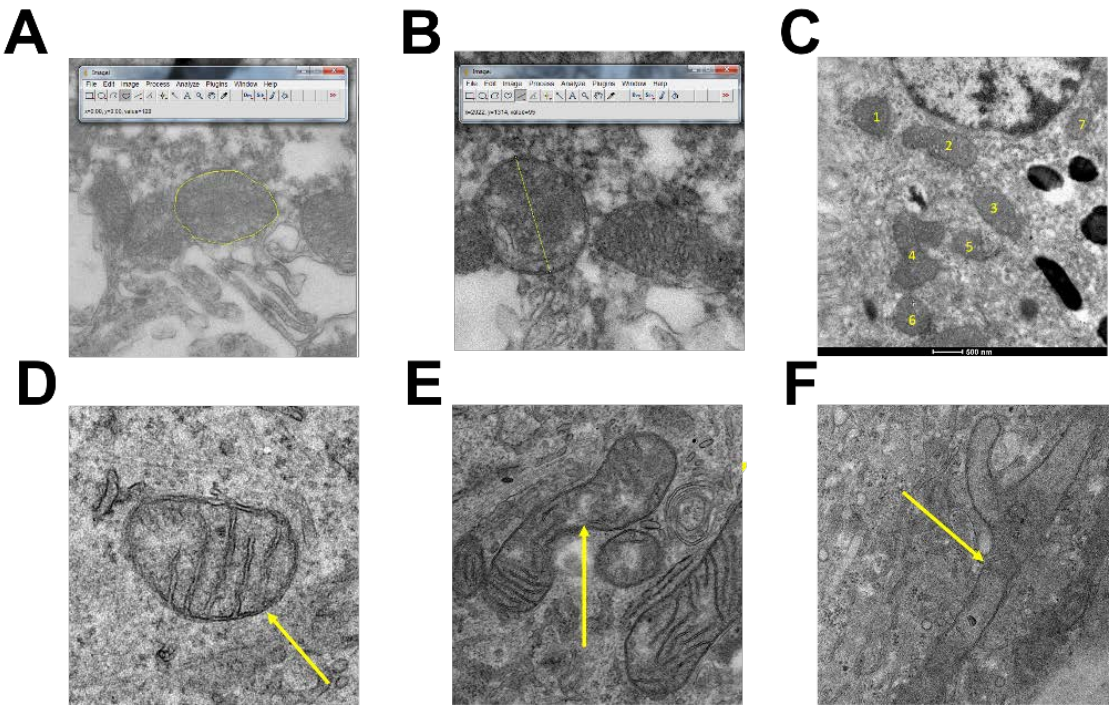

Figure 2.4. Quantification of mitochondria using Image J:

(A) Area measurements were calculated by freehand selection around every whole mitochondrion observed. (B) Diameter measurements were calculated by freehand lines at the largest part of every whole mitochondrion observed in each image. (C) Mitochondrial numbers were manually counted in each image. Mitochondria were manually classed into either (D) “fragmented”, (E) “short tubular” or (F) “long tubular“.

2.3.2. Heatmap generation and hierarchal clustering

Proteomics datasets were expressed as a heatmap using Morpheus matrix visualisation and analysis software (https://software.broadinstitute.org/morpheus/). In brief, the mean value from a complete dataset was subtracted from each value, the dataset was imported into the online software package and minimal/maximal points were adjusted based on the variance either side of zero. Hierarchal clustering was performed using an algorithm found on Morpheus matrix visualisation and analysis software. In brief, columns and rows were clustered using an average linkage method and a metric of one minus Pearson correlation.

2.3.3. STRING functional protein associations

The IL-33 "interactome" was assessed using the STRING database of known and predicted protein interactions (https://string-db.org/). The interactions include direct (physical) and indirect (functional) associations. In brief, gene-names were extracted from a proteomics dataset and copied into the online software package. The data was then assigned to either human or murine origin and expressed as a network. The PPI enrichment value (an indication that the given dataset has more interactions among themselves than what would be expected for a random set of proteins of similar size, drawn from the genome) above $P < 0.01$ was considered significant. Functional enrichments were assessed within the network based on biological processes (GO terms). Enrichments were expressed as a ranked analysis on both gene counts and false discovery rate.

2.3.4. Gene annotation enrichment analysis

The Database for Annotation, Visualization and Integrated Discovery (DAVID) v6.8 (https://david.ncifcrf.gov) was used for gene annotation enrichment analysis, functional annotation clustering and BioCarta/KEGG pathway mapping. This identified enriched biological themes, particularly GO terms within a dataset. A Benjamini-Hockberg corrected $P < 0.01$ was used as a significance threshold to adjust for false discovery rates.

2.3.5. Statistics

Data are presented as mean ± SD for technical replicates or mean ± SEM for biological replicates. Statistical analysis was performed using GraphPad Prism version 7.04. An unpaired two-tailed

Student's t test or a parametric ANOVA was used as specified for multiple comparisons between groups. $P < 0.05$ was considered significant.

2.4. Tables

2.4.1. Summary of agonists and recombinant proteins

Reagent	Company	Catalog number
LPS (0.5-1µg/ml ; Ultrapure from E-coli 0111:B4)	Invivogen	Cat tlrl-eblps
Poly (I:C) HMW (1-25µg/ml)	Invivogen	Cat tlrl-pic-5
Poly (I:C) LMW (10µg/ml)	Invivogen	Cat tlrl-picw
PGN-EB (10µg/ml)	Invivogen	Cat tlrl-pgneb
GPN ODN 2006 (10µg/ml)	Invivogen	Cat tlrl-2006
Recombinant human IL-33 (1-100ng/ml)	Enzo Life Sciences	Cat ALX-522-098-C010
Recombinant murine IL-33 (1-100ng/ml)	Enzo Life Sciences	Cat ALX-522-101-C010
Recombinant murine IL-3 (10ng/ml)	Preprotech	Cat 213-13
Recombinant human IL-1β (50ng/ml)	Invivogen	Cat rcyec-hil1b
Recombinant human IL-4 (10ng/ml)	R&D systems	Cat 204-IL-010
Recombinant human IL-6 (10ng/ml)	R&D systems	Cat 206-IL-010
Recombinant human IL-10 (10ng/ml)	Biolegend	Cat 571002
Recombinant human IL-17A (100ng/ml)	Preprotech	Cat 200-17
Recombinant human IL-22 (100ng/ml)	R&D systems	Cat 782-IL-010
Recombinant human TNFα (100ng/ml)	R&D systems	Cat 210-TA-005
Recombinant human IFN-γ (100U/ml)	Preprotech	Cat 300-02
Hydrogen peroxide (0.2-1mM)	Sigma Aldrich	Cat H1009
AICAR (1mM)	Tocris	Cat 2840
Compound C (40µM)	Millipore	Cat 171260

2.4.2. Western blotting antibodies

Antibody	Company	Catalog number
Rabbit monclonal anti-beta actin (1:2000)	Cell Signaling	Cat #4970
Rabbit monoclonal anti-beta tubulin (1:2000)	Cell Signaling	Cat #2146
Rabbit monoclonal anti-AMPKa (1:1000)	Cell Signaling	Cat #5831
Rabbit monoclonal anti-phospho AMPK (T172) (1:400)	Cell Signaling	Cat #2535
Rabbit monoclonal anti-ACC (1:1000)	Cell Signaling	Cat #3676
Rabbit monoclonal anti-phospho ACC (S79) (1:1000)	Cell Signaling	Cat #11818
Rabbit monoclonal anti-mTOR (1:800)	Cell Signaling	Cat #2983
Rabbit monoclonal anti-phospho mTOR (S2448) (1:800)	Cell Signaling	Cat #5536
Rabbit monoclonal anti-P70 S6 kinase (T421/S424) (1:1000)	Cell Signaling	Cat #9204
Rabbit monoclonal anti-phospho 4EBP1 (S65) (1:1000)	Cell Signaling	Cat #9456
Rabbit monoclonal anti-raptor (1:1000)	Cell Signaling	Cat #2280
Rabbit monoclonal anti-PI3 kinase p110a (1:500)	Cell Signaling	Cat #4255
Rabbit monoclonal anti-MPC2 (1:800)	Cell Signaling	Cat #46141
Rabbit monoclonal anti-MPC1 (1:1000)	Cell Signaling	Cat #14462
Rabbit monoclonal anti-catalase (1:1000)	Cell Signaling	Cat #12980
Mouse monoclonal anti-SOD1 (1:1000)	Cell Signaling	Cat #4266
Rabbit monoclonal anti-SOD2 (1:1000)	Cell Signaling	Cat #4266
Rabbit monoclonal anti-BCL2 (1:1000)	Abcam	Cat ab692
Rabbit monoclonal anti-survivin (1:1000)	Abcam	Cat ab76424
Goat polyclonal anti-IL-33 (1:1000)	R&D Systems	Cat AF3625
Mouse polyclonal Nessy-1 (anti IL-33) (1:1000)	ENZO Life Science	ALX-804-840-C100
Rabbit polyclonal anti-ST2 (1:1000)	Abcam	Cat ab25877
Rabbit Anti-Pyruvate Dehydrogenase E1-alpha subunit (phospho S293) antibody	Abcam	Cat ab92696

Rabbit Anti-Pyruvate Dehydrogenase E1-alpha subunit antibody	Abcam	Cat ab110334
Mouse monoclonal anti-RPE65 (1:1000)	Santa Cruz	Cat sc-390787
Mouse monoclonal anti-rhodopsin (1:1000)	Santa Cruz	Cat sc-57432
Rabbit monoclonal anti-pyruvate carboxylase (1:1000)	Abcam	Cat ab126707
Rabbit monoclonal anti-PKM2 (1:1000)	Cell signaling	Cat D78A4
Rabbit monoclonal anti-PKM1 (1:1000)	Cell signaling	Cat 7067S
Rabbit monoclonal anti-GLUT1 (1:2000)	Abcam	Cat ab115730
Total OXPHOS Human WB Antibody Cocktail (1:300)	Abcam	Cat ab110411
Rabbit polyclonal anti-SRSF3 (1:1000)	Abcam	Cat ab125124
Rabbit polyclonal anti-hnRNPA2B1 (1:1000)	Abcam	Cat ab31645
Rabbit polyclonal anti-hnRNPA1 (1:1000)	Abcam	Cat ab137780
Anti-rabbit IgG, HRP-linked Antibody (1:1500)	Cell Signaling	Cat #7074
Anti-mouse IgG, HRP-linked Antibody (1:1500)	Cell Signaling	Cat #7076
Donkey anti-goat IgG-HRP (1:2500)	Santa Cruz	Cat sc-2020

2.4.3. Primer sequences

Primers for RT-PCR	**Sequence (5'-)**
βACTIN forward	AGAGCTACGAGCTGCCTGAC
βACTIN reverse	AGCACTGTGTTGGCGTACAG
GLUT1 forward	TCACTGTGCTCCTGGTTTTCTG
GLUT1 reverse	CCTGTGCCTCCTGAGAGATCC
HK2 forward	TGATCGCCTGCTTATTCACGG
HK2 reverse	AACCGCCTAGAAATCTCCAGA
LDHA forward	TGGAGTGGAATGAATGTTGC
LDHA reverse	ATAGCCCAGGATGTGTAGCC
PFKP forward	ACCACAGTCCGGGCATGTAA

PFKP reverse	TGTCTCCAGCCCTAAGTCCA
GAPDH forward	ACCACAGTCCATGCCATCAC
GAPDH reverse	TCCACCACCCTGTTGCTGTA
PKM1 forward	ACCGCAAGCTGTTTGAAGAA
PKM1 reverse	TCCATGAGGTCTGTGGAGTG
PKM2 forward	GAGGCCTCCTTCAAGTGCT
PKM2 reverse	CCGACTTGGTGAGAGACGAT
ENO1 forward	GAATAAGAAGGCCTGGAGC
ENO1 reverse	TAGACACCACTGGGTAGTCC
SHDH forward	ATGGCGGTTCTCTGGAGGCTG
SHDH reverse	GAGCTTCCACAGCATGGCAAC
IL33 forward	CACCCCTCAAATGAATCAGG
IL33 reverse	GGAGCTCCACAGAGTGTTCC
PC forward	CCTTTGGGAATGGGGCGCTGTTTGT
PC reverse	ACAGAGTCGCTGGTGAGCCGAGTC
MPC1 forward	TGACCTTTGCTTTGTGTTGC
MPC1 reverse	CACCTTGGATCAATTGTGCT
MPC2 forward	CGATATGGCTAGACCAGCAG
MPC2 reverse	ACAGCGAACAAAGACCAATTT
PDK1 forward	CGGATCAGAACCGACACA
PDK1 reverse	ACTGAACCATTCTGGCTGGTGA
CS forward	GATTGTGCCCAATGTCCTCT
CS reverse	TTCATCTCCGTCATGCCATA
IDH1 forward	GGCGAGCAGCACAGAGAC

IDH1 reverse	TCACCCCAGATACCATCAGA
FH1 forward	CTACCCAAGCTCCCTCAGC
FH1 reverse	CAGGCAGGAGGGCTGAAG
HIF1α forward	TATGAGCCAGAAGAACTTTTAGGC
HIF1α reverse	CACCTCTTTTGGCAAGCATCCTG
PGC1α forward	GTCACCACCCAAATCCTTAT
PGC1α reverse	ATCTACTGCTGGAGACCTT
MYC forward	AGCGACTCTGAGGAGGAACAAGAA
MYC reverse	CGTAGTTGTGCTGATGTGTGGAGA
SIRT1 forward	TCGCAAAGGAACATAGACA
SIRT1 reverse	CTGTTGCAAAGGAACCATGACA
SIRT4 forward	CAGCAAGTCCTCCTCTGGAC
SIRT4 reverse	CCAGCCTACGAAGTTCTCG
CYTB forward	CCCCACAAACCCCATTACTAAACCCA
CYTB reverse	TTTCATCATGCGGAGATGTTGGATGG
16 S rRNA forward	GAGTGAAATTGACCTGCCCGTGAA
16 S rRNA reverse	TCTTAGCATGTACTGCTCGGAGGT
BGLOB forward	CTTGGGTTTCTGATAGGCAC
BGLOB reverse	CTTAGGGTTGCCCATAACAG
MFN1 forward	ATGGCAGAACCTGTTTCTCCACT
MFN1 reverse	GGAAGCAATTGGTTGGTTATATGGCCA
MFN2 forward	AATCTGAGGCGACTGGTGA
MFN2 reverse	CTCCTCCTGTTCGACAGTCA
OPA1 forward	GAAAGGGTCTGCTTGGTGAG

OPA1 reverse	CGCTTCTGTTGGGCATAG
PINK1 forward	TACCGTGCACCAGGAGAAG
PINK1 reverse	GCTTGGGACCTCTCTTGGAT
DRP1 forward	TGAAGGATGTCATGTCGGACC
DRP1 reverse	GTTGAGGACGTTGACTTGGCT
Il33 forward	CCTCCCCTGAGTACATCAATGACC
Il33 reverse	GTAGTAGCACCTGGTCTTGCTCTT
βActin forward	GCCCACTACTAAATCATTCGCA
βActin reverse	TAGACACTTGCTTACTGGCCAC

2.4.4. ELISA antibodies

Antibody	**Company**	**Catalog number**
Human IL-1β capture (1/60)	R&D Systems	DY201
Human IL-1β detection (1/60)	R&D Systems	DY201
Human IL-6 capture (1/40)	R&D Systems	DY206-05
Human IL-6 detection (1/60)	R&D Systems	DY206-05
Human IL-33 capture (1/60)	R&D Systems	DY3625B
Human IL-33 detection (1/60)	R&D Systems	DY3625B
Human ST2 capture (1/60)	R&D Systems	DY523B-05
Human ST2 detection (1/60)	R&D Systems	DY523B-05
Human malonyl coA-biotin antibody (1/100)	CUSABIO	CSB-E13877h

2.4.5. Seahorse parameters

Metabolic parameter	Equation	Definition
OCR/ECAR	(First OCR measurement)/(first ECAR measurement)	The ratio of mitochondrial OXPHOS to glycolytic lactate production.
Proton leak	(Difference between OCR after oligomycin and non-mitochondrial respiration)	Basal respiration not coupled to ATP-production. Can indicate mitochondrial damage or a mechanism to regulate ATP-production.
Non-mitochondrial respiration	(OCR measurement after antimycin-A/ rotenone)	Continued oxygen consumption as a result of a subset of cellular enzyme which consume oxygen after rotenone or antimycin A.
Basal respiration	(Difference between OCR before oligomycin and non-mitochondrial respiration)	Oxygen consumption under baseline conditions which results from both ATP-production and proton leak.
ATP production	(Difference between basal respiration and proton leak)	The decrease in OCR after ATP-synthase inhibitor oligomycin injection, signifies the amount of basal respiration utilized to drive ATP synthesis.
Maximal respiration	(Difference between maximum OCR post FCCP injection and non-mitochondrial respiration)	The maximal OCR reached through the injection of uncoupler FCCP mimics a physiological energy demand. This stimulates the ETC to operate at full capacity, leading to the rapid oxidation of TCA

		cycle substrates (amino acids, glucose and fatty acids).
Spare respiratory capacity	((Maximal respiration) / (basal respiration) x 100)	This measurement indicates both the ability of a cell to respond to a metabolic demand and how closely a cell is respiring to its theoretical maximum. An ability of a cell to respond to demand can indicate cell fitness and flexibility between metabolic pathways.
Glycolysis	(Difference between maximum ECAR rate before oligomycin and non-glycolytic acidification)	This measurement indicates the ability of cells to metabolise glucose to lactate under basal conditions.
Glycolytic capacity	(Difference between maximum ECAR rate after oligomycin and non-glycolytic acidification)	Oligomycin inhibits the ATP-synthase complex which shifts the energy production to glycolysis. The subsequent increase in ECAR indicates the theoretical maximal glycolytic capacity of a cell.
Glycolytic reserve	(Difference between glycolytic capacity and glycolysis)	This measurement indicates both the ability of a cell to respond to metabolic stress and how closely a cell is undergoing glycolytic metabolism compared to its theoretical glycolytic maximum. This can indicate

		flexibility between metabolic pathways.
Non-glycolytic acidification	(Last ECAR measurement before glucose injection)	ECAR in glucose-starved cells, prior to glucose injection. This is a result of other acidifying processes within a cell other than glycolysis.
Basal glycolysis (glycoPER)	(Last glycoPER measurement before rotenone/antimycin-A)	Proton efflux rate derived from glycolysis, discounting CO_2-dependent acidification.
Compensatory glycolysis	(Maximum glycoPER measurement after rotenone/antimycin-A)	Glycolytic rate in cells following the inhibition of oxidative phosphorylation and driving compensatory glycolytic adaptations to meet metabolic demand.
MitoOCR/glycoPER	([(Last OCR before rotenone/antimycin-A)-(minimum OCR after rotenone/antmycin-A)] / basal glycolysis)	A more refined ratio of mitochondrial OXPHOS to glycolytic lactate production, compared to OCR/ECAR.
Percentage PER from glycolysis	Glycolysis ((basal glycolysis/basal PER) x 100)	Percentage of ECAR which equates to lactate acidification.
CPT1-dependent respiration	(Difference between OCR before and after etomoxir)	The contribution of fatty acid oxidation through CPT-1 to maximal OCR.
MPC-dependent respiration	(Difference between OCR before and after UK5099)	The contribution of pyruvate oxidation through MPC to maximal OCR.

Chapter 3. AMP-activated kinase links metabolism and innate immunity in the retinal pigment epithelium

3.1. Introduction

The retina is referred to as an "immune privileged" tissue. The blood retinal barrier is a key structure in maintaining immune privilege; it describes a series of adaptations by the vascular endothelium and the RPE [455], whereby tight junction and adherens complexes are aptly formed in both cells. The BRB excludes circulating molecular toxins and microorganisms along with patrolling pro-inflammatory leukocytes [456]. With the absence of efferent lymphatics to the eye, immune homeostasis is maintained through hemopoietic immune cells such as microglia and resident macrophages/mast cells, as well as innate immune-competent tissue resident cells [457].

The RPE functions as a non-haematopoietic immune cell which responds to PAMPs and DAMPs through PRRs (e.g. TLR/NLR) [457]. Immune-mediated activation has been observed to have profound effect on aerobic glycolysis, the "Warburg effect", and leads to metabolic reprogramming in cells of both the innate and adaptive immune system (see section 1.9.) [5]. Metabolic alterations in RPE including the "Warburg effect" may contribute to inflammatory processes [286]. With progressing age, increased ROS production, the accumulation of mtDNA mutations and a decline in the function of CPT all contribute to a decline in bioenergetic function [86, 388, 389]. There is now increasing evidence that diminished mitochondrial health in RPE is suggested to play a prominent role in the pathogenesis of AMD [390, 391]. Indeed, a decline in bioenergetic health and the induction of the Warburg effect in RPE may impair its metabolic stability and ability to support the retina. This chapter investigates the role of the RPE as an innate immune competent cell and how its response to "immune stress" in the form of TLR activation (*via* synthetic ligands) impacts its metabolism. It is currently unknown to what extent the RPE can rapidly switch between metabolic pathways during quiescence and activation, and how this may be regulated (e.g. are there conserved mechanisms which occur in other activated innate immune cells).

The aims of this chapter are (1) to address the metabolic changes that occur with age; (2) define how immunological "stress" can define bioenergetic status in the RPE; (3) investigate the role of the metabolic regulator AMPK during innate immune activation.

3.2. Long-term *in vitro* cultivation of ARPE-19 induces changes in glycolytic metabolism and mitochondrial respiration

RPE cells require a massive metabolic output to provide functional support to the retina [6]. Whilst the mechanisms of AMD have yet to be elucidated, there is increasing evidence that mitochondrial deterioration, antioxidant defense, and mitophagy are likely drivers of pathogenesis. To understand how bioenergetic dysfunction may contribute to AMD, analysis of bioenergetic flux was used to examine metabolic status in RPE. Long-term *in vitro* cultivation of ARPE-19 lead to differences in their metabolic profile particularly the increase in basal oxidative phosphorylation (Fig. 3.1A and B) and decline in glycolytic function (Fig. 3.1C and D). I noted the decline in spare respiratory capacity (Fig. 3.1B) and increased proton leak (Fig. 3.1B), which may reflect a strain on mitochondrial function. Supporting the decline in glycolytic function, a reduction in *GLUT1* and *GAPDH* mRNA transcripts were observed (Fig. 3.1F).

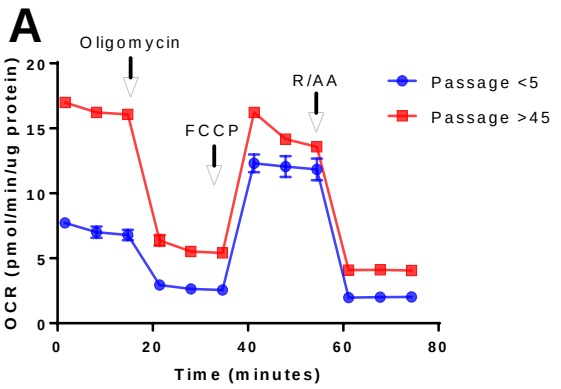
A
Oligomycin
FCCP
R/AA
Passage <5
Passage >45
OCR (pmol/min/ug protein)
Time (minutes)

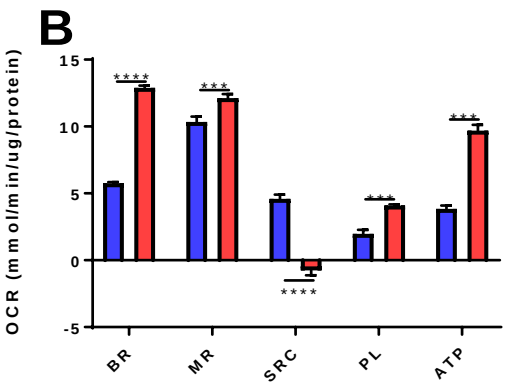
B
OCR (mmol/min/ug/protein)
BR
MR
SRC
PL
ATP

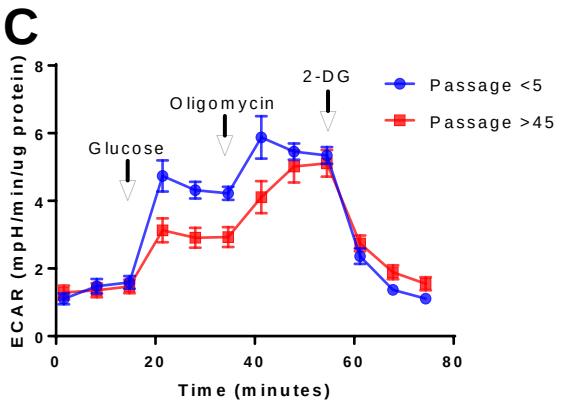
C
Glucose
Oligomycin
2-DG
Passage <5
Passage >45
ECAR (mpH/min/ug protein)
Time (minutes)

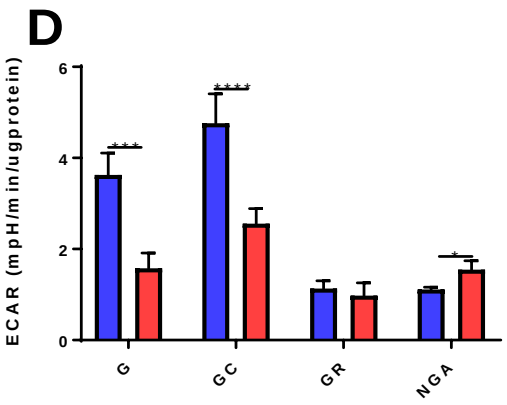
D
ECAR (mpH/min/ugprotein)
G
GC
GR
NGA

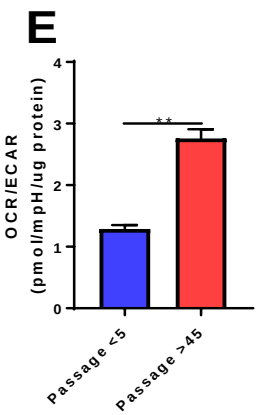
E
OCR/ECAR (pmol/mpH/ug protein)
Passage <5
Passage >45

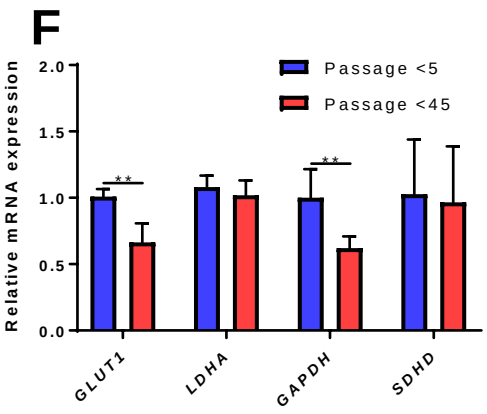
F
Passage <5
Passage <45
Relative mRNA expression
GLUT1
LDHA
GAPDH
SDHD

Figure 3.1. Long-term *in vitro* cultivation of ARPE-19 induces changes in glycolytic metabolism and mitochondrial respiration:

(A) Representative mitochondrial stress test measured with sequential injections of oligomycin, FCCP and rotenone/antimycin A. (B) mitochondrial parameters (BR- basal respiration; MR- maximal respiration; SRC- spare respiratory capacity; PL- proton leak; ATP- ATP-production) calculated from data shown in (A). (C) Representative glycolysis stress test measured with sequential injections of glucose, oligomycin and 2DG. (D) Glycolytic parameters (G- glycolysis; GC- glycolytic capacity; GR- glycolytic reserve; NGA- non-glycolytic acidification) calculated from data shown in (C). (E) Basal OCR and ECAR measurements expressed as the ratio OCR/ECAR. (F) Gene expression analysis of *GLUT1*, *LDHA, GAPDH* and *SDHD* mRNA transcripts, normalised to *β-ACTIN* as an internal control. Data are presented as means ± SD from three independent experiments performed in triplicates. Unpaired Student's T-test; **p*<0.05, ***p*<0.01, ****p*<0.005, *****p*<0.001.

3.3. Isolation and bioenergetic analysis of primary murine RPE

Extended cultivation of a cell line cannot replicate the complexities of an *in vivo* environment, including a lifetime of oxidative insults to the retina. For this reason, I isolated and cultured primary RPE from C57BL/6 mice. The isolated RPE purity was assessed by immunoblotting for RPE specific protein RPE65 and rhodopsin contamination from the neurosensory retina as previously described [453] (See materials and methods - Fig. 2.1.). After establishing a specific *ex vivo* RPE population, young (<10 weeks) and older (>18 months) primary RPE were isolated and subjected to bioenergetic analysis. The mitochondrial stress assay gave a characteristic profile in both groups (Fig. 3.2A), but there were significant changes in both maximal respiration (Fig. 3.2B) and glycolytic capacity (Fig. 3.2D). Parameters such as coupling efficiency and proton leak were found to be significantly altered in aged mice compared to their younger counterparts, in a fashion such that older RPE can be described as relatively impaired (Fig. 3.2C). Because of reduced ECAR observed in the aged population (Fig. 3.2E), there was a significant change in the basal OCR/ECAR (Fig. 3.2F).

Compared to the data obtained from long term *in vitro* cultivation of the ARPE-19 cell line, similar results were observed in terms of the reduced glycolytic function. In contrast to the “aged” ARPE-19 cell line, older primary RPE were not observed to display an increased basal OCR. Both groups exhibited reduced mitochondrial function.

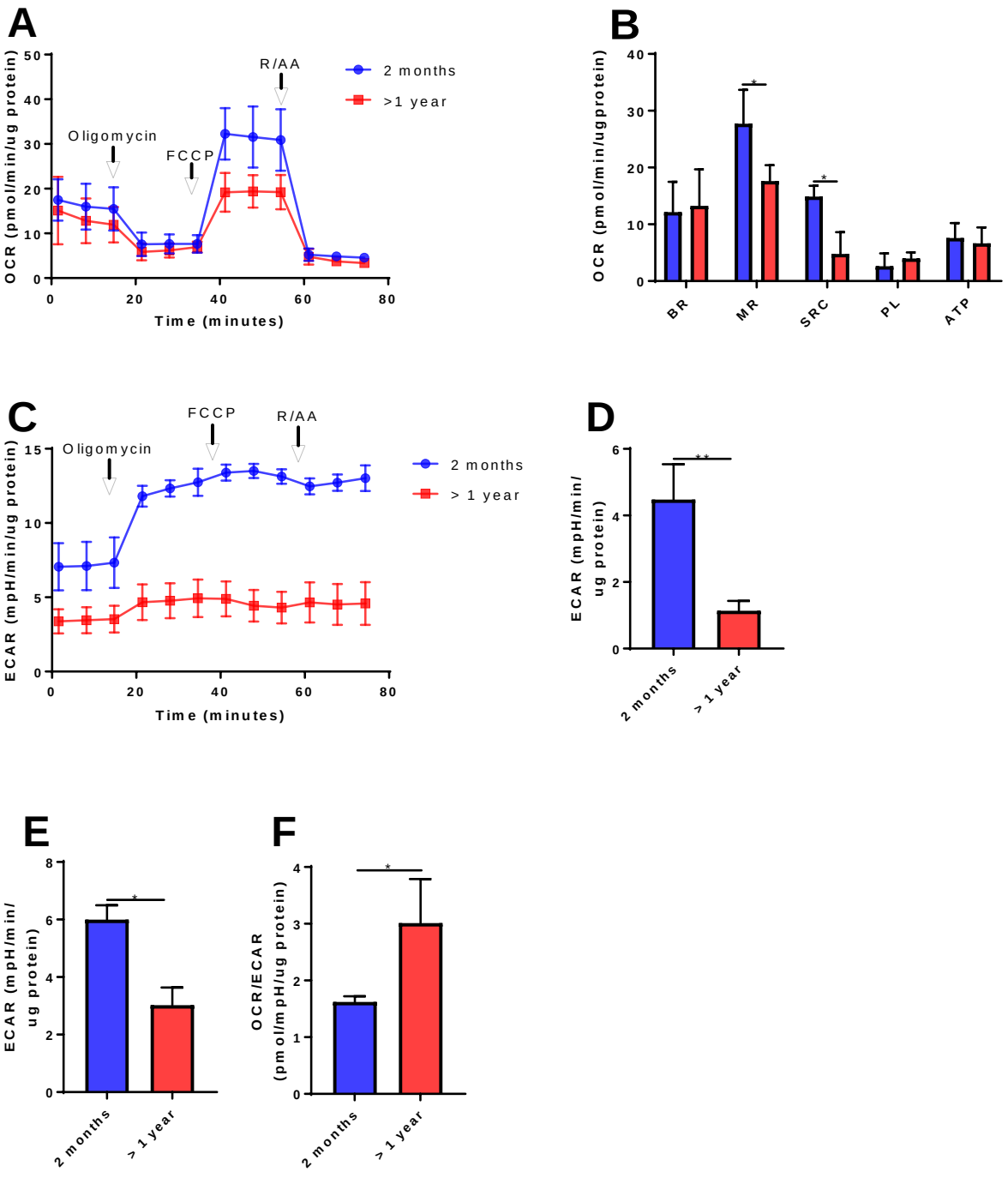
A
OCR (pmol/min/ug protein)
Time (minutes)
Oligomycin
FCCP
R/AA
2 months
>1 year
B
OCR (pmol/min/ugprotein)
BR
MR
SRC
PL
ATP
C
ECAR (mpH/min/ug protein)
Time (minutes)
Oligomycin
FCCP
R/AA
2 months
> 1 year
D
ECAR (mpH/min/ ug protein)
2 months
> 1 year
E
ECAR (mpH/min/ ug protein)
2 months
> 1 year
F
OCR/ECAR (pmol/mpH/ug protein)
2 months
> 1 year

Figure 3.2. Isolation and bioenergetics analysis of primary murine RPE:

(A) Representative mitochondrial stress test measured with sequential injections of oligomycin, FCCP and rotenone/antimycin A. (B) Mitochondrial parameters (BR- basal respiration; MR- maximal respiration; SRC- spare respiratory capacity; PL- proton leak; ATP- ATP-production) calculated from data shown in (B). (C) ECAR data from (A). (D) Glycolytic capacity calculated from ECAR values of data shown in (C). (E) Basal ECAR measurements. (F) OCR and ECAR measurements expressed as the ratio OCR/ECAR. Data presented as means ± SD from three independent experiments performed in triplicate. Unpaired Student's T-test; *p<0.05, **p<0.01, ***p<0.005, ****p<0.001.

3.4. Metabolic adaptations in ARPE-19 to TLR stimulation

Having established that ageing, both *in vitro* (with cell lines) or directly *ex vivo*, led to significant bioenergetic changes which were chronic and persistent, I then investigated whether RPE cells underwent bioenergetic modulation over short timescales, as might be expected in the event of inflammatory stimuli. To test this, I used PRR activation by PAMP/DAMP ligands.

TLRs are vital components for innate immunity; the RPE has a robust expression of TLRs 1-7,9 and 10 which that facilitate host defence against microbes [45]. In TLR-activated macrophages and DC, a switch to aerobic glycolysis has previously been reported [403, 416]. The impact of PAMP stimulus on RPE bioenergetics was investigated to identify if a similar metabolic shift occurs in the RPE. I chose to utilise agonists for TLR-3 due to a possible association with AMD [458] and TLR-4 because of its extensive study in the field of immunometabolism [416].

There was first a necessity to identify the effect of TLR agonists on ARPE-19 cell viability. Both LPS and Poly (I:C) treatment (based around doses found commonly in the literature [45, 427]) had no significant effect on LDH release after 24h (Fig. 3.3A-B). Using the doses of 1µg/ml for LPS and 10µg/ml for Poly (I:C), it was investigated to what extent RPE metabolism may be modulated over a time course of treatment. Cells were stimulated with agonists and OCR/ECAR measurements were taken at 30min, 1h, 2h, 6h, 12h, 24h and 48h. It was observed that Poly (I:C) treatment significantly increased the OCR/ECAR ratio between 12-24h, with the greatest significance observed at 24h of treatment (Fig. 3.3C). LPS treatment significantly decreased the OCR/ECAR ratio between 30min-6h of treatment. Having established the differential effects of each TLR agonist on RPE metabolism, I decided to test whether these occurred in a dose-response manner, at time points where each agonist exerted the most significant effect (24h for Poly (I:C) and 30min for LPS). Cells were treated with three doses of Poly (I:C) (5, 10 and 25 µg/ml) for 24h, it was found that the intermediate dose of Poly (I:C) (10µg/ml) elicited the greatest response in the OCR/ECAR ratio (Fig. 3.3E). Cells were treated for 30min with two doses of LPS (0.5 and 1 µg/ml) with a dose response observed (Fig. 3.3F).

The results of this section indicate the tolerability of the ARPE-19 cell line to both agonists in terms of LDH release. Both agonists exhibit differential effects on ARPE-19 metabolism accompanied by differential kinetics of the metabolic response.

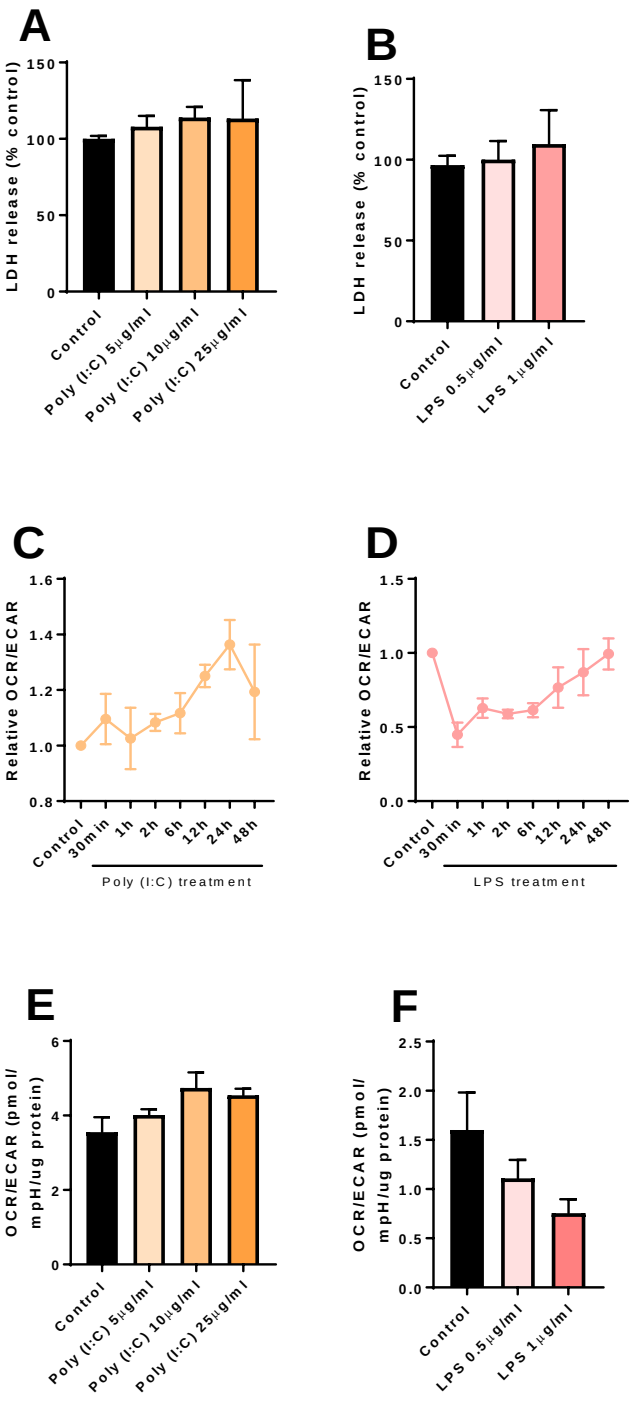
A
LDH release (% control)
150
100
50
0
Control
Poly (I:C) 5μg/ml
Poly (I:C) 10μg/ml
Poly (I:C) 25μg/ml
B
LDH release (% control)
150
100
50
0
Control
LPS 0.5μg/ml
LPS 1μg/ml
C
Relative OCR/ECAR
1.6
1.4
1.2
1.0
0.8
Control
30min
1h
2h
6h
12h
24h
48h
Poly (I:C) treatment
D
Relative OCR/ECAR
1.5
1.0
0.5
0.0
Control
30min
1h
2h
6h
12h
24h
48h
LPS treatment
E
OCR/ECAR (pmol/ mpH/ug protein)
6
4
2
0
Control
Poly (I:C) 5μg/ml
Poly (I:C) 10μg/ml
Poly (I:C) 25μg/ml
F
OCR/ECAR (pmol/ mpH/ug protein)
2.5
2.0
1.5
1.0
0.5
0.0
Control
LPS 0.5μg/ml
LPS 1μg/ml

Figure 3.3. Metabolic adaptations in ARPE-19 following TLR-stimulation:

(A) ARPE-19 cells were treated for 24h with varying doses of Poly (I:C) (5, 10 and 25µg/ml). Supernatants were taken and LDH levels were assessed using a commercial kit. LDH release was expressed as a (%) of an untreated control. (B) ARPE-19 cells were treated for 24h with varying doses of LPS (0.5 and 1µg/ml). Supernatants were taken and LDH levels were assessed using a commercial kit. LDH release was expressed as a (%) of an untreated control. (C) ARPE-19 cells were treated with Poly (I:C) (10µg/ml), basal OCR and ECAR measurements were taken at the indicated time points (0, 30min, 1h, 2h, 6h, 12h, 24h and 48h). (D) ARPE-19 cells were treated with LPS (1µg/ml), basal OCR and ECAR measurements were taken at the indicated time points (0, 30min, 1h, 2h, 6h, 12h, 24h and 48h). (E) ARPE-19 cells were treated with varying doses of Poly (I:C) (5, 10 and 25µg/ml), OCR and ECAR measurements were taken at 24h. (F) ARPE-19 cells were treated with varying doses of LPS (0.5 and 1µg/ml), OCR and ECAR measurements were taken at 30min. Data presented as means ± SD from (C-F) two and (A-B) three independent experiments performed in duplicate.

3.5. Toll-like receptor-3 and -4 agonists differentially modulate glycolysis and mitochondrial respiration in ARPE-19

The results from the previous section indicated that TLR-3 and TLR-4 agonists (Poly (I:C) and LPS, respectively) induced differential effects on RPE metabolism in terms of the "OXPHOS to glycolysis ratio". These results suggest varying kinetics of the response between the two agonists. Poly (I:C) stimulation has no immediate effect on metabolism until 12h onwards, where increased OXPHOS is observed and sustained until 48h. LPS stimulation on the other hand, elicits an immediate drop in the ratio of OXPHOS to glycolysis which returns to baseline after 12h. Considering these findings and having optimised doses and time points of interest for each agonist, it was necessary to further interrogate the metabolic responses that occur in the RPE.

Results from Figs 3.3C-D in the previous section showed that by 30min of LPS stimulation there was contemporaneous drop in OCR and increase in ECAR which was maintained until 6h. Poly (I:C) had little effect on ECAR or OCR in these time points, but it was plausible that a metabolic change could have occurred before 30min and not sustained. A similar experiment was conducted over a shorter timeframe to identify the kinetics of the metabolic response over minutes to hours. Real-time measurements indicated a rapid increase in ECAR accompanied by a drop in OCR in LPS-stimulated ARPE-19. The metabolic "switch" was observed by the first measurement (+3min post-injection). LPS promoted a 1.5-fold relative increase in the ECAR levels relative to resting controls, this was sustained until the end of the assay at (+2h post-injection). OCR measurements returned to the basal levels towards the end of the assay with values only significantly reduced within the first 90min (Fig. 3.4A-B). Poly (I:C) stimulation of cells was found to have no significant effect on either OCR or ECAR during the timeframe of this experiment (Fig. 3.4A-B).

Consequently, bioenergetic analysis was performed following stimulation of cells with either Poly (I:C) or LPS for 30min or 24h, respectively. Using a glycolysis stress test, the data showed that LPS stimulation increased glycolysis, but reduced glycolytic reserve, whereas Poly (I:C) stimulation increased both glycolytic capacity and reserve (Fig. 3.4C-D). Increased glycolytic capacity (and therefore glycolytic reserve) post-oligomycin is indicative of increased glycolytic flux for oxidative pyruvate catabolism (see materials and methods). A mitochondrial stress test identified reduced mitochondrial activity following LPS stimulation, in terms basal and maximal respiration (Fig. 3.4E-F). Poly (I:C) increased basal respiration yet had no significant effect on maximal respiration (Fig. 3.4E-F).

As Poly (I:C) is reported to display differential TLR-3 activation efficacy depending on which synthetic mimic is used [459], a Low molecular weight (LMW) Poly (I:C) was used to confirm the effects observed with the high molecular weight agonist. The use of two different synthetic agonists support the hypothesis that the effects observed are indeed specific to TLR-3 activation (see appendices section 10.3).

Collectively, this data shows that RPE cells undergo metabolic changes during a short timescale in response to inflammatory stimuli. These results suggest that activation of different TLRs in the RPE lead to distinct bioenergetic adaptations. In the context of TLR-4 activation, there is a rapid switch to "aerobic glycolysis" within minutes. Aerobic glycolysis (Warburg effect) is observed frequently in many cancer cells and activated immune cells and refers to the generation of ATP from glycolytic lactate production as opposed to mitochondrial metabolism (see section 1.9.1). LPS-stimulated ARPE-19 cells exhibit increased glycolysis at the expense of impaired mitochondrial function, suggesting the initiation of the Warburg effect in these cells. Poly (I:C)-stimulation increases mitochondrial function and oxidative glycolysis in ARPE-19 cells, yet this occurs much later after treatment.

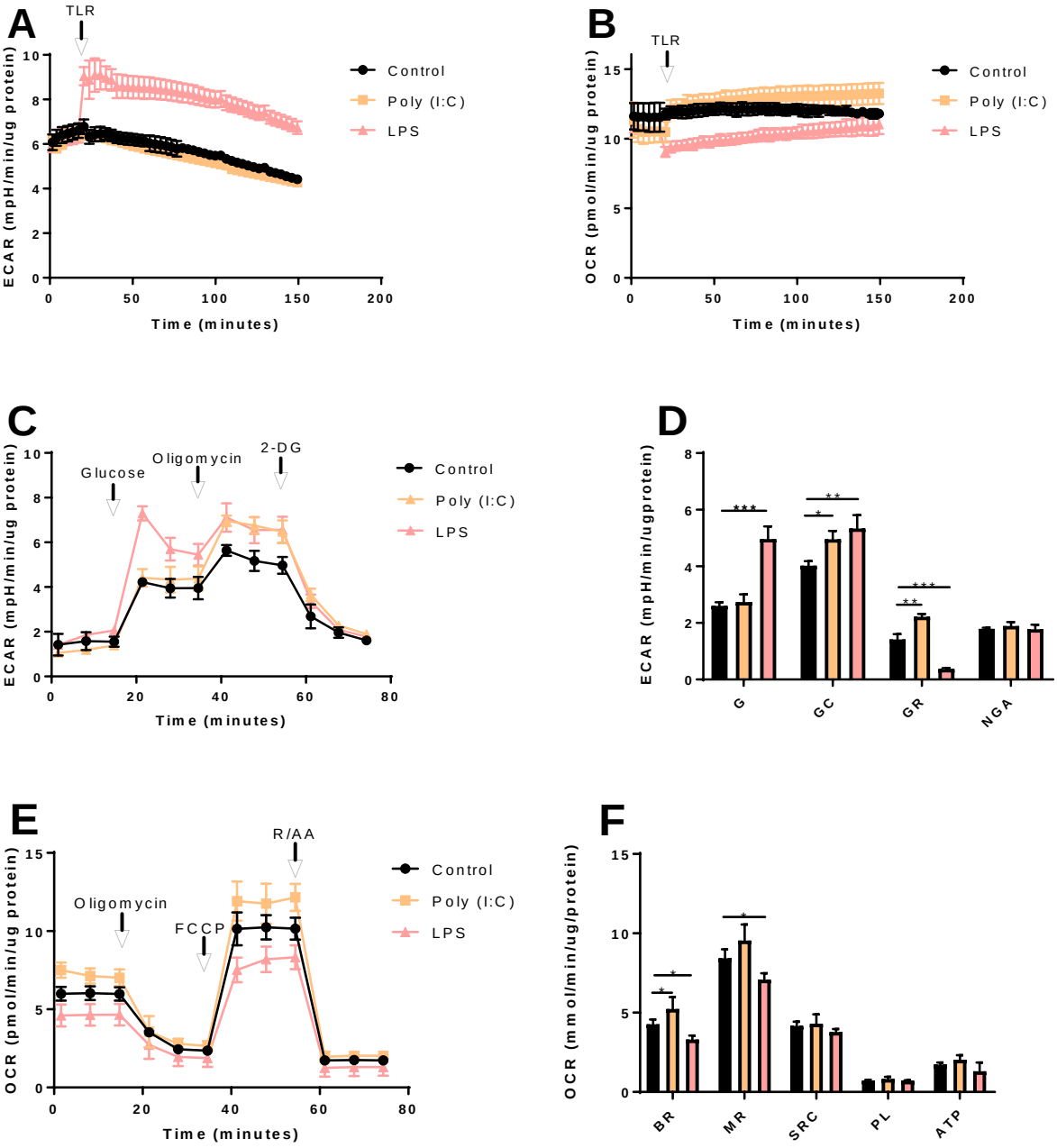
A
TLR
ECAR (mpH/min/ug protein)
Time (minutes)
Control
Poly (I:C)
LPS
B
TLR
OCR (pmol/min/ug protein)
Time (minutes)
Control
Poly (I:C)
LPS
C
Glucose
Oligomycin
2-DG
ECAR (mpH/min/ug protein)
Time (minutes)
Control
Poly (I:C)
LPS
D
ECAR (mpH/min/ugprotein)
G
GC
GR
NGA
E
Oligomycin
FCCP
R/AA
OCR (pmol/min/ug protein)
Time (minutes)
Control
Poly (I:C)
LPS
F
OCR (mmol/min/ug/protein)
BR
MR
SRC
PL
ATP

Figure 3.4. Toll-like receptor-3 and -4 agonists differentially modulate glycolysis and mitochondrial respiration in ARPE-19:

(A) Real-time changes in ECAR following injection of LPS (1µg/ml) or Poly (I:C) (10µg/ml). (B) Real-time changes in OCR following injection of LPS (1µg/ml) or Poly (I:C) (10µg/ml). (C) Representative glycolysis stress test measured with sequential injections of glucose, oligomycin and 2DG, following stimulation with LPS (30mins; 1µg/ml) or Poly (I:C) (24h; 10µg/ml). (D) Glycolysis parameters (G- glycolysis; GC- glycolytic capacity; GR- glycolytic reserve; NGA- non-glycolytic acidification) calculated from data shown in (C). (E) Representative mitochondrial stress test measured with sequential injections of Oligomycin, FCCP and rotenone/antimycin A, following stimulation with LPS (30mins; 1µg/ml) or Poly (I:C) (24h; 10µg/ml). (F) Mitochondrial parameters (BR- basal respiration; MR- maximal respiration; SRC- spare respiratory capacity; PL- proton leak; ATP- ATP-production) calculated from data shown in (E). Data presented as means ± SD, from two to three independent experiments performed in duplicate. (D and F) One-way ANOVA with Dunnet's multiple comparisons test, (G-H) Unpaired Student's T-test; *p<0.05, **p<0.01, ***p<0.005.

3.6. Glycolysis rate assay analysis of TLR-stimulated ARPE-19

A glycolysis rate assay was used to quantify the contribution of TCA cycle acidification to total ECAR. By subtracting the mitochondrial acidification from the total proton efflux rate (PER), a glycolytic PER (glycoPER) can be calculated to provide a more accurate quantification of lactate production by cells (see materials and methods). Following treatment of ARPE-19 with TLR agonists, it was observed that LPS stimulation lead to an increased glycoPER at basal levels, whilst both agonists increased glycoPER at compensatory levels (Fig. 3.5A-B). The mitoOCR/glycoPER ratio gives an indication of TCA activity within a cell, here it was identified that Poly (I:C)-stimulated ARPE-19 cells increased TCA activity (Fig. 3.5C). Furthermore, using both PER and glycoPER values, a percentage contribution of glycolysis and TCA acidification can be quantified. It was shown that LPS stimulated ARPE-19 had a greater percentage of PER from lactate production compared to a control, whereas Poly (I:C) treatment increased the percentage contribution from TCA acidification (Fig. 3.5D).

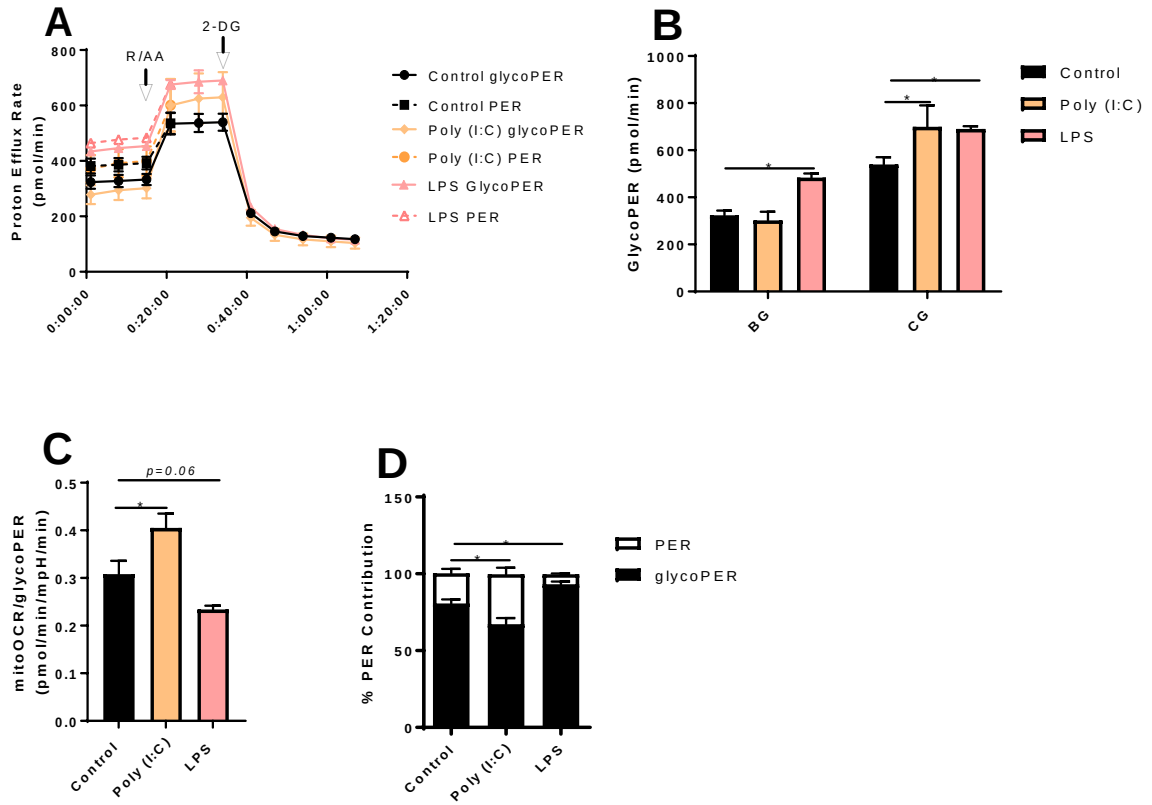

Figure 3.5. Glycolysis rate assay analysis of TLR-stimulated ARPE-19:

(A) Representative glycolysis rate assay measured with sequential injections of rotenone/antimycin A and 2DG, following stimulation with LPS (30min; 1µg/ml) or Poly (I:C) (24h; 10µg/ml). (B) Glycolysis rate parameters (BG- basal glycolysis; CG- compensatory glycolysis) calculated from (A). (C) Basal OCR and glycoPER measurements expressed as the ratio mitoOCR/glycoPER, following stimulation with LPS (30min; 1µg/ml) or Poly (I:C) (24h; 10µg/ml). Percentage contribution of glycolytic PER and non-glycolytic PER to total PER, following stimulation with LPS (30mins; 1µg/ml) or Poly (I:C) (24h; 10µg/ml). Data are expressed as means ± SD from two independent experiments performed in duplicate. One-way ANOVA with Dunnet's multiple comparisons test; *p<0.05, *p<0.01.

3.7. Effect of TLR agonists on primary murine RPE bioenergetics

To examine if the results obtained in ARPE-19 cells were truly indicative of the metabolic response of RPE to LPS and Poly (I:C), bioenergetic analysis was performed on primary cultured RPE. Basal OCR and ECAR measurements were taken pre and post injection of LPS and Poly (I:C) (Fig. 3.6A-B). It was observed that LPS treatment lead to a similar metabolic response to ARPE-19 cells, with a rapid increase of ECAR post-injection (Fig. 3.6A). This peaked at around 20min post injection of LPS and continued to fall until the end of the assay. LPS had no significant effect on the OCR post injection (Fig. 3.6B). Poly (I:C) stimulation had no significant effect on either OCR or ECAR measurements in the timeframe assessed (Fig. 3.6A-B). A mitochondrial stress test was used to further assess RPE OXPHOS parameters under stimulation of TLRs. Primary RPE cells were stimulated for 30min and 24h for LPS and Poly (I:C), respectively, based on time course data obtained using ARPE-19 in the previous chapter. It was observed that Poly (I:C) treatment had no significant effect on any parameters of mitochondrial respiration (Fig. 3.6C-D). LPS stimulation on the other hand, lead to a significant decrease in maximal respiration (post-injection of FCCP) and decreased spare respiratory capacity (Fig. 3.6C-D). The corresponding ECAR data of the mitochondrial stress test identified an increased glycolytic capacity of the RPE cells when stimulated with Poly (I:C) (Fig. 3.6E-F). LPS stimulation had no significant effect on glycolytic capacity (Fig. 3.6E-F). Primary RPE stimulated with Poly (I:C) for 24h had no significant changes in either OCR or ECAR measurements (Fig. 3.6C). RPE stimulated for 30min with LPS had a significantly reduced OCR/ECAR ratio.

Collectively, the data in this section indicates that primary murine RPE display a similar metabolic response to the human ARPE-19 cell line. LPS stimulation lead to increased glycolytic metabolism at the expense of mitochondrial capacity, suggesting a similar switch to aerobic glycolysis in these cells. LPS increased glycolysis for a shorter time period in primary murine RPE than ARPE-19 which may reflect fundamental differences in either metabolism or LPS sensitivity between the cells. Like ARPE-19 cells, Poly (I:C) stimulation of primary RPE was not accompanied by a switch to aerobic glycolysis. In contrast, no significant changes were observed to mitochondrial metabolism in Poly (I:C)-stimulated RPE compared to ARPE-19. There was however increased glycolytic capacity observed in both cell types. LMW Poly (I:C) stimulation of primary RPE was not assessed.

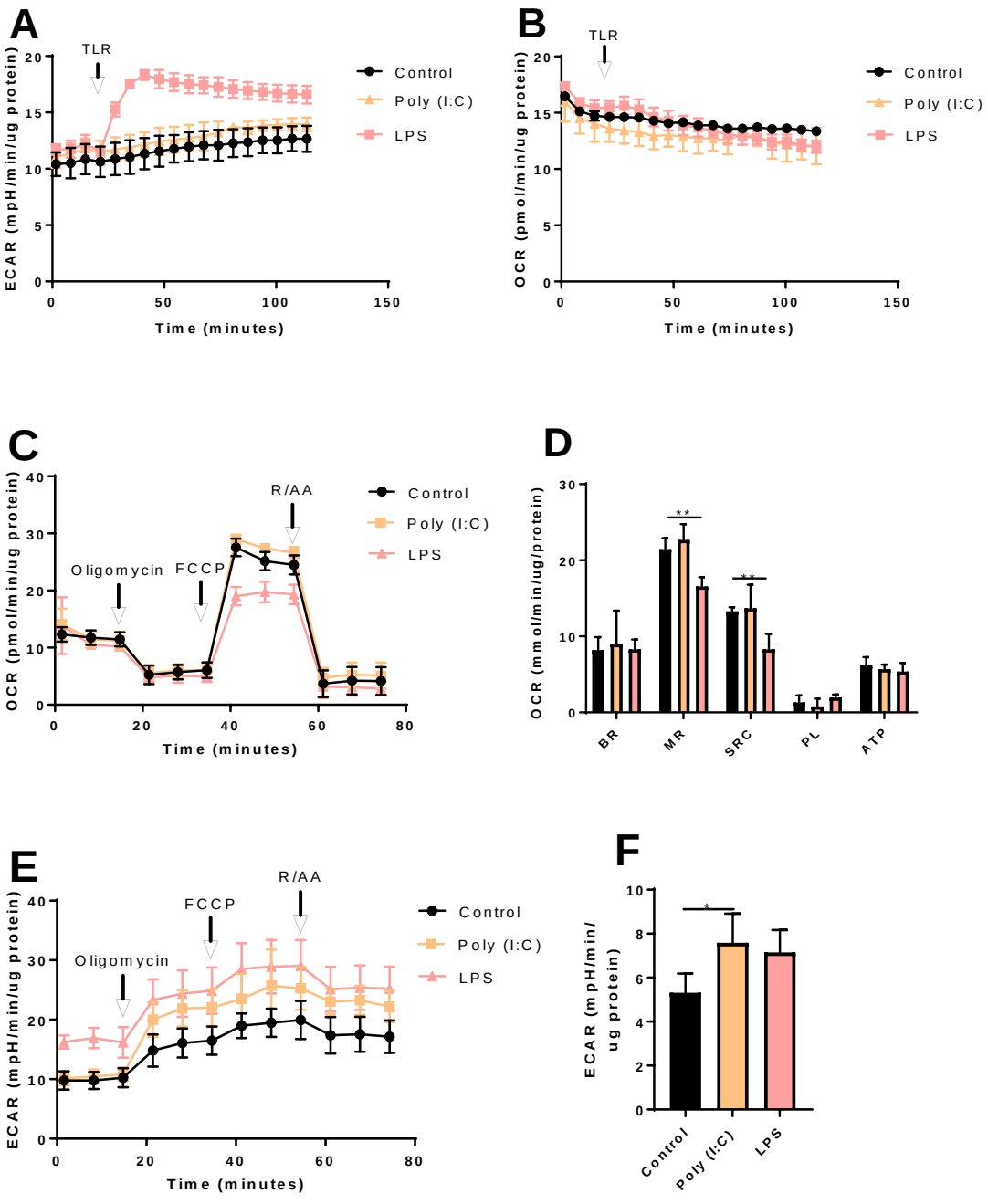
A
TLR
ECAR (mpH/min/ug protein)
Time (minutes)
Control
Poly (I:C)
LPS
B
TLR
OCR (pmol/min/ug protein)
Time (minutes)
Control
Poly (I:C)
LPS
C
Oligomycin
FCCP
R/AA
OCR (pmol/min/ug protein)
Time (minutes)
Control
Poly (I:C)
LPS
D
OCR (mmol/min/ug/protein)
**
**
BR
MR
SRC
PL
ATP
E
Oligomycin
FCCP
R/AA
ECAR (mpH/min/ug protein)
Time (minutes)
Control
Poly (I:C)
LPS
F
*
ECAR (mpH/min/ug protein)
Control
Poly (I:C)
LPS

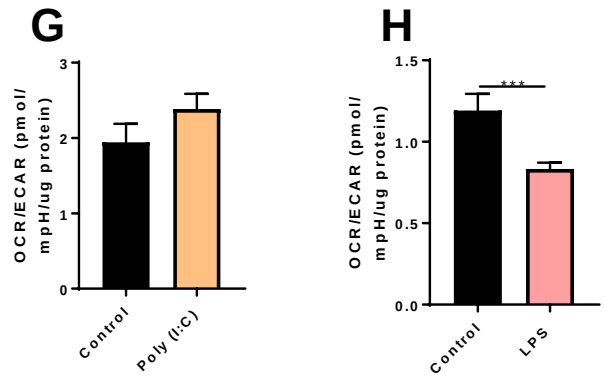

Figure 3.6. Effect of TLR agonists on primary murine RPE bioenergetics:

(A) Real-time changes in ECAR following injection of LPS (1µg/ml) or Poly (I:C) (10µg/ml). (B) Real-time changes in OCR following injection of LPS (1µg/ml) or Poly (I:C) (10µg/ml). (C) Representative mitochondrial stress test measured with sequential injections of Oligomycin, FCCP and rotenone/antimycin A, following stimulation with Poly (I:C) (24h; 10µg/ml) or LPS (30min; 1 µg/ml). (D) Mitochondrial parameters (BR- basal respiration; MR- maximal respiration; SRC- spare respiratory capacity; PL- proton leak; ATP- ATP-production) calculated from data shown in (C). (E) ECAR data from (C). (F) Glycolytic capacity calculated from (E). Basal OCR and ECAR measurements expressed as the ratio OCR/ECAR, (G) following 24h Poly (I:C) treatment (10µg/ml) or (H) 30mins LPS (1µg/ml). Data are expressed as means ± SD. (A-F) represents data from two independent experiments performed in duplicate. (G-H) represents data from two independent experiments performed in triplicate. Unpaired Student's T-test; ***p<0.001.

3.8. Poly (I:C) stimulation of ARPE-19 under hypoxia increases glycolysis

The photoreceptors are the most energy demanding cell within the retina, requiring full metabolic support from the RPE which receives 100% of the oxygen and nutrients from the choriocapillaris [382]. Glucose from the choroid fuels the whole retina, but must first cross the RPE for utilisation in photoreceptors [4]. Hypoxia is defined as a loss of oxygen supply from tissues. Initiation of hypoxia-induced metabolic stress in RPE is enough for the atrophy of photoreceptors, as glucose is utilised as an RPE fuel source rather than transported to the photoreceptors [382]. Inflammation and hypoxia exhibit a mutual dependence, with hypoxia-prompted inflammation, or inflammation during hypoxic conditions implicated in a range of human inflammatory diseases [460]. Contributors to tissue hypoxia during inflammation comprise of an increase in the metabolic demands of cells and increased cellular presence which therefore leads to a reduction in metabolic substrate abundance [461]. Additionally, replication of bacterium and multiplication of intracellular host pathogens can withdraw oxygen from infected cells [461]. Considering this, it is plausible that the initiation of inflammation in the retina would likely lead to a hypoxic retinal environment, with the RPE forced to utilize glycolytic consumption of glucose as opposed to mitochondrial OXPHOS. It therefore was of interest to see if the metabolic response to TLR-3 activation in the absence of oxygen would require increased aerobic lactate production instead of "coupling" glucose catabolism to the TCA cycle (as suggested from results in the previous sections).

ARPE-19 cells were cultured under hypoxic conditions for 24h. Hypoxia conditions in these experiments were 1% O_2, 94% N_2, and 5% CO_2 (as detailed in materials and methods). In order to first confirm hypoxia-induced metabolic stress, AMPK activation state was assessed in cell lysates. AMPK is an evolutionarily conserved energy sensor which responds to energetic stress through changes in AMP concentration (see section 1.8.5.3). During oxygen scarcity, restrictions in mitochondrial respiration lead to a decrease in the ATP/AMP ratio, which subsequently induce AMPK activation [462]. Western botting confirmed AMPK activation from control and treatment under hypoxia (Fig. 3.7A). In response to AMPK activation, cells up-regulate ATP generating pathways such β-oxidation, glycolysis and glucose uptake [344]. Hypoxia treatment significantly increased glycolytic metabolism in ARPE-19 cells (Fig. 3.7B-C). Both glycolysis and glycolytic capacity were significantly increased in response to hypoxia (Fig. 3.7B-C). Glycolytic reserve was significantly reduced (Fig. 3.7B-C), indicating cells had reduced oxidative glucose catabolism in the TCA.

ARPE-19 cells were stimulated with Poly (I:C) under hypoxia for 24h. It was found that AMPK (and its downstream activation target ACC) continued to retain their phosphorylation under stimulation of TLR-3 (Fig. 3.7A). The increased ECAR and lactate output following treatment indicates Poly (I:C)-stimulated cells metabolize pyruvate through LDHA in absence of oxygen (Fig. 3.7D-E). Interestingly, hypoxia treatment alone was unable to up-regulate basal ECAR or lactate output in ARPE-19 (Fig. 3.7D-E).

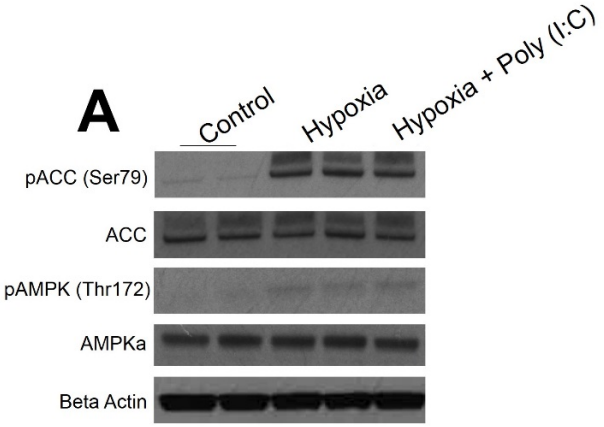
A
Control
Hypoxia
Hypoxia + Poly (I:C)
pACC (Ser79)
ACC
pAMPK (Thr172)
AMPKa
Beta Actin

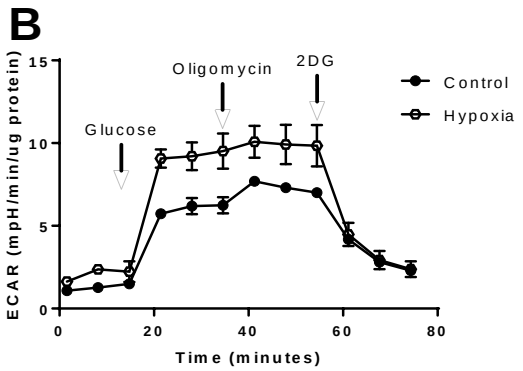
B
Glucose
Oligomycin
2DG
Control
Hypoxia
ECAR (mpH/min/ug protein)
Time (minutes)

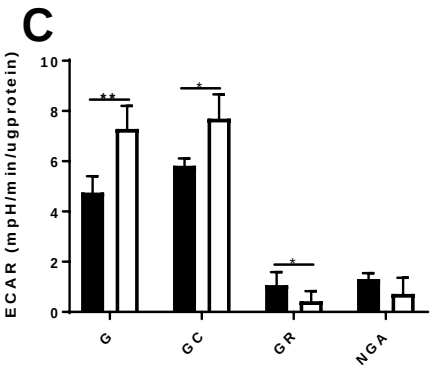
C
ECAR (mpH/min/ugprotein)
G
GC
GR
NGA

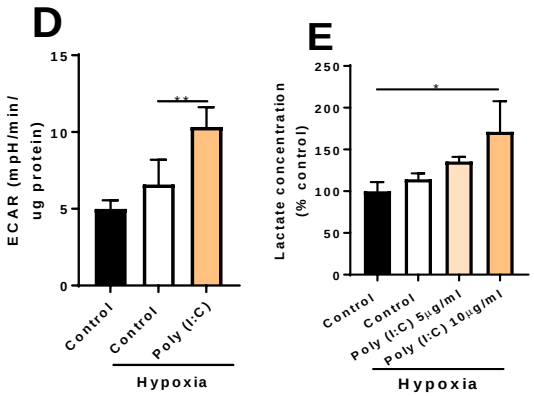
D
ECAR (mpH/min/ ug protein)
Control
Control
Poly (I:C)
Hypoxia
E
Lactate concentration (% control)
Control
Control
Poly (I:C) 5µg/ml
Poly (I:C) 10µg/ml
Hypoxia

Figure 3.7. Poly (I:C) stimulation of ARPE-19 under hypoxia increases glycolysis:

(A) ARPE-19 were treated with Poly (I:C) (10µg/ml) for 24h under 1% O_2; western blot analysis was used to determine the phosphorylation of AMPK and ACC following treatment. (B) Representative glycolysis stress test measured with sequential injections of glucose, oligomycin and 2DG following treatment of ARPE-19 for 24h under 1% O_2. (C) Glycolysis parameters (G- glycolysis; GC- glycolytic capacity; GR- glycolytic reserve; NGA- non-glycolytic acidification) calculated from data shown in (B). ARPE-19 were treated with Poly (I:C) (10µg/ml) for 24h under 1% O_2. (D) Basal ECAR measurements. (E) Extracellular lactate measurements were taken in the media and expressed as a percentage of the control. Data are expressed as means ± SD from two independent experiments performed in duplicates. (B) One-way ANOVA with Dunnet's multiple comparisons test, (C) One-way ANOVA with Tukey's multiple comparisons test; $^{**}p<0.01$.

3.9. Metabolic response of Müller glia and mast cells to TLR stimulation

To determine if the TLR-induced metabolic changes in RPE were cell specific, BMMCs and MIO-M1 Müller glial cells were used as comparators. Mast cells are key effector innate immune cells well known for their roles in allergic inflammation, but additionally play a key role in innate immune defence against pathogens; mast cells have a robust expression of functional TLRs observed [463]. Müller glia cells are the principle glial cell within the retina and contribute to innate immune defence *via* an expression of TLRs 2-6 [464]. These cells were used to compare the immediate metabolic responses of TLR activation in the RPE. The use of both an innate immune cell and a tissue-resident innate immune competent cell (like the RPE) provided excellent systems for studying the responses.

In a similar fashion to the RPE, MIO-M1 Müller glial cells displayed increased ECAR post-injection of LPS, but not Poly (I:C) (Fig. 3.8A). No significant changes to the OCR was observed with either agonist (Fig. 3.8B). BMMC increased ECAR with the injection of LPS and Poly (I:C) (Fig. 3.8C), OCR was also found to be increased with LPS, but not Poly (I:C) (Fig. 3.8D).

These results indicate the varied metabolic responses of cells to innate immune stimulation. Like the RPE, Müller glial cells display a similar immediate response to TLR-4 activation. TLR-3 activation was not accompanied by any metabolic changes. Longer-term Poly (I:C) treatment was observed to increase OXPHOS in the RPE, yet I did not investigate this response in Müller glia. Mast cells displayed an immediate metabolic response contrasting both the RPE and Müller glia. This may reflect core differences in the requirement of innate immune cells (such as mast cells) to respond rapidly to pathogens.

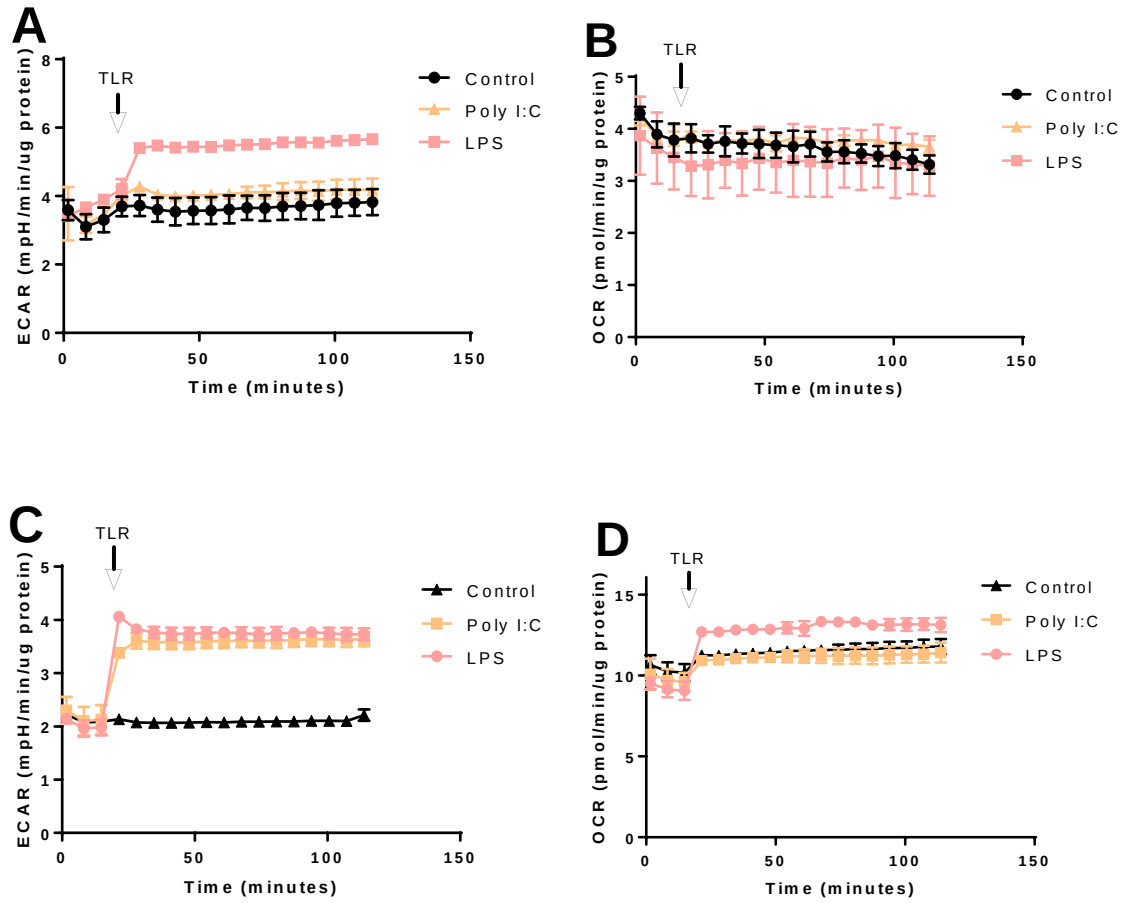

Figure 3.8. Metabolic response of Müller glia and BMMC to TLR stimulation:

Real-time ECAR (A) and OCR (B) measurements following injection of LPS (1µg/ml) or Poly (I:C) (10µg/ml) to MIO-M1. Real-time ECAR (C) and OCR (D) measurements following injection of LPS (1µg/ml) or Poly (I:C) (10µg/ml) to BMMC. Data are expressed as means ± SD from two independent experiments performed in duplicates.

3.10. Glycolysis is essential for TLR-mediated cytokine production

The data presented to this point has indicated that glycolytic metabolism is enhanced following stimulation of RPE cells with TLR-agonists. As suggested in previous studies, enhancing glycolysis rapidly provides ATP for cytokine production and cell effector functions. It was therefore of interest to determine whether glycolysis was necessary for inflammatory responses in the RPE and if impairment or forcing RPE cells to utilize other carbon sources would impair their cytokine production.

ARPE-19 cells were cultured in either (A) media without glucose, (B) without glucose but supplemented with lactate (a suppressor of glycolysis [465]) or (C) control media containing the hexokinase inhibitor 2DG. Cells were stimulated with either Poly (I:C) or LPS and innate immune responses were quantified through the output of inflammatory cytokines IL-1β and IL-6. As expected, treatment with Poly (I:C) and LPS elicited a robust expression of IL-1β and IL-6 (Fig. 9). Blocking glycolysis *via* any of the three described strategies significantly impaired the production of IL-1β and IL-6 (Fig. 9).

Taken together, this data indicates the requirement of glycolysis for efficient innate immune responses. Blocking the pathway with 2DG and depriving cells of glucose significantly reduces inflammatory responses. In addition to this, replacement of glucose with lactate (a metabolite readily converted to pyruvate) was unable to fully restore cytokine levels to that of stimulated cells in glucose-containing media.

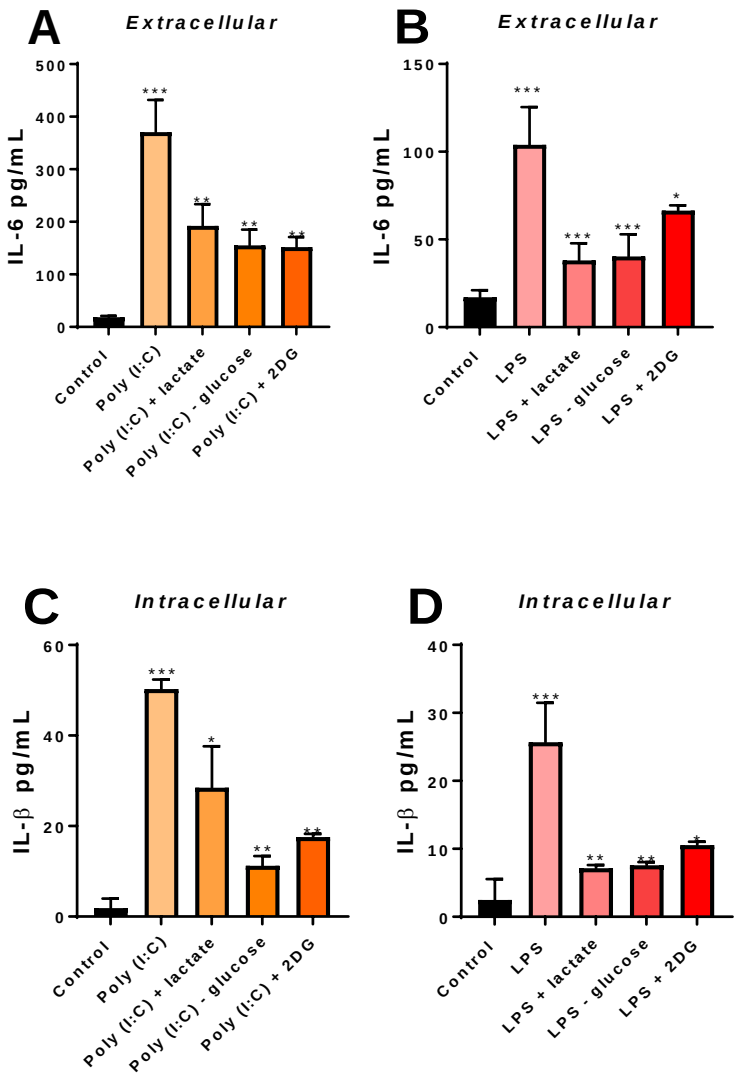

Figure 3.9. Glycolysis is essential for TLR-mediated cytokine production

ARPE-19 cells were treated for 24h with Poly (I:C) (10µg/ml) in either control media (25mM glucose), glucose-free media, glucose-free media with 25mM lactate or control media with 2DG (2.5mM). Cell culture supernatants were assessed for IL-6 release (A) and cell lysates were assessed for IL-1β (C). ARPE-19 cells were treated for 24h with LPS (1µg/ml) in either control media (25mM glucose), glucose-free media, glucose-free media with 25mM lactate or control media with 2DG (2.5mM). Cell culture supernatants were assessed for IL-6 release (B) and cell lysates were assessed for IL-1β (D). One-way ANOVA with Tukey's multiple comparisons test, * $p<0.05$, ** $p<0.01$, *** $p<0.001$.

3.11. TLR stimulation alters glucose consumption, transcriptional programs and the ATP/ADP ratio

Having established that TLR-stimulation enhances glycolysis (and is required for cytokine production), it was essential to confirm these results using a variety of additional *in vitro* assays and assessing the effects on the ARPE-19 transcriptome.

Glucose consumption was measured in the media of ARPE-19 and was observed to increase following TLR-stimulation (Fig. 3.10A). Considering the rapid switch to aerobic glycolysis with LPS treatment (observed using extracellular flux in the previous sections), it was logical to investigate the expression status of HIF-1α. HIF-1α is a master regulator of oxygen homeostasis, switching glucose metabolism from OXPHOS to glycolysis under low oxygen tensions. Normally HIF-1α is activated in response to hypoxia but can be induced by TLR stimulation in innate immune cells to reprogram their metabolism [466]. In response to LPS treatment, but not Poly (I:C), HIF-1α expression was observed to increase (Fig. 3.10B-C). Hypoxia treatment alone was used as a positive control (Fig. 3.10B-C). QPCR analysis identified increased glycolytic enzyme and GLUT1 expression in TLR-stimulated ARPE-19, however only Poly (I:C) increased the expression of TCA enzymes (Fig. 3.10D). Additionally, transcripts of metabolic regulators *HIF1α, PGC1α* and *MYC* were assessed. It was observed that Poly (I:C) treatment on the gene expression of any of these targets (Fig. 3.10D). LPS treatment significantly reduced the expression of *PGC1α* transcripts and increased the expression of *MYC* (Fig. 3.10D). This appears to fit with the hypothesis that LPS treatment increases glycolysis at the expense of OXPHOS, with PGC-1α promoting oxidative metabolism and mitochondrial biogenesis in cells [36], and MYC promoting the Warburg effect in cancer cells [467]. To confirm changes in transcription preceded translation of these key enzymes, western blotting was used to confirm the expression of three key targets, GLUT1, pyruvate carboxylase and PKM2. Comparable results were found, with Poly (I:C) treatment increasing GLUT1 and pyruvate carboxylase expression (Fig. 3.10E). LPS increased PKM2 at the protein level, supporting transcriptional changes (Fig. 3.10E). LPS additionally increased GLUT1 expression, suggesting that an increase of *GLUT1* mRNA may have been observed prior to the 24h time point assessed. Previously published results in macrophages showed that LPS treatment lead to a decreased ATP/ADP ratio, as there is a switch away from mitochondrial ATP production to glycolytic ATP production [468]. Consistent with these results, LPS treatment decreased the ATP/ADP ratio in ARPE-19 (Fig. 3.10G). Poly (I:C) treatment had no significant effect on the ATP/ADP ratio (Fig. 3.10G).

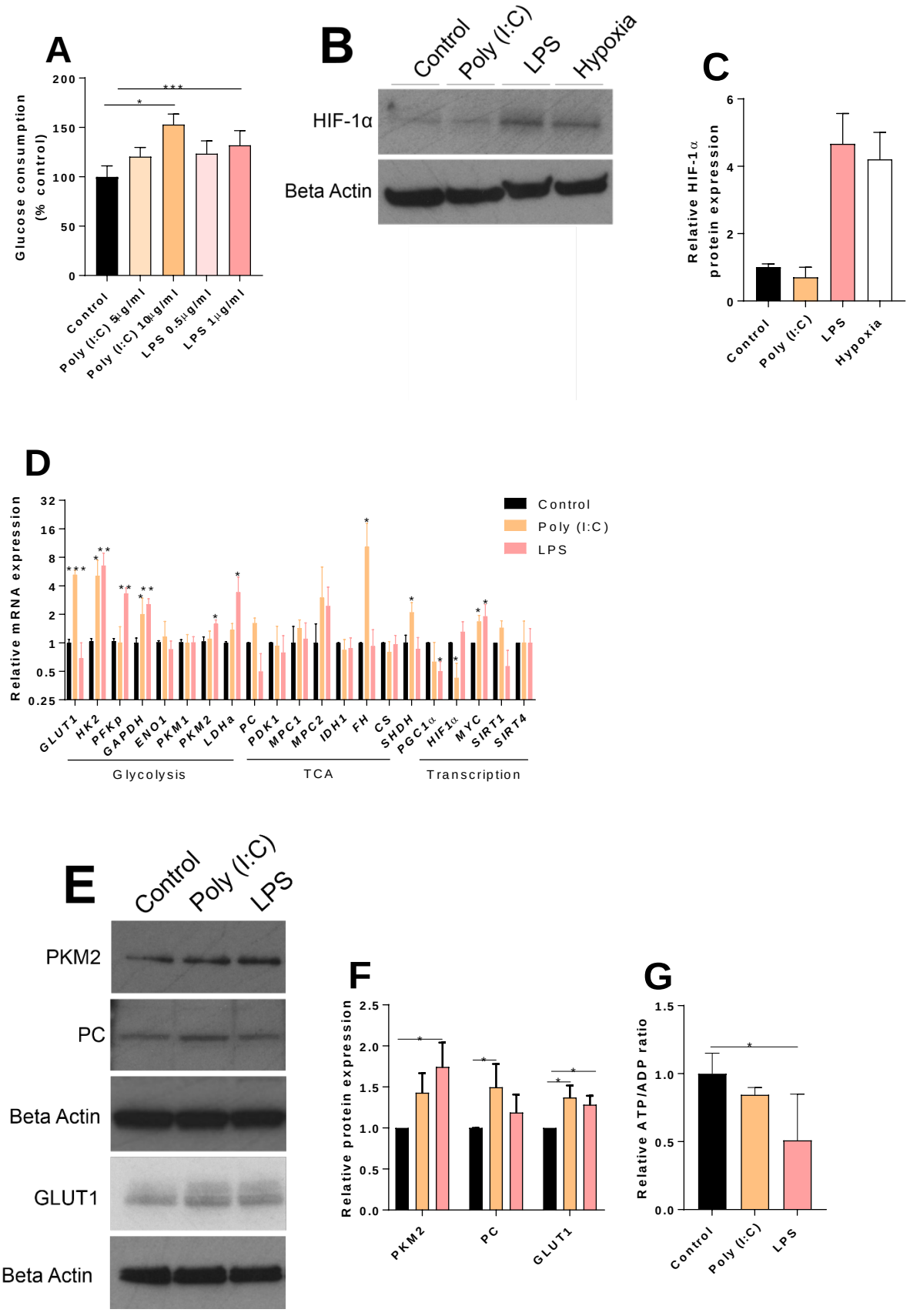
A
Glucose consumption (% control)
200
150
100
50
0
*
***
Control
Poly (I:C) 5μg/ml
Poly (I:C) 10μg/ml
LPS 0.5μg/ml
LPS 1μg/ml
B
Control
Poly (I:C)
LPS
Hypoxia
HIF-1α
Beta Actin
C
Relative HIF-1α protein expression
6
4
2
0
Control
Poly (I:C)
LPS
Hypoxia
D
Relative mRNA expression
32
16
8
4
2
1
0.5
0.25
Control
Poly (I:C)
LPS
GLUT1
HK2
PFKp
GAPDH
ENO1
PKM1
PKM2
LDHa
PC
PDK1
MPC1
MPC2
IDH1
FH
CS
SHDH
PGC1α
HIF1α
MYC
SIRT1
SIRT4
Glycolysis
TCA
Transcription
E
Control
Poly (I:C)
LPS
PKM2
PC
Beta Actin
GLUT1
Beta Actin
F
Relative protein expression
2.5
2.0
1.5
1.0
0.5
0.0
PKM2
PC
GLUT1
G
Relative ATP/ADP ratio
1.5
1.0
0.5
0.0
Control
Poly (I:C)
LPS

Figure 3.10. TLR-stimulation alters glucose consumption, transcriptional programs and the ATP/ADP ratio:

ARPE-19 cells were treated for 24h with Poly (I:C) (10μg/ml) or LPS (1μg/ml). (A) Supernatants were assessed for relative glucose consumption. (B) HIF-1α protein expression was assessed using western blotting. (C) Relative densitometry of (B). (D) Quantitative RT-PCR of glycolytic pathway enzymes (*HK, LDHA, PFKp, GAPDH, PKM1, PKM2* and *ENO1*), *GLUT1*, *PDK1*, *MPC1*, *MPC2* TCA cycle enzymes (*PC, IDH, FH, SDHD* and *CS*), *PGC1α, HIF1α, MYC, SIRT1* and *SIRT4* mRNA transcripts. (E) PKM2, pyruvate carboxylase and GLUT1 expression were assessed using western blotting. (F) Densitometry analysis of (E). (G) ATP and ADP levels were quantified following cell lysis and expressed as the ratio ATP/ADP. Data are expressed as means ± SD from (B-C) two and (A and D-G) three independent experiments performed in duplicate. One-way ANOVA with Dunnet's multiple comparisons test; *p<0.05, **p<0.01, ***p<0.005, ***p<0.001.

3.12. The immediate glycolytic switch following LPS stimulation is dependent on PDK1-mediated PDH inactivation

I next investigated the mechanisms involved in mediating the pronounced metabolic response to LPS stimulation in RPE cells. The PDH complex is responsible for the oxidative metabolism of pyruvate to acetyl-CoA for entry into the TCA cycle; PDH is inactivated *via* PDH-kinase-1 (PKD1) which phosphorylates of a highly conserved serine residue (Ser293) on the E1 subunit [469]. It was hypothesised that LPS treatment may lead to the phosphorylation (and therefore inactivation) of PDH, thus preventing mitochondrial pyruvate oxidation. As expected, LPS treatment increased the phosphorylation of PDH (Fig. 3.11A-B). To investigate whether PDK1 was required for the glycolytic response, in RPE cells, the inhibitor potassium dichloroacetate was used to inhibit PDK1 activity prior to TLR-4 activation. Potassium dichloroacetate incubation inhibited the increase in ECAR following LPS stimulation in RPE cells (Fig. 3.11C-D). Interestingly, potassium dichloroacetate treatment lead to a compensatory increase in OCR following LPS treatment (Fig. 3.11E-F), suggesting that mitochondrial pyruvate oxidation occurs in the absence of PDH inhibition. Collectively, these results support the hypothesis that LPS-treated cells divert pyruvate into lactate production rather than its oxidative metabolism.

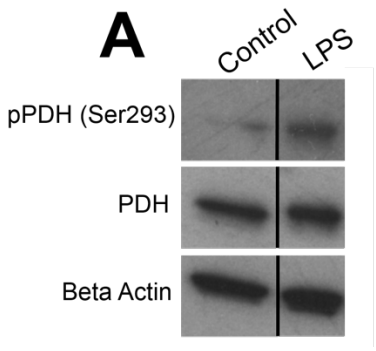
A
Control
LPS
pPDH (Ser293)
PDH
Beta Actin

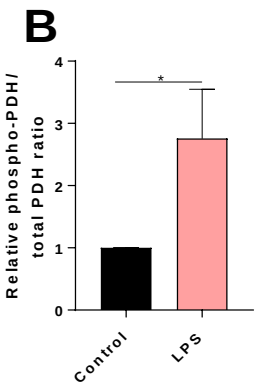
B
Relative phospho-PDH/ total PDH ratio
0
1
2
3
4
*
Control
LPS

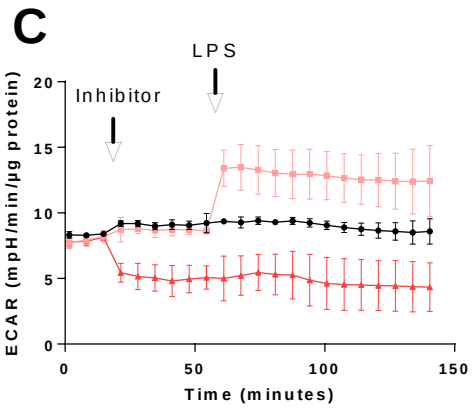
C
LPS
Inhibitor
ECAR (mpH/min/µg protein)
0
5
10
15
20
0
50
100
150
Time (minutes)

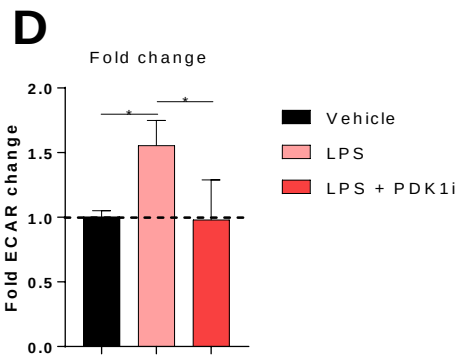
D
Fold change
Fold ECAR change
0.0
0.5
1.0
1.5
2.0
*
*
Vehicle
LPS
LPS + PDK1i

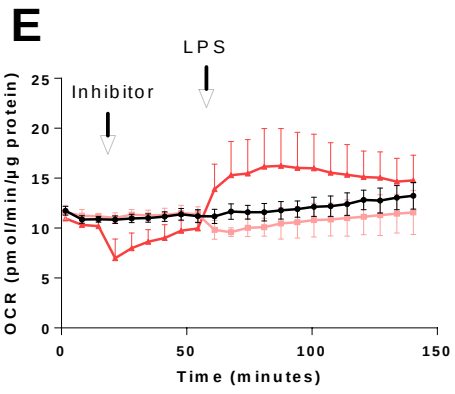
E
LPS
Inhibitor
OCR (pmol/min/µg protein)
0
5
10
15
20
25
0
50
100
150
Time (minutes)

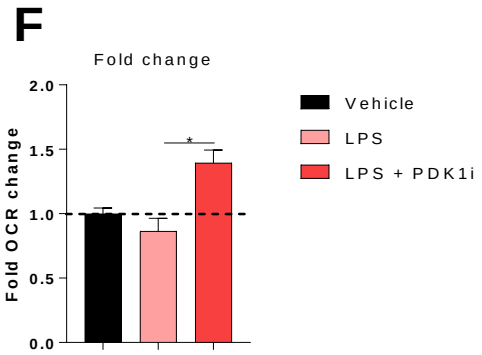
F
Fold change
Fold OCR change
0.0
0.5
1.0
1.5
2.0
*
Vehicle
LPS
LPS + PDK1i

Figure 3.11. The immediate glycolytic switch following LPS stimulation is dependent on PDK1-mediated PDH inactivation:

(A) ARPE-19 cells were treated for 2h with LPS (1μg/ml). Western blot analysis was used to determine the phosphorylation of pyruvate dehydrogenase. Black line indicates that samples were run on the same gel but were discontinuous. (B) Reprehensive densitometry from (A). (C) Real-time changes in ECAR following injection of DCA (PDKi; 20mM) and following injection of LPS (1μg/ml) to ARPE-19 cells. (D) Fold-ECAR change calculated from (C). (E) Real-time changes in OCR following injection of DCA (PDKi; 20mM) and following injection of LPS (1μg/ml) to ARPE-19 cells. (F) Fold-OCR change calculated from (E). Data are expressed as means ± SD from three independent experiments performed in duplicate. (A-C) One-way ANOVA with Dunnet's multiple comparisons test; *p<0.05, **p<0.01, ***p<0.005, ***p<0.001.

3.13. Mass spectroscopy-based metabolomics in TLR stimulated ARPE-19

To further confirm the differential bioenergetic adaptations to the RPE to TLR stimulation, I used a GC-MS approach to quantify total intracellular metabolites. This was carried out in collaboration with Dr. Emma Vincent (University of Bristol, UK) and the Metabolomics Core Facility (McGill University, Canada) to generate Fig 3.13.

SITA with [U-^{13}C]-glucose was used to assess the uptake of isotopically labelled glucose into metabolite pools following treatment with both TLR agonists. This approach allowed the quantification of C^{13} labelling into metabolite pools as cells approach steady-state equilibrium (schematic in Fig. 3.12.)

Cells were treated for with both Poly (I:C) and LPS for 24h and 2h respectively (as these were pre-optimised time points, at which significant effects on RPE metabolism were observed on the XF platform), followed by 2h of culture in [U-^{13}C]-glucose. Relative concentrations of C^{13}-labelled glyceraldehyde-3-phosphate, 3-phosphoglycerate, pyruvate and lactate were increased following LPS and Poly (I:C) treatment, suggesting increased glycolytic flux (Fig. 3.13A-D). LPS and Poly (I:C) treatment significantly increased the incorporation of glucose-derived carbon into TCA metabolites, including citrate (Fig. 3.13E), glutamate (Fig. 3.13G), succinate (Fig. 3.13H), fumarate (Fig. 3.13I), malate (Fig. 3.13J), oxaloacetate (Fig. 3.13K), and aspartate (Fig. 3.13L). No significant C^{13} enrichment was observed in α-ketoglutarate, regardless of treatment (Fig. 3.13F).

Collectively, these data indicate that TLR-stimulated cells increase the flux of glucose through the glycolytic pathway, indicated by increased C^{13} labelling in glycolytic intermediates. Furthermore, the relative abundance of unlabelled C^{12} intermediates of fumarate, succinate, aspartate and glutamate substantially increased with Poly (I:C) treatment, suggesting other fuels may contribute to these metabolite pools (Fig. 3.13G, H, I and L).

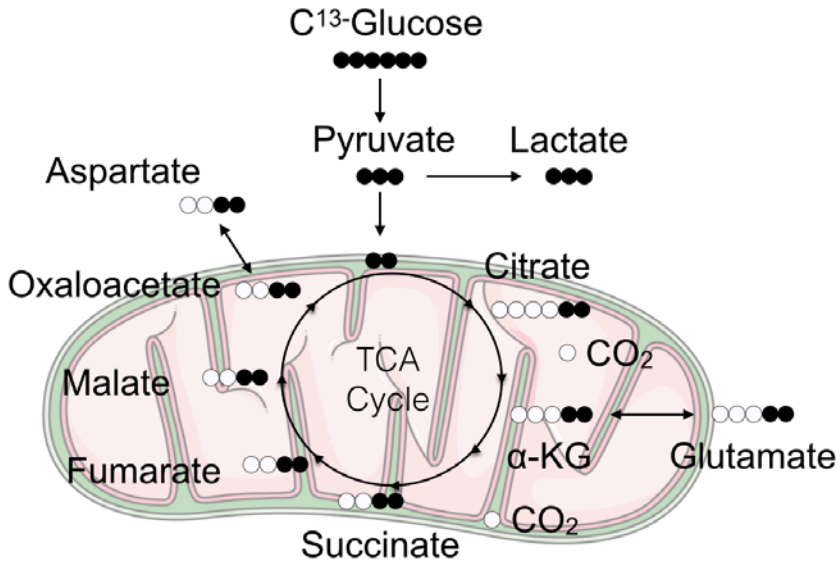

Figure 3.12. Schematic of glucose metabolism in the first turn of the TCA cycle

Glucose is taken up by cells and converted to pyruvate *via* a series of reactions termed glycolysis. Pyruvate is a key intersection in the network of metabolic pathways and has many fates including: transamination to form the amino acid alanine, cytosolic oxidation into lactate and mitochondrial oxidation into acetyl-coA *via* a loss of one carbon molecule as CO_2. The mitochondrial citric acid cycle utilizes the oxidation of pyruvate in the form of "bond energy" in the formation of NADH and $FADH_2$ which is used to make ATP in the ETC. Acetyl-coA combines with a four-carbon acceptor molecule oxaloacetate to form the six-carbon citrate. Citrate is converted to its isomer isocitrate and is then oxidized to yield CO_2 and a five-carbon metabolite α-ketoglutarate. α-ketoglutarate is then oxidized, releasing CO_2 and yielding the four-carbon succinate. In the fifth step, succinate is oxidized to form fumarate (a step yielding reduced FAD). Fumarate is then converted into malate *via* the nucleophilic addition of H_2O. In the final step of the citric acid cycle, oxaloacetate (the primary starting molecule) is regenerated *via* the oxidation of malate and reduction of NAD. An aminotransferase reaction takes place to convert oxaloacetate into aspartate for use in the malate-aspartate shuttle.

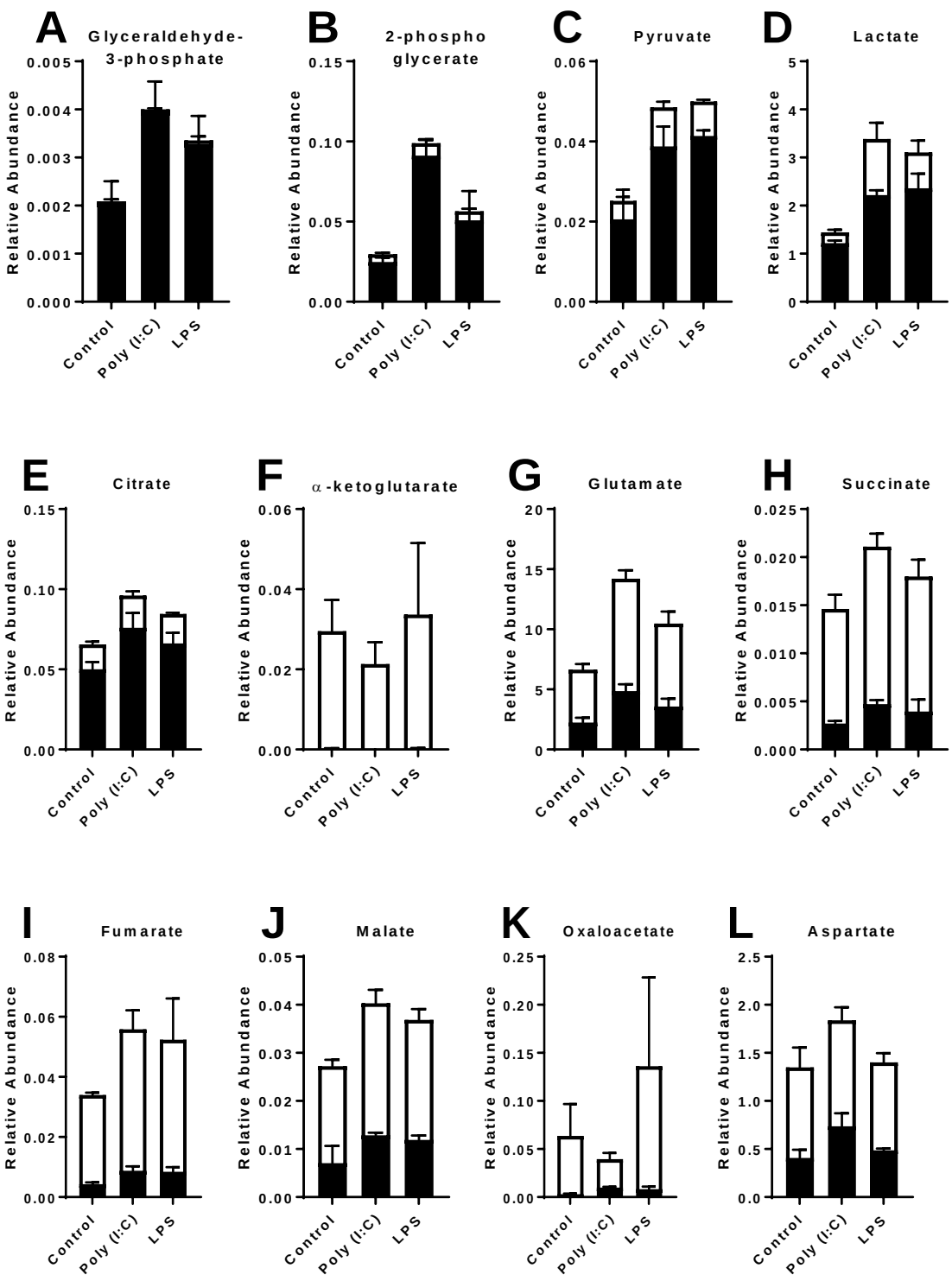
A
Glyceraldehyde-3-phosphate
B
2-phospho glycerate
C
Pyruvate
D
Lactate
E
Citrate
F
α-ketoglutarate
G
Glutamate
H
Succinate
I
Fumarate
J
Malate
K
Oxaloacetate
L
Aspartate
Relative Abundance
Control
Poly (I:C)
LPS

Figure 3.13. Glucose tracing in TLR-stimulated ARPE-19:

Cells were treated with Poly (I:C) (10µg/ml; 24h) or LPS (1µg/ml; 2h). Cells were incubated for 2h with media containing isotopically labelled glucose and GC-MS was used to quantify relative C^{13} (black) or C^{12} (white) incorporation into glyceraldehyde-3-phosphate (A), 3-phosphoglycerate (B), pyruvate (C), lactate (D), citrate (E), α-ketoglutarate (F), glutamate (G), succinate (H), fumarate (I), malate (J), oxaloacetate (K) and aspartate (L) metabolite pools. Represents data from three independent experiments.

3.14. Mitochondrial changes in TLR stimulated ARPE-19

Results from the previous sections indicate that TLR stimulation of RPE cells initiate metabolic reprogramming. LPS stimulation initiates aerobic glycolysis, whereas Poly (I:C) stimulation increases mitochondrial OXPHOS. Considering these observations, I further interrogated the changes to mitochondria which occur under innate immune activation. Mitochondria are hubs of metabolic activity, antiviral responses and cell death cascades which continually remodel their structure *via* nuclear GTPases to facilitate cell processes [470]. Dynamic changes in mitochondrial remodelling are acutely responsive to changes in cell metabolism [471] yet the impact of morphological changes on metabolic pathway utilisation have not been studied in great depth [472]. Generally, a deletion of any of the fission/fusion machinery impacts OXPHOS and glycolysis under basal conditions [473]. To investigate whether metabolic changes following TLR stimulation were accompanied with alterations to the RPE mitochondrial structure, samples were studied by transmission electron microscopy. This was carried out in collaboration with Dr. Chris Neal (University of Bristol, UK) who provided data shown in Figures 3.14A-E.

ARPE-19 cells were treated for the indicated time points with LPS or Poly (I:C), followed by fixation and imaging. It was observed that stimulation with Poly (I:C) increased mitochondrial size relative to an unstimulated control (Figs 3.14A and D). Similarly, LPS treatment increased RPE mitochondrial size (Fig. 3.14C-D). After treatment with both agonists, it was evident there were changes in the mitochondrial morphologies. Unstimulated cells showed mostly fragmented mitochondria (~77.5%) and short tubular mitochondria (~20%), long tubular mitochondria were observed at a low frequency (~2.5%) (Fig. 3.14E). When cells were stimulated with either Poly (I:C) or LPS there was shift in the morphologies, with decreased fragmented mitochondria, and an increase in long and short tubular mitochondria observed (Fig. 3.14E). The increased mitochondrial size and elongation suggested that mitochondrial fission and fusion processes were affected by TLR stimulation. Mitochondrial fission generates individual fragmented mitochondria which facilitate mitophagy [474], autophagy [475] and boost cell proliferative capacity [476]. “Fissed” mitochondria typically favour increased ROS production [477]. Mitochondrial fission is typically mediated by dynamin-related protein 1 (DRP1) which upon activation, scissions mitochondria at the outer membrane [472]. Mitochondrial fusion, and elongation into tubular networks, increases interactions between mitochondria and the endoplasmic reticulum to provide intercommunication during Ca^{2+} signalling [478]. Mitochondria elongation is initiated in response to nutrient stress to increase ATP synthase dimerization and activation under starvation [479]. Generally, oxidative metabolism stimulates elongation of

mitochondria to facilitate the assembly of quaternary respiratory chain super-complexes which maximize ETC activity [471, 472, 480]. Modulation of cristae remodelling dramatically affects RCS activity and respiratory-dependent growth [481]. Outer mitochondrial membrane (OMM) fusion is mediated by mitofusin-1 and -2 (MFN1/2), whereas inner mitochondrial membrane fusion is mediated by OPA1. PTEN-induced kinase 1 (PINK-1) has a key role in the regulation of mitophagy, whereby damaged and dysfunctional mitochondria are removed [482]. The transcription of nuclear-encoded mitochondrial fission/fusion enzymes was assessed by RT-PCR in LPS and Poly (I:C)-stimulated cells. Poly (I:C) treatment led to an increased expression of pro-fusion *MFN1*, *MFN2*, *OPA1* mRNA transcripts (Fig. 3.14F). A decrease in the transcription of pro-fission *DRP1* was also observed (Fig. 3.14F). LPS treatment increased the expression of *MFN1* and *MFN2*, yet there was no change to *OPA1* or *DRP1* expression (Fig. 3.14F). In addition, *PINK1* gene expression was increased with LPS treatment, yet remained unaffected by Poly (I:C) (Fig. 3.14F). Collectively, these data indicate that the changes in mitochondrial morphology are contemporaneous to transcriptional changes in fission and fusion genes, suggesting that TLR stimulation affects mitochondrial remodelling through canonical pathways.

The cellular content of mitochondria can influence oxidative capacity in the RPE [397]. The electron microscopy analysis showed, structural alterations that affected the mitochondria. This was followed up by an assessment of total mitochondrial number was affected. RT-PCR was used to estimate mitochondrial content through the amplification of two segments of the mitochondrial genome (the gene encoding cytochrome B and 16 S rRNA). These two sites were chosen due to both their stability and location in different regions of the genome [397]. Expression of both genes was normalized to the expression of the nuclear encoded β-globulin gene. No significant changes to mtDNA copy number was observed following treatment of cells with both TLR agonists (Fig. 3.14G). Whilst there were no changes observed to the mtDNA, it was of interest to identify whether the changes in metabolism were associated with alterations in the abundance of mitochondrial ETC complexes. To answer this question, I quantified the expression of mitochondrial ETC components using immunoblotting. Treatment with either agonist had little effect on the expression of ETC complexes, apart from complex III which was found to be significantly upregulated by Poly (I:C) treatment (Fig. 3.15A-B). Very-long chain specific acyl-coA dehydrogenase (ACAVDL) sits in the inner mitochondrial membrane and catalyses the first set in the β-oxidation of long chain fatty acids [483]. There was no significant change to the expression of this mitochondrial enzyme following stimulation of ARPE-19 with Poly (I:C) or LPS (Fig. 3.15A-B).

The results from this section show that the metabolic changes observed in TLR-stimulated ARPE-19 cells are accompanied by changes in mitochondrial morphologies. These are likely a result of transcriptional changes in fission/fusion genes which mediate mitochondrial remodelling. The changes to mitochondrial structure are not attributed to an increase in mitochondrial number or mitochondrial biogenesis, as the expression of ETC components and mtDNA remained constant.

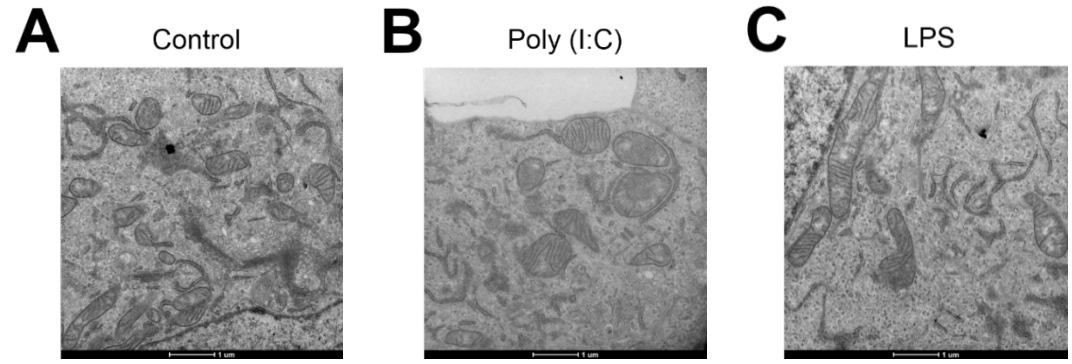
A
Control
B
Poly (I:C)
C
LPS

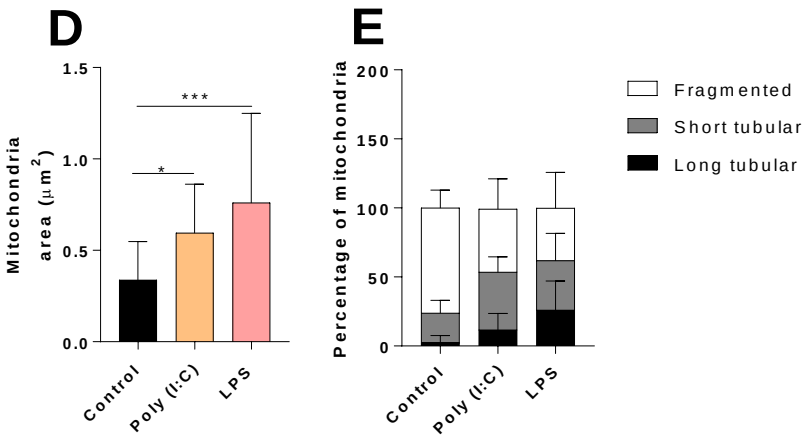
D
Mitochondria area (μm²)
1.5
1.0
0.5
0.0
***
*
Control
Poly (I:C)
LPS
E
Percentage of mitochondria
200
150
100
50
0
Fragmented
Short tubular
Long tubular
Control
Poly (I:C)
LPS

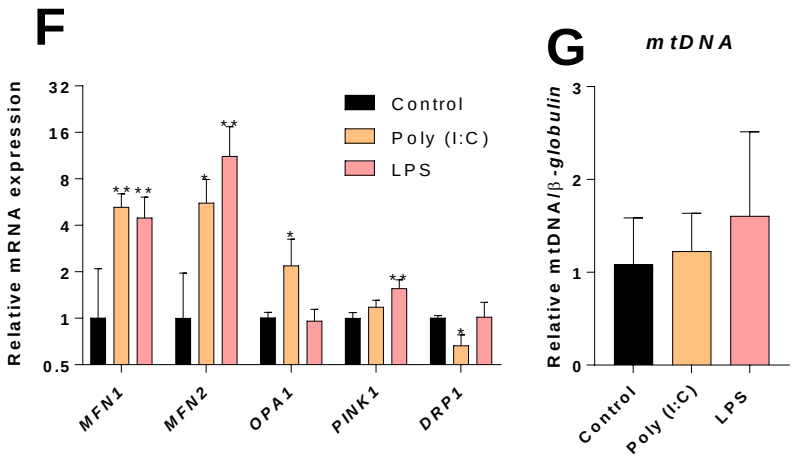
F
Relative mRNA expression
32
16
8
4
2
1
0.5
Control
Poly (I:C)
LPS
MFN1
MFN2
OPA1
PINK1
DRP1
G
mtDNA
Relative mtDNA/β-globulin
3
2
1
0
Control
Poly (I:C)
LPS

Figure 3.14. Mitochondrial changes of TLR-stimulated ARPE-19:

Representative transmission electron microscopy of ARPE-19 mitochondria either untreated (A), stimulated with Poly (I:C) (10µg/ml) (B) or LPS (1µg/ml) for 24h (C). Magnification 9300x. (D) Mitochondrial area was calculated using ImageJ. (E) Quantification of mitochondrial morphology into either fragmented, short tubular or long tubular phenotypes. (F) Quantitative RT-PCR was performed to assess the mitochondrial fission and fusion enzymes *MFN1*, *MFN2*, *OPA1*, *PINK1* and *DRP1* mRNA transcripts. (G) Quantitative RT-PCR was performed to assess mitochondrial content; this was estimated from the amplification of *CTYB* and 16S rRNA relative to *BGLOB* mRNA transcripts. Data expressed as relative mean from three independent experiments. One-way ANOVA with Dunnet's multiple comparisons test; *p<0.05, **p<0.01, ***p<0.005, ***p<0.001.

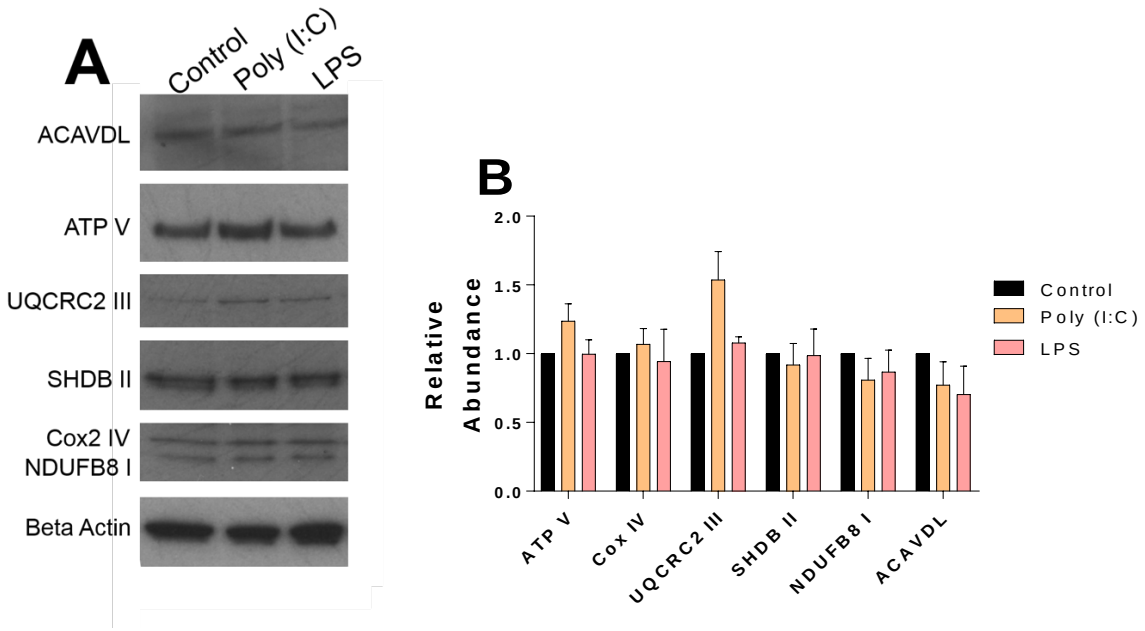

Figure 3.15. Expression of ETC components in TLR-stimulated ARPE-19:

ARPE-19 were stimulated with either Poly (I:C) (10µg/ml) (B) or LPS (1µg/ml) for 24h. (A) Western blot analysis was used to determine the expression of ETC complexes (ATP synthase V, Cox2 IV, UQCRC2 III, SHDB II and NDUFB8 I) and ACAVDL. (B) Relative densitometry was calculated from (H) using ImageJ. Bands were normalised to a loading control (Beta Actin). Represents two independent blots.

3.15. Effect of TLR-agonists on AMP-activated kinase activation status in ARPE-19.

Having demonstrated that different TLR stimulation initiates divergent metabolic reprogramming and morphological adaptations in RPE mitochondria, there remained a question of how this may be mechanistically regulated in the RPE. The data presented heretofore demonstrates that LPS stimulation of RPE drives a rapid switch to aerobic glycolysis. Poly (I:C) stimulation on the other hand increases oxidative glucose metabolism and TCA activity. Considering observations made in dendritic cells whereby LPS-stimulation was accompanied by a rapid in-activation of the AMP-activated kinase AMPK to facilitate a shift to aerobic glycolysis [403], it was hypothesised that different TLR-induced metabolic responses may be governed by the AMPK activation status in the RPE.

AMPK is a key regulator of cellular metabolism, that plays a central role in maintaining energy homeostasis by switching on catabolic pathways that generate ATP, whilst simultaneously inhibiting anabolic, ATP consuming pathways such as protein/sterol/fatty acid synthesis, which contribute to cell-cycle progression (see section 1.8.5.3.) [344]. AMPK is a well described negative regulator of the Warburg effect, with a loss of AMPK-dependent signalling in cancer cells enough to stabilize normoxic HIF-1α, promoting aerobic glycolysis and biomass accumulation *via* lipid synthesis [311]. The overall effects activation of AMPK are compatible with the view of AMPK as a tumour suppressor promoting oxidative metabolism characteristic of quiescent anti-inflammatory cells [345]. Indeed, anti-inflammatory cytokines promote AMPK activation and the generation of M2 macrophages [484].

In view of previous experiments performed using seahorse analysis - whereby LPS stimulation initiated rapid metabolic changes within minutes – it was of interest to observe how TLR-4 activation affected AMPK activation status over a short-term period. ARPE-19 cells were stimulated with LPS for either 0, 20, 40 or 60min and western blotting was used to determine the activation of AMPK *via* its immediate downstream target (and surrogate for activation) Acetyl Co-A carboxylase (ACC). Alike previously published work [403, 484], AMPK activation was observed to diminish rapidly after exposure to LPS (Fig. 3.16A-B). Having observed that the inactivation of AMPK (and subsequent activation of ACC) occurs within the early time points of LPS stimulation, 30min was chosen as a time point to measure the phosphorylation of AMPK on Thr172 in its activation loop. Stimulation with LPS for 30 min reduced the phosphorylation (and activation) of AMPK and ACC (Fig. 3.16C-E).

The rapid suppression of AMPK during RPE activation (*via* TLR-4) led to the hypothesis that AMPK may function to antagonise the switch to aerobic glycolysis, and therefore is rapidly inactivated upon LPS stimulation. As Poly (I:C)-stimulation RPE was not accompanied by a similar metabolic switch, it was of interest to investigate AMPK activation status following the activation of TLR-3. ARPE-19 cells were cultured in the presence or absence of Poly (I:C) for 24h. It was observed that treatment of cells increased the phosphorylation of AMPK Thr172 and its downstream target ACC on Ser79 (Fig. 3.16F-H) suggesting increased activity of AMPK and subsequent inactivation of ACC.

To examine whether the metabolic phenotypes associated with AMPK activation or inactivation were observed with LPS or Poly (I:C) treatment, I subsequently investigated the fatty acid oxidation and synthesis pathways. As previously discussed, AMPK activation opposes anabolic pathways such as fatty acid synthesis whilst promoting catabolic fatty acid oxidation. Confirming the varying effects on AMP activation status, I observed that LPS and Poly (I:C) treatment of RPE cells differentially affected these two pathways. With Poly (I:C) treatment, there was a significant increase in fatty acid oxidation (as quantified through a mitochondrial stress test, including the third injection of CPT1 inhibitor etomoxir) (Fig. 3.17A-B). LPS on the other hand, significantly reduced fatty acid oxidation (Fig. 3.17A-B). Fatty acid synthesis was assessed by quantification of malonyl CoA, a core metabolite in this pathway. Malonyl coA is formed in the reaction catalysed by ACC and is transferred to the terminal thiol group of acyl carrier protein [292]. Moreover, malonyl CoA inhibits the rate limiting step of β-oxidation through an association with CPT1. Treatment with LPS increased malonyl coA (as previously described in macrophages [485]), whereas Poly (I:C) treated cells exhibited reduced malonyl coA (Fig. 3.17C).

Collectively, the data from this section indicate a potential mechanism whereby the two TLR agonists exert differential effects on RPE metabolism. Suppression of AMPK and subsequent activation of ACC is enough to permit the Warburg effect and fatty acid synthesis in LPS-stimulated cells. In the context of Poly (I:C) treatment, the sustained activation of AMPK opposes this metabolic shift, allowing cells to continue utilising mitochondrial OXPHOS as opposed to metabolic reprogramming into an aerobically glycolytic signature.

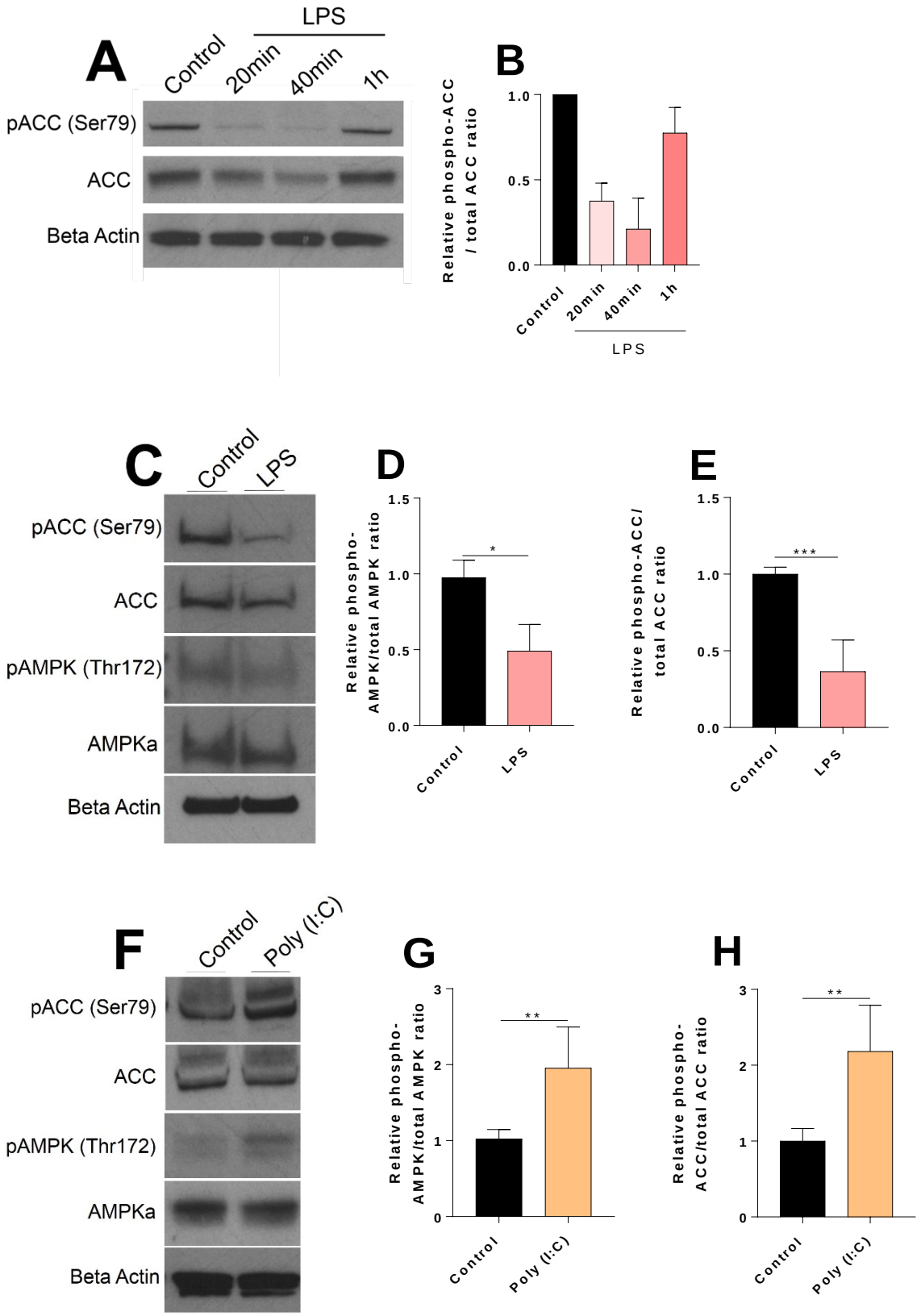
A
LPS
Control
20min
40min
1h
pACC (Ser79)
ACC
Beta Actin
B
Relative phospho-ACC / total ACC ratio
1.0
0.5
0.0
Control
20min
40min
1h
LPS
C
Control
LPS
pACC (Ser79)
ACC
pAMPK (Thr172)
AMPKa
Beta Actin
D
Relative phospho-AMPK/total AMPK ratio
1.5
1.0
0.5
0.0
*
Control
LPS
E
Relative phospho-ACC/ total ACC ratio
1.5
1.0
0.5
0.0
***
Control
LPS
F
Control
Poly (I:C)
pACC (Ser79)
ACC
pAMPK (Thr172)
AMPKa
Beta Actin
G
Relative phospho-AMPK/total AMPK ratio
3
2
1
0
**
Control
Poly (I:C)
H
Relative phospho-ACC/total ACC ratio
3
2
1
0
**
Control
Poly (I:C)

Figure 3.16. Effect of TLR agonists on AMP-activated kinase activation status in ARPE-19:

(A) Cells were treated with 1μg/ml LPS for 0, 20, 40 and 60min. Western blot analysis was used to determine AMPK activation *via* its downstream surrogate ACC. (B) Densitometry analysis of P-ACC/ACC over the indicated time points of LPS treatment. (C) Cells were treated with LPS (1μg/ml) for 30min. Western blot analysis was used to determine the activation of P-AMPK/AMPK and P-ACC/ACC following treatment. (D) Densitometry analysis of P-AMPK/AMPK. (E) Densitometry analysis of P-ACC/ACC. (F) Cells were treated with Poly (I:C) (10μg/ml) for 24h. Western blot analysis was used to determine the phosphorylation of AMPK and ACC following treatment. (G) Densitometry analysis of P-AMPK/AMPK. (H) Densitometry analysis of P-ACC/ACC. Data are expressed as means ± SD from (A-B) two or (C-H) three independent blots. Unpaired Student's T-test; *p<0.05, ***p<0.001.

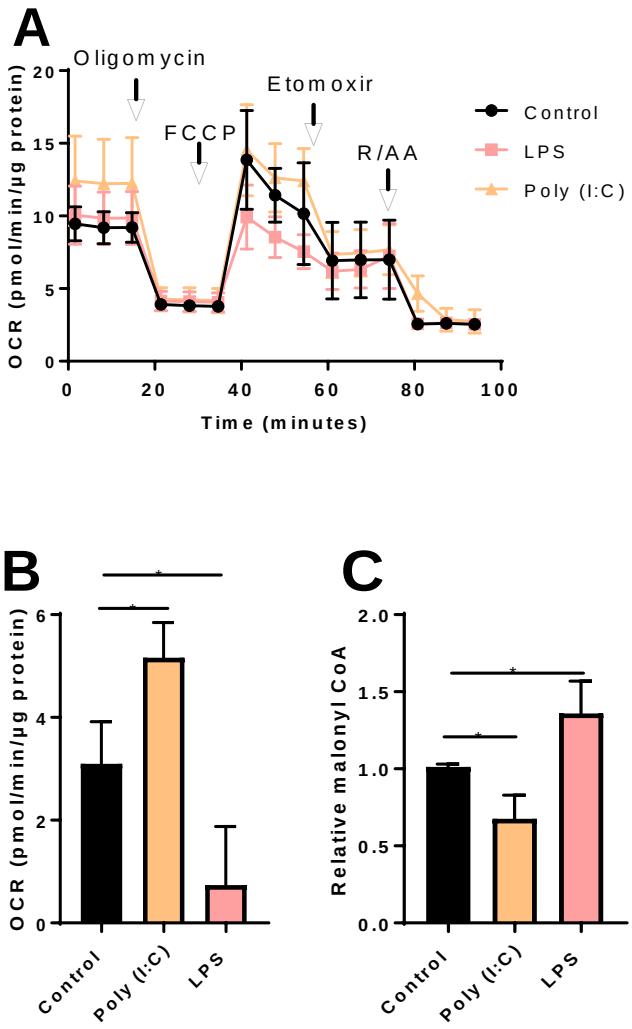

Figure 3.17. Effect of TLR-agonists on fatty acid metabolism:

(A) ARPE-19 were treated for 24h with Poly (I:C) (10µg/ml) or 30min with LPS (1µg/ml); a mitochondrial stress test with a third injection of etomoxir (10µg/ml) was used to assess fatty acid oxidation. (B) Analysis of data shown in (A). (C) ARPE-19 were treated for 24h with either Poly (I:C) (10µg/ml) or LPS (1µg/ml); relative malonyl coA levels were assessed in cell lysates. Data expressed as relative mean from three independent experiments. One-way ANOVA with Dunnet's multiple comparisons test; *p<0.05, **p<0.01, ***p<0.005, ***p<0.001.

3.16. Effect of TLR agonists on mammalian target of rapamycin signalling in ARPE-19.

Due to the opposing effects of Poly (I:C) and LPS on AMPK activation, the downstream mTOR signalling pathway was examined. mTOR is modulated by a variety of cellular signals, including insulin, cytokines, TLRs and amino acids (see section 1.8.5.3.) [434]. Considering the modulation of AMPK activation status *via* differential TLR stimuli, it was of interest to investigate the downstream mTORC1 and PI3K signalling pathways.

ARPE-19 cells were cultured for 24h with Poly (I:C) and western blotting of mTOR/PI3K components was performed. Poly (I:C)-stimulation was observed to increase mTOR phosphorylation (and therefore activation) at the catalytic subunit (Ser 2448) (Fig. 3.18A-B). Downstream of mTOR is the mitogen activated Ser/Thr protein kinase p-70 S6 kinase, a key player in cell growth and proliferation through the regulation of translation [486]. p-70 S6 kinase is commonly used as a surrogate of mTOR activation. Poly (I:C)-stimulation increased the expression of p-70 S6 kinase (Fig. 3.18A and C). Interestingly, Poly (I:C) reduced the expression of mTORC1 subunit Raptor (Fig. 3.21A and C). Cells stimulated for 24h with Poly (I:C) showed no significant change in the expression of catalytic PI3K subunit p110 (Fig. 3.18A and C). This suggests PI3K activation as an early event in the signalling cascade and may explain why there is no change in the phosphorylation status when stimulated with Poly (I:C) for 24h.

Stimulation with LPS for 30min upregulated the expression of catalytic PI3K subunit p110 (Fig. 3.18D and F). Downstream of PI3K, LPS treatment lead to increased activation of mTOR at the catalytic Ser 2448 subunit (this was notably larger than the Poly (I:C)-induced expression) and immediate downstream mTORC1 target p-70 S6 kinase (Fig. 3.18D-F). LPS had no effect on the expression of Raptor (Fig. 3.18D and F). The phosphorylation status of Raptor or the expression of GβL was not assessed for either LPS or Poly (I:C) treatment.

These data indicate that both TLR agonists activate the mTORC1 pathway despite the observed differences in AMPK activation status. As previously mentioned, the mTOR system incorporates a variety of environmental cues (including that of AMPK and PI3K activation). This suggests that even with prominent AMPK activation under a Poly (I:C) stimuli, mTORC1 signalling is still significantly enhanced. Notably, the LPS-induced mTORC1 response was greater than that of Poly (I:C), which may encompass the negative regulation conferred by active AMPK. However, the kinetics of LPS and Poly (I:C) treatments are completely dissimilar (as a result of different time points of stimulation) so it is

difficult to make comparisons between the two groups. Poly (I:C) may activate mTOR/PI3K at earlier time points, but this was not investigated in this body of work.

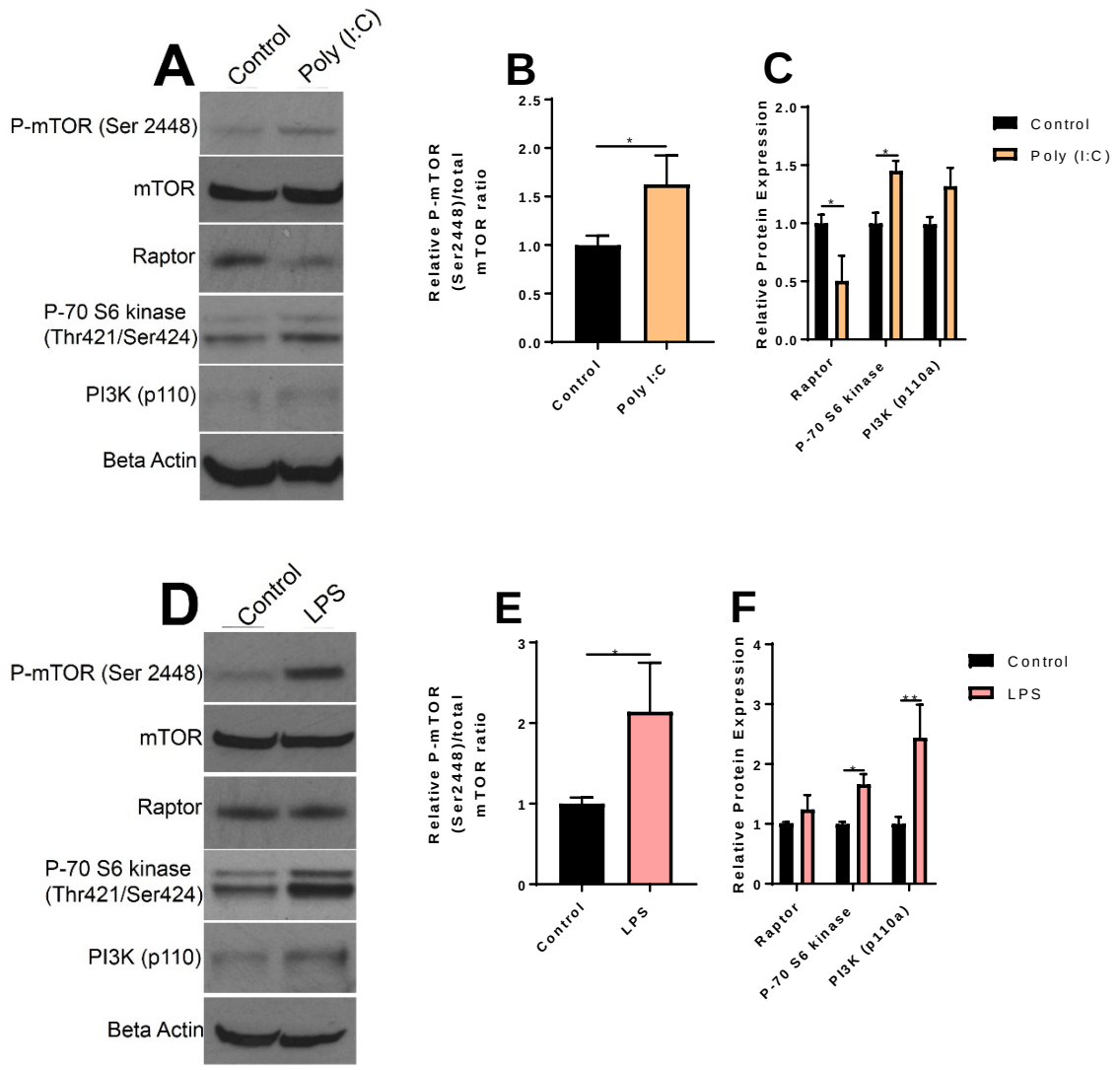

Figure 3.18. Effect of TLR-agonists on mammalian target of rapamycin signalling in ARPE-19:

(A) Cells were treated with Poly (I:C) (10µg/ml) for 6h. Western blot analysis was used to determine the activation of the PI3K/mTOR pathway following treatment. (B) Densitometry analysis of P-mTOR/mTOR. (C) Densitometry analysis of Raptor, p-70 S6 kinase and PI3K. (D) Cells were treated with LPS (1µg/ml) for 30min. Western blot analysis was used to determine the activation of the PI3K/mTOR pathway following treatment. (E) Densitometry analysis of P-mTOR/mTOR. (F) Densitometry analysis of p-70 S6 kinase and PI3K. Data are expressed as means ± SD from three independent blots. Unpaired Student's T-test; *p<0.05, **p<0.01.

3.17. AMP-activated kinase agonists differentially affect ARPE-19 metabolism.

The data presented in the previous sections indicate a potential mechanism for the differential effects of TLR-3 and -4 activation on RPE metabolism. LPS inactivates AMPK by dephosphorylation of Thr172 enabling engagement anabolic processes and a "Warburg-like" switch away from oxidative pyruvate metabolism. Poly (I:C) on the other hand, activates AMPK to induce a state of pseudo-starvation, which may prevent aerobic glycolysis in the RPE. To further explore how AMPK may regulate metabolism in the RPE, a pharmacological activator (AICAR) and inhibitor (compound C) of AMPK were utilised.

Due to the reported toxicity of both compounds [487, 488], an initial time-course experiment was conducted to investigate the tolerability of both compounds to the RPE at doses used commonly in experiments on other cell lines [426, 427, 489]. It was observed that 24h of treatment with either compound led to significant LDH release (Fig. 3.19A). Cell viability was significantly decreased from as early as 2h following compound C treatment (Fig. 3.19B). The effect of AICAR treatment on cell viability was only detected at 24h (Fig. 3.19B). Based on these results, a 1h treatment of both compounds was used to carry out the following experiments to minimise cell death. It was confirmed by western blot that AICAR and compound C increased/decreased AMPK Thr172 phosphorylation, respectively (Fig 3.19C). Pharmacological activation and inhibition of AMPK had opposing effects on the OCR/ECAR ratio (Fig. 3.19D). The ATP/ADP ratio showed that compound C treatment significantly reduced the cellular production of ATP, whereas AICAR had minimal effect (Fig. 3.19E). A mitochondrial stress test identified significant increases in maximal respiration and spare respiratory capacity following AICAR treatment (Fig. 3.19F and G). Compound C treatment decreased the maximal respiration yet had no significant effect on the spare respiratory capacity, basal metabolism or ATP-production (Fig. 3.19F and G). This supports previous work which showed that pharmacological AMPK activation boosted spare respiratory capacity [489]. AICAR was additionally observed to decrease glucose consumption and lactate output in keeping with previous studies [489]; compound C had no significant effect on the consumption of glucose or lactate production (Fig. 3.19H-I). Collectively, these data are consistent with the hypothesis that AMPK is promoting oxidative phosphorylation rather than aerobic glycolysis during innate immune responses [345].

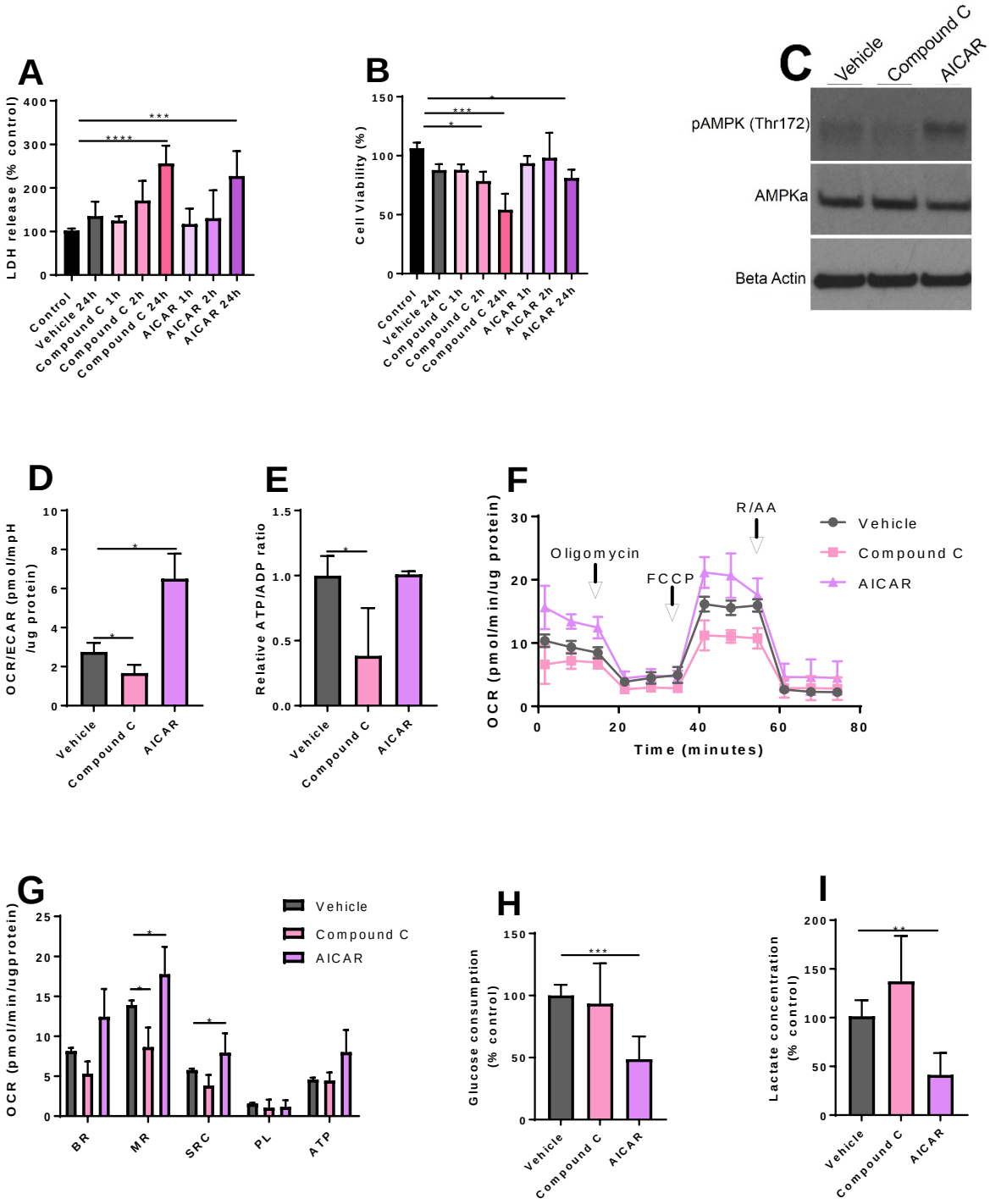
A
LDH release (% control)
400
300
200
100
0
***
****
Control
Vehicle 24h
Compound C 1h
Compound C 2h
Compound C 24h
AICAR 1h
AICAR 2h
AICAR 24h
B
Cell Viability (%)
150
100
50
0
*
***
*
Control
Vehicle 24h
Compound C 1h
Compound C 2h
Compound C 24h
AICAR 1h
AICAR 2h
AICAR 24h
C
Vehicle
Compound C
AICAR
pAMPK (Thr172)
AMPKa
Beta Actin
D
OCR/ECAR (pmol/mpH /ug protein)
10
8
6
4
2
0
*
*
Vehicle
Compound C
AICAR
E
Relative ATP/ADP ratio
1.5
1.0
0.5
0.0
*
Vehicle
Compound C
AICAR
F
OCR (pmol/min/ug protein)
30
20
10
0
Oligomycin
FCCP
R/AA
Vehicle
Compound C
AICAR
0
20
40
60
80
Time (minutes)
G
OCR (pmol/min/ugprotein)
25
20
15
10
5
0
*
*
*
Vehicle
Compound C
AICAR
BR
MR
SRC
PL
ATP
H
Glucose consumption (% control)
150
100
50
0
***
Vehicle
Compound C
AICAR
I
Lactate concentration (% control)
200
150
100
50
0
**
Vehicle
Compound C
AICAR

Figure 3.19. AMP-activated kinase agonists differentially affect ARPE-19 metabolism:

Cells were treated with AICAR (1mM) or Compound C (40µM) for the indicated time points. (A) LDH release was quantified in supernatants and expressed as a percentage of an untreated control. (B) Cell viability was quantified using an MTT assay and expressed as a percentage of the untreated control. Cells were pre-treated for 1h prior to XF assays. (D) Basal OCR and ECAR measurements expressed as the ratio OCR/ECAR. (E) Cellular ATP and ADP levels were quantified in lysed cells after 2h of treatment. (F) Representative mitochondrial stress test measured with sequential injections of Oligomycin, FCCP and rotenone/antimycin A. (G) Mitochondrial parameters (BR- basal respiration; MR- maximal respiration; SRC- spare respiratory capacity; PL- proton leak; ATP- ATP-production) calculated from data shown in (F). Cell supernatants were collected after 24h. (H) Lactate release was quantified in supernatants and expressed relative to an untreated control. (I) Glucose consumption assessed and expressed as a percentage of the mean untreated control. Both (H-I) were normalised to cell viability calculated from (B). Data are expressed as means ± SD. (A-B) and (H-I) represent three independent experiments performed in duplicate. (D-F) represent two independent experiments performed in duplicates. (C) Represents three independent blots. One-way ANOVA with Dunnet's multiple comparisons test; *p<0.05, **p<0.01, ***p<0.005, ***p<0.001.

3.18. Activation of AMP-activated kinase attenuates aerobic glycolysis in ARPE-19.

The results from the previous sections indicate that in the RPE, AMPK is a negative regulator of aerobic glycolysis. This applies to RPE both under quiescent/unstimulated conditions and under "stress" conditions such as TLR stimulation. Boosting AMPK activity *via* the small molecule activator AICAR drastically inhibits glycolytic metabolism and lactate output in RPE cells, whereas inhibition attenuates mitochondrial function and sustains glycolysis. In the context of TLR stimulation, LPS treatment rapidly inactivates AMPK which likely augments the switch to aerobic glycolysis. Poly (I:C) on the other hand, activates AMPK which likely prevents a similar metabolic reprogramming to LPS.

Considering these findings, and to further examine the role of AMPK on innate inflammatory responses, the effect of AMPK activation on the LPS-induced immediate metabolic switch was assessed. ARPE-19 cells were pre-treated in the presence or absence of AICAR for 1h prior to XF analysis. Basal OCR and ECAR measurements were taken before and after an injection of LPS. Due to the previously presented effects of AICAR on basal metabolism (see section 3.17.), OCR and ECAR data was normalised as "relative ECAR/OCR", prior to LPS injection to assess the relative changes in both parameters. LPS-induced increases in ECAR were attenuated by the pre-treatment of cells with AICAR (Fig. 3.20A-B). AMPK activation blunted the initial decrease in OCR following LPS stimulation (Fig. 3.20C-D). The decreased OCR post injection of LPS was observed to return to basal levels more rapidly with the pre-treatment of AICAR (Fig. 3.20C). As AMPK was already activated with Poly (I:C) stimulation, the effect of AICAR pre-treatment on the initial metabolic changes following Poly (I:C) injection was not investigated.

Collectively, the data from this section strengthen the hypothesis of AMPK as a negative regulator of aerobic glycolysis in the RPE. AMPK activation was enough to completely dampen the LPS-induced metabolic switch.

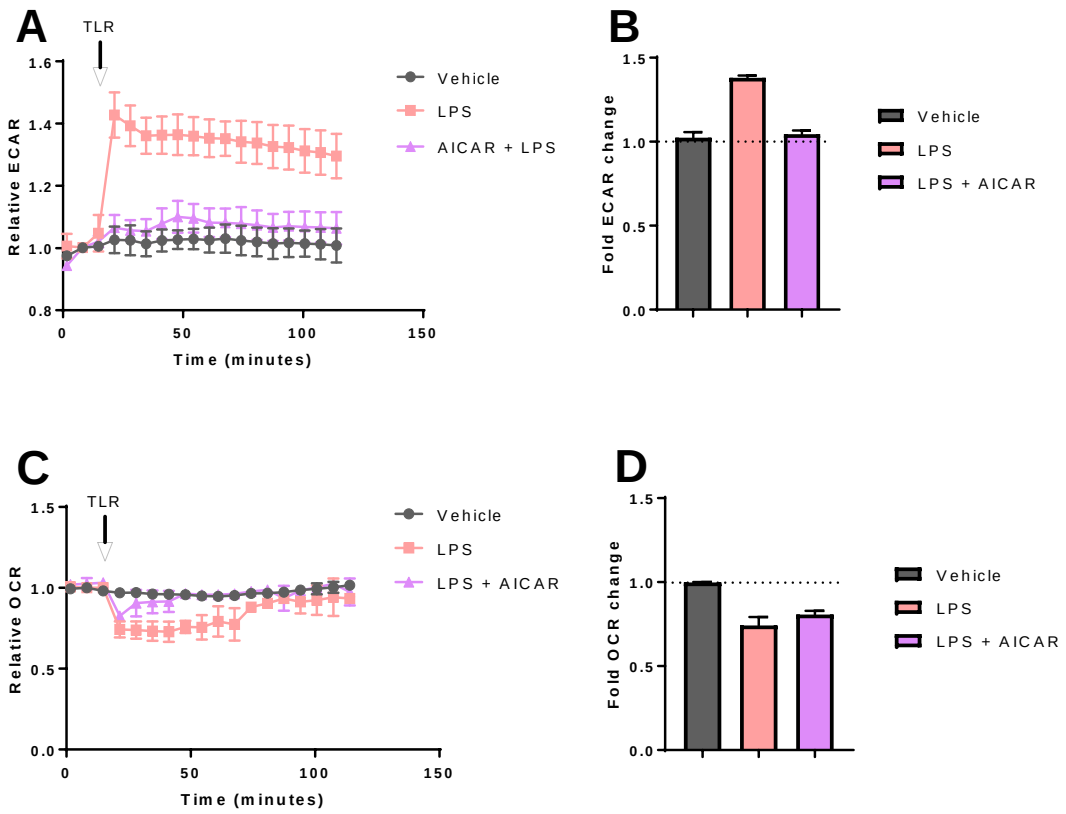

Figure 3.20. Activation of AMPK attenuates aerobic glycolysis in ARPE-19:

Cells were pre-treated with AICAR (1mM) for 1h prior to real-time measurements of ECAR (A) or OCR (C) following injection of LPS (1µg/ml). Changes in ECAR (B) or OCR (D) post injection of LPS. Data are expressed as means ± SD from (A-D) two experiments with two technical repeats.

3.19. Activation of AMP-activated kinase attenuates translation of *IL33* in ARPE-19.

RPE cells have been previously shown to respond to TLR agonists, inducing the expression of IL-33 which contributes to the regulation of tissue homeostasis [8]. For this reason, the effect of AMPK on IL-33 expression was investigated. Modulation of the activity of AMPK by pharmacological activation had no effect on the transcription of *IL33* mRNA (Fig. 3.21A) yet there was reduced expression of IL-33 protein (Fig. 3.21B), suggesting that AICAR affected constitutive IL-33 translation. mRNA stability and decay rates are another mechanism whereby gene expression is influenced in mammalian cells [490], however this was not assessed in this body of work. Pre-treatment with both compounds reduced the LPS and Poly (I:C)-induced translation of *IL33* mRNA into IL-33 protein (Fig. 3.21C-F).

The mTORC1 complex is a central regulator of protein translation, when activated it phosphorylates and inactivates 4EB-P1 (an e1F4F sequestering protein). Free e1F4F is a platform protein for eukaryotic initiation factor 4E and G (eIF4E/G) which together bind to the 7-methyl-GTP cap present at the 5' of each mRNA to initiate mRNA translation [486]. Because of the effect of AICAR on *IL33* translation, it was necessary to investigate the activity of the mTORC1 complex. Both AMPK modulation decreased the expression of mTORC1 complex component Raptor and downstream signalling components p-70 S6 kinase and P 4EB-P1 (Fig. 3.21G-H) indicating a mechanism whereby *IL33* mRNA translation is regulated in the RPE under metabolic stress through the AMPK/mTOR axis.

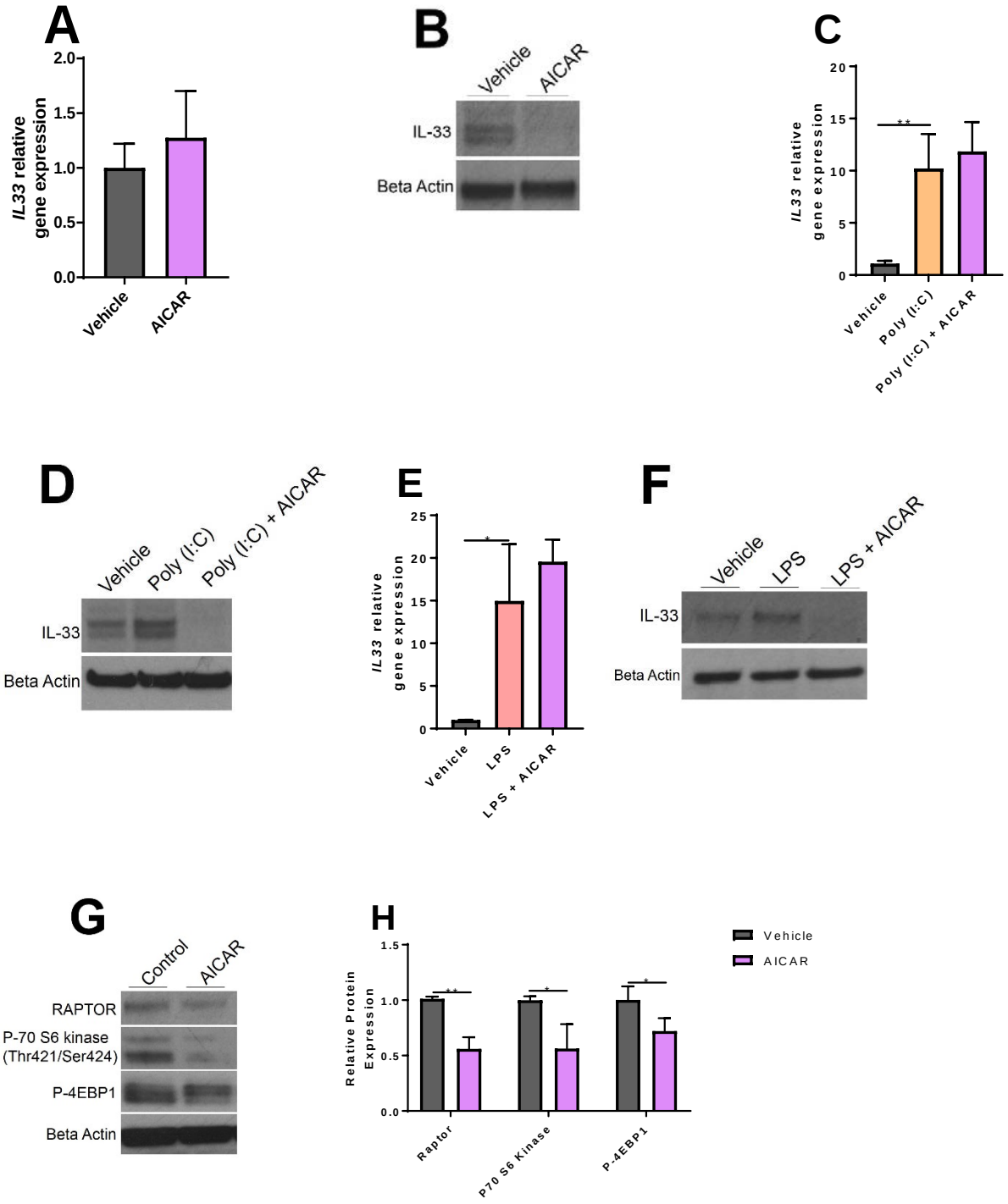
A
IL33 relative gene expression
2.0
1.5
1.0
0.5
0.0
Vehicle
AICAR
B
Vehicle
AICAR
IL-33
Beta Actin
C
IL33 relative gene expression
20
15
10
5
0
**
Vehicle
Poly (I:C)
Poly (I:C) + AICAR
D
Vehicle
Poly (I:C)
Poly (I:C) + AICAR
IL-33
Beta Actin
E
IL33 relative gene expression
25
20
15
10
5
0
*
Vehicle
LPS
LPS + AICAR
F
Vehicle
LPS
LPS + AICAR
IL-33
Beta Actin
G
Control
AICAR
RAPTOR
P-70 S6 kinase (Thr421/Ser424)
P-4EBP1
Beta Actin
H
Relative Protein Expression
1.5
1.0
0.5
0.0
**
*
*
Raptor
P70 S6 Kinase
P-4EBP1
Vehicle
AICAR

Figure 3.21. Activation of AMPK attenuates translation of *IL33* in ARPE-19:

Cells were treated for 24h with AICAR (1mM) and IL-33 expression was assessed at both the RNA level (A) or at the protein level (B). Cells were pre-treated with AICAR (1mM) for 1h prior to treatment with Poly (I:C) (10μg/ml) for 24h. IL-33 expression was assessed at both the RNA level (C) or at the protein level (D). Cells were pre-treated with AICAR (1mM) for 1h prior to treatment with LPS (1ug/ml). IL-33 expression was assessed at both the RNA level (E) or at the protein level (F). (G-H) Cells were treated for 24h with AICAR (1mM), mTORC1 activation was assessed western blotting analysis of RAPTOR, p70 S6 kinase and P-4EBP1. Data are expressed as means ± SD. (A, C and E) represent three independent experiments performed with duplicates. (B, D, F and G) represent two and (H) represents three independent blots. (H) One-way ANOVA with Dunnet's multiple comparisons test, (C and E) One-way ANOVA with Tukey's multiple comparisons test; *p<0.05, **p<0.01.

3.20. Discussion.

It remains unresolved how RPE cell metabolism is regulated following immune activation to maintain retinal homeostasis and retinal function. As mitochondrial dysfunction and inflammatory processes are likely underlying mechanisms driving early AMD disease progression, it is probable that defects in the ability of RPE to respond to tissue stress signals exacerbate homeostatic regulatory immune responses to altered dysregulated inflammatory state. The rationale behind this chapter is that under stress, RPE cells adapt their metabolic profile to provide ATP for bioenergetically expensive processes. As cells or organisms age, a decline in mitochondrial health [491] may limit the ability of a cell to divert bioenergetic sources for a rapid generation of ATP.

Results obtained in this chapter suggest that the energy sensor AMPK is a critical node linking innate immune and metabolic function within the RPE. I have shown that AMPK functions to limit aerobic glycolysis and anabolic metabolism, whilst simultaneously increasing mitochondrial function. In the context of innate immune activation, altering the activation state of AMPK allows different TLR activation to elicit alternate RPE metabolic phenotypes. In the case of TLR-4 signalling, AMPK is rapidly inactivated, permitting an immediate switch to aerobic glycolysis and the augmentation of anabolic amino-acid/ fatty acid biosynthesis pathways (Fig. 3.22). Conversely, TLR-3 signalling activates AMPK, providing a key metabolic checkpoint which antagonises pro-anabolic metabolism and the "Warburg effect" to permit functional mitochondrial OXPHOS.

Age, leading to progressive biological changes over time, remains one of the most obvious predisposing factors for the development of AMD [492]. Any cell with replicative potential may undergo cellular senescence (often allied with aging), where a non-dividing state is reached in otherwise mitotically competent cells [493]. RPE cells have been shown to reach a senescent state both *in vitro* culture and *in situ* [492]. To examine how aging and senescence may contribute to bioenergetic dysfunction in RPE, Seahorse analysis was carried out on RPE aged both *in vitro* and *in vivo*. Long-term *in vitro* cultivation leads to the development of RPE with reduced glycolytic and mitochondrial function, yet an increased metabolic demand in terms of a significantly increased OCR. Interestingly, the increased mitochondrial activity exhibited in these cells may be indicative of a switch to a senescence-associated secretory phenotype, where increased fatty acid oxidation fuels the release of secretory proteins that may contribute to increased sterile inflammation within the tissue [494, 495]. RPE from aged mice are more representative of the multifaceted *in vivo* environment faced

during a lifespan. Parameters associated with impaired mitochondrial health were found to be more prominent in aged RPE, such as proton leak and coupling efficiency. The observation that aged murine RPE have an reduced capacity to utilize mitochondrial respiration and glycolysis compared with younger cells supports results from aged human RPE, where both glycolysis and mitochondrial reserve capacity were diminished [496].

Inflammation and metabolism are intertwined, with cells rapidly modulating their metabolic pathways to generate effective responses against pathogen invasion followed by the restoration of tissue homeostasis. Microbial products such as LPS and Poly (I:C) activate TLR which leads to the output of cell-type specific pro-inflammatory cytokines [45]. RPE display responsiveness to Poly (I:C) and LPS, which is in keeping with previous studies [45, 286]. LPS stimulation is a well-known inducer of aerobic glycolysis within immune and non-immune cells [5]. TLR-4 stimulation decreases AMPK activation in macrophages [497] and AMPK has been shown to agonise LPS-induced glucose consumption in dendritic cells [403]. A recent study demonstrated a role for AMPK in LPS-challenged monocytes, whereby under glucose deprovision, AMPK activation drives oxidative metabolism of fatty acids and a rapid respiratory burst [498].

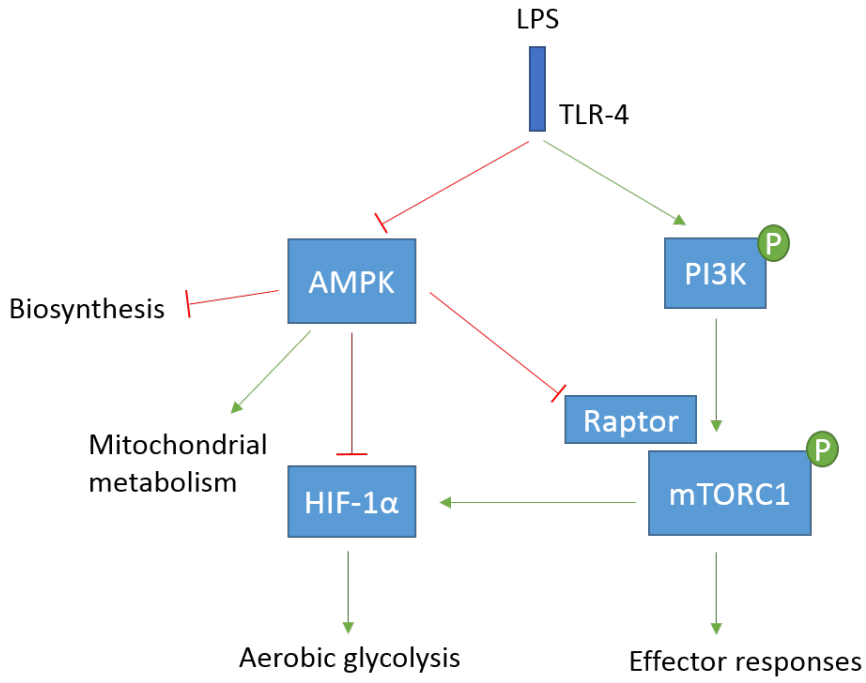

Figure 3.22. Signalling events in LPS-stimulated RPE which promote aerobic glycolysis:

LPS signals through TLR-4 in the RPE leading to immediate changes in RPE metabolism. AMPK is inactivated *via* dephosphorylation of Thr172 on the catalytic subunit. AMPK promotes catabolism and opposes anabolism, therefore in its activation, FAS and amino-acid biosynthesis from glucose occurs. AMPK opposes the metabolic switch to aerobic glycolysis *via* inhibition of the mTORC1-HIF-1α axis. LPS inhibits AMPK allowing increased normoxic stabilisation of HIF-1α to occur and subsequently a metabolic switch to aerobic glycolysis. LPS activates anabolic mTOR signalling through PI3K.

It was anticipated that Poly (I:C) activated cells would undergo a similar switch to aerobic glycolysis as observed in other cell types [499, 500]. Yet interestingly, Poly (I:C) stimulation led to the activation of AMPK and an increase in OXPHOS. This increase in mitochondrial activity was attributed to both the increased flux of glucose-derived carbon into the TCA cycle and the activation of a fatty acid oxidation metabolic program. These results confirm observations made in bone marrow-derived dendritic cells, whereby Poly (I:C) and TLR-9 agonist CpG have been shown to promote both fatty acid oxidation and mitochondrial pyruvate oxidation [419].

Fatty acid synthesis and cholesterol biosynthesis pathways are upregulated in virus-infected cells in order to support the generation of progeny. Viruses typically inactivate AMPK to promote these anabolic pathways, whilst inhibiting catabolic fatty acid oxidation [501]. Pharmacological inhibition of fatty acid oxidation has previously been shown to impact the ability of cells to control viral replication [502]. AMPK activation has been shown to limit a broad array of viral infections, including Rift Valley Fever virus, through inhibiting the rate limiting step (ACC) of the fatty acid synthesis pathway [503]. This suggests a potential mechanism for AMPK in ocular viral defence; *via* inhibiting ACC, fatty acid synthesis repression diverts free fatty acids that could otherwise be used in viral replication. Additionally, the effects of AMPK extend beyond metabolic reprogramming during infection, with antiviral defence mediated through the modulation of stimulator of IFN genes (STING) [504].

AMPK, when activated endeavours to maintain energetic homeostasis by increasing ATP production and limiting energetic expenditure [344]. In the RPE, both strategies are engaged, and bioenergetically expensive processes (such as cytokine expression) are halted. A similar effect is observed in nutrient starved murine T-cells, whereby AMPK activation reduces the translation of *Ifng* mRNA [428]. The results obtained suggest a critical role for AMPK in the translation of *IL33* mRNA and limitation of the "Warburg effect". It is essential to note the potential off-target effects through pharmacological manipulation of AMPK using small molecule activators/inhibitors; data obtained should be interpreted with care [505, 506].

Hypoxia is an activator of AMPK; through alterations in the AMP:ATP ratio, AMPK strives to restore energy homeostasis through the promotion of catabolic processes [344]. Poly (I:C) was capable of sustaining AMPK activation under hypoxia to further up-regulate glycolysis. Considering, the observation that *HIF1α* transcripts were reduced with Poly (I:C) treatment, it is interesting that RPE

cells are still able to function under hypoxic conditions and upregulate glycolytic metabolism. Unsurprisingly, hypoxia treatment alone was enough to increase glycolysis in the RPE. Mouse models using the genetic induction RPE hypoxia, impact its ability to support nutrient availability within the retina [507].

The mTOR network is more of a general regulator of metabolism compared to AMPK, and therefore must integrate multiple environmental cues to augment the inflammatory response [434]. Both TLR agonists activated the mTOR pathway, despite the alternate effects on AMPK phosphorylation status. This suggests that whilst AMPK is activated by Poly (I:C), the inhibitory effects on mTOR are overcome by PI3K activation. Interestingly, Poly (I:C) was found to decrease the expression of Raptor. Raptor interacts with HIF-1α *via* an mTOR signalling motif in HIF-1α, thereby promoting HIF-1α activity [361]. As GβL is reported to stimulate the kinase activity of mTORC1 independently of Raptor [508], this may permit mTOR signalling to continue, whilst restricting the ability of the cell to undergo a HIF-1α-dependent switch to aerobic glycolysis (Fig. 3.23). Interestingly, silencing of Raptor diminishes the expression *HIF1α* mRNA transcripts [311], indicating a mechanism independent of AMPK whereby Poly (I:C)-stimulation could limit the aerobic glycolytic switch.

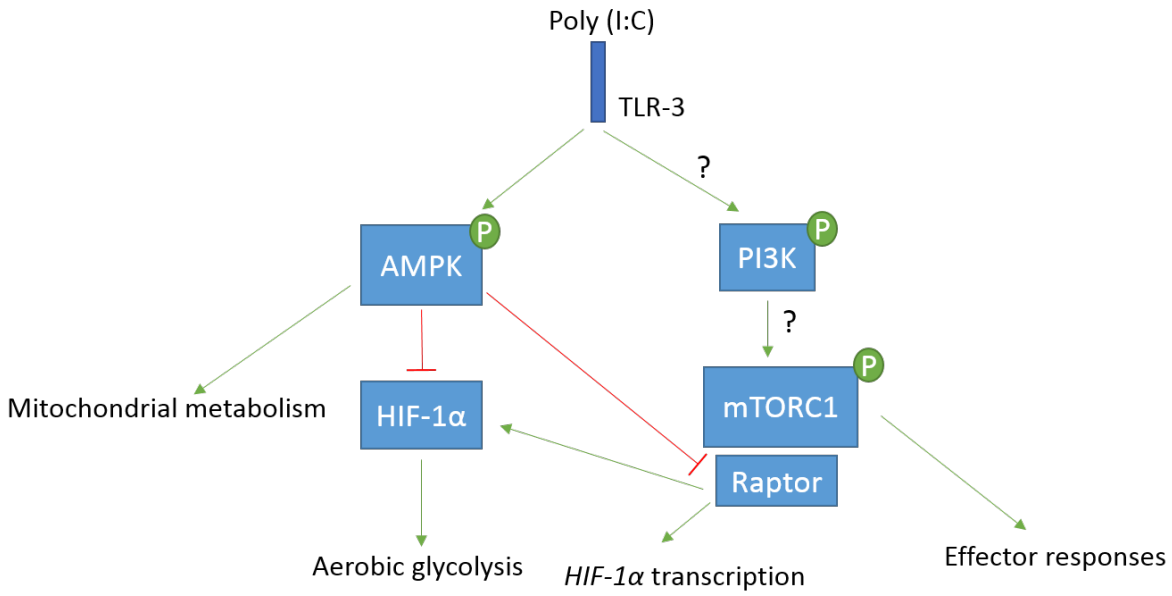

Figure 3.23. Signalling events in Poly (I:C)-stimulated RPE which limit aerobic glycolysis:

The synthetic analogy of dsRNA, Poly (I:C) is recognised by TLR-3. TLR-3 activation leads to the downstream activation of AMPK which promotes mitochondrial metabolism. Activation of mTORC1 is possibly mediated by PI3K in RPE cells as an early signalling event in response to Poly (I:C). The mTORC1 complex remains active, despite the downregulation of regulatory subunit Raptor, to maintain effector responses (such as gene transcription of antiviral genes). The absence of Raptor limits *HIF1α* gene transcription therefore antagonising aerobic glycolysis.

The concept of a metabolic 'retinal ecosystem' that was recently introduced by Hurley et al, suggests that energy homeostasis in retina and RPE relies on a complex and specialized metabolic interplay between metabolically distinct cells in the retina and RPE and has implications for retinal diseases [4]. That study suggests that dysfunctional mitochondrial activity with age restricts the concentration of glucose able to reach the photoreceptors and consequently reduces the lactate available to the RPE as a fuel source. This increased reliance on glycolysis may upset the "metabolic ecosystem" and lead to photoreceptor death. Indeed, as previously mentioned, hypoxia-induced metabolic stress and the induction of glycolysis in RPE cells leads to photoreceptor atrophy [382]. The results in this chapter – when applied to the context of a "metabolic ecosystem" – suggest that increased RPE glycolysis observed following TLR "stimulation" may have an adverse effect on the photoreceptor metabolism and subsequently, health.

PRR activation and the subsequent effects on RPE metabolism were assessed *via* the use of commercially available TLR agonists in this study. Typically, innate inflammatory responses occur as a result of microbial stimulation. However, as the eye exhibits a degree of immune-privilege [1], frequent TLR "stimulation" *via* bacterial and viral-derived PAMP ligands is improbable. In chronic conditions a form of "sterile" inflammation can occur in response to uncontrolled activation of PRR *via* self-derived ligands. TLRs bind and are activated by putative endogenous ligands (e.g. proteins, polysaccharides, phospholipids, nucleic acids and proteoglycans). There is now increasing evidence that endogenous ligand-TLR signalling occurs during pathological conditions such as tissue damage and repair under sterile inflammation [87]. Degenerating RPE-derived drusen components are likely drivers of innate sterile immune responses within the eye which manifest as TLR activation [41].

In summary, the results presented in this chapter identify variances in metabolic profiles in TLR-stimulated, and aging RPE both *in vitro* and *ex vivo*. The AMPK activation state restricts the "Warburg effect" in RPE following innate immune activation and limits the translation of *IL33* during disruption of energetic homeostasis.

Chapter 4. Extracellular interleukin-33 modulates retinal pigment epithelium bioenergetics

4.1. Introduction

Interleukin-33 (IL-33) is a newly discovered member of the IL-1 superfamily of cytokines [509]. IL-33 initiates signalling through a heterodimeric receptor complex comprised of its cognate receptor ST2 and IL-1RAcP [132]. Alternative splicing of ST2 generates a soluble extracellular form which acts as a decoy receptor for IL-33-dependent signalling [245]. It was initially proposed that IL-33, like IL-1β and IL-18 required cleavage for release and bioactivity because the protein lacked a clear signal peptide. IL-33 release was later found to not require inflammasome activation, with optimum bioactivity occurring at full-length; and rather, caspase-mediated cleavage inactivated IL-33 [233]. Full length pro-IL-33 is released from barrier cells following cellular damage and PRR activation and acts as an endogenous danger signal ("alarmin") to alert the immune system to tissue injury [9]. Typically, IL-33 is associated with Th2 responses as ST2 is expressed at high levels on mast cells and Th2 lymphocytes [9].

IL-33 plays an important role in several diseases, such as, chronic gastrointestinal inflammation [12], allergic diseases/ anaphylaxis [13], cardiovascular disease [14], choroidal angiogenesis [8] and Alzheimer's [15]. In experimental autoimmune uveitis, IL-33 moderates disease severity [16]. In a phototoxic model of retinal degeneration, IL-33 contributed to an upregulated chemokine and cytokine output from Müller Glia, leading to the recruitment of mononuclear phagocytes, and ultimately contributing to photoreceptor loss and diminished retinal integrity [17]. IL-33 was released as a 19-kD cleavage product from activated Müller Glia in the absence of cell death, implicating inflammasome mediated cleavage and inactivation of IL-33 [233]. As TLR-dependent up-regulation of IL-33 by RPE does not influence cell viability [8], it is likely that this is an adaptive response to maintain homeostasis.

How IL-33 exerts effects on ST2 expressing cells are not fully established. Evidence suggests IL-33 binds to its heterodimeric receptor complex and recruits the adaptor proteins MyD88 (also used by other TLRs [60]) and interleukin-1 receptor-associated kinase (IRAK), this leads to the activation of MAPK and NF-KB through the activity of TRAF6 [133]. ST2 activation is known to drive phosphorylation of ERK1/2, JNK1/2 and AKT pathways to facilitate the production and release of cytokines and chemokines [133]. IL-33 signalling has been shown to lead to broad transcriptional changes in cells modulating hundreds of genes depending on cell type. A detailed macrophage phosphoproteome analysis identified changes in over 600 proteins with IL-33 stimulation [510]. Microarray analysis of

human epithelium identified close to 1400 gene transcripts differentially regulated by IL-33 [511]. There is currently no uniform picture of the extent of intracellular gene induction regulated by IL-33/ST2 signalling. Therefore, between cell types it is unknown to what degree IL-33 influences transcriptional adaptations in innate immune response genes.

Recent exploitation of the cytoplasmic hybrid technique for representative mtDNA haplotypes of AMD populations, revealed alterations in IL-33 expression and altered bioenergetics [18]. IL-33 likely drives changes in transcription and intracellular signalling pathways to permit innate immune defence. As detailed in the previous chapter, innate immune signalling has been shown to be accompanied by metabolic reprogramming to bioenergetically support the demand of an innate immune response by an RPE cell. Collectively this led the investigation into the role of IL-33 in the regulation of RPE metabolism with a focus on the extracellular signalling activities.

4.2. Effect of recombinant human IL-33 on ARPE-19 basal metabolism and viability

Expression of the IL-33 cognate receptor ST2 has been previously demonstrated on RPE cells [8]. It was hypothesised that activation of RPE through the IL-33/ST2 signalling axis may be accompanied by metabolic changes like that of TLR activation considering their convergence on multiple conserved signalling pathways.

Although previously published work indicated the safety and tolerability of RPE cells to recombinant IL-33 [8], I first confirmed these results by assessing cell viability (MTT) and LDH release (indicative of cell cytotoxicity) in ARPE-19 cells stimulated for 24h with varying doses of rhIL-33 (Fig. 4.1A-B). Having established that IL-33 had no significant effect of the health of ARPE-19 cells, I investigated the initial metabolic responses to IL-33/ST2 signalling using seahorse XF. As IL-33/ST2 signalling is a rapid process in epithelial cells, leading to ERK activation and NF-kB nuclear translocation within minutes [512], it was of interest to see if there were metabolic change which accompanied immediate signalling cascades following ST2 activation; similarly to that of LPS activation of TLR-4 (see chapter 3). I utilised a similar experimental set-up as with TLR agonists (see section 3.4.), taking basal OCR and ECAR measurements every 7min over a 2h time frame, post injection of rhIL-33. No metabolic changes were observed in either ECAR or OCR measurements post injection of rhIL-33 (Fig. 4.1C-D). To investigate whether metabolic changes would occur later post stimulation, ARPE-19 cells were subsequently treated with varying doses of rhIL-33 (100-1ng/ml) for 12h. However, no significant effect was observed in terms of basal OCR or ECAR (Fig. 4.1E). ARPE-19 cells treated for an additional 12h (total 24h) with rhIL-33 showed a dose dependent increase in the basal OCR/ECAR ratio (Fig. 4.1E).

Collectively, these data suggest that RPE cells undergo metabolic changes in response to IL-33 stimulation for 24h. The increase in the OCR/ECAR ratio is indicative of an increase in OXPHOS over glycolysis. The metabolic changes observed with rhIL-33 at 24h occurred in the absence of changes to cell viability.

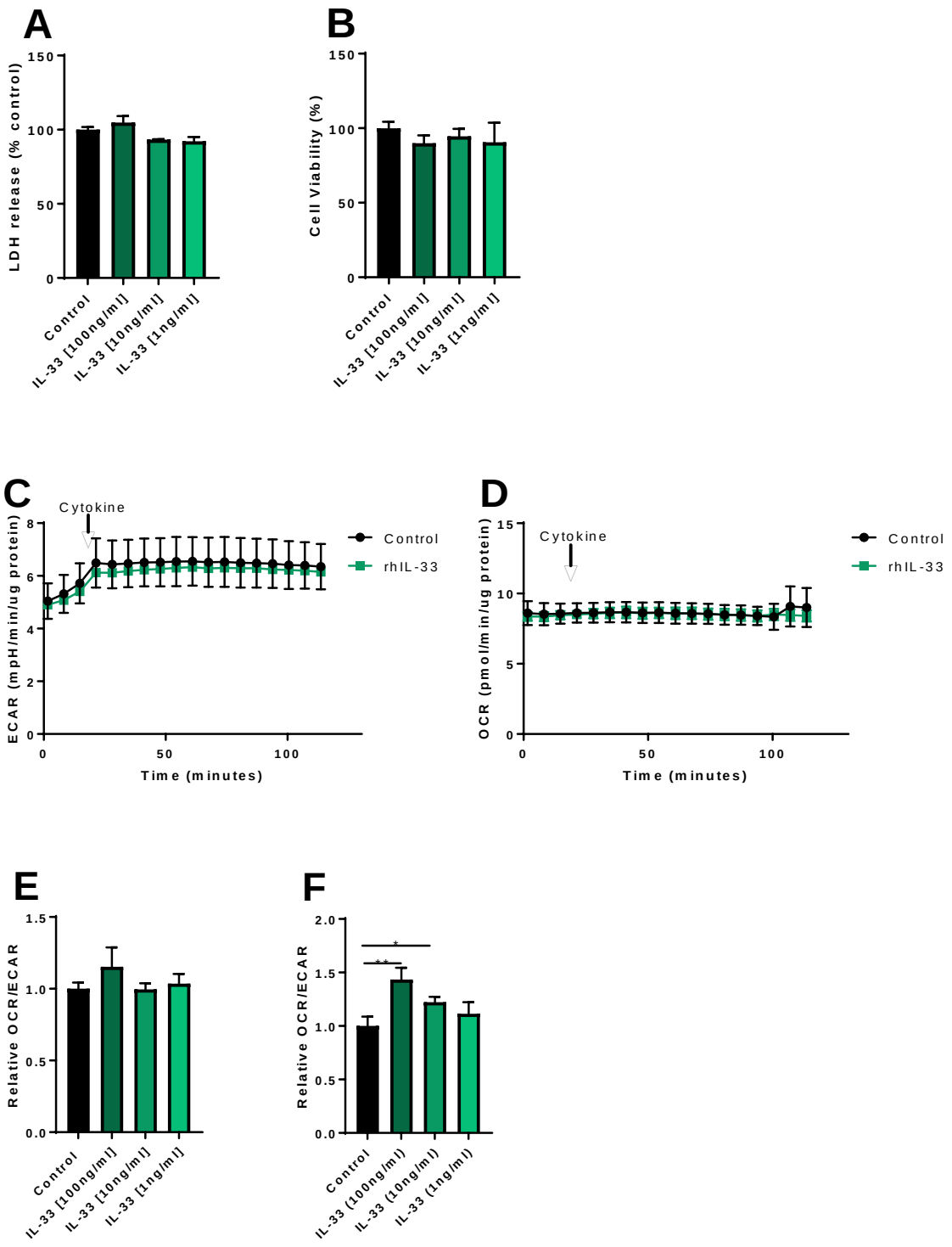
A
LDH release (% control)
150
100
50
0
Control
IL-33 [100ng/ml]
IL-33 [10ng/ml]
IL-33 [1ng/ml]
B
Cell Viability (%)
150
100
50
0
Control
IL-33 [100ng/ml]
IL-33 [10ng/ml]
IL-33 [1ng/ml]
C
Cytokine
ECAR (mpH/min/ug protein)
8
6
4
2
0
0
50
100
Time (minutes)
Control
rhIL-33
D
Cytokine
OCR (pmol/min/ug protein)
15
10
5
0
0
50
100
Time (minutes)
Control
rhIL-33
E
Relative OCR/ECAR
1.5
1.0
0.5
0.0
Control
IL-33 [100ng/ml]
IL-33 [10ng/ml]
IL-33 [1ng/ml]
F
Relative OCR/ECAR
2.0
1.5
1.0
0.5
0.0
*
**
Control
IL-33 (100ng/ml)
IL-33 (10ng/ml)
IL-33 (1ng/ml)

Figure 4.1. Effect of recombinant human IL-33 on ARPE-19 basal metabolism and viability:

Cells were treated for 24h with rhIL-33. (A) LDH release was quantified in supernatants and expressed relative to an untreated control, (B) Cell viability was quantified using an MTT assay and expressed as a percentage of the untreated control. (C) Real-time ECAR measurements post injection of 100ng/ml rhIL-33. (D) Real-time OCR measurements post injection of 100ng/ml rhIL-33. Basal OCR/ECAR ratio 12h (E) and 24h (F) after treatment with rhIL-33. Data are expressed as means ± SD. (A-B) Represent data from four independent experiments performed with four technical repeats. (C-D) Represents data from two independent experiments performed in triplicate. (E-F) Represent data from three independent experiments performed with no technical repeats. One-way ANOVA with Dunnet's multiple comparisons test; *p<0.05, **p<0.01.

4.3. Effect of recombinant human IL-33 on ARPE-19 glycolytic and mitochondrial metabolism

To further investigate the effects of IL-33 on ARPE-19 metabolism, additional experiments were performed using pre-optimised "metabolic tests" on the XF platform (as shown in chapter 3). A glycolysis stress test was used to examine glycolytic parameters following treatment of rhIL-33. No significant changes were observed in glycolysis (post glucose injection), yet there was an increase in glycolytic capacity (post oligomycin) and glycolytic reserve (Fig. 4.2A-B). This suggested that there was an increased ability of IL-33 treated cells to accommodate increased ATP demand by increasing glycolytic flux. I subsequently utilised a mitochondrial stress test to evaluate mitochondrial respiration in IL-33-stimulated RPE. This test identified increases in oxidative metabolism following treatment, particularly increases in basal, maximal and spare capacity (Fig. 4.2C-D). Collectively these results indicate that IL-33 stimulation of ARPE-19 leads to increased glycolytic and mitochondrial metabolism.

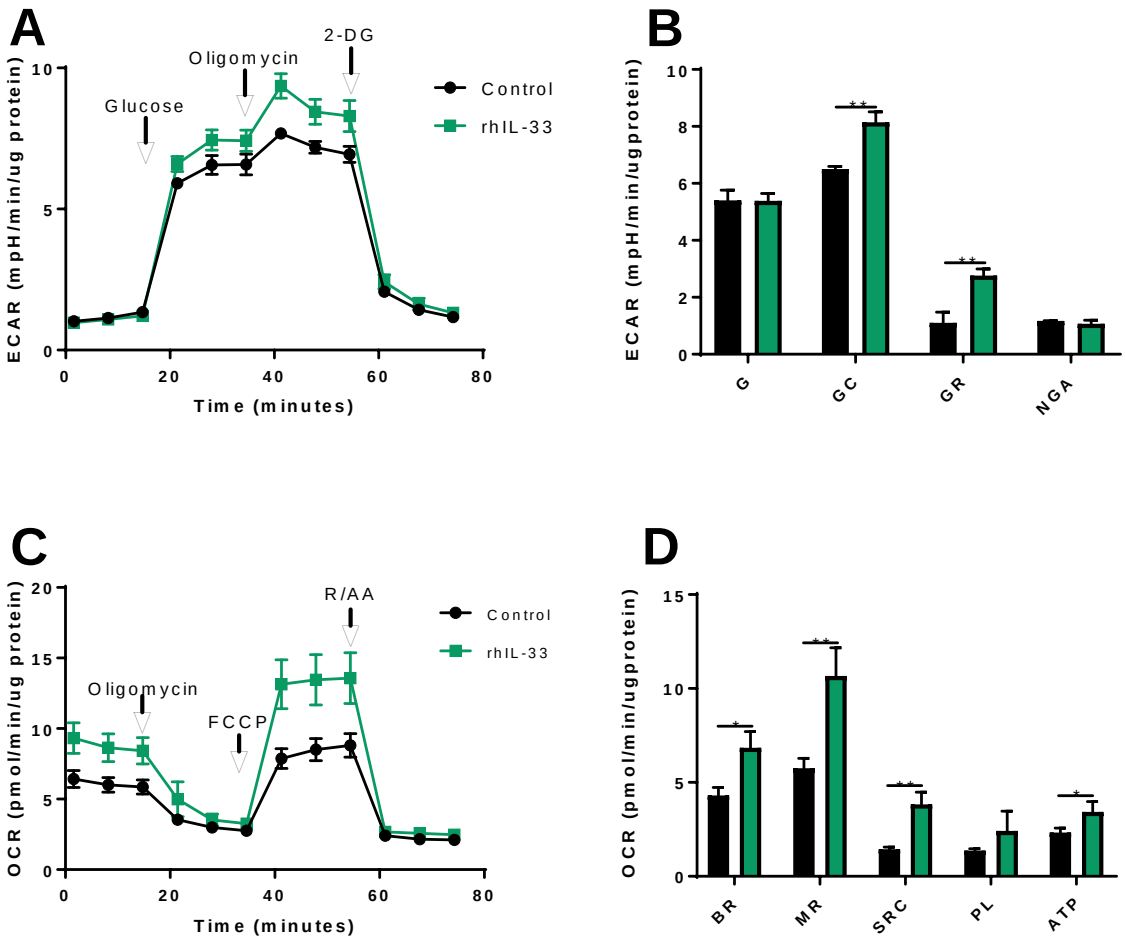

Figure. 4.2. Effect of recombinant human IL-33 on ARPE-19 glycolytic and mitochondrial metabolism:

(A) Representative glycolysis stress test measured with sequential injections of glucose, oligomycin and 2DG, following stimulation with rhIL-33 (100ng/ml) for 24h. (B) Glycolysis parameters (G- glycolysis; GC- glycolytic capacity; GR- glycolytic reserve; NGA- non-glycolytic acidification) calculated from data shown in (A). (C) Representative mitochondrial stress test measured with sequential injections of Oligomycin, FCCP and rotenone/antimycin A, following stimulation with rhIL-33 (100ug/ml) for 24h. (D) Mitochondrial parameters (BR- basal respiration; MR- maximal respiration; SRC- spare respiratory capacity; PL- proton leak; ATP- ATP-production) calculated from data shown in (C). Data are expressed as means ± SD from three independent experiments performed in triplicates. Unpaired Student's T-test; *p<0.05, **p<0.01.

4.4. Effect of recombinant murine IL-33 on primary murine RPE bioenergetics

To investigate whether the metabolic changes observed with IL-33 treatment were not limited to this immortalised cell line but represented an ability of RPE to adapt its metabolism under stress, primary murine RPE were also used. Like the ARPE-19 cell-line, rmIL-33 was observed to have no effect on immediate metabolic responses post-injection (Fig. 4.3A-B). Primary RPE were stimulated for 24h with rmIL-33 and a mitochondrial stress analysis was used to identify changes to mitochondrial respiration. It was observed that IL-33 treatment increased oxidative metabolism; with basal and maximal respiration increased post treatment (Fig. 4.3C-D). No significant changes were observed to spare respiratory capacity (Fig. 4.3C-D). rmIL-33 increased the OCR/ECAR ratio of the primary RPE (Fig. 4.3E).

IL-33 signals through its cognate receptor comprised of ST2 and IL-1RAcP [133]. To determine if the effects of IL-33 were due to IL-33/ST2 signalling, primary murine RPE were isolated from mice lacking the ST2 receptor gene (*Il1rl1*$^{-/-}$). Both WT and *Il1rl1*$^{-/-}$ RPE were stimulated for 24h with rmIL-33 and the OCR/ECAR ratio was measured. This showed that the effect of rmIL-33 on the primary isolated RPE was dependent on ST2 expression (Fig. 4.3F).

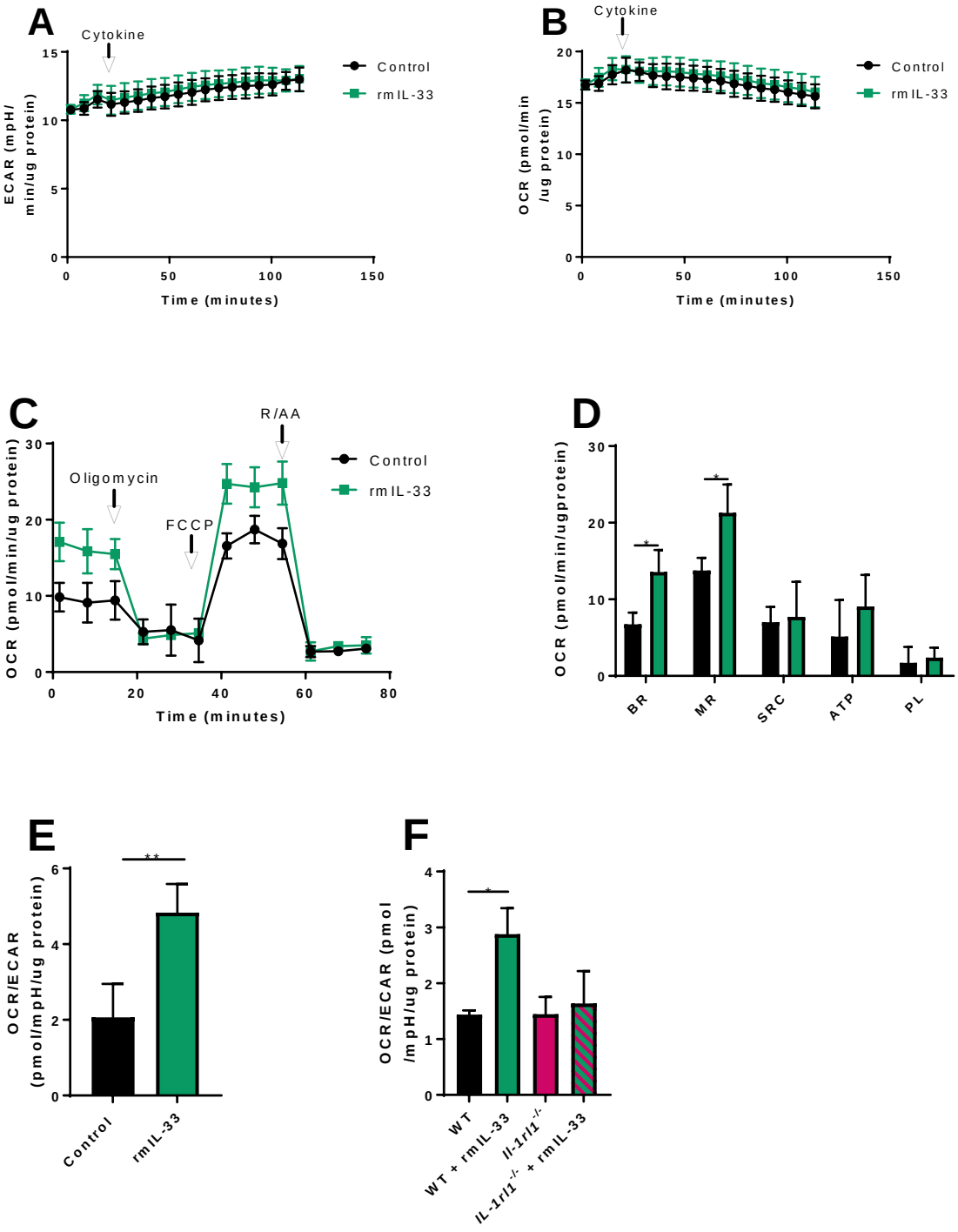
A
Cytokine
ECAR (mpH/ min/ug protein)
Time (minutes)
Control
rmIL-33
B
Cytokine
OCR (pmol/min /ug protein)
Time (minutes)
Control
rmIL-33
C
Oligomycin
FCCP
R/AA
OCR (pmol/min/ug protein)
Time (minutes)
Control
rmIL-33
D
OCR (pmol/min/ugprotein)
BR
MR
SRC
ATP
PL
E
OCR/ECAR (pmol/mpH/ug protein)
Control
rmIL-33
F
OCR/ECAR (pmol /mpH/ug protein)
WT
WT + rmIL-33
Il-1rl1-/-
IL-1rl1-/- + rmIL-33

Figure 4.3. Effect of recombinant murine IL-33 on primary murine RPE bioenergetics:

(A) Real-time changes in ECAR following injection of rmIL-33 (100ng/ml). (B) Real-time changes in OCR following injection of rmIL-33 (100ng/ml). (C) Representative mitochondrial stress test measured with sequential injections of oligomycin, FCCP and rotenone/antimycin A. (D) mitochondrial parameters (BR- basal respiration; MR- maximal respiration; SRC- spare respiratory capacity; PL- proton leak; ATP- ATP-production) calculated from data shown in (C). (E) Basal OCR and ECAR measurements expressed as the ratio OCR/ECAR, following 24h rmIL-33 treatment (100ng/ml). (F) Basal OCR and ECAR measurements expressed as the ratio OCR/ECAR, following 24h rmIL-33 treatment (100ng/ml) to either WT or *Il1rl1* KO mice. Data are expressed as means ± SD from either (A, B, E and F) two independent experiments performed in triplicates or (C-D) three independent experiments performed in triplicates. (C-E) Unpaired Student's T-test; *p<0.05, **p<0.01. (F) One-way ANOVA with Dunnet's multiple comparisons test; *p<0.05.

4.5. Metabolic response of mast cells and Müller glia to recombinant IL-33

The results from the previous sections indicate that IL-33 stimulation of RPE cells elicits metabolic reprogramming and an increase in mitochondrial metabolism. To identify whether these effects were specific to the RPE, or ubiquitous within other ST2 expressing cells, two additional cell types were utilised: mast cells and Müller glia.

Mast cells express high levels of ST2 and are potently activated by IL-33 [513]. Considering this, the mast cell was an excellent candidate to determine whether the metabolic effects observed with IL-33 treatment were specific to the RPE. To determine whether IL-33 elicited any metabolic changes in mast cells, real-time measurements of ECAR and OCR were taken post-injection of IL-33. rmIL-33 had no effect on the basal OCR or ECAR measurements (Fig. 4.4A-B). A mitochondrial stress test was coupled to this assay (2h post injection) to determine the effect of rmIL-33 on mitochondrial metabolism. There was no significant effect of treatment on mast cell OXPHOS parameters (Fig. 4.4B-C). Using the corresponding ECAR data generated from this assay, it was observed that there were no significant changes to the glycolytic capacity post-injection of oligomycin (Fig, 4.4D). Treatment of mast cells for 24h with rmIL-33 had no significant effect on OXPHOS parameters (Fig, 4.4E-F), glycolytic capacity (Fig, 4.4G) or basal OCR/ECAR ratio in mast cells (Fig. 4.4H). As a positive control for mast cell activation and degranulation, the degranulating agent calcimycin [514] was also used as a positive control. It was observed that calcimycin treatment induced a rapid increase in mast cell glycolytic metabolism post injection (Fig. 4.4A-B).

GFAP+ Müller glia have been observed to highly express transmembrane ST2 after light exposure to the retina [17]. IL-33 was observed to elicit a robust expression of cytokine and chemokine expression from Müller glia cells in an autocrine manner [17]. To further investigate the role of IL-33 signalling on cellular metabolism, the response of Müller glia to rhIL-33 was additionally investigated. Real-time measurements of ECAR and OCR were taken post-injection of rhIL-33, however there were no significant changes observed (Fig. 4.5A-B). Treatment of Müller glia for 24h with rhIL-33 had no significant effect on the mitochondrial function of Müller glia (Fig. 4.5C-D), glycolytic capacity (Fig. 4.5E), or the OCR/ECAR ratio (Fig. 4.5F).

Taken together, the results from this section indicate that the effects of IL-33 on cellular metabolism in the retina may be specific to the RPE. Other ST2 expressing cells such as human Müller glia and murine mast cells displayed no significant metabolic alterations when treated with the cytokine.

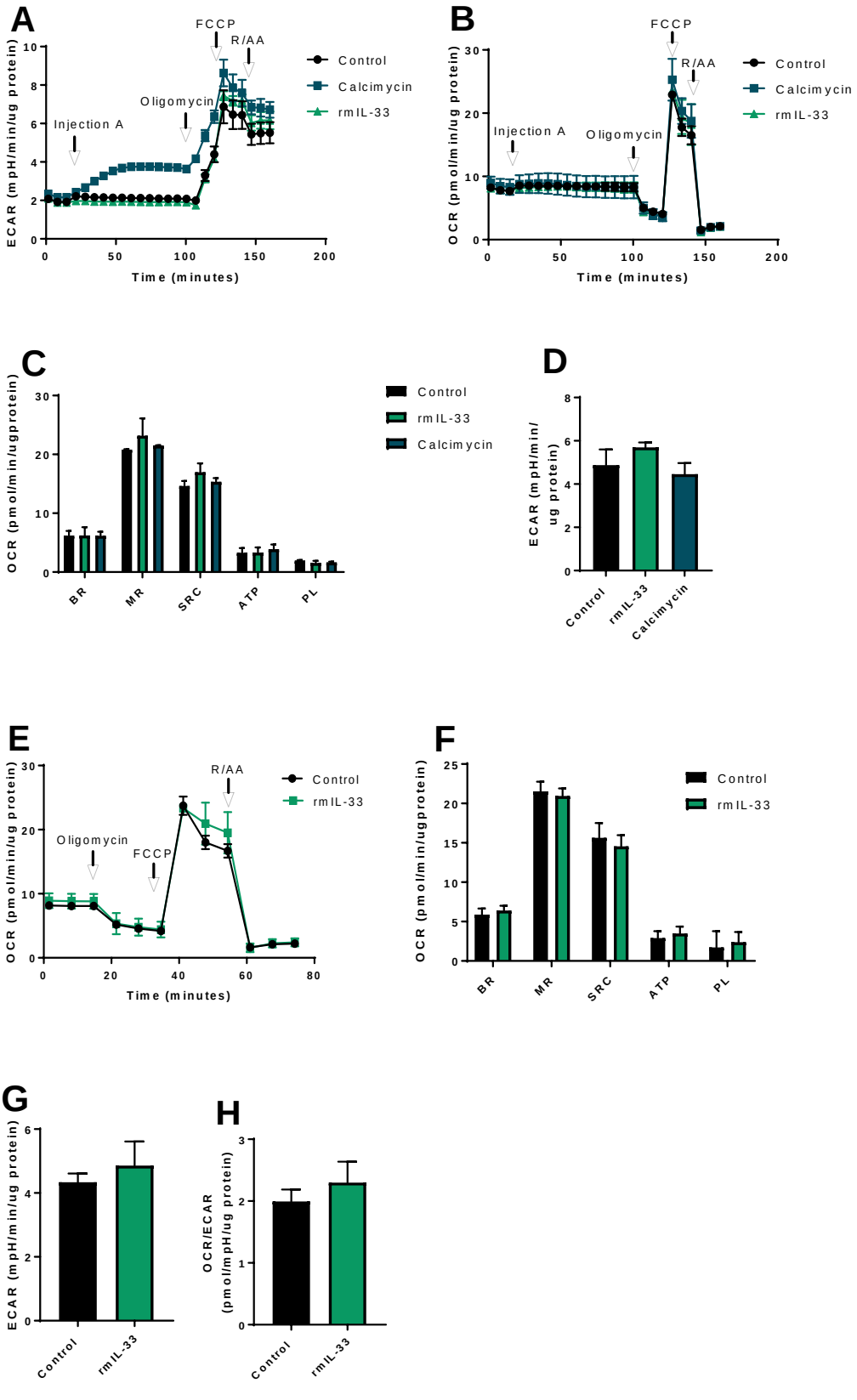
A
ECAR (mpH/min/ug protein)
Time (minutes)
Injection A
Oligomycin
FCCP
R/AA
Control
Calcimycin
rmIL-33
B
OCR (pmol/min/ug protein)
Time (minutes)
Injection A
Oligomycin
FCCP
R/AA
Control
Calcimycin
rmIL-33
C
OCR (pmol/min/ugprotein)
BR
MR
SRC
ATP
PL
Control
rmIL-33
Calcimycin
D
ECAR (mpH/min/ ug protein)
Control
rmIL-33
Calcimycin
E
OCR (pmol/min/ug protein)
Time (minutes)
Oligomycin
FCCP
R/AA
Control
rmIL-33
F
OCR (pmol/min/ugprotein)
BR
MR
SRC
ATP
PL
Control
rmIL-33
G
ECAR (mpH/min/ug protein)
Control
rmIL-33
H
OCR/ECAR (pmol/mpH/ug protein)
Control
rmIL-33

Figure 4.4. Metabolic response of BMMC to recombinant IL-33:

(A) Real-time changes in ECAR following injection of rmIL-33 (100ng/ml) or Calcimycin (50nM) to BMMC (B) Real-time changes in OCR following injection of rmIL-33 (100ng/ml) or Calcimycin (50nM) to BMMC. Sequential mitochondrial stress test measured with sequential injections of oligomycin, FCCP and rotenone/antimycin A. (C) mitochondrial parameters (BR- basal respiration; MR- maximal respiration; SRC- spare respiratory capacity; PL- proton leak; ATP- ATP-production) calculated from data shown in (B). (D) glycolytic capacity calculated from data shown in (A). (E) Mitochondrial stress test analysis following rmIL-33 treatment (100ng/ml) of BMMC. (F) mitochondrial parameters (BR- basal respiration; MR- maximal respiration; SRC- spare respiratory capacity; PL- proton leak; ATP- ATP-production) calculated from data shown in (E). (G) Glycolytic capacity calculated from the corresponding ECAR data to (E). (H) Basal OCR and ECAR measurements expressed as the ratio OCR/ECAR, following 24h rmIL-33 treatment (100ng/ml) of BMMC. Data are expressed as means ± SD. A-C represents data from two experiments performed in duplicate. E-H represents data from two experiments performed in triplicates.

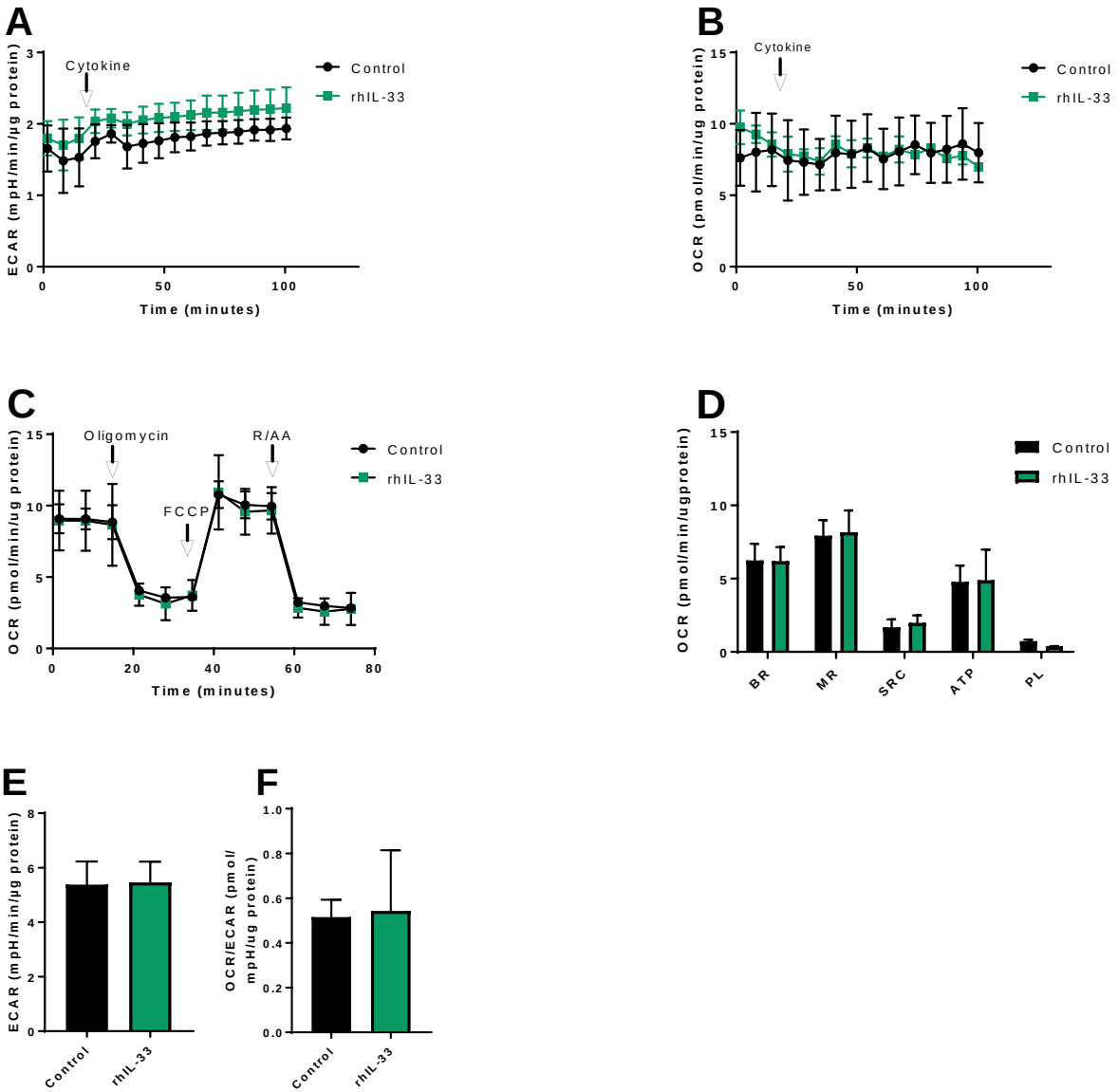
A
Cytokine
Control
rhIL-33
ECAR (mpH/min/µg protein)
Time (minutes)
B
Cytokine
Control
rhIL-33
OCR (pmol/min/ug protein)
Time (minutes)
C
Oligomycin
R/AA
FCCP
Control
rhIL-33
OCR (pmol/min/ug protein)
Time (minutes)
D
Control
rhIL-33
OCR (pmol/min/ugprotein)
BR
MR
SRC
ATP
PL
E
ECAR (mpH/min/µg protein)
Control
rhIL-33
F
OCR/ECAR (pmol/ mpH/ug protein)
Control
rhIL-33

Figure 4.5. Metabolic response of Müller glia to recombinant IL-33:

(A) Real-time changes in ECAR following injection of rmIL-33 (100ng/ml) to Müller glia. (B) Real-time changes in OCR following injection of rmIL-33 (100ng/ml) to Müller glia. (C) Mitochondrial stress test analysis following 24h rmIL-33 treatment (100ng/ml) of Müller glia. (D) mitochondrial parameters (BR- basal respiration; MR- maximal respiration; SRC- spare respiratory capacity; PL- proton leak; ATP- ATP-production) calculated from data shown in (C). (E) Glycolytic capacity calculated from the corresponding ECAR data from (C). (F) Basal OCR and ECAR measurements expressed as the ratio OCR/ECAR, following 24h rmIL-33 treatment (100ng/ml) of Müller glia. Data are expressed as means ± SD. (A-B) represents data from two experiments performed in duplicate. (B-H) represents data from two experiments performed in triplicates.

4.6. Glucose consumption, lactate production and metabolic gene transcription in IL-33-stimulated ARPE-19

To confirm the results in the previous sections using the XF platform, I utilized several alternative assays to measure RPE metabolism. Glucose consumption was first measured in the media of ARPE-19 cells treated with rhIL-33 for 24h. This showed no statistically significant change between the unstimulated and rhIL-33 groups (*p=0.067*) (Fig. 4.6A).

RT-PCR analysis of metabolic genes (encoding glycolytic and TCA cycle enzymes and nuclear transcription factors) was performed. This indicated that in the glycolysis pathway there was significantly increased expression of *GLUT1* (responsible for glucose import) and *PKM2* transcripts with rhIL-33 treatment compared to an untreated control (Fig. 4.6B). An increase in GLUT1, but not PKM2 expression was observed at the protein level (Fig. 4.6C-D). In terms of the TCA cycle, increased expression of *IDH1*, *FH*, *CS* and *SDHD* transcripts were observed in the rhIL-33 treatment group (Fig. 4.6B). rhIL-33 treatment additionally increased the transcription of "master metabolic regulators" *MYC* and *SIRT1* (Fig. 4.6B).

Lactate output was measured in the media as a direct quantification of glycolytic activity, and there was no statistically significant change observed (*p=0.057*) (Fig. 4.6E). The ATP/ADP ratio was assessed to identify if a metabolic shift with rhIL-33 treatment was accompanied by augmented ATP production. It was observed that ARPE-19 treated with rhIL-33 displayed an increased ATP/ADP ratio (Fig. 4.6F), suggesting increased mitochondrial activity and ATP production.

The PDH complex catalyses the irreversible decarboxylation of pyruvate into Acetyl-CoA, which feeds into the TCA cycle for oxidative metabolism *via* NADH production [469]. PDH is therefore critical in connecting the glycolysis pathway to the TCA cycle. PDH is regulated by PDK1 which phosphorylates and inactivates PDH on a highly conserved serine residue [469]. It was observed that rhIL-33 increased the expression (but not activation status) of PDH relative to an unstimulated control (Fig. 4.6G-H). This indicates that increased PDH expression likely results in increased oxidative pyruvate catabolism in the mitochondria. Collectively these results confirm previously observed results that IL-33 treatment increases glycolytic and mitochondrial metabolism in the RPE.

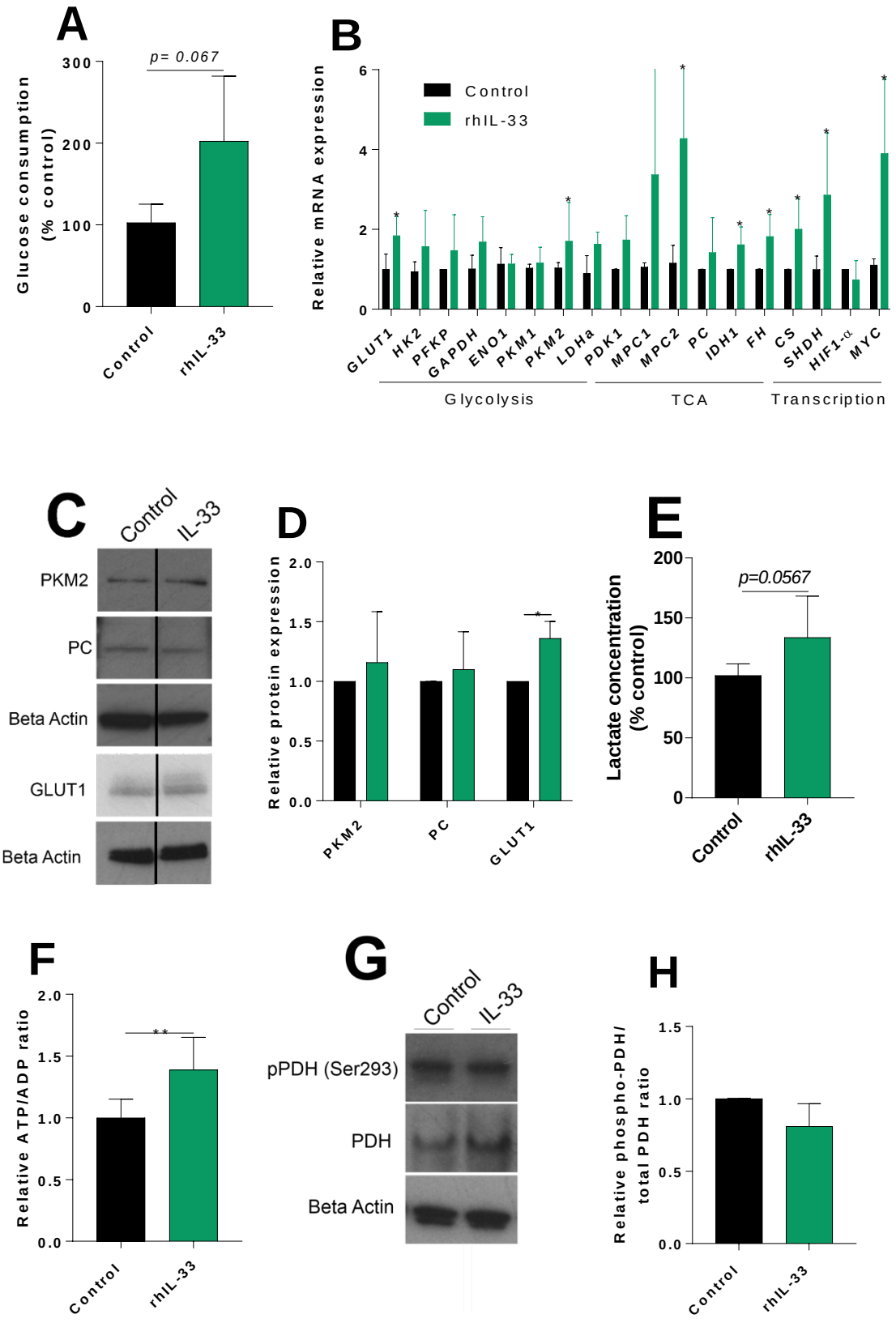
A
p= 0.067
Glucose consumption (% control)
300
200
100
0
Control
rhIL-33
B
Relative mRNA expression
6
4
2
0
Control
rhIL-33
GLUT1
HK2
PFKP
GAPDH
ENO1
PKM1
PKM2
LDHa
PDK1
MPC1
MPC2
PC
IDH1
FH
CS
SHDH
HIF1-α
MYC
Glycolysis
TCA
Transcription
C
Control
IL-33
PKM2
PC
Beta Actin
GLUT1
Beta Actin
D
Relative protein expression
2.0
1.5
1.0
0.5
0.0
PKM2
PC
GLUT1
E
p=0.0567
Lactate concentration (% control)
200
150
100
50
0
Control
rhIL-33
F
Relative ATP/ADP ratio
2.0
1.5
1.0
0.5
0.0
Control
rhIL-33
G
Control
IL-33
pPDH (Ser293)
PDH
Beta Actin
H
Relative phospho-PDH/ total PDH ratio
1.5
1.0
0.5
0.0
Control
rhIL-33

Figure 4.6. Glucose consumption, lactate production and glycolysis gene transcription in IL-33-stimulated ARPE-19:

ARPE-19 cells were stimulated for 24h with rhIL-33 (100ng/ml). (A) Supernatants were assessed for relative glucose consumption. (B) Quantitative RT-PCR of glycolytic pathway enzymes (*HK, LDHA, PFKP, GAPDH, PKM1, PKM2* and *ENO1*), *GLUT1*, *PDK1*, *MPC1*, *MPC2*, TCA cycle enzymes (*PC, IDH1, FH, SDHD* and *CS*), *PGC1α, HIF1α, MYC, SIRT1* and *SIRT4* mRNA transcripts. (C) Extracellular lactate measurements were taken in the media and expressed as a percentage of the mean untreated control. (D) ATP and ADP levels were quantified following cell lysis and expressed as the ratio ATP/ADP. (E) Western blot analysis was used to determine the phosphorylation of pyruvate dehydrogenase. (F) Reprehensive densitometry from (E). Data are expressed as means ± SD. (A and C) Represents data from three independent experiments performed in triplicate. (B and D) Represents data from three independent experiments performed in duplicate. (F and G) Represent two independent blots. Unpaired Student's T-test; *p<0.05, **p<0.01.

4.7. Mass spectroscopy-based metabolomics in IL-33-stimulated ARPE-19

The data shown in the previous sections indicate that IL-33 stimulated RPE cells (but not other ST2 expressing cells) specifically undergo metabolic reprogramming accompanied by increased TCA activity and glycolytic metabolism. To further investigate the metabolic changes which occur, a mass-spectroscopy-based approach was used to quantify total intracellular metabolites following treatment of ARPE-19 with rhIL-33.

SITA with [U-^{13}C]-glucose was used to assess the uptake of isotopically labelled glucose into metabolite pools following treatment with rhIL-33. This approach allowed the quantification of C^{13} labelling into metabolite pools as cells approach steady-state equilibrium (see schematic in Fig. 3.12). Cells were treated for the indicated time points with rhIL-33, followed by 2h of culture in [U-^{13}C]-glucose. Relative concentrations of C^{13}-labelled labelled glyceraldehyde-3-phosphate, 3-phosphoglycerate, pyruvate and lactate were increased in the rhIL-33 treatment group, suggesting increased glycolytic flux (Fig. 4.7A-D). Significantly enriched C^{13} labelling was also observed in TCA metabolites citrate (Fig. 4.7E), succinate (Fig. 4.7H), fumarate (Fig. 4.7I), malate (Fig. 4.7J) and oxaloacetate (Fig. 4.7K) in the IL-33 treatment group. No C^{13} labelling was observed in α-ketoglutarate, yet there was a significant reduction of the unlabelled metabolite pool with IL-33 treatment (Fig. 4.7F). No significant changes were observed in glutamate (Fig. 4.7G) or aspartate (Fig. 4.7L) between treatment groups.

These data indicate that glycolytic metabolism is increased in cells stimulated with IL-33, as observed by the increased C^{13} flux into glycolytic intermediates. Moreover, increased labelling in TCA cycle metabolites confirms the increased pyruvate oxidation and mitochondrial activity observed in previous sections.

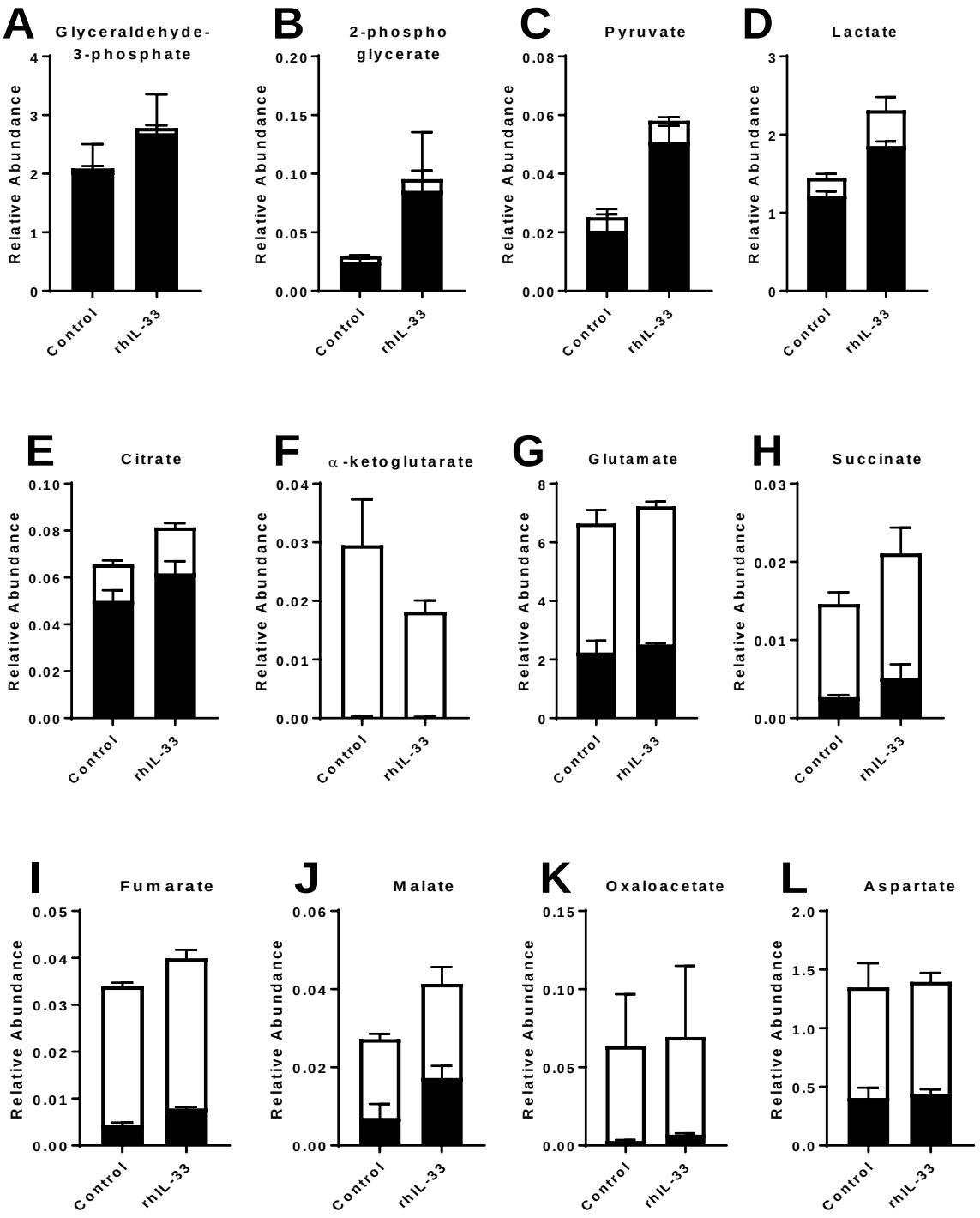
A
Glyceraldehyde-3-phosphate
B
2-phospho glycerate
C
Pyruvate
D
Lactate
E
Citrate
F
α-ketoglutarate
G
Glutamate
H
Succinate
I
Fumarate
J
Malate
K
Oxaloacetate
L
Aspartate
Relative Abundance
Control
rhIL-33

Figure 4.7. Glucose tracing in IL-33-stimulated ARPE-19:

Cells were treated with IL-33 (100ng/ml; 24h). Cells were incubated for 2h with media containing isotopically labelled glucose and GC-MS was used to quantify relative C^{13} (black) or C^{12} (white) incorporation into glyceraldehyde-3-phosphate (A), 3-phosphoglycerate (B), pyruvate (C), lactate (D), citrate (E), α-ketoglutarate (F), glutamate (G), succinate (H), fumarate (I), malate (J), oxaloacetate (K) and aspartate (L) metabolite pools. Represents data from three independent experiments.

4.8. Mitochondrial morphology of IL-33-treated ARPE-19

Results from the previous sections indicate that IL-33/ST2 signalling in RPE cells initiates metabolic reprogramming, increasing both glycolysis and mitochondrial OXPHOS. Considering these observations, I further interrogated the changes to mitochondria which occur in innate immunity *via* cytokine/cytokine receptor signalling. As previously mentioned (see section 3.14.), mitochondrial dynamics is essential to the maintenance of organelle quality control and adaptation to bioenergetic parameters (e.g. nutrient supply, energy demand and pathway efficiency) [473]. Opposing mitochondrial morphologies (mediated by fission or fusion) are linked with different bioenergetic programs, with increased mitochondrial fragmentation in anabolic cells associated with increased proton leak. Mitochondrial fragmentation and leak permit increased TCA flux for anabolism in a situation of aerobic glycolytic metabolism [515]. Inhibition of mitochondrial fission machinery prompts mitochondrial elongation, accompanied bioenergetically by increased OXPHOS [472]. To investigate whether metabolic changes following exposure of RPE cells to IL-33 were accompanied with alterations to mitochondrial structure, samples were studied by transmission electron microscopy.

ARPE-19 cells were treated for 24h with rhIL-33, followed by fixation and imaging. Stimulation with rhIL-33 had little effect on the size of mitochondria compared to an unstimulated control (Fig. 4.8A-C). rhIL-33 elicited changes to RPE mitochondrial morphologies. Unstimulated cells showed mostly fragmented mitochondria (77.5%) and short tubular mitochondria. Long tubular mitochondria were observed at a low frequency (2.5%). With treatment of rhIL-33, there was a 10-fold increase in the frequency of long tubular mitochondria (27.4%) at the expense of fragmented mitochondria which dropped to around 50% of total mitochondria (Fig. 4.8D). The increased frequency of elongated mitochondria suggested that mitochondrial fission/fusion enzymes were affected by IL-33 treatment. Considering this, the transcription of nuclear-encoded mitochondrial fission/fusion enzymes was assessed by RT-PCR in ARPE-19 cells exposed to IL-33. IL-33 treatment lead to increased expression of the OMM-localized, pro-fusion, *OPA1* gene transcripts (Fig. 4.8E). Conversely, IL-33 treatment was also accompanied by an upregulation of *DRP1*, which is involved in mitochondrial fission (Fig. 4.8E). DRP1 is inactivated by phosphorylation on a conserved subunit, however the protein expression of DRP1 and its phosphorylation status was not investigated in this body of work. No significant changes were found in the transcription of pro-fusion *MFN1* or *MFN2*, or mitophagy regulator *PINK1* (Fig. 4.8E). The data presented so far indicates that IL-33 treatment drives elongation of RPE mitochondria. This shift in the mitochondrial morphologies was not as profound as that of TLR stimulation (see chapter 3),

likely due to reduced transcriptional changes in fission/fusion genes. RT-PCR was used to estimate mitochondrial content through the amplification of two segments of the mitochondrial genome (the gene encoding cytochrome B and 16 S rRNA). Expression of both genes was normalized to the expression of the nuclear encoded β-globulin gene. No significant changes to mtDNA copy number was observed following treatment of cells with IL-33.

To further explore mitochondrial structure during the metabolic changes associated with IL-33 signalling, the expression of ETC components were assessed using western blotting. ARPE-19 cells were stimulated for 24h with rhIL-33, total protein was isolated and a commercially available preoptimized OXPHOS antibody cocktail was used to assess protein expression. IL-33 treatment was observed to significantly up-regulate the protein expression of Cox2 (complex IV), UQCRC2 (complex III), SHDB (complex II) and NDUFB8 (complex I) (Fig. 4.9A-B). No significant changes were observed in the expression of the ATP synthase complex (Fig. 4.9A-B).

The data presented in this section show that structural changes in mitochondria are observed in response to IL-33 signalling. IL-33 has little effect on mitochondrial biogenesis but affects both mitochondrial remodelling and the expression of ETC components. This suggests that the changes observed to metabolic function in the previous sections are likely to be attributed to the increased capacity of mitochondria to undergo OXPHOS (through increased ETC components) rather than increased mitochondrial numbers. By altering the functionality of mitochondria rather than their abundance, IL-33 stimulation endows increased oxidative potential in RPE cells.

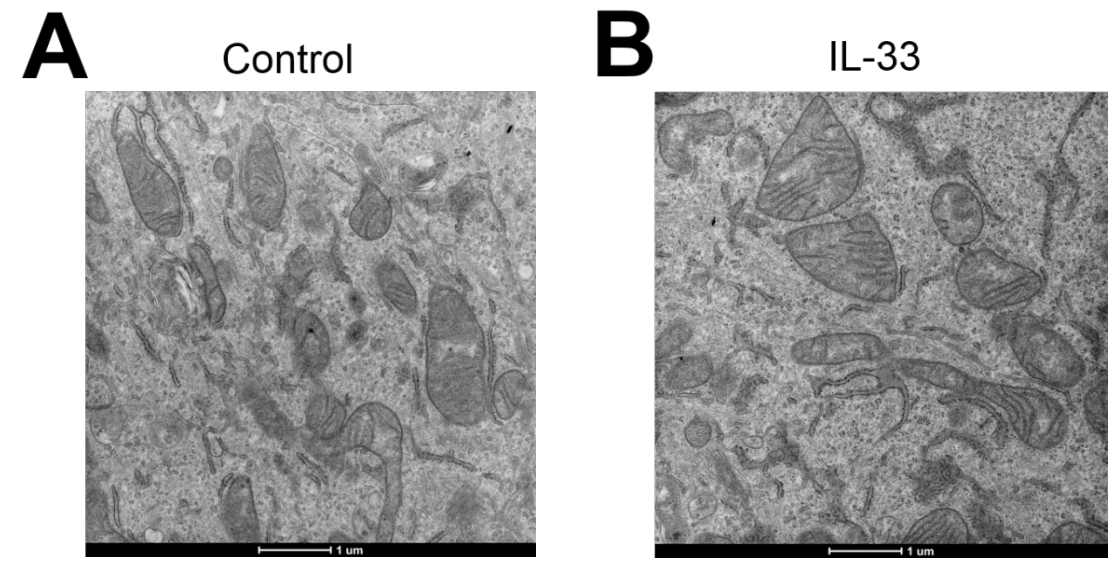
A
Control
B
IL-33
1 um
1 um

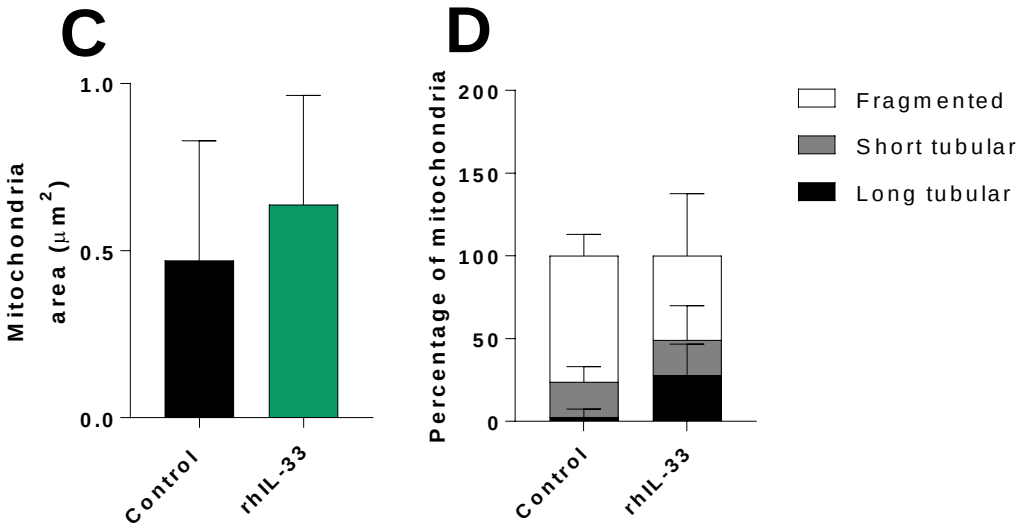
C
Mitochondria area (μm²)
1.0
0.5
0.0
Control
rhIL-33
D
Percentage of mitochondria
200
150
100
50
0
Control
rhIL-33
Fragmented
Short tubular
Long tubular

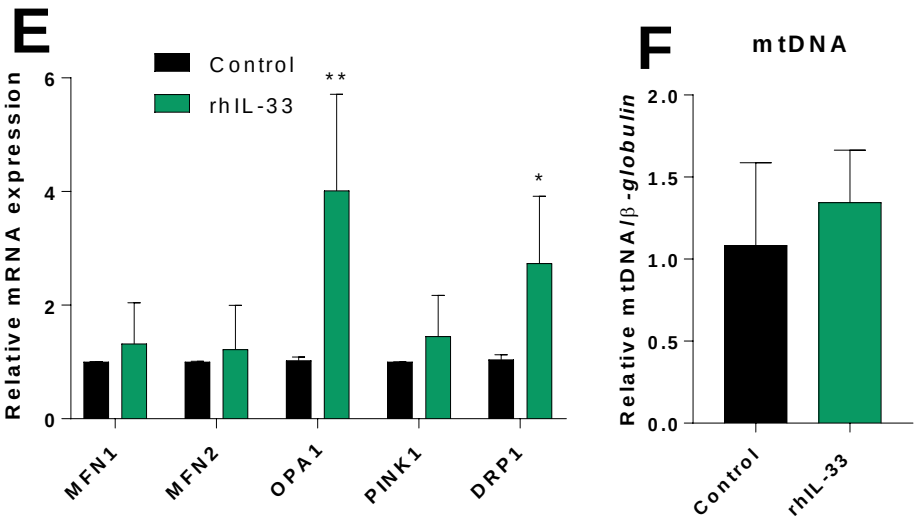
E
Relative mRNA expression
Control
rhIL-33
6
4
2
0
**
*
MFN1
MFN2
OPA1
PINK1
DRP1
F
mtDNA
Relative mtDNA/β-globulin
2.0
1.5
1.0
0.5
0.0
Control
rhIL-33

Figure 4.8. Mitochondrial morphologies in IL-33-stimulated ARPE-19:

Representative transmission electron microscopy of ARPE-19 mitochondria either untreated (A) stimulated with rhIL-33 for 24h (B). Magnification 9300x. (C) Mitochondrial area was calculated using ImageJ. (D) Quantification of mitochondrial morphology into either fragmented, short tubular or long tubular phenotypes. (E) Quantitative RT-PCR was performed to assess the mitochondrial fission and fusion enzymes *MFN1*, *MFN2*, *OPA1*, *PINK1* and *DRP1* mRNA transcripts. (F) Quantitative RT-PCR was performed to assess mitochondrial content; this was estimated from the amplification of *CTYB* and 16S rRNA relative to *BGLOB* mRNA transcripts. One-way ANOVA with Dunnet's multiple comparisons test; *p<0.05, **p<0.01.

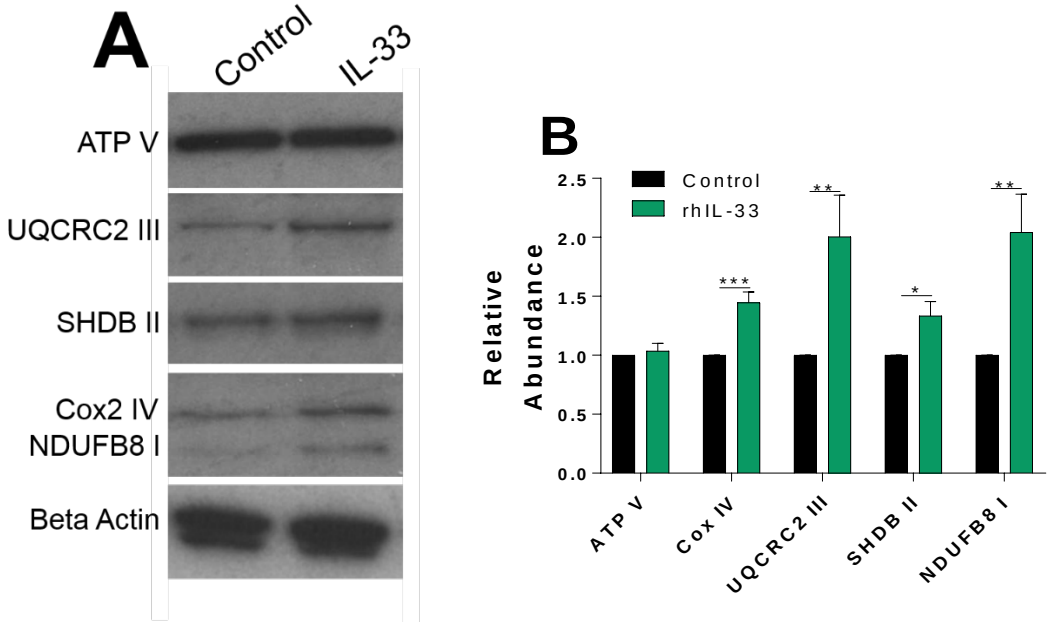

Figure 4.9. Expression of ETC components in IL-33-stimulated ARPE-19:

ARPE-19 were stimulated with rhIL-33 (100ng/ml) for 24h. (A) Western blot analysis was used to determine the expression of ETC complexes (ATP synthase V, Cox2 IV, UQCRC2 III, SHDB II and NDUFB8 I). (B) Relative densitometry was calculated from (H) using ImageJ. Represents two independent blots.

4.9. Effect of IL-33 on AMP-activated kinase activation status in ARPE-19

The data presented in the previous sections has shown that IL-33/ST2 signalling drives metabolic changes in the RPE towards oxidative mitochondrial metabolism. Glycolysis is also increased but it appears that IL-33 does not elicit an immediate "Warburg-like" metabolic switch to aerobic glycolysis (like LPS stimulated RPE (see chapter 3), but rather utilises the mitochondrial TCA cycle. The metabolic changes in IL-33 stimulated cells were accompanied by structural alterations to mitochondria and increased expression of OXPHOS components. Whilst there was a clear increase in mitochondrial metabolism with IL-33 treatment, the underlying mechanisms whereby TCA cycle/ETC activity was boosted remained elusive.

Data from the previous chapter indicated that mitochondrial OXPHOS was regulated by the activation status of AMPK in the RPE. AMPK signalling was observed to limit the Warburg effect in RPE cells in response to TLR-3 and -4 stimulation. Comparable to TLR-3 activated RPE, bioenergetic adaptations which followed IL-33/ST2 signalling in the RPE, were increased OXPHOS and a restriction of aerobic glycolysis, occurring at a later time-point of 24h post-stimulation. It is well known that AMPK activation limits the Warburg effect and drives increased mitochondrial metabolism in cells [311, 344]. It was therefore of interest to determine whether IL-33/ST2 signalling in the RPE elicits bioenergetic adaptations through the activation of AMPK.

ARPE-19 cells were stimulated with rhIL-33 for 24h and the activation of AMPK was assessed by western blot analysis. IL-33 was observed to increase the phosphorylation (and activation) of AMPK (Fig. 4.10A-B). Downstream of AMPK, there was a non-significant increase of the phosphorylation of ACC ($p=0.054$) (Fig. 4.10A and C). Collectively this supports the hypothesis that IL-33 signalling is not accompanied by a shift to aerobic glycolysis but rather maintains the activity of mitochondrial OXPHOS, likely through the sustained activation of AMPK and the limitation of anabolic signalling.

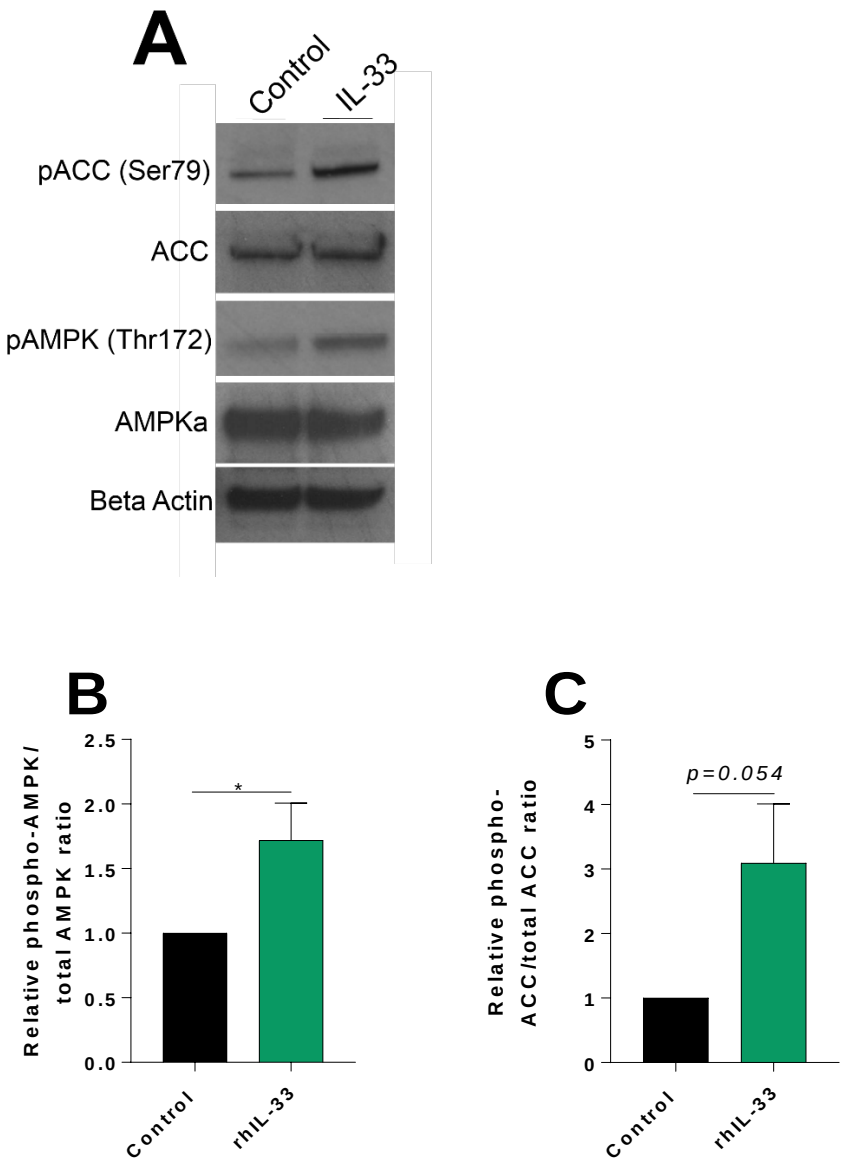

Figure 4.10. Effect of IL-33 on AMP-activated kinase activation status in ARPE-19:

(A) Cells were treated with rhIL-33 (100ug/ml) for 24h. Western blot analysis was used to determine the phosphorylation of AMPK and ACC following treatment. (B) Densitometry analysis of P-AMPK/AMPK. (C) Densitometry analysis of P-ACC/ACC. Data are expressed as means ± SD from two independent blots. Unpaired Student's T-test; *p<0.05.

4.10. Effect of IL-33 pre-treatment on hydrogen peroxide-mediated oxidative stress

Given the functional significance of IL-33/ST2 signalling on both AMPK activation and mitochondrial capacity, it was hypothesised this could be exploited to protect against oxidative damage to the RPE. As AMD progresses, there is an increase in chronic photo-oxidative stress. This results in the production of reactive oxygen intermediates which initiate RPE dysfunction and death [516]. The RPE is susceptible to the noxious effects of oxidative stress as a result of its high levels of metabolic activity, high oxygenation and exposure to photosensitizers such as lipofuscin [3]. As a comparator for RPE oxidative stress and cytotoxicity, H_2O_2 was used as an *in vitro* platform of inducing reactive oxygen species within the RPE [517]. Increased oxidative stress (*via* H_2O_2) in RPE cells manifest in ATP depletion, receptor-interacting serine/threonine-protein kinase 3 (RIPK3) aggregation, membrane breakdown and HMGB1 release (all key features of necrosis) [517]. Oxidative stress-mediated cell death in RPE cells has been shown to occur through necrosis rather than apoptosis, autophagy or pyroptosis [517]. The use of H_2O_2 in this body of work enabled the formation of a platform of RPE degeneration secondary to oxidative stress. As anticipated dose and time-dependent relationships were observed between H_2O_2 concentrations and cell viability (Fig. 4.11A). Cell viability was measured using the MTT assay to provide a direct readout of the cytotoxicity of treatments. I used the two doses of H_2O_2 (0.2mM and 1mM) at 24h of treatment as this was the time point which elicited significant variation between the two doses, which was not observed at 12h, and preserved a level of cell viability which was lost at 48h (Fig. 4.11A).

To test the hypothesis that IL-33 may confer a protective effect against oxidative stress in RPE cells, ARPE-19 cells were co-treated with both H_2O_2 and rhIL-33 for 24h. It was found that co-treatment of rhIL-33 and H_2O_2 had no protective effect on cell viability at either dose (Fig. 4.11B). Considering the observation that IL-33 undergoes oxidation-induced conformational changes, responsible for terminating biological activity upon ST2 binding [236], I hypothesised that the co-treatment with hydrogen peroxide may terminate its biological activity. In order to overcome this problem and to assess if IL-33 was protective against oxidative stress, ARPE-19 cells were pre-treated with different doses of rhIL-33 for 12h prior to exposure to H_2O_2 for 24h. It was observed that IL-33 pre-treatment (at any of the doses investigated) had no significant effect on cell viability following treatment of 0.2mM H_2O_2 (Fig. 4.11C). At the higher dose of H_2O_2 (1mM), IL-33 pre-treatment was observed to increase cell viability (Fig. 4.11C). To confirm the effects of IL-33 in promoting RPE survival during oxidative stress using cell viability (MTT) as a read-out, cell cytotoxicity was also measured using LDH release into cell culture supernatants. LDH release is indicative of loss of cell membrane integrity and

cell necrosis which can be attributed to treatment cytotoxicity. H_2O_2 treatment at the greater dose of 1mM significantly increased the LDH release into ARPE-19 supernatants (Fig. 4.11D). Pre-treatment of ARPE-19 cells with low concentrations of IL-33 (1-10ng/ml) were protective against the 1mM H_2O_2-induced cytotoxicity (Fig. 4.11D).

These data indicate an ability of IL-33 to protect against H_2O_2-mediated oxidative damage to the RPE. Interestingly, IL-33 was ineffective in protecting against cytotoxicity when treated in combination with H_2O_2. This was likely a result of impaired bioactivity, although it was not investigated in this body of work whether H_2O_2 conferred structural changes to the IL-33 polypeptide, rendering its signalling ineffective. Pre-treatment of cells with IL-33 positively influenced RPE survival in high levels of oxidative damage. However, as this was only assessed after 12h of pre-treatment and 24h of H_2O_2 treatment, there is little indication on how long the protective effect of IL-33 remains in RPE cells under oxidative stress, or how long the pre-treatment must be to elicit significant effects.

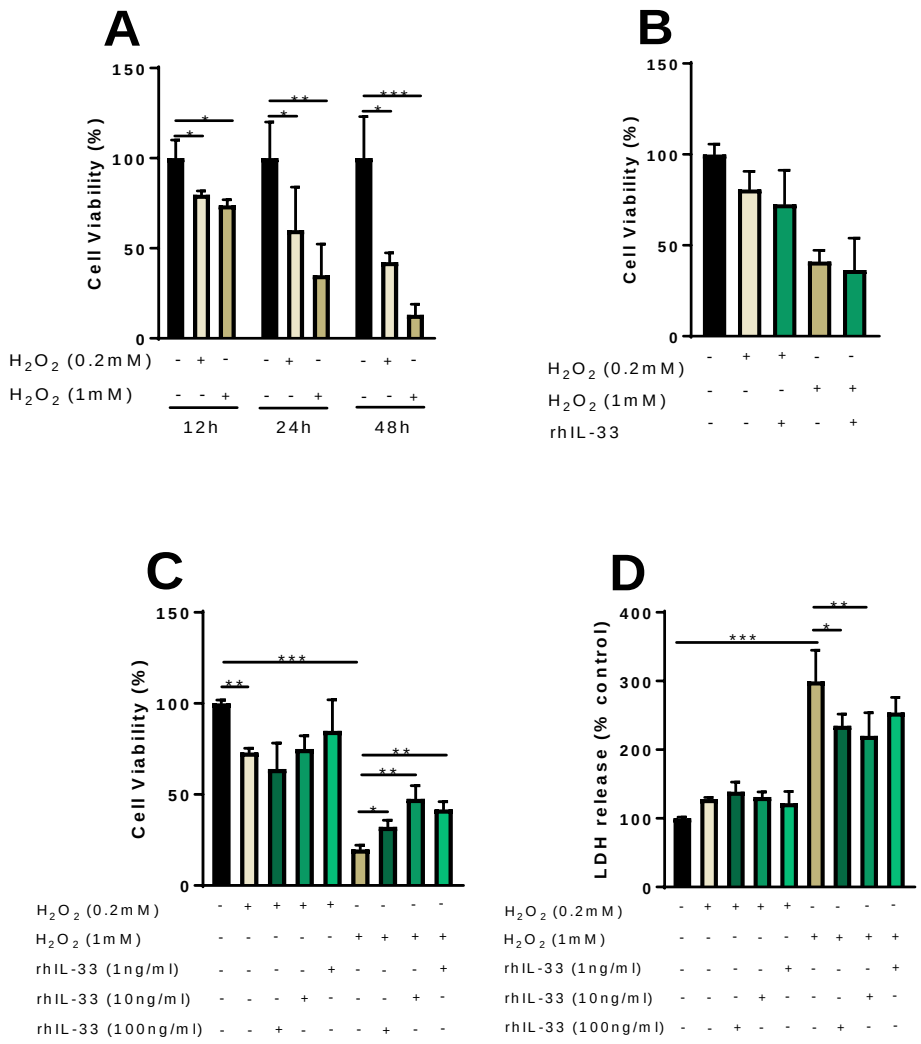

Figure 4.11. Effect of IL-33 pre-treatment on hydrogen peroxide-mediated oxidative stress:

(A) ARPE-19 were exposed to hydrogen peroxide (0.2 and 1mM), cell viability was quantified using an MTT assay and expressed as a percentage of the untreated control. (B) Cell viability was quantified following co-treatment with either hydrogen peroxide (0.2 and 1mM) or hydrogen peroxide (0.2 and 1mM) and rhIL-33 (100ng/ml) for 24h. Cells were pre-treated with rhIL-33 (1-100ng/ml) for 12h before exposure to hydrogen peroxide (0.2 and 1mM) for 24h. (C) Cell viability was quantified using an MTT assay and expressed as a percentage of the untreated control. (D) LDH release was quantified in supernatants and expressed relative to an untreated control. Data are expressed as means ± SD. Represents data from three independent experiments performed with four technical repeats. (A and B) One-way ANOVA with Dunnet's multiple comparisons test, (C and D) One-way ANOVA with Tukey's multiple comparisons test; *p<0.05, **p<0.01, ***p<0.005.

4.11. Effect of IL-33 on ST2 expression

The results obtained in the previous section indicated that IL-33 augmented RPE survival over short periods of oxidative stress. Interestingly, the lower doses of IL-33 (1 and 10ng/ml) were observed to confer a greater degree of protection in terms of both cell viability (MTT) and H_2O_2-mediated cytotoxicity (LDH release). It was hypothesised that "dose-response" kinetics of IL-33 may be attenuated by the release of decoy receptor sST2 into the cell culture supernatants. sST2 lacks the transmembrane and extracellular components required for signalling and is found in the extracellular space whereby it binds and sequesters IL-33 to neutralise IL-33/ (membrane bound) ST2 signalling. Previous reports have shown that exogenous recombinant IL-33 administration increases the secretion of sST2 from cells [227]. To confirm that in ARPE-19 cells, rhIL-33 dose-dependently increases the secretion of sST2, a commercial ELISA was used to determine the secreted sST2 into the supernatants. rhIL-33 treatment for 24h lead to a dose-dependent increase in the secretion of sST2 into the supernatants (Fig. 4.12A). Increased sST2 expression was also confirmed intracellularly at the protein level using western blot analysis (Fig. 4.12B-C). No changes were observed in the expression of the membrane-bound ST2 receptor following treatment with rhIL-33 (Fig. 4.12B). Collectively these data indicate that IL-33 promotes the expression and secretion of sST2 from RPE cells. As IL-33 is a biologically potent cytokine, this is likely a mechanism to control proinflammatory signalling.

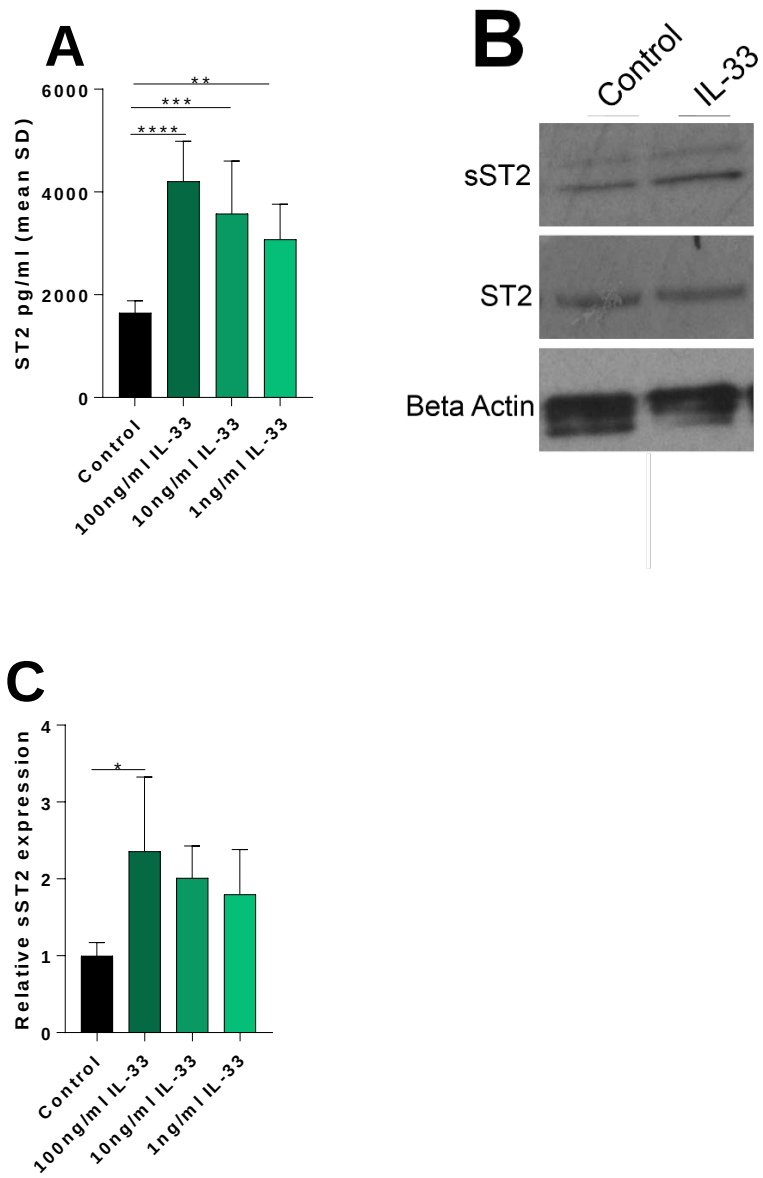

Figure 4.12. Effect of IL-33 on ST2 expression:

ARPE-19 cells were treated with varying does of rhIL-33 (100-1ng/ml) for 24h. (A) ST2 expression was quantified in supernatants using a commercial ELISA kit. (B) Western blot analysis was utilised to confirm the expression of ST2. (C) Densitometry analysis of ST2 expression. Data are expressed as means ± SD. (A) Represents data from three independent experiments performed with four technical repeats. (B and C) Represents data from two independent experiments performed with two technical repeats. One-way ANOVA with Tukey's multiple comparisons test; *p<0.05, **p<0.01, ***p<0.005, ***p<0.001.

4.12. Protection against mitochondrial dysfunction by IL-33

Corroborating the above data that demonstrate a protective effect of IL-33 against hydrogen-peroxide-induced stress, it was of interest to further refine the findings in the context of RPE metabolic health. With oxidative stress and mitochondrial damage, there is impaired mitochondrial and glycolytic activity in RPE cells [397, 518]. Indeed, as AMD disease severity progresses, there is increased mitochondrial damage observed in the RPE [396] To validate the *in vitro* platform of oxidative stress, extracellular flux analysis was used to determine the metabolism of ARPE-19 cells following treatment with H_2O_2. Treatment with H_2O_2 (1mM) for 24h resulted in altered mitochondrial function as established by decreased basal respiration, maximal respiration, spare respiratory capacity and ATP-production (Fig. 4.13A-B). H_2O_2 treatment lead to reduced basal ECAR and glycolytic capacity (Fig. 4.13C-D) signifying reduced glycolytic energy metabolism.

Subsequent to confirming extracellular flux as a read-out of mitochondrial damage, I investigated how pre-treatment with IL-33 would affect metabolic health. ARPE-19 were first pre-treated with rhIL-33 (100ng/ml) for 12h (as this was observed to protect against H_2O_2 in the LDH and MTT assays). Basal respiratory measurements were taken, and hydrogen peroxide was then injected. rhIL-33 treatment increased the OCR measurements post hydrogen peroxide (Fig. 4.13E). No significant "protection" was observed in ECAR post injection (Fig. 4.13F). To understand how the mitochondrial capacity may be altered with oxidative stress, a mitochondrial stress was utilised with an acute primary injection of H_2O_2 (Fig. 4.13G). It was observed that H_2O_2 reduced the maximal mitochondrial respiration and spare respiratory capacity (Fig. 4.13H). rhIL-33 pre-treatment of the cells for 24h prior to treatment significantly increased the maximal respiration and the spare respiratory capacity of the cells post H_2O_2 treatment (Fig. 4.13G-H). The top dose of 100ng/ml rhIL-33 was observed to elicit the greatest protection to the cells in this assay (Fig. 4.13G-H).

Combined, this data supports the observations from the preceding sections whereby IL-33 pre-treatment of cells was protective against H_2O_2-induced cytotoxicity. In this section I have shown that H_2O_2 treatment impairs mitochondrial function and glycolytic capacity. Pre-treating RPE cells with IL-33 protected against acute mitochondrial dysfunction, yet this was investigated on different time scales (1h vs 24h of H_2O_2 treatment) to the previous section so it is unknown to what extent mitochondrial function is sustained in IL-33 treated cells.

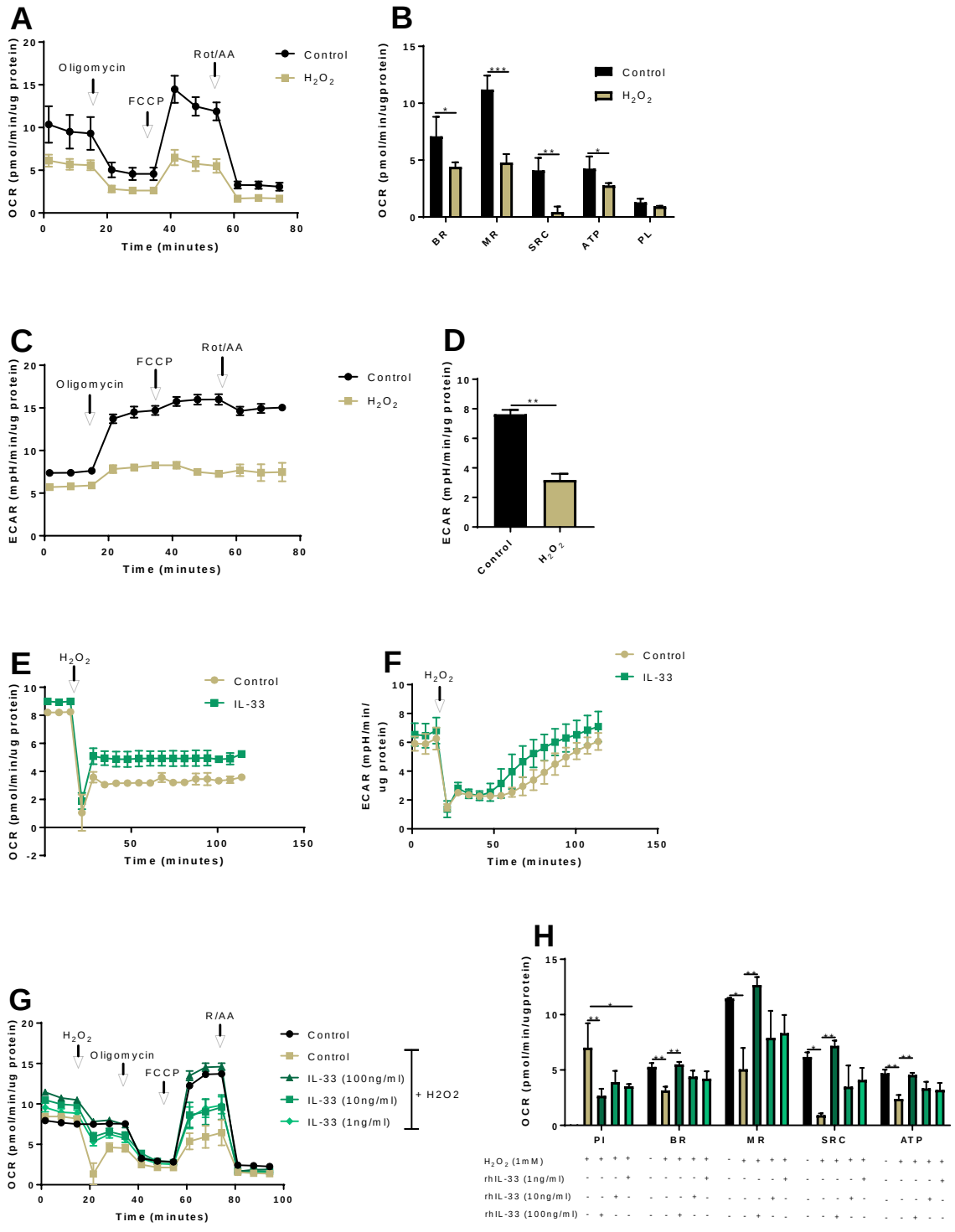

4.13. Protection against mitochondrial dysfunction by IL-33:

ARPE-19 were treated with hydrogen peroxide (1mM) for 24h. (A) Mitochondrial stress test analysis (B) Mitochondrial parameters (BR- basal respiration; MR- maximal respiration; SRC- spare respiratory capacity; PL- proton leak; ATP- ATP-production) calculated from data shown in (A). (C) Corresponding ECAR data from (A). (D) Glycolytic capacity was calculated from (C). ARPE-19 were pre-treated with rhIL-33 (100ng/ml) for 12h. (E) Real-

time OCR readings post-injection of hydrogen peroxide (1mM) (F) Real-time ECAR readings post-injection of hydrogen peroxide (1mM). (G) Representative modified mitochondrial stress test measured with sequential injections of hydrogen peroxide, Oligomycin, FCCP and rotenone/antimycin A, following stimulation with rhIL-33 (100ng/ml) for 24h. (H) Mitochondrial stress parameters (PI- ΔOCR post H_2O_2; MR- maximal respiration; SRC- spare respiratory capacity; PL- proton leak; ATP- ATP-production) calculated from data shown in (G). Data are expressed as means ± SD except for (H) which is expressed as means ± SEM. (A-D) Represents data from two experiment performed with three technical repeats. (E-F) Represents data from three experiment performed with three technical repeats. (G-H) Represents data from three independent experiments performed with no technical repeats. One-way ANOVA with Tukey's multiple comparisons test; *p<0.05, **p<0.01.

4.13. Effect of IL-33 on expression of antioxidant enzymes, survival proteins and transcription factors

To investigate the potential mechanistic basis for the ability of IL-33 treatment to protect against oxidative damage, the expression of antioxidant enzymes was assessed in ARPE-19 following rhIL-33 stimulation. The cellular antioxidant capacity has a significant impact on how the cell responds to an oxidative challenge. Antioxidant enzymes and redox sensitive genes are essential to the maintenance of a healthy environment post oxidative insult. The major enzymes involved in the removal of ROS are SOD1 and SOD2 enzymes (responsible for the conversion of superoxide radicals *to* H_2O_2) and catalase and glutathione peroxidase (enzymes responsible for the later conversion of H_2O_2 into H_2O) [519, 520]. It was found that the treatment of ARPE-19 cells with rhIL-33 had no significant effect on the expression of catalase, SOD1 or SOD2 (Fig. 4.14A).

Since AMPK has been implicated in upregulating BCL-2/survivin expression [521], I examined the possibility that in addition to the metabolic effects described in the previous section, IL-33/AMPK promoted cell survival by upregulating anti-apoptotic factors such as survivin and BCL-2. It was observed that rhIL-33 had no significant effect on the expression of either anti-apoptotic protein (Fig. 4.14B).

The transcriptional coactivator, PGC-1α is a well-studied mediator of mitochondrial function. Previous work has shown that PGC-1α increases mitochondrial function and protects against oxidative damage in the RPE [36]. It is also known that AMPK activation increases *PGC1α* expression and activates PGC-1α by direct phosphorylation [522]. SIRT-1 has a major role in cellular metabolism, epigenetic regulation and directly associates with a variety of transcriptional co-factors (including PGC-1α) which confer protection against oxidative damage [523]. I examined the possibility IL-33/ST2 signalling influenced PGC-1α expression in the RPE, which could serve as a possible mechanism to protect against oxidative stress. It was observed that IL-33 treatment increased the expression of *PGC1α* and PGC-1α protein. No significant changes were observed in the gene expression of *SIRT1* following treatment with rhIL-33 (Fig. 4.14C).

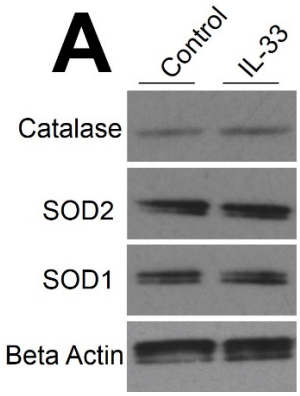
A
Control
IL-33
Catalase
SOD2
SOD1
Beta Actin

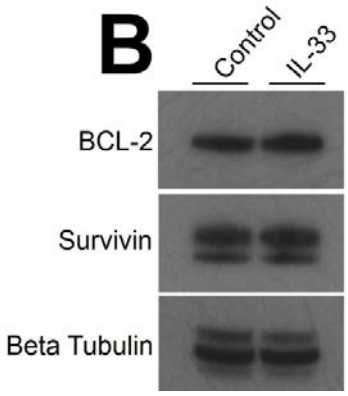
B
Control
IL-33
BCL-2
Survivin
Beta Tubulin

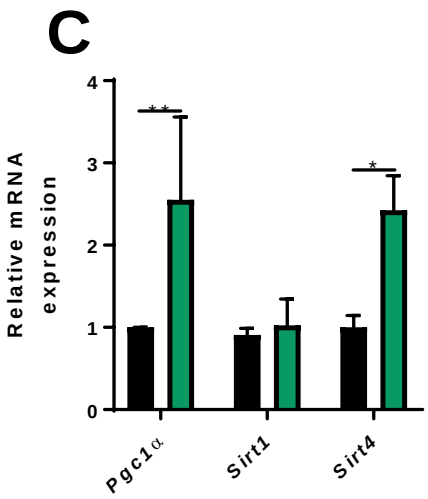
C
Relative mRNA expression
0
1
2
3
4
**
*
Pgc1α
Sirt1
Sirt4

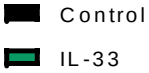
Control
IL-33

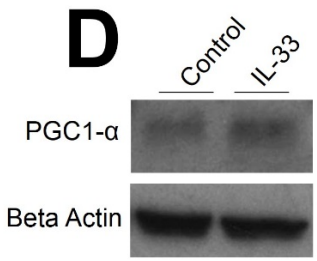
D
Control
IL-33
PGC1-α
Beta Actin

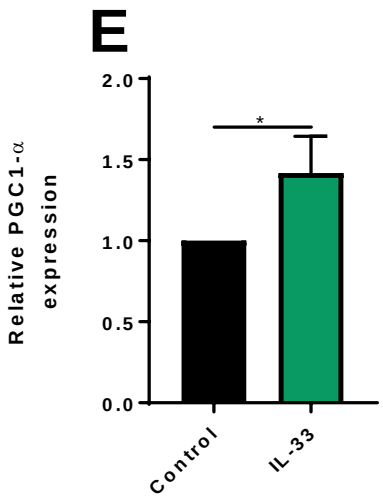
E
Relative PGC1-α expression
0.0
0.5
1.0
1.5
2.0
*
Control
IL-33

Figure 4.14. Effect of IL-33 on expression of antioxidant enzymes, survival proteins and transcription factors:

ARPE-19 were treated with rhIL-33 (100ug/ml) for 24h. (A) Western blot analysis of antioxidant enzymes: catalase, superoxide dismutase-1 and superoxide dismutase-2. (B) Western blot analysis of antiapoptotic enzymes: survivin and B-cell lymphoma 2. (C) Quantitative RT-PCR of *PGC1α, SIRT1 and SIRT4.* Data are expressed as means ± SD. (A-B) Represents data from two independent blots, (C) represents data from three independent experiments performed in triplicate. Unpaired Student's T-test; $^{**}p<0.01$.

4.14. Discussion.

Key changes in innate immune cell metabolic regulatory events are initiated in response to both nutrient and oxygen deprivation, but additionally in response to DAMPS and other cell derived signalling events. One example of this is the polarisation of macrophages to an M2 phenotype by IL-4 or IL-13; under these conditions M2 macrophage activation is maintained by increased fatty acid oxidation and OXPHOS [524]. In this chapter I have presented data that IL-33 initiates metabolic reprogramming in the innate immune-competent RPE cell with increased metabolic flux through the glycolysis pathway and into the TCA cycle. IL-33 bolsters mitochondrial activity and protects against oxidative damage, likely through the increased expression of PGC-1α and other metabolic regulators. These data indicate that activation of the IL-33/ST2 axis is supported metabolically by mitochondrial respiration. This likely permits a generation of ATP for bioenergetically expensive innate immune responses. Moreover, the increased mitochondrial activity and antioxidant response conferred by IL-33 may have implications for the oxidative damage response in RPE degeneration.

IL-33 functions extracellularly as an "alarmin" molecule; when released extracellularly following cellular damage/stress, exposure to allergens or infection with viruses, it potently activates immune (and non-immune) cells expressing its receptor ST2 [146]. The metabolic adaptations of the RPE to IL-33 signalling may reflect the need to reprogram its metabolism to support the bioenergetic demands of cytokine and chemokine production. However, mast cell activation by IL-33 also elicits a robust output of inflammatory cytokines and chemokines [13], yet a metabolic change was not observed. Future work should aim to address whether the IL-33/ST2 signalling axis is specific to the RPE or whether other ST2 expressing cells undergo metabolic changes when activated.

The basis of investigating the role of IL-33 on RPE metabolism was centred around a study investigating mtDNA haplotypes in AMD [18]. mtDNA can mediate cellular bioenergetics and expression levels of nuclear genes related to complement, inflammation and apoptosis [18]. This study - using cybrid RPE cells with representative mtDNA haplotypes - demonstrated that different mtDNA variants exhibit a difference in ATP levels, lactate production and metabolic (glycolytic) enzyme expression, which further dictates altered expression of nuclear encoded genes in complement, innate immunity, apoptosis and pro-inflammatory signalling pathways [18, 390]. One component of the innate immune signalling pathways found to alter significantly in RPE according to mtDNA content was IL-33 [18]. These "high-risk" AMD RPE cybrids exhibit both reduced mitochondrial metabolism and expression of

IL-33 [18]. Therefore, there are contemporaneous changes in RPE metabolism and expression of IL-33 when mtDNA change is observed. The notion is that IL-33 acts as a signal in the RPE to adapt or maintain its mitochondrial metabolism.

Consistent with prior reports within cancer cells [443] and fibroblasts [442] IL-33/ST2 signalling was identified to be accompanied with increased metabolic activity (particularly in the glycolysis pathway). My findings here indicate that IL-33 increases glucose uptake (through the increased expression of GLUT1) and flux through glycolysis supported by both increased expression of glycolytic enzymes and carbon tracing data. C^{13} glucose SITA indicated that for the major part, increased glycolytic consumption was accompanied by flux into the TCA cycle which along with increased expression of key TCA cycle enzymes may account for the upregulated mitochondrial capacity in IL-33 stimulated RPE. This suggests that future work should aim to identify the contribution of glycolysis and mitochondrial pyruvate entry to the augmented oxygen consumption under an IL-33 stimulus. It is probable (as a Th2 cytokine capable of eliciting M2 macrophage polarisation [278]) that IL-33 may induce metabolic reprogramming in the RPE through comparable pathways to IL-4 and IL-13 activated macrophages. In these conditions IL-4/IL-13 signal *via* the mTORC2/IRF4/STAT6 axis to promote oxidative glucose metabolism and support fatty acid metabolism [439]. It would also be of interest to identify if this effect on the RPE is indeed specific to IL-33 "alarmin" signalling, or whether other Th2 cytokines (such as IL-4/IL-13) facilitate a similar metabolic signature.

The data presented in this chapter suggests that IL-33 promotes RPE oxidative pyruvate metabolism, yet the effects on mitochondrial capacity is unlikely to be solely attributed to increased glycolytic flux into the TCA cycle. Future experiments employing alterative isotopically labelled analytes will permit a greater understanding of additional metabolic pathways modulated by IL-33. Activation of AMPK and expression of mitochondrial fusion genes (e.g. OPA-1) may additionally drive fatty acid oxidation under an IL-33 stimulus. Indeed, increased mitochondrial fusion in T-cells generates increased oxidative potential, largely dependent on fatty acid oxidation [472].

Activation of AMPK appears to be associated with the counter regulation of inflammatory pathways in innate immune cells [345]. Stimulation of macrophages with anti-inflammatory cytokines (specifically IL-10, TGF-β and IL-4) drive the activation of AMPK, which in turn suppresses pro-inflammatory responses [497] and promotes OXPHOS through the inhibition of mTORC1 [525]. The

activation of AMPK may contribute to the regulation of mTORC1 in the RPE in order to suppress high rates of aerobic glycolysis and loss of mitochondrial integrity [525], whilst simultaneously supporting mitochondrial oxidative metabolism and biogenesis [345]. Future work should aim to interrogate not only canonical ST2 signalling pathways in the RPE (i.e. MyD88/NF-kB) but the input of mTORC1/2 signalling in response to IL-33. AMPK activation *via* IL-33/ST2 signalling may be of great significance *in vivo*, whereby AMPK stimulation prevents loss of the photoreceptors and RPE in three models of retinal degeneration [384]. Whilst in this study metformin was utilised to mediate protection *via* the induction of oxidative damage response and mitochondrial biogenesis transcriptional changes [384], there are emerging studies which question the effectiveness of metformin as an AMPK activator [505].

The data indicated that IL-33 signalling protected RPE cells against the noxious effects of oxidative stress. IL-33 release is regulated by oxidative stress and antioxidants within airway epithelium [240], reported to reduce ROS production in fibroblasts [14] and directly enhance the activity of SOD in cardiomyocytes [288]. However, the data here identified no change to antioxidant enzyme expression but rather an increase in metabolic flux and mitochondrial activity. Whilst not examined entirely here, future work should aim to identify if IL-33 pre-treatment enables the RPE to have an increased protective response (rather than increased basal expression) under oxidative stress in terms of antioxidant enzymes and mitochondrial biogenesis. TFAM, and NRF1 are both key mediators of mitochondrial biogenesis and mtDNA maintenance [384]. Although these were not examined following IL-33 stimulation, future work should aim to assess their involvement to the IL-33-induced RPE stress response. The protection against oxidative damage may likely be attributed to increased expression of PGC-1α following treatment of RPE with IL-33. ARPE-19 and human foetal RPE cells overexpressing PGC-1α have previously been shown to increase mitochondrial mass, mitochondrial respiration and strongly induce the expression of antioxidant genes which protect the RPE from oxidant-mediated cell death [36]. Increased function of PGC-1α could improve the increased oxidative stress and reduced metabolism observed in AMD without affecting RPE survival or function [36]. It is worth noting however, that cultured RPE cells from AMD patients have been shown to exhibit increased PGC-1α expression compared to non-AMD controls [397]. In the context of the "metabolic ecosystem" hypothesis [4], bolstering both glycolysis and OXPHOS in the RPE may have adverse effects on photoreceptor health. If IL-33 signalling increases the glucose consumption and flux through glycolysis and the TCA cycle, less glucose would (in theory) be able to traverse to the photoreceptors to support their program of highly glycolytic metabolism [4]. Future studies are warranted to test whether the regulation of mitochondrial function could have beneficial effects for RPE survival in *in vivo* models of oxidative stress and retinal degeneration.

It was of interest to note that even the lower doses of IL-33 (1ng/ml) could still influence RPE responses and viability, consistent with reports that low levels of circulating cytokines can modulate human brain function [526]. While high extracellular levels (100ng/ml) of IL-33 are physiologically unlikely within the retinal microenvironment of patients (with or without AMD) [527], one cannot eliminate a local high concentration of IL-33 which may occur at a site of tissue damage [528].

In summary, the results presented in this chapter identify IL-33/ST2 signalling in the RPE to be accompanied by a metabolic adaptation of increased mitochondrial activity, likely to support the effector functions of the RPE in "stress" conditions. Activation of AMPK by IL-33 to reduce oxidative stress and expand mitochondrial capacity provide evidence for an attractive immunotherapeutic-mediated approach to halt retinal degeneration in early AMD development.

Chapter 5. Nuclear interleukin-33 regulates cellular metabolism in the retinal pigment epithelium

5.1. Introduction

IL-33 is constitutively expressed in the inner retina, RPE and choroid [529], as well as in epithelial cells, endothelial cells, and fibroblasts [217]. IL-33 is expressed in the nucleus of these cells during homeostasis at a high level [217]. During inflammation the expression of this protein can be further upregulated, whilst still retaining the nuclear localization [530]. In the RPE, IL-33 is upregulated by exposure to TLR-3 and TLR-4 ligands LPS and Poly (I:C), respectively (see chapter 3). Full-length unprocessed IL-33 is released from the nucleus after necrotic cellular damage and displays potent biological activity [233]. IL-33 cytokine activity is therefore constrained by its subcellular localization and regulated through proteolytic cleavage [233, 531]. Full length IL-33 is bioactive [233]. Cleavage by caspases in the IL-1 cytokine domain process IL-33 into inactive forms during apoptosis [233]. Processing by neutrophil-derived or environmental allergen proteases can generate processed forms of IL-33 with augmented cytokine activity [235, 285]. Nuclear localization of full-length IL-33 appears to be a property that is observed universally across all IL-33-producing cells of both human and murine origin. Nuclear IL-33 exhibits a chromatin-binding motif which permits an association with the histone heterodimer H2A-H2B [256]. The chromatin-binding motif (contained within the nuclear domain) is evolutionarily conserved in all IL-33 sequences, implicating a role in chromatin association [254].

A largely unanswered question concerning the biology of IL-33 is the significance of its nuclear localisation. Other nuclear alarmins (e.g. HMGB1 and IL-1α) are considered to display dual functionality, "moonlighting" as transcription factors through their ability to bind DNA [532, 533]. Roles for nuclear IL-33 have previously been described in the transcriptional repression of NF-kB [10, 254], leading to the proposed theory that it also has dual functionality, acting both extracellularly and as a nuclear factor regulating gene transcription. Despite multiple studies describing a role for IL-33 in transcriptional regulation [257, 258, 534], recent reports which provide evidence that endogenous nuclear IL-33 is not a dominant regulator of gene expression raise questions over this conclusion [230, 263].

A recent study suggested a novel epigenetic role for IL-33 as shown in the maintenance of uncoupled metabolism in adipose tissue [19]. This combined with results detailed in the previous chapter (whereby activation of the IL-33/ST2 axis in the RPE drives metabolic changes), and the altered IL-33 expression observed in AMD hybrids [18], lead to the hypothesis that IL-33 may act an intranuclear regulator of RPE metabolic pathways as well as at the extracellular level. Therefore, the primary

objective of this chapter was to test if genetic modulation of the expression status of intracellular nuclear IL-33 could have any effect on the control of RPE metabolism.

5.2. Establishing knockdown and overexpression of IL-33 in ARPE-19 using siRNA and CRISPR cas9

In order to answer the hypothesis of this chapter "*does intracellular IL-33 expression status influence RPE metabolism?*", there remained a need to first achieve stable knockdown (KD) and overexpression of full-length nuclear IL-33 in the RPE. Continuing with the use of ARPE-19 as an RPE model system, I first optimised genetic modulation of IL-33 in this cell line. To KD IL-33 in ARPE-19 cells, four preselected siRNA duplexes each targeting different sequences of the human *IL33* gene were utilized. The effectiveness of siRNA KD was confirmed both at the protein and gene level (Fig. 5.1A-C). Additionally, ARPE-19 cells were genetically engineered to constitutively overexpress IL-33 using a CRISPR-cas9 system. The CRISPR/synergistic activation mediator (SAM) transcription activation system enabled the upregulation of IL-33 by utilising a D10 deactivated Cas9 nuclease fused to a VP64 activation domain, in conjunction with a single guide RNA (MS2) and an IL-33-specific single guide RNA engineered to bind the MS2-p65-HSF-1 fusion protein [535]. The effectiveness of CRISPR-cas9 overexpression was confirmed both at the gene and protein level in whole cell lysates (Fig. 5.1D, E, G). As IL-33 functions as a dual function cytokine, residing both within the nucleus and functioning extracellularly [9], there was a necessity to identify the subcellular location of IL-33 following overexpression. Like previous studies [136, 260, 263], constitutive nuclear expression of IL-33 was observed in ARPE-19 cells (Fig. 5.1F). When IL-33 was overexpressed using the activation plasmid, nuclear retention was still observed (Fig. 5.1F). Immunoblotting for nuclear histone 3 and cytoplasmic β-Actin expression was conducted to confirm specificity in the nuclear and cytoplasmic lysates (Fig. 5.1F).

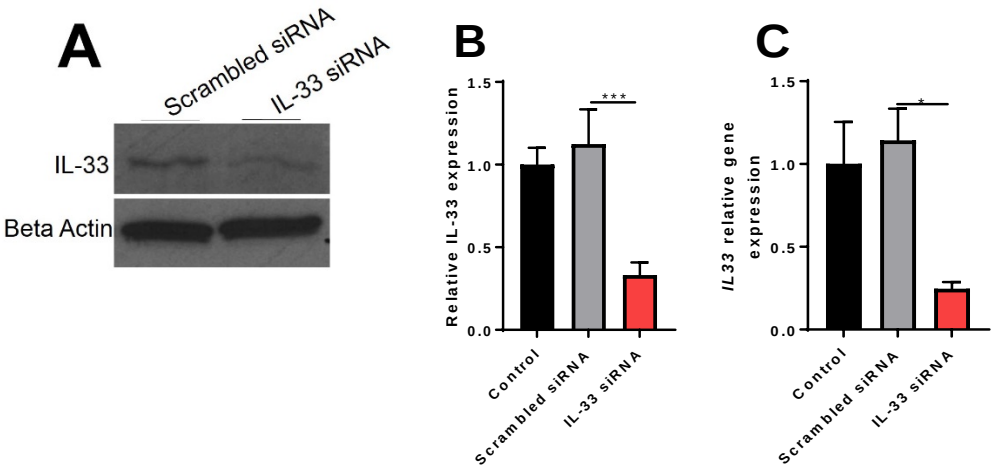
A
Scrambled siRNA
IL-33 siRNA
IL-33
Beta Actin
B
Relative IL-33 expression
1.5
1.0
0.5
0.0
***
Control
Scrambled siRNA
IL-33 siRNA
C
IL33 relative gene expression
1.5
1.0
0.5
0.0
*
Control
Scrambled siRNA
IL-33 siRNA

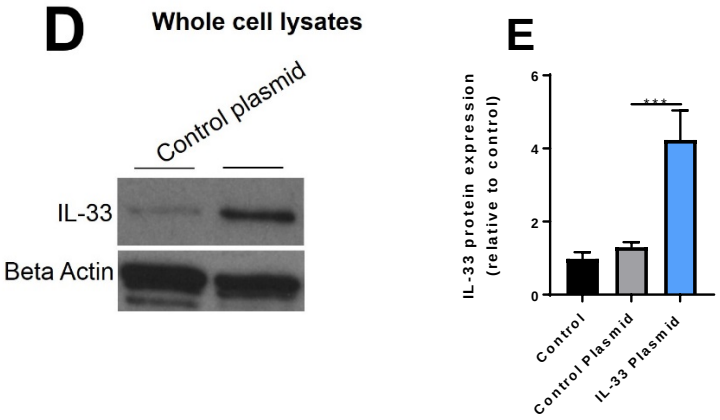
D
Whole cell lysates
Control plasmid
IL-33
Beta Actin
E
IL-33 protein expression (relative to control)
6
4
2
0
***
Control
Control Plasmid
IL-33 Plasmid

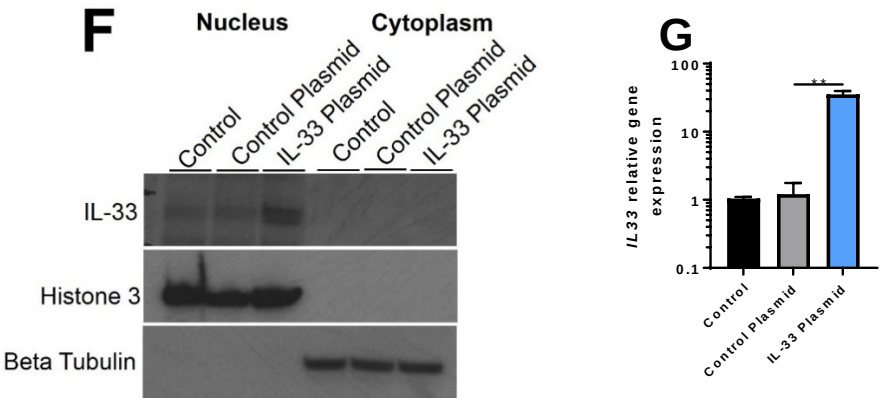
F
Nucleus
Cytoplasm
Control
Control Plasmid
IL-33 Plasmid
Control
Control Plasmid
IL-33 Plasmid
IL-33
Histone 3
Beta Tubulin
G
IL33 relative gene expression
100
10
1
0.1
**
Control
Control Plasmid
IL-33 Plasmid

Figure 5.1. Establishing knockdown and overexpression of IL-33 in ARPE-19 using siRNA and CRISPR-cas9:

ARPE-19 were transfected for 48h with either scrambled siRNA or a pre-selected mixture of 4 siRNA duplexes targeting the human *IL33* gene. (A) Representative immunoblot of IL-33 protein expression following transfection. (B) Densitometry analysis of IL-33 protein expression. (C) Quantitative RT-PCR of *IL33* mRNA transcripts. ARPE-19 were transfected for 48h with either a scrambled gDNA plasmid or an *IL33* activation gDNA plasmid. (D) Representative immunoblot of IL-33 protein expression following transfection. (E) Densitometry analysis of IL-33 protein expression. (F) Representative immunoblot of IL-33 subcellular location following transfection. (G) Quantitative RT-PCR of *IL33* mRNA transcripts. Data are expressed as means ± SD. (A, B, D, E, F) Represents data from three independent blots, (C and G) represents data from three independent experiments performed in triplicate. One-way ANOVA with Tukey's multiple comparisons test; *p<0.05, **p<0.01, ***p<0.005.

5.3. Toxicity and IL-33 release in transfected ARPE-19

Considering the observations from the previous chapter -whereby recombinant IL-33 drove metabolic changes to the RPE - there remained a necessity to investigate (A) whether IL-33 is released from RPE cells in health or stress and (b) (if the previous proved to be correct) whether altering the expression status with siRNA or CRISPR-cas9 would simply alter the output of IL-33 secreted, and drive metabolic changes to the RPE in an autocrine or paracrine manner (Fig 5.2). As IL-33 lacks a traditional signal sequence or a non-canonical export pathway, previous studies have suggested that its release occurs only through necrotic mechanisms, allowing the full-length cytokine to reach the extracellular milieu [530].

In order to measure the release of IL-33 into cell culture supernatants, a commercial ELISA was used. ARPE-19 cells were first treated with increasing doses of H_2O_2 to induce cellular necrosis through oxidative stress. Consistent with previously reported observations, increased IL-33 release from the ARPE-19 cells was observed with increasing cell death (Fig 5.3A-B). In the untreated group, IL-33 release was not reliably detected within the culture supernatant (Fig 5.3A). The mean concentration of IL-33 was 7± 2 pg/ml and below the assay detection limit of 23.4 pg/ml and therefore unreliable to construe as constitutive release from the cells. To further assess, cell supernatants were analysed from ARPE-19 cells transfected with an IL-33 siRNA or a scrambled control siRNA for 48h. IL-33 was detected in the supernatants of all groups but again below the detection limits of the ELISA (control (10.1± 4 pg/ml), scrambled siRNA (11.6± 4.6 pg/ml) and siRNA (9.12± 6 pg/ml)) (Fig. 5.3A). Transfection with either siRNA had no significant effect on the LDH release of the target cells (Fig. 5.3C). As there were no detectable differences between the groups, and IL-33 was not detected above an accurate threshold in supernatants, I concluded that under these culture conditions IL-33 is not constitutively released from ARPE-19 and the “below sensitivity” concentrations of IL-33 present may be a result of low levels of cell death which occur within a cell culture system.

There remained a need to investigate whether IL-33 would be secreted from cells transfected with an IL-33 overexpression plasmid. Cell culture supernatants were taken post transfection for 48h and an ELISA was used to determine the release of IL-33. It was observed that in all groups, IL-33 release was below the detection limits of the assay. The IL-33 concentrations in the supernatants were control - 4.7± 2 pg/ml, control plasmid - 7.6± 5.6 pg/ml and IL-33 plasmid - 17.1± 6.5 pg/ml (Fig. 5.3C). Transfection of cells with both plasmids significantly increased the LDH release, however it was

observed that the IL-33 plasmid elicited increased cytotoxicity compared to the control plasmid (Fig. 5.3D).

Considering these observations, it was necessary to optimise the transfection strategy of both plasmids to elicit a similar amount of toxicity and (in theory) IL-33 release in the ARPE-19 system. The rationale behind this was: if the IL-33 plasmid is more cytotoxic that the control plasmid, any results observed when looking at the metabolic profiles may be skewed by both IL-33 release and damage to the cells. Additionally, it was essential to optimise the IL-33 plasmid to induce the greatest IL-33 expression with the lowest cytotoxicity. In the first set of experiments, the concentration of the IL-33 activation plasmid was titrated around a pre-optimised concentration of 1µg (1.5-0.25µg) and *IL33* expression was assessed using RT-PCR. Unsurprisingly, it was found that increasing concentrations of the IL-33 activation plasmid dose dependently increased the expression of *IL33* (Fig. 5.3E). Supernatants were assessed for the release of LDH and IL-33 protein. It was found that titrating the activation plasmid had little effect on the LDH release between titration groups, yet there was still a significant cytotoxicity in the IL-33 activation plasmid groups compared to that of the scrambled control (Fig. 5.3F). In terms of the IL-33 release from the transfected cells, levels in supernatants were below the reliable detection limits of the ELISA (Fig. 5.3G). This showed although the IL-33 activation plasmid was more cytotoxic to the cells than the control, titrating the transfection dose had little effect on the cell viability. Considering this, I kept the concentration of the plasmid at 1.5 µg, whilst titrating out different doses of the transfection reagent around a pre-optimised volume of 10µL (15-2.5µL). *IL33* expression was first assessed using RT-PCR. A "bell curve" distribution pattern was observed in terms of *IL33*, with the maximum expression observed at 10µL (Fig. 5.3H). Following this, supernatants were then assessed for the release of LDH and IL-33. A dose response was observed, leading to increased LDH release with increasing transfection reagent volume (Fig. 5.3I). IL-33 release into the cell culture supernatants was below the assay detection limits (Fig. 5.3J).

These results highlighted that in order to minimise the difference of toxicity between the two treatment groups, an alternate dose of transfection reagent would need to be used for the control plasmid. The IL-33 plasmid appeared to be more cytotoxic than the control plasmid, even when its concentration was reduced. Altering the concentration of transfection reagent appeared to be the pivotal factor in reducing cytotoxicity. Considering this, it was necessary in future experiments to utilise 10µL of transfection reagent for the IL-33 plasmid and 15µL of transfection reagent for the control plasmid. These volumes elicited a similar cytotoxicity (362± 31 %LDH release (control plasmid)

and 346± 17 %LDH release (IL-33 plasmid)) from the transfected cells. Optimising the toxicity conferred from plasmid transfection enabled a more reliable assessment of the cell biology in transfected cells and ruled out confounding factors such as IL-33 autocrine/paracrine activation of ST2 and mitochondrial dysfunction with increasing cytotoxicity. These experiments indicate that IL-33 is not released from ARPE-19 cells constitutively or under genetic modulation *via* siRNA knockdown or CRISPR overexpression. Therefore, any effect observed in terms of altering the expression status is due to the intracellular endogenous effects of the cytokine rather than extracellular release and exogenous signalling through ST2.

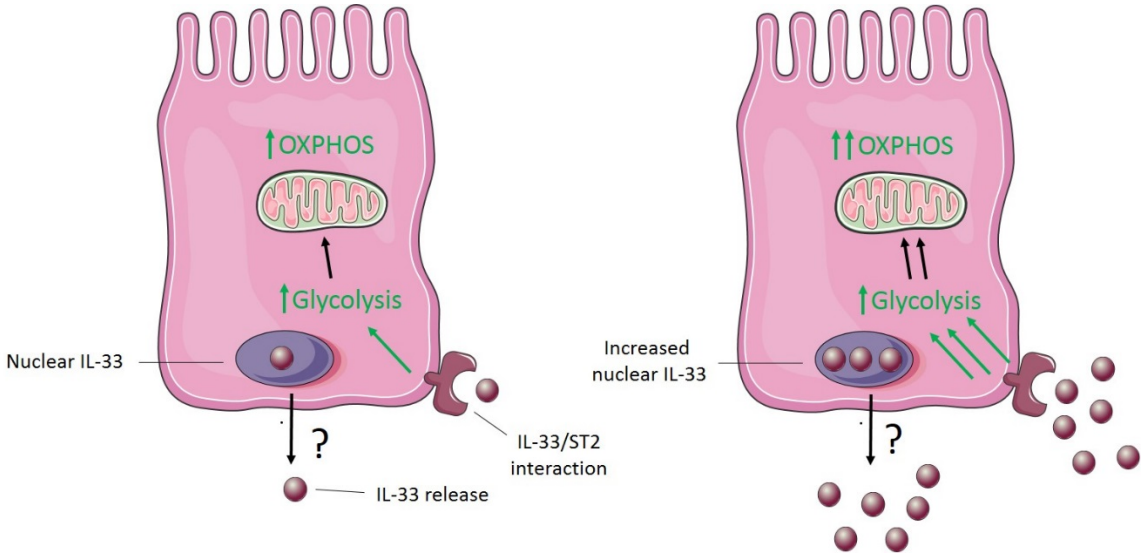

Figure 5.2. Would the overexpression of IL-33 drive RPE metabolic reprogramming in an autocrine/paracrine manner?:

As detailed in chapter 4, IL-33 activates RPE cells through ST2 signalling and increases both glycolysis and mitochondrial OXPHOS. During cellular homeostasis IL-33 is observed in the nuclear of epithelial cells. Whether IL-33 is constitutively released from epithelial cells is currently unknown, due to a lack of a signal sequence for Golgi-mediated release. The consensus appears to be that full-length IL-33 is released extracellularly upon cell death or damage. In the context of RPE cells constitutively overexpressing IL-33, questions emerge as to (A) whether its nuclear expression is retained and (B) whether it is released into the extracellular milieu. If IL-33 overexpression lead to its extracellular release, it is plausible that through autocrine (or paracrine activation), bioenergetic changes could be observed in the RPE which may be falsely interpreted as an intracellular effect of the cytokine.

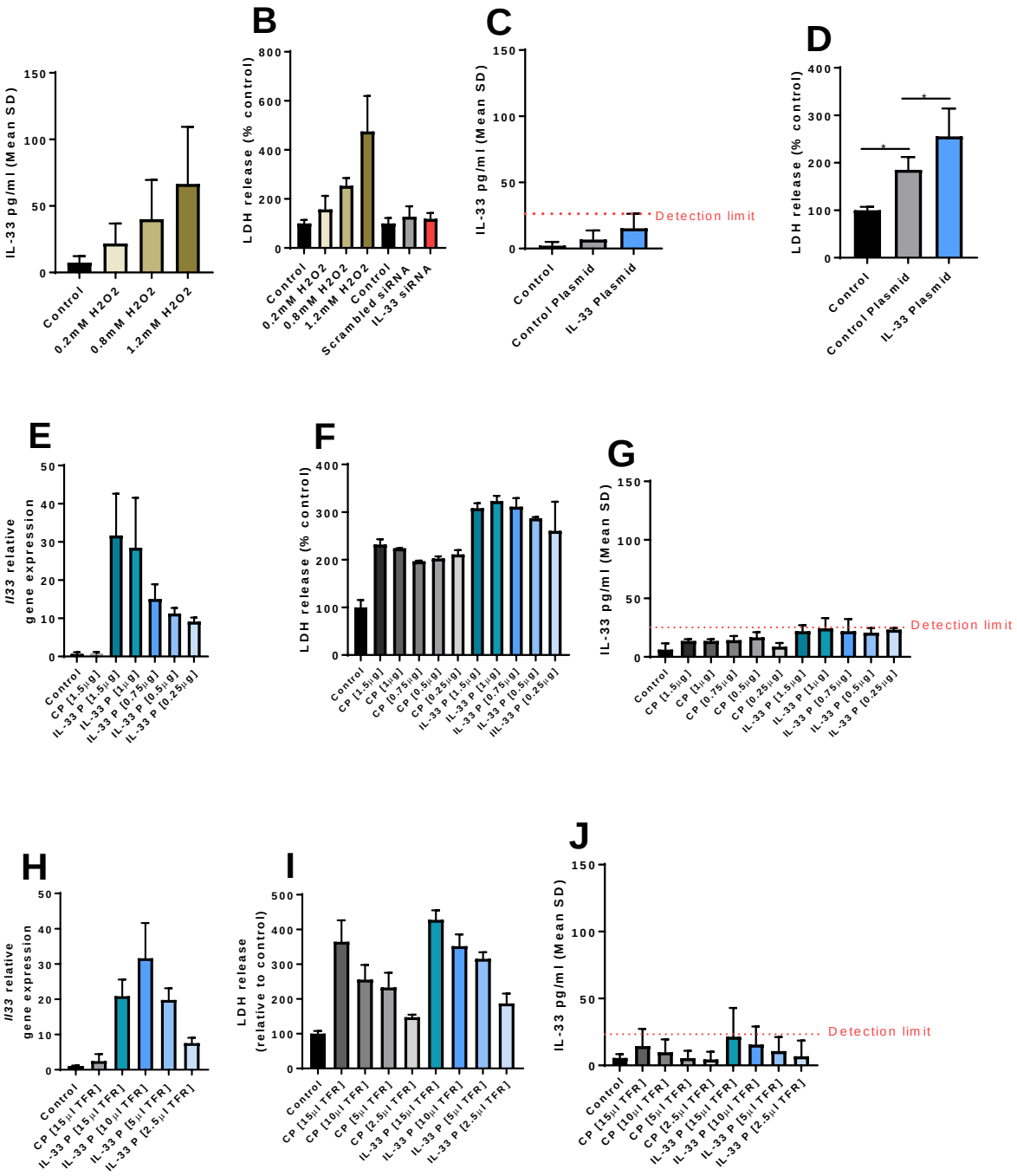
A
IL-33 pg/ml (Mean SD)
Control
0.2mM H2O2
0.8mM H2O2
1.2mM H2O2
B
LDH release (% control)
Control
0.2mM H2O2
0.8mM H2O2
1.2mM H2O2
Control
Scrambled siRNA
IL-33 siRNA
C
IL-33 pg/ml (Mean SD)
Detection limit
Control
Control Plasmid
IL-33 Plasmid
D
LDH release (% control)
*
*
Control
Control Plasmid
IL-33 Plasmid
E
Il33 relative gene expression
Control
CP [1.5µg]
IL-33 P [1.5µg]
CP [1µg]
IL-33 P [1µg]
CP [0.75µg]
IL-33 P [0.75µg]
CP [0.5µg]
IL-33 P [0.5µg]
CP [0.25µg]
IL-33 P [0.25µg]
F
LDH release (% control)
Control
CP [1.5µg]
IL-33 P [1.5µg]
CP [1µg]
IL-33 P [1µg]
CP [0.75µg]
IL-33 P [0.75µg]
CP [0.5µg]
IL-33 P [0.5µg]
CP [0.25µg]
IL-33 P [0.25µg]
G
IL-33 pg/ml (Mean SD)
Detection limit
Control
CP [1.5µg]
IL-33 P [1.5µg]
CP [1µg]
IL-33 P [1µg]
CP [0.75µg]
IL-33 P [0.75µg]
CP [0.5µg]
IL-33 P [0.5µg]
CP [0.25µg]
IL-33 P [0.25µg]
H
Il33 relative gene expression
Control
CP [15µl TFR]
IL-33 P [15µl TFR]
CP [10µl TFR]
IL-33 P [10µl TFR]
CP [5µl TFR]
IL-33 P [5µl TFR]
CP [2.5µl TFR]
IL-33 P [2.5µl TFR]
I
LDH release (relative to control)
Control
CP [15µl TFR]
IL-33 P [15µl TFR]
CP [10µl TFR]
IL-33 P [10µl TFR]
CP [5µl TFR]
IL-33 P [5µl TFR]
CP [2.5µl TFR]
IL-33 P [2.5µl TFR]
J
IL-33 pg/ml (Mean SD)
Detection limit
Control
CP [15µl TFR]
IL-33 P [15µl TFR]
CP [10µl TFR]
IL-33 P [10µl TFR]
CP [5µl TFR]
IL-33 P [5µl TFR]
CP [2.5µl TFR]
IL-33 P [2.5µl TFR]

Figure 5.3. Toxicity and IL-33 release in transfected ARPE-19:

ARPE-19 were transfected for 48h with either scrambled siRNA or a pre-selected mixture of 4 siRNA duplexes targeting the human *IL33* gene; or treated for 24h with varying doses of H_2O_2 (0.2-1.2mM). (A) IL-33 was quantified in supernatants using an ELISA. (B) LDH release was quantified in supernatants and expressed relative to an untreated control. ARPE-19 were transfected for 48h with either a scrambled gDNA plasmid or an *IL33* activation gDNA plasmid. (C) IL-33 was quantified in supernatants using an ELISA. (D) LDH release was quantified in supernatants and expressed relative to an untreated control. ARPE-19 were transfected for 48h with varying concentrations of either a scrambled gDNA plasmid or an *IL33* activation gDNA plasmid. (E) Quantitative RT-PCR of *IL33* mRNA transcripts. (F) LDH release was quantified in supernatants and expressed relative to an untreated control. (G) IL-33 was quantified in supernatants using an ELISA. ARPE-19 were transfected for 48h with either a scrambled gDNA plasmid or an *IL33* activation gDNA plasmid. Varying concentrations of the plasmid transfection reagent were utilised. (H) Quantitative RT-PCR of *IL33* mRNA transcripts. (I) LDH release was quantified in supernatants and expressed relative to an untreated control. (J) IL-33 was quantified in supernatants using an ELISA. Represents data from two independent experiments run in duplicate. One-way ANOVA with Tukey's multiple comparisons test; *p<0.05.

5.4. Effect of IL-33 genetic modulation on ARPE-19 metabolism

Following optimisation of transfection in the previous two sections, ARPE-19 cells were obtained either exhibiting IL-33 knockdown or overexpression using siRNA or CRISPR-cas9, respectively. The first set of experiments to assess the role of nuclear IL-33 in the metabolism of the RPE utilised the XF platform. Mitochondrial stress analysis identified reduced maximal respiration and spare respiratory capacity in the IL-33 siRNA compared to the scrambled siRNA (Fig. 5.4A-B). There were no significant changes observed in the basal respiration or proton leak (Fig. 5.4A-B). ATP-production post oligomycin was increased (Fig. 5.4A-B). Transfection of ARPE-19 cells with a control scrambled siRNA had no significant effect on mitochondrial fitness (Fig. 5.4A-B). Collectively the results from the mitochondrial stress analysis indicated that the ability of the RPE to respond metabolically under "stress" conditions was impaired when IL-33 expression was reduced. After identification of defects in mitochondrial metabolism using the mitochondrial stress test, I chose to investigate how glycolytic metabolism may be affected by the loss of IL-33. A glycolysis stress test identified increased glycolysis and glycolytic capacity following IL-33 KD, yet there was no change in non-glycolytic acidification or glycolytic reserve (Fig. 5.4C-D). Transfection of the cells with a control scrambled plasmid had no effect on glycolytic function (Fig. 5.4C-D). As the ECAR values plateaued after the initial glycose injection in the absence of IL-33 and failed to respond to the injection of the ATP synthase inhibitor oligomycin, this suggested that IL-33 KD cells relied more on aerobic lactate production rather than mitochondrial glucose utilisation. Indeed, the reduced OCR/ECAR ratio indicated the increased aerobic glycolysis compared to mitochondrial activity in the IL-33 KD cells (Fig. 5.4E).

Following these sets of experiments, a similar experimental pipeline was used in the context of IL-33 overexpression. First a mitochondrial stress test to assess the effect of constitutive IL-33 overexpression on RPE metabolism was carried out. In comparison to the control plasmid, the IL-33 plasmid elicited a significant increase in basal respiration, ATP-production and maximal respiration (Fig. 5.4F-G). There was a non-significant increase in the spare-respiratory capacity of IL-33 plasmid group ($p=0.08$) (Fig. 5.4F-G). No-significant changes were observed in the mitochondrial proton leak (Fig. 5.4F-G). The transfection of a control scrambled plasmid had no significant effect on any mitochondrial respiratory parameter, indicating the results obtained were specific to altered IL-33 expression (Fig. 5.4F-G). Together the results from the mitochondrial stress test indicated that with IL-33 overexpression, ARPE-19 cells had improved mitochondrial fitness and maximal respiration. Glucose-starved cells were subjected to a glycolysis stress test to identify changes in glycolytic parameters. It was observed that IL-33 overexpression significantly increased both glycolysis,

glycolytic capacity and glycolytic reserve (Fig. 5.4H-I). Transfection with a control plasmid had no significant effect on glycolytic function in cells (Fig. 5.4H-I). No significant changes were observed in the OCR/ECAR ratio with IL-33 overexpression (Fig. 5.4J). These results indicated that glycolytic function was increased with IL-33 expression. The ECAR values did not plateau after the glucose injection and continued to increase post-inhibition of ATP synthase (Fig. 5.4H). This suggested that although glycolysis was increased, glucose continued to remain a substrate for mitochondrial OXPHOS.

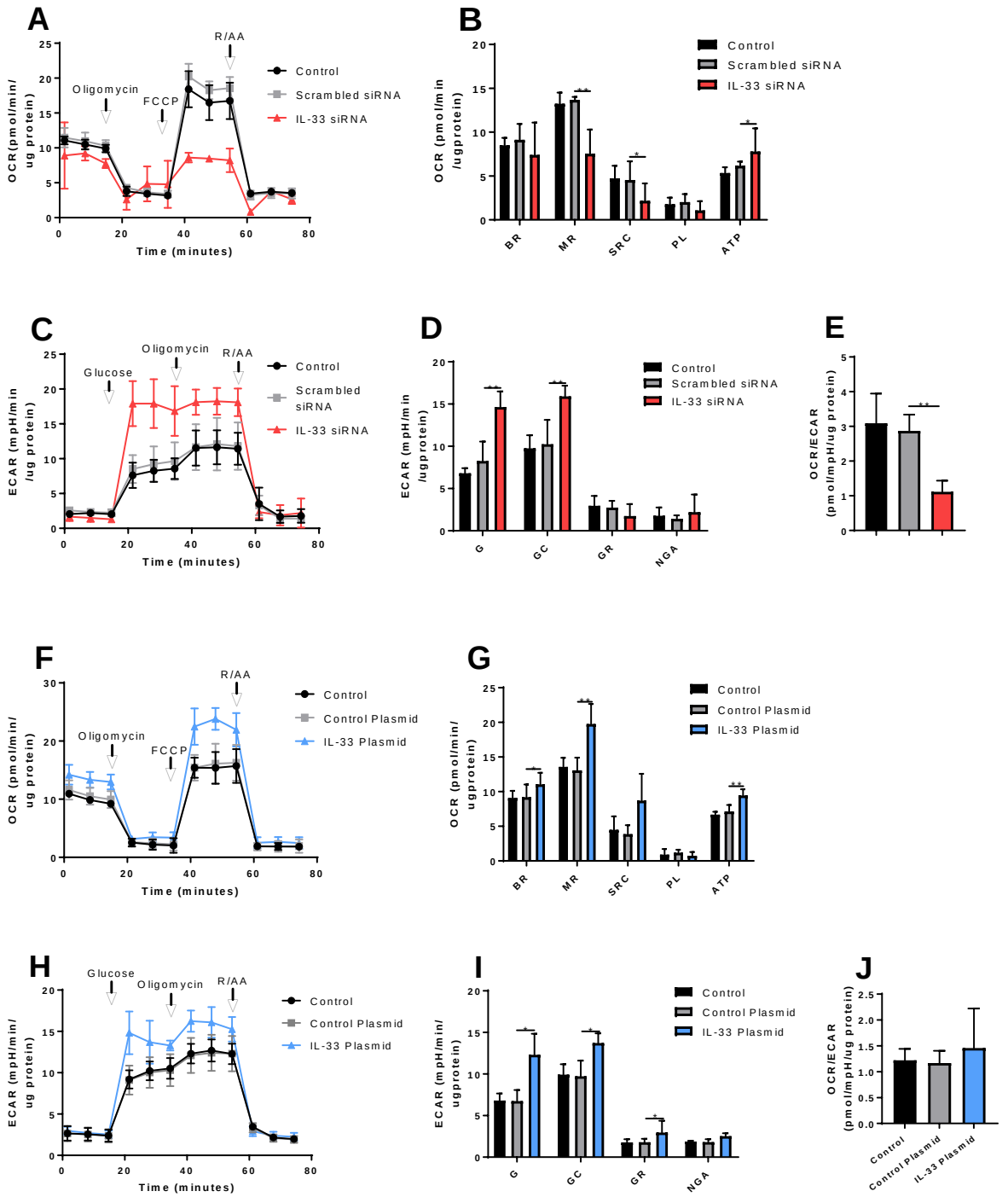
A
OCR(pmol/min/ ug protein)
Oligomycin
FCCP
R/AA
Control
Scrambled siRNA
IL-33 siRNA
Time (minutes)
B
OCR (pmol/min /ugprotein)
Control
Scrambled siRNA
IL-33 siRNA
BR
MR
SRC
PL
ATP
C
ECAR (mpH/min /ug protein)
Glucose
Oligomycin
R/AA
Control
Scrambled siRNA
IL-33 siRNA
Time (minutes)
D
ECAR (mpH/min /ugprotein)
Control
Scrambled siRNA
IL-33 siRNA
G
GC
GR
NGA
E
OCR/ECAR (pmol/mpH/ug protein)
F
OCR (pmol/min/ ug protein)
Oligomycin
FCCP
R/AA
Control
Control Plasmid
IL-33 Plasmid
Time (minutes)
G
OCR (pmol/min/ ugprotein)
Control
Control Plasmid
IL-33 Plasmid
BR
MR
SRC
PL
ATP
H
ECAR (mpH/min/ ug protein)
Glucose
Oligomycin
R/AA
Control
Control Plasmid
IL-33 Plasmid
Time (minutes)
I
ECAR (mpH/min/ ugprotein)
Control
Control Plasmid
IL-33 Plasmid
G
GC
GR
NGA
J
OCR/ECAR (pmol/mpH/ug protein)
Control
Control Plasmid
IL-33 Plasmid

Figure 5.4. Effect of IL-33 genetic modulation on ARPE-19 metabolism:

ARPE-19 were transfected for 48h with either scrambled siRNA or a pre-selected mixture of 4 siRNA duplexes targeting the human *IL33* gene. (A) Representative mitochondrial stress test measured with sequential injections of Oligomycin, FCCP and rotenone/antimycin A (B) Mitochondrial stress parameters (BR- basal respiration; MR- maximal respiration; SRC- spare respiratory capacity; PL- proton leak; ATP- ATP-production) calculated from (A). (C) Representative glycolysis stress test measured with sequential injections of glucose, oligomycin and 2DG. (D) Glycolysis stress parameters (G- glycolysis; GC- glycolytic capacity; GR- glycolytic reserve; NGA- non-glycolytic acidification) calculated from (C). (E) Basal OCR and ECAR measurements expressed as the ratio OCR/ECAR. ARPE-19 were transfected for 48h with either a scrambled gDNA plasmid or an *IL33* activation gDNA plasmid. (F) Representative mitochondrial stress test measured with sequential injections of oligomycin, FCCP and rotenone/antimycin A (G) Mitochondrial stress parameters (BR- basal respiration; MR- maximal respiration; SRC- spare respiratory capacity; PL- proton leak; ATP- ATP-production) calculated from (F). (H) Representative glycolysis stress test measured with sequential injections of glucose, oligomycin and 2DG. (I) Glycolysis stress parameters (G- glycolysis; GC- glycolytic capacity; GR- glycolytic reserve; NGA- non-glycolytic acidification) calculated from (H). (J) Basal OCR and ECAR measurements expressed as the ratio OCR/ECAR. Data are expressed as means ± SD. Represents data from six independent experiments performed with either two or no technical repeats. One-way ANOVA with Tukey's multiple comparisons test; *p<0.05, **p<0.01, ***p<0.005.

5.5. Bioenergetic analysis of *Il33*$^{-/-}$ and *Il1rl1*$^{-/-}$ primary murine RPE

To investigate the role of IL-33 further, I performed a bioenergetic analysis of primary RPE derived from *Il33*$^{-/-}$ mice. This was carried out to assess the metabolic effects of IL-33 loss in another system.

Using a mitochondrial stress test, it was observed that in comparison to WT, *Il33*$^{-/-}$ mice had reduced maximal respiration and spare respiratory capacity (Fig. 5.5A-B). No significant changes were observed in basal respiration, ATP-production or non-mitochondrial oxygen consumption (Fig. 5.5A-B). Like IL-33 KD ARPE-19 cells, I observed that primary *Il33*$^{-/-}$ RPE had increased glycolysis, and yet lacked glycolytic reserve, measured post-oligomycin (Fig. 5.5C-D). There was no significant effect on the OCR/ECAR ratio (Fig. 5.5E). Together, these results mirror IL-33 inhibition caused by siRNA knock-down and suggest a change in the relative importance of glycolysis over OXPHOS in the absence of IL-33.

The results from the previous sections suggest that altered IL-33 release and autocrine signalling does not contribute to the metabolic changes of transfected cells. However, it remained possible that autocrine IL-33 signalling could play a role and there remained a need to identify if the effects of IL-33 loss (or overexpression) required receptor engagement. IL-33 binds and signals through its cognate receptor ST2 (encoded by *Il1rl1*) [133], and therefore targeting this signalling pathway addressed the question of whether ST2 is required for optimal metabolic function in the RPE. To address this, bioenergetic analysis was performed of primary RPE derived from *Il1rl1*$^{-/-}$ mice. A mitochondrial stress test was used to assess the activity and function of mitochondria in both WT and *Il1rl1*$^{-/-}$ mice. No significant changes were observed in mitochondrial respiration between groups (Fig. 5.5E-F). Following this, a glycolysis stress test was utilised to assess the key parameters of glycolytic flux within the isolated RPE cells. No significant changes were observed in glycolytic metabolism between *Il1rl1*$^{-/-}$ and WT controls (Fig. 5.5G-H). There was no significant effect on the OCR/ECAR ratio (Fig. 5.5I). Together these results show that a loss of ST2 expression has no effect on the metabolism of RPE. Furthermore, these results indicate that the effect of IL-33 loss is not dependent on ST2 signalling.

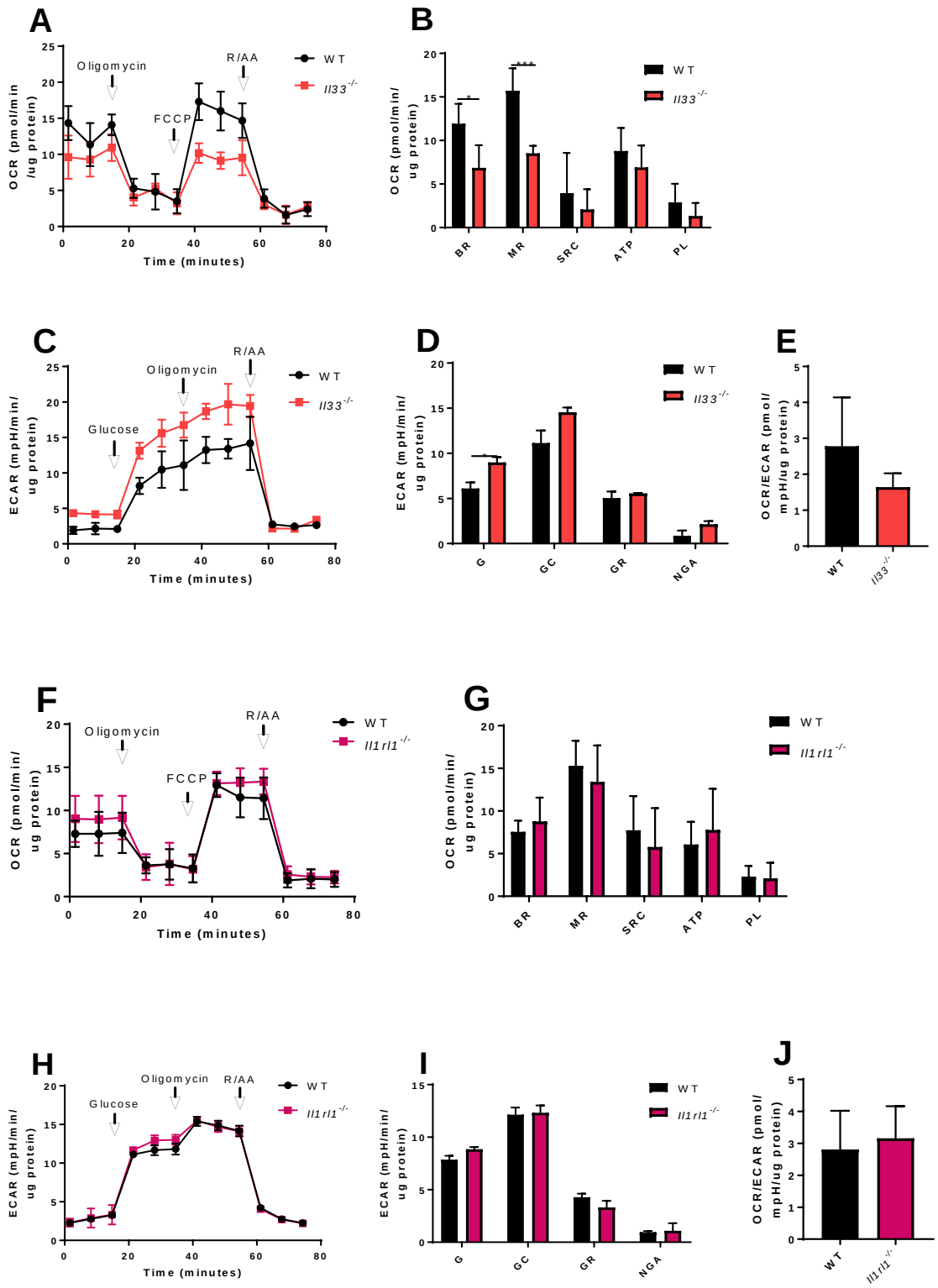
A
Oligomycin
FCCP
R/AA
WT
Il33-/-
OCR (pmol/min /ug protein)
Time (minutes)
B
WT
Il33-/-
OCR (pmol/min/ ug protein)
BR
MR
SRC
ATP
PL
C
Glucose
Oligomycin
R/AA
WT
Il33-/-
ECAR (mpH/min/ ug protein)
Time (minutes)
D
WT
Il33-/-
ECAR (mpH/min/ ug protein)
G
GC
GR
NGA
E
OCR/ECAR (pmol/ mpH/ug protein)
WT
Il33-/-
F
Oligomycin
FCCP
R/AA
WT
Il1rl1-/-
OCR (pmol/min/ ug protein)
Time (minutes)
G
WT
Il1rl1-/-
OCR (pmol/min/ ug protein)
BR
MR
SRC
ATP
PL
H
Glucose
Oligomycin
R/AA
WT
Il1rl1-/-
ECAR (mpH/min/ ug protein)
Time (minutes)
I
WT
Il1rl1-/-
ECAR (mpH/min/ ug protein)
G
GC
GR
NGA
J
OCR/ECAR (pmol/ mpH/ug protein)
WT
Il1rl1-/-

Figure 5.5. Bioenergetic analysis of *Il33*$^{-/-}$ and *Il1rl1*$^{-/-}$ primary murine RPE:

Primary RPE were isolated from WT or *Il33*$^{-/-}$ mice. (A) Representative mitochondrial stress test measured with sequential injections of oligomycin, FCCP and rotenone/antimycin A. (B) Mitochondrial parameters (BR- basal respiration; MR- maximal respiration; SRC- spare respiratory capacity; PL- proton leak; ATP- ATP-production) calculated from data shown in (A). (C) Representative glycolysis stress test measured with sequential injections of glucose, oligomycin and 2DG. (D) Glycolysis stress parameters (G- glycolysis; GC- glycolytic capacity; GR- glycolytic reserve; NGA- non-glycolytic acidification) calculated from (C). (E) Basal OCR and ECAR measurements expressed as the ratio OCR/ECAR. Primary RPE were isolated from WT or *Il1rl1*$^{-/-}$ mice. (F) Representative mitochondrial stress test measured with sequential injections of oligomycin, FCCP and rotenone/antimycin A. (G) Mitochondrial parameters (BR- basal respiration; MR- maximal respiration; SRC- spare respiratory capacity; PL- proton leak; ATP- ATP-production) calculated from data shown in (F). (H) Representative glycolysis stress test measured with sequential injections of glucose, oligomycin and 2DG. (I) Glycolysis stress parameters (G- glycolysis; GC- glycolytic capacity; GR- glycolytic reserve; NGA- non-glycolytic acidification) calculated from (H). (J) Basal OCR and ECAR measurements expressed as the ratio OCR/ECAR. Data presented as means ± SD. (A, B and E) Represents data from three mice per group. (C-D) Represents data from two mice per group. Unpaired Student's T-test; *p<0.05, **p<0.01, ***p<0.005.

5.6. Glucose consumption, lactate production, ATP/ADP ratio and glycolysis/TCA gene transcription in ARPE-19 with IL-33 genetic modulation

The results from the previous sections indicate that altering IL-33 expression status has an impact on the metabolism of RPE cells by a cell intrinsic mechanism. In the absence of IL-33, there appeared to be increased aerobic glycolysis, potentially at the expense of mitochondrial function. When IL-33 was overexpressed, both glycolysis and mitochondrial function increased. To extend these observations further using the XF platform, I tested alternative readouts of metabolism.

Starting with the IL-33 KD cells, glucose consumption was assessed in the supernatants using a commercial glucose assay. No significant changes were observed in the glucose consumption between any group (Fig. 5.6A). Following this, I assessed the lactate output in the supernatants of IL-33 KD cells. Lactate output is used as a direct readout of aerobic glycolysis and therefore, one would expect the readout from the seahorse assay to match lactate production. The assay indicated that there was a significant increase in lactate production in the IL-33 siRNA group compared to that of a scrambled siRNA control (Fig. 5.6B). No significant changes were observed between the scrambled control and untreated cells, indicating the effects of the IL-33 siRNA were not a result of the transfection process (Fig. 5.6B). The ATP/ADP ratio gives an indication of the balance between ATP synthesis and ATP consumption in a cell. The ratio of ATP and ADP present was assessed, and it was found that IL-33 KD had no significant effect on this (Fig. 5.6C) suggesting the balance of ATP synthesis and consumption was not altered. To assess how metabolism relevant genes were affected by IL-33 KD, RT-PCR analysis of selected mRNAs encoding glycolytic and TCA cycle enzymes and nuclear transcription factors was performed. In the glycolysis pathway, KD of IL-33 with siRNA increased the expression of *LDHA* and *GAPDH* transcripts (Fig. 5.6D). *PKM2* (the alternatively spliced isoform of pyruvate kinase) transcript levels were reduced with KD (Fig. 5.6D). In the TCA cycle, only the expression of *PC* (pyruvate carboxylase (PC)) was significantly reduced by IL-33 KD, no significant changes were observed in the transcription of other TCA cycle enzymes (Fig. 5.6D). Out of the five transcriptional regulators assessed, only the gene expression of *SIRT4* was affected by IL-33 KD (Fig. 5.6D). Interestingly, *SIRT4* was a gene target upregulated with exogenous IL-33 expression in the previous chapter (see Fig. 4.15.). Together these results supported the earlier conclusions but indicated that the increased aerobic lactate production was not a result of upregulated glycolysis, as no changes were observed in glucose uptake by cells. The RT-PCR results pointed to transcriptional changes that occur with IL-33 KD in the glycolysis and TCA pathways. Up-regulation of lactate dehydrogenase-A expression may account for the increased lactate protection observed. However, the lack of mitochondrial capacity observed in

the previous chapter could not attributed to reduced expression of TCA cycle enzymes, with only the anaplerotic enzyme pyruvate carboxylase affected in the context of IL-33 KD.

Similar experiments were used to obtain a greater insight into the mechanisms governing metabolic changes occurring with upregulated IL-33 expression. In cells transfected with an IL-33 activation plasmid, there was increased glucose consumption in the supernatants compared to a control plasmid (Fig. 5.6E). Lactate output was also assessed to determine if aerobic glycolysis was also increased in cells, yet no significant changes were observed in the supernatants (Fig. 5.6F). The ATP/ADP ratio was measured in cells constitutively overexpressing IL-33 to identify if the metabolic changes were accompanied by a shift in ATP synthesis. No significant changes were observed in the ATP/ADP ratio, suggesting that the balance of synthesis to consumption remained unaltered (Fig. 5.6G). Pan glycolysis, pan TCA and transcriptional metabolic enzyme expression was assessed using RT-PCR. This permitted a greater understanding of how these metabolic pathways are influenced by IL-33. With transfection of the IL-33 plasmid, I found that there was an increased expression of multiple targets in glycolysis and the TCA cycle. IL-33 overexpression increased the transcript abundance of *GLUT1* (responsible for glucose import into the cell), and the glycolytic enzymes *PFKP, ENO1* and both *PKM* isoforms (Fig. 5.6H). In terms of the TCA cycle enzymes, increased transcripts were observed in *PDH*, *IDH1*, *FH*, *CH* and *SDHD* (Fig. 5.6H). Nuclear located transcriptional regulators of metabolism were also observed to be affected by the overexpression of IL-33. *MYC* transcripts were significantly increased, yet the expression of *SIRT1* was significantly reduced (Fig. 5.6H). These data strengthen those of section 5.4. which show that increasing nuclear IL-33 expression *via* CRISPR-cas9 leads to an increase in both RPE glycolysis and OXPHOS. The increased glucose uptake from these cells and increased transcription of glycolytic enzymes support the increased glycolysis shown using the seahorse. Moreover, the lack of increased lactate production and increased expression of TCA cycle enzymes supports the hypothesis that glucose may be used as a substrate for mitochondrial OXPHOS and overexpression increases its flux into the TCA cycle.

PDH is a key metabolic checkpoint which bridges both glycolysis and the TCA cycle. PDH is responsible for the conversion of pyruvate to acetyl-CoA for entry into the TCA cycle and inactivated by the PDK1-dependent phosphorylation of a serine residue (Ser293) on the E1 subunit [469]. To identify whether nuclear IL-33 influenced oxidative glucose metabolism, there remained a necessity to identify if the activity of PDH was affected by IL-33 expression status. Cell lysates were taken from both scrambled siRNA/ IL-33 siRNA and control plasmid/ IL-33 plasmid transfected cells and an immunoblot was

performed for both PDH and phosphorylated PDH (Ser293). With IL-33 KD there was no significant change in the activation status of PDH (Fig. 5.6I-J). When IL-33 was overexpressed, there was decreased phosphorylation of the Ser293 residue, and therefore increased activation compared to the control plasmid (Fig. 5.6I and K). This indicates, collectively that in the context of IL-33 overexpression there is increased flux through glycolysis and the TCA cycle. The activation of pyruvate kinase by IL-33 overexpression suggests that there is increased entry of pyruvate into the TCA cycle. However, as IL-33 KD had no effect of the activation status of PDH, it is unlikely that IL-33 regulates metabolic function in the RPE through PDH. The increased PDH activity with IL-33 is likely secondary to an alternative step bridging glycolysis and the TCA cycle.

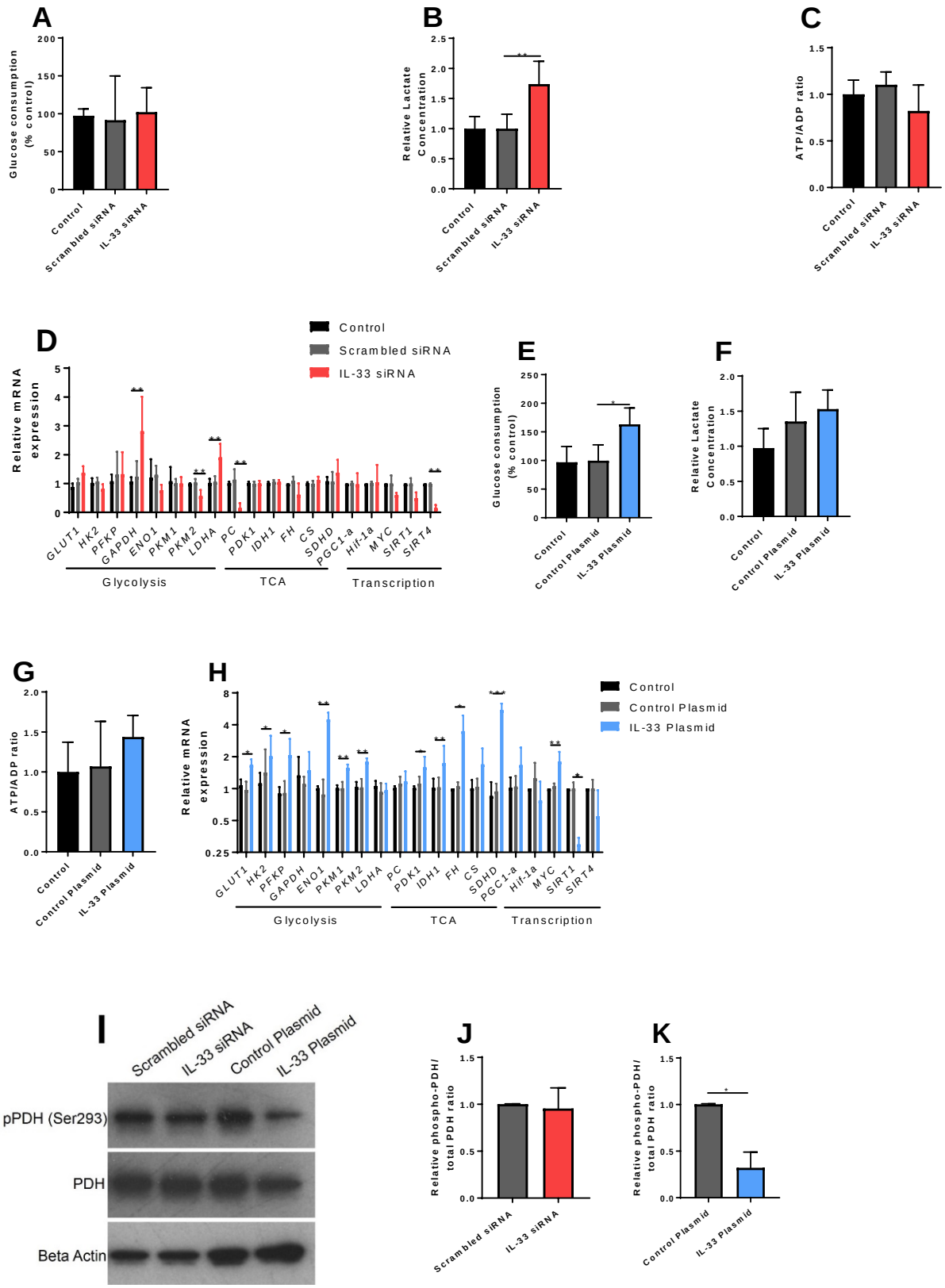
A
Glucose consumption (% control)
Control
Scrambled siRNA
IL-33 siRNA
B
Relative Lactate Concentration
C
ATP/ADP ratio
D
Control
Scrambled siRNA
IL-33 siRNA
Relative mRNA expression
GLUT1 HK2 PFKP GAPDH ENO1 PKM1 PKM2 LDHA PC PDK1 IDH1 FH CS SDHD PGC1-a Hif-1a MYC SIRT1 SIRT4
Glycolysis
TCA
Transcription
E
Glucose consumption (% control)
Control Plasmid
IL-33 Plasmid
F
Relative Lactate Concentration
G
ATP/ADP ratio
H
Relative mRNA expression
I
Scrambled siRNA
IL-33 siRNA
Control Plasmid
IL-33 Plasmid
pPDH (Ser293)
PDH
Beta Actin
J
Relative phospho-PDH/ total PDH ratio
K
Relative phospho-PDH/ total PDH ratio

Figure 5.6. Glucose consumption, lactate production, ATP/ADP ratio and glycolysis/TCA gene transcription in ARPE-19 with IL-33 genetic modulation:

ARPE-19 were transfected for 48h with either scrambled siRNA or a pre-selected mixture of 4 siRNA duplexes targeting the human *IL33* gene. (A) Supernatants were assessed for relative glucose consumption. (B) Extracellular lactate measurements were taken in the media and expressed as a percentage of the mean untreated control. (C) ATP and ADP levels were quantified following cell lysis and expressed as the ratio ATP/ADP. (D) Quantitative RT-PCR of glycolytic pathway enzymes (*HK2, LDHA, PFKP, GAPDH, PKM1, PKM2* and *ENO1*), *GLUT1, HIF1α, PGC1α, SIRT1, SIRT4,* and TCA cycle enzymes (*SDHD, PDK1, IDH1, FH* and *CS*) mRNA transcripts. ARPE-19 were transfected for 48h with either a scrambled gDNA plasmid or an *IL33* activation gDNA plasmid. (E) Supernatants were assessed for relative glucose consumption. (F) Extracellular lactate measurements were taken in the media and expressed as a percentage of the mean untreated control. (G) ATP and ADP levels were quantified following cell lysis and expressed as the ratio ATP/ADP. (H) Quantitative RT-PCR of glycolytic pathway enzymes (*HK, LDHA, PFKP, GAPDH, PKM1, PKM2* and *ENO1*), *GLUT1, HIF1α, PGC1α, SIRT1, SIRT4,* and TCA cycle enzymes (*SDHD, PDK1, IDH1, FH* and *CS*) mRNA transcripts. (I-K) Western blot analysis was used to determine the phosphorylation of pyruvate dehydrogenase following transfection. Data are expressed as means ± SD. (A-C, E-G) Represents data from two independent experiments performed in duplicate. (D and H) Represents data from three independent experiments performed in duplicate. One-way ANOVA with Tukey's multiple comparisons test; **p*<0.05, ***p*<0.01, ****p*<0.005. (I-K) Represents data from two independent blots. Unpaired Student's t-test; **p*<0.05.

5.7. Contribution of pyruvate import and fatty oxidation to the metabolism of IL-33 knockdown or overexpressing ARPE-19

The results in the previous sections have demonstrated that IL-33 expression is a critical determinant of ARPE-19 metabolism. When nuclear IL-33 is reduced, mitochondrial spare respiratory capacity is impaired at the expense of aerobic glycolysis. Although there was an increase in lactate production (despite no overall increase in glycolytic uptake), this was not attributable to reduced PDH activity. Considering this there remained a necessity to identify the extent to which pyruvate was utilised as a substrate for OXPHOS. When IL-33 was overexpressed, there was an increase in both glycolysis and OXPHOS accompanied by increased glucose uptake, broad transcriptional changes in glycolysis and TCA pathway genes, and increased end-point glycolysis activity into the TCA cycle *via* PDH. In view of these results, the logical next step was to consider if the increased mitochondrial function was solely a result of increased pyruvate import.

Pyruvate is the end-point metabolite of glucose metabolism and the breakdown of many amino acids. It is produced within the cytosol and requires facilitated transport into the mitochondria for further degradation [536]. Pyruvate import is mediated through the MPC consisting of components MPC1/2 [536]. These two inner mitochondrial membrane proteins (MPC1 and MPC2) form a 150kDa complex and are essential for the transport of pyruvate into the mitochondria [537]. A modified mitochondrial stress test with the additional injection of the MPC-specific inhibitor UK5099 [538] was used to assess the contribution of aerobic glucose metabolism to total OCR. In ARPE-19 cells that overexpress IL-33, the increased maximal respiration was largely due to increased pyruvate-dependent respiration (Fig. 5.7A-B). UK5099 treatment reduced the maximal OCR to a similar level of the control plasmid (Fig. 5.7A). When a similar experiment was performed on IL-33 siRNA cells it was observed that pyruvate-dependent respiration had a significantly reduced contribution to maximal OCR (Fig. 5.7C-D).

To assess if pyruvate metabolism was the only component affected by the altered expression of IL-33, or if other metabolic pathways feeding into the TCA cycle were involved, a similar experiment was conducted to assess fatty acid oxidation. Fatty acids are significant metabolic intermediates, because they can be used for lipid synthesis, protein modification, or degradation through β-oxidation to maintain ATP generation through oxidative phosphorylation [539]. The rate limiting step in the β-oxidation process is the transfer of free fatty acids from the cytosol into the mitochondria by carnitine palmitoyltransferase-1 (CPT-1) [539]. A modified mitochondrial stress test with the additional

injection of the CPT1 inhibitor etomoxir was used to assess the contribution of β-oxidation to maximal OCR. Etomoxir treatment post mitochondrial uncoupling significantly reduced the OCR, however between control plasmid and IL-33 plasmid groups this reduction was not significant (Fig. 5.7E-F). With IL-33 loss, we observed that β-oxidation was significantly increased (Fig. 5.7G-H), suggesting that β-oxidation is upregulated in the absence of IL-33 to compensate for defects in pyruvate metabolism.

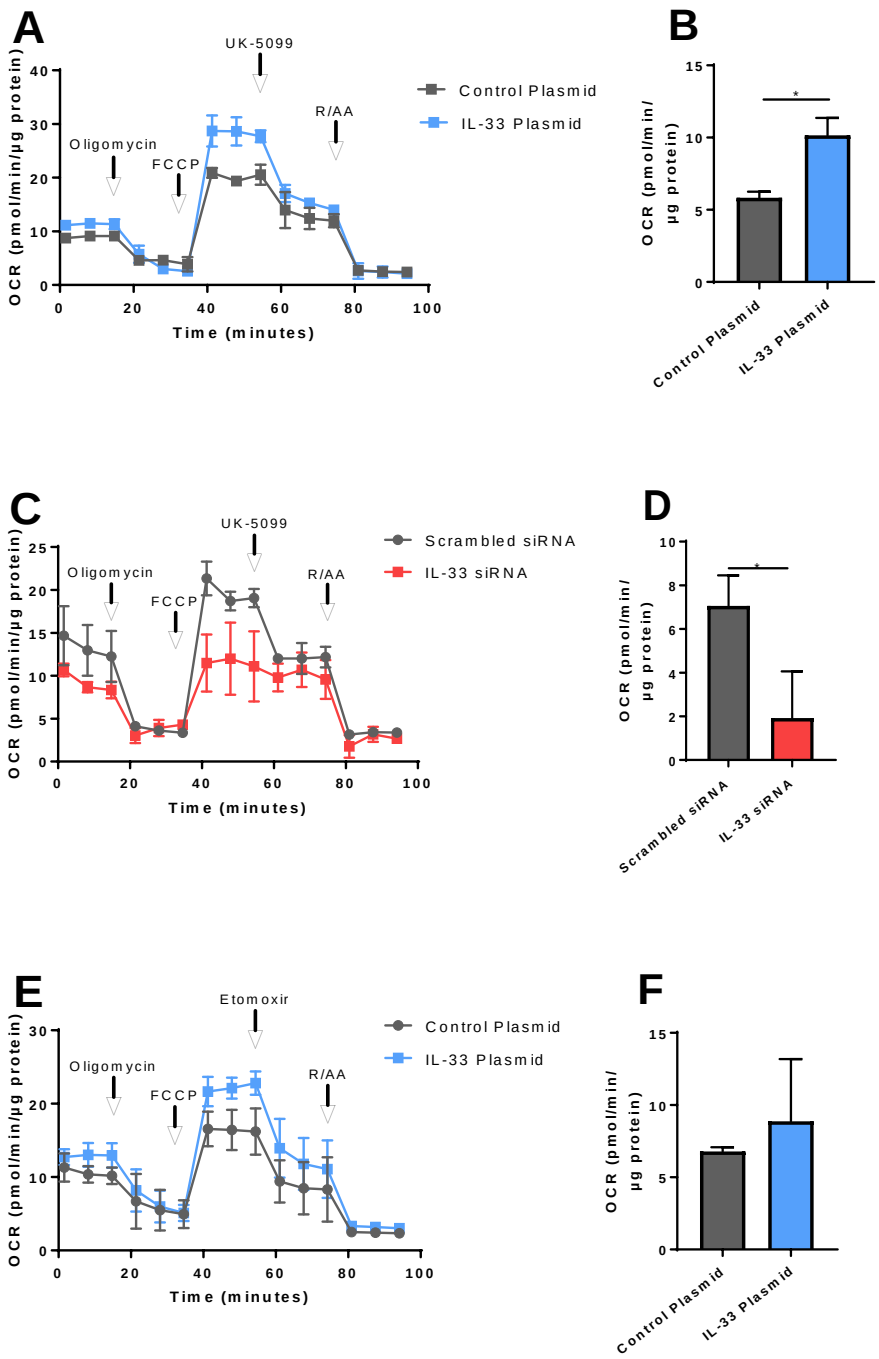
A
UK-5099
R/AA
Oligomycin
FCCP
Control Plasmid
IL-33 Plasmid
OCR (pmol/min/µg protein)
Time (minutes)
B
OCR (pmol/min/ µg protein)
Control Plasmid
IL-33 Plasmid
C
UK-5099
Oligomycin
FCCP
R/AA
Scrambled siRNA
IL-33 siRNA
OCR (pmol/min/µg protein)
Time (minutes)
D
OCR (pmol/min/ µg protein)
Scrambled siRNA
IL-33 siRNA
E
Etomoxir
Oligomycin
FCCP
R/AA
Control Plasmid
IL-33 Plasmid
OCR (pmol/min/µg protein)
Time (minutes)
F
OCR (pmol/min/ µg protein)
Control Plasmid
IL-33 Plasmid

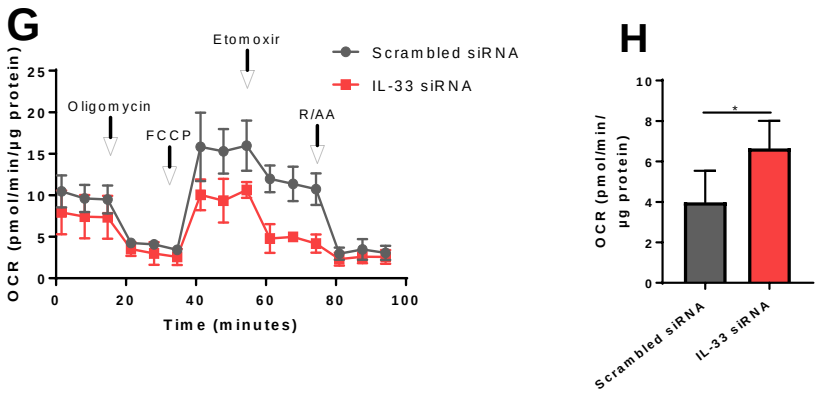

Figure 5.7. Contribution of pyruvate import and fatty oxidation to the metabolism of IL-33 knockdown or overexpressing ARPE-19:

ARPE-19 were transfected for 48h with either a scrambled gDNA plasmid/ *IL33* activation gDNA plasmid or with either scrambled siRNA or a pre-selected mixture of 4 siRNA duplexes targeting the human *IL33* gene. (A) Representative modified mitochondrial stress test measured with sequential injections of oligomycin, FCCP, UK-5099 (40µM) and rotenone/antimycin A. (B) Parameter calculated from (A). (C) Representative modified mitochondrial stress test measured with sequential injections of oligomycin, FCCP, UK-5099 (40µM) and rotenone/antimycin A. (D) Parameter calculated from (C). (E) Representative modified mitochondrial stress test measured with sequential injections of oligomycin, FCCP, etomoxir (200µM) and rotenone/antimycin A. (F) Parameter calculated from (E). (G) Representative modified mitochondrial stress test measured with sequential injections of oligomycin, FCCP, etomoxir (200µM) and rotenone/antimycin A. (H) Parameter calculated from (G). Data are expressed as means ± SD. Represents data from three independent experiments performed in triplicate. Unpaired Student's t-test; *p<0.05.

5.8. Glucose pathway tracing in IL-33 knockdown or overexpressing ARPE-19

To confirm that IL-33 influenced pyruvate oxidation in ARPE-19, I utilised SITA analysis to trace the flux of glucose through glycolysis and into the TCA cycle. SITA with [U-^{13}C]-glucose allowed me to assess the uptake of isotopically labelled glucose into metabolite pools following KD or overexpression of IL-33. Quantifying C^{13} labelling in different metabolite pools as cells approach steady-state equilibrium allows a true defect in pyruvate import into the mitochondria to be detected.

To assess the effect of IL-33 KD on glucose metabolism in ARPE-19, GC-MS was used to measure the abundance of intracellular glycolysis and TCA cycle metabolites in samples. As cells were cultured with C^{13}-isotopically labelled glucose, the C^{13} abundance of these metabolites could be solely attributed to a glucose carbon source. In the glycolysis pathway, there were no significant changes in the relative abundances of glyceraldehyde-3-phosphate, 3-phosphoglycerate, 2-phosphoglycerate or pyruvate (Fig. 5.8A-D). There was, however, a significant increase in the relative abundance of lactate in the IL-33 siRNA compared to the scrambled siRNA control (Fig. 5.8E), matching the observed increase in extracellular lactate in the preceding sections. Glucose-derived pyruvate constitutes a major source of acetyl-coA which serves as a key carbon input into the TCA cycle [540]. Acetyl-coA enters at the citrate synthase step and combines with oxaloacetate to form citrate [540]. Citrate C^{13} enrichment was observed to be significantly decreased in the IL-33 siRNA compared to the scrambled siRNA control (Fig. 5.8F). Relative abundances of C^{13}-labelled succinate and malate were also reduced by IL-33 siRNA treatment (Fig. 5.8G and I). However, no significant changes were observed in the abundance of C^{13}-labelled fumarate, malate, oxaloacetate and aspartate (Fig. 5.8H, J-L). `These results support the earlier conclusions and suggest that there is a defect in pyruvate entry into the TCA cycle when IL-33 is reduced. The carbon tracing data indicates that pyruvate is metabolized into lactate rather than entering the TCA cycle to form citrate.

For each metabolite, signals were monitored at the nominal *m/z* (M0) and at all detectable naturally labelled mass isotopomers (M+X). MID patterns of a given metabolite can yield essential information into the flux between interacting metabolic pathways. Labelling patterns using C^{13}-labelled glucose then highlight differential flux from glycolysis and pyruvate input into the TCA cycle. Glucose-derived pyruvate can enter the TCA cycle through either PDH or PC (Figure 5.9). The citrate M+2/pyruvate M+3 ratio can serve as a surrogate for PDH activity, while the citrate M+3/pyruvate M+3 ratio is used as a surrogate of PC activity [541].

With IL-33 siRNA there was an increased enrichment of M+3 pyruvate (Fig. 5.10A), indicating an increased abundance of glucose-derived pyruvate and a reduced utilization of these carbons in the TCA cycle [541]. KD of IL-33 significantly reduced both the citrate M+2/pyruvate M+3 (Figure 5.10B) and citrate M+3/pyruvate M+3 (Figure 5.10C) ratios suggesting a decrease in the activity of both PDH and PC complexes.

After performing the experiments in the context of IL-33 loss, I assessed how glucose metabolism was affected by IL-33 overexpression. In a similar manner, cells were cultured with an C^{13}-isotopically labelled glucose tracer permitting the identification of glucose derived metabolite abundances within ARPE-19 cells. In the glycolysis pathway, there were significant increases in the relative metabolite abundances of C^{13}-isotopically labelled glyceraldehyde-3-phosphate, 3-phosphoglycerate and 2-phosphoglycerate (Fig. 5.11A-C). No significant changes were observed in the relative abundances of the glycolysis "end-point" metabolites pyruvate or lactate (Fig. 5.11D-E). In the TCA cycle, there was a significant increase in C^{13}-enrichment in all metabolites assessed (Fig. 5.11F-L), indicating that glucose-derived TCA cycle activity was up-regulated with IL-33 overexpression.

Overexpression of IL-33 lead to a decrease in the enrichment of M+3 pyruvate (Fig. 5.12A). There was a significant increase in the citrate M+2/pyruvate M+3 ratio (Fig. 5.12B), suggesting that PDH activity was augmented with IL-33 plasmid treatment. No significant changes were observed in the citrate M+3/pyruvate M+3 ratio with IL-33 overexpression (Fig. 5.12C), indicating that increased pyruvate entry into the TCA cycle was largely dependent on PDH rather PC activity. With IL-33 overexpression a significant increase in citrate M+6 was observed (Fig. 5.12D). This pattern will occur in citrate when both oxaloacetate and malate carbons are derived from glucose. Increased M+4 aspartate (Fig. 5.12E) and malate (Fig. 5.12F) indicate the increased TCA cycling which occurs with IL-33 overexpression. When TCA cycling increases, the production rate of labelled TCA metabolites may be greater than their consumption rate. If this is the case, C^{13} labelling may be increased in amino acid metabolites which branch off the glycolysis pathway (e.g. alanine, which is transaminated *via* glutamic pyruvic transaminase 1/2) [542]. With IL-33 overexpression, there was an observed decrease in M+3 alanine (Fig. 5.12G) indicating the increased consumption of glucose carbons into the TCA cycle.

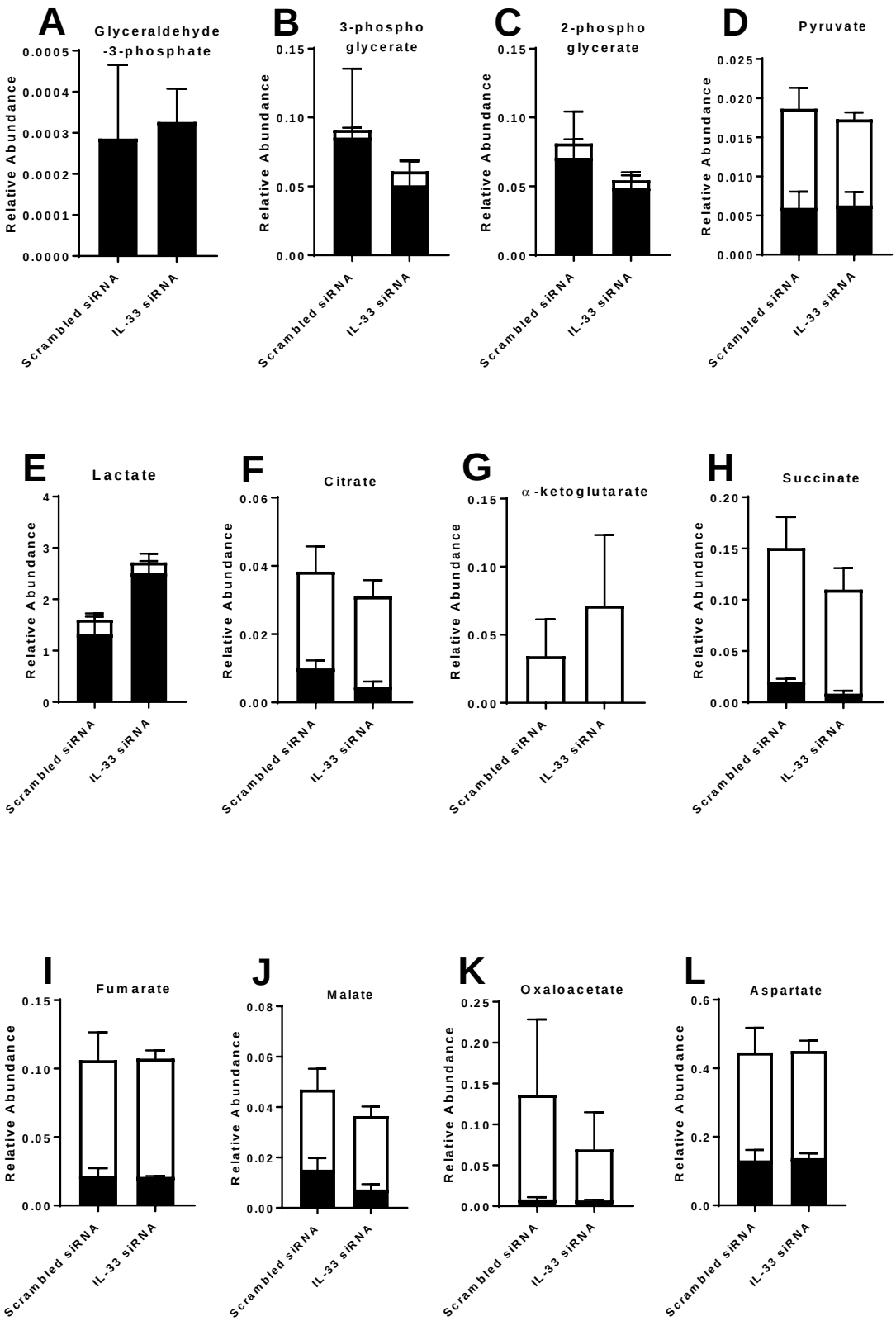
A
Glyceraldehyde -3-phosphate
B
3-phospho glycerate
C
2-phospho glycerate
D
Pyruvate
E
Lactate
F
Citrate
G
α-ketoglutarate
H
Succinate
I
Fumarate
J
Malate
K
Oxaloacetate
L
Aspartate
Relative Abundance
Scrambled siRNA
IL-33 siRNA

Figure 5.8. Glucose tracing in ARPE-19 with IL-33 knockdown:

ARPE-19 were transfected for 48h with either scrambled siRNA or a pre-selected mixture of 4 siRNA duplexes targeting the human *IL33* gene. Cells were incubated for 2h with media containing isotopically labelled glucose and GC-MS was used to quantify relative C^{13} (black) or C^{12} (white) incorporation into glyceraldehyde-3-phosphate (A), 3-phosphoglycerate (B), 2-phosphoglycerate (C), pyruvate (D), lactate (E), citrate (F), α-ketoglutarate (G), succinate (H), fumarate (I), malate (J), oxaloacetate (K) and aspartate (L) metabolite pools. Data expressed as means ± SD from three independent experiments.

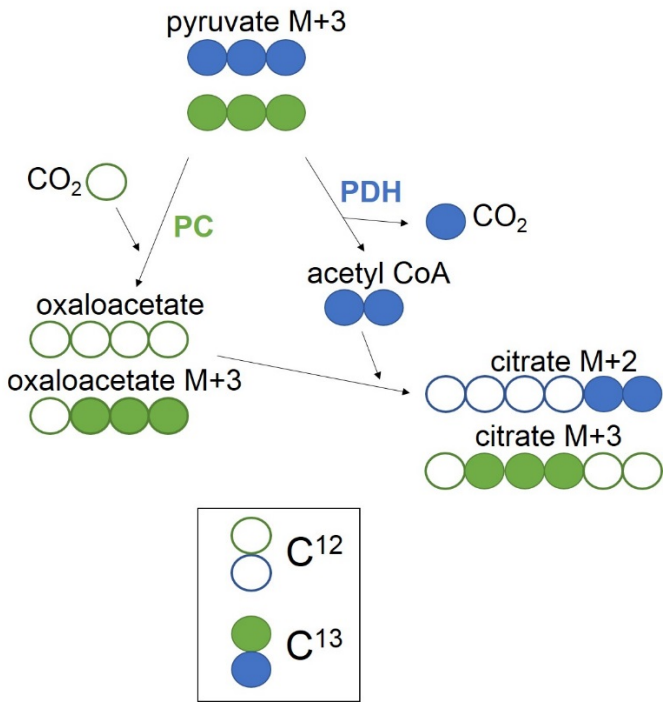

Figure 5.9. Citrate labelling from C^{13}-glucose *via* pyruvate dehydrogenase and pyruvate carboxylase activity in the first turn of the TCA cycle:

Isotopologue distribution in citrate can be used to obtain a clearer representation of pathways feeding into the TCA cycle. Glucose-derived pyruvate can pass into the TCA cycle *via* either oxidation into acetyl-coA by the PDH complex or the anaplerotic generation of oxaloacetate through PC. Activation of PDH will conventionally form M+2 citrate, as positions C1 and C2 are labelled with the glucose-derived tracer. In contrast, activation of PC conventionally forms M+3 oxaloacetate, which in turn forms M+3 citrate as positions C3, C4 and C5 are labelled with C^{13}. The citrate M+2/pyruvate M+3 ratio can serve as a surrogate for PDH activity, whereas the citrate M+3/pyruvate M+3 ratio can be a surrogate for PC. Adapted from [541].

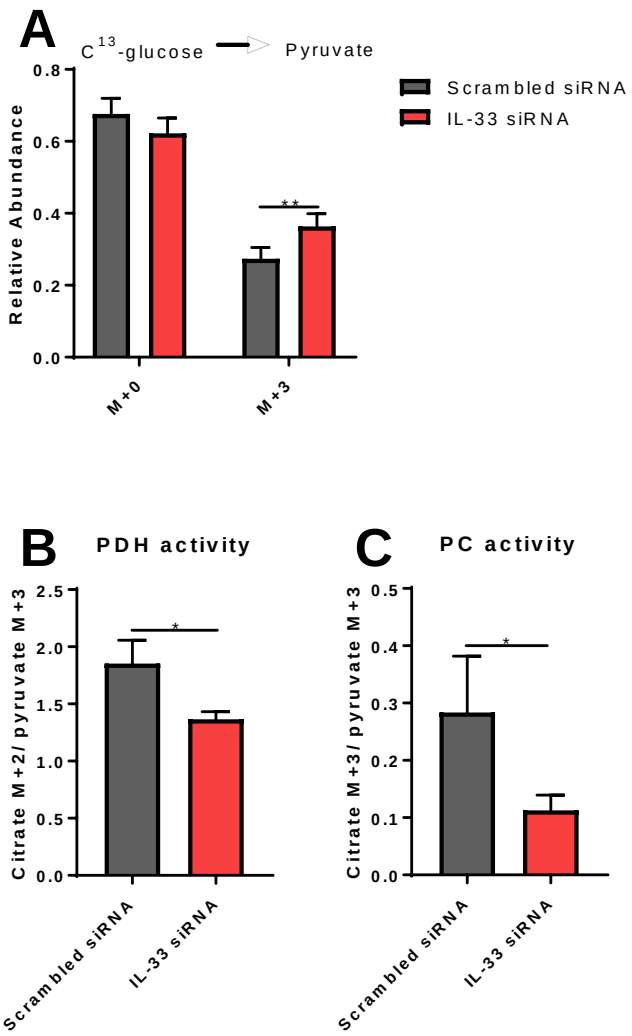

Figure 5.10. Differential citrate labelling from C^{13}-glucose in ARPE-19 with IL-33 knockdown:

ARPE-19 were transfected for 48h with either scrambled siRNA or a pre-selected mixture of 4 siRNA duplexes targeting the human *IL33* gene. Cells were incubated for 2h with media containing isotopically labelled glucose and GC-MS was used to quantify relative C^{13} incorporation. (A) Mass isotopomer distribution of [U-^{13}C]-glucose-derived carbon into pyruvate. This data indicates the raw abundances of the indicated isotopomers in the pyruvate metabolite pool. (B) Citrate m+2/pyruvate m+3 ratio can be a surrogate for PDH activity. (C) Citrate m+3/pyruvate m+3 ratio can be a surrogate for PC activity. Data expressed as relative mean from three independent experiments. Unpaired Student's T-test; *p<0.05; *p<0.01.

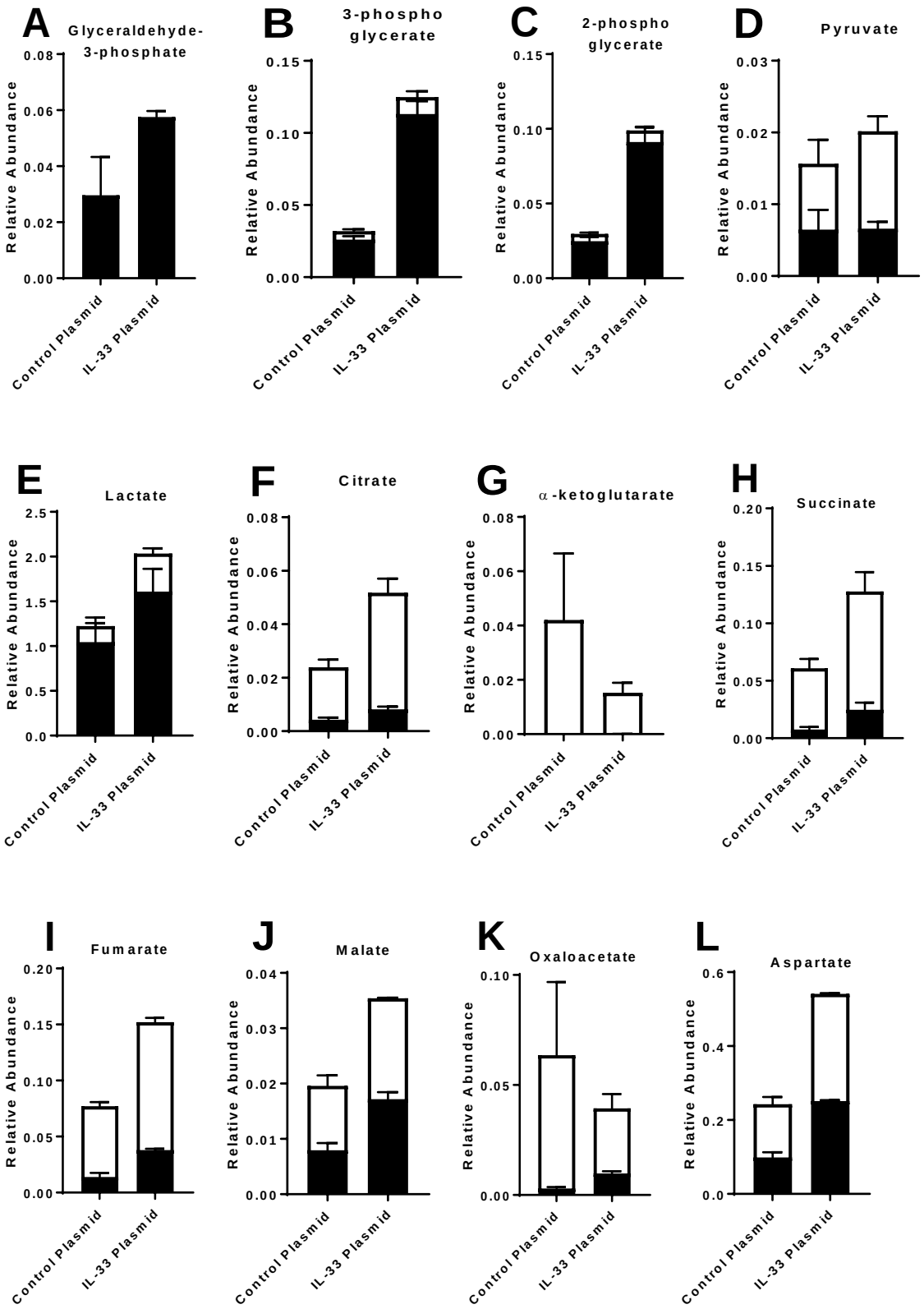
A
Glyceraldehyde-3-phosphate
B
3-phospho glycerate
C
2-phospho glycerate
D
Pyruvate
E
Lactate
F
Citrate
G
α-ketoglutarate
H
Succinate
I
Fumarate
J
Malate
K
Oxaloacetate
L
Aspartate
Relative Abundance
Control Plasmid
IL-33 Plasmid

Figure 5.11. Glucose tracing in ARPE-19 constitutively overexpressing IL-33:

ARPE-19 were transfected for 48h with either a scrambled gDNA plasmid/ *IL33* activation gDNA plasmid. Cells were incubated for 2h with media containing isotopically labelled glucose and GC-MS was used to quantify relative C^{13} (black) or C^{12} (white) incorporation into glyceraldehyde-3-phosphate (A), 3-phosphoglycerate (B), 2-phosphoglycerate (C), pyruvate (D), lactate (E), citrate (F), α-ketoglutarate (G), succinate (H), fumarate (I), malate (J), oxaloacetate (K) and aspartate (L) metabolite pools. Data expressed as relative mean from three independent experiments.

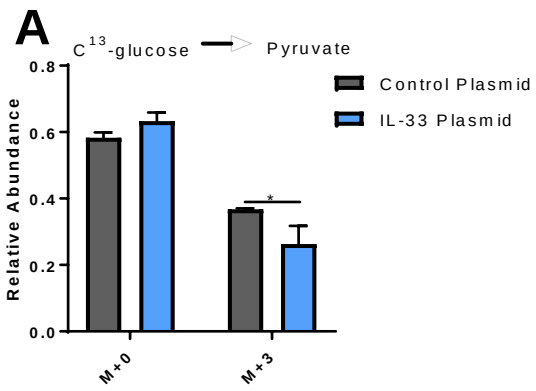
A
C13-glucose
Pyruvate
Control Plasmid
IL-33 Plasmid
Relative Abundance
0.8
0.6
0.4
0.2
0.0
*
M+0
M+3

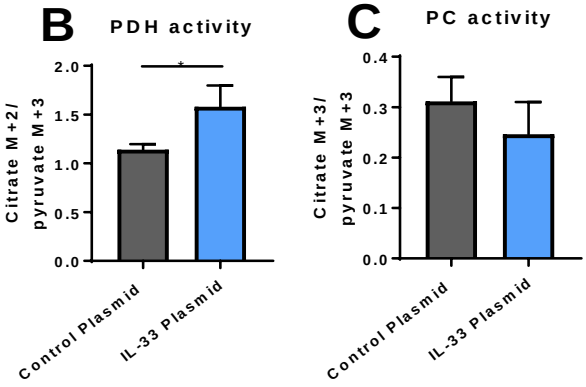
B
PDH activity
Citrate M+2/ pyruvate M+3
2.0
1.5
1.0
0.5
0.0
*
Control Plasmid
IL-33 Plasmid
C
PC activity
Citrate M+3/ pyruvate M+3
0.4
0.3
0.2
0.1
0.0
Control Plasmid
IL-33 Plasmid

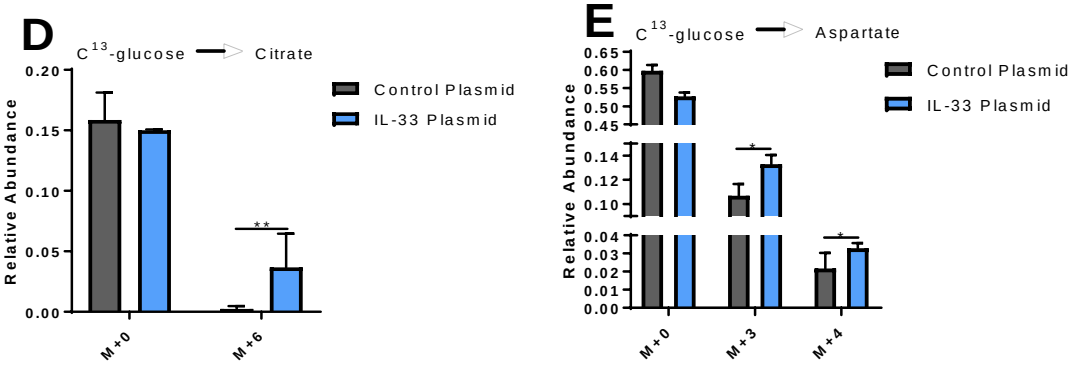
D
C13-glucose
Citrate
Control Plasmid
IL-33 Plasmid
Relative Abundance
0.20
0.15
0.10
0.05
0.00
**
M+0
M+6
E
C13-glucose
Aspartate
Control Plasmid
IL-33 Plasmid
Relative Abundance
0.65
0.60
0.55
0.50
0.45
0.14
0.12
0.10
0.04
0.03
0.02
0.01
0.00
*
*
M+0
M+3
M+4

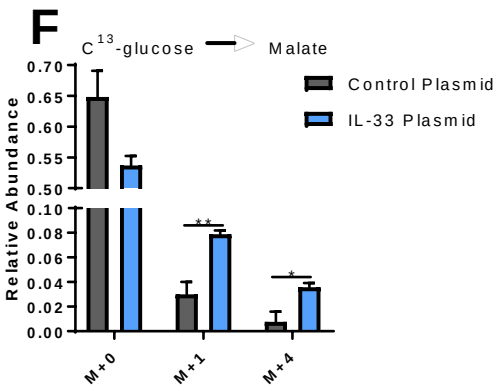
F
C13-glucose
Malate
Control Plasmid
IL-33 Plasmid
Relative Abundance
0.70
0.65
0.60
0.55
0.50
0.10
0.08
0.06
0.04
0.02
0.00
**
*
M+0
M+1
M+4

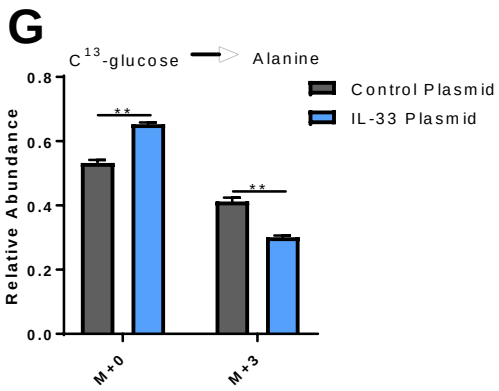
G
C13-glucose
Alanine
Control Plasmid
IL-33 Plasmid
Relative Abundance
0.8
0.6
0.4
0.2
0.0
**
**
M+0
M+3

Figure 5.12. ARPE-19 overexpressing IL-33 exhibit increased TCA cycling:

ARPE-19 were transfected for 48h with either a scrambled gDNA plasmid/ *IL33* activation gDNA plasmid. Cells were incubated for 2h with media containing isotopically labelled glucose and GC-MS was used to quantify relative C^{13} incorporation. (A) Mass isotopomer distribution of [U-^{13}C]-glucose-derived carbon into pyruvate. This data indicates the raw abundances of the indicated isotopomers in the pyruvate metabolite pool. (B) Citrate m+2/pyruvate m+3 ratio can be a surrogate for PDH activity. (C) Citrate m+3/pyruvate m+3 ratio can be a surrogate for PC activity. Mass isotopomer distribution of [U-^{13}C]-glucose-derived carbon into citrate, malate, aspartate and alanine. The distribution of m+6 citrate (D), m+3 and m+4 aspartate (E), m+1 and m+4 malate (F), and m+3 alanine (G) was determined by GC-MS. This data indicates the raw abundances of the indicated isotopomers in their respective metabolite pools. Data expressed as relative mean from three independent experiments. Unpaired Student's T-test; *p<0.05; *p<0.01.

5.9. IL-33 regulates the expression of MPC1 and 2 in ARPE-19 cells

Collectively the data presented so far suggest that nuclear IL-33 is a regulator of pyruvate oxidative metabolism in the RPE. When over expressed, there is increased glycolytic flux into the TCA cycle, which boosts OXPHOS likely through increased PDH activity. The absence of IL-33 reduces OXPHOS activity as pyruvate is "metabolically redirected" into lactate production. Whilst the data indicated a *bona fide* alteration to pyruvate metabolism when IL-33 was either lost or overexpressed, there remained a need to identify the molecular mechanisms.

As detailed in the previous section, the use of the MPC inhibitor UK5099 indicated that MPC-dependent pyruvate entry and mitochondrial oxidation was affected by IL-33 expression. These results suggested that in the absence of IL-33, defects in the entry of pyruvate into the mitochondria were present. When IL-33 was overexpressed, increased pyruvate entered the TCA cycle for OXPHOS. Considering these results, I investigated whether altering IL-33 expression would alter MPC expression in transfected ARPE-19. Altered MPC1/MPC2 expression results in significant metabolic disorders and has been previously shown to contribute to the Warburg effect in cancer cells [295].

RT-PCR was used to identify the gene expression of nuclear encoded *MPC1* and *MPC2* genes following modulation of IL-33 using either siRNA or CRISPR-cas9. KD of IL-33 using siRNA significantly reduced the abundance of both *MPC1* and *MPC2* mRNA transcripts (Fig. 5.13A). Overexpression of IL-33 lead to increased *MPC1* but had no significant effect on *MPC2* mRNA expression (Fig. 5.13B). To confirm that the differences in gene transcription matched translation (and therefore protein expression), immunoblotting was performed for both MPC1 and MPC2 proteins. Transfection of ARPE-19 with IL-33 siRNA significantly reduced the protein expression of both MPC components relative to a scrambled siRNA control (Fig. 5.13C-D). In contrast ARPE-19 transfected with an IL-33 overexpression plasmid increased MPC1 expression, yet no significant effect was observed in MPC2 expression relative to a control activation plasmid (Fig. 5.13E-F).

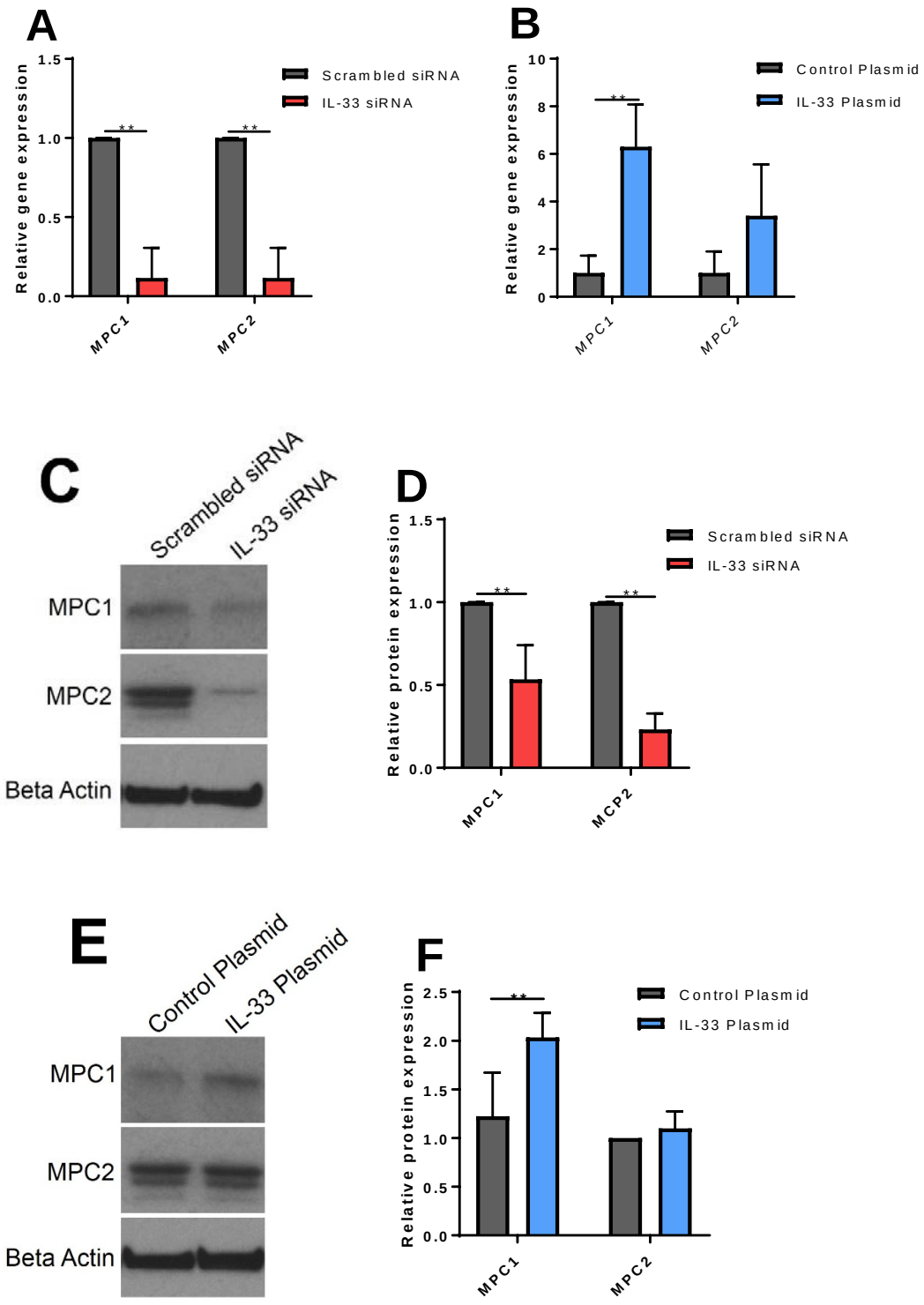
A
Relative gene expression
1.5
1.0
0.5
0.0
**
**
Scrambled siRNA
IL-33 siRNA
MPC1
MPC2
B
Relative gene expression
10
8
6
4
2
0
**
Control Plasmid
IL-33 Plasmid
MPC1
MPC2
C
Scrambled siRNA
IL-33 siRNA
MPC1
MPC2
Beta Actin
D
Relative protein expression
1.5
1.0
0.5
0.0
**
**
Scrambled siRNA
IL-33 siRNA
MPC1
MCP2
E
Control Plasmid
IL-33 Plasmid
MPC1
MPC2
Beta Actin
F
Relative protein expression
2.5
2.0
1.5
1.0
0.5
0.0
**
Control Plasmid
IL-33 Plasmid
MPC1
MPC2

Figure 5.13. IL-33 regulates the expression of MPC1 and 2 in ARPE-19 cells:

(A) ARPE-19 were transfected for 48h with either scrambled siRNA or a pre-selected mixture of 4 siRNA duplexes targeting the human *IL33* gene; RNA was extracted, and RT-PCR was used to determine the expression of *MPC1* and *MPC2.* (B) ARPE-19 were transfected for 48h with either a scrambled gDNA plasmid or an *IL33* activation gDNA plasmid; RNA was extracted, and RT-PCR was used to determine the expression of *MPC1* and *MPC2.* (C-D) ARPE-19 were transfected for 48h with either scrambled siRNA or a pre-selected mixture of 4 siRNA duplexes targeting the human *IL33* gene; protein was extracted, and western blot analysis was used to determine the expression of MPC1 and MPC2. (E-F) ARPE-19 were transfected for 48h with either a scrambled gDNA plasmid or an *IL33* activation gDNA plasmid; protein was extracted, and western blot analysis was used to determine the expression of MPC1 and MPC2. (A-B) Represents data from three independent experiments performed in triplicate. (C-F) Represents data from three independent western blots. Unpaired Student's T-test; *p<0.01.

5.10. Recombinant IL-33 is unable to rescue metabolic defects with IL-33 loss

Results presented in both this chapter and chapter 4 suggest differential roles of the cytokine on RPE metabolism through intracellular interactions ST2 dependent extracellular alarmin activity. Extracellular IL-33/ST2 signalling was accompanied with increased metabolic activity (particularly in the glycolysis pathway/TCA cycle). Similarly, increases in the nuclear expression of IL-33 lead to augmented glycolytic flux into the TCA cycle, whereas KD/loss of endogenous IL-33 impaired TCA activity. Considering these findings, I considered whether IL-33 signalling *via* ST2 could overcome the metabolic defects observed in the RPE with IL-33 loss.

To address this hypothesis, primary RPE were isolated from both WT and *Il33*$^{-/-}$ mice and treated with rmIL-33 for 24h; following this, XF analysis was performed to identify metabolic changes. A mitochondrial stress test was utilised to investigate mitochondrial metabolism. As previously detailed, IL-33 loss impairs primary RPE spare respiratory capacity, whereas treatment with exogenous IL-33 boosts RPE OXPHOS capacity. The addition of rmIL-33 to primary *Il33*$^{-/-}$ RPE was unable to restore impaired mitochondrial function (Fig. 5.14A-C). A complimentary experiment was performed in human ARPE-19 cells. IL-33 KD was first induced using siRNA; following KD cells were incubated for 24h in the presence or absence of rhIL-33. The addition of rhIL-33 to the IL-33 KD cells was unable to alleviate impaired mitochondrial function (Fig. 5.14D-F). These data indicate that regulation of metabolic properties by intrinsic IL-33 is independent from IL-33 receptor dependent signalling.

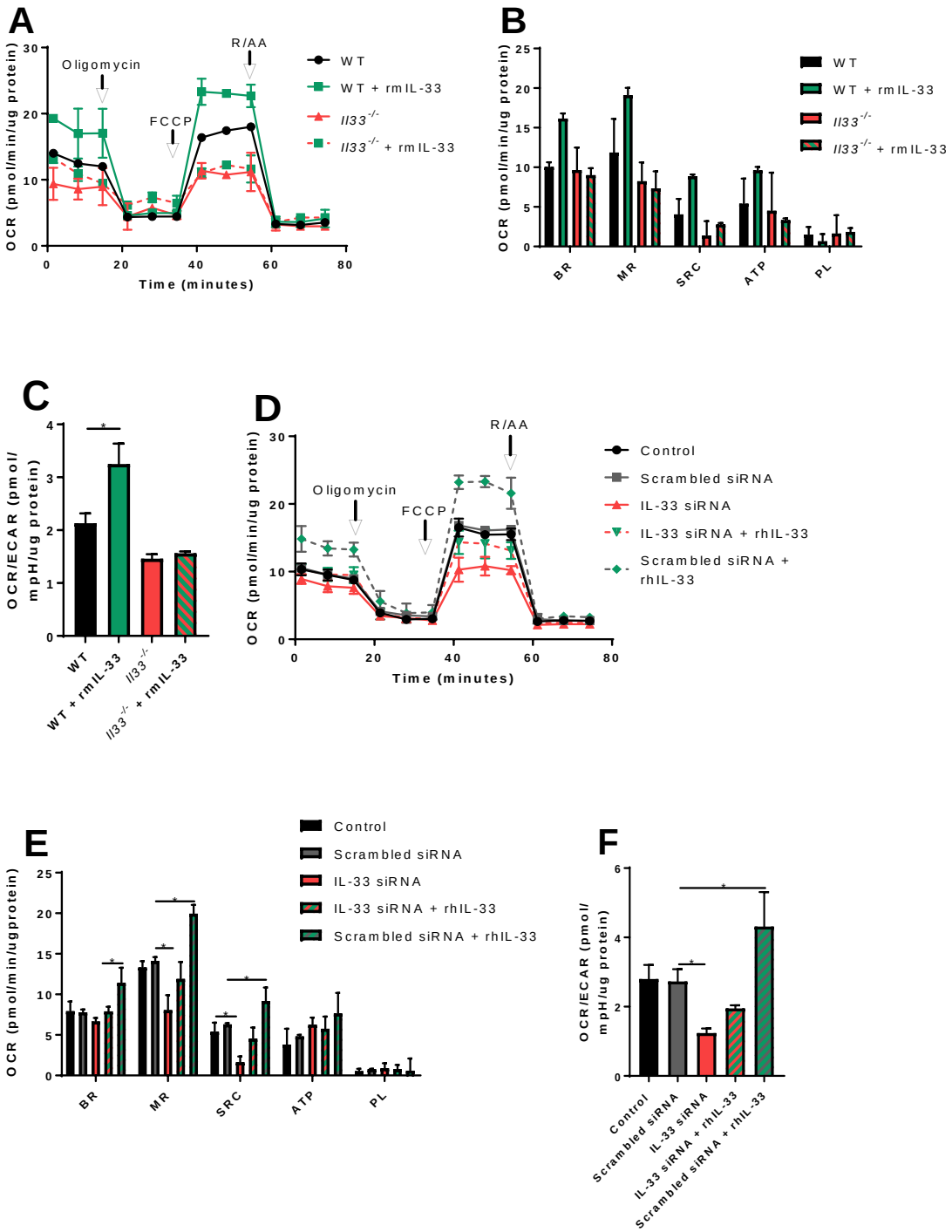
A
OCR (pmol/min/ug protein)
Oligomycin
FCCP
R/AA
WT
WT + rmIL-33
Il33-/-
Il33-/- + rmIL-33
Time (minutes)
B
OCR (pmol/min/ug protein)
WT
WT + rmIL-33
Il33-/-
Il33-/- + rmIL-33
BR
MR
SRC
ATP
PL
C
OCR/ECAR (pmol/ mpH/ug protein)
WT
WT + rmIL-33
Il33-/-
Il33-/- + rmIL-33
D
OCR (pmol/min/ug protein)
Oligomycin
FCCP
R/AA
Control
Scrambled siRNA
IL-33 siRNA
IL-33 siRNA + rhIL-33
Scrambled siRNA + rhIL-33
Time (minutes)
E
OCR (pmol/min/ugprotein)
Control
Scrambled siRNA
IL-33 siRNA
IL-33 siRNA + rhIL-33
Scrambled siRNA + rhIL-33
BR
MR
SRC
ATP
PL
F
OCR/ECAR (pmol/ mpH/ug protein)
Control
Scrambled siRNA
IL-33 siRNA
IL-33 siRNA + rhIL-33
Scrambled siRNA + rhIL-33

Figure 5.14. Recombinant IL-33 fails to reverse the effects of IL-33 loss in the RPE:

Primary RPE were isolated from WT or *Il33*$^{-/-}$ mice and treated for 24h with rmIL-33 (100ng/ml). (A) Representative mitochondrial stress test measured with sequential injections of oligomycin, FCCP and rotenone/antimycin A. (B) OXPHOS parameters calculated from data shown in (A). (C) Basal OCR and ECAR measurements expressed as the ratio OCR/ECAR. ARPE-19 were transfected for 48h with either scrambled siRNA or a pre-selected mixture of 4 siRNA duplexes targeting the human *IL33* gene. Cells were treated for a further 24h with rhIL-33. (D) Representative mitochondrial stress test measured with sequential injections of oligomycin, FCCP and rotenone/antimycin A. (E) OXPHOS parameters calculated from data shown in (D). (F) Basal OCR and ECAR measurements expressed as the ratio OCR/ECAR. (100ng/ml). Data presented as means ± SD. (A-C) Represents data from two mice per group. (D-F) Represents data from four independent experiments run with no technical repeats. One-way ANOVA with Tukey's multiple comparisons test; *p<0.05.

5.11. RPE mitochondrial analysis with alternate IL-33 expression status

Recent studies have determined a novel role for IL-33 in the maintenance of mitochondrial respiration. Mitochondria from *Il33*$^{-/-}$ and *Il1rl1*$^{-/-}$ beige and brown adipocytes were observed to exhibit reduced OXPHOS and expression of ETC components; moreover, electron microscopy demonstrated functional defects in mitochondrial structure [19]. Given the pronounced changes in metabolism in absence/overexpression of IL-33 I used transmission electron microscopy to identify visible structural changes in primary murine RPE mitochondria. Compared to WT mitochondria, *Il33*$^{-/-}$ mitochondria were smaller, elongated and more irregular in size (Fig. 5.15A-B, F). Image analysis of mitochondrial samples showed that mitochondrial diameter was decreased in *Il33*$^{-/-}$ cells (Fig. 5.15C). No significant changes were observed in mitochondrial area (Fig. 5.15D), but there was increased mitochondrial number/field in the *Il33*$^{-/-}$ group (Fig. 5.15E). Additionally, retinal sections from *Il33*$^{-/-}$ mice stained with MitoGreen™ were observed to have increased mitochondrial density (Fig. 5.15G-H). Mitochondrial staining was localised to the RPE, outer plexiform layer and inner plexiform layer (Fig. 5.15G).

A similar experimental pipeline was used to assess mitochondrial structure in ARPE-19 cells exhibiting IL-33 KD (*via* siRNA). Electron microscopy was used to identify structural changes in the IL-33 siRNA group compared to a scrambled siRNA control (Fig. 5.16A-C). Image analysis identified significant alterations to both the mitochondrial diameter (Fig. 5.16D) and area (Fig. 5.16E) in the IL-33 siRNA group compared to a scrambled siRNA control. Interestingly, transfection with the scrambled siRNA alone elicited changes to the mitochondrial diameter (Fig. 5.16D). After transfection with the IL-33 siRNA, it was apparent there were changes to mitochondrial morphologies. Unstimulated cells showed typically fragmented mitochondria (62.4%) and short tubular mitochondria (32%), long tubular mitochondria were observed at a lower frequency of (5.6%) (Fig. 5.16E). This was similar in the scrambled siRNA transfected group, with fragmented mitochondria (67.3%), short tubular mitochondria (13.1%) and long tubular mitochondria (19.6%). In the IL-33 siRNA group, the frequency of mitochondrial morphologies was altered, with almost all mitochondria observed as fragmented (97.4%), with very few tubular mitochondria observed (Fig. 5.16F). The increased mitochondrial size and elongation suggested that mitochondrial fission and fusion processes (see section 3.14) were affected by IL-33 KD. The transcription status of nuclear-encoded mitochondrial fission/fusion enzymes was assessed by RT-PCR in ARPE-19 cells transfected with either scrambled or IL-33 siRNA. In response to IL-33 KD there was no changes observed to the transcription of *DRP1* (involved in mitochondrial fission), *MFN2* and *OPA1* (both involved in mitochondrial fusion) or *PINK1* (a regulator of mitophagy) mRNA transcripts (Fig. 5.16G). Surprisingly, IL-33 KD significantly upregulated the

expression of *MFN1*, an enzyme involved in OMM fusion (Fig. 5.16G). Collectively, the QPCR data suggested that the mitochondrial fission (and generation of fragmented mitochondria) was not as a result to IL-33-mediated transcriptional reprogramming of fission/fusion genes. As DRP1 is regulated by phosphorylation, it is plausible that its activation state is altered in the absence of IL-33. This, however, was not investigated in this body of work.

As the electron microscopy analysis showed structural alterations that affected the mitochondria, this was followed up by an assessment of total mitochondrial number was affected. RT-PCR was used to estimate mitochondrial content through the amplification of cytochrome B and 16 S rRNA transcripts [397]. An increased mitochondrial copy number was observed in the absence of IL-33 compared to a scrambled siRNA control (Fig. 5.16H). Following establishing the increased mitochondrial mass in the IL-33 KD group, it was of interest to identify if there were alterations in the abundance of mitochondrial ETC complexes, as quantified by immunoblotting. It was observed that IL-33 siRNA treatment significantly increased the expression of complexes IV, III and II (Fig. 5.17A-B). No significant changes were observed to the expression of the ATP synthase complex (complex V) and complex I (Fig. 5.17A-B).

Having established that IL-33 loss - both in murine RPE sections and human cell line cultures – leads to changes in mitochondria architecture (albeit varied between mouse and human), mitochondrial density and the expression of ETC components, it was necessary to examine how IL-33 overexpression would influence mitochondrial structure. Again, using electron microscopy, it was determined that overexpression of IL-33 significantly altered the structure of ARPE-19 mitochondria (Fig. 5.18A-C). although, no significant changes were observed to either mitochondrial diameter (Fig. 5.18D) or mitochondrial area (Fig. 5.18E) when IL-33 was overexpressed, there was a significant shift in the percentage of tubular mitochondria, compared to a scrambled plasmid control (Fig. 5.18F). In the control plasmid group, fragmented mitochondria were observed at the highest frequency (45.3%), with long tubular and short tubular mitochondria observed at 27.2% and 27.5%, respectively (Fig. 5.18F). In the IL-33 plasmid group, the percentage of fragmented mitochondria had shifted to 10.4%. Long tubular and short tubular mitochondria were observed at a higher frequency in these images, occurring at 52.6% and 37%, respectively (Fig. 5.18F). Like the IL-33KD experiments, mitochondrial morphologies were affected by IL-33 overexpression. To investigate if the alterations in mitochondrial morphology were attributed to nuclear-encoded mitochondrial fission/fusion enzymes, I utilized RT-PCR to determine their gene expression. IL-33 overexpression led to increased mRNA expression of

the pro-fusion enzyme *MFN2* (Fig. 5.19G). *PINK1* mRNA transcripts were found to be significantly decreased with IL-33 overexpression (Fig. 5.18G). No significant changes were observed to the expression of *MFN1*, *OPA1* and *DRP1* (Fig. 5.18G). Collectively, these data indicate that mitochondrial remodelling occurs with IL-33 overexpression, increasing the frequency of "fused" mitochondria. Although *MFN2* expression status was altered by the overexpression of IL-33 its role in mitochondrial remodelling was not investigated further.

To investigate if mitochondrial number was affected by the overexpression of IL-33, mtDNA copy number was quantified using RT-PCR. However, no significant changes in mitochondrial copy number were observed (Fig. 5.18H). Whilst mitochondria number remained unchanged, it was of interest to see if the changes in mitochondria structure and function were accompanied by alterations to the expression of ETC components. Using immunoblotting, the expression of complexes V-I were quantified in ARPE-19 cells transfected with either a control plasmid or an IL-33 activation plasmid. It was observed that overexpression of IL-33 had no significant effect on the protein expression of complexes V, IV and II (Fig. 5.19A-B). Interestingly, IL-33 overexpression significantly reduced the expression of complexes I and III (Fig. 5.19A-B).

Taken together, the results from this section indicate that the previously described metabolic changes observed in the RPE with changes in IL-33 expression status are concurrent with alterations in mitochondrial structure, morphology and expression of functional components. Primary RPE from *Il33*$^{-/-}$ mice exhibited alterations to mitochondrial morphology and increased mitochondrial number. Although mitochondrial structural changes were observed in ARPE-19 cells with transient IL-33 KD, these were towards a higher proportionality of fragmented punctate mitochondria, rather than short (and to a lesser extent) long tubular, as observed in from *Il33*$^{-/-}$ mice. IL-33 KD, both transiently and germline KO, led to increased mitochondrial abundance. Moreover, IL-33 siRNA treated ARPE-19 cells exhibited increased abundance of ETC components compared to a scrambled siRNA. IL-33 overexpression equally altered both mitochondrial structure and morphology. IL-33 overexpressing cells shifted their mitochondrial ultrastructure towards fused networks.

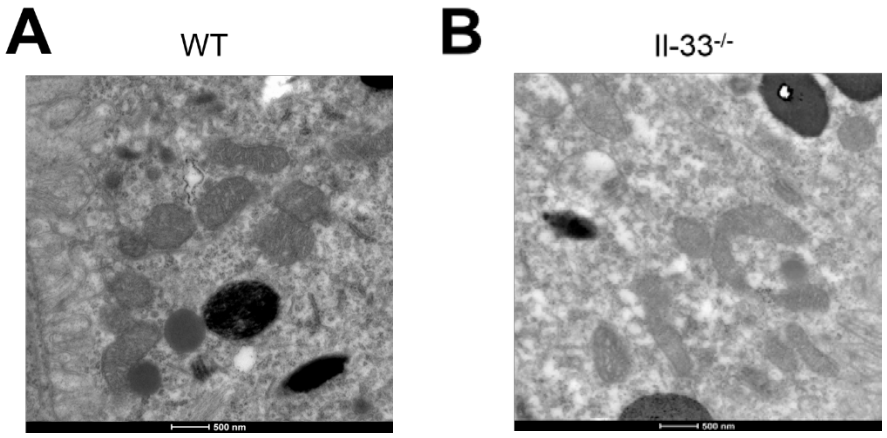
A
WT
B
Il-33-/-
500 nm
500 nm

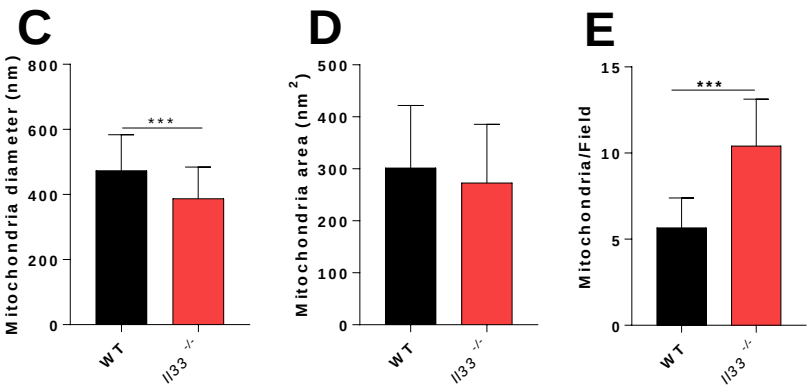
C
Mitochondria diameter (nm)
800
600
400
200
0
***
WT
Il33 -/-
D
Mitochondria area (nm2)
500
400
300
200
100
0
WT
Il33 -/-
E
Mitochondria/Field
15
10
5
0
***
WT
Il33 -/-

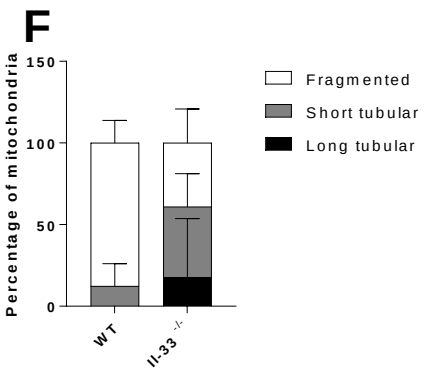
F
Percentage of mitochondria
150
100
50
0
WT
Il-33 -/-
Fragmented
Short tubular
Long tubular

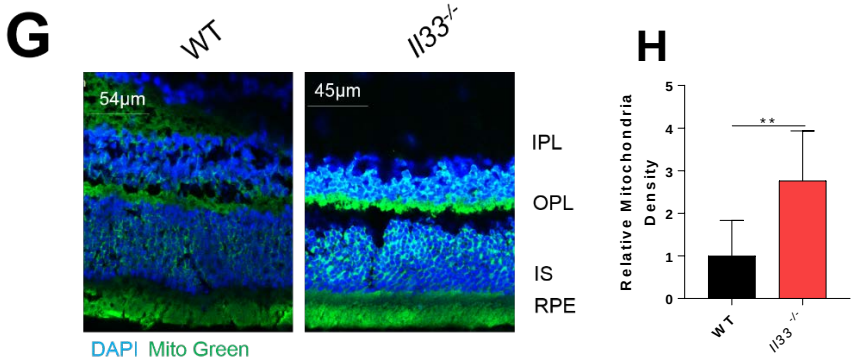
G
WT
Il33-/-
54µm
45µm
IPL
OPL
IS
RPE
DAPI Mito Green
H
Relative Mitochondria Density
5
4
3
2
1
0
**
WT
Il33 -/-

Figure 5.15. Mitochondrial analysis of *Il33*$^{-/-}$ RPE:

Representative transmission electron microscopy of RPE from (A) WT and (B) *Il33*$^{-/-}$ mice. Magnification 9300x. (C) Mitochondrial diameter, (B) mitochondrial area and (C) mitochondrial number were calculated using ImageJ from transmission electron microscopy images of RPE from WT and *Il33*$^{-/-}$ mice (as detailed in methods). (F) Quantification of mitochondrial morphology into either fragmented, short tubular or long tubular phenotypes. (G) Eyes from both WT and *Il33*$^{-/-}$ mice were collected and sections or RPE/choroid whole-mounts were prepared. Representative confocal images of sections show the mitochondrial content in the retina (MitoGreen™ was used to analyse mitochondrial density). (H) Quantitative MFI analysis from confocal images displayed in (G). Data are expressed as means ± SD from three independent experiments. Unpaired Student's T-test; *p<0.05, ***p<0.001.

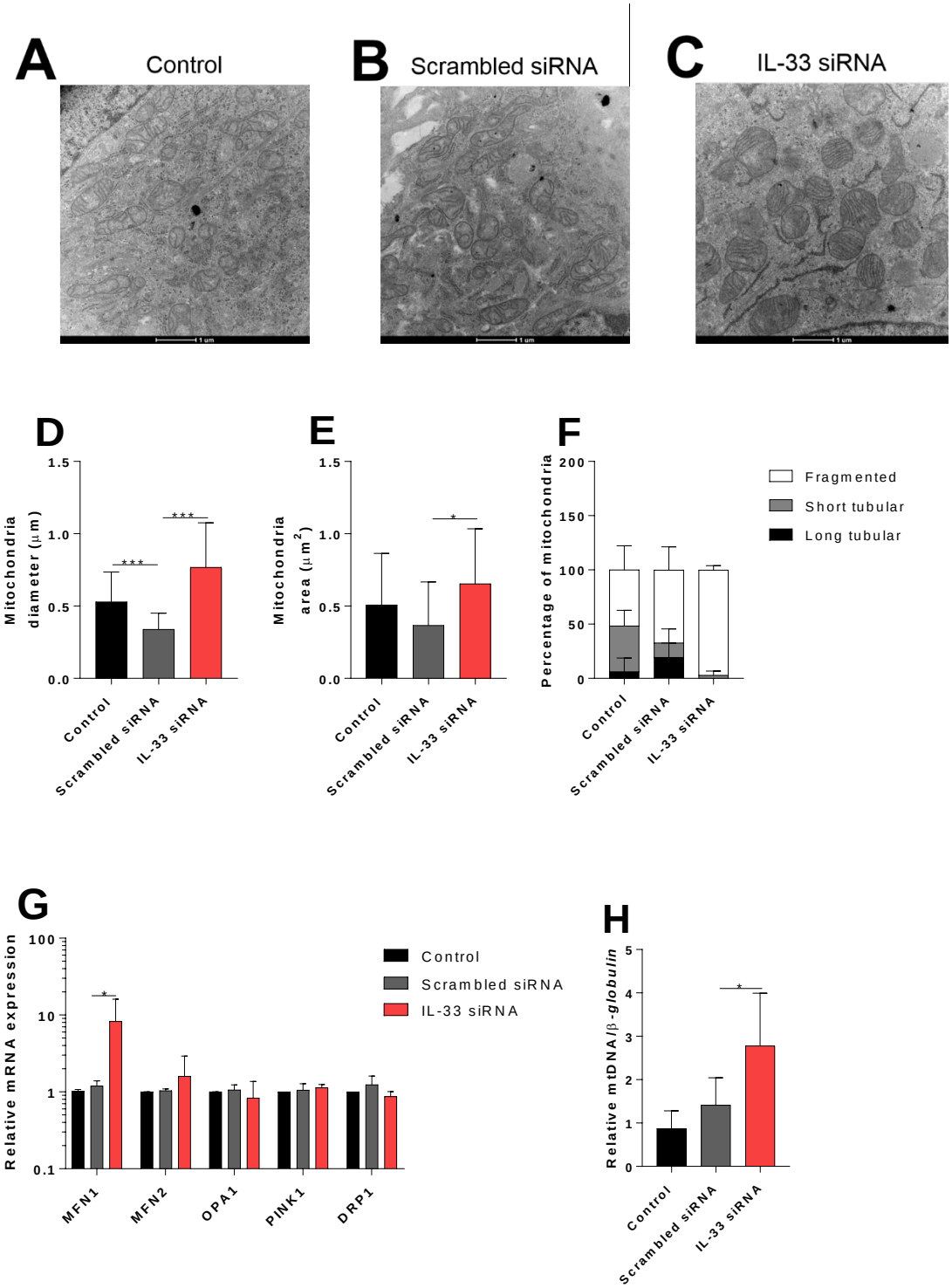
A
Control
B
Scrambled siRNA
C
IL-33 siRNA
D
Mitochondria diameter (μm)
1.5
1.0
0.5
0.0
***
***
Control
Scrambled siRNA
IL-33 siRNA
E
Mitochondria area (μm²)
1.5
1.0
0.5
0.0
*
Control
Scrambled siRNA
IL-33 siRNA
F
Percentage of mitochondria
200
150
100
50
0
Fragmented
Short tubular
Long tubular
Control
Scrambled siRNA
IL-33 siRNA
G
Relative mRNA expression
100
10
1
0.1
*
Control
Scrambled siRNA
IL-33 siRNA
MFN1
MFN2
OPA1
PINK-1
DRP1
H
Relative mtDNA/β-globulin
5
4
3
2
1
0
*
Control
Scrambled siRNA
IL-33 siRNA

Figure 5.16. Mitochondrial analysis of ARPE-19 with IL-33 knockdown:

Representative transmission electron microscopy of ARPE-19 from (A) untreated, (B) scrambled siRNA transfected and (C) IL-33 siRNA transfected. (D) Mitochondrial diameter and (E) area were calculated using ImageJ. (F) Quantification of mitochondrial morphology into either fragmented, short tubular or long tubular phenotypes. (G) Quantitative RT-PCR was performed to assess mitochondrial content; this was estimated from the amplification of *CTYB* and 16S rRNA relative to *BGLOB* mRNA transcripts. Data are presented as means ± SD from three independent experiments. One-way ANOVA with Dunnet's multiple comparisons test; *p<0.05, ***p<0.005.

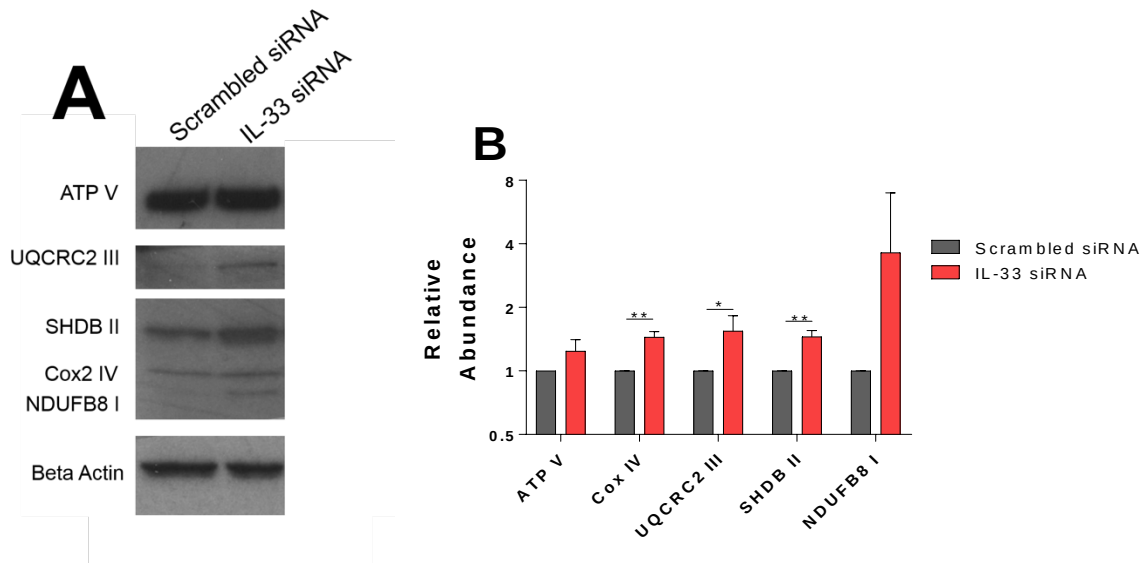

Figure 5.17. Expression of ETC components in ARPE-19 with IL-33 knock-down:

(A) ARPE-19 cells were transfected with either a scrambled siRNA or an IL-33 siRNA. Western blot analysis was used to determine the expression of ETC complexes (ATP synthase V, Cox2 IV, UQCRC2 III, SHDB II and NDUFB8 I). (B) Relative densitometry was calculated from (G) using ImageJ.

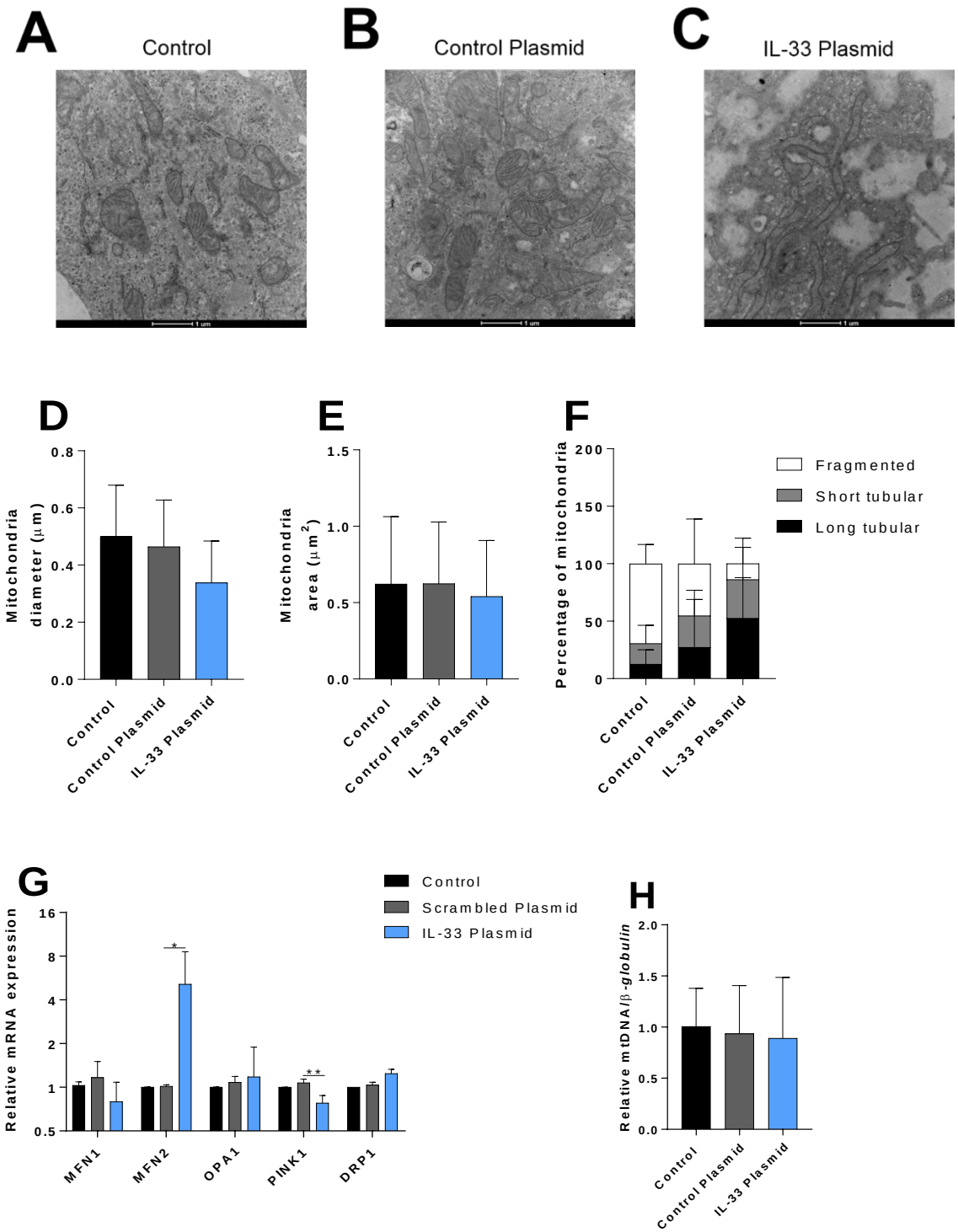
A
Control
B
Control Plasmid
C
IL-33 Plasmid
D
Mitochondria diameter (μm)
0.8
0.6
0.4
0.2
0.0
Control
Control Plasmid
IL-33 Plasmid
E
Mitochondria area (μm²)
1.5
1.0
0.5
0.0
Control
Control Plasmid
IL-33 Plasmid
F
Percentage of mitochondria
200
150
100
50
0
Fragmented
Short tubular
Long tubular
Control
Control Plasmid
IL-33 Plasmid
G
Relative mRNA expression
16
8
4
2
1
0.5
Control
Scrambled Plasmid
IL-33 Plasmid
*
**
MFN1
MFN2
OPA1
PINK1
DRP1
H
Relative mtDNA/β-globulin
2.0
1.5
1.0
0.5
0.0
Control
Control Plasmid
IL-33 Plasmid

Figure 5.18. Mitochondrial analysis of ARPE-19 cells with IL-33 overexpression:

Representative transmission electron microscopy of ARPE-19 from (A) untreated, (B) control plasmid transfected and (C) IL-33 plasmid transfected. (D) Mitochondrial diameter and (E) area were calculated using ImageJ. (F) Quantification of mitochondrial morphology into either fragmented, short tubular or long tubular phenotypes. (G) Quantitative RT-PCR was performed to assess mitochondrial content; this was estimated from the amplification of *CTYB* and 16S rRNA relative to *BGLOB* mRNA transcripts. Data are presented as means ± SD from three independent experiments. One-way ANOVA with Dunnet's multiple comparisons test; **p*<0.05, ****p*<0.005.

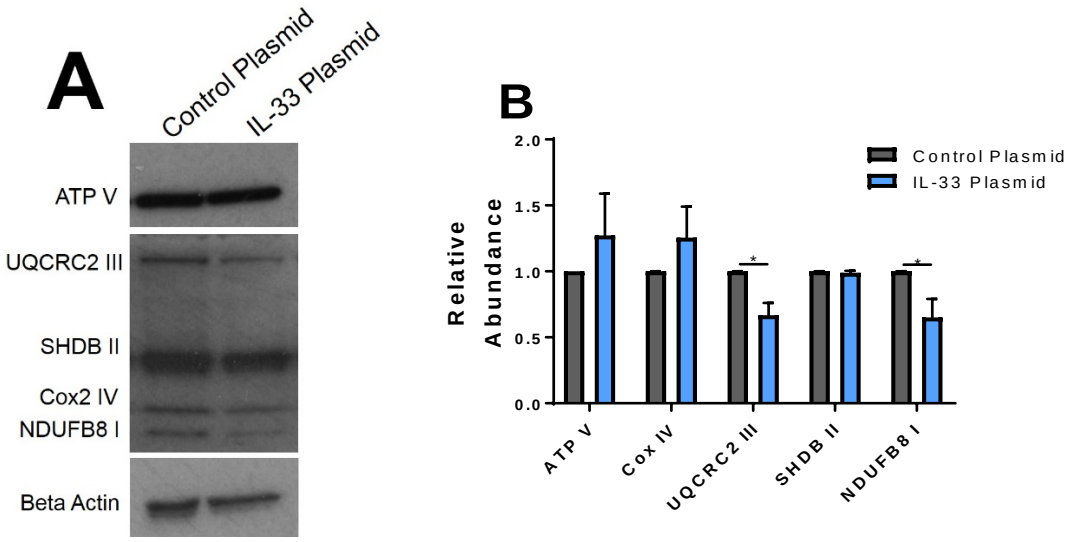

Figure 5.19. Expression of ETC components in ARPE-19 with IL-33 overexpression:

(A) ARPE-19 cells were transfected with either a control plasmid or an IL-33 activation plasmid. Western blot analysis was used to determine the expression of ETC complexes (ATP synthase V, Cox2 IV, UQCRC2 III, SHDB II and NDUFB8 I). (B) Relative densitometry was calculated from (G) using ImageJ.

5.12. Discussion

In this chapter I have addressed a central question in the biology of IL-33 focusing on the role that endogenous IL-33 plays regulating cellular function. These results demonstrate that endogenous IL-33 expression status influences metabolic regulation in RPE cells. IL-33 loss in RPE cells increases aerobic glycolysis at the expense of oxidative glucose catabolism, as IL-33 was found to regulate pyruvate import into the mitochondria through the MPC complex. Cells overexpressing IL-33 display increased expression of MPC complex components and activity of pyruvate dehydrogenase to facilitate increased pyruvate flux into the TCA cycle. This may have implications for innate immune activation of the RPE whereby metabolic changes are accompanied by an increase in the expression of nuclear IL-33.

The intracellular properties of IL-33 remain poorly defined to date and it is currently unknown to what extent nuclear localised IL-33 exerts effects on gene expression, although within the literature it is reported as a difunctional cytokine, acting both as a "nuclear transcription factor" and extracellular ligand for ST2-dependent signalling [256]. IL-33 is constitutively expressed in mainly epithelial cells and fibroblasts during homeostasis [137], with expression levels augmented during inflammation [146, 543]. Following cellular damage or stress IL-33 is released and acts as a potent pro-inflammatory cytokine [243]. Emerging evidence suggests that functions of IL-33 do not extend beyond its extracellular ability to activate ST2-expressing cells; and its unique nuclear localisation and chromatin binding properties are simply evolutionary conserved mechanisms which relate to storage for cytokine release and bioactivity [230, 263]. These conclusions are in contrast with other recent findings, providing a plethora of experimental data which suggests a nuclear role for the cytokine (e.g. regulation of Nf-kB activity [10, 259, 260], binding to homeobox binding motifs in the promoter regions of *IL1RL1, IL6 and CCL5* [257] or *Il13* [258] and an extensive nuclear interactome converging on transcriptional and chromatin remodelling factors [261].

My findings strongly support the conclusion that nuclear localised IL-33 plays an essential part in mitochondrial respiration in the RPE. These results attribute a dual-function to IL-33 in the cellular context of the RPE. Cells lacking IL-33 display abnormal mitochondrial respiration, with diminished spare respiratory capacity. This is consistent with observations in adipose tissue where isolated mitochondria from *Il33*$^{-/-}$ (and *Il1rl1*$^{-/-}$) mice exhibited profound respiratory defects, including reduced OXPHOS, and enzymatic activity of ETC complexes II and IV [19]. It is therefore of note that RPE from

Il1rl1$^{-/-}$ deficient mice did not exhibit bioenergetic changes. The same study identified an increased expression of genes involved in the catabolism of fatty acids, glucose and amino acids in *Il33*$^{-/-}$ adipose tissue suggesting a similar compensatory mechanism as I report in the RPE in the face of reduced mitochondrial function [19]. This study identified a mechanism whereby IL-33 indirectly affects mitochondrial function through the alternative splicing of *UCP1* mRNA transcripts [19]. UCP1 is localised to the inner mitochondrial membrane and plays a key role in the regulation of energy expenditure through uncoupling substrate oxidation from ATP production [544]. Until recently it was believed that UCP1 expression was exclusive to brown adipose tissue. Recent studies have identified *Ucp1* in white adipose tissue, pancreatic islets, skeletal muscle, rat and mouse thymus [545-547]. UCP1 expression has been observed in both bovine and human retina [548, 549], and the *UCP1* −3826A/G polymorphism is associated with diabetic retinopathy [549]. It would be of interest to investigate (A) whether *UCP1* is expressed in human RPE and (if so) (B) is IL-33 involved in its alternative splicing therefore contributing to defects in mitochondrial function with IL-33 loss.

Multiple lines of evidence suggest that the increased aerobic glycolysis seen with IL-33 loss in the RPE occurs at the expense of oxidative glucose catabolism, as IL-33 impairs pyruvate import into the mitochondria through the MPC complex. Support for this was obtained from IL-33KD ARPE-19, where reduced expression of both MPC1 and MPC2 was found. These are known to be essential proteins in the facilitated transport of pyruvate into the mitochondria [537]. Furthermore, cells overexpressing IL-33 displayed reduced aerobic glycolysis as mitochondrial activity was increased. The increased expression of MPC complex components and activity of pyruvate dehydrogenase was accompanied by an increased consumption and oxidation of glucose within the TCA cycle. The increased spare respiratory capacity was found to be attributed to pyruvate import following the use of the MPC-specific inhibitor UK5099 (Fig. 7E) [294]. I found that IL-33 is a key mediator of transcriptional changes to glycolytic and TCA cycle genes, which either drive the RPE into aerobic glycolysis or mitochondrial metabolism in its absence or presence, respectively. Altered MPC1/MPC2 expression results in significant metabolic disorders and has been previously shown to contribute to the Warburg effect in cancer cells [295]. An increased reliance on glycolysis may lead to RPE dysfunction and increase the metabolic burden placed upon the photoreceptors; although future work will be required to assess if retinal degeneration is accelerated in mice lacking IL-33.

Carbon tracing data with C^{13}-glucose supports the hypothesis that IL-33 loss impairs pyruvate import in the RPE. Indeed, loss of C^{13} enrichment was observed in the first three TCA cycle intermediates,

increased lactate enrichment and reduced enzymatic activities of PDH and PC. As the C^{13} enrichment was maintained in the remainder of TCA metabolites from fumarate onwards, this suggests that glucose may be redirected into other metabolite pools and fed back into the TCA cycle at different entry points. Pyruvate supports the biosynthesis of alanine, valine, isoleucine and leucine. Glucogenic valine and isoleucine enter the TCA cycle *via* succinate-coA, whereas leucine and alanine enter *via* acetyl-coA and pyruvate respectively. One can speculate that the TCA cycle may be maintained through a metabolic "shunt" *via* fatty acid synthesis and catabolism effectively bypassing pyruvate entry. This, however, is purely theoretical and will require further investigation into these pathways in the RPE.

Although alterations to MPC expression likely contributes to the bioenergetic differences observed in RPE cells with alternate IL-33 expression, it is unlikely that this alone regulates the altered flux of glucose-derived carbon into the TCA cycle. In the context of IL-33 overexpression, there was an increased abundance of C^{13} labelling in many glycolytic intermediates, indicating increased glycolytic flux. It is dubious that MPC1 upregulation alone is responsible for an upregulation of glycolysis, and so a question emerges as to which other regulatory nodes are affected by IL-33. *GLUT1, MYC* and multiple glycolytic enzyme mRNA transcripts were found to be upregulated with IL-33 overexpression suggesting an influence of pro-glycolytic pathways.

In addition to this, future work will be required to examine the extent to which glutamine metabolism and fatty acid oxidation maintain the TCA cycle in the absence of pyruvate entry. Fatty acid oxidation was assessed in the context of IL-33 KD using a modified seahorse analysis including etomoxir treatment, with significant effects were observed. However, many effects of etomoxir are regarded as "off target" nonspecific effects (*via* the disruption of coA homeostasis/ inhibition of mitochondrial ETC complex 1) which have led to its use as a CPT1 inhibitor to be questioned [298, 550]. As a result of this, further work using isotopically labelled palmitate will be required to assess how β-oxidation is impacted by changes in pyruvate metabolism. Glutamine metabolism can be assessed using isotopically labelled glutamine and may additionally provide insight into how mitochondrial metabolism is supported in the absence of IL-33.

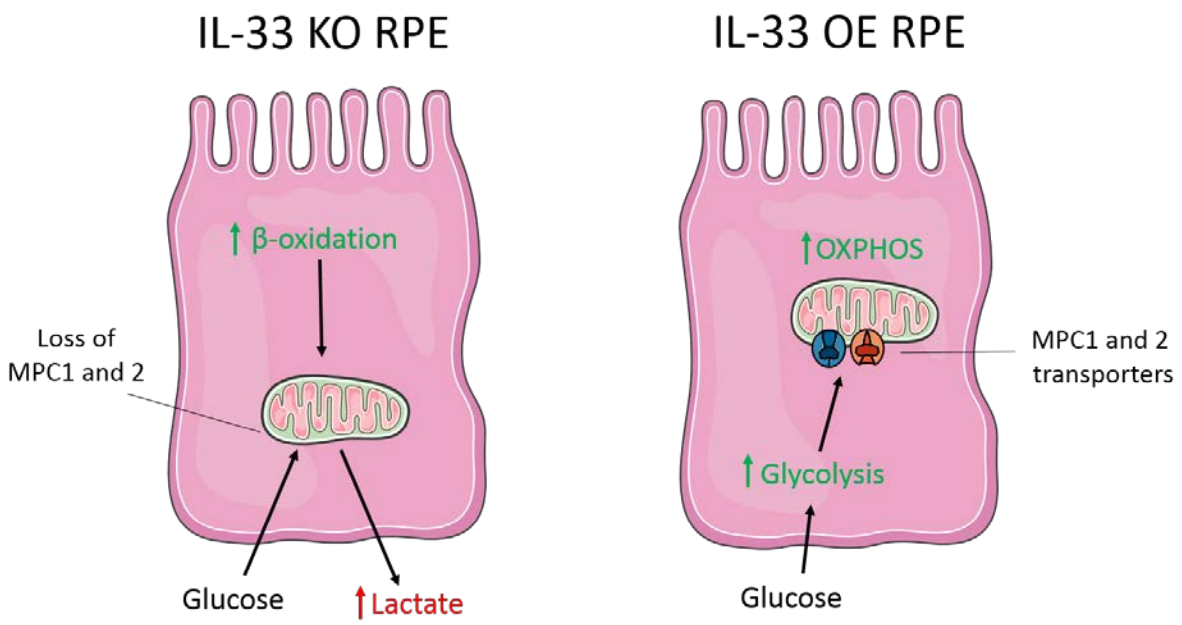

Figure 5.20. IL-33 regulates RPE metabolic phenotype:

In an IL-33-deficient RPE (*left*), glucose enters through surface GLUT1 transporters and is metabolised through glycolysis to produce pyruvate. As MPC1 and 2 expression is lost, pyruvate is metabolically rediverted to produce lactate, which is then exported. As pyruvate does not undergo oxidative catabolism, a functional TCA cycle, and thus ATP levels are maintained through increased fatty acid oxidation. In an IL-33-overexpressing RPE (*right*), increased levels of glucose enter the cell through the increased expression of cell surface GLUT1. Increased glycolysis lead to the production of pyruvate, which enters the mitochondrion through increased expression of MPC1 and 2. Mitochondrial pyruvate oxidation provides increased levels of OXPHOS and greatly enhances the RPE respiratory capacity. RPE, retinal pigment epithelium; GLUT1, glucose transporter 1; MPC, mitochondrial pyruvate carrier; OXPHOS, oxidative phosphorylation; KO, knock-out; OE, overexpression.

While these experiments have uncovered a role for IL-33 in mitochondrial respiration in RPE, a key question that emerges from this work is how does IL-33 regulate expression of MPC1/2 in RPE to facilitate the transport of pyruvate. One could speculate a likely (direct or indirect) nuclear interaction with either *MPC* promoter regions, an *MPC* regulating transcriptional factor or splicing machinery that influence expression of *MPC* transcript variants. Future research exploiting high-throughput approaches (e.g CHIP-sequencing and/or proteomics of the IL-33 interactome) will provide a clearer understanding of the regulation of RPE metabolism by IL-33 and will benefit the understanding of extent, to which nuclear IL-33 exerts effects on the cellular function. Whilst this chapter has looked at the effects of IL-33 genetic modulation at basal state metabolism, the role of nuclear IL-33 in "stress"-induced changes has not been examined. Inflammatory mediators mediate cellular metabolic adaptations and lead to the increased expression of nuclear IL-33, essential for cellular responses [223, 229, 551]. As nuclear IL-33 is reportedly involved in the regulation of HIF1-α [442], and HIF1-α is a critical regulator of the Warburg effect in immune cells [345], it would be of interest to uncover the role (if any) of IL-33 in the regulation of bioenergetic responses to inflammatory stress.

Dynamic changes in mitochondrial morphology are suggested to regulate mitochondrial metabolism [472]. The elongated mitochondrial phenotype observed in the *Il33*$^{-/-}$ group was reminiscent of previously published data whereby reduced bioenergetic capacity and mitochondrial elongation were observed in LPS-stimulated monocytes [552]. It is worth considering the observation that in IL-15 polarised T-memory cells, mitochondrial elongation and fusion promote increased mitochondrial mass and bioenergetic capacity [472]. The conflict between these data indicate the need to further decipher the role of mitochondrial dynamics in metabolic reprogramming. In the context of T-memory cells, increased cristae remodelling promoted a metabolic shift to increased β-oxidation and OXPHOS [472]. Considering that RPE in the absence of IL-33 have diminished pyruvate utilisation yet still maintain basal OCR, it is plausible that changes in alternate pathway engagement (e.g. fatty acid oxidation) support TCA cycle activity under metabolic stress. Moreover, a bioenergetic program of increased mitochondrial abundance, mitochondrial ATP-production (as shown by seahorse) and expression of ETC components in IL-33 KD cells may be established to compensate a lack of ATP derived from oxidative glucose catabolism.

In conclusion, I have identified that IL-33 acts at a point that controls a key metabolic checkpoint, antagonising the Warburg effect to ensure the functional stability of the RPE. The identification of IL-33 as a key regulator of mitochondrial metabolism suggests roles for the cytokine that go beyond its extracellular "alarmin" activities. For example, when RPE is under stress, IL-33 contributes to minimise

the effects of oxidative damage to the RPE and bolster mitochondrial metabolism. IL-33 exerts control over mitochondrial respiration in RPE by facilitating pyruvate import into mitochondria *via* up regulation of MPC expression and may be systemically integrated by the capacity of RPE to maintain homeostasis. Therefore, as well as identifying a molecular pathway for activation of mitochondrial respiration in RPE, my results demonstrate that intrinsic cellular IL-33 acts as a metabolic regulator exerting profound effects on retinal metabolism.

Chapter 6. A proteomics-based approach to determine the role of nuclear interleukin-33

6.1. Introduction

Cytokines are mediators of intercellular communication through the activation of surface receptors, upon release into the extracellular environment. Classically, cytokines contain a signal sequence which permits their processing through the Golgi pathway, ultimately leading to constitutive release or sequestration into granules for release upon activation [553]. A subset of cytokines, including multiple IL-1 family members and HMGB1 do not exhibit a signal sequence and instead remain localised to the nucleus [554]. These nuclear cytokines have been dubbed “alarmins” as a result of their potent cytokine activity occurring upon cell damage/necrosis and release into the extracellular milieu. In addition to their function extracellularly upon release, many alarmins exhibit nuclear functions [554].

IL-33 is constitutively expressed in barrier cells (e.g fibroblasts, endothelial cells and epithelium) [9]. When released from necrotic or damaged cells, it functions to alert immune cells expressing its cognate receptor ST2 (mast cells, ILC2s, Tregs and Th2 CD4 cells) of nearby tissue disruption [134]. IL-33 has multiple cellular targets (see chapter 1) and has arose as a critical immune regulator with pleiotropic activities in type 1, type 2 and regulatory immune responses, and underlying key mechanisms in allergic, infectious and chronic inflammatory diseases [134]. IL-33 is unique as an alarmin, in the sense that release from necrotic cells primes the immune system for allergic responses. Furthermore, polymorphisms in the genes encoding IL-33 and ST2 have been identified as major susceptibility loci for human asthma [282]. Consequently, therapeutic targeting of the IL-33/ST2 axis has emerged as a novel therapeutic in allergic disorders.

Despite being extensively studied in terms of its extracellular signalling, a clear nuclear function for IL-33 remains ambiguous. A largely unanswered question in the biology of IL-33 is the functional significance of both nuclear localisation and chromatin binding. IL-33 binds directly to chromatin nucleosome acidic patch comprised of histones H2A and H2B, which is critical in the regulation of chromatin remodelling [256]. This chromatin binding domain has a strikingly high sequence similarity to that of latency-associated nuclear antigen (LANA), which is responsible for the attachment of viral genomes to mitotic chromosomes [256]. Additionally, IL-33 promotes chromatin compaction [254]. Despite these findings, no key IL-33 nuclear targets have been elucidated. Recent work has suggested that IL-33 may exhibit nuclear localisation solely to regulate its potent cytokine activity, and therefore protecting against lethal inflammation [230]. In this model, IL-33 is sequestered to the nuclei of barrier cells, so that in the event of cell damage, full length IL-33 could be released and activate ST2 expressing

cells. Whilst an interesting model, two key questions emerge. One: Why are nuclear levels of IL-33 so high; two: does IL-33 have nuclear functions, like other alarmins.

In this chapter, I utilised a proteomics-based approach to address the functional significance of nuclear localisation of IL-33 in epithelial cells; focusing on the RPE as model epithelial cell with constitutively high levels of IL-33 expression. This approach allowed an identification of the IL-33 interacting networks in the nucleus of epithelial cells and indicated how alterations to IL-33 expression status directly influenced the RPE cell proteome.

6.2. Using tandem mass-tagging to identify the IL-33 interactome in both human and murine RPE

In order to establish a nuclear function of IL-33, nuclear localisation of IL-33 was first confirmed in the RPE. Previous studies had identified IL-33 expression in different parts of the retina. IL-33 was expressed by cells in the RPE, inner nuclear layer (INL), with expression localized to the nuclei of Müller glial cells and retinal endothelial cells [8]. Previously I identified nuclear IL-33 expression in the ARPE-19 cell line (both constitutively, and when genetically engineered to overexpress IL-33 using CRISPR-cas9 (see chapter 5) It was also important to identify the subcellular localisation in primary murine RPE. Cells were pooled from multiple eyes to generate the numbers required for sub cellular fractionation. Following fractioning lysates into nuclear and cytoplasmic proportions, immunoblotting was used to confirm the nuclear localisation of IL-33 in primary murine RPE cells. As a control, immunoblotting of IL-33 was not observed in primary RPE derived from *Il33*$^{-/-}$ mice (Fig. 6.1A).

I next sought to better understand how nuclear IL-33 regulates RPE cell function. In published studies, IL-33 is suggested to regulate cancer cell function predominantly through the recruitment and/or regulation of a range of binding proteins [261]. This reflects a disease setting and may not accurately capture the physiological interaction repertoire of IL-33. To conduct a high-resolution, global, unbiased proteomic analysis of the complete IL-33 interactome of RPE cells I performed TMT-labelling of antibody-bead eluate prepared with two anti-IL-33 antibodies validated for their ability to "pull-down" IL-33 in both human and mouse RPE cell lysates (Fig. 6.1B-C).

To control for non-specific binding, blank beads (and no antibody [555]) were incubated with the lysates to validate the binding of IL-33 targets. In order to pass the target selection criteria, IL-33

interacting proteins (present in all three samples). Binding targets were further filtered based on an abundance ratio of >1.5 (anti-IL-33 vs beads alone). This was repeated using two different antibodies (Nessy-1 and R&D anti-IL-33) to validate the interactome. This controlled quantitative approach validated the specificity and reproducibility of the method and enabled the application of a filtering criteria to the proteomics data to define the IL-33 interactome in human and mouse cells.

This analysis revealed an extensive RPE IL-33 interactome in both human and mouse. Contextualised to the size other interactomes, the IL-33 interactome was around a similar level to that of other transcription factors or signalling molecules identified with TMT analysis [556-558]. Using the selected criteria for significance, 260 human and 159 mouse proteins interacting with IL-33 were identified. Of these, 80 were found in both situations.

Functional analysis of the IL-33 interactome was conducted using the STRING database (version 11) [559]. This allowed protein-protein interaction data to be retrieved and the "functional association" (i.e. a specific and productive functional relationship between two proteins, likely contributing to a common biological pathway) to be identified. STRING interactions are derived from multiple sources: (1) known experimental interactions from primary databases, (2) pathway knowledge from databases, (3) interactions are predicted *de novo* by several algorithms and (4) pre-computed ortholog relations. Data inputs to STRING provide assessment and integration of protein–protein interactions, including direct (physical) and indirect (functional) associations. The IL-33 interactome showed high interconnectivity around two nodes using STRING analysis (Fig. 6.1E). Upon further investigation, these nodes were found to be significantly enriched with proteins involved in node A: translation and node B: RNA splicing (Fig. 6.1E). Gene ontology analysis of both biological and cellular processes [Database for Annotation, Visualization and Integrated Discovery (DAVID) bioinformatics database] represented within the data set identified significantly enriched terms associated with translation, gene expression, RNA splicing, cellular metabolic pathways, cytoskeleton, pyruvate metabolism, chromatin structure and regulation of RNA splicing (Fig. 6.1F). Enriched pathways exhibited a Benjamini-Hochberg corrected p-value of <0.01. Interestingly, translation and the regulation of chromatin structure were key pathways identified in the nuclear IL-33 interactome of a previous study [261].

Taken together, the results from this section demonstrate nuclear localisation IL-33 in both human (cell line) and murine (primary cells) RPE. Using proteomics analysis of the pull-down, I observed a large interactome of proteins with IL-33 affinity. Whilst this does not confirm a nuclear role for IL-33, it supports the possibility that whilst in the nucleus IL-33 plays a role (either directly or indirectly) in the regulation of these pathways.

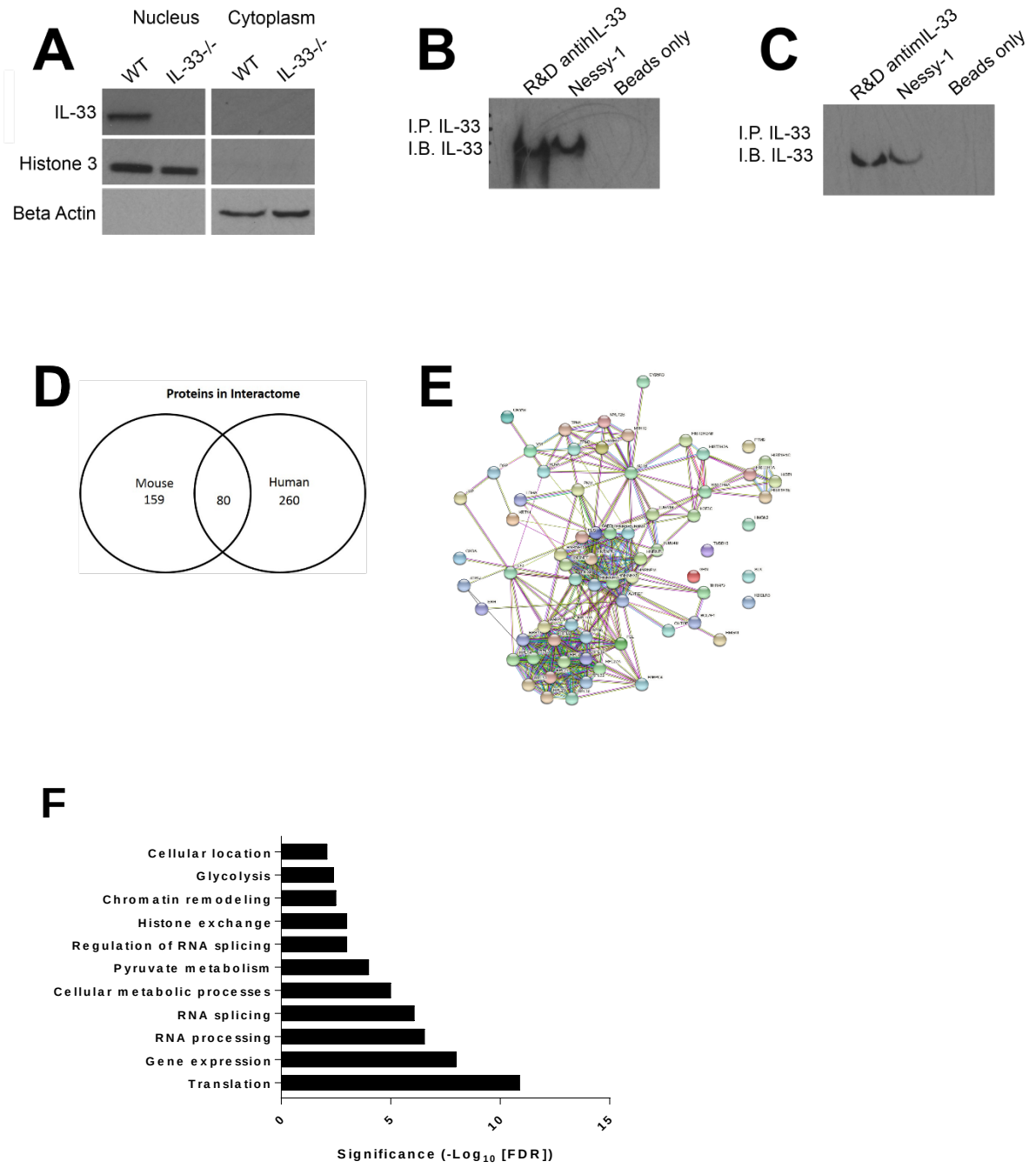

Figure 6.1. Tandem mass-tagging identifies the IL-33 interactome in both human and murine RPE:

(A) Cell lysates from both WT and *Il33* deficient mice were separated into nuclear or cytoplasmic fractions to determine IL-33 subcellular location. (B) Immunoprecipitation of IL-33 in ARPE-19 with two independent antibodies. (C) Immunoprecipitation of IL-33 in primary RPE with two independent antibodies. (D) Venn diagram of proteins identified in IL-33 pull-down TMT analysis. (E) Mapped interactions of proteins identified in IL-33 pull-down TMT analysis using STRING. Interactions include direct (physical) and indirect (functional)

associations. (F) Pathway analysis of proteins identified in IL-33 pull-down TMT analysis using DAVID. Data are expressed from three independent experiments. (A) represents pooled data from three mice.

6.3. The IL-33 interactome in primary human podocyte cells

Having identified an interaction network of nuclear IL-33 in human and murine RPE, it was necessary to investigate nuclear IL-33 in the context of another IL-33 expressing epithelial cell, the podocyte (kindly gifted by Dr. Gavin Welsh, University of Bristol). Podocytes are specialised epithelial cells located on the urinary side of the glomerular filtration barrier [560]. Importantly, podocytes, similarly to RPE become terminally differentiated after birth, with little ability to re-enter the cell cycle and proliferate [561]. This allowed me to test a terminally differentiated epithelial cell from a completely different biological setting. To first validate the expression of IL-33, immunoblotting was performed on whole podocyte cell lysates (Fig. 6.2A). Having established that IL-33 is expressed in podocyte cells and has robust pull-down by both antibodies, proteomics was used to investigate proteins with IL-33 affinity. A similar selection pipeline was utilised for protein identification, based on an abundance ratio of >1.5 (IL-33 pulldown vs beads alone) and presence in the pull down from two antibodies.

This analysis revealed an extensive human podocyte IL-33 interactome of 135 proteins which passed the selection criteria. Functional analysis of the IL-33 interactome was conducted using the STRING data base. This identified the presence of three main nodes of interconnectivity based on direct and indirect protein-protein interactions. These corresponded to enriched pathways with proteins involved in translation (node A), RNA splicing (node B) and cytoskeletal regulation (node C) (Fig. 6.2B). This was like the RPE interactome in terms of protein enrichment in translation and splicing pathways. However, the podocyte interactome displayed a degree of interconnectivity around cytoskeletal protein enrichment which was not observed in the RPE STRING analysis. Gene ontology analysis using the DAVID bioinformatics database identified significant biological and cellular processes enriched within the dataset. These corresponded to translation, cell-cell adhesion, RNA splicing, RNA recognition, cytoskeleton, histone binding, chromatin assembly and glycolysis (Fig. 6.2C). Between the podocyte and RPE interactomes there were a total of 88 conserved proteins with IL-33 affinity (Fig. 6.2D).

The data presented in this section indicates the presence of nuclear IL-33 in another specialised epithelial cell and suggests a similar nuclear interactome between the two cell types. This set of experiments were required to identify conserved IL-33 targets and pathways between the two cell types, suggesting that IL-33 nuclear function is ubiquitous to other epithelial cells.

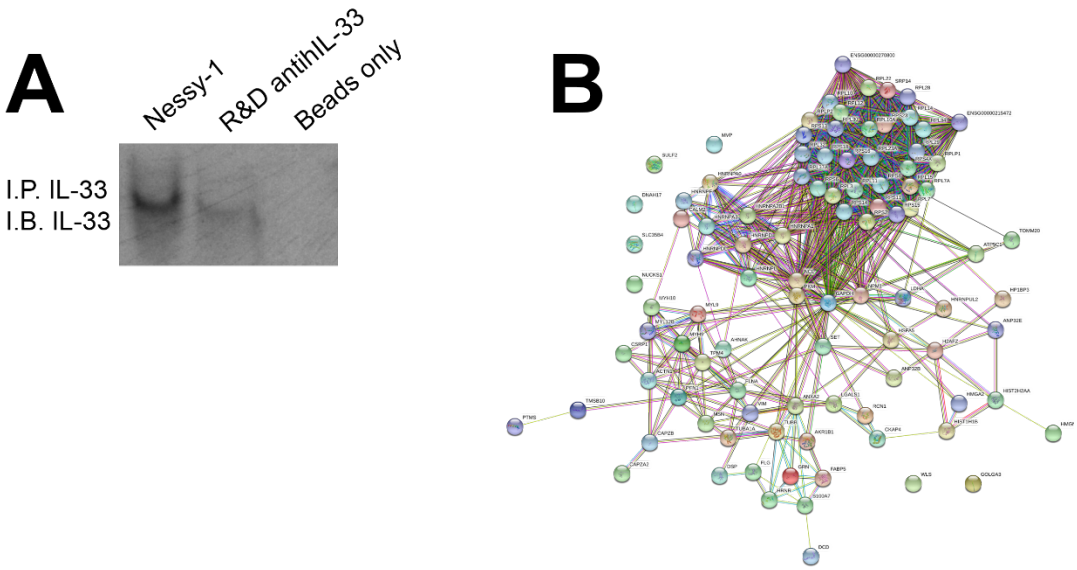
A
Nessy-1
R&D antihIL-33
Beads only
I.P. IL-33
I.B. IL-33
B
C
Golgi apperatus
Gluconeogenesis
Glycolysis
Chromatin assembly
Histone binding
Cytoskeleton
RNA binding
RNA recognition
RNA splicing
Cell-cell adhesion
Translation
0
10
20
30
40
Significance (-Log10 [p value])
D
Human RPE
260
88
Human podocyte
135

Figure 6.2. Tandem mass-tagging identifies the IL-33 interactome in human podocytes:

(A) Immunoprecipitation of IL-33 in primary podocytes with two independent antibodies. (B) Mapped interactions of proteins identified in IL-33 pull-down TMT analysis using STRING. Interactions include direct (physical) and indirect (functional) associations. (C) Pathway analysis of proteins identified in IL-33 pull-down TMT analysis using DAVID. (D) Venn diagram of proteins identified in IL-33 pull-down TMT analysis in ARPE-19 and primary podocytes. Data are expressed from three independent experiments.

6.4. Immune-stimulation of ARPE-19 cells modulates IL-33 interactions

Previous work has identified that IL-33 expression is upregulated in the RPE in response to inflammatory stimulus [8]. This is not restricted to the RPE, with increased IL-33 expression observed in multiple cell types in response to TLR and cytokine receptor stimulation [9]. There is little evidence of inducible release and secretion in these cells, with the increased IL-33 localised to the nucleus [9]. Considering the observations in the previous section, whereby a large array of proteins was found to display affinity for IL-33 in a basal state, I hypothesised that this interactome may be subject to alterations upon stimulation, with IL-33 functioning as a key node in the transcriptional response to danger signals. Indeed, a loss of endogenous IL-33 negatively impairs IFN-γ-induced cytokine production in oesophageal epithelial cells [534].

RPE cells were first exposed to an array of inflammatory stimuli to identify signalling pathways which upregulate the expression of nuclear IL-33. I chose inflammatory mediators with known cognate receptor complexes expressed on the RPE and/or reported changes in RPE function upon stimulation [8, 63, 562-566]. As two positive controls I included TLR-3 and -4 agonists Poly (I:C) and LPS, which have been previously shown to up regulate IL-33 in the RPE (see chapter 3/ [8]). In addition to this, I chose to assess agonists for TLRs 2 and 9 (peptidoglycan (PGN) and CpG oligodeoxynucleotide for TLR-2 and -9, respectively) as these have been reported to be expressed in RPE cells [62]. In addition to TLR agonists, I investigated if the cytokines IL-1β, IL-4, IL-6 IL-10, IL-17A, IL-22, TNFα and IFN-γ elicited an increased expression of nuclear IL-33. Doses of all agonists/cytokine were based around commonly used concentrations found within the literature [8, 63, 562-566]. After stimulation for 24h with each cytokine/TLR agonist listed above, cell lysates were split into a nuclear fraction and IL-33 expression was assessed using immunoblotting. All four TLR agonists upregulated the expression of IL-33, although this effect was greater in LPS and PGN than Poly (I:C) or CpG (Fig. 6.3A-B). Out of the panel of 8 cytokines assessed for their ability to increase IL-33 expression, changes were only observed with IL-1β, IL-6 and IFN-γ (Fig. 6.3A-B).

Following this, I proceeded to investigate how the IL-33 interactome was altered under immune stimulation, whereby ARPE-19 cells increased their nuclear IL-33 expression. The IL-33 interactome was investigated in two conditions promoting IL-33 expression (LPS and Poly (I:C)) and one condition where IL-33 remained unaffected (TNFα). Cells were unstimulated or treated with either LPS, Poly (I:C) or TNFα for 24h. Following treatment immunoprecipitation against IL-33 was performed on the cell

lysate and eluted antibody-bead complexes were analysed using TMT-labelling. In response to LPS treatment, 67 variant proteins were observed (FDR 5% and p<0.01). Only 42 of these were passed the selection criteria of p<0.01 and >50%-fold change, 23 of which were up-regulated and 19 down-regulated (Fig. 6.4A; Table 10.6.1, page 410). There were no proteins absent in either control or LPS samples. Functional analysis of the LPS-stimulated IL-33 interactome was conducted using the STRING data base. It was observed that in the up-regulated group of proteins, there were two main nodes of interconnectivity, whereby their interactions were clustered around groups of biologically connected proteins. These areas of interaction enrichment were comprised of proteins with the following biological processes (GO terms), node A: RNA catabolism, translation initiation and mRNA metabolic processes; node B: nucleosome assembly, nucleosome organization and DNA conformational change. Following this, gene ontology analysis of both biological and cellular processes represented within the data set identified significantly enriched terms associated with negative regulation of gene expression, chromosome organisation, chromatin silencing, histone exchange and chromatin remodelling (Fig. 6.4B). In the down regulated group of proteins, there was one node of interconnectivity among the proteins which corresponded to GO terms such as: RNA binding, ribosome and pre-mRNA binding (Fig. 6.4C). In addition to this, gene ontology analysis was conducted on the data set to identify overrepresented pathways. It was found that in the down-regulated data set, significant enrichment was observed in translation initiation, RNA processing, gene expression and mRNA splicing (Fig. 6.4D). STRING analysis identified one cluster of proteins involved in translation initiation (Fig. 6.4E).

A similar analysis was performed on ARPE-19 cells in response to the TLR-3 agonist, Poly (I:C). Following treatment 41 variant proteins were observed (FDR 5% and p<0.01). Of these, 40 proteins were observed to be above the selection criteria of a >50%-fold change, 27 of which were up-regulated and 13 down-regulated (Fig. 6.5A; Table 10.6.2, page 411). There were no proteins absent in either control or Poly (I:C) samples. Functional analysis of the Poly (I:C)-stimulated IL-33 interactome was conducted using the both STRING and DAVID data bases. It was observed that in the up-regulated set of proteins there were large areas of interconnectivity, with proteins forming a clustered node corresponding to pathogenic/E.coli infection (Fig. 6.5B). A PPI enrichment of p=1.27e-09 was observed indicating significant enrichment in pathways than what would be expected for a list of proteins of similar size, drawn randomly from the genome. Such an enrichment indicates that the proteins are at least partially biologically connected, as a group (http://version10.string-db.org). Gene ontology analysis was subsequently conducted to identify significantly enriched biological processes within the altered proteins. In the data set of 27 proteins, significantly enriched terms were found associated with translation, microtubule, glycolysis, cell-cell adhesion and ribosome (Fig. 6.5C). It was of interest

to note four glycolytic enzymes associated with IL-33 were increased upon Poly (I:C) stimulation (Table 6.2). It is well known that many glycolytic enzymes "moonlight" in the nucleus where they have diverse roles in the regulation of transcription, translation and chromatin stability (see section 1.8.5.1.). I then proceeded to investigate the downregulated set of proteins present in the Poly (I:C)-stimulated interactome. After inputting these proteins into the STRING software, it was clear that there were two clusters of proteins. Cluster A corresponded to GO terms such as translational initiation and SRP-dependent protein targeting to the membrane (Fig. 6.5E). Cluster B was observed to include GO terms such as the spliceosome and mRNA processing (Fig. 6.5D). Gene ontology analysis of both biological and cellular processes represented within the data set identified significantly enriched terms associated with viral transcription, translation initiation and ribosome (Fig. 6.5D).

In addition to the studies performed on the Poly (I:C) or LPS-stimulated cells, it was essential to investigate how IL-33 interactions would change in response to a stimulus not observed to increase IL-33 expression in ARPE-19 cells. Out of all the inflammatory stimuli used, I chose to investigate TNFα for several reasons: (1) TNFα is a proinflammatory cytokine and therefore its effects on the IL-33 interactome would be more comparable to TLR signalling; (2) Its effects are better studied in RPE cells (including ARPE-19 [566]) and therefore one could concur a TNFα response would be more representative of RPE activation than IL-17A, IL-4 and IL-22, where cognate receptor expression is observed but the downstream effects are unfamiliar. I performed a similar experiment to the previous two sections, immunoprecipticating IL-33 after exposure to TNFα. Despite no observed change in IL-33 expression with TNFα, 10 variant proteins found between the unstimulated and stimulated conditions ($p<0.01$ and FDR 5%). Of these 10 proteins, 8 were above the selection criteria of a >50%-fold change (Table 10.6.3, page 413). Interestingly all proteins were observed to be down regulated in the TNFα treated IL-33 pull down compared to an untreated control. Using STRING analysis, I observed that these proteins clustered around a central node of consisting of enrichment of terms including translation and the negative regulation of gene expression (Fig. 6.6A).

Between the three treatment groups, there were small overlaps in IL-33-interacting partners. Poly (I:C) and LPS stimulated interactomes shared 5 conserved proteins, whereas TNFα and Poly (I:C) exhibited 6. No conserved proteins were found in the IL-33 interactomes of LPS and TNFα-stimulated cells, and therefore between all groups assessed (Fig. 6.6B).

Taken together, the results obtained within this section indicate a plasticity in the IL-33 interactome in response to immune stressors. To date, the biological significance of nuclear IL-33 upregulation after activation remains unsolved.

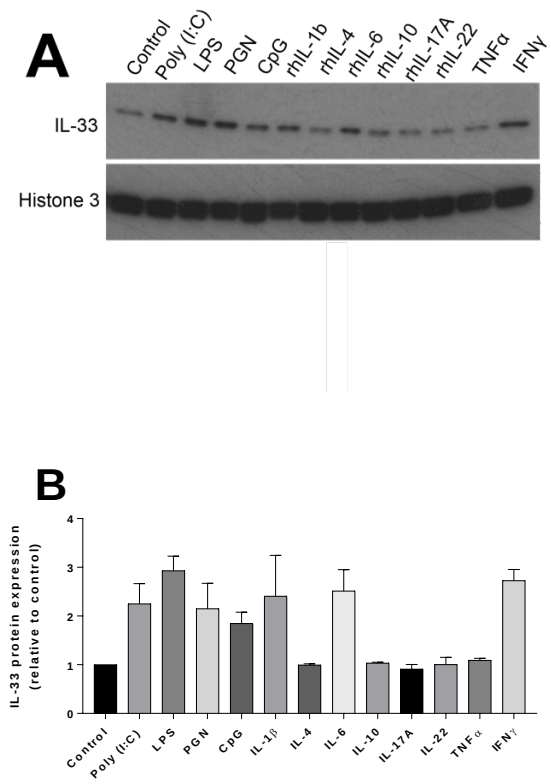

Figure 6.3. Stimulated nuclear IL-33 production in ARPE-19 cells:

(A) Cells were treated for 24h with either Poly (I:C) (10µg/ml), LPS (1µg/ml), PGN (50ng/ml), CpG (10µg/ml), rhIL-1β (50ng/ml), rhIL-4 (10ng/ml), rhIL-6 (10ng/ml), rhIL-10 (10ng/ml), rhIL-17A (100ng/ml), rhIL-22 (100ng/ml), TNFα (50ng/ml) or IFN-γ (100ng/ml). Nuclear lysates were fractionated, and immunoblotting was used to assess IL-33 expression. (B) Densitometry analysis of (A). Represents data from two independent blots.

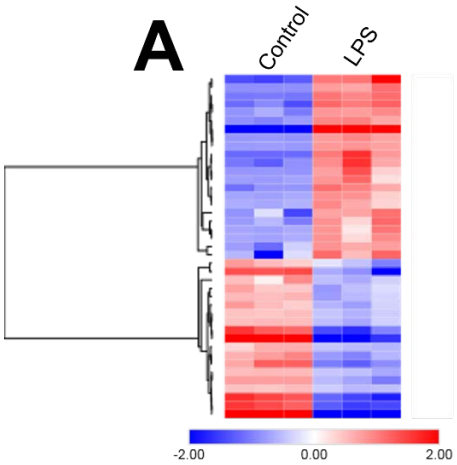
A
Control
LPS
-2.00
0.00
2.00

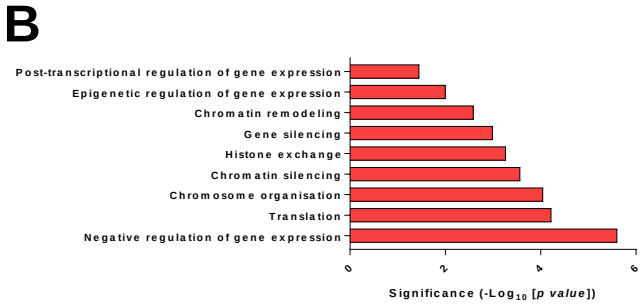
B
Post-transcriptional regulation of gene expression
Epigenetic regulation of gene expression
Chromatin remodeling
Gene silencing
Histone exchange
Chromatin silencing
Chromosome organisation
Translation
Negative regulation of gene expression
0
2
4
6
Significance (-Log10 [p value])

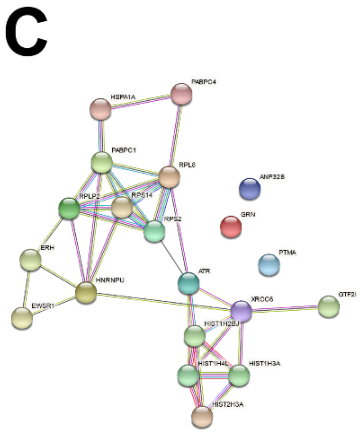
C
PABPC4
HSPA1A
PABPC1
RPL6
ANP32B
RPLP2
RPS14
GRN
RPS12
ERH
PTMA
ATR
HNRNPU
XRCC6
GTF2I
EWSR1
HIST1H2BJ
HIST1H4L
HIST1H3A
HIST2H3A

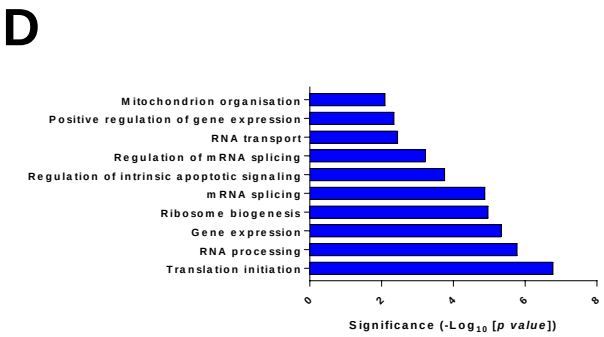
D
Mitochondrion organisation
Positive regulation of gene expression
RNA transport
Regulation of mRNA splicing
Regulation of intrinsic apoptotic signaling
mRNA splicing
Ribosome biogenesis
Gene expression
RNA processing
Translation initiation
0
2
4
6
8
Significance (-Log10 [p value])

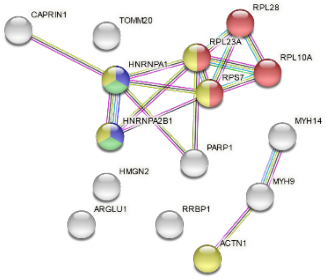
E
CAPRIN1
TOMM20
RPL28
RPL23A
RPL10A
HNRNPA1
RPS7
HNRNPA2B1
MYH14
PARP1
HMGN2
MYH9
ARGLU1
RRBP1
ACTN1

Figure 6.4. LPS stimulation alters the IL-33 interactome in ARPE-19 cells:

Cells were either unstimulated or treated for 24h with LPS (1μg/ml). (A) Heatmap of differentially expressed proteins observed in IL-33 pull down. (B) Pathway analysis of proteins up-regulated in IL-33 pull-down TMT analysis using DAVID. (C) Mapped interactions of proteins up-regulated in IL-33 pull-down TMT analysis using STRING. (D) Pathway analysis of proteins down-regulated in IL-33 pull-down TMT analysis using DAVID. (E) Mapped interactions of proteins down-regulated in IL-33 pull-down TMT analysis using STRING. Data are expressed from three independent experiments.

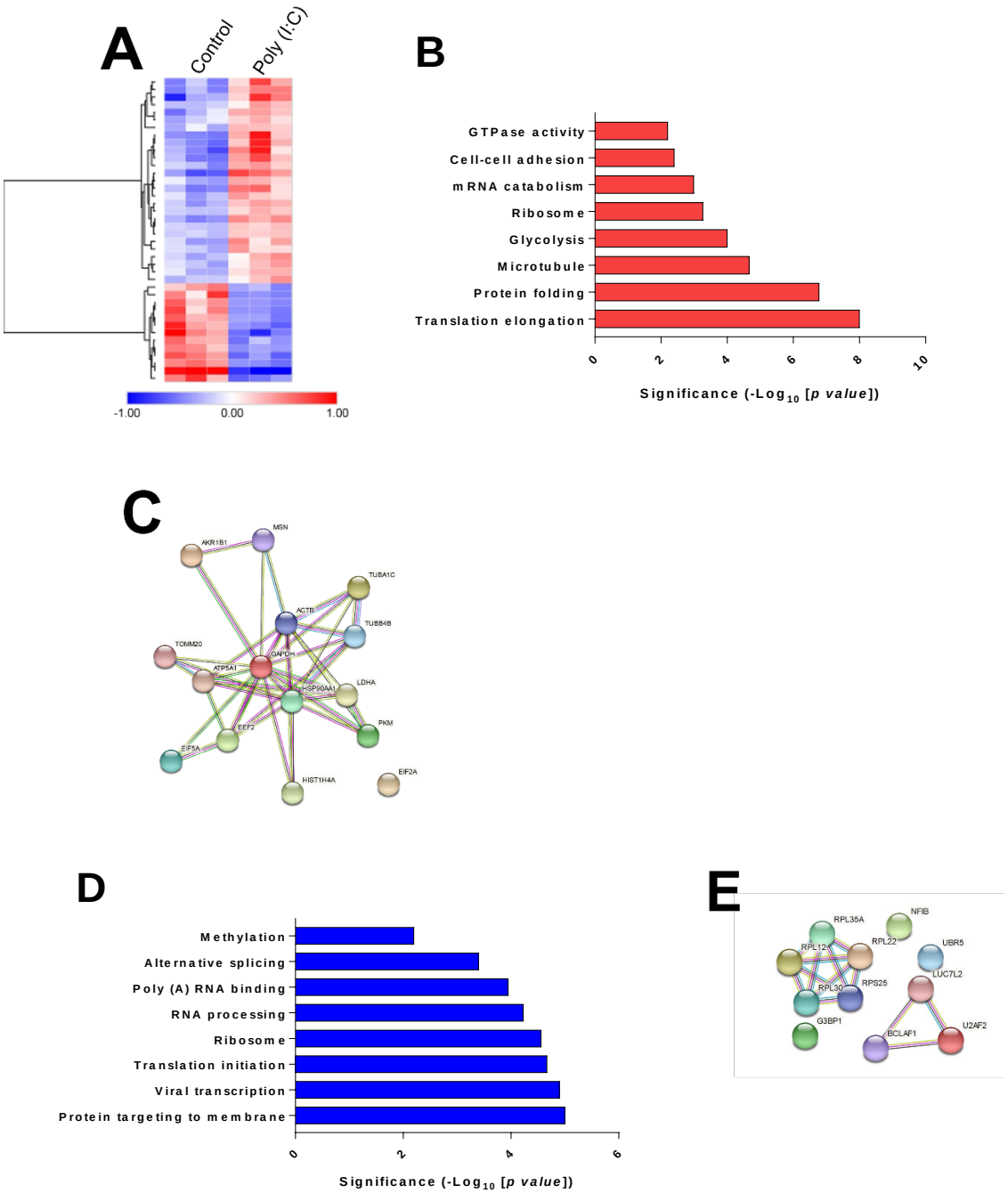
A
Control
Poly (I:C)
-1.00
0.00
1.00
B
GTPase activity
Cell-cell adhesion
mRNA catabolism
Ribosome
Glycolysis
Microtubule
Protein folding
Translation elongation
0
2
4
6
8
10
Significance (-Log10 [p value])
C
MSN
AKR1B1
TUBA1C
ACTB
TUBB4B
TOMM20
GAPDH
ATP5A1
HSP90AA1
LDHA
PKM
EEF2
EIF5A
EIF2A
HIST1H4A
D
Methylation
Alternative splicing
Poly (A) RNA binding
RNA processing
Ribosome
Translation initiation
Viral transcription
Protein targeting to membrane
0
2
4
6
Significance (-Log10 [p value])
E
RPL35A
NFIB
RPL12
RPL22
UBR5
LUC7L2
RPL30
RPS25
G3BP1
BCLAF1
U2AF2

Figure 6.5. Poly (I:C) stimulation alters the IL-33 interactome in ARPE-19 cells:

Cells were either unstimulated or treated for 24h with Poly (I:C) (10μg/ml). (A) Heatmap of differentially expressed proteins observed in IL-33 pull down. (B) Pathway analysis of proteins up-regulated in IL-33 pull-down TMT analysis using DAVID. (C) Mapped interactions of proteins up-regulated in IL-33 pull-down TMT analysis using STRING. (D) Pathway analysis of proteins down-regulated in IL-33 pull-down TMT analysis using DAVID. (E) Mapped interactions of proteins down-regulated in IL-33 pull-down TMT analysis using STRING. Data are expressed from three independent experiments.

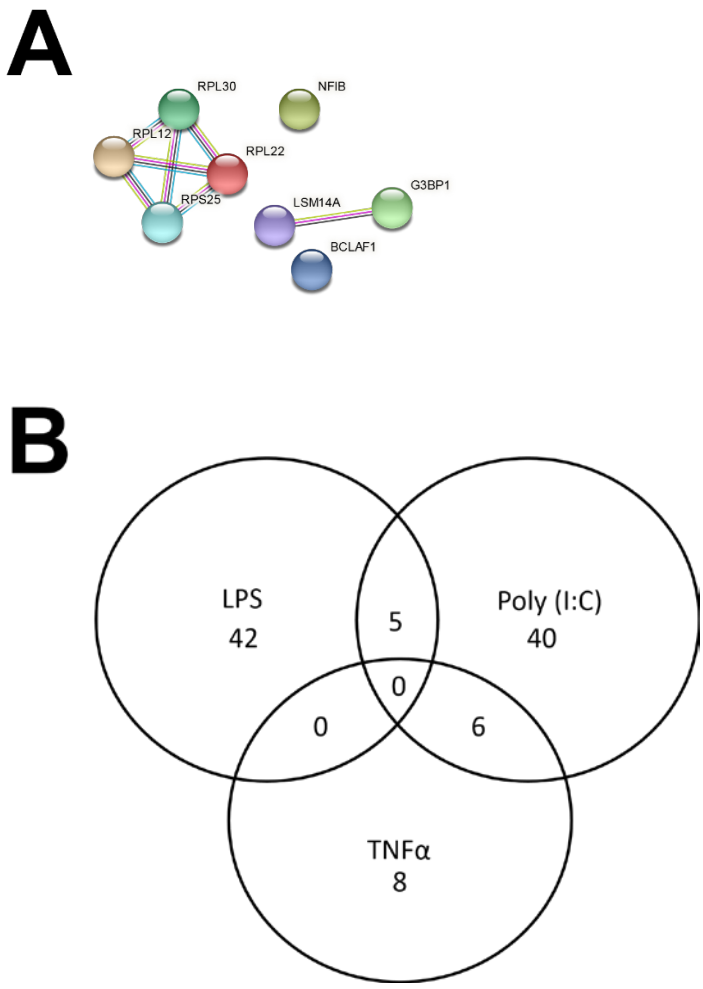

Figure 6.6. STRING analysis of IL-33 interactome following TNFα stimulation:

(A) Cells were either unstimulated or treated for 24h with TNFα (50ng/ml). Mapped interactions of proteins down-regulated in IL-33 pull-down TMT analysis using STRING. (B) Venn diagram of differentially regulated proteins found in the IL-33 interactomes of LPS, Poly (I:C) or TNFα-stimulated cells. Data are expressed from three independent experiments.

6.5. A global proteomic approach to analyse endogenous IL-33 function in ARPE-19 cells

In the previous sections I have identified a large IL-33 interaction network in epithelial cells corresponding to protein involved in translation, RNA splicing and other nuclear processes. In order to confirm that these interactions were functional it was subsequently investigated whether a loss of nuclear IL-33 would affect the total proteome in RPE cells. I chose to utilise proteomics as opposed to transcriptomics due to the significant enrichment of post-transcriptional pathways (i.e splicing/ translation) in the data sets.

Previous studies have utilised a large-scale proteomic approach to analyse the effect of endogenous IL-33 cell proteome, however these studies have largely focussed on endothelial cells [230]. To identify IL-33 regulated proteins in RPE cells, I performed TMT-based proteomics in ARPE-19 cells exhibiting IL-33 silencing by siRNA. Cells transfected with a scrambled siRNA were used as a control. IL-33 knockdown was first confirmed by immunoblotting (Fig. 6.7A). Proteomics identified a total of 8341 proteins identified in all six experiments (three scrambled siRNA and three IL-33 siRNA). A false discovery rate of 5% was applied in the identification of differentially modulated proteins. Out of the total of 8341 proteins, 2368 were found to be significantly changed between scrambled and IL-33 siRNA samples ($p<0.01$). However only 857 proteins were above the cut-off of a >25% fold change [567] (368 total upregulated and 489 total down regulated) (Fig. 6.7B-C). As a positive control for silencing, I observed a significant decrease of IL-33 (~4-fold) (Fig. 6.7B). Gene ontology analysis (DAVID) of the proteomics data indicated that knock down of endogenous IL-33 induced the expression of proteins with significantly enriched terms associated with mitochondrion, protein transport, fatty acid metabolism, mRNA splicing, TCA cycle, WD40-repeat domain and amino acid metabolism (Fig. 6.7D). Conversely, pathway analysis of downregulated proteins represented within the data set indicated significant enrichment in terms such as: nucleotide binding, cell-cell adhesion, chaperone, cell cycle, NADP oxoreductase, mitochondrial matrix and DNA condensation (Fig. 6.7D).

Taken together, the proteome-wide analysis indicated that multiple biological pathways may be affected by IL-33 loss in epithelial cells. Within the up-regulated data set there appeared to be a large focus on cellular bioenergetics, with a selection of significantly enriched GO terms highlighting mitochondrial metabolism and pathways such as fatty acid oxidation which feed into the TCA cycle.

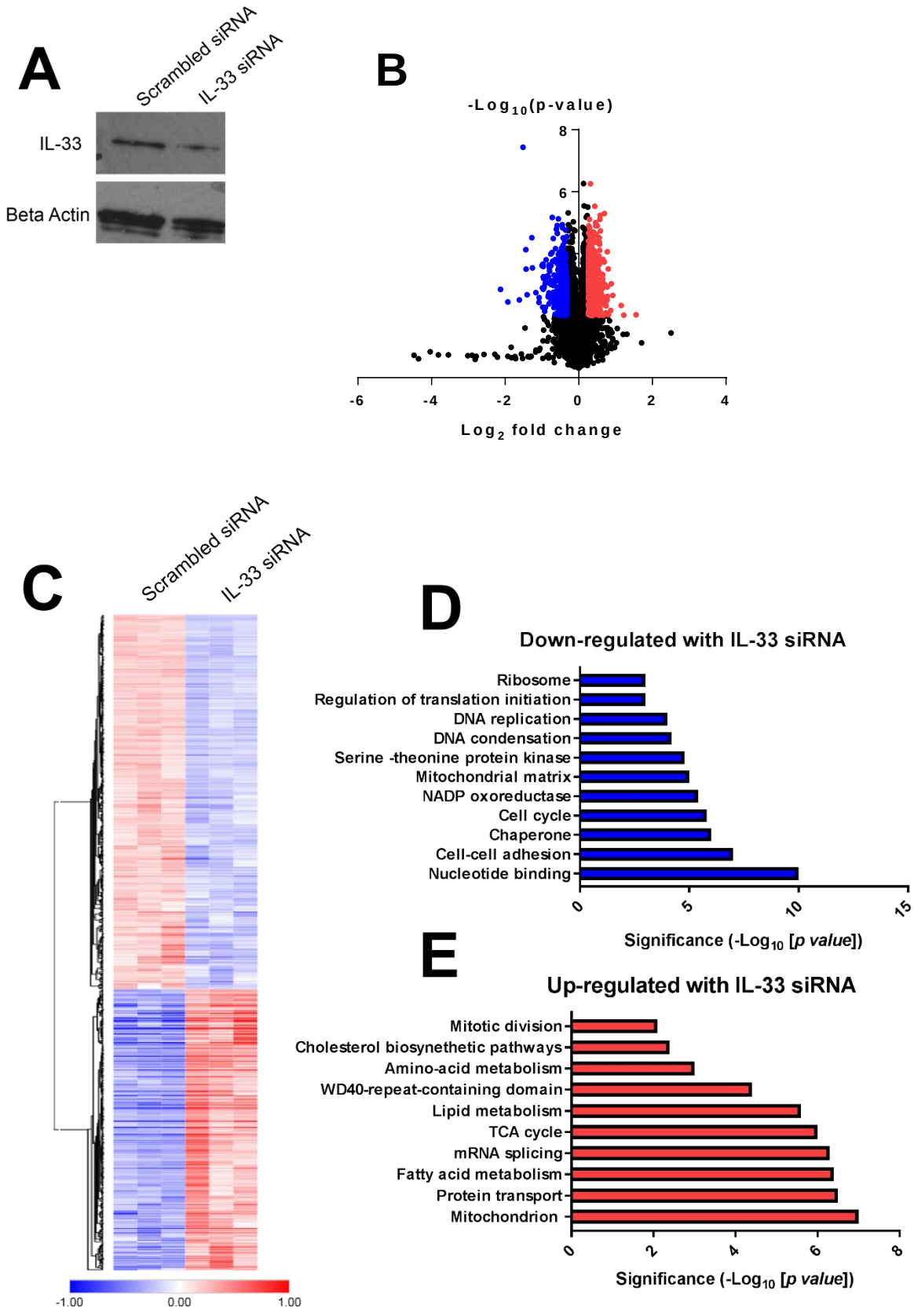
A
Scrambled siRNA
IL-33 siRNA
IL-33
Beta Actin
B
-Log10(p-value)
8
6
-6
-4
-2
0
2
4
Log2 fold change
C
Scrambled siRNA
IL-33 siRNA
-1.00
0.00
1.00
D
Down-regulated with IL-33 siRNA
Ribosome
Regulation of translation initiation
DNA replication
DNA condensation
Serine -theonine protein kinase
Mitochondrial matrix
NADP oxoreductase
Cell cycle
Chaperone
Cell-cell adhesion
Nucleotide binding
0
5
10
15
Significance (-Log10 [p value])
E
Up-regulated with IL-33 siRNA
Mitotic division
Cholesterol biosynethetic pathways
Amino-acid metabolism
WD40-repeat-containing domain
Lipid metabolism
TCA cycle
mRNA splicing
Fatty acid metabolism
Protein transport
Mitochondrion
0
2
4
6
8
Significance (-Log10 [p value])

Figure 6.7. Effect of IL-33 loss on the ARPE-19 proteome:

ARPE-19 were transfected for 48h with either scrambled siRNA or a pre-selected mixture of 4 siRNA duplexes targeting the human *IL33* gene. (A) Representative immunoblot of IL-33 protein expression following transfection. (B) Volcano plot displaying fold change (log2) of proteomic data reveals differentially expressed proteins in whole cell lysates following transfection. (C) Heatmap of differentially expressed proteins in whole cell lysates following transfection (FDR <5%, $p<0.01$ and >1.25-fold expression). (D) Pathway analysis of proteins induced with IL-33 KD. (E) Pathway analysis of proteins suppressed with IL-33 KD. Data are expressed from three independent experiments.

6.6. A global proteomic approach to analyse endogenous IL-33 function in primary murine RPE

Having established that ARPE-19 cells treated with IL-33 siRNA pools exhibited global proteomic changes, it was essential to investigate if a similar shift in the RPE proteome was observed in primary RPE from mice lacking endogenous IL-33 in comparison to WT counterparts. This experiment tested whether the observed protein changes were specific to a loss of IL-33 and rather than off target effects of gene silencing. Having isolated RPE cell lysates from both WT and *Il33*$^{-/-}$ mice, I proceeded to analyse respective proteomes using TMT. There was a total of 9529 proteins identified in all six samples (three WT and three *Il-33*$^{-/-}$). Of these proteins, 501 were observed to be significantly changed ($p<0.01$) in the *Il33*$^{-/-}$ murine RPE proteome compared to the WT control. When a selection criteria of a fold change >25% was applied to the data set, only 417 proteins were taken forward. Of these 417 proteins, 45 were down-regulated and 372 were up-regulated (Fig. 6.8B). Following identification of differentially regulated proteins in the RPE proteome, I used the DAVID software to perform pathway enrichment analysis of both data sets. In the down-regulated protein set, I observed a significant enrichment in clusters corresponding to nucleosome core, histone and chromatin silencing, myosin complex, tight junction, cell adhesion and actin filament binding, and extracellular matrix remodelling (Fig. 6.8C). In the up-regulated protein data set, there was significant enrichment in clusters corresponding to mitochondrial metabolism, fatty acid oxidation, zinc ion homeostasis, oxidoreductase and innate immunity (Fig. 6.8D).

The data collected from the primary RPE proteome further supports a role for nuclear IL-33. Taken together, the data presented in this section shows that loss of IL-33 at the germline level leads to significant alterations in the RPE proteome, thus indicating that IL-33 acts as a key node in the control of protein expression. Noted was the reduced total number of significantly down-regulated proteins compared to that of significantly upregulated within the data set; this corresponded to a ~8-fold change (45 vs 372). This, however, may be attributed to the fact that these samples were taken from cells *ex vivo* compared to an *in vitro* cell line system.

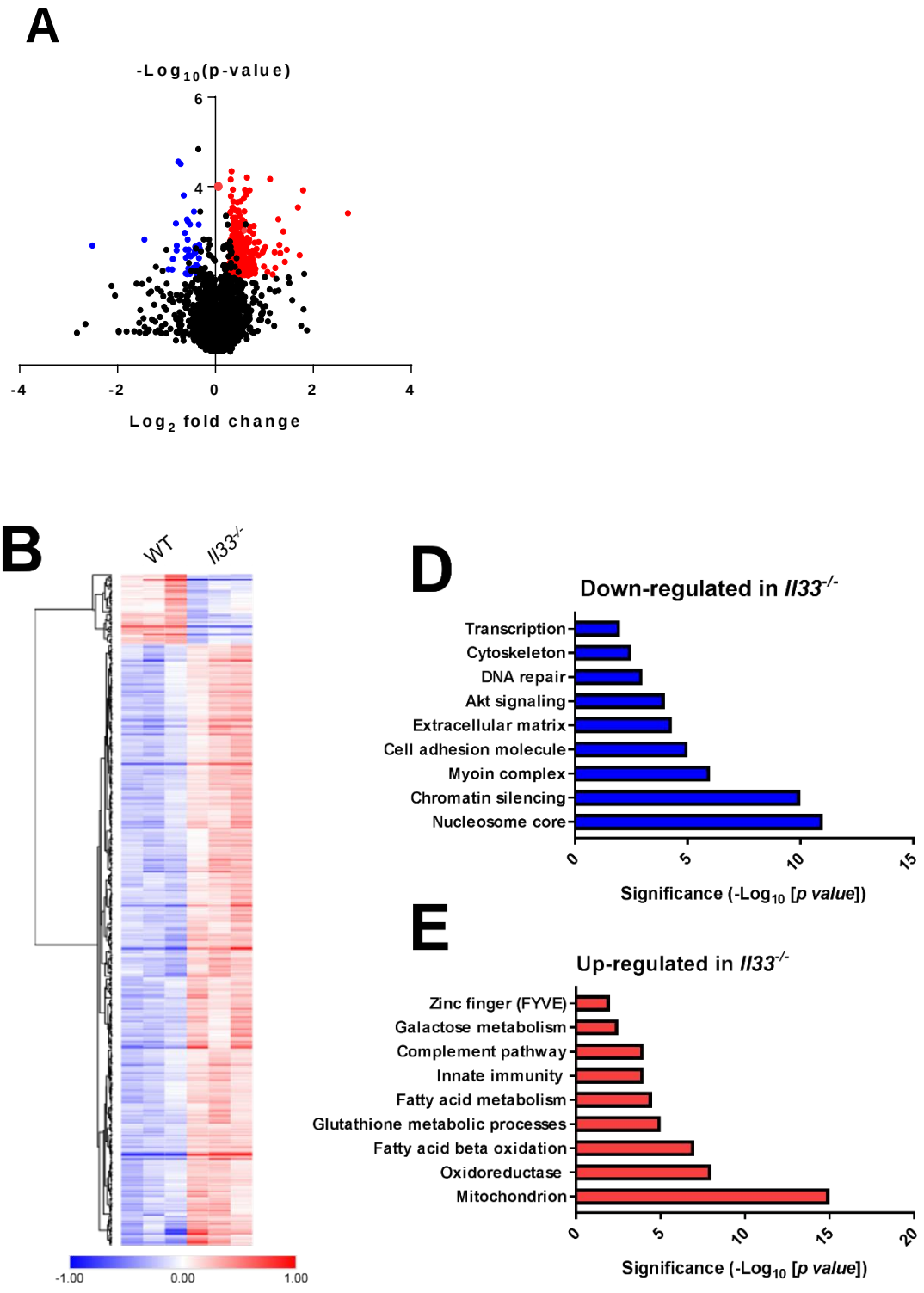
A
-Log10(p-value)
6
4
-4
-2
0
2
4
Log2 fold change
B
WT
Il33-/-
-1.00
0.00
1.00
D
Down-regulated in Il33-/-
Transcription
Cytoskeleton
DNA repair
Akt signaling
Extracellular matrix
Cell adhesion molecule
Myoin complex
Chromatin silencing
Nucleosome core
0
5
10
15
Significance (-Log10 [p value])
E
Up-regulated in Il33-/-
Zinc finger (FYVE)
Galactose metabolism
Complement pathway
Innate immunity
Fatty acid metabolism
Glutathione metabolic processes
Fatty acid beta oxidation
Oxidoreductase
Mitochondrion
0
5
10
15
20
Significance (-Log10 [p value])

Figure 6.8. Whole proteome analysis of WT and *Il33*$^{-/-}$ primary RPE:

Primary RPE cell lysates were isolated from WT or *Il33*$^{-/-}$ mice. (A) Volcano plot displaying fold change (log2) of differentially expressed proteins in primary RPE cell lysates. (B) Heatmap of differentially expressed proteins in whole cell lysates (FDR <5%, p<0.01 and >1.25-fold expression). (D) Pathway analysis of proteins induced in *Il33*$^{-/-}$ RPE. (E) Pathway analysis of proteins suppressed *Il33*$^{-/-}$ RPE. Data are expressed from three independent experiments.

6.7. Overexpression of nuclear IL-33 alters the ARPE-19 proteome

As previously discussed, an important question in the biology of IL-33 is the role of endogenous intracellular nuclear IL-33 in the regulation of cellular function. It has been long proposed that IL-33 is a dual function cytokine with relative roles in extracellular signalling and in the nucleus where it controls gene expression [10]. In the previous two sections of this chapter I have provided evidence of a nuclear role for IL-33 in the RPE whereby its loss, both *in vitro* (siRNA) and at the germline level (mice lacking endogenous IL-33) exhibited functional biological changes, as indicated by proteome-wide analysis. Having established that a loss of IL-33 elicits proteomic changes in RPE cells, I further assessed proteomic changes in RPE cells constitutively overexpressing IL-33 by CRISPR-cas9.

Prior to examining proteomic changes, up-regulation of nuclear IL-33 was confirmed by immunoblotting (Fig. 6.9A). Following establishment of efficient plasmid transfection and increased IL-33 expression, I performed proteome-wide analysis on whole cell lysates from both control plasmid and IL-33 plasmid transfected cells. Proteomics identified a total of 8117 proteins identified in all six experiments (three control plasmid and three IL-33 plasmid). A false discovery rate of 5% was applied in the identification of differentially modulated proteins. Out of these proteins, 1240 were observed to be significantly modulated ($p<0.01$), yet only 421 of these variant proteins passed the selection criteria of >25% fold change. Out of these proteins, 244 were found to be up-regulated and 177 were found to be down-regulated (Fig. 6.9B-C). IL-33 was not found within the total number of proteins observed within each group and therefore, there was no positive control for this experiment. Despite this, I used DAVID to identify pathways that were induced or repressed from the proteins identified in IL-33 overexpressing cells. While gene ontologies associated with cell-cell adhesion, nucleotide binding, carbon metabolism, actin binding and RNA binding were repressed in IL-33 overexpressing ARPE-19, gene ontologies associated with cell-cell adhesion, chaperone, glycolysis, amino acid biosynthesis, proteasome and NFκB signalling were all induced with IL-33 overexpression (Fig. 6.9D-E).

Collectively, these data demonstrate that the augmented presence of nuclear IL-33 alters a consistent proteomic shift in ARPE-19 cells under the conditions tested. Gene ontologies for glycolysis and other carbon metabolic pathways were highlighted in the data set, indicating that increased glycolytic flux may be observed under these conditions, consistent with observations made in chapter 5.

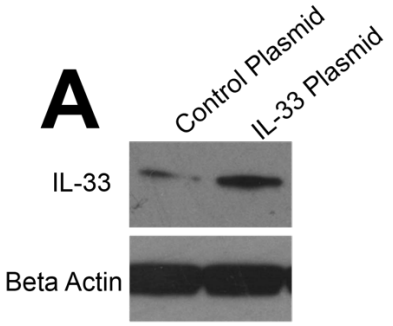
A
Control Plasmid
IL-33 Plasmid
IL-33
Beta Actin

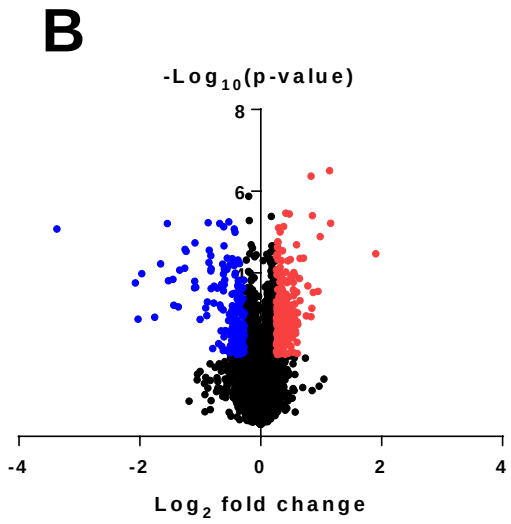
B
-Log10(p-value)
8
6
-4
-2
0
2
4
Log2 fold change

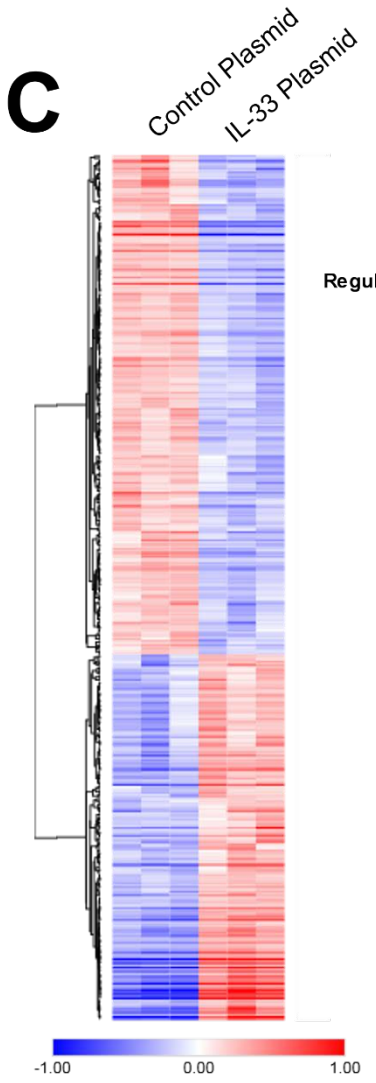
C
Control Plasmid
IL-33 Plasmid
-1.00
0.00
1.00

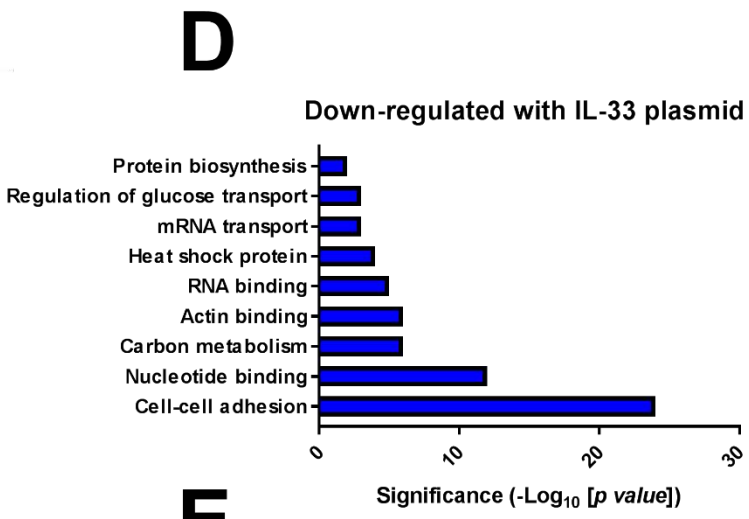
D
Down-regulated with IL-33 plasmid
Protein biosynthesis
Regulation of glucose transport
mRNA transport
Heat shock protein
RNA binding
Actin binding
Carbon metabolism
Nucleotide binding
Cell-cell adhesion
0
10
20
30
Significance (-Log10 [p value])

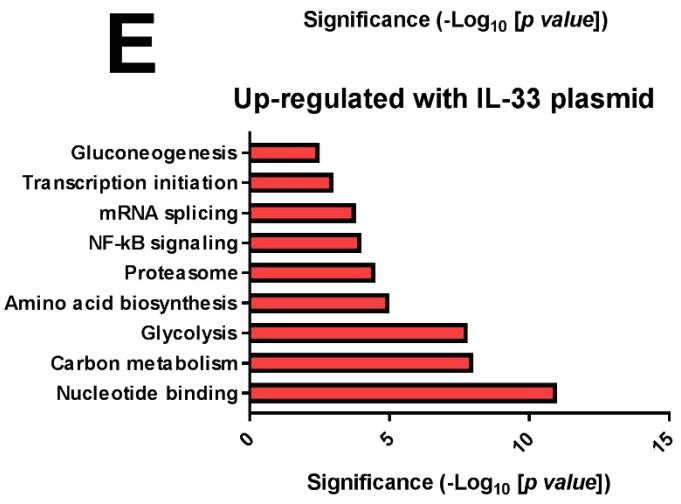
E
Up-regulated with IL-33 plasmid
Gluconeogenesis
Transcription initiation
mRNA splicing
NF-kB signaling
Proteasome
Amino acid biosynthesis
Glycolysis
Carbon metabolism
Nucleotide binding
0
5
10
15
Significance (-Log10 [p value])

Figure 6.9. Effect of IL-33 overexpression on the ARPE-19 proteome:

ARPE-19 were transfected for 48h with either control plasmid or an IL-33 activation plasmid. (A) Representative immunoblot of IL-33 protein expression following transfection. (B) Volcano plot displaying fold change (log2) of proteomic data reveals differentially expressed proteins in whole cell lysates following transfection. (C) Heatmap of differentially expressed proteins in whole cell lysates following transfection (FDR <5%, $p<0.01$ and >1.25-fold expression). (D) Pathway analysis of proteins induced with IL-33 OE. (E) Pathway analysis of proteins suppressed with IL-33 OE. Data are expressed from three independent experiments.

6.8. IL-33 interacts with components of the PKM splicing complex in ARPE-19 cells, but not primary RPE

Within the data sets from the previous sections, a large focus of gene ontologies associated with the proteomic changes appeared to focus around aspects of cellular metabolism. In IL-33 knock-down RPE cells, aspects of mitochondrial metabolism were significantly enriched within the data sets. Conversely, overexpression of IL-33 was accompanied by significant enrichment in gene ontologies involving the glycolysis pathway. Whilst unsurprising considering the observations made in chapter 5 (whereby IL-33 was observed to promote glycolytic flux and oxidative mitochondrial catabolism of pyruvate), this indicated an opportunity to further investigate the molecular mechanisms governing the control of metabolism by nuclear IL-33.

A major control point of glycolysis is the regulation of pyruvate kinase splicing (see section 1.8.5.2.). Indeed, multiple studies have identified key roles for PKM2 in metabolic reprogramming of cancer cells [330]. PKM1 and PKM2 are generated by exclusive alternative splicing of the *PKM* mRNA, a mechanism largely driven by the activity of MYC [331]. In the glycolytic pathway, pyruvate kinase is a rate limiting enzyme that catalyses the final reaction of PEP into pyruvate. PKM2 is responsible for augmented glycolytic activity in its tetramer form yet when dimerized, PKM2 translocates to the nucleus where it interacts with HIF-1α and promotes the expression of a glycolytic gene program [328]. Using the data generated in section 6.1, I found that IL-33 interacted with multiple factors involved in the regulation of PKM2 splicing, including SRSF3, hnRNPA1, hnRNPA2B1, PTB, and even PKM2 itself (Fig. 6.10A). In order to confirm these interactions, IL-33 was co-immunoprecipitated for SRSF3, hnRNPA1 and hnRNPA2B1, which were confirmed to be both present in the input (cell lysate) and also in the IL-33 pull-down, suggesting an interaction between these factors and IL-33 (Fig. 6.10B). This, however, was restricted to the human RPE cell-line, with IL-33 not observed to interact with any of these factors in primary murine RPE. Due to a lack of interaction in the proteomics data, immunoprecipitation-immunoblotting experiments were not performed.

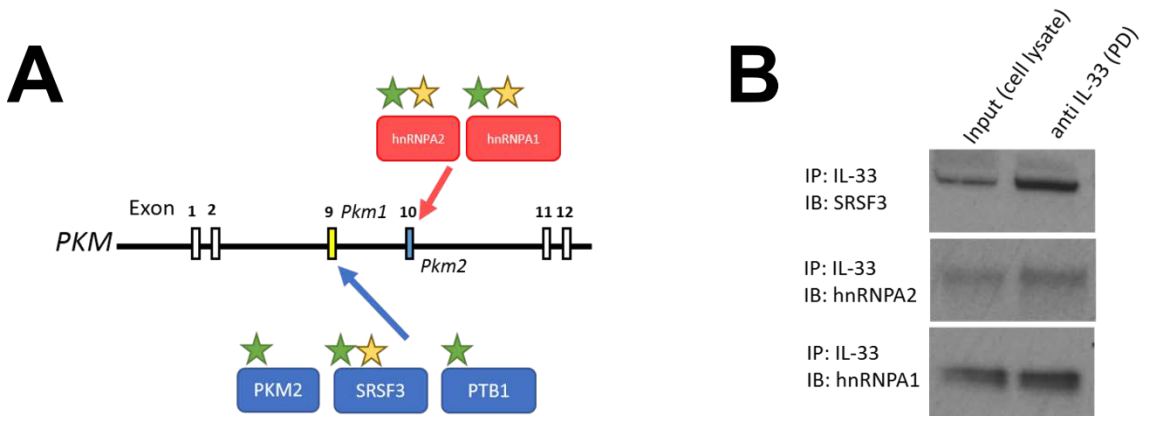

Figure 6.10. IL-33 interacts with components of the PKM splicing complex in ARPE-19 cells:

(A) Schematic of splicing of the *PKM* gene. Green stars indicate presence in the IL-33 pull-down TMT analysis. Yellow stars indicate a physical interaction by IL-33 I.P. and western blotting. (B) IL-33 was immunoprecipitated in ARPE-19 cells. Western blotting was used to confirm the presence of SRSF3, HNRNPA1 and HNRNPA2. Data are expressed from three independent experiments.

6.9. Differential expression patterns of pyruvate kinase are regulated by IL-33 in human but not murine RPE cells

The results from the previous section appeared to suggest an interaction between IL-33 and components of the PKM splicing machinery in an *in vitro* ARPE-19 system. This was supported by interactions both *via* TMT-labelling proteomics and immunoprecipitation experiments. Interestingly, this did not appear to be the case in the context of primary murine RPE cells. In order to further investigate the fundamental differences between the two cell types, I investigated the levels of PKM1 and PKM2 abundances in the total proteome of both WT mice RPE and untreated ARPE-19 cell lysates. In the ARPE-19 cell lysates, PKM2 was the dominant isoform, with an abundance ~4-fold greater than PKM1 (Fig. 6.11A). Similarly, PKM2 was the predominant isoform in the primary RPE cell lysates. However, from the total proteomics data only the one isoform could be detected (Fig. 6.11B). In order to confirm, primary RPE cell lysates from WT and *Il33*$^{-/-}$ mice were probed for both PKM1 and PKM2. Immunoblotting indicated that PKM2 was the predominant isoform, with no PKM1 expression detected (Fig. 6.11C). Although PKM2 has been demonstrated as the predominant isoform in the retina (particularly photoreceptors) [568, 569], no study has identified which isoform is expressed by RPE cells. No changes were observed in the expression of PKM2 between WT and *Il33*$^{-/-}$ groups (Fig. 6.11C). Upon further investigation of the PKM splicing factors hnRNPA1, hnRNPA2B1 and SRFS3, it was revealed that there were no significant changes between WT and *Il33*$^{-/-}$ groups (Fig. 6.11D). In the ARPE-19 cell lysates, expression of both PKM1 and PKM2 was confirmed by immunoblotting (Fig. 6.11E). In addition to this, it was observed that modulation of the IL-33 expression status altered PKM1/PKM2 ratio. With IL-33 siRNA, an increase of PKM1 was observed as PKM2 levels dropped (Fig. 6.11E). Conversely, with IL-33 overexpression, PKM1 levels dropped whilst the expression of PKM2 increased (Fig. 6.11E). Upon further investigation of the ARPE-19 proteomics data, it was clear that alteration of IL-33 expression by either siRNA or CRISPR-cas9 differentially modulated the expression of PKM splicing components (Fig. 6.11F-G). In the context of IL-33 knock down, protein expression of both hnRNPA1 and hnRNPA2B1 were significantly increased, yet expression of SRSF3 was decreased (Fig. 6.11F). Proteomics confirmed that knockdown of IL-33 increased the PKM1/PKM2 ratio (Fig. 6.11F). With IL-33 overexpression, protein expression of both PKM1, hnRNPA1 and hnRNPA2B1 were significantly decreased (Fig. 6.11G). In addition to this, SRSF3 and PKM2 were increased (Fig. 6.11G).

These data indicate fundamental differences in the metabolism of pyruvate in ARPE-19 cells compared to primary RPE. Although both cell types express PKM2 as their predominant isoform, PKM1 is expressed in ARPE-19 cells. Expression of these two isoforms (albeit at differing abundances) permits

modulation of the splicing machinery and an upregulation of the pro-glycolytic PKM2 isoform compared to a basal state. In ARPE-19 cells PKM splicing appears to be regulated by IL-33, with altered expression of PKM1/PKM2 isoforms, and components of the splicing machinery observed with alterations in IL-33 expression. As primary murine RPE only express one isoform of PKM, it is unlikely alternative splicing occurs and thus ruling out a role for nuclear IL-33 in its regulation.

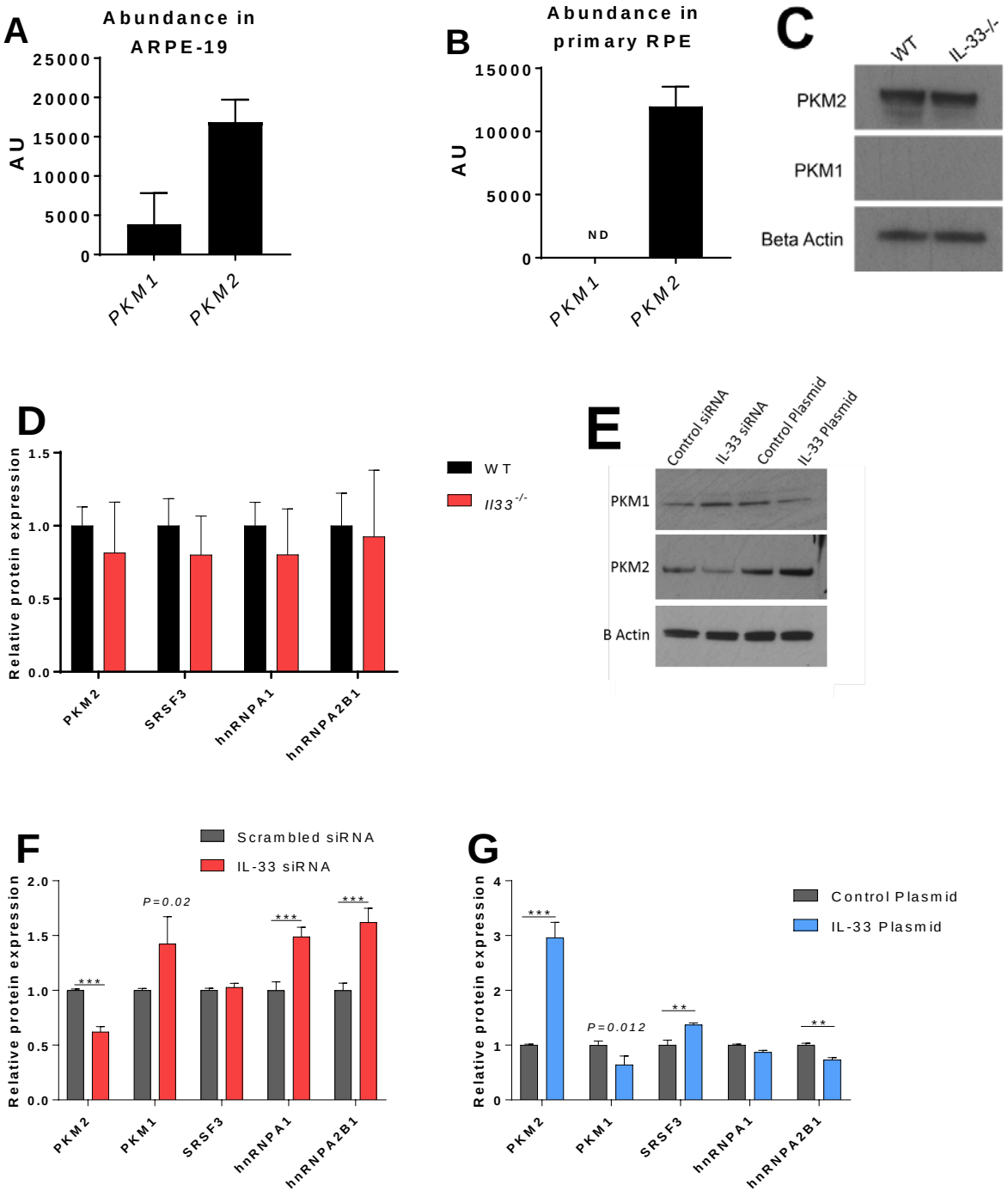
A
Abundance in ARPE-19
AU
25000
20000
15000
10000
5000
0
PKM1
PKM2
B
Abundance in primary RPE
AU
15000
10000
5000
0
ND
PKM1
PKM2
C
WT
IL-33-/-
PKM2
PKM1
Beta Actin
D
Relative protein expression
1.5
1.0
0.5
0.0
PKM2
SRSF3
hnRNPA1
hnRNPA2B1
WT
Il33-/-
E
Control siRNA
IL-33 siRNA
Control Plasmid
IL-33 Plasmid
PKM1
PKM2
B Actin
F
Scrambled siRNA
IL-33 siRNA
Relative protein expression
2.0
1.5
1.0
0.5
0.0
***
P=0.02
***
***
PKM2
PKM1
SRSF3
hnRNPA1
hnRNPA2B1
G
Control Plasmid
IL-33 Plasmid
Relative protein expression
4
3
2
1
0
***
P=0.012
**
**
PKM2
PKM1
SRSF3
hnRNPA1
hnRNPA2B1

Figure 6.11. IL-33 regulates *PKM* splicing in ARPE-19 cells, but not primary murine RPE:

(A) Abundance count of PKM1 and PKM2 in ARPE-19 cell lysates using TMT labelling. (B) (A) Abundance count of PKM1 and PKM2 in primary RPE cell lysates using TMT labelling. (C) Immunoblot of PKM1 and PKM2 expression in cell lysates from WT and or *Il33*$^{-/-}$ mice. (D) Relative expression of PKM2 and splicing factors using proteome datasets generated in Fig. 6.8. (E) Immunoblot of PKM1 and PKM2 expression in cell lysates from ARPE-19 cells transfected with either scrambled siRNA/IL-33 siRNA or a control plasmid/IL-33 activation plasmid. (F) Relative expression of PKM2 and splicing factors using proteome datasets generated in Fig 6.9. (G) Relative expression of PKM2 and splicing factors using proteome datasets generated in Fig 6.7. Data are expressed as means ± SD from three independent experiments. Unpaired Student's T-test; $^{**}p<0.01$, $^{***}p<0.005$.

6.10. Discussion

The IL-1 family cytokine IL-33 has well-described extracellular roles in the initiation of innate immune responses and type 2 immune responses [231]. Activation of ST2 expressing cells by IL-33 has been well described within the literature. One aspect of IL-33 biology which remains enigmatic is that of its unique nuclear localisation and binding to chromatin. In this chapter I have addressed the biological significance of IL-33 nuclear localisation and how this affects epithelial cell function *in vitro* and *ex vivo.* Important observations were: that (A) IL-33 retains its nuclear localisation *in vitro* under multiple conditions of inflammatory stress; (B) whilst in the nucleus, multiple proteins display high affinity for IL-33; (C) upon activation of multiple innate immune signalling components, IL-33 exhibits alterations in the abundance of various binding partners, as identified by interactome analysis; (D) In the nucleus, IL-33 affects homeostatic protein expression as assessed by three independent strategies: 1. proteome-wide profiling of RPE cells engineered to overexpress IL-33 *via* CRISPR-cas9, 2. RPE cells transiently silenced *via* IL-33 siRNA pools and 3. *ex vivo* from RPE cell lysates of mice from WT or IL-33 deficient backgrounds and (E) IL-33 interacts with key components of the splicing machinery in epithelial cells, however only functional roles for IL-33 in the regulation of an RPE cell line have been described. Taken together, these proteomics studies support a view of dual functionality in IL-33, acting as both a nuclear regulator and extracellular cytokine.

RPE cells were an ideal system for this investigation on the basis of three key points: (1) they signify a major source of endogenously derived IL-33 within the eye (along with Müller glia) [17]; (2) although a specialized form in the context of RPE, all epithelial cells are known to express IL-33 at high levels, a phenomenon not observed in branches of the endothelial tree [134]; (3) functional changes were previously observed in terms of regulating the metabolism of RPE cells when endogenous IL-33 expression was genetically manipulated (see chapter 5). Considering the previously characterised metabolic changes regulated by endogenous IL-33, any metabolic alterations would likely be downstream of endogenous functional roles.

IL-33 has been linked to the regulation of transcription in previous studies [10], although precise mechanisms supporting these observations are unknown. I confirmed that nuclear IL-33 interacts with chromatin histone components, supporting a nuclear role, and TMT proteomics identified proximal interactions with components of the translation and splicing machinery, various factors involved in the modulation of chromatin dynamics and nuclear localised metabolic enzymes, including members

of the glycolytic pathway. These results suggest that IL-33 may have diverse roles within the nucleus of RPE cells which differ from its traditional view as a transcriptional repressor.

A recent study focusing on the role of IL-33 in cancer cells, suggests key roles for the cytokine in core epigenetic pathways, including transcriptional initiation and chromatin remodelling [261]. In this study, binding of multiple epigenetic factors (including WD Repeat Domain 82 (WDR82), SWI/SNF-related matrix-associated actin-dependent regulator of chromatin subfamily B member 1 (SMARC1), TAF9 RNA polymerase II, TATA box binding protein (TBP)-associated factor (TAF9), Bromodomain-containing protein 4 (BRD4) and HDAC4) to IL-33 was observed. IL-33 was observed to be a critical core component of the WDR82 chromatin complex, a key regulatory step of H3K4 trimethylation [261]. In addition to this, IL-33 bound to various chromatin modifiers essential for the modulation of NF-κB-target genes, such as *Ccl5* [261]. Whilst, none of the listed above proteins were key IL-33 interaction targets in the RPE, one cannot rule out a context where IL-33 which may be aberrantly modulated in the squamous cell carcinoma. I identified WD repeat and FYVE domain containing 1 (WDFY1) to be a key IL-33 target in the interactome analysis, and as one of the most significantly up-regulated proteins in whole proteome analyses from both mouse and human cells. As WDFY1 is a critical adaptor protein in the TLR-3/4 signalling pathways [570] (responsible for the recruitment of TRIF and subsequent NF-κB activation), it is plausible that IL-33 acts *via* alternate mechanisms to control the transcription of NF-κB-target genes in the RPE.

It was interesting to note that the IL-33 interactome exhibited a degree of plasticity, with stimulation from immune-mediated stress signals enough to alter the abundance of different binding partners. Furthermore, even signals not observed to alter IL-33 expression status (i.e. TNFα) were observed to have effects on the interactome. This suggests that IL-33 may act as a nuclear node in multiple cytokine signalling pathways where previously regarded as redundant. In both TNFα and Poly (I:C) treatment settings, one key transcription factor was found to have a much lower protein abundance in the IL-33 pull-down compared to other significantly altered targets (>10-15-fold). This corresponded to nuclear factor 1 (NF1), a key transcription factor containing an unusual DNA binding domain [571]. NF1 family members interact with chromatin to promote both gene repression and activation by binding to DNA dyad symmetric consensus site or half-site sequence TTGGC(N5)GCCAA [571]. NF1 activity (for the most part) correlates with increased expression of target genes and is associated with higher levels of active promoter methylation marks such as H3K4me3 and H3K36me3, implicating them predominantly as activators of transcription [571]. Future work will be required to investigate the

interactions between IL-33 and NF1, both in basal and stimulated states, to better understand the role of IL-33 in the regulation of gene expression.

From the proteomics datasets generated in this chapter, it was evident that proteins involved in core cellular metabolic pathways were significantly enriched. This was unsurprising considering my previous observations in chapter 5. In the IL-33 siRNA and *Il33*$^{-/-}$ data sets, many mitochondrial proteins were significantly up-regulated, including targets in FAO, glutaminolysis, TCA and mitochondrial biogenesis pathways. Interestingly, significant enrichment of mitochondrial metabolic pathways have been highlighted in an RNA-sequencing experiment of *Il33*$^{-/-}$ adipocytes previously [19]. On the other hand, IL-33 overexpressing cells had multiple glycolytic enzymes and key targets in amino acid/ fatty acid biosynthesis pathways significantly up-regulated. These observations suggest that in the context of IL-33 loss, cells appear to favour a more quiescent metabolic state, whereby catabolic pathways fuel the TCA cycle. With IL-33 overexpression an anabolic metabolic state appears to predominate, favouring glycolytic metabolism to support biosynthetic demands. This correlates to a degree with data obtained in the previous chapter and may explain observations made, including: (A) why glycolytic flux was augmented with IL-33 overexpression and (B) how basal mitochondrial metabolism was maintained despite the loss of IL-33 and lack of pyruvate oxidation in the TCA cycle.

Whilst searching for a downstream target which could mediate the bioenergetic adaptations observed in RPE cells, I observed that IL-33 interacted with the splicing machinery of the *PKM* gene in ARPE-19 cells. Whist the mechanisms underlying the interactions (and to what degree IL-33 influenced their function) were unknown, it was clear that upon modulation of IL-33 expression status, alterations in the abundances of various splicing factors were observed, correlating to differential expression of PKM isoforms PKM1 and PKM2. This, however, was not observed in primary RPE cells, indicating that regulation of PKM splicing by IL-33 may not be a property observed *in vivo*, but rather that of a cell line adapted to a two-dimensional culture environment. This observation highlights the need to utilise a combination of both primary cells and cell lines to validate and translate observations on RPE function from *in vitro* studies, to the *in vivo* environment. Much of the current understanding of RPE function originates from i*n vitro* studies using various “RPE-esque” cell lines. Although frequently used in RPE research, it is unclear to what extend these cells are representative of a “true” RPE cell. Indeed, studies have shown that once brought into culture, primary RPE cells quickly lose their specialised function and expression of key markers, expressing characteristics of cells from a mesenchymal origin [572]. Furthermore, differential protein profiling experiments of primary vs immortalised RPE cells

indicated that none of the commonly used cell lines (including ARPE-19) exhibited a protein expression signature found in native RPE [572]. Expression of the PKM1 isoform in ARPE-19 cell lines may act as a survival advantage *in vitro*. Whilst not a key regulator of *PKM* splicing in RPE cells, it would be of interest to investigate IL-33 has any role in the alternative splicing of *PKM* in other epithelial cells expressing both isoforms of PKM.

It was apparent from the total proteome experiments that IL-33 exhibited a *bone fide* nuclear role, with three unique experiments (two in the context of IL-33 loss and one with IL-33 overexpression) displaying significant alterations to protein expression compared to either WT controls or control nucleotides *via* transfections. Whilst, the mechanism of IL-33 in the nucleus remains unclear, future work utilising the generated data sets from this chapter may allow the identification of key pathways and IL-33-target proteins. The involvement of IL-33 in the regulation of splicing machinery may be an interesting avenue to follow considering the observations made with PKM in ARPE-19 cells, and considering recent work which has suggested a role for nuclear IL-33 in the regulation of UCP1 splicing [19]. Additionally, as IL-33 was observed to bind to core chromatin components and affect key epigenetic components, it would be of interest to observe the key DNA binding sites of IL-33 and its effects on the epigenetic landscape.

Despite the observations made in this chapter, it is essential to note the work of previous studies indicating that there no evidence for a role of nuclear IL-33 in epithelial cells and endothelial cells. The first of these studies utilised a cell line lacking constitutive IL-33 expression and following transfection (with a vector permitting doxycycline (Dox)-inducible expression of IL-33) analysed the transcriptome [263]. In this study, the only transcript observed to be regulated by IL-33 overexpression was that of *Il-33* itself. Following a subsequent series of elegant experiments, this study concluded that IL-33 slowly dissociates from cells as part of an IL-33-histone high-molecular weight complex which synergistically augments ST2 receptor activation. Thus, proposing that nuclear retention and chromatin binding constitute a post-translational mechanism to regulate ST2-mediated bioactivity [263]. One potential caveat of this study is the use of a cell line lacking constitutive IL-33 expression. Upon dox-mediated induction of IL-33, nuclear translocation and histone binding was observed, but not changes in transcription. Although one would expect induction of a foreign “nuclear factor” (as IL-33 is dubbed within the literature) to elicit transcriptional alterations, it is plausible that IL-33 is not required as an epigenetic node in these cells and therefore is not constitutively expressed. Considering observations made in this body of work and others [19], as IL-33 interacts with key translational and spliceosome constituents, it may be that IL-33 acts post transcriptionally on the translatome. This,

however, will require further investigation into the roles of protein translation/ splicing machinery with IL-33 affinity.

Another study (of similar experimental set up to this chapter) took a proteomics-based approach and observed no reproducible effect of nuclear IL-33 silencing on total protein expression in primary human endothelial cells [230]. A well-designed study in the sense that two independent RNA silencing strategies were applied to endothelial cells. This allowed robust identification of the IL-33 induced proteome without potential off-target effects associated with siRNA transfection. Although endothelial cells constitute a major source of endogenous IL-33 in human tissues [217], there appear to be fundamental species related differences in the endothelial vasculature trees of humans and mice. In murine endothelial cells from blood vessels, IL-33 is not expressed constitutively, and its nuclear expression is exclusively observed in a chronic inflammatory state [134]. To further examine the role of IL-33, it will be necessary to investigate how homeostatic cell function is altered cells constitutively expressing IL-33. Whilst not considered in the study, it would be of interest to interrogate the role of nuclear IL-33 during chronic disease states, where significantly increased expression is observed.

The lack of "clear cut" nuclear functions for the cytokine can be likely attributed to the fact that cell lines vary in the expression of their IL-33 splice variants [573]. This in turn, may impact functional roles [574]. It is therefore critical to understand what splice isoforms are expressed in RPE cells and indeed additional cell types before attributing endogenous faction (or in the case of previous studies, lack of).

The sequestration of IL-33 to the nucleus may likely serve as a mechanism of controlling its potent extracellular signalling activities in a variety of tissues. Despite an observed nuclear function in RPE cells under the conditions tested in this body of work, it is plausible that these may be context and cell specific, with IL-33 selected for during evolution to act solely as a local alarmin upon cell damage without exhibiting nuclear transcriptional repressor properties. In a recent study, deletion of the chromatin-binding nuclear domain of IL-33 dramatically affects immune homeostasis in mice. When not actively targeted to the nucleus, there was constitutive IL-33 release into the serum, leading ultimately to lethal eosinophil-dominated inflammation [531]. This provides evidence that a lack of signal peptide and a nuclear localisation may be related to IL-33 mode of action, with sequestration necessary to limit the potent extracellular biological activity.

In conclusion, the data presented in this chapter indicate that nuclear IL-33 regulates protein expression of human and murine RPE cells. These support the current view of IL-33 as a dual function protein including functional roles in the nucleus. As IL-33 and its nuclear interactions are enhanced or dampened in response to inflammatory cues indicates that IL-33 acts as a key node to maintain cellular homeostasis and likely facilitate innate immune responses separate from its extracellular functions.

Chapter 7. Final discussion and future directions

The RPE cell layer endows functional support to the entire retina. The importance of these cells is evident, with RPE loss contributing to the pathogenesis of several retinal degenerative diseases, including AMD. To sustain its numerous functions in photoreceptor phagocytosis, nutrient transport and the maintenance of tissue immune homeostasis, RPE are highly metabolically active. The metabolism of RPE cells revolves around a functional mitochondrial TCA cycle, whereby carbon inputs from fatty acids, lactate and amino acids (such as proline and glutamine) support OXPHOS [6, 379]. Although capable of carrying out glycolysis, glucose is largely unused by the RPE as a fuel source, and instead traverses the monolayer to support other cells within the retina such as photoreceptors, which depend on a highly glycolytic program. Work from Hurley et al., has informed us on how the cells within the retina are co-dependent on each other both functionally and metabolically [4]. Increasing the dependence of RPE cells to the use of glucose as a fuel source has dire consequences for the rest of the retina. As glucose concentrations fall on the apical side of the RPE, photoreceptors starve and degrade. Indeed, a lack of mitochondrial function (naturally occurring with age and enhanced in AMD) forces RPE to utilise glycolysis to survive, at the expense of photoreceptors.

Whilst targeting metabolism in the RPE appears to be a tractable hypothesis for the prevention of AMD, one cannot ignore additional confounding factors implicated in disease pathogenesis. Despite its multifaceted aetiology, immune dysfunction appears to be a central player. Clinical and genetic data support a role for the immune system in AMD pathogenesis in particular, innate immunity and the regulation of the complement pathway [2]. A functional immune response is critical for retinal homeostasis, yet evidence points towards the overactivation and dysregulation of these responses in AMD. Obscuring the understanding of inflammatory contributions to disease pathogenesis are the mechanisms underlying the “initial switch” from homeostatic to chronic low-grade inflammation. The balance between immune activation and regulation involves intrinsic control through soluble mediators at the cellular level. If homeostasis is perturbed following tissue stress in the retina, para-inflammatory responses remain unchecked and manifest in augmented tissue damage. Tissue damage itself further increases endogenous sterile inflammatory signals (e.g alarmin release), and the cycle continues. One defining feature of AMD development is the build-up of drusen deposits, predicted to be of RPE origin. Drusen is comprised of many immune-stimulating components such as oxidised lipids and complement factors. It is unknown if drusen is the trigger for the initial inflammatory response or participates in the heightened sterile inflammation later in disease progression.

Work from O'Neill has highlighted the "Warburg effect" in context to immune cell activation [5]. Extrapolating from observations made almost a century ago (whereby tumour cells preferentially use aerobic glycolysis for survival), it is appreciated that macrophages, dendritic cells, and many other cells of the innate and adaptive arms of the immune cell tree, undergo metabolic reprogramming in response to "stress signals", namely that of TLR and cytokine receptor signalling. Metabolic changes in innate immune cells plays a predominant role in the regulation of cellular phenotype; mitochondria themselves play a central role in the regulation of IL-1 expression, inflammasome activation and the generation of ROS through reverse ETC flux [412]. These studies show the interconnectivity (and to an extent) co-dependency of core metabolic pathways in inflammatory responses. For example, the up regulation of glycolysis in LPS activated macrophages not only supports the bioenergetic demands of cytokine secretion and phagocytosis but also feeds the pentose phosphate, fatty acid synthesis and serine biosynthesis pathways which support ribose for nucleotides, amino acids for protein synthesis and malonyl coA, which influences translation of key inflammatory mRNAs [485].

The RPE is critical to the maintenance of immune privilege within the retina. As an innate-immune competent cell, the RPE respond to inflammatory cues through a rich expression of PAMP and DAMP receptors [45]. Data presented in this thesis shows that in a similar manner to macrophages, RPE cells exhibit a plasticity between metabolic pathways which permits a bioenergetic switch from mitochondrial OXPHOS to aerobic glycolysis under conditions of innate immune stress. The initial metabolic switch is almost certainly a protective response, bolster flux through ATP-producing pathways to support cytokine production and respond to extracellular danger signals by attracting innate immune cells. Whilst this adaptive metabolic response permits the RPE to main homeostasis in health, it raises concerns for the heightened para-inflammatory environment observed in AMD.

If one is to appreciate the theory of a metabolic ecosystem within the retina [4], it is easy to see how the interplay between innate immune and metabolic dysfunction may accelerate AMD progression. Under healthy conditions, glucose is passed to the photoreceptors as a fuel source, leaving mitochondrial metabolism to support the RPE. With age and early AMD development, it is now appreciated that a bioenergetic switch occurs in the RPE towards an increased reliance on glycolytic metabolism. With age (and implicated in AMD development) RPE exhibit increased strain on mitochondria function and abundance of dysfunctional mitochondria, as mitophagy/autophagy housekeeping pathways are impaired [575]. Cybrid RPE cells, created from AMD risk haplogroups, indicate that mitochondrial variants themselves determine the bioenergetic switch to aerobic

glycolysis [18]. With a reliance on glycolysis, comes the breakdown of the symbiotic metabolic relationship shared between RPE and photoreceptors. Glucose is passed through the glycolysis pathway and exits as lactate. Although, lactate could normally be used as an RPE fuel source [4], the diminished mitochondrial function prevents enough ATP generation from oxidative lactate/pyruvate metabolism. Consequently, little glucose passes through to the photoreceptors and they begin to starve, and ultimately degrade. A similar mechanism likely occurs in the face of uncontrolled para-inflammatory responses observed in the AMD RPE. Endogenous-derived signals activate innate immune receptors present on the RPE (such as TLR-4), permitting a switch to aerobic glycolysis. Chronic low-grade inflammation has the potential to constantly rewire the metabolism of RPE cells towards a program of increased aerobic glycolysis. This state of augmented glycolysis once again negatively impacts the metabolic co-dependency of RPE and photoreceptors, as glucose is effectively prevented from traversing the RPE without being consumed for ATP production (Figure 7.1). Whilst considered individually here, it is likely that the development of AMD is based on interactions between both innate immune and metabolic dysfunction. An RPE forced into a glycolytic state by a decline in mitochondrial function lacks the ability to switch between metabolic pathways under stress. This occurs naturally over the course of a lifetime regardless of AMD development. We see in normal aging mice, a complete loss of any RPE glycolytic capacity. A lack of ability to adapt metabolically likely limits the ability of RPE cells to adequately respond and maintain homeostasis in the retina, leading to a downwards spiral of uncontrolled inflammation.

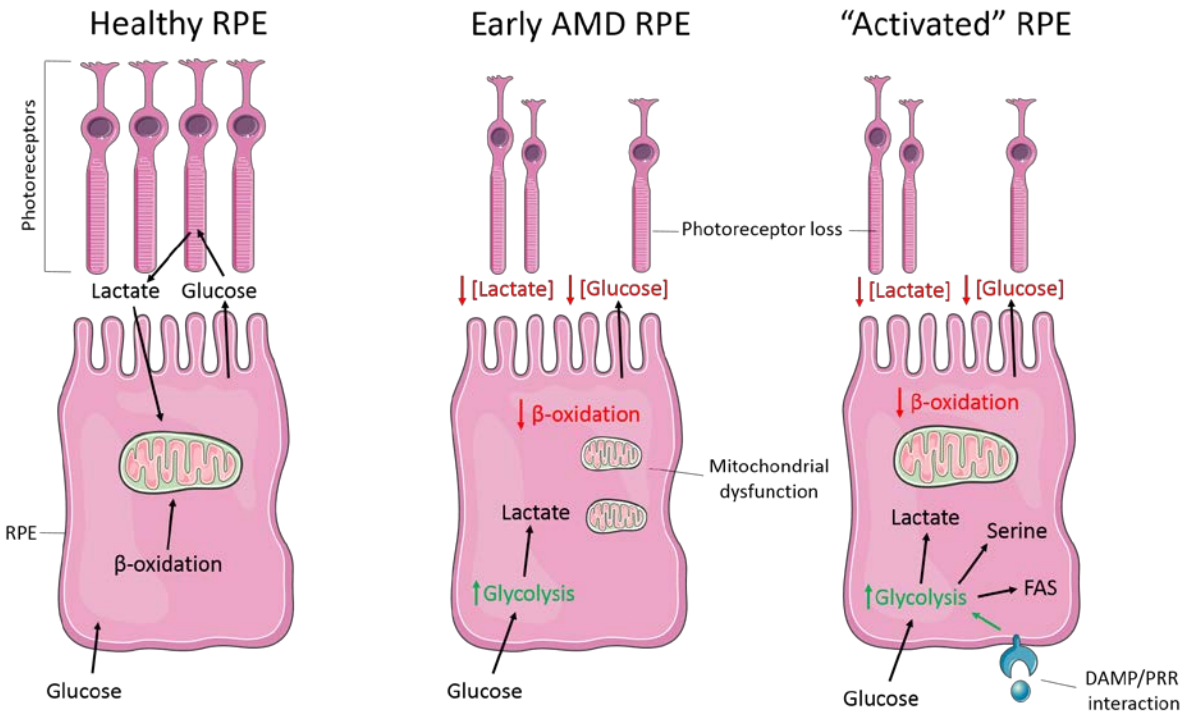

Figure 7.1. Interplay between metabolic dysfunction and low-grade inflammation in AMD pathogenesis: In a heathy retina (left), RPE cells take up glucose through GLUT1 transporters, yet is not used as a metabolic substrate. Instead, glucose from the choroidal blood flow is shuttled to the photoreceptors for use in aerobic glycolysis. Lactate produced in the photoreceptors is taken up by RPE monocarboxylate transporters and enters the mitochondrial TCA cycle as pyruvate. Photoreceptors also supply RPE cells with lipids from the degradation of photoreceptor outer segments. These lipids are used to generate ATP in mitochondrial β-oxidation. In AMD (middle), a bioenergetic switch to glycolysis occurs, as dysfunctional mitochondria limit the cell's ability to generate ATP through oxidative phosphorylation. This limits the concentration of glucose transported to the photoreceptors, leading to starvation and death. Mitochondrial dysfunction impairs the ability of RPE cells to process lipids from degraded photoreceptor outer segments, leading to the accumulation in RPE. A similar bioenergetic switch may occur in the RPE under conditions of chronic low-grade inflammation. The constant interaction between tissue-derived danger associated molecular patterns (DAMPS) and DAMP receptors/ cytokines and cytokine receptors present on the RPE surface lead to metabolic rewiring into aerobic glycolysis through an up-regulation of hypoxia-inducible factor α (HIF-1α). Increased RPE glycolysis renders the RPE less able to support the photoreceptors and subsequently leads to their starvation and death. β-oxidation is similarly reduced as the RPE switches away from mitochondrial metabolism, leading to the accumulation of outer-segment lipids. RPE, retinal pigment epithelium; AMD, age-related macular degeneration; FAS, fatty acid synthesis; DAMP, danger-associated molecular pattern; PRR, pattern recognition receptor; ATP, adenosine triphosphate; GLUT1, glucose transporter 1. Adapted from [4].

Data presented in this thesis has highlighted the metabolic adaptations of the RPE to other immune-derived stress signals, namely the TLR-3 agonist Poly (I:C) and alarmin IL-33. Unlike TLR-4 activation, TLR-3 ligation was accompanied by an increase in mitochondrial OXPHOS, mediated by activation of AMPK. Whilst activation of this pathway was not accompanied by a bioenergetic switch to aerobic glycolysis, flux through the glycolysis pathway was still augmented. This has highlighted the differential metabolic response of the RPE to varying signalling pathways likely to be activated in the context of the low-grade chronic parainflammatory environment of AMD. Despite the differential metabolic outcomes in terms of aerobic glycolysis vs oxidative glucose catabolism in response to immune stimulation, it is evident that "activated" RPE cells increase their glucose consumption. This, as highlighted in previous sections, would have adverse effects for the photoreceptors. Although, endogenous TLR-3 agonists can elicit retinal degeneration *in vivo* [576], it is unknown to what extent RPE metabolism is altered *in vivo* and if this contributes to photoreceptor loss.

A limitation of the work presented in this thesis is that the metabolism of RPE was assessed *ex vivo* and *in vitro* and therefore may not be truly representative of the *in vivo* metabolic environment whereby RPE cells scarcely use glucose as a fuel source. When primary RPE cells are cultured *ex vivo* they adopt a metabolic program of glycolysis and lactate production. The work conducted in this study assumed that these pathways may be redundant *in vivo*, using *in vitro* studies to answer the question "*does metabolic reprogramming occur in the RPE in response to immune stressors?*" and subsequently assess the underlying molecular mechanisms. Whilst this work has unravelled some interesting conclusions on RPE behaviours, future work should aim to explore some of the observations made in this study, with the focus on investigating if RPE cells adapt their metabolism to glycolysis *in vivo* following activation of PAMP or DAMP-mediated signalling pathways.

The groundwork of this thesis was built on the overarching hypothesis that the induction of the Warburg effect in RPE generates an IL-33 signature that regulates cellular gene responses and prevents unwanted immune activation. It was originally hypothesised that changes in the tissue environment are signals to drive changes in RPE metabolism, resulting in a direct signal to activate inflammation. Whilst immune activation could be perceived as adverse, in the context of RPE and retina, a consequence of this is the "protective" response conferred by

increased IL-33 production. Whilst we now appreciate a metabolic switch does indeed occur in response to immune stressors, it is important to note the multifaceted nature of such a response in terms of both the "metabolic ecosystem" and the concurrent production of IL-33. The initial up-regulation of IL-33 is almost certainly a protective response to cellular stress. During injury, RPE cells are destroyed, liberating IL-33 into the extracellular milieu. Once released, IL-33 signals to nearby cells to alert the immune system of tissue damage and dysfunction. IL-33 can also act in a paracrine/autocrine manner on RPE cells within the monolayer to preserve cellular function through increasing overall bioenergetic demands. There is much interest in the ability to protect against noxious damage to the RPE in the form of oxidative stress (a key early event in AMD progression [577]) and the observation of IL-33 to protect against oxidative damage has exciting implications. One cannot, ignore the fact that IL-33 is a highly pro-inflammatory cytokine with many pleiotropic functions [9]. Whilst in the context of bolstering RPE mitochondrial function, use of therapeutic IL-33 appears attractive, there is however, evidence that IL-33 is released from Müller cells and contributes to photoreceptor loss through recruitment of mononuclear phagocytes (macrophage/microglia) [17]. As previously stated, the initial IL-33 release is protective, leading to the co-ordination of immune responses and attempt to repair tissue damage [8]. The increased IL-33 expression observed in areas of macular degeneration [17] supports the alarmin nature of the cytokine in response to RPE cell loss and lesions. However, with an attempt to maintain homeostasis comes the price of undesired inflammation and starvation of photoreceptors through rewiring of RPE glucose metabolism. Therefore, one can argue the context-dependent protective or damaging effects of IL-33 depend on both the location and degree of insult.

It is of interest to assess the role of IL-33 in the context of other ST2-expressing cells in the retina (namely mononuclear cells, Müller glia and mast cells) in response to RPE death during early AMD. Data presented in chapter 4 highlighted that the metabolic effects of IL-33/ST2 signalling appear to be specific to RPE. This, however, does not rule out that IL-33 has no effect on Müller glia and mast cells. The caveat with investigating Müller glia is that high levels of ST2 are only expressed when "active" (e.g. following exposure to phototoxic light in animal models). Upon ligation of ST2, IL-33 induces the expression of chemokines and cytokines [17]. Müller glia are important in the maintenance of laminar structure, neuronal survival,

metabolic homeostasis and repair of the damaged retina [578]; understanding how these processes may be altered following activation of the IL-33/ST2 axis require further investigation. The main source of IL-33 is in the nucleus of Müller glia in the normal retina, suggesting a key role of these cells in immune-mediated repair processes [17]. Interestingly, the deletion of IL-33 in murine models of photoreceptor detachment leads to persistent Müller gliosis and augmented degeneration [579]. These results suggest that IL-33 negatively regulates Müller glia to protect against inflammatory photoreceptor damage. Macrophages and microglia are key ST2 expressing myeloid cells [580], and key contributors to immune homeostasis in the retina [41]. One can extrapolate from previous observations that IL-33 signalling in retinal myeloid cells establishes a homeostatic tissue tone. The observation that IL-33 protects against EAU through the polarisation of M2 macrophages [16] has interesting implications for AMD whereby macrophage subtype shifts towards an M1 phenotype [581]. In the brain, IL-33 serves to protects against tissue injury through the polarization of microglia to an M2 phenotype with enhanced IL-10 production, critical for neuronal survival [582]. We now understand that a functional interface is observed between the RPE and macrophage; impairing RPE function through perturbation of autophagy or mitochondrial function is sufficient to recruit macrophages which phagocytose the damaged RPE [518]. A consequence of this however, is macrophage inflammasome activation and proangiogenic inflammatory responses [518]. As Th2 cytokines suppress these responses [583], it is likely that the IL-33 released in the context acts to subvert noxious pro-angiogenic responses [8] without suppressing macrophage phagocytotic functions [15]. Mast cells are abundant in the choroid and play a key role in the regulation of choroidal inflammation, they exhibit high expression of ST2 and are an important target of release IL-33 [200, 203]. The role of mast cells in AMD pathogenesis is currently unknown. Studies suggest that increased mast cell degranulation may drive early AMD, with an increased choroidal mast cell number observed in AMD tissue [584]. Further research suggests that tryptase (a highly abundant mast cell secretory granule-derived serine protease) is released during degranulation of choroidal mast cells, accumulating at the basement membrane in high levels in GA patients [585]. One important function of IL-33 is that it does not induce degranulation of mast cells, but rather “fine tunes” and potentiates IgE-mediated mast cell responses [203]. In addition to this, IL-33 orchestrates the initiation of the mast cell-mediated inflammatory response through the production of pro-inflammatory cytokines (IL-6 and TNFα) and Th2 cytokines (IL-5, IL-10 and IL-13) [205]. As

mast cells are implicated in disease development, interrogating the RPE/mast cell IL-33/ST2 axis is essential for furthering our understanding of IL-33 release in the context of early AMD pathology.

One aspect of this thesis entailed investigating how IL-33 release regulates homeostasis through maintenance of RPE function. As previously discussed, IL-33 acts in an autocrine manner when released to increase RPE mitochondrial respiration which protects against oxidative damage. I have additionally discussed how IL-33 likely serves to protect retinal homeostasis through recruitment of mononuclear cells and mast cells. Whilst these are essential to discuss, there is a need to consider how IL-33 functions in conditions of cellular stress below a threshold to which RPE are damaged and IL-33 is not released (potentially akin to the earliest stages of AMD development). Although, chronic low-grade inflammation is likely to contribute to RPE death through un-controlled tissue destruction, the initial response of RPE to cellular stress is not that of immediate death but rather activation of innate immune pathways. A consequence of RPE stress is the up-regulation of intrinsic IL-33 which retains its localisation in the nucleus. Studies show that IL-33 release from cells is unlikely to occur without damage due to a lack of signal sequence and canonical processing pathway (like that of IL-1β and IL-18) [134]. Therefore, IL-33, exhibiting nuclear localization signals and containing a homeobox Helix-Turn-Helix DNA binding motif ubiquitous to many transcription factors [136], likely contributes to the regulation of cellular function through nuclear mechanisms in the absence of cell death.

The nuclear role of IL-33 in the RPE was first assessed through probing protein interaction networks. The data presented in chapter 6 highlighted a robust IL-33 interaction network in RPE cells of both human and murine origin, converging on core histone-modifying and chromatin remodelling complexes (as expected considering previous observations [261]). As IL-33 was found to interact with components of the translation machinery, I hypothesised that IL-33 may also be involved in post-transcriptional regulation and this led to further proteomics-based experiments exploring the effect of IL-33 loss (or augmented expression) on the RPE proteome. Collectively, these data indicated that IL-33 directly impacted protein expression in RPE cells and emphasised a *bone fide* intrinsic role. The observation that alterations of IL-33 expression status in human and murine RPE cells led to a proteomic signature with enrichment in targets in metabolic function was of interest considering observations made in chapter 5. Therefore, one can assume that a consequence of nuclear IL-33 up-regulation in response to immune stress is for the control of the core-biosynthetic pathways. Upregulation of glycolysis in RPE cells through the action of nuclear IL-33, likely serves as an adaptive

mechanism, allowing the RPE to respond bioenergetically to the demands of an innate immune response (Figure 7.2).

While the role of endogenous IL-33 in the regulation of immune cell metabolism is multifaceted (discussed to a greater extent in section 1.9.3), it appears that its function converges on aspects of glycolytic and central carbon metabolism. In macrophages overexpressing IL-33, increased glucose uptake and lactate production are observed suggesting increases in glycolytic flux [444]. Cancer lines transfected to overexpress IL-33 exhibit a similar shift in metabolism [443]. Additionally, knockdown of endogenous IL-33 in synovial fibroblasts reduces HIF-1α expression [442]. These observations suggest that IL-33 is a key regulator of the glycolysis pathway and supports observations presented in this thesis, whereby overexpression of IL-33 in human RPE cells augmented glycolytic flux and pyruvate entry into the TCA cycle. The paradox that IL-33 appears to increase glycolytic metabolism when overexpressed and knocked-down in the RPE endows a level of complexity to its endogenous functions. Whilst data presented in chapter 5 indicates that RPE cells lacking IL-33 have increased ECAR (and lactate production) this does not necessarily translate to increased glycolysis. Through employing SITA, I found that IL-33 does not increase C^{13}-glucose labelling in any other metabolite except for lactate. Upon further investigation I observed defects in the expression of key pyruvate transporters MPC1 and 2 with IL-33 KD. Faults in the expression of these key import proteins are likely contributors to the increased ECAR observed (rather than glycolytic flux) as pyruvate is reduced to lactate. One cannot rule out the contribution of TCA cycle acidification to ECAR under these test conditions, as increased flux of fatty acid metabolites appear to support the TCA cycle. The metabolic phenotype of IL-33 KD RPE therefore appears to be that of increased mitochondrial fatty acid oxidation rather than enhanced glycolysis. Supporting the view of IL-33 as a key metabolic regulator, proteomic signatures from three lines of investigation identified significant enrichment of metabolic pathways that supported the functional analysis (seahorse). Pathway analysis of IL-33 overexpressing cells showed that up-regulation of glycolytic proteins formed one of the highest significance functional annotation clusters. Vice versa, RPE cells lacking IL-33 displayed increased enrichment of clusters containing proteins of mitochondrial metabolism and fatty acid oxidation. It is of interest to note that similar gene expression ontologies were significantly enriched in *Il33*$^{-/-}$ adipocytes [19], suggesting conserved roles in metabolic regulation across cell types. A schematic showing the metabolic phenotypes observed with alterations to IL-33 expression is shown in Figure 7.2.

Translating the observations made in this thesis regarding IL-33 expression and metabolic phenotype into the *in vivo* environment has interesting implications for RPE health and AMD pathogenesis. A previous observation that IL-33 expression status was altered in RPE cybrids from AMD "high-risk" haplotypes [18] highlighted contemporaneous changes in RPE metabolism and expression of IL-33 when mtDNA content changes. It was thus proposed that IL-33 acts as a signal in the RPE to adapt or maintain mitochondrial metabolism; a down-regulation in the expression status (as observed in "high-risk" AMD groups) would therefore have adverse effects on RPE metabolism and accelerate disease progression. Taking experimental data from chapter 5 into consideration, one would anticipate that this would be the case considering a loss of IL-33 impairs RPE spare respiratory capacity (suggesting damage to mitochondrial health). A decline in RPE mitochondrial function in animal models (e.g. loss of antioxidant enzymes in SOD1, SOD2 and NRF2-deficient mice [586-588] and loss of OXPHOS in mitochondrial transcription factor A-deficient mice [383]) leads to phenotypes resembling the clinical features of AMD development, namely RPE degeneration, photoreceptor decline of function and lipofuscin accumulation. However, we find no observable ocular phenotype in young IL-33-deficient mice (Unpublished data, Matthew Campbell, Trinity College Dublin). This raises the question on how clear metabolic differences observed *ex vivo* and *in vitro* do not translate into a phenotype *in vivo* which would impair RPE function. If we return our attention to the observation that RPE cells are not glycolytic *in vivo* it becomes clear how IL-33 loss may not be deleterious for retinal health. When RPE are cultured ex vivo they rapidly dedifferentiate [589] and switch to the use of glycolytic metabolism [381]. As IL-33 regulates the expression of MPC1 and 2, this manifests in the apparent increase in lactate production as RPE are forced to utilise glucose as a substrate. *In vivo,* glucose passes through the RPE monolayer and is utilised by photoreceptors [4]. An impairment in glucose-derived carbon input into the TCA cycle is therefore unlikely to affect RPE (unless required to adapt under stress) as their metabolism is supported by lactate, amino-acid and fatty acid catabolism [6, 374, 379]. It was interesting to note that the TCA cycle, mitochondrion and fatty acid oxidation were all significantly enriched GO terms in proteomics experiments from primary RPE lysates of *Il33*$^{-/-}$ mice. As these were not from *ex vivo* cultures, it suggested that core mitochondrial pathways were up-regulated in the absence of IL-33 *in vivo* and were not an adaptive response to maintain TCA cycle activity in the absence of pyruvate import. In addition to this, increased mitochondrial staining of retinal sections and mitochondrial number from EM

experiments suggest that mitochondria activity is augmented *in vivo*. Extrapolating from results in macrophages [444], upregulation IL-33 which likely serves to rewire RPE metabolism and enhance inflammatory responses. With defects in glucose metabolism with IL-33 loss, RPE cells likely exhibit an impaired ability to respond to endogenous stress signals, leaving chronic inflammation to persist unchecked. Future directions of this work will aim to observe how RPE cells with differential IL-33 expression respond to inflammatory signalling.

Taken together, this does not necessarily translate to the hypothesis that increasing IL-33 expression in RPE cells (whether that be through targeted gene therapy etc.) could be an attractive therapeutic adjuvant for early AMD. As previously discussed, IL-33 upregulation in cells serves as a switch to up-regulate glycolytic flux, providing rapid ATP synthesis for functional responses. The initial metabolic switch is protective from the point of view that RPE cells can respond and control inflammatory responses, but this likely occurs at the expense of photoreceptors (although there is no experimental data to show this to date). Depriving photoreceptors of glucose for extended periods leads to starvation and degeneration. Indeed, transgenic enhancement of mTOR-dependent glycolysis in mice leads to a progressive regional loss of photoreceptors [383]. Future work will be required to examine how overexpression of IL-33 affects RPE and photoreceptor health *in vivo*. Furthermore, as the regulation of IL-33 and concurrent metabolic shifts are likely a tightly regulated process, further work will be required to identify whether a down-regulation of IL-33 is required to restore the RPE β-oxidation program (see Figure 7.2.) In order to further understand the role played by intrinsic IL-33 during the innate response, work from this thesis will also need to be translated into the *in vivo* environment. *In vivo* C^{13} labelling will be essential to understand IL-33-mediated metabolic reprogramming without confounding factors, such as the adaptation of RPE to *in vitro* culture environment. As mentioned, transgenic models of IL-33-overexpressing RPE will likely be required to assess how enhancing RPE glycolysis will impact the rest of the retina.

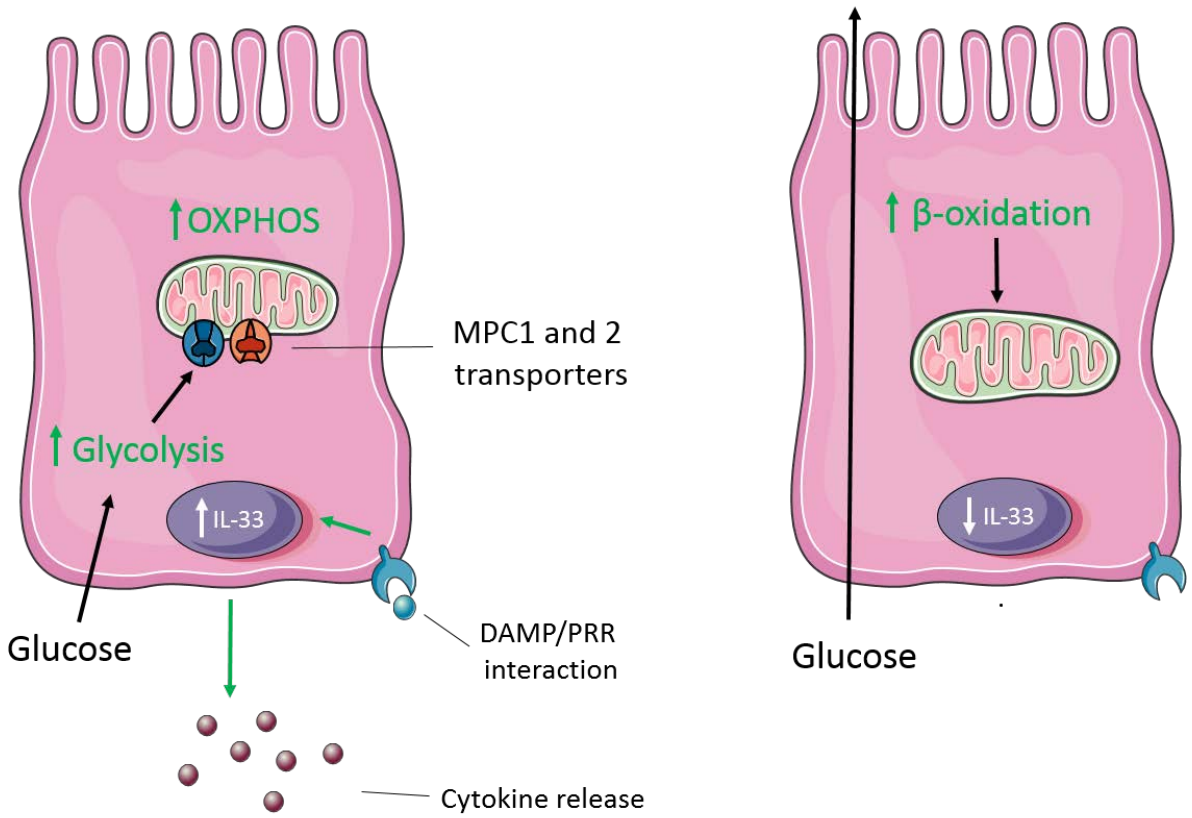

Figure 7.2. IL-33 regulates RPE metabolic adaptations in response to immune stressors:

In a heathy retina, RPE cells take up glucose through GLUT1 transporters, yet is not used as a metabolic substrate. Instead, glucose from the choroidal blood flow is shuttled to the photoreceptors for use in aerobic glycolysis. RPE cells are supported through β-oxidation and amino acid catabolic pathways, which feed into the TCA cycle. In response to innate immune stress signals (*left*), RPE cells increase the expression of nuclear IL-33 which in turn reprograms RPE metabolism towards a program of enhanced glycolysis. Pyruvate enters the mitochondrial through MPC 1 and 2 and is oxidised to produce ATP. The enhanced ATP produced from glycolysis is required to fuel the production and release of immunomodulatory cytokines. Downregulation of IL-33 (*right*) elicits a metabolic shift towards mitochondrial β-oxidation. As pyruvate entry into the mitochondria is impaired, ATP-production is likely supported by β-oxidation and glucose passage through the retina may be restored. IL-33, interleukin-33; MPC, mitochondrial pyruvate carrier; DAMP, danger-associated molecular pattern; PRR, pattern recognition receptor; RPE, retinal pigment epithelium; ATP, adenosine triphosphate; GLUT1, glucose transporter 1.

.

Data has demonstrated a key intrinsic role for the nuclear cytokine IL-33 in RPE cells. Despite gaining insight into how altering IL-33 expression status influences protein expression and thus basic cellular function (metabolism), the underlying endogenous function(s) of IL-33 remain elusive. Homology studies of the IL-33 protein indicated the presence of a helix-turn-helix domain [136] which when combined with its constitutive nuclear expression has led to the broad assumption that IL-33 binds directly to DNA. ChIP-RT-PCR studies have reported enrichment of IL-33 at the promoters of *IL13* and *IL1RL1* [254, 257] [258]. Despite these findings, there is insufficient evidence of IL-33 DNA binding and the mechanisms of its nuclear function. This likely stems to much of the research converging on its extracellular cytokine activity. However, this may be a result of a lack of suitable IL-33-specific ChIP-grade antibodies or simply that IL-33 does not exhibit DNA binding.

The preliminary experimental data (presented in appendices 10.5, page 405) suggests that the Nessy-1 antibody may unsuitable for ChIP, despite functioning well for immunoprecipitation and immunoblotting (see chapter 6). Library preparation was successful, yet peak splitting analysis revealed an extremely low peak number compared to what one might expect to see from a typical non-histone protein (99 with Nessy-1 compared to ~5,000 [590]). Despite a low peak number attained from the Nessy-1 antibody, ChIP peaks were investigated further to reveal a small number of annotated genes with IL-33 affinity. Most of these corresponded to non-coding regions/pseudogenes (indicative of background signal), leaving only 15 protein coding genes; none of which corresponded to *IL1RL1* or *IL13* (genes displaying an affinity for IL-33 in previous studies [257] [258]) (Table 10.6.4, page 414).

One may argue that that IL-33 may not exhibit extensive DNA binding in ARPE-19 cells and the small list of genes are in fact *bona fide* interactions. This, however, will require further investigation with additional IL-33 antibody(s). Moreover, a single biological replicate is insufficient to create conclusions on lack of nuclear function. Although, the data presented does not fit the hypothesis that IL-33 binds to DNA and exerts function on gene expression, there is uncertainty in the authenticity and reliability of the peaks.

As discussed in the conclusion of chapter 6, it is essential to take into consideration the contexts whereby IL-33 may not display “dual functional” properties and is localised to the nucleus to sequester its potent biological activity [230, 263]. IL-33 is undeniably a potent inflammatory cytokine with the

capacity to elicit overt inflammation when not sequestered to the nucleus [531]. Indeed, IL-33 lacking an N-terminal chromatin-binding domain is readily secreted from Müller glia and contributes to ST2-dependent inflammation and retinal cell loss [17]. Whilst the data presented in this thesis and a mass of other experimental evidence suggests an intrinsic role for IL-33 [10, 19, 223, 260, 261, 442], the observations that IL-33 has no transcriptional properties in certain systems cannot be ignored.

In summary, this thesis has explored the ability of the RPE to adapt metabolically to stress signals. I find that intrinsic IL-33 functions as a metabolic checkpoint to potentiate a bioenergetic switch to glycolysis, which in turn supports the bioenergetic demands of innate immune responses. Non-canonical intrinsic IL-33 responses likely serve to maintain metabolic and immune function, particularly within sensitive tissues such as the retina. The benefits of keeping RPE metabolic function and uncontrolled inflammatory responses in check is clear, especially when we consider the degenerative diseases such as AMD whereby a bioenergetic crisis and chronic inflammation likely contribute to the underlying pathology. Debatably, further investigation into the molecular mechanisms governing these processes will elucidate novel approaches that serve to prevent further disease development and restore tissue homeostasis.

The future directions of this work will be to investigate the nature of metabolic coupling within the retina and how this is influenced under conditions of innate immunological stress. As previously discussed, a caveat of this thesis is the lack of translation from *in vitro* studies and therefore, a lack of understanding to how metabolic reprogramming occurs *in vivo* when we consider the unique metabolic relationship shared between RPE cells, photoreceptors and Müller glia. The emergence of techniques such as *in vivo* C^{13} labelling will allow us to assess to what extent RPE glycolytic reprogramming occurs in animal models of innate immune stress, and how this affects export of metabolic intermediates into the retina. In addition to this, the translation of this work into an *in vivo* environment will allow us to dissect visual function and photoreceptor health, which one cannot achieve in 2D cell culture studies. This is essential for furthering our understanding of the complex interplay between innate immune responses and energy metabolism. It will be important to further assess the molecular mechanisms whereby intracellular immune-derived signals, drive metabolic adaptations of the RPE. Thus, we can employ alternative approaches that can target the “protective” aspects of innate immunity and restore metabolic health in the RPE, forestalling the insidious development of AMD.

Chapter 8. References

1. Whitcup, S.M., et al., *The role of the immune response in age-related macular degeneration.* Int J Inflam, 2013. **2013**: p. 348092.
2. Ambati, J., J.P. Atkinson, and B.D. Gelfand, *Immunology of age-related macular degeneration.* Nat Rev Immunol, 2013. **13**(6): p. 438-51.
3. Strauss, O., *The retinal pigment epithelium in visual function.* Physiol Rev, 2005. **85**(3): p. 845-81.
4. Kanow, M.A., et al., *Biochemical Adaptations Of The Retina And Retinal Pigment Epithelium Support A Metabolic Ecosystem In The Vertebrate Eye.* bioRxiv, 2017.
5. O'Neill, L.A.J., R.J. Kishton, and J. Rathmell, *A guide to immunometabolism for immunologists.* Nat Rev Immunol, 2016. **16**(9): p. 553-565.
6. Du, J., et al., *Reductive carboxylation is a major metabolic pathway in the retinal pigment epithelium.* Proceedings of the National Academy of Sciences, 2016. **113**(51): p. 14710-14715.
7. Qin, S., *Roles for AMP-activated protein kinase in RPE cell function.* Adv Exp Med Biol, 2012. **723**: p. 745-51.
8. Theodoropoulou, S., et al., *Interleukin-33 regulates tissue remodelling and inhibits angiogenesis in the eye.* J Pathol, 2016.
9. Martin, N.T. and M.U. Martin, *Interleukin 33 is a guardian of barriers and a local alarmin.* Nat Immunol, 2016. **17**(2): p. 122-31.
10. Ali, S., et al., *The dual function cytokine IL-33 interacts with the transcription factor NF-kappaB to dampen NF-kappaB-stimulated gene transcription.* J Immunol, 2011. **187**(4): p. 1609-16.
11. Garlanda, C., C.A. Dinarello, and A. Mantovani, *The interleukin-1 family: back to the future.* Immunity, 2013. **39**(6): p. 1003-18.
12. Lopetuso, L.R., S. Chowdhry, and T.T. Pizarro, *Opposing Functions of Classic and Novel IL-1 Family Members in Gut Health and Disease.* Front Immunol, 2013. **4**: p. 181.
13. Saluja, R., et al., *The role of the IL-33/IL-1RL1 axis in mast cell and basophil activation in allergic disorders.* Mol Immunol, 2015. **63**(1): p. 80-5.
14. Sanada, S., et al., *IL-33 and ST2 comprise a critical biomechanically induced and cardioprotective signaling system.* J Clin Invest, 2007. **117**(6): p. 1538-49.
15. Fu, A.K.Y., et al., *IL-33 ameliorates Alzheimer's disease-like pathology and cognitive decline.* Proceedings of the National Academy of Sciences, 2016. **113**(19): p. E2705-E2713.
16. Barbour, M., et al., *IL-33 attenuates the development of experimental autoimmune uveitis.* European Journal of Immunology, 2014. **44**(11): p. 3320-3329.
17. Xi, H., et al., *IL-33 amplifies an innate immune response in the degenerating retina.* The Journal of Experimental Medicine, 2016.
18. Kenney, M.C., et al., *Inherited mitochondrial DNA variants can affect complement, inflammation and apoptosis pathways: insights into mitochondrial-nuclear interactions.* Hum Mol Genet, 2014. **23**(13): p. 3537-51.
19. Odegaard, Justin I., et al., *Perinatal Licensing of Thermogenesis by IL-33 and ST2.* Cell, 2016. **166**(4): p. 841-854.
20. Forrester, J.V., et al., *Chapter 1 - Anatomy of the eye and orbit*, in *The Eye (Fourth Edition)*, J.V. Forrester, et al., Editors. 2016, W.B. Saunders. p. 1-102.e2.

21. Whitmore, S.S., et al., *Transcriptomic analysis across nasal, temporal, and macular regions of human neural retina and RPE/choroid by RNA-Seq.* Experimental eye research, 2014. **129**: p. 93-106.
22. Caspi, R.R., *A look at autoimmunity and inflammation in the eye.* The Journal of clinical investigation, 2010. **120**(9): p. 3073-3083.
23. Thumann, G., et al., *Chapter 16 - Cell Biology of the Retinal Pigment Epithelium*, in *Retina (Fifth Edition)*, S.J. Ryan, et al., Editors. 2013, W.B. Saunders: London. p. 401-414.
24. Boulton, M. and P. Dayhaw-Barker, *The role of the retinal pigment epithelium: Topographical variation and ageing changes.* Eye, 2001. **15**: p. 384.
25. Bergersen, L., et al., *Cellular and subcellular expression of monocarboxylate transporters in the pigment epithelium and retina of the rat.* Neuroscience, 1999. **90**(1): p. 319-331.
26. Pautler, E.L. and C. Tengerdy, *Transport of acidic amino acids by the bovine pigment epithelium.* Experimental Eye Research, 1986. **43**(2): p. 207-214.
27. Harik, S.I., et al., *Glucose transporters are abundant in cells with "occluding" junctions at the blood-eye barriers.* Proc Natl Acad Sci U S A, 1990. **87**(11): p. 4261-4.
28. Kevany, B.M. and K. Palczewski, *Phagocytosis of Retinal Rod and Cone Photoreceptors.* Physiology, 2010. **25**(1): p. 8-15.
29. Rakoczy, P.E., et al., *Distribution of cathepsin D in human eyes with or without age-related maculopathy.* Exp Eye Res, 1999. **69**(4): p. 367-74.
30. Keeling, E., et al., *Impaired Cargo Clearance in the Retinal Pigment Epithelium (RPE) Underlies Irreversible Blinding Diseases.* Cells, 2018. **7**(2).
31. Mazzitello, K.I., et al., *Formation and growth of lipofuscin in the retinal pigment epithelium cells.* Physical review. E, Statistical, nonlinear, and soft matter physics, 2009. **80**(5 Pt 1): p. 051908-051908.
32. Simó, R., et al., *The Retinal Pigment Epithelium: Something More than a Constituent of the Blood-Retinal Barrier—Implications for the Pathogenesis of Diabetic Retinopathy.* Journal of Biomedicine and Biotechnology, 2010. **2010**: p. 15.
33. Cai, J., et al., *Oxidative damage and protection of the RPE.* Progress in Retinal and Eye Research, 2000. **19**(2): p. 205-221.
34. Tate, D.J., Jr., M.V. Miceli, and D.A. Newsome, *Phagocytosis and H2O2 induce catalase and metallothionein gene expression in human retinal pigment epithelial cells.* Investigative Ophthalmology & Visual Science, 1995. **36**(7): p. 1271-1279.
35. Miceli, M.V., M.R. Liles, and D.A. Newsome, *Evaluation of Oxidative Processes in Human Pigment Epithelial Cells Associated with Retinal Outer Segment Phagocytosis.* Experimental Cell Research, 1994. **214**(1): p. 242-249.
36. Iacovelli, J., et al., *PGC-1α Induces Human RPE Oxidative Metabolism and Antioxidant Capacity.* Investigative Ophthalmology & Visual Science, 2016. **57**(3): p. 1038-1051.
37. Kay, P., Y.C. Yang, and L. Paraoan, *Directional protein secretion by the retinal pigment epithelium: roles in retinal health and the development of age-related macular degeneration.* Journal of Cellular and Molecular Medicine, 2013. **17**(7): p. 833-843.
38. Cayouette, M., et al., *Pigment epithelium-derived factor delays the death of photoreceptors in mouse models of inherited retinal degenerations.* Neurobiol Dis, 1999. **6**(6): p. 523-32.

39. De, S., et al., *Human retinal pigment epithelium cell changes and expression of alphaB-crystallin: a biomarker for retinal pigment epithelium cell change in age-related macular degeneration.* Arch Ophthalmol, 2007. **125**(5): p. 641-5.
40. Zhou, R. and R.R. Caspi, *Ocular immune privilege.* F1000 biology reports, 2010. **2**: p. 3.
41. Dick, A.D., *Doyne lecture 2016: intraocular health and the many faces of inflammation.* Eye, 2017. **31**(1): p. 87-96.
42. Farrokh-Siar, L., et al., *Human fetal retinal pigment epithelium suppresses the activation of CD4(+) and CD8(+) T-cells.* Graefes Arch Clin Exp Ophthalmol, 1999. **237**(11): p. 934-9.
43. Horie, S., et al., *Human retinal pigment epithelium-induced CD4+CD25+ regulatory T cells suppress activation of intraocular effector T cells.* Clinical Immunology, 2010. **136**(1): p. 83-95.
44. Detrick, B. and J.J. Hooks, *Immune regulation in the retina.* Immunol Res, 2010. **47**(1-3): p. 153-61.
45. Kumar, M.V., et al., *Innate immunity in the retina: Toll-like receptor (TLR) signaling in human retinal pigment epithelial cells.* J Neuroimmunol, 2004. **153**(1-2): p. 7-15.
46. Percopo, C.M., et al., *Cytokine-mediated activation of a neuronal retinal resident cell provokes antigen presentation.* J Immunol, 1990. **145**(12): p. 4101-7.
47. Doyle, S.L., et al., *NLRP3 has a protective role in age-related macular degeneration through the induction of IL-18 by drusen components.* Nat Med, 2012. **18**(5): p. 791-8.
48. Zhang, S., et al., *Interleukin-17A Induces IL-1beta Secretion From RPE Cells Via the NLRP3 Inflammasome.* Invest Ophthalmol Vis Sci, 2016. **57**(2): p. 312-9.
49. Holtkamp, G.M., et al., *Retinal Pigment Epithelium-immune System Interactions: Cytokine Production and Cytokine-induced Changes.* Progress in Retinal and Eye Research, 2001. **20**(1): p. 29-48.
50. Kim, Y.H., et al., *Regulated secretion of complement factor H by RPE and its role in RPE migration.* Graefes Arch Clin Exp Ophthalmol, 2009. **247**(5): p. 651-9.
51. Yoshida, A., et al., *Differential Chemokine Regulation by Th2 Cytokines during Human RPE–Monocyte Coculture.* Investigative Ophthalmology & Visual Science, 2001. **42**(7): p. 1631-1638.
52. Rein, D.B., et al., *Forecasting Age-Related Macular Degeneration Through the Year 2050: The Potential Impact of New Treatments.* Archives of Ophthalmology, 2009. **127**(4): p. 533-540.
53. Rosenfeld, P.J., et al., *Ranibizumab for Neovascular Age-Related Macular Degeneration.* New England Journal of Medicine, 2006. **355**(14): p. 1419-1431.
54. van Lookeren Campagne, M., et al., *Mechanisms of age-related macular degeneration and therapeutic opportunities.* J Pathol, 2014. **232**(2): p. 151-64.
55. Ambati, J., et al., *Age-Related Macular Degeneration: Etiology, Pathogenesis, and Therapeutic Strategies.* Survey of Ophthalmology, 2003. **48**(3): p. 257-293.
56. Copland, D.A., et al., *A Perspective of AMD Through the Eyes of ImmunologyAMD, Immunology, and Inflammation.* Investigative Ophthalmology & Visual Science, 2018. **59**(4): p. AMD83-AMD92.
57. Chen, M. and H. Xu, *Parainflammation, chronic inflammation and age-related macular degeneration.* Journal of leukocyte biology, 2015. **98**(5): p. 713-725.

58. Janeway, C.A., Jr. and R. Medzhitov, *Innate immune recognition.* Annu Rev Immunol, 2002. **20**: p. 197-216.
59. Cooper, M.D. and M.N. Alder, *The Evolution of Adaptive Immune Systems.* Cell, 2006. **124**(4): p. 815-822.
60. Bryant, C.E. and T.P. Monie, *Mice, men and the relatives: cross-species studies underpin innate immunity.* Open Biol, 2012. **2**(4): p. 120015.
61. Akira, S., K. Takeda, and T. Kaisho, *Toll-like receptors: critical proteins linking innate and acquired immunity.* Nat Immunol, 2001. **2**(8): p. 675-680.
62. Mai, K., et al., *Role of toll-like receptors in human iris pigment epithelial cells and their response to pathogen-associated molecular patterns.* J Inflamm (Lond), 2014. **11**: p. 20.
63. Ebihara, N., et al., *Distinct functions between toll-like receptors 3 and 9 in retinal pigment epithelial cells.* Ophthalmic Res, 2007. **39**(3): p. 155-63.
64. Kawasaki, T. and T. Kawai, *Toll-like receptor signaling pathways.* Frontiers in immunology, 2014. **5**: p. 461-461.
65. Hoebe, K., et al., *Upregulation of costimulatory molecules induced by lipopolysaccharide and double-stranded RNA occurs by Trif-dependent and Trif-independent pathways.* Nat Immunol, 2003. **4**(12): p. 1223-1229.
66. Chen, G., et al., *NOD-Like Receptors: Role in Innate Immunity and Inflammatory Disease.* Annual Review of Pathology: Mechanisms of Disease, 2009. **4**(1): p. 365-398.
67. Ting, J.P.Y., et al., *The NLR Gene Family: A Standard Nomenclature.* Immunity, 2008. **28**(3): p. 285-287.
68. Lopez-Castejon, G. and D. Brough, *Understanding the mechanism of IL-1beta secretion.* Cytokine Growth Factor Rev, 2011. **22**(4): p. 189-95.
69. Baroja-Mazo, A., et al., *The NLRP3 inflammasome is released as a particulate danger signal that amplifies the inflammatory response.* Nat Immunol, 2014. **15**(8): p. 738-748.
70. Perregaux, D. and C.A. Gabel, *Interleukin-1 beta maturation and release in response to ATP and nigericin. Evidence that potassium depletion mediated by these agents is a necessary and common feature of their activity.* J Biol Chem, 1994. **269**(21): p. 15195-203.
71. Shimada, K., et al., *Oxidized mitochondrial DNA activates the NLRP3 inflammasome during apoptosis.* Immunity, 2012. **36**(3): p. 401-14.
72. Sanman, L.E., et al., *Disruption of glycolytic flux is a signal for inflammasome signaling and pyroptotic cell death.* Elife, 2016. **5**: p. e13663.
73. Heid, M.E., et al., *Mitochondrial reactive oxygen species induces NLRP3-dependent lysosomal damage and inflammasome activation.* J Immunol, 2013. **191**(10): p. 5230-8.
74. Murakami, T., et al., *Critical role for calcium mobilization in activation of the NLRP3 inflammasome.* Proc Natl Acad Sci U S A, 2012. **109**(28): p. 11282-7.
75. Elinav, E., et al., *NLRP6 inflammasome regulates colonic microbial ecology and risk for colitis.* Cell, 2011. **145**(5): p. 745-57.
76. Kayagaki, N., et al., *Non-canonical inflammasome activation targets caspase-11.* Nature, 2011. **479**(7371): p. 117-21.
77. Sarma, J.V. and P.A. Ward, *The Complement System.* Cell and tissue research, 2011. **343**(1): p. 227-235.

78. Hovingh, E.S., B. van den Broek, and I. Jongerius, *Hijacking Complement Regulatory Proteins for Bacterial Immune Evasion.* Front Microbiol, 2016. **7**: p. 2004.
79. Luo, C., et al., *Complement expression in retinal pigment epithelial cells is modulated by activated macrophages.* Experimental Eye Research, 2013. **112**: p. 93-101.
80. Varela, J.C. and S. Tomlinson, *COMPLEMENT: AN OVERVIEW FOR THE CLINICIAN.* Hematology/oncology clinics of North America, 2015. **29**(3): p. 409-427.
81. Huber-Lang, M., et al., *Generation of C5a in the absence of C3: a new complement activation pathway.* Nature Medicine, 2006. **12**: p. 682.
82. Kolev, M., G.L. Friec, and C. Kemper, *Complement — tapping into new sites and effector systems.* Nature Reviews Immunology, 2014. **14**: p. 811.
83. Medzhitov, R., *Origin and physiological roles of inflammation.* Nature, 2008. **454**(7203): p. 428-435.
84. Mangge, H., et al., *Inflammation, adiponectin, obesity and cardiovascular risk.* Curr Med Chem, 2010. **17**(36): p. 4511-20.
85. Lathe, R., A. Sapronova, and Y. Kotelevtsev, *Atherosclerosis and Alzheimer--diseases with a common cause? Inflammation, oxysterols, vasculature.* BMC Geriatr, 2014. **14**: p. 36.
86. Shaw, P.X., et al., *Oxidative stress, innate immunity, and age-related macular degeneration.* AIMS molecular science, 2016. **3**(2): p. 196-221.
87. Yu, L., L. Wang, and S. Chen, *Endogenous toll-like receptor ligands and their biological significance.* Journal of cellular and molecular medicine, 2010. **14**(11): p. 2592-2603.
88. Hageman, G.S., et al., *A common haplotype in the complement regulatory gene factor H (HF1/CFH) predisposes individuals to age-related macular degeneration.* Proc Natl Acad Sci U S A, 2005. **102**(20): p. 7227-32.
89. Fagerness, J.A., et al., *Variation near complement factor I is associated with risk of advanced AMD.* Eur J Hum Genet, 2009. **17**(1): p. 100-4.
90. Francis, P.J., et al., *Polymorphisms in C2, CFB and C3 are associated with progression to advanced age related macular degeneration associated with visual loss.* J Med Genet, 2009. **46**(5): p. 300-7.
91. Tuo, J., et al., *The involvement of sequence variation and expression of CX3CR1 in the pathogenesis of age-related macular degeneration.* Faseb j, 2004. **18**(11): p. 1297-9.
92. Falk, M.K., et al., *CX3CL1/CX3CR1 and CCL2/CCR2 chemokine/chemokine receptor complex in patients with AMD.* PLoS One, 2014. **9**(12): p. e112473.
93. Yang, Z., et al., *Toll-like receptor 3 and geographic atrophy in age-related macular degeneration.* N Engl J Med, 2008. **359**(14): p. 1456-63.
94. Zareparsi, S., et al., *Toll-like receptor 4 variant D299G is associated with susceptibility to age-related macular degeneration.* Hum Mol Genet, 2005. **14**(11): p. 1449-55.
95. Zhu, Y., et al., *C5a and toll-like receptor 4 crosstalk in retinal pigment epithelial cells.* Mol Vis, 2015. **21**: p. 1122-9.
96. Kindzelskii, A.L., et al., *Toll-Like Receptor 4 (TLR4) of Retinal Pigment Epithelial Cells Participates in Transmembrane Signaling in Response to Photoreceptor Outer Segments.* The Journal of General Physiology, 2004. **124**(2): p. 139-149.
97. Yi, H., et al., *Novel role for the innate immune receptor Toll-like receptor 4 (TLR4) in the regulation of the Wnt signaling pathway and photoreceptor apoptosis.* PLoS One, 2012. **7**(5): p. e36560.
98. Guven, M., et al., *Toll-Like Receptors 2 and 4 Polymorphisms in Age-Related Macular Degeneration.* Curr Eye Res, 2016. **41**(6): p. 856-61.

99. Cho, Y., et al., *Toll-like receptor polymorphisms and age-related macular degeneration: replication in three case-control samples.* Invest Ophthalmol Vis Sci, 2009. **50**(12): p. 5614-8.
100. Kaneko, H., et al., *DICER1 deficit induces Alu RNA toxicity in age-related macular degeneration.* Nature, 2011. **471**(7338): p. 325-30.
101. Bernard, J.J., et al., *Ultraviolet radiation damages self noncoding RNA and is detected by TLR3.* Nat Med, 2012. **18**(8): p. 1286-1290.
102. Klein, M.L., et al., *Progression of geographic atrophy and genotype in age-related macular degeneration.* Ophthalmology, 2010. **117**(8): p. 1554-9, 1559.e1.
103. Zhou, P., et al., *Toll-like receptor 3 C1234T may protect against geographic atrophy through decreased dsRNA binding capacity.* Faseb j, 2011. **25**(10): p. 3489-95.
104. Ma, L., et al., *Association of toll-like receptor 3 polymorphism rs3775291 with age-related macular degeneration: a systematic review and meta-analysis.* Scientific Reports, 2016. **6**: p. 19718.
105. Patel, A.K. and A.S. Hackam, *Toll-like receptor 3 (TLR3) protects retinal pigmented epithelium (RPE) cells from oxidative stress through a STAT3-dependent mechanism.* Molecular Immunology, 2013. **54**(2): p. 122-131.
106. Ehlers, M. and J.V. Ravetch, *Opposing effects of Toll-like receptor stimulation induce autoimmunity or tolerance.* Trends Immunol, 2007. **28**(2): p. 74-9.
107. Liu, R.T., et al., *Inflammatory mediators induced by amyloid-beta in the retina and RPE in vivo: implications for inflammasome activation in age-related macular degeneration.* Invest Ophthalmol Vis Sci, 2013. **54**(3): p. 2225-37.
108. Asgari, E., et al., *C3a modulates IL-1beta secretion in human monocytes by regulating ATP efflux and subsequent NLRP3 inflammasome activation.* Blood, 2013. **122**(20): p. 3473-81.
109. Kauppinen, A., et al., *Oxidative stress activates NLRP3 inflammasomes in ARPE-19 cells--implications for age-related macular degeneration (AMD).* Immunol Lett, 2012. **147**(1-2): p. 29-33.
110. Tarallo, V., et al., *DICER1 loss and Alu RNA induce age-related macular degeneration via the NLRP3 inflammasome and MyD88.* Cell, 2012. **149**(4): p. 847-59.
111. Doyle, S.L., et al., *IL-18 Attenuates Experimental Choroidal Neovascularization as a Potential Therapy for Wet Age-Related Macular Degeneration.* Science Translational Medicine, 2014. **6**(230): p. 230ra44-230ra44.
112. Nozaki, M., et al., *Drusen complement components C3a and C5a promote choroidal neovascularization.* Proc Natl Acad Sci U S A, 2006. **103**(7): p. 2328-33.
113. Anderson, D.H., et al., *Characterization of β amyloid assemblies in drusen: the deposits associated with aging and age-related macular degeneration.* Experimental Eye Research, 2004. **78**(2): p. 243-256.
114. Anderson, O.A., A. Finkelstein, and D.T. Shima, *A2E Induces IL-1ß Production in Retinal Pigment Epithelial Cells via the NLRP3 Inflammasome.* PLOS ONE, 2013. **8**(6): p. e67263.
115. Zhou, J., et al., *Complement activation by photooxidation products of A2E, a lipofuscin constituent of the retinal pigment epithelium.* Proc Natl Acad Sci U S A, 2006. **103**(44): p. 16182-7.
116. Anderson, D.H., et al., *The pivotal role of the complement system in aging and age-related macular degeneration: Hypothesis re-visited.* Progress in Retinal and Eye Research, 2010. **29**(2): p. 95-112.

117. Edwards, A.O., et al., *Complement Factor H Polymorphism and Age-Related Macular Degeneration.* Science, 2005. **308**(5720): p. 421.
118. Gold, B., et al., *Variation in factor B (BF) and complement component 2 (C2) genes is associated with age-related macular degeneration.* Nature Genetics, 2006. **38**: p. 458.
119. Klaver, C.C., et al., *Complement Component C3 and Risk of Age-Related Macular Degeneration.* Investigative Ophthalmology & Visual Science, 2008. **49**(13): p. 2663-2663.
120. Klein, R.J., et al., *Complement factor H polymorphism in age-related macular degeneration.* Science, 2005. **308**(5720): p. 385-9.
121. Toomey, C.B., et al., *Regulation of age-related macular degeneration-like pathology by complement factor H.* Proceedings of the National Academy of Sciences of the United States of America, 2015. **112**(23): p. E3040-E3049.
122. Fritsche, L.G., et al., *Age-related macular degeneration: genetics and biology coming together.* Annu Rev Genomics Hum Genet, 2014. **15**: p. 151-71.
123. Netea, M.G., et al., *Inflammasome-Independent Regulation of IL-1-Family Cytokines.* Annual Review of Immunology, 2015. **33**(1): p. 49-77.
124. Sims, J.E. and D.E. Smith, *The IL-1 family: regulators of immunity.* Nat Rev Immunol, 2010. **10**(2): p. 89-102.
125. Abderrazak, A., et al., *NLRP3 inflammasome: From a danger signal sensor to a regulatory node of oxidative stress and inflammatory diseases.* Redox Biology, 2015. **4**: p. 296-307.
126. Miller, A.C., et al., *Decreased content of the IL1 alpha processing enzyme calpain in murine bone marrow-derived macrophages after treatment with the benzene metabolite hydroquinone.* Toxicol Lett, 1994. **74**(2): p. 177-84.
127. Dunne, A. and L.A. O'Neill, *The interleukin-1 receptor/Toll-like receptor superfamily: signal transduction during inflammation and host defense.* Sci STKE, 2003. **2003**(171): p. re3.
128. Wang, P., et al., *The interleukin-1-related cytokine IL-1F8 is expressed in glial cells, but fails to induce IL-1beta signalling responses.* Cytokine, 2005. **29**(6): p. 245-50.
129. Nakanishi, K., et al., *Interleukin-18 regulates both Th1 and Th2 responses.* Annu Rev Immunol, 2001. **19**: p. 423-74.
130. Lee, J.-K., et al., *Differences in signaling pathways by IL-1β and IL-18.* Proceedings of the National Academy of Sciences of the United States of America, 2004. **101**(23): p. 8815-8820.
131. Nold, M.F., et al., *IL-37 is a fundamental inhibitor of innate immunity.* Nat Immunol, 2010. **11**(11): p. 1014-1022.
132. Dinarello, C., et al., *IL-1 family nomenclature.* Nat Immunol, 2010. **11**(11): p. 973.
133. Schmitz, J., et al., *IL-33, an interleukin-1-like cytokine that signals via the IL-1 receptor-related protein ST2 and induces T helper type 2-associated cytokines.* Immunity, 2005. **23**(5): p. 479-90.
134. Liew, F.Y., J.P. Girard, and H.R. Turnquist, *Interleukin-33 in health and disease.* Nat Rev Immunol, 2016. **16**(11): p. 676-689.
135. Onda, H., et al., *Identification of genes differentially expressed in canine vasospastic cerebral arteries after subarachnoid hemorrhage.* J Cereb Blood Flow Metab, 1999. **19**(11): p. 1279-88.

136. Baekkevold, E.S., et al., *Molecular characterization of NF-HEV, a nuclear factor preferentially expressed in human high endothelial venules.* Am J Pathol, 2003. **163**(1): p. 69-79.
137. Moussion, C., N. Ortega, and J.P. Girard, *The IL-1-like cytokine IL-33 is constitutively expressed in the nucleus of endothelial cells and epithelial cells in vivo: a novel 'alarmin'?* PLoS One, 2008. **3**(10): p. e3331.
138. Ohno, T., et al., *Caspase-1, caspase-8, and calpain are dispensable for IL-33 release by macrophages.* J Immunol, 2009. **183**(12): p. 7890-7.
139. Talabot-Ayer, D., et al., *The mouse interleukin (Il)33 gene is expressed in a cell type- and stimulus-dependent manner from two alternative promoters.* J Leukoc Biol, 2012. **91**(1): p. 119-25.
140. Nile, C.J., et al., *Expression and regulation of interleukin-33 in human monocytes.* Immunology, 2010. **130**(2): p. 172-80.
141. Abston, E.D., et al., *IL-33 independently induces eosinophilic pericarditis and cardiac dilation: ST2 improves cardiac function.* Circ Heart Fail, 2012. **5**(3): p. 366-75.
142. Xu, D., et al., *IL-33 exacerbates autoantibody-induced arthritis.* J Immunol, 2010. **184**(5): p. 2620-6.
143. Athari, S.K., et al., *Collagen-induced arthritis and imiquimod-induced psoriasis develop independently of interleukin-33.* Arthritis Res Ther, 2016. **18**(1): p. 143.
144. Korhonen, P., et al., *Immunomodulation by interleukin-33 is protective in stroke through modulation of inflammation.* Brain Behav Immun, 2015. **49**: p. 322-36.
145. Pomeshchik, Y., et al., *Interleukin-33 treatment reduces secondary injury and improves functional recovery after contusion spinal cord injury.* Brain Behav Immun, 2015. **44**: p. 68-81.
146. Cayrol, C. and J.-P. Girard, *IL-33: an alarmin cytokine with crucial roles in innate immunity, inflammation and allergy.* Current Opinion in Immunology, 2014. **31**: p. 31-37.
147. Boraschi, D. and A. Tagliabue, *The interleukin-1 receptor family.* Seminars in Immunology, 2013. **25**(6): p. 394-407.
148. Loiarro, M., V. Ruggiero, and C. Sette, *Targeting TLR/IL-1R Signalling in Human Diseases.* Mediators of Inflammation, 2010. **2010**: p. 674363.
149. Ali, S., et al., *IL-1 receptor accessory protein is essential for IL-33-induced activation of T lymphocytes and mast cells.* Proc Natl Acad Sci U S A, 2007. **104**(47): p. 18660-5.
150. Funakoshi-Tago, M., et al., *TRAF6 is a critical signal transducer in IL-33 signaling pathway.* Cellular Signalling, 2008. **20**(9): p. 1679-1686.
151. Zhao, Q. and G. Chen, *Role of IL-33 and its receptor in T cell-mediated autoimmune diseases.* BioMed research international, 2014. **2014**: p. 587376-587376.
152. Xu, D., et al., *Selective Expression of a Stable Cell Surface Molecule on Type 2 but Not Type 1 Helper T Cells.* The Journal of Experimental Medicine, 1998. **187**(5): p. 787.
153. Löhning, M., et al., *T1/ST2 is preferentially expressed on murine Th2 cells, independent of interleukin 4, interleukin 5, and interleukin 10, and important for Th2 effector function.* Proceedings of the National Academy of Sciences, 1998. **95**(12): p. 6930.
154. Monticelli, L.A., et al., *Innate lymphoid cells promote lung-tissue homeostasis after infection with influenza virus.* Nature Immunology, 2011. **12**: p. 1045.

155. Smithgall, M.D., et al., *IL-33 amplifies both Th1- and Th2-type responses through its activity on human basophils, allergen-reactive Th2 cells, iNKT and NK Cells.* International Immunology, 2008. **20**(8): p. 1019-1030.
156. Bourgeois, E., et al., *The pro-Th2 cytokine IL-33 directly interacts with invariant NKT and NK cells to induce IFN-γ production.* European Journal of Immunology, 2009. **39**(4): p. 1046-1055.
157. Baumann, C., et al., *T-bet– and STAT4–dependent IL-33 receptor expression directly promotes antiviral Th1 cell responses.* Proceedings of the National Academy of Sciences, 2015. **112**(13): p. 4056.
158. Bonilla, W.V., et al., *The Alarmin Interleukin-33 Drives Protective Antiviral CD8⁺ T Cell Responses.* Science, 2012. **335**(6071): p. 984.
159. Schiering, C., et al., *The alarmin IL-33 promotes regulatory T-cell function in the intestine.* Nature, 2014. **513**: p. 564.
160. Komai-Koma, M., et al., *IL-33 Activates B1 Cells and Exacerbates Contact Sensitivity.* The Journal of Immunology, 2011. **186**(4): p. 2584.
161. Sattler, S., et al., *IL-10-producing regulatory B cells induced by IL-33 (Breg(IL-33)) effectively attenuate mucosal inflammatory responses in the gut().* Journal of Autoimmunity, 2014. **50**(100): p. 107-122.
162. Peine, M., R.M. Marek, and M. Löhning, *IL-33 in T Cell Differentiation, Function, and Immune Homeostasis.* Trends in Immunology, 2016. **37**(5): p. 321-333.
163. Yang, Q., et al., *IL-33 synergizes with TCR and IL-12 signaling to promote the effector function of CD8+ T cells.* European Journal of Immunology, 2011. **41**(11): p. 3351-3360.
164. Salmond, R.J., et al., *IL-33 induces innate lymphoid cell-mediated airway inflammation by activating mammalian target of rapamycin.* J Allergy Clin Immunol, 2012. **130**(5): p. 1159-1166.e6.
165. Guo, L., et al., *IL-1 family members and STAT activators induce cytokine production by Th2, Th17, and Th1 cells.* Proceedings of the National Academy of Sciences, 2009. **106**(32): p. 13463.
166. Meisel, C., et al., *Regulation and Function of T1/ST2 Expression on CD4⁺ T Cells: Induction of Type 2 Cytokine Production by T1/ST2 Cross-Linking.* The Journal of Immunology, 2001. **166**(5): p. 3143.
167. Nabekura, T., J.P. Girard, and L.L. Lanier, *IL-33 receptor ST2 amplifies the expansion of NK cells and enhances host defense during mouse cytomegalovirus infection.* J Immunol, 2015. **194**(12): p. 5948-52.
168. Montecino-Rodriguez, E., et al., *Distinct Genetic Networks Orchestrate the Emergence of Specific Waves of Fetal and Adult B-1 and B-2 Development.* Immunity, 2016. **45**(3): p. 527-539.
169. Arima, H., et al., *Notch1-Activated B Cells Have an Immunomodulatory Function Enhancing Th2 and Treg Immune Response Via IL-33-ST2 Pathway.* Blood, 2016. **128**(22): p. 130.
170. Mauri, C. and M.R. Ehrenstein, *The 'short' history of regulatory B cells.* Trends Immunol, 2008. **29**(1): p. 34-40.
171. Artis, D. and H. Spits, *The biology of innate lymphoid cells.* Nature, 2015. **517**(7534): p. 293-301.
172. Neill, D.R., et al., *Nuocytes represent a new innate effector leukocyte that mediates type-2 immunity.* Nature, 2010. **464**(7293): p. 1367-70.

173. Hoyler, T., et al., *The transcription factor GATA-3 controls cell fate and maintenance of type 2 innate lymphoid cells.* Immunity, 2012. **37**(4): p. 634-48.
174. Stier, M.T., et al., *IL-33 promotes the egress of group 2 innate lymphoid cells from the bone marrow.* The Journal of Experimental Medicine, 2018. **215**(1): p. 263-281.
175. Rak, G.D., et al., *IL-33-Dependent Group 2 Innate Lymphoid Cells Promote Cutaneous Wound Healing.* Journal of Investigative Dermatology, 2016. **136**(2): p. 487-496.
176. Johnston, L.K. and P.J. Bryce, *Understanding Interleukin 33 and Its Roles in Eosinophil Development.* Frontiers in Medicine, 2017. **4**: p. 51.
177. Drissen, R., et al., *Distinct myeloid progenitor-differentiation pathways identified through single-cell RNA sequencing.* Nat Immunol, 2016. **17**(6): p. 666-676.
178. Suzukawa, M., et al., *Interleukin-33 enhances adhesion, CD11b expression and survival in human eosinophils.* Lab Invest, 2008. **88**(11): p. 1245-53.
179. Willebrand, R. and D. Voehringer, *IL-33-Induced Cytokine Secretion and Survival of Mouse Eosinophils Is Promoted by Autocrine GM-CSF.* PLOS ONE, 2016. **11**(9): p. e0163751.
180. Cherry, W.B., et al., *A novel IL-1 family cytokine, IL-33, potently activates human eosinophils.* J Allergy Clin Immunol, 2008. **121**(6): p. 1484-90.
181. Bouffi, C., et al., *IL-33 Markedly Activates Murine Eosinophils by an NF-κB–Dependent Mechanism Differentially Dependent upon an IL-4–Driven Autoinflammatory Loop.* The Journal of Immunology, 2013. **191**(8): p. 4317.
182. Wen, T., et al., *Eosinophil adoptive transfer system to directly evaluate pulmonary eosinophil trafficking in vivo.* Proc Natl Acad Sci U S A, 2013. **110**(15): p. 6067-72.
183. Pecaric-Petkovic, T., et al., *Human basophils and eosinophils are the direct target leukocytes of the novel IL-1 family member IL-33.* Blood, 2009. **113**(7): p. 1526.
184. Suzukawa, M., et al., *An IL-1 Cytokine Member, IL-33, Induces Human Basophil Activation via Its ST2 Receptor.* The Journal of Immunology, 2008. **181**(9): p. 5981.
185. Silver, M.R., et al., *IL-33 synergizes with IgE-dependent and IgE-independent agents to promote mast cell and basophil activation.* Inflammation Research, 2010. **59**(3): p. 207-218.
186. Le, H.T., et al., *IL-33 Priming Regulates Multiple Steps of the Neutrophil-Mediated Anti-Candida albicans Response by Modulating TLR and Dectin-1 Signals.* The Journal of Immunology, 2012. **189**(1): p. 287.
187. Hueber, A.J., et al., *IL-33 induces skin inflammation with mast cell and neutrophil activation.* European Journal of Immunology, 2011. **41**(8): p. 2229-2237.
188. Enoksson, M., et al., *Intraperitoneal influx of neutrophils in response to IL-33 is mast cell–dependent.* Blood, 2013. **121**(3): p. 530.
189. Carri, et al., *Endogenous IL-33 Deficiency Exacerbates Liver Injury and Increases Hepatic Influx of Neutrophils in Acute Murine Viral Hepatitis.* Mediators of Inflammation, 2017. **2017**: p. 15.
190. Sun, B., et al., *Characterization and allergic role of IL-33-induced neutrophil polarization.* Cellular And Molecular Immunology, 2018.
191. Xu, J., et al., *IL33-mediated ILC2 activation and neutrophil IL5 production in the lung response after severe trauma: A reverse translation study from a human cohort to a mouse trauma model.* PLOS Medicine, 2017. **14**(7): p. e1002365.
192. Liang, Y., et al., *IL-33 induces immunosuppressive neutrophils via a type 2 innate lymphoid cell/IL-13/STAT6 axis and protects the liver against injury in LCMV infection-induced viral hepatitis.* Cellular And Molecular Immunology, 2018.

193. Moritz, D.R., et al., *The IL-1 receptor-related T1 antigen is expressed on immature and mature mast cells and on fetal blood mast cell progenitors.* J Immunol, 1998. **161**(9): p. 4866-74.
194. Drube, S., et al., *The receptor tyrosine kinase c-Kit controls IL-33 receptor signaling in mast cells.* Blood, 2010. **115**(19): p. 3899-906.
195. Allakhverdi, Z., et al., *Cutting Edge: The ST2 Ligand IL-33 Potently Activates and Drives Maturation of Human Mast Cells.* The Journal of Immunology, 2007. **179**(4): p. 2051.
196. Wang, J.-X., et al., *IL-33/ST2 axis promotes mast cell survival via BCLXL.* Proceedings of the National Academy of Sciences, 2014. **111**(28): p. 10281.
197. Moulin, D., et al., *Interleukin (IL)-33 induces the release of pro-inflammatory mediators by mast cells.* Cytokine, 2007. **40**(3): p. 216-225.
198. Ho, L.H., et al., *IL-33 induces IL-13 production by mouse mast cells independently of IgE-FcεRI signals.* Journal of Leukocyte Biology, 2007. **82**(6): p. 1481-1490.
199. Andrade, M.V., et al., *Amplification of cytokine production through synergistic activation of NFAT and AP-1 following stimulation of mast cells with antigen and IL-33.* European Journal of Immunology, 2011. **41**(3): p. 760-772.
200. Morita, H., et al., *An Interleukin-33-Mast Cell-Interleukin-2 Axis Suppresses Papain-Induced Allergic Inflammation by Promoting Regulatory T Cell Numbers.* Immunity, 2015. **43**(1): p. 175-86.
201. Cho, K.A., et al., *IL-33 induces Th17-mediated airway inflammation via mast cells in ovalbumin-challenged mice.* Am J Physiol Lung Cell Mol Physiol, 2012. **302**(4): p. L429-40.
202. Ball, D.H., et al., *IL-33/ST2 signalling and crosstalk with FcεRI and TLR4 is targeted by the parasitic worm product, ES-62.* Scientific Reports, 2018. **8**(1): p. 4497.
203. Joulia, R., et al., *IL-33 fine tunes mast cell degranulation and chemokine production at the single-cell level.* Journal of Allergy and Clinical Immunology, 2017. **140**(2): p. 497-509.e10.
204. Komai-Koma, M., et al., *Interleukin-33 amplifies IgE synthesis and triggers mast cell degranulation via interleukin-4 in naïve mice.* Allergy, 2012. **67**(9): p. 1118-1126.
205. Enoksson, M., et al., *Mast Cells as Sensors of Cell Injury through IL-33 Recognition.* The Journal of Immunology, 2011. **186**(4): p. 2523.
206. Murray, P.J. and T.A. Wynn, *Protective and pathogenic functions of macrophage subsets.* Nature Reviews Immunology, 2011. **11**: p. 723.
207. Kurowska-Stolarska, M., et al., *IL-33 amplifies the polarization of alternatively activated macrophages that contribute to airway inflammation.* J Immunol, 2009. **183**(10): p. 6469-77.
208. Joshi, A.D., et al., *Interleukin-33 contributes to both M1 and M2 chemokine marker expression in human macrophages.* BMC Immunology, 2010. **11**(1): p. 52.
209. Mayuzumi, N., H. Matsushima, and A. Takashima, *IL-33 Promotes DC Development in BM Culture by Triggering GM-CSF Production.* European journal of immunology, 2009. **39**(12): p. 3331-3342.
210. Matta, B.M., et al., *IL-33 is an unconventional Alarmin that stimulates IL-2 secretion by dendritic cells to selectively expand IL-33R/ST2+ regulatory T cells.* J Immunol, 2014. **193**(8): p. 4010-20.
211. Rank, M.A., et al., *IL-33–activated dendritic cells induce an atypical TH2-type response.* Journal of Allergy and Clinical Immunology, 2009. **123**(5): p. 1047-1054.

212. Dominguez, D., et al., *Exogenous IL-33 Restores Dendritic Cell Activation and Maturation in Established Cancer.* J Immunol, 2017. **198**(3): p. 1365-1375.
213. Tominaga, S., *A putative protein of a growth specific cDNA from BALB/c-3T3 cells is highly similar to the extracellular portion of mouse interleukin 1 receptor.* FEBS Lett, 1989. **258**(2): p. 301-4.
214. Yagami, A., et al., *IL-33 Mediates Inflammatory Responses in Human Lung Tissue Cells.* The Journal of Immunology, 2010. **185**(10): p. 5743.
215. Pastorelli, L., et al., *Epithelial-derived IL-33 and its receptor ST2 are dysregulated in ulcerative colitis and in experimental Th1/Th2 driven enteritis.* Proceedings of the National Academy of Sciences, 2010. **107**(17): p. 8017.
216. Macari, S., et al., *ST2 regulates bone loss in a site-dependent and estrogen-dependent manner.* J Cell Biochem, 2018.
217. Pichery, M., et al., *Endogenous IL-33 is highly expressed in mouse epithelial barrier tissues, lymphoid organs, brain, embryos, and inflamed tissues: in situ analysis using a novel Il-33-LacZ gene trap reporter strain.* J Immunol, 2012. **188**(7): p. 3488-95.
218. Miller, A.M., et al., *IL-33 reduces the development of atherosclerosis.* The Journal of Experimental Medicine, 2008. **205**(2): p. 339.
219. Demyanets, S., et al., *Components of the interleukin-33/ST2 system are differentially expressed and regulated in human cardiac cells and in cells of the cardiac vasculature.* Journal of Molecular and Cellular Cardiology, 2013. **60**(100): p. 16-26.
220. Sakai, N., et al., *Interleukin-33 is hepatoprotective during liver ischemia/reperfusion in mice.* Hepatology, 2012. **56**(4): p. 1468-78.
221. Mildner, M., et al., *Primary sources and immunological prerequisites for sST2 secretion in humans.* Cardiovasc Res, 2010. **87**(4): p. 769-77.
222. Pavlou, S., et al., *Investigating the role of interleukin-33 (IL33) in Muller cells.* Investigative Ophthalmology & Visual Science, 2015. **56**(7): p. 406-406.
223. Kunisch, E., et al., *IL-33 regulates TNF-alpha dependent effects in synovial fibroblasts.* Int J Mol Med, 2012. **29**(4): p. 530-40.
224. Guo, Z., et al., *IL-33 promotes airway remodeling and is a marker of asthma disease severity.* Journal of Asthma, 2014. **51**(8): p. 863-869.
225. Mahapatro, M., et al., *Programming of Intestinal Epithelial Differentiation by IL-33 Derived from Pericryptal Fibroblasts in Response to Systemic Infection.* Cell Rep, 2016. **15**(8): p. 1743-56.
226. Heyen, L., et al., *Lung epithelium is the major source of IL-33 and is regulated by IL-33-dependent and IL-33-independent mechanisms in pulmonary cryptococcosis.* Pathogens and Disease, 2016. **74**(7): p. ftw086-ftw086.
227. Scott, L.M., et al., *Production and regulation of interleukin-1 family cytokines at the materno-fetal interface.* Cytokine, 2017.
228. Sundlisaeter, E., et al., *The alarmin IL-33 is a notch target in quiescent endothelial cells.* Am J Pathol, 2012. **181**(3): p. 1099-111.
229. Küchler, A.M., et al., *Nuclear Interleukin-33 Is Generally Expressed in Resting Endothelium but Rapidly Lost upon Angiogenic or Proinflammatory Activation.* The American Journal of Pathology, 2008. **173**(4): p. 1229-1242.
230. Gautier, V., et al., *Extracellular IL-33 cytokine, but not endogenous nuclear IL-33, regulates protein expression in endothelial cells.* Scientific Reports, 2016. **6**: p. 34255.
231. Lamkanfi, M. and V.M. Dixit, *IL-33 raises alarm.* Immunity, 2009. **31**(1): p. 5-7.

232. Zhao, W. and Z. Hu, *The enigmatic processing and secretion of interleukin-33.* Cell Mol Immunol, 2010. **7**(4): p. 260-262.
233. Cayrol, C. and J.-P. Girard, *The IL-1-like cytokine IL-33 is inactivated after maturation by caspase-1.* Proceedings of the National Academy of Sciences, 2009. **106**(22): p. 9021-9026.
234. Lüthi, A.U., et al., *Suppression of Interleukin-33 Bioactivity through Proteolysis by Apoptotic Caspases.* Immunity, 2009. **31**(1): p. 84-98.
235. Lefrançais, E., et al., *IL-33 is processed into mature bioactive forms by neutrophil elastase and cathepsin G.* Proceedings of the National Academy of Sciences, 2012. **109**(5): p. 1673-1678.
236. Cohen, E.S., et al., *Oxidation of the alarmin IL-33 regulates ST2-dependent inflammation.* Nat Commun, 2015. **6**: p. 8327.
237. Scott, I.C., et al., *Interleukin-33 is activated by allergen- and necrosis-associated proteolytic activities to regulate its alarmin activity during epithelial damage.* Scientific Reports, 2018. **8**(1): p. 3363.
238. Kearley, J., et al., *Cigarette Smoke Silences Innate Lymphoid Cell Function and Facilitates an Exacerbated Type I Interleukin-33-Dependent Response to Infection.* Immunity, 2015. **42**(3): p. 566-579.
239. Jackson, D.J., et al., *IL-33-dependent type 2 inflammation during rhinovirus-induced asthma exacerbations in vivo.* Am J Respir Crit Care Med, 2014. **190**(12): p. 1373-82.
240. Uchida, M., et al., *Oxidative stress serves as a key checkpoint for IL-33 release by airway epithelium.* Allergy, 2017. **72**(10): p. 1521-1531.
241. Kouzaki, H., et al., *The Danger Signal, Extracellular ATP, Is a Sensor for an Airborne Allergen and Triggers IL-33 Release and Innate Th2-Type Responses.* The Journal of Immunology, 2011.
242. Sundnes, O., et al., *Epidermal Expression and Regulation of Interleukin-33 during Homeostasis and Inflammation: Strong Species Differences.* Journal of Investigative Dermatology, 2015. **135**(7): p. 1771-1780.
243. Cayrol, C. and J.-P. Girard, *Interleukin-33 (IL-33): A nuclear cytokine from the IL-1 family.* Immunological Reviews, 2017. **281**(1): p. 154-168.
244. Sweet, M.J., et al., *A novel pathway regulating lipopolysaccharide-induced shock by ST2/T1 via inhibition of Toll-like receptor 4 expression.* J Immunol, 2001. **166**(11): p. 6633-9.
245. Yanagisawa, K., et al., *Presence of a novel primary response gene ST2L, encoding a product highly similar to the interleukin 1 receptor type 1.* FEBS Letters, 1993. **318**(1): p. 83-87.
246. Leung, B.P., et al., *A novel therapy of murine collagen-induced arthritis with soluble T1/ST2.* J Immunol, 2004. **173**(1): p. 145-50.
247. Hayakawa, H., et al., *Soluble ST2 blocks interleukin-33 signaling in allergic airway inflammation.* J Biol Chem, 2007. **282**(36): p. 26369-80.
248. Yin, H., et al., *Adenovirus-mediated overexpression of soluble ST2 provides a protective effect on lipopolysaccharide-induced acute lung injury in mice.* Clinical & Experimental Immunology, 2011. **164**(2): p. 248-255.
249. Smith, D.E., et al., *The soluble form of IL-1 receptor accessory protein enhances the ability of soluble type II IL-1 receptor to inhibit IL-1 action.* Immunity, 2003. **18**(1): p. 87-96.

250. Bulek, K., et al., *The Essential Role of Single Ig IL-1 Receptor-Related Molecule/Toll IL-1R8 in Regulation of Th2 Immune Response.* The Journal of Immunology, 2009. **182**(5): p. 2601-2609.
251. Wald, D., et al., *SIGIRR, a negative regulator of Toll-like receptor-interleukin 1 receptor signaling.* Nat Immunol, 2003. **4**(9): p. 920-927.
252. Zhao, J., et al., *F-box protein FBXL19-mediated ubiquitination and degradation of the receptor for IL-33 limits pulmonary inflammation.* Nat Immunol, 2012. **13**(7): p. 651-8.
253. Yamamoto, Y., et al., *Generation of highly stable IL-18 based on a ligand–receptor complex structure.* Biochemical and Biophysical Research Communications, 2004. **317**(1): p. 181-186.
254. Carriere, V., et al., *IL-33, the IL-1-like cytokine ligand for ST2 receptor, is a chromatin-associated nuclear factor in vivo.* Proc Natl Acad Sci U S A, 2007. **104**(1): p. 282-7.
255. Koo, J.H., et al., *Cell membrane penetrating function of the nuclear localization sequence in human cytokine IL-1alpha.* Mol Biol Rep, 2014. **41**(12): p. 8117-26.
256. Roussel, L., et al., *Molecular mimicry between IL-33 and KSHV for attachment to chromatin through the H2A–H2B acidic pocket.* EMBO reports, 2008. **9**(10): p. 1006-1012.
257. Shao, D., et al., *Nuclear IL-33 regulates soluble ST2 receptor and IL-6 expression in primary human arterial endothelial cells and is decreased in idiopathic pulmonary arterial hypertension.* Biochem Biophys Res Commun, 2014. **451**(1): p. 8-14.
258. Ni, Y., et al., *The Deubiquitinase USP17 Regulates the Stability and Nuclear Function of IL-33.* Int J Mol Sci, 2015. **16**(11): p. 27956-66.
259. Lee, E.J., et al., *Interleukin-33 acts as a transcriptional repressor and extracellular cytokine in fibroblast-like synoviocytes in patients with rheumatoid arthritis.* Cytokine, 2016. **77**: p. 35-43.
260. Choi, Y.-S., et al., *Nuclear IL-33 is a transcriptional regulator of NF-κB p65 and induces endothelial cell activation.* Biochemical and Biophysical Research Communications, 2012. **421**(2): p. 305-311.
261. Serrels, B., et al., *IL-33 and ST2 mediate FAK-dependent antitumor immune evasion through transcriptional networks.* Sci Signal, 2017. **10**(508).
262. Kakkar, R., et al., *Interleukin 33 as a Mechanically Responsive Cytokine Secreted by Living Cells.* Journal of Biological Chemistry, 2012. **287**(9): p. 6941-6948.
263. Travers, J., et al., *Chromatin regulates IL-33 release and extracellular cytokine activity.* Nature communications, 2018. **9**(1): p. 3244-3244.
264. Vogelmann, J., et al., *Roles of chromatin insulator proteins in higher-order chromatin organization and transcription regulation.* Nucleus (Austin, Tex.), 2011. **2**(5): p. 358-369.
265. Miller, A.M., et al., *Interleukin-33 induces protective effects in adipose tissue inflammation during obesity in mice.* Circulation research, 2010. **107**(5): p. 650-658.
266. Mok, M.Y., et al., *Serum levels of IL-33 and soluble ST2 and their association with disease activity in systemic lupus erythematosus.* Rheumatology, 2010. **49**(3): p. 520-527.
267. Hoogerwerf, J.J., et al., *Soluble ST2 plasma concentrations predict mortality in severe sepsis.* Intensive Care Med, 2010. **36**(4): p. 630-7.
268. Granne, I., et al., *ST2 and IL-33 in Pregnancy and Pre-Eclampsia.* PLoS ONE, 2011. **6**(9): p. e24463.

269. Bhardwaj, A. and J.L. Januzzi, Jr., *ST2: a novel biomarker for heart failure.* Expert Rev Mol Diagn, 2010. **10**(4): p. 459-64.
270. Ho, J.E., et al., *Common genetic variation at the IL1RL1 locus regulates IL-33/ST2 signaling.* J Clin Invest, 2013. **123**(10): p. 4208-18.
271. Humphreys, N.E., et al., *IL-33, a potent inducer of adaptive immunity to intestinal nematodes.* J Immunol, 2008. **180**(4): p. 2443-9.
272. Yasuda, K., et al., *Contribution of IL-33-activated type II innate lymphoid cells to pulmonary eosinophilia in intestinal nematode-infected mice.* Proc Natl Acad Sci U S A, 2012. **109**(9): p. 3451-6.
273. Hung, L.Y., et al., *IL-33 drives biphasic IL-13 production for noncanonical Type 2 immunity against hookworms.* Proc Natl Acad Sci U S A, 2013. **110**(1): p. 282-7.
274. Hepworth, M.R., M. Maurer, and S. Hartmann, *Regulation of type 2 immunity to helminths by mast cells.* Gut Microbes, 2012. **3**(5): p. 476-81.
275. Kropf, P., et al., *Organ-specific distribution of CD4+ T1/ST2+ Th2 cells in Leishmania major infection.* Eur J Immunol, 2002. **32**(9): p. 2450-9.
276. Rostan, O., et al., *The IL-33/ST2 axis is associated with human visceral leishmaniasis and suppresses Th1 responses in the livers of BALB/c mice infected with Leishmania donovani.* MBio, 2013. **4**(5): p. e00383-13.
277. Piehler, D., et al., *T1/ST2 promotes T helper 2 cell activation and polyfunctionality in bronchopulmonary mycosis.* Mucosal Immunol, 2013. **6**(2): p. 405-14.
278. Nelson, M.P., et al., *IL-33 and M2a Alveolar Macrophages Promote Lung Defense against the Atypical Fungal Pathogen Pneumocystis murina.* Journal of immunology (Baltimore, Md. : 1950), 2011. **186**(4): p. 2372-2381.
279. Alves-Filho, J.C., et al., *Interleukin-33 attenuates sepsis by enhancing neutrophil influx to the site of infection.* Nat Med, 2010. **16**(6): p. 708-12.
280. Prefontaine, D., et al., *Increased expression of IL-33 in severe asthma: evidence of expression by airway smooth muscle cells.* J Immunol, 2009. **183**(8): p. 5094-103.
281. Barlow, J.L., et al., *IL-33 is more potent than IL-25 in provoking IL-13-producing nuocytes (type 2 innate lymphoid cells) and airway contraction.* J Allergy Clin Immunol, 2013. **132**(4): p. 933-41.
282. Ohno, T., et al., *Interleukin-33 in allergy.* Allergy, 2012. **67**(10): p. 1203-14.
283. Shimizu, M., et al., *Functional SNPs in the distal promoter of the ST2 gene are associated with atopic dermatitis.* Hum Mol Genet, 2005. **14**(19): p. 2919-27.
284. Haenuki, Y., et al., *A critical role of IL-33 in experimental allergic rhinitis.* J Allergy Clin Immunol, 2012. **130**(1): p. 184-94.e11.
285. Cayrol, C., et al., *Environmental allergens induce allergic inflammation through proteolytic maturation of IL-33.* Nature Immunology, 2018. **19**(4): p. 375-385.
286. Theodoropoulou, S., et al., *Toll-like receptor activation of retinal pigment epithelial cells induces a glycolytic shift and increase of IL-33 expression.* Investigative Ophthalmology & Visual Science, 2014. **55**(13): p. 79-79.
287. Gadani, S.P., et al., *The glia-derived alarmin IL-33 orchestrates the immune response and promotes recovery following CNS injury.* Neuron, 2015. **85**(4): p. 703-9.
288. Zhang, H.-F., et al., *Altered serum levels of IL-33 in patients with advanced systolic chronic heart failure: correlation with oxidative stress.* Journal of Translational Medicine, 2012. **10**(1): p. 120.

289. Stankovic, M.S., et al., *Effects of IL-33/ST2 pathway in acute inflammation on tissue damage, antioxidative parameters, magnesium concentration and cytokines profile.* Exp Mol Pathol, 2016. **101**(1): p. 31-7.
290. Ohno-Matsui, K., *Parallel findings in age-related macular degeneration and Alzheimer's disease.* Prog Retin Eye Res, 2011. **30**(4): p. 217-38.
291. Chapuis, J., et al., *Transcriptomic and genetic studies identify IL-33 as a candidate gene for Alzheimer's disease.* Mol Psychiatry, 2009. **14**(11): p. 1004-1016.
292. Stryer, L., *Biochemistry*. 1998.
293. Costello, L.C. and R.B. Franklin, *'Why do tumour cells glycolyse?': from glycolysis through citrate to lipogenesis.* Molecular and cellular biochemistry, 2005. **280**(1-2): p. 1-8.
294. Halestrap, A.P., *The mitochondrial pyruvate carrier. Kinetics and specificity for substrates and inhibitors.* Biochemical Journal, 1975. **148**(1): p. 85-96.
295. Gray, L.R., S.C. Tompkins, and E.B. Taylor, *Regulation of pyruvate metabolism and human disease.* Cell Mol Life Sci, 2014. **71**(14): p. 2577-604.
296. Csibi, A., et al., *The mTORC1 Pathway Stimulates Glutamine Metabolism and Cell Proliferation by Repressing SIRT4.* Cell, 2013. **153**(4): p. 840-854.
297. DeBerardinis, R.J., et al., *The Biology of Cancer: Metabolic Reprogramming Fuels Cell Growth and Proliferation.* Cell Metabolism, 2008. **7**(1): p. 11-20.
298. Divakaruni, A.S., et al., *Etomoxir Inhibits Macrophage Polarization by Disrupting CoA Homeostasis.* Cell Metabolism, 2018. **28**(3): p. 490-503.e7.
299. Weinberg, S.E. and N.S. Chandel, *Futility sustains memory T cells.* Immunity, 2014. **41**(1): p. 1-3.
300. Nicholls, D.G. and R.M. Locke, *Thermogenic mechanisms in brown fat.* Physiological Reviews, 1984. **64**(1): p. 1-64.
301. Heytler, P.G. and W.W. Prichard, *A new class of uncoupling agents — Carbonyl cyanide phenylhydrazones.* Biochemical and Biophysical Research Communications, 1962. **7**(4): p. 272-275.
302. Vander Heiden, M.G., L.C. Cantley, and C.B. Thompson, *Understanding the Warburg Effect: The Metabolic Requirements of Cell Proliferation.* Science (New York, N.Y.), 2009. **324**(5930): p. 1029-1033.
303. Palsson-McDermott, E.M. and L.A.J. O'Neill, *The Warburg effect then and now: From cancer to inflammatory diseases.* BioEssays, 2013. **35**(11): p. 965-973.
304. Macintyre, A.N. and J.C. Rathmell, *Activated lymphocytes as a metabolic model for carcinogenesis.* Cancer Metab, 2013. **1**(1): p. 5.
305. Boroughs, L.K. and R.J. DeBerardinis, *Metabolic pathways promoting cancer cell survival and growth.* Nature cell biology, 2015. **17**(4): p. 351-359.
306. Dang, C.V., *MYC, metabolism, cell growth, and tumorigenesis.* Cold Spring Harb Perspect Med, 2013. **3**(8).
307. Wang, R., et al., *The Transcription Factor Myc Controls Metabolic Reprogramming upon T Lymphocyte Activation.* Immunity, 2011. **35**(6): p. 871-882.
308. Semenza, G.L., *HIF-1: upstream and downstream of cancer metabolism.* Current opinion in genetics & development, 2010. **20**(1): p. 51-56.
309. Semenza, G.L., *Hypoxia-inducible factors in physiology and medicine.* Cell, 2012. **148**(3): p. 399-408.

310. Cairns, R.A., et al., *Metabolic targeting of hypoxia and HIF1 in solid tumors can enhance cytotoxic chemotherapy.* Proc Natl Acad Sci U S A, 2007. **104**(22): p. 9445-50.
311. Faubert, B., et al., *AMPK is a negative regulator of the Warburg effect and suppresses tumor growth in vivo.* Cell Metab, 2013. **17**(1): p. 113-24.
312. Simabuco, F.M., et al., *p53 and metabolism: from mechanism to therapeutics.* Oncotarget, 2018. **9**(34): p. 23780-23823.
313. Puzio-Kuter, A.M., *The Role of p53 in Metabolic Regulation.* Genes & cancer, 2011. **2**(4): p. 385-391.
314. Scarpulla, R.C., *Metabolic control of mitochondrial biogenesis through the PGC-1 family regulatory network.* Biochimica et biophysica acta, 2011. **1813**(7): p. 1269-1278.
315. McGuirk, S., et al., *PGC-1α supports glutamine metabolism in breast cancer.* Cancer & metabolism, 2013. **1**(1): p. 22-22.
316. Finck, B.N. and D.P. Kelly, *PGC-1 coactivators: inducible regulators of energy metabolism in health and disease.* J Clin Invest, 2006. **116**(3): p. 615-22.
317. St-Pierre, J., et al., *Suppression of Reactive Oxygen Species and Neurodegeneration by the PGC-1 Transcriptional Coactivators.* Cell, 2006. **127**(2): p. 397-408.
318. van der Knaap, J.A. and C.P. Verrijzer, *Undercover: gene control by metabolites and metabolic enzymes.* Genes Dev, 2016. **30**(21): p. 2345-2369.
319. Liu, T.F. and C.E. McCall, *Deacetylation by SIRT1 Reprograms Inflammation and Cancer.* Genes & Cancer, 2013. **4**(3-4): p. 135-147.
320. Locasale, J.W., *Serine, glycine and one-carbon units: cancer metabolism in full circle.* Nature Reviews Cancer, 2013. **13**: p. 572.
321. Li, B., et al., *Fructose-1,6-bisphosphatase opposes renal carcinoma progression.* Nature, 2014. **513**: p. 251.
322. Huangyang, P. and M.C. Simon, *Hidden features: exploring the non-canonical functions of metabolic enzymes.* Dis Model Mech, 2018. **11**(8).
323. Chang, C., et al., *AMPK-Dependent Phosphorylation of GAPDH Triggers Sirt1 Activation and Is Necessary for Autophagy upon Glucose Starvation.* Molecular Cell, 2015. **60**(6): p. 930-940.
324. Zhai, D., et al., *Disruption of the nuclear p53-GAPDH complex protects against ischemia-induced neuronal damage.* 2014. **7**(1): p. 20.
325. Castonguay, Z., et al., *Nuclear lactate dehydrogenase modulates histone modification in human hepatocytes.* Biochemical and Biophysical Research Communications, 2014. **454**(1): p. 172-177.
326. Lee, S.M., et al., *A nucleocytoplasmic malate dehydrogenase regulates p53 transcriptional activity in response to metabolic stress.* Cell Death And Differentiation, 2009. **16**: p. 738.
327. Altenberg, B. and K.O. Greulich, *Genes of glycolysis are ubiquitously overexpressed in 24 cancer classes.* Genomics, 2004. **84**(6): p. 1014-20.
328. Dong, G., et al., *PKM2 and cancer: The function of PKM2 beyond glycolysis.* Oncology letters, 2016. **11**(3): p. 1980-1986.
329. Takenaka, M., et al., *Alternative splicing of the pyruvate kinase M gene in a minigene system.* 1996. **235**(1-2): p. 366-371.
330. Dayton, T.L., T. Jacks, and M.G. Vander Heiden, *PKM2, cancer metabolism, and the road ahead.* EMBO Rep, 2016. **17**(12): p. 1721-1730.

331. David, C.J., et al., *HnRNP proteins controlled by c-Myc deregulate pyruvate kinase mRNA splicing in cancer.* Nature, 2010. **463**(7279): p. 364-368.
332. Wang, Z., et al., *Exon-centric regulation of pyruvate kinase M alternative splicing via mutually exclusive exons.* J Mol Cell Biol, 2012. **4**(2): p. 79-87.
333. Clower, C.V., et al., *The alternative splicing repressors hnRNP A1/A2 and PTB influence pyruvate kinase isoform expression and cell metabolism.* Proc Natl Acad Sci U S A, 2010. **107**(5): p. 1894-9.
334. Hsu, M.-C. and W.-C.J.M.C. Hung, *Pyruvate kinase M2 fuels multiple aspects of cancer cells: from cellular metabolism, transcriptional regulation to extracellular signaling.* 2018. **17**(1): p. 35.
335. Jurica, M.S., et al., *The allosteric regulation of pyruvate kinase by fructose-1,6-bisphosphate.* Structure, 1998. **6**(2): p. 195-210.
336. Ashizawa, K., et al., *An in vitro novel mechanism of regulating the activity of pyruvate kinase M2 by thyroid hormone and fructose 1, 6-bisphosphate.* Biochemistry, 1991. **30**(29): p. 7105-11.
337. Lunt, S.Y., et al., *Pyruvate kinase isoform expression alters nucleotide synthesis to impact cell proliferation.* Mol Cell, 2015. **57**(1): p. 95-107.
338. Anastasiou, D., et al., *Inhibition of pyruvate kinase M2 by reactive oxygen species contributes to cellular antioxidant responses.* Science, 2011. **334**(6060): p. 1278-83.
339. Christofk, H.R., et al., *Pyruvate kinase M2 is a phosphotyrosine-binding protein.* Nature, 2008. **452**(7184): p. 181-6.
340. *Cytosolic thyroid hormone-binding protein is a monomer of pyruvate kinase.* Proceedings of the National Academy of Sciences, 1990. **87**(4): p. 1625.
341. Yang, W. and Z. Lu, *Pyruvate kinase M2 at a glance.* J Cell Sci, 2015. **128**(9): p. 1655-60.
342. Luo, W., et al., *Pyruvate Kinase M2 Is a PHD3-Stimulated Coactivator for Hypoxia-Inducible Factor 1.* Cell, 2011. **145**(5): p. 732-744.
343. Zoncu, R., A. Efeyan, and D.M. Sabatini, *mTOR: from growth signal integration to cancer, diabetes and ageing.* Nat Rev Mol Cell Biol, 2011. **12**(1): p. 21-35.
344. Hardie, D.G., F.A. Ross, and S.A. Hawley, *AMPK: a nutrient and energy sensor that maintains energy homeostasis.* Nat Rev Mol Cell Biol, 2012. **13**(4): p. 251-262.
345. O'Neill, L.A.J. and D.G. Hardie, *Metabolism of inflammation limited by AMPK and pseudo-starvation.* Nature, 2013. **493**(7432): p. 346-355.
346. Woods, A., et al., *LKB1 Is the Upstream Kinase in the AMP-Activated Protein Kinase Cascade.* Current Biology, 2003. **13**(22): p. 2004-2008.
347. Marsin, A.S., et al., *Phosphorylation and activation of heart PFK-2 by AMPK has a role in the stimulation of glycolysis during ischaemia.* Curr Biol, 2000. **10**(20): p. 1247-55.
348. Egan, D.F., et al., *Phosphorylation of ULK1 (hATG1) by AMP-activated protein kinase connects energy sensing to mitophagy.* Science, 2011. **331**(6016): p. 456-61.
349. Kim, J., et al., *AMPK and mTOR regulate autophagy through direct phosphorylation of Ulk1.* Nat Cell Biol, 2011. **13**(2): p. 132-41.
350. Kim, J., et al., *AMPK and mTOR regulate autophagy through direct phosphorylation of Ulk1.* Nature cell biology, 2011. **13**(2): p. 132-141.
351. Grahame Hardie, D., *Regulation of AMP-activated protein kinase by natural and synthetic activators.* Acta Pharmaceutica Sinica B, 2016. **6**(1): p. 1-19.
352. Laplante, M. and D.M. Sabatini, *mTOR signaling at a glance.* Journal of Cell Science, 2009. **122**(20): p. 3589.

353. Saxton, R.A. and D.M. Sabatini, *mTOR Signaling in Growth, Metabolism, and Disease.* Cell, 2017. **168**(6): p. 960-976.
354. Wang, Y., et al., *miR-130a upregulates mTOR pathway by targeting TSC1 and is transactivated by NF-κB in high-grade serous ovarian carcinoma.* Cell Death And Differentiation, 2017. **24**: p. 2089.
355. Huang, J. and B.D. Manning, *The TSC1-TSC2 complex: a molecular switchboard controlling cell growth.* The Biochemical journal, 2008. **412**(2): p. 179-190.
356. Gwinn, D.M., et al., *AMPK phosphorylation of raptor mediates a metabolic checkpoint.* Mol Cell, 2008. **30**(2): p. 214-26.
357. Wolfson, R.L. and D.M. Sabatini, *The Dawn of the Age of Amino Acid Sensors for the mTORC1 Pathway.* Cell Metab, 2017. **26**(2): p. 301-309.
358. Sun, Q., et al., *Mammalian target of rapamycin up-regulation of pyruvate kinase isoenzyme type M2 is critical for aerobic glycolysis and tumor growth.* Proc Natl Acad Sci U S A, 2011. **108**(10): p. 4129-34.
359. Deblon, N., et al., *Chronic mTOR inhibition by rapamycin induces muscle insulin resistance despite weight loss in rats.* British journal of pharmacology, 2012. **165**(7): p. 2325-2340.
360. Waickman, A.T. and J.D. Powell, *mTOR, metabolism, and the regulation of T-cell differentiation and function.* Immunological reviews, 2012. **249**(1): p. 43-58.
361. Land, S.C. and A.R. Tee, *Hypoxia-inducible factor 1alpha is regulated by the mammalian target of rapamycin (mTOR) via an mTOR signaling motif.* J Biol Chem, 2007. **282**(28): p. 20534-43.
362. Delgoffe, G.M., et al., *The kinase mTOR regulates the differentiation of helper T cells through the selective activation of signaling by mTORC1 and mTORC2.* Nat Immunol, 2011. **12**(4): p. 295-303.
363. Linke, M., et al., *mTORC1 and mTORC2 as regulators of cell metabolism in immunity.* FEBS letters, 2017. **591**(19): p. 3089-3103.
364. Schieke, S.M., et al., *The Mammalian Target of Rapamycin (mTOR) Pathway Regulates Mitochondrial Oxygen Consumption and Oxidative Capacity.* 2006. **281**(37): p. 27643-27652.
365. Pollizzi, K.N., et al., *mTORC1 and mTORC2 selectively regulate CD8(+) T cell differentiation.* J Clin Invest, 2015. **125**(5): p. 2090-108.
366. Oh, W.J. and E. Jacinto, *mTOR complex 2 signaling and functions.* Cell cycle (Georgetown, Tex.), 2011. **10**(14): p. 2305-2316.
367. Calnan, D.R. and A. Brunet, *The FoxO code.* Oncogene, 2008. **27**: p. 2276.
368. Zhang, L., et al., *Mammalian Target of Rapamycin Complex 2 Controls CD8 T Cell Memory Differentiation in a Foxo1-Dependent Manner.* Cell Rep, 2016. **14**(5): p. 1206-1217.
369. Mueckler, M. and B. Thorens, *The SLC2 (GLUT) family of membrane transporters.* Molecular Aspects of Medicine, 2013. **34**(2–3): p. 121-138.
370. Rizzolo, L.J., *Glucose Transporters in Retinal Pigment Epithelium Development*, in *Ocular Transporters In Ophthalmic Diseases And Drug Delivery: Ophthalmology Research*, J. Tombran-Tink and C.J. Barnstable, Editors. 2008, Humana Press: Totowa, NJ. p. 185-199.
371. Senanayake, P.d., et al., *Glucose utilization by the retinal pigment epithelium: Evidence for rapid uptake and storage in glycogen, followed by glycogen utilization.* Experimental Eye Research, 2006. **83**(2): p. 235-246.

372. Takagi, H., et al., *Characterization of glucose transporter in cultured human retinal pigment epithelial cells: gene expression and effect of growth factors.* Invest Ophthalmol Vis Sci, 1994. **35**(1): p. 170-7.
373. Hurley, J.B., K.J. Lindsay, and J. Du, *Glucose, lactate, and shuttling of metabolites in vertebrate retinas.* Journal of neuroscience research, 2015. **93**(7): p. 1079-1092.
374. Adijanto, J., et al., *The retinal pigment epithelium utilizes fatty acids for ketogenesis.* The Journal of biological chemistry, 2014. **289**(30): p. 20570-20582.
375. Warburg, O., *The Metabolism of Carcinoma Cells.* The Journal of Cancer Research, 1925. **9**(1): p. 148.
376. Karunadharma, P.P., et al., *Mitochondrial DNA damage as a potential mechanism for age-related macular degeneration.* Investigative ophthalmology & visual science, 2010. **51**(11): p. 5470-5479.
377. Miceli, M.V., D.A. Newsome, and G.W. Schriver, *Glucose uptake, hexose monophosphate shunt activity, and oxygen consumption in cultured human retinal pigment epithelial cells.* Investigative Ophthalmology & Visual Science, 1990. **31**(2): p. 277-283.
378. Philp, N.J., et al., *Loss of MCT1, MCT3, and MCT4 expression in the retinal pigment epithelium and neural retina of the 5A11/basigin-null mouse.* Invest Ophthalmol Vis Sci, 2003. **44**(3): p. 1305-11.
379. Chao, J.R., et al., *Human retinal pigment epithelial cells prefer proline as a nutrient and transport metabolic intermediates to the retinal side.* 2017. **292**(31): p. 12895-12905.
380. Yam, M., et al., *Proline mediates metabolic communication between retinal pigment epithelial cells and the retina.* 2019.
381. Glocklin, V.C. and A.M. Potts, *THE METABOLISM OF RETINAL PIGMENT CELL EPITHELIUM. II. RESPIRATION AND GLYCOLYSIS.* Invest Ophthalmol, 1965. **4**: p. 226-34.
382. Kurihara, T., et al., *Hypoxia-induced metabolic stress in retinal pigment epithelial cells is sufficient to induce photoreceptor degeneration.* Elife, 2016. **5**.
383. Zhao, C., et al., *mTOR-mediated dedifferentiation of the retinal pigment epithelium initiates photoreceptor degeneration in mice.* J Clin Invest, 2011. **121**(1): p. 369-83.
384. Xu, L., et al., *Stimulation of AMPK prevents degeneration of photoreceptors and the retinal pigment epithelium.* Proceedings of the National Academy of Sciences, 2018. **115**(41): p. 10475.
385. Navarro, A. and A. Boveris, *The mitochondrial energy transduction system and the aging process.* American Journal of Physiology - Cell Physiology, 2007. **292**(2): p. C670.
386. Boffoli, D., et al., *DECLINE WITH AGE OF THE RESPIRATORY-CHAIN ACTIVITY IN HUMAN SKELETAL-MUSCLE.* Biochimica Et Biophysica Acta-Molecular Basis of Disease, 1994. **1226**(1): p. 73-82.
387. Benzi, G., et al., *The mitochondrial electron transfer alteration as a factor involved in the brain aging.* Neurobiology of Aging, 1992. **13**(3): p. 361-368.
388. Liu, J., D.W. Killilea, and B.N. Ames, *Age-associated mitochondrial oxidative decay: Improvement of carnitine acetyltransferase substrate-binding affinity and activity in brain by feeding old rats acetyl-l- carnitine and/or R-α-lipoic acid.* Proceedings of the National Academy of Sciences, 2002. **99**(4): p. 1876-1881.

389. Hiona, A., et al. *Mitochondrial DNA mutations induce mitochondrial dysfunction, apoptosis and sarcopenia in skeletal muscle of mitochondrial DNA mutator mice*. PloS one, 2010. **5**, e11468 DOI: 10.1371/journal.pone.0011468.
390. Udar, N., et al., *Mitochondrial DNA haplogroups associated with age-related macular degeneration.* Invest Ophthalmol Vis Sci, 2009. **50**(6): p. 2966-74.
391. SanGiovanni, J.P., et al., *Mitochondrial DNA variants of respiratory complex I that uniquely characterize haplogroup T2 are associated with increased risk of age-related macular degeneration.* PLoS One, 2009. **4**(5): p. e5508.
392. da Cunha, F.M., N.Q. Torelli, and A.J. Kowaltowski, *Mitochondrial Retrograde Signaling: Triggers, Pathways, and Outcomes.* Oxidative medicine and cellular longevity, 2015. **2015**: p. 482582-482582.
393. Patrushev, M., et al., *Mitochondrial permeability transition triggers the release of mtDNA fragments.* Cell Mol Life Sci, 2004. **61**(24): p. 3100-3.
394. Cline, S.D., *Mitochondrial DNA damage and its consequences for mitochondrial gene expression.* Biochim Biophys Acta, 2012. **1819**(9-10): p. 979-91.
395. Meissner, C., et al., *The 4977bp deletion of mitochondrial DNA in human skeletal muscle, heart and different areas of the brain: A useful biomarker or more?* Experimental Gerontology, 2008. **43**(7): p. 645-652.
396. Terluk, M.R., et al., *Investigating mitochondria as a target for treating age-related macular degeneration.* J Neurosci, 2015. **35**(18): p. 7304-11.
397. Ferrington, D.A., et al., *Altered bioenergetics and enhanced resistance to oxidative stress in human retinal pigment epithelial cells from donors with age-related macular degeneration.* Redox Biology, 2017. **13**: p. 255-265.
398. Golestaneh, N., et al., *Dysfunctional autophagy in RPE, a contributing factor in age-related macular degeneration.* Cell Death Dis, 2017. **8**(1): p. e2537.
399. Kanow, M.A., et al., *Biochemical adaptations of the retina and retinal pigment epithelium support a metabolic ecosystem in the vertebrate eye.* eLife, 2017. **6**: p. e28899.
400. Brown, E.E., et al., *Mitochondrial oxidative stress in the retinal pigment epithelium (RPE) led to metabolic dysfunction in both the RPE and retinal photoreceptors.* Redox Biology, 2019. **24**: p. 101201.
401. Curcio, C.A., N.E. Medeiros, and C.L. Millican, *Photoreceptor loss in age-related macular degeneration.* Investigative Ophthalmology & Visual Science, 1996. **37**(7): p. 1236-1249.
402. Aït-Ali, N., et al., *Rod-Derived Cone Viability Factor Promotes Cone Survival by Stimulating Aerobic Glycolysis.* Cell, 2015. **161**(4): p. 817-832.
403. Krawczyk, C.M., et al., *Toll-like receptor-induced changes in glycolytic metabolism regulate dendritic cell activation.* Blood, 2010. **115**(23): p. 4742-9.
404. Rodriguez-Prados, J.C., et al., *Substrate fate in activated macrophages: a comparison between innate, classic, and alternative activation.* J Immunol, 2010. **185**(1): p. 605-14.
405. Dang, E.V., et al., *Control of T(H)17/T(reg) balance by hypoxia-inducible factor 1.* Cell, 2011. **146**(5): p. 772-84.
406. Doughty, C.A., et al., *Antigen receptor-mediated changes in glucose metabolism in B lymphocytes: role of phosphatidylinositol 3-kinase signaling in the glycolytic control of growth.* Blood, 2006. **107**(11): p. 4458-65.

407. Keppel, M.P., et al., *Activation-specific metabolic requirements for NK Cell IFN-γ production.* Journal of immunology (Baltimore, Md. : 1950), 2015. **194**(4): p. 1954-1962.
408. Michl, J., D.J. Ohlbaum, and S.C. Silverstein, *2-Deoxyglucose selectively inhibits Fc and complement receptor-mediated phagocytosis in mouse peritoneal macrophages. I. Description of the inhibitory effect.* J Exp Med, 1976. **144**(6): p. 1465-83.
409. Hamilton, J.A., G. Vairo, and S.R. Lingelbach, *CSF-1 stimulates glucose uptake in murine bone marrow-derived macrophages.* Biochem Biophys Res Commun, 1986. **138**(1): p. 445-54.
410. Jones, N., et al., *Bioenergetic analysis of human peripheral blood mononuclear cells.* Clinical & Experimental Immunology, 2015. **182**(1): p. 69-80.
411. Shi, L.Z., et al., *HIF1alpha-dependent glycolytic pathway orchestrates a metabolic checkpoint for the differentiation of TH17 and Treg cells.* J Exp Med, 2011. **208**(7): p. 1367-76.
412. O'Neill, L.A.J. and E.J. Pearce, *Immunometabolism governs dendritic cell and macrophage function.* The Journal of Experimental Medicine, 2016. **213**(1): p. 15.
413. Roiniotis, J., et al., *Hypoxia prolongs monocyte/macrophage survival and enhanced glycolysis is associated with their maturation under aerobic conditions.* J Immunol, 2009. **182**(12): p. 7974-81.
414. Kolev, M., et al., *Complement Regulates Nutrient Influx and Metabolic Reprogramming during Th1 Cell Responses.* Immunity. **42**(6): p. 1033-1047.
415. van der Windt, Gerritje J.W., et al., *Mitochondrial Respiratory Capacity Is a Critical Regulator of CD8+ T Cell Memory Development.* Immunity, 2012. **36**(1): p. 68-78.
416. Kelly, B. and L.A.J. O'Neill, *Metabolic reprogramming in macrophages and dendritic cells in innate immunity.* Cell Res, 2015. **25**(7): p. 771-784.
417. Palsson-McDermott, E.M., et al., *Pyruvate kinase M2 regulates Hif-1alpha activity and IL-1beta induction and is a critical determinant of the warburg effect in LPS-activated macrophages.* Cell Metab, 2015. **21**(1): p. 65-80.
418. Yang, E., et al., *Antimicrobial activity of bacteriocin-producing lactic acid bacteria isolated from cheeses and yogurts.* AMB Express, 2012. **2**(1): p. 48.
419. Wu, D., et al., *Type 1 Interferons Induce Changes in Core Metabolism that Are Critical for Immune Function.* Immunity, 2016. **44**(6): p. 1325-1336.
420. Garedew, A., S.O. Henderson, and S. Moncada, *Activated macrophages utilize glycolytic ATP to maintain mitochondrial membrane potential and prevent apoptotic cell death.* Cell Death Differ, 2010. **17**(10): p. 1540-1550.
421. Vats, D., et al., *Oxidative metabolism and PGC-1beta attenuate macrophage-mediated inflammation.* Cell Metab, 2006. **4**(1): p. 13-24.
422. Panday, A., et al., *NADPH oxidases: an overview from structure to innate immunity-associated pathologies.* Cell Mol Immunol, 2015. **12**(1): p. 5-23.
423. Blagih, J. and Russell G. Jones, *Polarizing Macrophages through Reprogramming of Glucose Metabolism.* Cell Metabolism, 2012. **15**(6): p. 793-795.
424. Theodoropoulou, S., et al., *Role of interleukin 33/ST2 axis in the immune-mediated pathogenesis of age-related macular degeneration.* Lancet, 2015. **385 Suppl 1**: p. S97.
425. MacIver, N.J., et al., *The liver kinase B1 is a central regulator of T cell development, activation, and metabolism.* J Immunol, 2011. **187**(8): p. 4187-98.

426. Guo, Y., et al., *AMPK Inhibition Blocks ROS-NFκB Signaling and Attenuates Endotoxemia-Induced Liver Injury.* PLOS ONE, 2014. **9**(1): p. e86881.
427. Turner, M.L., et al., *Glucose Availability and AMP-Activated Protein Kinase Link Energy Metabolism and Innate Immunity in the Bovine Endometrium.* PLOS ONE, 2016. **11**(3): p. e0151416.
428. Blagih, J., et al., *The Energy Sensor AMPK Regulates T Cell Metabolic Adaptation and Effector Responses In Vivo.* Immunity, 2015. **42**(1): p. 41-54.
429. Nath, N., et al., *5-aminoimidazole-4-carboxamide ribonucleoside: a novel immunomodulator with therapeutic efficacy in experimental autoimmune encephalomyelitis.* J Immunol, 2005. **175**(1): p. 566-74.
430. Park, D.W., et al., *Activation of AMPK enhances neutrophil chemotaxis and bacterial killing.* Mol Med, 2013. **19**: p. 387-98.
431. Marsin, A.S., et al., *The stimulation of glycolysis by hypoxia in activated monocytes is mediated by AMP-activated protein kinase and inducible 6-phosphofructo-2-kinase.* J Biol Chem, 2002. **277**(34): p. 30778-83.
432. Qin, S. and G.A. Rodrigues, *Differential roles of AMPKα1 and AMPKα2 in regulating 4-HNE-induced RPE cell death and permeability.* Experimental Eye Research, 2010. **91**(6): p. 818-824.
433. Qin, S., *Blockade of MerTK Activation by AMPK Inhibits RPE Cell Phagocytosis.* Adv Exp Med Biol, 2016. **854**: p. 773-8.
434. Weichhart, T., M. Hengstschlager, and M. Linke, *Regulation of innate immune cell function by mTOR.* Nat Rev Immunol, 2015. **15**(10): p. 599-614.
435. Peng, T., T.R. Golub, and D.M. Sabatini, *The Immunosuppressant Rapamycin Mimics a Starvation-Like Signal Distinct from Amino Acid and Glucose Deprivation.* Molecular and Cellular Biology, 2002. **22**(15): p. 5575.
436. Weichhart, T., et al., *The TSC-mTOR Signaling Pathway Regulates the Innate Inflammatory Response.* Immunity, 2008. **29**(4): p. 565-577.
437. Moon, J.-S., et al., *mTORC1-Induced HK1-Dependent Glycolysis Regulates NLRP3 Inflammasome Activation.* Cell Reports, 2015. **12**(1): p. 102-115.
438. Pearce, E.L., et al., *Enhancing CD8 T-cell memory by modulating fatty acid metabolism.* Nature, 2009. **460**: p. 103.
439. Huang, Stanley C.-C., et al., *Metabolic Reprogramming Mediated by the mTORC2-IRF4 Signaling Axis Is Essential for Macrophage Alternative Activation.* Immunity, 2016. **45**(4): p. 817-830.
440. Malik, D., et al. *Human retinal transmitochondrial cybrids with J or H mtDNA haplogroups respond differently to ultraviolet radiation: implications for retinal diseases*. PloS one, 2014. **9**, e99003 DOI: 10.1371/journal.pone.0099003.
441. Caslin, H.L., et al., *Inhibiting Glycolysis and ATP Production Attenuates IL-33-Mediated Mast Cell Function and Peritonitis.* 2018. **9**(3026).
442. Hu, F., et al., *Hypoxia-inducible factor-1alpha and interleukin 33 form a regulatory circuit to perpetuate the inflammation in rheumatoid arthritis.* PLoS One, 2013. **8**(8): p. e72650.
443. Wang, C., et al., *IL-33 signaling fuels outgrowth and metastasis of human lung cancer.* Biochemical and Biophysical Research Communications, 2016. **479**(3): p. 461-468.
444. Xu, H., et al., *Deficiency in IL-33/ST2 Axis Reshapes Mitochondrial Metabolism in Lipopolysaccharide-Stimulated Macrophages.* Front Immunol, 2019. **10**: p. 127.

445. Chen, M., et al., *Characterization of a spontaneous mouse retinal pigment epithelial cell line B6-RPE07.* Invest Ophthalmol Vis Sci, 2008. **49**(8): p. 3699-706.
446. McCleland, M.L., et al., *Lactate dehydrogenase B is required for the growth of KRAS-dependent lung adenocarcinomas.* Clin Cancer Res, 2013. **19**(4): p. 773-84.
447. Limb, G.A., et al., *In Vitro Characterization of a Spontaneously Immortalized Human Müller Cell Line (MIO-M1).* Investigative Ophthalmology & Visual Science, 2002. **43**(3): p. 864-869.
448. Oboki, K., et al., *IL-33 is a crucial amplifier of innate rather than acquired immunity.* Proc Natl Acad Sci U S A, 2010. **107**(43): p. 18581-6.
449. Fernandez-Godino, R., D.L. Garland, and E.A. Pierce, *Isolation, culture and characterization of primary mouse RPE cells.* Nat. Protocols, 2016. **11**(7): p. 1206-1218.
450. Alexopoulou, L., et al., *Recognition of double-stranded RNA and activation of NF-κB by Toll-like receptor 3.* Nature, 2001. **413**: p. 732.
451. Lee, B.L., et al., *Caspase-11 auto-proteolysis is crucial for noncanonical inflammasome activation.* The Journal of Experimental Medicine, 2018. **215**(9): p. 2279.
452. Kim, S., et al., *Characterizing the genetic basis of innate immune response in TLR4-activated human monocytes.* Nat Commun, 2014. **5**: p. 5236.
453. Wei, H., et al., *An easy, rapid method to isolate RPE cell protein from the mouse eye.* Experimental Eye Research, 2016. **145**: p. 450-455.
454. McGuirk, S., et al., *PGC-1α supports glutamine metabolism in breast cancer.* 2013. **1**(1): p. 22.
455. Runkle, E.A., P.M. Titchenell, and D.A. Antonetti, *Molecular Regulation of Endothelial Cell Tight Junctions and the Blood-Retinal Barrier*, in *Visual Dysfunction in Diabetes: The Science of Patient Impairment and Health Care*, J. Tombran-Tink, C.J. Barnstable, and T.W. Gardner, Editors. 2012, Springer New York: New York, NY. p. 123-141.
456. Bharadwaj, A.S., et al., *Role of the retinal vascular endothelial cell in ocular disease.* Progress in retinal and eye research, 2013. **32**: p. 102-180.
457. Nussenblatt, R.B., et al., *Immune Responses in Age-Related Macular Degeneration and a Possible Long-term Therapeutic Strategy for Prevention.* American Journal of Ophthalmology. **158**(1): p. 5-11.e2.
458. *Geographic Atrophy in Age-Related Macular Degeneration and TLR3.* New England Journal of Medicine, 2009. **360**(21): p. 2251-2256.
459. Zhou, Y., et al., *TLR3 activation efficiency by high or low molecular mass poly I:C.* Innate Immun, 2013. **19**(2): p. 184-92.
460. Bartels, K., A. Grenz, and H.K. Eltzschig, *Hypoxia and inflammation are two sides of the same coin.* Proceedings of the National Academy of Sciences, 2013. **110**(46): p. 18351-18352.
461. Eltzschig, H.K. and P. Carmeliet, *Hypoxia and inflammation.* The New England journal of medicine, 2011. **364**(7): p. 656-665.
462. Mungai, P.T., et al., *Hypoxia triggers AMPK activation through reactive oxygen species-mediated activation of calcium release-activated calcium channels.* Molecular and cellular biology, 2011. **31**(17): p. 3531-3545.
463. Sandig, H. and S. Bulfone-Paus, *TLR signaling in mast cells: common and unique features.* Frontiers in immunology, 2012. **3**: p. 185-185.

464. Lin, X., et al., *The expression of Toll-like receptors in murine Müller cells, the glial cells in retina.* 2013. **34**(8): p. 1339-1346.
465. Faubert, B., et al., *Lactate Metabolism in Human Lung Tumors.* Cell, 2017. **171**(2): p. 358-371.e9.
466. Spirig, R., et al., *Effects of TLR agonists on the hypoxia-regulated transcription factor HIF-1alpha and dendritic cell maturation under normoxic conditions.* PLoS One, 2010. **5**(6): p. e0010983.
467. Wahlström, T. and M. Arsenian Henriksson, *Impact of MYC in regulation of tumor cell metabolism.* Biochimica et Biophysica Acta (BBA) - Gene Regulatory Mechanisms, 2015. **1849**(5): p. 563-569.
468. Mills, E.L., et al., *Succinate Dehydrogenase Supports Metabolic Repurposing of Mitochondria to Drive Inflammatory Macrophages.* Cell, 2016. **167**(2): p. 457-470.e13.
469. Patel, M.S. and L.G. Korotchkina, *Regulation of mammalian pyruvate dehydrogenase complex by phosphorylation: complexity of multiple phosphorylation sites and kinases.* Experimental &Amp; Molecular Medicine, 2001. **33**: p. 191.
470. Nunnari, J. and A. Suomalainen, *Mitochondria: In Sickness and in Health.* Cell, 2012. **148**(6): p. 1145-1159.
471. Mishra, P. and D.C. Chan, *Metabolic regulation of mitochondrial dynamics.* The Journal of Cell Biology, 2016. **212**(4): p. 379.
472. Buck, Michael D., et al., *Mitochondrial Dynamics Controls T Cell Fate through Metabolic Programming.* Cell, 2016. **166**(1): p. 63-76.
473. Liesa, M. and Orian S. Shirihai, *Mitochondrial Dynamics in the Regulation of Nutrient Utilization and Energy Expenditure.* Cell Metabolism, 2013. **17**(4): p. 491-506.
474. Frank, M., et al., *Mitophagy is triggered by mild oxidative stress in a mitochondrial fission dependent manner.* Biochimica et Biophysica Acta (BBA) - Molecular Cell Research, 2012. **1823**(12): p. 2297-2310.
475. Youle, R.J. and M. Karbowski, *Mitochondrial fission in apoptosis.* Nature Reviews Molecular Cell Biology, 2005. **6**: p. 657.
476. Taguchi, N., et al., *Mitotic phosphorylation of dynamin-related GTPase Drp1 participates in mitochondrial fission.* J Biol Chem, 2007. **282**(15): p. 11521-9.
477. Yu, T., J.L. Robotham, and Y. Yoon, *Increased production of reactive oxygen species in hyperglycemic conditions requires dynamic change of mitochondrial morphology.* Proceedings of the National Academy of Sciences of the United States of America, 2006. **103**(8): p. 2653.
478. de Brito, O.M. and L. Scorrano, *Mitofusin 2 tethers endoplasmic reticulum to mitochondria.* Nature, 2008. **456**: p. 605.
479. Gomes, L.C., G.D. Benedetto, and L. Scorrano, *During autophagy mitochondria elongate, are spared from degradation and sustain cell viability.* Nature Cell Biology, 2011. **13**: p. 589.
480. Mishra, P., et al., *Proteolytic Cleavage of Opa1 Stimulates Mitochondrial Inner Membrane Fusion and Couples Fusion to Oxidative Phosphorylation.* Cell Metabolism, 2014. **19**(4): p. 630-641.
481. Cogliati, S., et al., *Mitochondrial Cristae Shape Determines Respiratory Chain Supercomplexes Assembly and Respiratory Efficiency.* Cell, 2013. **155**(1): p. 160-171.
482. King, L. and H. Plun-Favreau, *Chapter 5 - Mitophagy*, in *Parkinson's Disease*, P. Verstreken, Editor. 2017, Academic Press: San Diego. p. 139-177.

483. Cairns, A.P., et al., *Very-long-chain acyl-coenzyme A dehydrogenase deficiency— a new cause of myoglobinuric acute renal failure.* Nephrology Dialysis Transplantation, 2000. **15**(8): p. 1232-1234.
484. Sag, D., et al., *Adenosine 5'-monophosphate-activated protein kinase promotes macrophage polarization to an anti-inflammatory functional phenotype.* Journal of immunology (Baltimore, Md. : 1950), 2008. **181**(12): p. 8633-8641.
485. Galván-Peña, S., et al., *Malonylation of GAPDH is an inflammatory signal in macrophages.* Nature Communications, 2019. **10**(1): p. 338.
486. Showkat, M., M.A. Beigh, and K.I. Andrabi, *mTOR Signaling in Protein Translation Regulation: Implications in Cancer Genesis and Therapeutic Interventions.* Molecular Biology International, 2014. **2014**: p. 14.
487. Liu, X., et al., *The AMPK inhibitor compound C is a potent AMPK-independent antiglioma agent.* Mol Cancer Ther, 2014. **13**(3): p. 596-605.
488. Ceschin, J., et al., *Disruption of Nucleotide Homeostasis by the Antiproliferative Drug 5-Aminoimidazole-4-carboxamide-1-beta-d-ribofuranoside Monophosphate (AICAR).* J Biol Chem, 2015. **290**(39): p. 23947-59.
489. Vincent, E.E., et al., *Differential effects of AMPK agonists on cell growth and metabolism.* Oncogene, 2015. **34**(28): p. 3627-3639.
490. Ross, J., *mRNA stability in mammalian cells.* Microbiological reviews, 1995. **59**(3): p. 423-450.
491. Payne, B.A.I. and P.F. Chinnery, *Mitochondrial dysfunction in aging: Much progress but many unresolved questions.* Biochimica et biophysica acta, 2015. **1847**(11): p. 1347-1353.
492. Kozlowski, M.R., *RPE cell senescence: A key contributor to age-related macular degeneration.* Medical Hypotheses, 2012. **78**(4): p. 505-510.
493. Rodier, F. and J. Campisi, *Four faces of cellular senescence.* J Cell Biol, 2011. **192**(4): p. 547-56.
494. Perez-Mancera, P.A., A.R.J. Young, and M. Narita, *Inside and out: the activities of senescence in cancer.* Nat Rev Cancer, 2014. **14**(8): p. 547-558.
495. Tchkonia, T., et al., *Cellular senescence and the senescent secretory phenotype: therapeutic opportunities.* The Journal of Clinical Investigation, 2013. **123**(3): p. 966-972.
496. Rohrer, B., M. Bandyopadhyay, and C. Beeson, *Reduced Metabolic Capacity in Aged Primary Retinal Pigment Epithelium (RPE) is Correlated with Increased Susceptibility to Oxidative Stress*, in *Retinal Degenerative Diseases: Mechanisms and Experimental Therapy*, C. Bowes Rickman, et al., Editors. 2016, Springer International Publishing: Cham. p. 793-798.
497. Sag, D., et al., *Adenosine 5'-monophosphate-activated protein kinase promotes macrophage polarization to an anti-inflammatory functional phenotype.* J Immunol, 2008. **181**(12): p. 8633-41.
498. Raulien, N., et al., *Fatty Acid Oxidation Compensates for Lipopolysaccharide-Induced Warburg Effect in Glucose-Deprived Monocytes.* Frontiers in Immunology, 2017. **8**: p. 609.
499. Pantel, A., et al., *Direct type I IFN but not MDA5/TLR3 activation of dendritic cells is required for maturation and metabolic shift to glycolysis after poly IC stimulation.* PLoS Biol, 2014. **12**(1): p. e1001759.

500. Everts, B., et al., *TLR-driven early glycolytic reprogramming via the kinases TBK1-IKK[epsiv] supports the anabolic demands of dendritic cell activation.* Nat Immunol, 2014. **15**(4): p. 323-332.
501. Raniga, K. and C. Liang, *Interferons: Reprogramming the Metabolic Network against Viral Infection.* Viruses, 2018. **10**(1): p. 36.
502. Munger, J., et al., *Systems-level metabolic flux profiling identifies fatty acid synthesis as a target for antiviral therapy.* Nat Biotechnol, 2008. **26**(10): p. 1179-86.
503. Moser, T.S., D. Schieffer, and S. Cherry, *AMP-Activated Kinase Restricts Rift Valley Fever Virus Infection by Inhibiting Fatty Acid Synthesis.* PLOS Pathogens, 2012. **8**(4): p. e1002661.
504. Prantner, D., D.J. Perkins, and S.N. Vogel, *AMP-activated Kinase (AMPK) Promotes Innate Immunity and Antiviral Defense through Modulation of Stimulator of Interferon Genes (STING) Signaling.* The Journal of biological chemistry, 2017. **292**(1): p. 292-304.
505. Vincent, E.E., et al., *Differential effects of AMPK agonists on cell growth and metabolism.* Oncogene, 2014. **34**: p. 3627.
506. Chung, E.J., et al., *AICAR suppresses TNF-α-induced complement factor B in RPE cells.* Scientific Reports, 2017. **7**: p. 17651.
507. Kurihara, T., et al., *Hypoxia-induced metabolic stress in retinal pigment epithelial cells is sufficient to induce photoreceptor degeneration.* eLife, 2016. **5**: p. e14319.
508. Kim, D.-H., et al., *GβL, a Positive Regulator of the Rapamycin-Sensitive Pathway Required for the Nutrient-Sensitive Interaction between Raptor and mTOR.* Molecular Cell, 2003. **11**(4): p. 895-904.
509. Schmitz, J., et al., *IL-33, an Interleukin-1-like Cytokine that Signals via the IL-1 Receptor-Related Protein ST2 and Induces T Helper Type 2-Associated Cytokines.* Immunity, 2005. **23**(5): p. 479-490.
510. Pinto, S.M., et al., *Quantitative phosphoproteomic analysis of IL-33-mediated signaling.* Proteomics, 2015. **15**(2-3): p. 532-544.
511. Maywald, R.L., et al., *IL-33 activates tumor stroma to promote intestinal polyposis.* Proc Natl Acad Sci U S A, 2015. **112**(19): p. E2487-96.
512. Lin, J., et al., *A Novel Interleukin 33/ST2 Signaling Regulates Inflammatory Response in Human Corneal Epithelium.* PLOS ONE, 2013. **8**(4): p. e60963.
513. Hueber, A.J., et al., *IL-33 induces skin inflammation with mast cell and neutrophil activation.* Eur J Immunol, 2011. **41**(8): p. 2229-37.
514. Allen, J.D., et al., *p21-activated kinase regulates mast cell degranulation via effects on calcium mobilization and cytoskeletal dynamics.* Blood, 2009. **113**(12): p. 2695.
515. Liesa, M. and Orian S. Shirihai, *Mitochondrial Networking in T Cell Memory.* Cell, 2016. **166**(1): p. 9-10.
516. Suzuki, M., et al., *Chronic photo-oxidative stress and subsequent MCP-1 activation as causative factors for age-related macular degeneration.* Journal of Cell Science, 2012. **125**(10): p. 2407.
517. Hanus, J., et al., *Induction of necrotic cell death by oxidative stress in retinal pigment epithelial cells.* Cell Death Dis, 2013. **4**: p. e965.
518. Liu, J., et al., *Impairing autophagy in retinal pigment epithelium leads to inflammasome activation and enhanced macrophage-mediated angiogenesis.* Scientific Reports, 2016. **6**.

519. Candas, D. and J.J. Li, *MnSOD in Oxidative Stress Response-Potential Regulation via Mitochondrial Protein Influx.* Antioxidants & Redox Signaling, 2014. **20**(10): p. 1599-1617.
520. Ng, C.F., et al., *The rate of cellular hydrogen peroxide removal shows dependency on GSH: Mathematical insight into in vivo H2O2 and GPx concentrations.* Free Radical Research, 2007. **41**(11): p. 1201-1211.
521. Sullivan, L.B. and N.S. Chandel, *Mitochondrial metabolism in TCA cycle mutant cancer cells.* Cell Cycle, 2014. **13**(3): p. 347-8.
522. Jäger, S., et al., *AMP-activated protein kinase (AMPK) action in skeletal muscle via direct phosphorylation of PGC-1α.* Proceedings of the National Academy of Sciences, 2007. **104**(29): p. 12017.
523. Golestaneh, N., et al., *Repressed SIRT1/PGC-1alpha pathway and mitochondrial disintegration in iPSC-derived RPE disease model of age-related macular degeneration.* J Transl Med, 2016. **14**(1): p. 344.
524. Huang, S.C.-C., et al., *Cell-intrinsic lysosomal lipolysis is essential for alternative activation of macrophages.* Nature Immunology, 2014. **15**: p. 846.
525. Ip, W.K.E., et al., *Anti-inflammatory effect of IL-10 mediated by metabolic reprogramming of macrophages.* Science (New York, N.Y.), 2017. **356**(6337): p. 513-519.
526. Pollmächer, T., et al., *Low levels of circulating inflammatory cytokines—Do they affect human brain functions?* Brain, Behavior, and Immunity, 2002. **16**(5): p. 525-532.
527. Nassar, K., et al., *Serum cytokines as biomarkers for age-related macular degeneration.* Graefes Arch Clin Exp Ophthalmol, 2015. **253**(5): p. 699-704.
528. Currie, H.N., et al., *Spatial cytokine distribution following traumatic injury.* Cytokine, 2014. **66**(2): p. 112-118.
529. Theodoropoulou, S., et al., *Interleukin-33 regulates tissue remodelling and inhibits angiogenesis in the eye.* J Pathol, 2017. **241**(1): p. 45-56.
530. Molofsky, A.B., A.K. Savage, and R.M. Locksley, *Interleukin-33 in Tissue Homeostasis, Injury, and Inflammation.* Immunity, 2015. **42**(6): p. 1005-19.
531. Bessa, J., et al., *Altered subcellular localization of IL-33 leads to non-resolving lethal inflammation.* J Autoimmun, 2014. **55**: p. 33-41.
532. Lotze, M.T. and K.J. Tracey, *High-mobility group box 1 protein (HMGB1): nuclear weapon in the immune arsenal.* Nature Reviews Immunology, 2005. **5**: p. 331.
533. Werman, A., et al., *The precursor form of IL-1alpha is an intracrine proinflammatory activator of transcription.* Proc Natl Acad Sci U S A, 2004. **101**(8): p. 2434-9.
534. Shan, J., et al., *Interferon γ-Induced Nuclear Interleukin-33 Potentiates the Release of Esophageal Epithelial Derived Cytokines.* PloS one, 2016. **11**(3): p. e0151701-e0151701.
535. Konermann, S., et al., *Genome-scale transcriptional activation by an engineered CRISPR-Cas9 complex.* Nature, 2015. **517**(7536): p. 583-8.
536. Halestrap, A.P., *The mitochondrial pyruvate carrier: has it been unearthed at last?* Cell Metab, 2012. **16**(2): p. 141-3.
537. Herzig, S., et al., *Identification and functional expression of the mitochondrial pyruvate carrier.* Science, 2012. **337**(6090): p. 93-6.

538. Halestrap, A.P., *The mechanism of the inhibition of the mitochondrial pyruvate transportater by alpha-cyanocinnamate derivatives.* The Biochemical journal, 1976. **156**(1): p. 181-183.
539. Deberardinis, R.J., J.J. Lum, and C.B. Thompson, *Phosphatidylinositol 3-kinase-dependent modulation of carnitine palmitoyltransferase 1A expression regulates lipid metabolism during hematopoietic cell growth.* J Biol Chem, 2006. **281**(49): p. 37372-80.
540. Owen, O.E., S.C. Kalhan, and R.W. Hanson, *The key role of anaplerosis and cataplerosis for citric acid cycle function.* J Biol Chem, 2002. **277**(34): p. 30409-12.
541. Courtney, K.D., et al., *Isotope Tracing of Human Clear Cell Renal Cell Carcinomas Demonstrates Suppressed Glucose Oxidation In Vivo.* Cell Metabolism, 2018. **28**(5): p. 793-800.e2.
542. Le, A., et al., *Glucose-independent glutamine metabolism via TCA cycling for proliferation and survival in B-cells.* Cell Metabolism, 2012. **15**(1): p. 110-121.
543. *Pineda-Torres M, Flores-Espinosa P, Espejel-Nunez A, Estrada-Gutierrez G, Flores-Pliego A, Maida-Claros R, et al. Evidence of an immunosuppressive effect of progesterone upon in vitro secretion of proinflammatory and prodegradative factors in a model of choriodecidual infection. BJOG 2014, doi:10.1111/1471-0528.13113*.
544. Azzu, V. and M.D. Brand, *The on-off switches of the mitochondrial uncoupling proteins.* Trends in Biochemical Sciences, 2010. **35**(5): p. 298-307.
545. Carroll, A.M., et al., *Identification of a functioning mitochondrial uncoupling protein 1 in thymus.* J Biol Chem, 2005. **280**(16): p. 15534-43.
546. Nagase, I., et al., *Expression of uncoupling protein in skeletal muscle and white fat of obese mice treated with thermogenic beta 3-adrenergic agonist.* J Clin Invest, 1996. **97**(12): p. 2898-904.
547. Li, B., et al., *Skeletal muscle respiratory uncoupling prevents diet-induced obesity and insulin resistance in mice.* Nature Medicine, 2000. **6**: p. 1115.
548. Cui, Y., et al., *Expression modification of uncoupling proteins and MnSOD in retinal endothelial cells and pericytes induced by high glucose: The role of reactive oxygen species in diabetic retinopathy.* Experimental Eye Research, 2006. **83**(4): p. 807-816.
549. Brondani, L.A., et al., *The UCP1 −3826A/G Polymorphism Is Associated with Diabetic Retinopathy and Increased UCP1 and MnSOD2 Gene Expression in Human Retina.* Investigative Ophthalmology & Visual Science, 2012. **53**(12): p. 7449-7457.
550. Raud, B., et al., *Etomoxir Actions on Regulatory and Memory T Cells Are Independent of Cpt1a-Mediated Fatty Acid Oxidation.* Cell Metabolism, 2018. **28**(3): p. 504-515.e7.
551. Oshio, T., et al., *Nuclear expression of IL-33 in epidermal keratinocytes promotes wound healing in mice.* Journal of Dermatological Science, 2017. **85**(2): p. 106-114.
552. Lachmandas, E., et al., *Microbial stimulation of different Toll-like receptor signalling pathways induces diverse metabolic programmes in human monocytes.* Nature Microbiology, 2016. **2**: p. 16246.
553. Stanley, A.C. and P. Lacy, *Pathways for Cytokine Secretion.* Physiology, 2010. **25**(4): p. 218-229.
554. Bertheloot, D. and E. Latz, *HMGB1, IL-1alpha, IL-33 and S100 proteins: dual-function alarmins.* Cell Mol Immunol, 2017. **14**(1): p. 43-64.

555. Trinkle-Mulcahy, L., et al., *Identifying specific protein interaction partners using quantitative mass spectrometry and bead proteomes.* The Journal of cell biology, 2008. **183**(2): p. 223-239.
556. Morgan, R.G., et al., *LEF-1 drives aberrant β-catenin nuclear localization in myeloid leukemia cells.* Haematologica, 2019. **104**(7): p. 1365-1377.
557. Durrant, T.N., et al., *In-depth PtdIns(3,4,5)P3 signalosome analysis identifies DAPP1 as a negative regulator of GPVI-driven platelet function.* Blood Adv, 2017. **1**(14): p. 918-932.
558. Guard, S.E., et al., *The nuclear interactome of DYRK1A reveals a functional role in DNA damage repair.* Scientific Reports, 2019. **9**(1): p. 6539.
559. Szklarczyk, D., et al., *STRING v11: protein-protein association networks with increased coverage, supporting functional discovery in genome-wide experimental datasets.* Nucleic Acids Res, 2019. **47**(D1): p. D607-d613.
560. Hurcombe, J.A., et al., *Podocyte GSK3 is an evolutionarily conserved critical regulator of kidney function.* Nature Communications, 2019. **10**(1): p. 403.
561. Sun, Y., et al., *The Expression and Significance of Neuronal Iconic Proteins in Podocytes.* PLOS ONE, 2014. **9**(4): p. e93999.
562. Abe, T., et al., *Interleukin-1beta and barrier function of retinal pigment epithelial cells (ARPE-19): aberrant expression of junctional complex molecules.* Invest Ophthalmol Vis Sci, 2003. **44**(9): p. 4097-104.
563. Chen, Y., et al., *The Effects of Th17 Cytokines on the Inflammatory Mediator Production and Barrier Function of ARPE-19 Cells.* PLOS ONE, 2011. **6**(3): p. e18139.
564. Kutty, R.K., et al., *Differential regulation of microRNA-146a and microRNA-146b-5p in human retinal pigment epithelial cells by interleukin-1beta, tumor necrosis factor-alpha, and interferon-gamma.* Mol Vis, 2013. **19**: p. 737-50.
565. Fasler-Kan, E., et al., *Activation of the JAK-STAT intracellular pathway in human retinal pigment epithelial cell line ARPE-19*, in *International Journal of Interferon, Cytokine and Mediator Research*. 2010. p. 127-136.
566. An, E., H. Gordish-Dressman, and Y. Hathout, *Effect of TNF-alpha on human ARPE-19-secreted proteins.* Molecular vision, 2008. **14**: p. 2292-2303.
567. Ting, L., et al., *Normalization and statistical analysis of quantitative proteomics data generated by metabolic labeling.* Molecular & cellular proteomics : MCP, 2009. **8**(10): p. 2227-2242.
568. Rajala, A., et al., *Pyruvate kinase M2 regulates photoreceptor structure, function, and viability.* Cell death & disease, 2018. **9**(2): p. 240-240.
569. Rajala, R.V.S., et al., *The Warburg Effect Mediator Pyruvate Kinase M2 Expression and Regulation in the Retina.* Scientific Reports, 2016. **6**: p. 37727.
570. Hu, Y.H., et al., *WDFY1 mediates TLR3/4 signaling by recruiting TRIF.* EMBO Rep, 2015. **16**(4): p. 447-55.
571. Fane, M., et al., *Nuclear factor one transcription factors as epigenetic regulators in cancer.* 2017. **140**(12): p. 2634-2641.
572. Glenn, J.V., et al., *Proteomic profiling of human retinal pigment epithelium exposed to an advanced glycation-modified substrate.* Graefe's archive for clinical and experimental ophthalmology = Albrecht von Graefes Archiv fur klinische und experimentelle Ophthalmologie, 2012. **250**(3): p. 349-359.

573. Tsuda, H., et al., *Novel Splice Variants of IL-33: Differential Expression in Normal and Transformed Cells.* Journal of Investigative Dermatology, 2012. **132**(11): p. 2661-2664.
574. Hong, J., et al., *Identification of constitutively active interleukin 33 (IL-33) splice variant.* J Biol Chem, 2011. **286**(22): p. 20078-86.
575. Fisher, C.R. and D.A. Ferrington, *Perspective on AMD Pathobiology: A Bioenergetic Crisis in the RPEA Bioenergetic Crisis Underlies AMD Pathology.* Investigative Ophthalmology & Visual Science, 2018. **59**(4): p. AMD41-AMD47.
576. Kleinman, M.E., et al., *Short-interfering RNAs induce retinal degeneration via TLR3 and IRF3.* Mol Ther, 2012. **20**(1): p. 101-8.
577. Cano, M., et al., *Cigarette smoking, oxidative stress, the anti-oxidant response through Nrf2 signaling, and Age-related Macular Degeneration.* Vision Res, 2010. **50**(7): p. 652-64.
578. Bringmann, A., et al., *Muller cells in the healthy and diseased retina.* Prog Retin Eye Res, 2006. **25**(4): p. 397-424.
579. Pavlou, S., et al., *Deletion of interleukin-33 (IL33) results in persistent Müller cell activation during retinal detachment*. 2016.
580. Kakkar, R. and R.T. Lee, *The IL-33/ST2 pathway: therapeutic target and novel biomarker.* Nat Rev Drug Discov, 2008. **7**(10): p. 827-40.
581. Cao, X., et al., *Macrophage polarization in the maculae of age-related macular degeneration: a pilot study.* Pathology international, 2011. **61**(9): p. 528-535.
582. Yang, Y., et al., *ST2/IL-33-Dependent Microglial Response Limits Acute Ischemic Brain Injury.* J Neurosci, 2017. **37**(18): p. 4692-4704.
583. Wu, W.-K., et al., *IL-4 Regulates Specific Arg-1+ Macrophage sFlt-1–Mediated Inhibition of Angiogenesis.* The American Journal of Pathology, 2015. **185**(8): p. 2324-2335.
584. Bhutto, I.A., et al., *Increased choroidal mast cells and their degranulation in age-related macular degeneration.* The British journal of ophthalmology, 2016. **100**(5): p. 720-726.
585. McLeod, D.S., et al., *Mast Cell-Derived Tryptase in Geographic Atrophy.* Investigative ophthalmology & visual science, 2017. **58**(13): p. 5887-5896.
586. Imamura, Y., et al., *Drusen, choroidal neovascularization, and retinal pigment epithelium dysfunction in SOD1-deficient mice: a model of age-related macular degeneration.* Proceedings of the National Academy of Sciences of the United States of America, 2006. **103**(30): p. 11282-11287.
587. Justilien, V., et al., *SOD2 knockdown mouse model of early AMD.* Invest Ophthalmol Vis Sci, 2007. **48**(10): p. 4407-20.
588. Zhao, Z., et al., *Age-Related Retinopathy in NRF2-Deficient Mice.* PLOS ONE, 2011. **6**(4): p. e19456.
589. Alge, C.S., et al., *Comparative Proteome Analysis of Native Differentiated and Cultured Dedifferentiated Human RPE Cells.* Investigative Ophthalmology & Visual Science, 2003. **44**(8): p. 3629-3641.
590. Thomas, R., et al., *Features that define the best ChIP-seq peak calling algorithms.* Brief Bioinform, 2017. **18**(3): p. 441-450.

Chapter 9. Research output

9.1. Publications

Scott LM, Vincent EE, Hudson N, Neal C, Lavelle E, Campbell M, Halestrap AP, Dick AD & Theodoropoulou S. *Interleukin-33 regulates metabolic reprogramming of the retinal pigment epithelium in responses to immune stressors*. JCI Insight (In revision).

Ou K, Mertsch S, Theodoropoulou S, Wu J, Liu J, Copland DA, **Scott LM**, Dick AD, Schrader S & Liu L. *Müller cells stabilise vasculature through hypoxic preconditioning*. Cell Physiol Biochem 2019;52(4):668-680.

9.2. Presentations

9.2.1. Oral presentations

Scott LM, Vincent EE, Dick, AD & Theodoropoulou S. *Interleukin-33 regulates mitochondrial function in the retinal pigment epithelium maintaining immune homeostasis*. European Association for Vision and Eye Research Annual Meeting, 3rd-6th October 2018, Nice, France.

9.2.2. Poster presentations

Scott LM, Theodoropolou S & Dick AD. *AMP-activated kinase links metabolism and innate immunity in the retinal pigment epithelium*. University of Bristol School of Cellular and Molecular Medicine Away Day, 5th January 2017, Bristol, UK.

Scott LM, Theodoropolou S & Dick AD. *AMP-activated kinase links metabolism and innate immunity in the retinal pigment epithelium*. Oxford, Bristol, Cardiff, Southampton Ophthalmology Alliance Meeting, 2nd June 2017, Southampton, UK.

Scott LM, Dick AD & Theodoropolou S. *AMP-activated kinase links metabolism and innate immunity in the retinal pigment epithelium*. University of Bristol Infection and Immunity Away Day 21st June 2017, Bristol, UK.

Scott LM, Dick AD & Theodoropolou S. *AMP-activated kinase and interleukin-33 regulate metabolic function in the retinal pigment epithelium.* University of Bristol School of Cellular and Molecular Medicine Away Day, 11th January 2018, Bristol, UK.

Scott LM, Vincent EE, Dick, AD & Theodoropoulou S. *Interleukin-33 regulates mitochondrial function in the retinal pigment epithelium maintaining immune homeostasis*. European Association for Vision and Eye Research Annual Meeting, 3rd-6th October 2018, Nice, France.

Scott LM, Vincent EE, Dick, AD & Theodoropoulou S. *Interleukin-33 regulates mitochondrial function in the retinal pigment epithelium maintaining immune homeostasis*. University of Bristol School of Cellular and Molecular Medicine Away Day, 10th January 2019, Bristol, UK.

Scott LM, Vincent EE, Hudson N, Copland DA, Heesom K, Campbell M, Halestrap A, Dick AD & Theodoropoulou S. *Mapping interleukin-33 to metabolic function in the retinal pigment epithelium*. Association of Research in Vision and Ophthalmology Annual Meeting, 27th April – 2nd May 2019, Vancouver, Canada.

Chapter 10. Appendices

10.1. Detection of “metabolic switching” on the XF platform

To identify potential metabolic changes to the RPE under innate immune “stress”, there was a need to observe if: (A) the RPE was able to rapidly alter its metabolism and (B) if the Seahorse XFp can detect these changes in real-time. Together the experiments were designed to observe whether a potent metabolic signal could induce real-time metabolic changes to the RPE. Lactate was chosen as a suitable signal due to its well-described ability to suppress glycolysis in cancer cells [463]. Lactate has a described role in suppressing RPE glycolysis and is used as an RPE fuel source [4]. In order to assess the changes to ARPE-19 metabolism, basal OCR and ECAR measurements were taken before and after an injection of lactate. It was found that lactate dose-dependently increased OCR measurements and suppressed ECAR measurements post injection (Fig. 10.1A-B). This data indicated that rapid changes in metabolism could be identified in RPE cells.

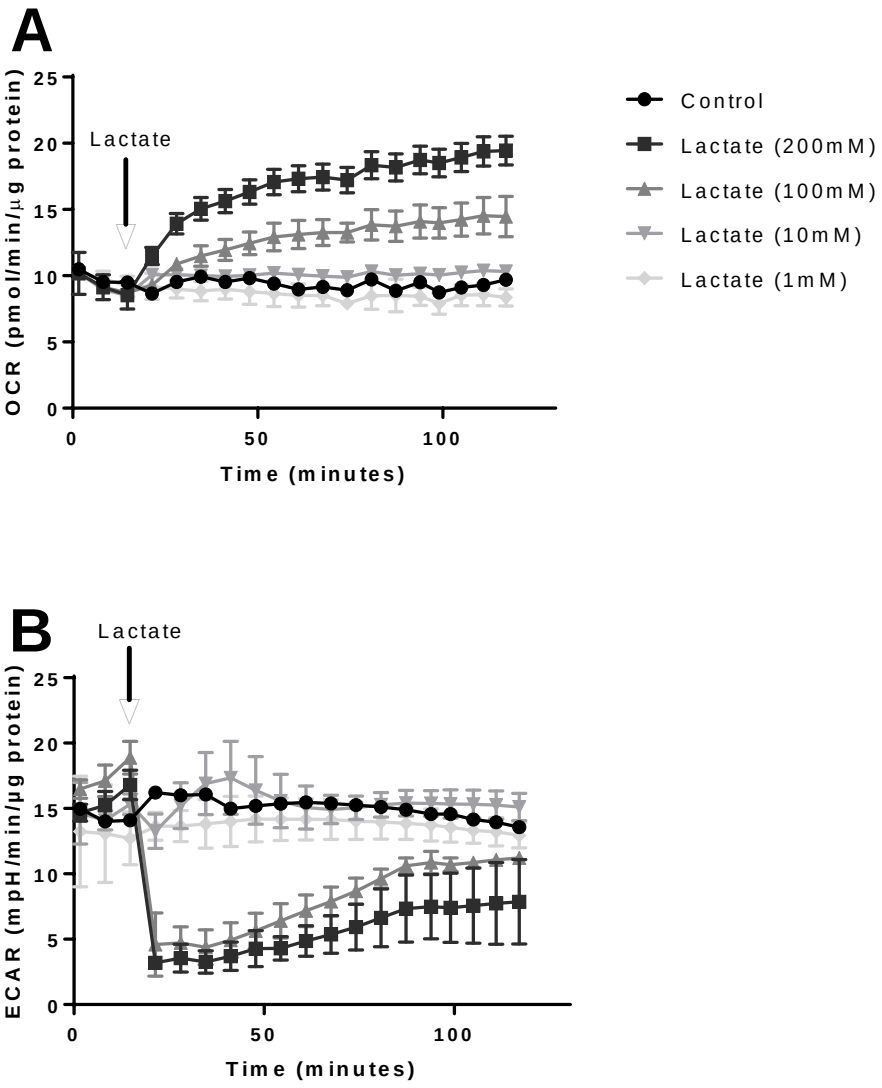

Figure 10.1. Metabolic switching in ARPE-19 cells:

The ability of lactate to suppress glycolysis and increase oxidative phosphorylation in ARPE-19 cells was assessed on the XFp platform. Varying doses of lactate was injected into ports of XFp cartridges and OCR (A) or ECAR (B) measurements were taken for over 100min. Data presented as means ± SD from two independent experiments performed in triplicates.

10.2. Detection of alternate bioenergetic profiles

Extracellular bioflux analysis allows quantification of the ATP-producing respiratory processes via measurement of OCR for oxidative phosphorylation and ECAR for glycolysis. These are subsequently utilized to determine various metabolic parameters, which can be used to examine the "bioenergetic status" of a cell. Because bioflux is a cell-type specific process, it was important to first identify if alternate parameters (such as the Warburg effect) could be observed using cells with distinct known metabolic characteristics. I chose to utilize the ARPE-19 (as a typically OXPHOS utilizing cell [376]) and as a comparator, the colon cancer cell line SW1463 (highly glycolytic cells established from a grade III solid rectal adenocarcinoma [444]). A glycolysis stress test was utilised to measure the glycolytic function in these cells (as detailed in materials and methods). It was found that SW1463 were significantly more glycolytic than ARPE-19 yet lacked glycolytic reserve post-oligomycin injection (Fig. 10.2A-B). The lack of glycolytic reserve indicated that the SW1463 cells relied less on mitochondrial ATP production compared to ARPE-19. A mitochondrial stress test was utilised to measure the mitochondrial function in these cells (as detailed in materials and methods). It was found that SW1463 cells had reduced basal and maximal respiration compared to ARPE-19 cells (Fig. 10.2C-D). The reduced OCR/ECAR in the SW1463 cells further highlighted the increased reliance on glycolysis over OXPHOS (Fig. 10.2E).

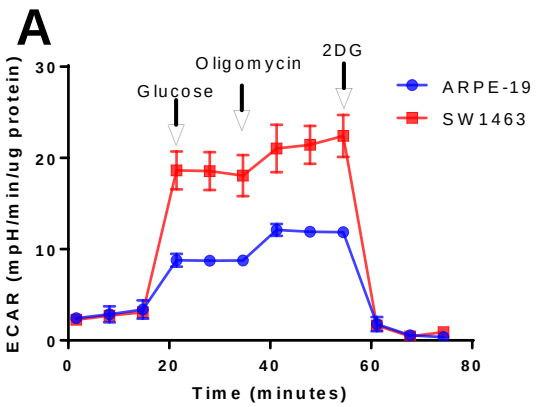
A
Glucose
Oligomycin
2DG
ARPE-19
SW1463
ECAR (mpH/min/ug protein)
Time (minutes)

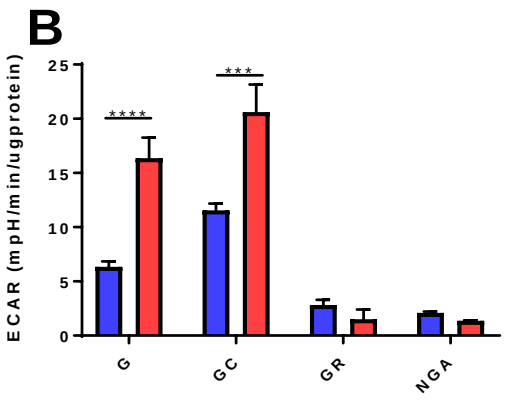
B
ECAR (mpH/min/ugprotein)
G
GC
GR
NGA

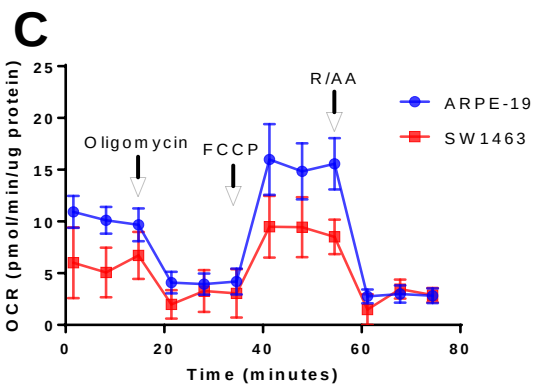
C
Oligomycin
FCCP
R/AA
ARPE-19
SW1463
OCR (pmol/min/ug protein)
Time (minutes)

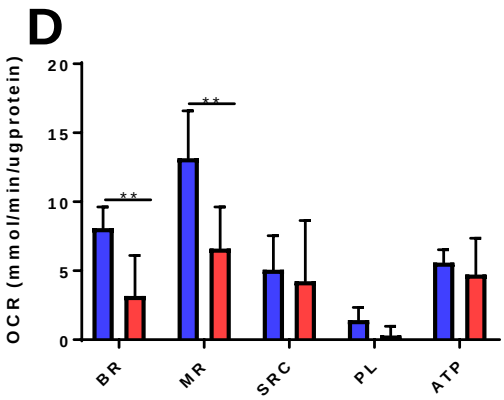
D
OCR (mmol/min/ugprotein)
BR
MR
SRC
PL
ATP

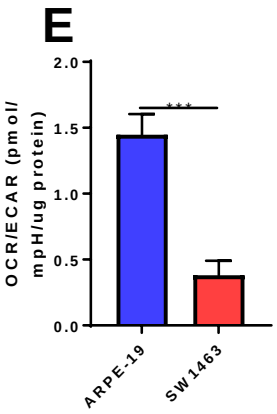
E
OCR/ECAR (pmol/ mpH/ug protein)
ARPE-19
SW1463

Figure 10.2. Comparative bioflux analysis indicates SW1463 colon cancer cells exhibit increased glycolysis compared to ARPE-19:

(A) Representative glycolysis stress test measured with sequential injections of glucose, oligomycin and 2DG (B) Glycolysis parameters (G- glycolysis; GC- glycolytic capacity; GR- glycolytic reserve; NGA- non-glycolytic acidification) calculated from data shown in (A). (C) Representative mitochondrial stress test measured with sequential injections of oligomycin, FCCP and rotenone/antimycin-A. (D) Mitochondrial parameters (BR- basal respiration; MR- maximal respiration; SRC- spare respiratory capacity; PL- proton leak; ATP- ATP-production) calculated from data shown in (C). (E) Basal OCR and ECAR measurements expressed as the ratio OCR/ECAR. (F) Data presented as means ± SD from two independent experiments performed in triplicates. (B-C) One-way ANOVA with Tukey's multiple comparisons test, (D) Unpaired Student's T-test; *p<0.05, **p<0.01, ***p<0.005, ****p<0.001.

10.3. Low-molecular weight Poly (I:C) has similar effects to the high-molecular weight agonist on ARPE-19 metabolism

Treatment of ARPE-19 cells with LMW Poly (I:C) for 24h had no significant effect on the cytotoxicity (Fig. 10.3A). Having confirmed that the LMW displayed similar tolerability by ARPE-19 cells, I proceeded to undertake metabolic analysis.

Post injection of LMW Poly (I:C) there were no changes observed in real-time ECAR or OCR measurements (Fig. 10.3B-C). A mitochondrial stress test was used to identify changes in OXPHOS parameters. It was found that treatment of ARPE-19 cells for 24h with 10μg/ml of LMW Poly (I:C) increased mitochondrial respiration. Basal respiration and maximal respiration were both significantly increased (Fig. 10.3D-E). No significant changes were observed to spare respiratory capacity or any deleterious mitochondrial parameter (Fig. 10.3D-E). The corresponding ECAR data was used to identify how basal glycolysis and glycolytic capacity were affected by LMW Poly (I:C) stimulation. It was observed – post oligomycin injection – that cells pre-treated with LMW poly (I:C) for 24h had increased glycolytic capacity (Fig. 10.3F-G). The OCR and ECAR data were expressed as the ratio OCR/ECAR to reflect OXPHOS/lactate production levels. There was a significant increase in OCR/ECAR ratio (Fig. 10.3H).

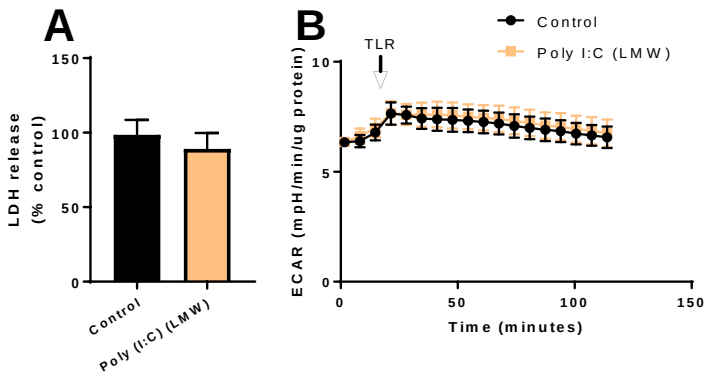
A
LDH release (% control)
150
100
50
0
Control
Poly (I:C) (LMW)
B
TLR
Control
Poly I:C (LMW)
ECAR (mpH/min/ug protein)
10
5
0
0
50
100
150
Time (minutes)

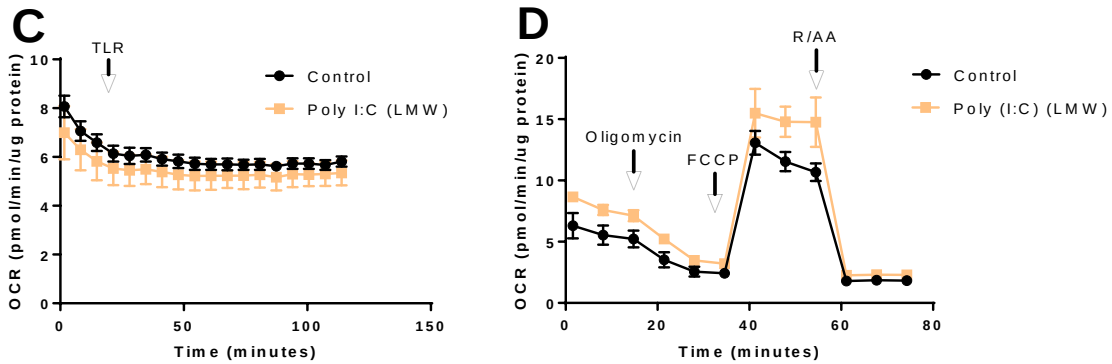
C
TLR
Control
Poly I:C (LMW)
OCR (pmol/min/ug protein)
10
8
6
4
2
0
0
50
100
150
Time (minutes)
D
R/AA
Oligomycin
FCCP
Control
Poly (I:C) (LMW)
OCR (pmol/min/ug protein)
20
15
10
5
0
0
20
40
60
80
Time (minutes)

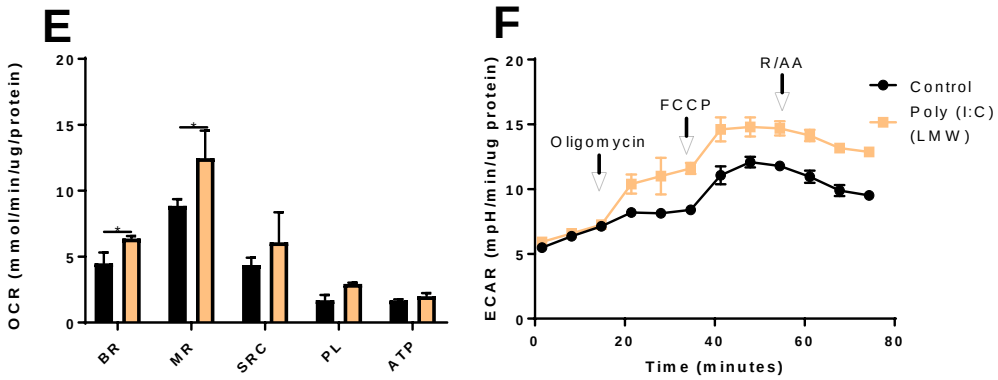
E
OCR (mmol/min/ug/protein)
20
15
10
5
0
BR
MR
SRC
PL
ATP
F
R/AA
FCCP
Oligomycin
Control
Poly (I:C) (LMW)
ECAR (mpH/min/ug protein)
20
15
10
5
0
0
20
40
60
80
Time (minutes)

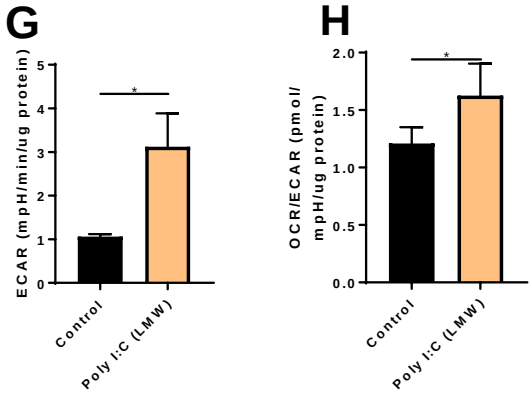
G
ECAR (mpH/min/ug protein)
5
4
3
2
1
0
Control
Poly I:C (LMW)
H
OCR/ECAR (pmol/ mpH/ug protein)
2.0
1.5
1.0
0.5
0.0
Control
Poly I:C (LMW)

Figure 10.3. Low-molecular weight Poly (I:C) has similar effects to the high-molecular weight agonist on ARPE-19 metabolism:

(A) ARPE-19 cells were treated for 24h with LMW Poly (I:C) (10μg/ml). Supernatants were taken and LDH levels were assessed using a commercial kit. LDH release was expressed as a (%) of an untreated control. (B) Real-time changes in ECAR following injection of LMW Poly (I:C) (10μg/ml). (C) Real-time changes in OCR following injection of LMW Poly (I:C) (10μg/ml). (D) Representative mitochondrial stress test measured with sequential injections of Oligomycin, FCCP and rotenone/antimycin A, following stimulation with LMW Poly (I:C) (24h; 10μg/ml). (E) Mitochondrial parameters (BR- basal respiration; MR- maximal respiration; SRC- spare respiratory capacity; PL- proton leak; ATP- ATP-production) calculated from data shown in (D). (F) ECAR data from (D). (G) Glycolytic capacity calculated from (F). (H) Basal OCR and ECAR measurements expressed as the ratio OCR/ECAR, after 24h LMW Poly (I:C) (10μg/ml) treatment. Data presented as means ± SD, from two independent experiments performed in triplicate. Unpaired Student's T-test; *p<0.05.

10.4. Validation of recombinant IL-33 bioactivity

I chose to use recombinant mouse (ALX-522-101-C010) and human recombinant IL-33 (ALX-522-098 C010) from Enzo Life Sciences Ltd (see Section 2.2.1) [8]. Prior to assessing the role of IL-33 on RPE metabolism, there was a necessity to validate the bioactivity of both human and murine rIL-33 in RPE cells. A previous study identified transcriptional changes in an IL-33-stimulated murine cell line, whereby increased *Il33* and *Mpc-1* mRNA transcripts were observed [16]. I decided to repeat this experiment in both human ARPE-19 and murine B6RPE-07 cell lines exposed to varying doses of rIL-33 for 24h, using the expression changes of *IL33*/*Il33* mRNA as a positive control for the recombinant proteins. Both RPE cell lines were observed to exhibit a dose-dependent increase in the expression of *IL33* or *Il33* in response to rhIL-33 or rmIL-33, respectively (Fig. 10.4A-B). Collectively, these preliminary results provide a bioactivity control for both recombinant proteins.

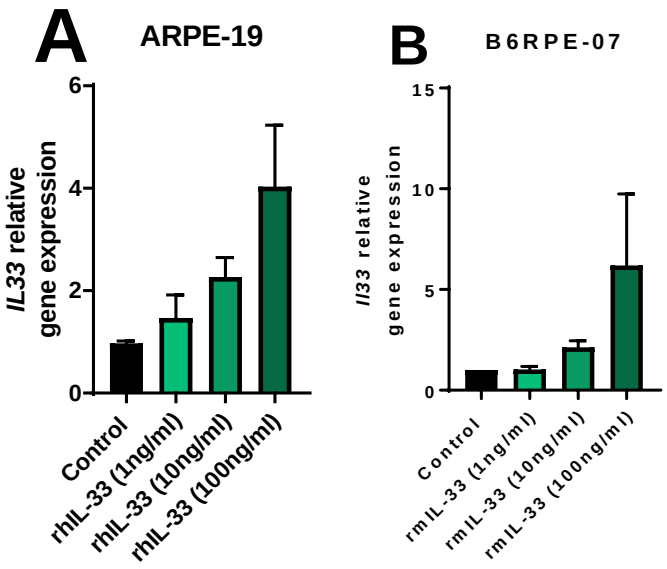

Figure 10.4. Validation of recombinant IL-33 bioactivity:

(A) ARPE-19 cells were treated for 24h in the presence or absence of rhIL-33 (1-100ng/ml). RNA was isolated, converted to cDNA and RT-PCR was used to assess the expression of *IL33.* (B) B6RPE-07 cells were treated for 24h in the presence or absence of rmIL-33 (1-100ng/ml). RNA was isolated, converted to cDNA and RT-PCR was used to assess the expression of *Il33 or IL33.* Represents data from one experiment with two biological repeats.

10.5. Nessy-1 antibody test and small-scale ChIP sequencing

To determine the role of IL-33 in DNA binding, A ChIP reaction was carried out using 30µg of human ARPE-19 epithelial cells chromatin and anti-IL-33 antibody (Nessy-1). In the absence of a suitable commercially available ChIP/ChIP-seq grade antibody for IL-33, Nessy-1 was chosen as a preliminary antibody for two reasons: firstly, it was observed to successfully pull-down IL-33 in the experiments detailed in chapter 6; secondly, Nessy-1 was used successfully to show the binding of IL-33 to the *IL1RL1* promoter (ChIP-RT-PCR) and co-immunoprecipitation of SUV39H1 in a previous study [256]. The ChIP DNA was processed into a standard Illumina ChIP-Seq library and sequenced to generate >5 million reads. Reads were aligned to the human genome (hg38), and after removal of duplicate and non-uniquely mapped reads, ~6.5 million alignments were obtained. A signal map capturing fragment densities along the genome was generated and visualized in the Integrated Genome Browser (IGB). In addition, MACS peak finding was performed to identify the most significant peaks. Using a default cut-off of p-value <1e-7 (without control file), only 99 peaks were identified (after ENCODE blacklist filtering). Typically, antibody validations for non-histone proteins which pass this criterion exhibit a peak number of around 5,000 [588].

Further investigation into the peaks identified from the Nessy-1 test revealed that almost two thirds (63/99) of these corresponded to repetitive/centromeric/near-telomeric regions with no gene annotation. The remaining 36 peaks with gene annotations are summarised in Table 10.4, Appendices. Of these, only 15 peaks corresponded to protein encoding genes, with 19 peaks corresponding to pseudogenes or non-coding RNA. It was essential to note that gene position varied across the genes with no enrichment in promoter or exon regions. Indeed, most peaks corresponded to upstream or downstream gene regions indicative of no clear regulatory function.

Six Integrated Genome Browser 9.0.2 (IGB) screenshots are enclosed (Fig. 10.5-7), showing different chromosomes and regions of the genome. Each image shows the IL-33 data in the top track (blue colour), followed by a track with red marks indicating the location of the filtered MACS peaks. The bottom two data tracks of the screenshots (black colour) show a negative ("input control") and positive ChIP-Seq assay (historical, unrelated data) for comparison and as illustration. These "control tracks" were generated from 5 million tags, and IGB y-axis scales were adjusted to make all tracks comparable. The bottom 2 tracks show the RefSeq gene annotations in green.

Based on the background-level number of peaks identified and the essentially flat appearance of the signal map in the genome browser, it suggested that this antibody test was likely unsuccessful. As there was no positive control available for Nessy-1, the antibody validation assay did not include an actual positive control with the same chromatin. Instead, the reactions were carried out in batches with other ChIP-Seq assays using validated antibodies at Active Motif Laboratories, Carlsbad, USA. The latter reactions serve thus as technical controls for the present antibody validation.

Taken together, the results obtained in this section suggest that Nessy-1 may not be a suitable antibody for ChIP of IL-33 and therefore future work should aim to investigate an alternate antibody and proceed with small-scale sequencing.

A

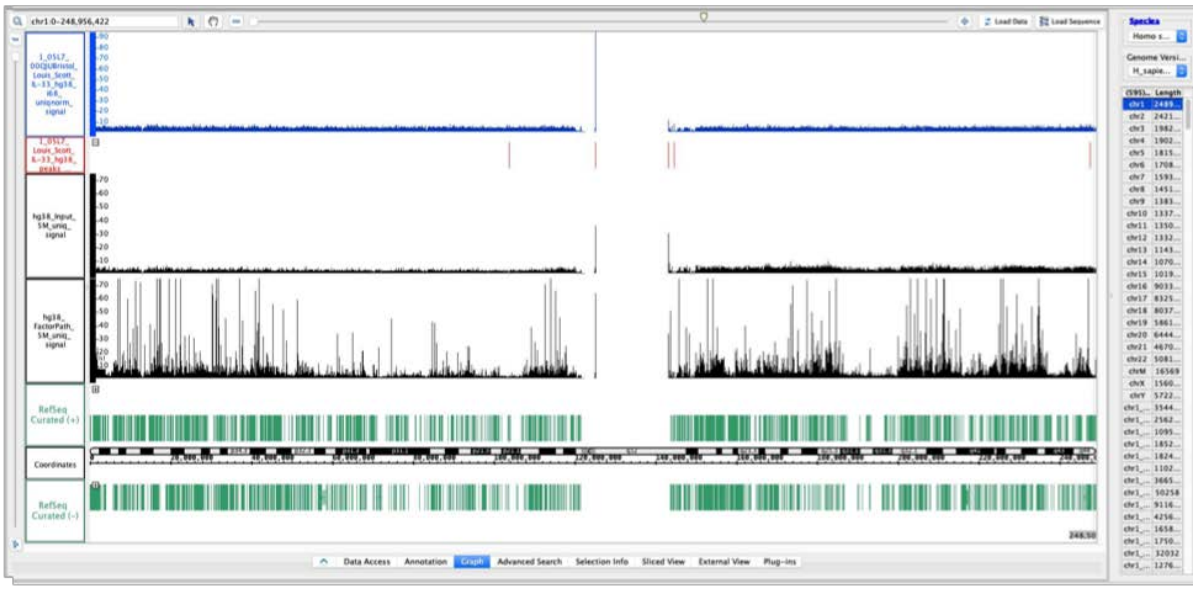

B

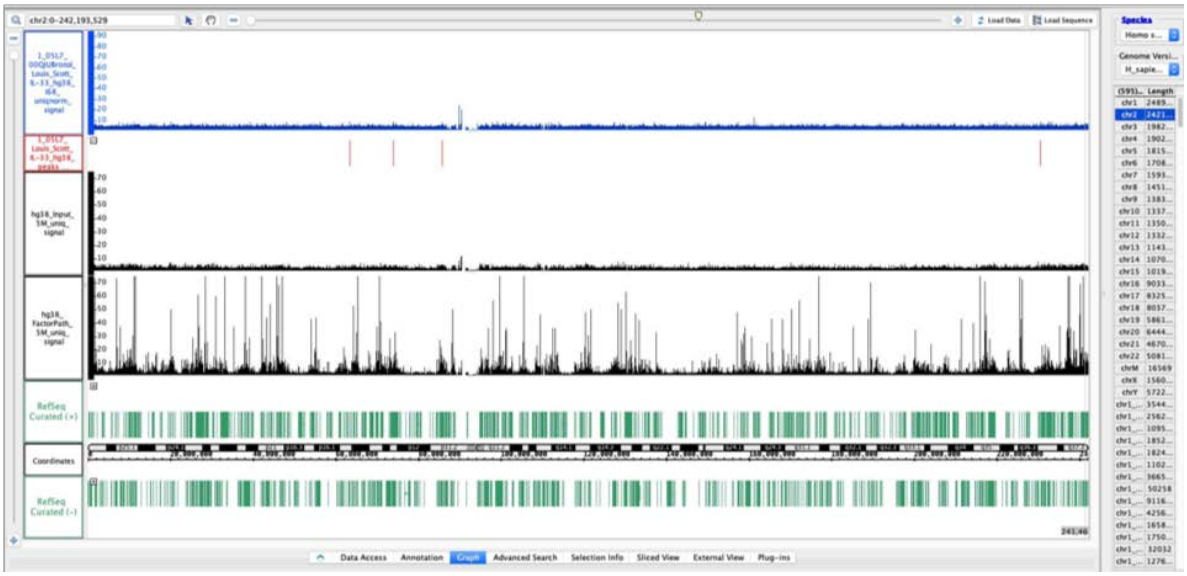

Figure 10.5. Small-scale DNA sequencing reveals few Nessy-1 binding sites in chromosomes one and two:

Integrated Genome Browser was used to determine Nessy-1 affinity DNA sites on (A) chromosome one and (B) chromosome two following ChIP and small-scale DNA sequencing. Nessy-1 data track (blue), followed by a track indicating the location of the filtered MACS peaks (red). The bottom two data tracks of the screenshots (black) show a negative ("input control") and positive ChIP-Seq assay (historical, unrelated data) for comparison and as illustration. These "control tracks" were generated from 5 million tags, and IGB y-axis scales were adjusted to make all tracks comparable. The bottom 2 tracks show the RefSeq gene annotations in green.

A

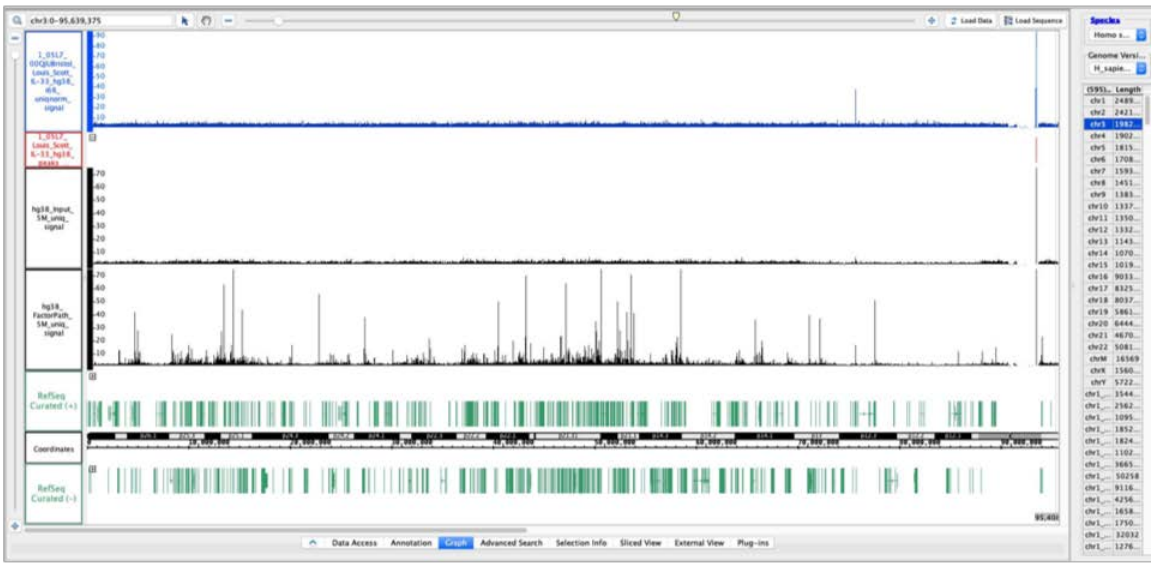

B

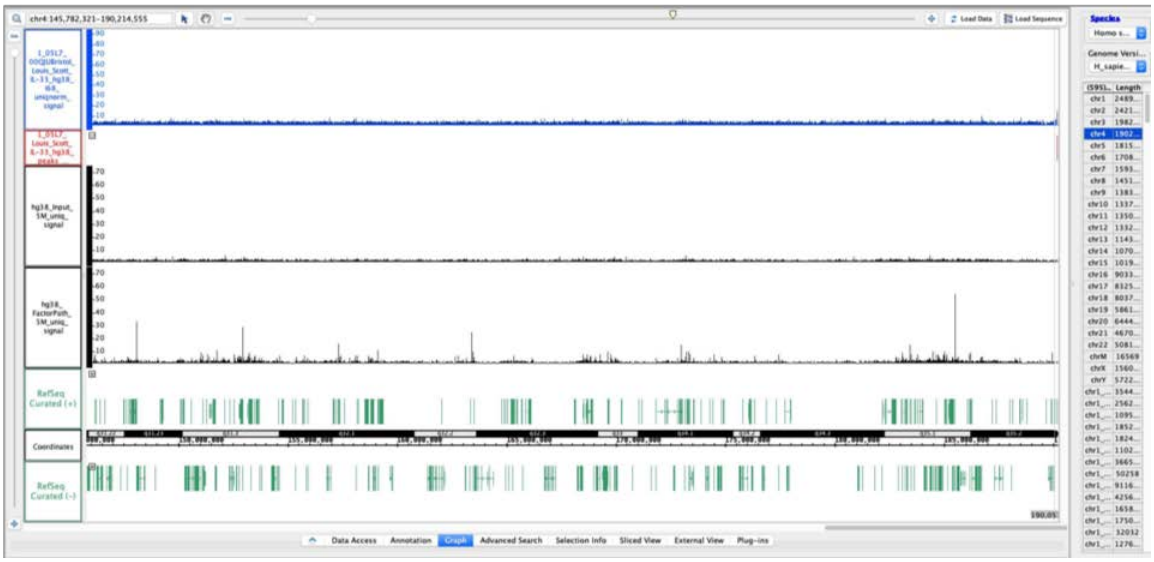

Figure 10.6. Small-scale DNA sequencing reveals few Nessy-1 binding sites in chromosomes three and four:

Integrated Genome Browser was used to determine Nessy-1 affinity DNA sites on (A) chromosome three and (B) chromosome four following ChIP and small-scale DNA sequencing. Nessy-1 data track (blue), followed by a track indicating the location of the filtered MACS peaks (red). The bottom two data tracks of the screenshots (black) show a negative ("input control") and positive ChIP-Seq assay (historical, unrelated data) for comparison and as illustration. These "control tracks" were generated from 5 million tags, and IGB y-axis scales were adjusted to make all tracks comparable. The bottom 2 tracks show the RefSeq gene annotations in green.

A

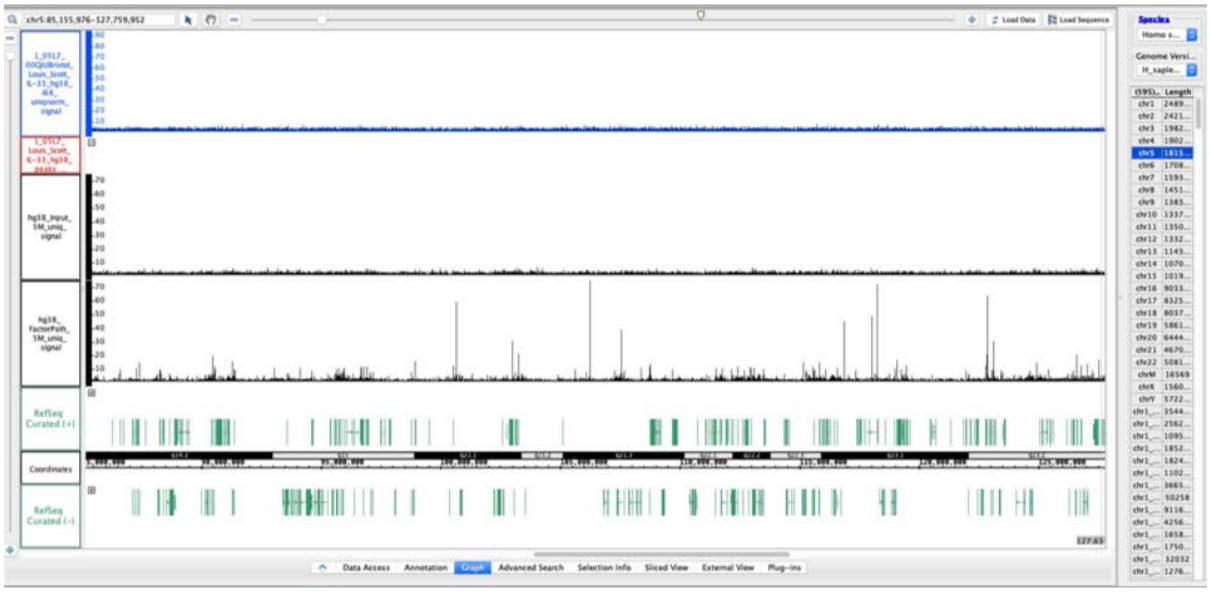

B

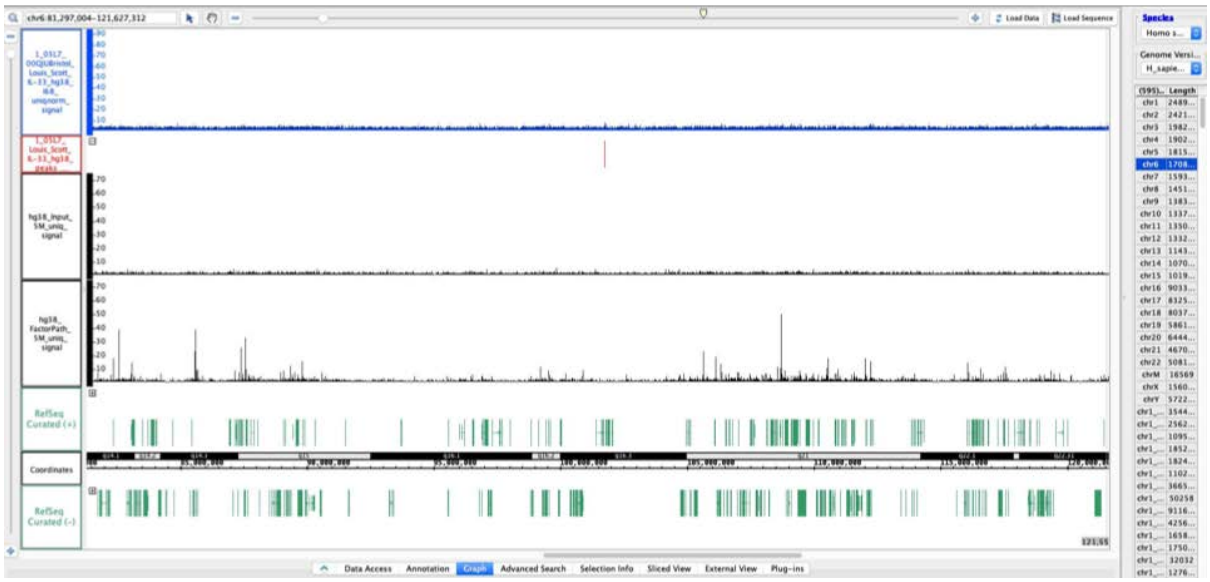

Figure 10.7. Small-scale DNA sequencing reveals few Nessy-1 binding sites in chromosomes five and six:

Integrated Genome Browser was used to determine Nessy-1 affinity DNA sites on (A) chromosome five and (B) chromosome six following ChIP and small-scale DNA sequencing. Nessy-1 data track (blue), followed by a track indicating the location of the filtered MACS peaks (red). The bottom two data tracks of the screenshots (black) show a negative ("input control") and positive ChIP-Seq assay (historical, unrelated data) for comparison and as

illustration. These “control tracks” were generated from 5 million tags, and IGB y-axis scales were adjusted to make all tracks comparable. The bottom 2 tracks show the RefSeq gene annotations in green.

10.6. Tables

10.6.1. Differentially expressed IL-33-interacting proteins following LPS stimulation

Protein	Fold change (LPS vs control)
40S ribosomal protein S14	3.123487
Serine/threonine-protein kinase ATR	1.913947
General transcription factor II-I	1.869565
Histone H3.2	1.811798
X-ray repair cross-complementing protein 6	1.781768
Histone H3.1	1.747967
SWI/SNF-related matrix-associated actin-dependent regulator of chromatin subfamily A	1.699605
Histone H2B type 1-J	1.641221
Prothymosin alpha	1.578947
60S ribosomal protein	1.575092
Granulins	1.567436
Heat shock 70kDa protein 8 isoform 1 variant	1.556092
RNA-binding protein EWS	1.556092
Histone H4	1.546763
40S ribosomal protein S2	1.546763
ABC transporter ATP-binding protein	1.539379
Polyadenylate-binding protein 1	1.537545
Heterogeneous nuclear ribonucleoprotein U	1.532067
Acidic leucine-rich nuclear phosphoprotein 32 family member B	1.532067
Enhancer of rudimentary homolog	1.530249
60S acidic ribosomal protein P2	1.523022
Polyadenylate-binding protein	1.517647
Non-histone chromosomal protein HMG-17	0.144514

Myosin-14	0.144811
Heterogeneous nuclear ribonucleoprotein K	0.146297
Myosin	0.146593
Actinin	0.149836
Mitochondrial import receptor subunit TOM20	0.151592
Heterogeneous nuclear ribonucleoprotein AB	0.151592
60S ribosomal protein L23a	0.16138
60S ribosomal protein L10a	0.163925
Heterogeneous nuclear ribonucleoproteins A2/B1	0.178277
Ribosome-binding protein 1	0.1918
40S ribosomal protein S7	0.219289
Poly [ADP-ribose] polymerase	0.263242
60S ribosomal protein L28	0.267032
Fus-like protein	0.313059
Caprin-1	0.316345
Alternative protein CHST9	0.320679
Heterogeneous nuclear ribonucleoprotein A1	0.456714
Heterogeneous nuclear ribonucleoprotein A3	0.481648

10.6.2. Differentially expressed IL-33 interacting proteins following Poly (I:C) stimulation

Protein	**Fold change (Poly (I:C) vs control)**
L-lactate dehydrogenase A	3.361564
Aldose reductase	3.225166
Alpha-enolase	3.077091
Protein transport protein sec16	2.646907
Pyruvate kinase M2 isoform	2.632353
Epididymis luminal secretory protein 52	2.559402

Glyceraldehyde-3-phosphate dehydrogenase	2.534081
Prothymosin alpha	2.409938
Eukaryotic translation initiation factor 4A, isoform 1	2.38403
ATP synthase subunit alpha	2.24605
Elongation factor 1-alpha	1.93407
Tubulin alpha chain	1.902827
Tubulin beta-4B chain	1.824503
Histone H4	1.79562
Histone H2B	1.683208
Moesin	1.681967
mRNA cap guanine-N7 methyltransferase	1.666031
Eukaryotic translation initiation factor 2A	1.663866
Eukaryotic translation initiation factor 5A-1	1.636071
Mitochondrial import receptor subunit TOM20	1.63197
Actin, cytoplasmic 1	1.618684
Autoantigen La	1.602317
Liver histone H1e	1.572554
Ribosomal protein L3	1.55
Elongation factor 2	1.541401
Serine/threonine-protein phosphatase	1.534639
Heterogeneous nuclear ribonucleoprotein AB	1.527969
60S ribosomal protein L35a	0.491538
Chromosome-associated kinesin KIF4A variant	0.487546
60S ribosomal protein	0.450539
Splicing factor U2AF	0.438163
Ras-GTPase-activating protein SH3-domain-binding protein	0.433944
ATP-dependent RNA helicase	0.422881
40S ribosomal protein S25	0.408405
Bcl-2-associated transcription factor 1	0.4006
Putative RNA-binding protein Luc7-like 2	0.377295

60S ribosomal protein L22	0.353086
Ribosomal protein L30	0.339869
E3 ubiquitin-protein ligase UBR5	0.332685
eIF4G1 variant protein	0.245236
Nuclear factor 1	0.072939

10.6.3. Differentially expressed IL-33 interacting proteins following TNFα stimulation

Protein	Fold change (TNFα vs control)
Nuclear factor 1	0.098835
60S ribosomal protein L12	0.477248
Ribosomal protein L30	0.351307
ATP-dependent RNA helicase DDX3X	0.490478
60S ribosomal protein L22	0.417284
40S ribosomal protein S25	0.387931
Bcl-2-associated transcription factor 1	0.480006
eIF4G1 variant protein	0.416249

10.6.4. Gene intervals identified from small-scale Nessy-1 ChIP-sequencing

Gene	Protein	Position (distance to start)	Peak summit
FAM230C	Family With Sequence Similarity 230 (RNA gene)	In gene (18,287)	18,212,112
LOC642643	Family With Sequence Similarity 230 Member A (RNA gene)	Upstream (-3,111)	18,730,624
DUX4L21	Double Homeobox 4 Like 21 (Pseudogene)	Downstream (9071)	133,689,440
FAM230C	Family With Sequence Similarity 230 (RNA gene)	In gene (16,815)	18,212,112
LOC102723981	Long Intergenic Non-Protein Coding RNA 234	Upstream (-3,111)	18,730,624
LOC105379474	Long Intergenic Non-Protein Coding RNA 932	Upstream (-2,255)	8,220,000
TIMP2	TIMP Metallopeptidase Inhibitor 2	Downstream (9071)	133,689,440
TEKT4P2	MAFF Interacting Protein-Like	In gene (18,287)	18,213,584
MGC39584	Family With Sequence Similarity 27 Member C (RNA gene)	Upstream (-5,345)	190,179,536
MGC39584	Family With Sequence Similarity 27 Member C (RNA gene)	Upstream (-4,978)	33,491,488
MGC39584	Family With Sequence Similarity 27 Member C (RNA gene)	In gene (1,893)	9,819,168
LOC105372752	Long Intergenic Non-Protein Coding RNA 53727	Downstream (18,467)	25,448,032
LOC105379516	Long Intergenic Non-Protein Coding RNA 9516	Upstream (-8,051)	12,175,104

LOC102723390	Long Intergenic Non-Protein Coding RNA 3390	Upstream (-4,051)	29,500,960
MIR6724-4	MicroRNA 6724-4	Upstream (-7077)	8,442,384
LOC105369207	Uncharacterized LOC105369207 (RNA gene)	Downstream (16671)	57,210,208
GLIS3	GLIS Family Zinc Finger 3	In gene (36,554)	4,273,952
LOC105376368	Uncharacterized LOC105376368 (RNA gene)	In gene (14609)	4,164,848
SLC7A8	Solute Carrier Family 7 Member 8	In gene (40,300)	23,143,360
LOC105379211	Long Intergenic Non-Protein Coding RNA (9211)	In gene (2,071)	20,341,440
ZNF236	Zinc Finger Protein 236	Downstream (148639)	21,854,336
MBP	Myelin Basic Protein	Upstream (-9278)	76,971,200
FEM1A	Fem-1 Homolog A	Downstream (7,436)	4,799,152
WDPCP	WD Repeat Containing Planar Cell Polarity Effector	In gene (492,281)	63,348,544
STAMBP	STAM Binding Protein	In gene (316)	73,857,712
SP100	SP100 Nuclear Antigen	In gene (84404)	230,500,560
COL23A1	Collagen Type XXIII Alpha 1 Chain	In gene (5,003)	178,585,552

GCSAML	Germinal Center Associated Signaling And Motility Like	In gene (6,740)	247,513,798
DUX4L22	Double Homeobox 4 Like 22 (Pseudogene)	Downstream (10749)	133,687,808
MSI2	Musashi RNA Binding Protein 2	In gene (322,902)	57,579,472
LOC105379516	Uncharacterized LOC105379516 (RNA gene)	Upstream (-4,035)	12,171,088
LOC102723981	Uncharacterized LOC102723981 (RNA gene)	Upstream (-3,217)	190,181,664
GRIK2	Glutamate Ionotropic Receptor Kainate Type Subunit 2	In gene (342,820)	101,736,528
AMY1C	Amylase Alpha 1C	In gene (342,820)	101,736,528
FAM90A19P	Family With Sequence Similarity 90 Member A19, Pseudogene	Upstream (-5564)	7,765,232
FAM91A1	Family With Sequence Similarity 91 Member A1	In gene (34,945)	123,803,384